SINGLE-STAGE, SLURRY-CATALYZED CO-PROCESSING DEVELOPMENTS

John G. Gatsis, Carl L. Lea, and Mark A. Miller
UOP Research Center
Des Plaines, Illinois, 60017

INTRODUCTION

UOP is currently in the sixth year of a co-processing research program sponsored by the U. S. Department of Energy (DOE). Earlier work, under completed contract DE-AC22-84PC70002, has been reported in a series of papers and reports (1-7). The overall objectives, to evaluate the technical feasibility of the co-processing concept and to establish a co-processing process data base, were met. The concept of single-stage, slurry-catalyzed co-processing was successfully demonstrated in laboratory batch experiments (1). The concept was further extended to include continuous bench-scale operations (2). Good long-term operability of the process was demonstrated in the continuous pilot plant for nearly 2,000 hours on stream (3). Typical yields and conversions from this run are shown in Table 1. A method of recovering the catalyst was developed and demonstrated on the laboratory scale. Catalyst recovery exceeded 95%. On the basis of the long-term operability and catalyst recovery studies, a conceptual commercial design was completed for a co-processing unit integrated with a 100,000 BPSD conventional refinery (3,4).

The overall objective of the current contract, DE-AC22-87PC79818, is to extend and optimize the single-stage, slurry-catalyzed co-processing scheme. Specific objectives are to improve and define catalyst utilization and costs, determine the process response to changes in resid composition and different coals, investigate the process response to changes in key operating variables, define optimum operating conditions, and reassess the economics of co-processing.

Catalyst economics play a major role in determining the overall profitability of slurry-phase co-processing. Consequently, much work has been devoted to exploring new catalyst systems and improving catalyst activity, dispersion, and recovery techniques. A new catalyst that is more active than the previous reference catalyst was identified in autoclave screening tests. This molybdenum-based catalyst is currently being evaluated in the continuous bench-scale unit. A study of the effect of catalyst concentration and increased process severity on product yields and plant operability has recently been completed and is the subject of this paper.

EFFECTS OF CATALYST CONCENTRATION AND INCREASED PROCESS SEVERITY

Program Objective

The overall objective of the current work is to study the interaction of catalyst concentration and increased process severity in the continuous bench-scale unit. A specific objective is to determine the optimum conversion level required to produce high liquid yields by selective catalytic conversion as opposed to thermal conversion. This study should lead to a better understanding of how the catalyst

functions and how it can best be utilized in co-processing to accelerate reactions and decrease intrinsic activation energy. Previous experience has indicated that optimum operation is achieved at less-severe operations, where undesirable regressive recombination reactions are minimized.

Continuous Bench-Scale Operations

A simplified block diagram of the pilot plant is shown in Figure 1. The unit contains many of the essential features of the commercial flow scheme and is equipped to quantitatively measure the hydrogen consumption in the operations. The slurry feed (finely ground coal, petroleum vacuum resid, and catalyst) is combined with a hydrogen-rich recycle gas and is preheated before it enters the bottom of an upflow reactor. The products from the reactor are separated into gas and oil streams in the high-pressure separator (HPS). The gas stream from the HPS is combined with makeup hydrogen before being recycled back to the incoming fresh feed. A portion of the oil stream from the HPS is recycled back to the incoming fresh feed, and the remainder is sent to a stripper. The lighter hydrocarbon stream from the stripper is sent to a debutanizer, where it is separated into C_{4-} and C_{5+} products. The heavier hydrocarbon stream from the stripper is sent to a vacuum fractionator to recover an overhead stream (light oil and vacuum gas oil) and a bottoms stream containing catalyst, coal minerals, insoluble carbonaceous material, and nondistillable hydrocarbons.

Feedstocks

The feedstocks used for this study were reference feedstocks, Lloydminster vacuum resid, designated as R10, and Illinois No. 6 coal designated as C1.4. Feed properties are given in Tables 2 and 3.

Lloydminster vacuum resid (950°F$^+$, 120-150 Pen.) was obtained from a commercial refinery in Canada.

Illinois Coal No. 6 was obtained by the Kentucky Center for Energy Research Laboratory from the Burning Star Mine. Grinding (thru 200 mesh) and drying were done by Empire Coke Company of Holt, Alabama. The preparation procedure and equipment have been previously described (5).

Process Conditions

For each given catalyst concentration, a temperature survey was conducted with a 2:1 mixture of resid to coal, at 3000 psig and base WHSV. The reactor temperature was increased in a stepwise manner from 420°C until evidence of thermal degradation or reactor fouling was observed. Heptane insoluble conversion, which is primarily controlled by catalytic effects, was monitored to determine the process response to temperature. Three catalyst concentrations, 0.50, 0.12 and 0.05 wt-% Mo, were studied.

0.50 wt-% Mo Catalyst Temperature Study

The first study was made with 0.50 wt-% molybedum (Mo) catalyst, measured on a metal per moisture and ash free feed (MAFF) basis. The run was started at 422°C, and the temperature was increased in a

stepwise manner. Six test conditions (422, 427, 440, 451, 457, and 467°C) were run. The plant operated well, even at the higher processing temperatures and showed no evidence of either thermal degradation or reactor fouling. Surprisingly, the conversions showed a steady increase with temperature, with no sign of decrease even at 467°C. The unconverted coal (toluene insolubles less ash) did not show the characteristic increase that is typically observed as a result of coking at higher temperatures (Figure 2). Heptane insoluble conversion also showed a steady increase with temperature (Figure 3). Previous studies showed a rapid decline in heptane insoluble conversions at temperatures greater than about 430°C and coking and plugging problems limiting plant operability above about 435°C (2). The decline in conversions and increase in coking with increased temperature may be attributed to retrograde reactions in which asphaltenes in the petroleum feedstock and those formed by thermal breakup of the coal polymerize and eventually form coke. In the presence of an effective hydrogenation catalyst and hydrogen, these reactive intermediates may be preferentially converted to stable lower-molecular-weight products. However, at high temperatures, the rates of the retrogressive thermal reactions possibly exceed those of the beneficial catalytic reactions, and pitch and coke are formed at the expense of the more-desirable lighter liquid products.

Two major differences between this study and the earlier temperature studies were observed, and these differences may account for the improved high-temperature conversions and plant stability. The catalyst was changed from a catalyst based on vanadium (V) to a more-active Mo-based catalyst, and a liquid recycle stream from the bottom of the HPS to the reactor inlet was included. Space velocity was maintained constant in each study, but the addition of the liquid recycle stream (5:1 recycle to fresh feed) resulted in greater mixing and higher velocity through the reactor. The improved high-temperature conversions and plant stability may be due to better contacting of the reactive fragments with hydrogen and catalyst (as a result of increased reactor backmixing), or to the decreased relative contact between the coke precursors and the hot reactor walls due to greater superficial liquid velocities in the reactor. Hydrodynamic differences from the recycle may have also affected the flow regime, heat transfer characteristics, or gas void fraction in the reactor. How much of the improved high-temperature conversion and operability is due to the catalyst and how much is due to improved hydrodynamics resulting from use of liquid recycle is not known at this time. Further reactor modeling studies are required to thoroughly understand these phenomena.

The greatest impact of the higher temperature was the 40 wt-% increase in nondistillable conversion (Figure 4), without significant carbon loss to retrograde reactions, and only about 6% increase in light-ends yields (Figure 5). Table 4 compares the yields and product properties at 427, 451, and 467°C. The product distribution gives the expected trends with increasing temperature: an increase of lighter fractions (C_1-C_4, C_5-177°C, and 177-343°C) and a decrease of heavier fractions (343-510°C and 510°C+). The quality of the liquid product improved with increasing temperature. The API gravity and hydrogen content of the product increased, and heptane insolubles, sulfur, and nitrogen levels decreased.

0.12 wt-% Mo Catalyst Temperature Study

This run was started at 427°C, and as in the previous run, the temperature was increased in a stepwise manner. Six test conditions (427, 432, 438, 446, 451, and 459°C) were run. Plant operations were again reasonably good, and there was no evidence of thermal degradation or reactor fouling. As in the prior run, all of the conversions continued to increase with temperature over the range studied. The unconverted coal showed a steady decrease with temperature (Figure 6), and the heptane-insoluble conversion increased with temperature (Figure 7). The yields and product properties at 427, 446, and 459°C are compared in Table 5. The yields of lighter fractions (C_1-C_4, C_5-177°C, and 177-343°C) increased and the heavier fractions (343-510°C and 510°C+) decreased with increasing temperature. The increases in nondistillable conversion (Figure 8), and light-ends yields (Figure 9) were comparable to the 0.50% Mo case. The quality of the liquid product improved with increasing temperature. The API and hydrogen content increased, and heptane insolubles, sulfur, and nitrogen levels decreased, though to a lesser extent than in the 0.50% Mo case.

0.05 wt-% Mo Catalyst Temperature Study

The third temperature study was conducted with a 0.05 wt-% Mo catalyst concentration. The objective of this run was to determine the low-concentration and high-temperature operability limits of the plant. Four test conditions (428, 447, 456,and 462°C) were run. Even with this low catalyst concentration, the plant operations were reasonably good, and there was no evidence of either thermal degradation or reactor fouling over the temperature range studied. As in the previous runs, all of the conversions continued to increase with temperature, and the yields and product properties follow similar trends. The yield of unconverted MAF coal, heptane insolubles, and nondistillable conversions and light-ends yield versus temperature are shown in Figures 10-13. Yields and product properties at 428, 447, and 462°C are compared in Table 6.

Effect Of Catalyst Concentration

An understanding of the effect of catalyst concentration at increased process severity is important to the co-processing concept. Increased conversion of petroleum resid and coal to lighter products can be achieved by increasing process severity. However, at these high conversion levels, increased hydrogen consumption and the nonselective production of light ends also occur. Degradation reactions and the fouling and coking tendency of the resid-coal mixture also tend to increase at high-severity conditions. At very high severities, thermal effects greatly predominate over catalytic effects and further accelerate the problems associated with yield loss, product stability, and coking. A wide range of nondistillable conversion levels can be achieved, merely by increasing the reactor temperature. The more-difficult task and an important part of UOP's program is to determine the optimum conversion level that produces high liquid yields by selective catalytic conversion, as opposed to thermal conversion, and reduces the problems associated with high severity operation.

Nondistillable conversion, which increased with increasing

temperature, was about the same for the different catalyst concentrations over the entire temperature range investigated (Figure 16). This result indicates that nondistillable conversion is primarily controlled by thermal effects and is not catalytically induced. Coal conversion (Figure 14) and heptane insoluble conversion (Figure 15) were more responsive to catalyst concentration, indicating that catalyst plays a role in coal and heptane-insoluble conversion. The 0.05 wt-% Mo catalyst gave slightly higher heptane insoluble conversion (Figure 15) than the 0.12 wt-% Mo. The liquid product properties were also equal to or better than the properties of the 0.12 wt-% Mo catalyst. This can be accounted for by improved catalyst dispersion for the 0.05 wt-% Mo catalyst. The effect of catalyst concentration was more pronounced at temperatures below about 440°C. At the higher temperatures, the effect of catalyst concentration diminishes, and virtually identical performance is obtained irrespective of catalyst concentration. The fact that the effect of catalyst concentration was more pronounced at the low temperature and its effect diminished at the high temperature indicates that hydrogenation, which is catalytically induced and is favored at low temperature, is being promoted by the catalyst. The catalyst provides hydrogen in an active form for stabilization of the coal-derived free radicals at the onset of coal dissolution and for the conversion of asphaltenes to thermally stable oil-soluble products. Thus, the catalyst beneficially effects the ultimate conversion and product distribution. The liquid-product properties (Tables 4, 5, and 6) followed the same trends as the coal and heptane-insoluble conversions; i.e., they improved with higher catalyst concentration, and the improvement diminished with increasing temperature. Increases in API, hydrogen content, conversion of asphaltenes, and removal of heteroatoms are primarily controlled by catalytic effects that predominate at the lower temperatures.

Two questions may be asked: what is the role of the catalyst at the higher temperature, and is it indeed needed? To answer these questions, UOP has planned a run with no catalyst. This run will provide a baseline for determining whether improved high temperature operability was due solely to improved hydrodynamics resulting from the use of liquid recycle, or whether the catalyst also plays an important role, even at very low concentrations.

CONCLUSIONS

The beneficial effects of increased catalyst concentration were more pronounced at lower temperatures (below about 440°C). The advantage of high catalyst concentration diminished at higher temperatures, where thermal effects dominate over catalytic effects. High nondistillable conversions, without excessive carbon loss to retrograde reactions and light-ends yields, were demonstrated. The improved operability of co-processing at high temperatures represents an important advance that may significantly improve the process economics.

REFERENCES

(1) J. G. Gatsis, et. al., "Coal Liquefaction Co-Processing," Proceedings of DOE Direct Liquefaction Contractors' Review Meeting, Nov. 19-21, 1985.

(2) J. G. Gatsis, et. al., "Continuous Bench-Scale Single-Stage Slurry Catalyzed Co-Processing," Proceedings of DOE Direct Liquefaction Contractors' Review Meeting, Oct. 20-22, 1986.

(3) J. G. Gatsis, et. al., "Continuous Bench-Scale Single-Stage Slurry Catalyzed Co-Processing," Proceedings of DOE Direct Liquefaction Contractors' Review Meeting, Oct. 6-8, 1987.

(4) D. A. Nafis, et. al., "Bench-Scale Co-Processing," Proceedings of DOE Direct Liquefaction Contractors' Review Meeting, Oct. 4-6, 1988.

(5) C. P. Luebke, et. al., "Coal Liquefaction Co-Processing Topical Report Number 1," Prepared for the United States Department of Energy under Contract No. DE-AC22-84PC70002, June 1, 1987.

(6) J. G. Gatsis, et. al., "Coal Liquefaction Co-Processing Topical Report Number 2," Prepared for the United States Department of Energy under Contract No. DE-AC22-84PC70002, Aug. 19, 1988.

(7) D. A. Nafis, et. al., "Coal Liquefaction Co-Processing Final Report," Prepared for the United States Department of Energy Under Contract No. DE-AC22-84PC70002.

(8) D. A. Nafis, et. al., "UOP Co-Processing Developments," Proceedings of DOE Direct Liquefaction Contractors' Review Meeting, Oct. 2-4, 1989.

Table 1

Run 19 Long-Term Operability Study

Conditions:

Coal: Ill. No. 6 (C1.2)
Resid: Lloydminster Vacuum Resid (R8)
Catalyst: 1.0 wt-% V (K1.0)
Resid-Coal: 2:1
Temperature: 425°C
Pressure: 3,000 psig

Yields, wt-% MAF Coal and Resid	
H_2S	2.2
NH_3	0.4
H_2O	5.0
C_1-C_4	2.7
C_5-371°C	28.5
371-510°C	26.3
510+°C	33.7
Unc. MAF Coal*	3.7
H_2 Consumption	(2.5)
	100.0

Conversions, wt-%	
MAF Coal	89.3
Heptane Insolubles	79.5
510+°C Nondist.	56.8
371+°C Nondist.	35.7

Table 2

Petroleum Resid Analysis

Resid	Lloydminster Vacuum Resid (R10)
API Gravity	6.6
Specific Gravity	1.0246
Distillation, °C	
IBP, vol-%	379
5	455
10	473
20	509
EP	512
Vol-% over at EP	22.0
Analysis, wt-%	
Carbon	83.6
Hydrogen	10.3
Sulfur	4.77
Nitrogen	0.59
Heptane Insolubles	13.56
Carbon Residue (MCRT)	17.39

Table 3

Coal Analysis

Coal	Illinois No. 6 (Cl.4)
Proximate Analysis (AR Basis), wt-%	
Volatile Matter	38.84
Fixed Carbon (1)	45.80
Moisture	4.08
Ash	11.28
Ultimate Analysis (AR Basis), wt-%	
Carbon	66.75
Hydrogen (2)	4.66
Sulfur	2.91
Nitrogen	1.34
Oxygen (1)	8.98
Ash	11.28
Moisture	4.08

(1) By difference
(2) Corrected for moisture

Table 4

Effect of Severity on Yields and Product Properties

0.50 wt-% Mo Catalyst

Temperature, °C	427	451	467
Yields, wt-% MAFF			
$H_2O + CO_x$	2.20	4.22	6.11
H_2S	2.26	3.11	3.11
NH_3	0.21	0.63	0.22
C_1-C_4 (Light Ends)	2.33	6.75	8.91
C_5-177°C (Naphtha)	5.90	17.17	25.46
171-343°C (Distillate)	17.61	31.54	32.59
343-510°C (VGO)	26.52	22.12	15.90
510°C+ (Resid)	40.82	15.27	8.37
Unc. MAF Coal	4.51	2.87	2.95
H_2 Consumption	(2.37)	(3.66)	(3.61)
TOTAL	100.00	100.00	100.00
C_{5+} Total Liquid Product			
MAFF, wt-%	90.85	86.10	82.32
API Gravity	13.3	24.4	28.6
Carbon, wt-%	86.36	86.99	85.76
Hydrogen, wt-%	10.38	11.04	11.23
Sulfur, wt-%	1.66	0.61	0.47
Nitrogen, wt-%	0.79	0.57	0.84
Heptane Insolubles, wt-%	8.64	4.61	3.38
MCRT, wt-%	12.84	7.36	6.36

Table 5

Effect of Severity on Yields and Product Properties

0.12 wt-% Mo Catalyst

Temperature, °C	427	446	459
Yields, wt-% MAFF			
$H_2O + CO_x$	6.7	4.0	4.3
H_2S	1.6	3.3	3.5
NH_3	0.2	0.4	0.8
C_1-C_4 (Light Ends)	2.5	5.5	9.1
C_5-177°C (Naphtha)	5.4	12.0	14.5
177-343°C (Distillate)	17.6	24.0	36.0
343-510°C (VGO)	29.2	26.1	22.9
510+°C (Resid)	34.0	24.2	10.3
Unc. MAF Coal	5.6	3.6	2.3
H_2 Consumption	(2.8)	(2.9)	(3.6)
TOTAL	100.0	100.0	100.0
C_{5+} Total Liquid Product			
MAFF, wt-%	86.2	86.3	83.7
API Gravity	12.9	17.0	19.9
Carbon, wt-%	84.7	84.0	84.4
Hydrogen, wt-%	10.0	10.3	11.0
Sulfur, wt-%	2.1	1.4	1.1
Nitrogen, wt-%	0.9	0.8	0.4
Heptane Insolubles, wt-%	9.8	9.1	3.1
MCRT, wt-%	12.7	11.2	6.2

Table 6

Effect of Severity on Yields and Product Properties

0.05 wt-% Mo Catalyst

Temperature, °C	428	447	462
Yields, wt-% MAFF			
$H_2O + CO_x$	1.67	2.00	3.64
H_2S	2.51	3.28	3.64
NH_3	0.34	0.49	0.42
C_1-C_4 (Light Ends)	2.75	5.68	9.10
C_5-177°C (Naphtha)	5.69	13.69	23.43
173-343°C (Distillate)	11.04	25.65	27.92
343-510°C (VGO)	30.65	24.47	17.92
510°C+ (Resid)	40.66	24.03	14.66
Unc. MAF Coal	6.76	3.67	2.62
H_2 Consumption	(2.07)	(2.96)	(3.35)
TOTAL	100.00	100.00	100.00
C_{5+} Total Liquid Product			
MAFF, wt-%	88.04	87.84	83.93
API Gravity	11.4	18.7	25.4
Carbon, wt-%	84.4	84.8	85.0
Hydrogen, wt-%	10.4	10.9	11.3
Sulfur, wt-%	2.4	1.5	0.9
Nitrogen, wt-%	0.7	0.7	0.7
Heptane Insolubles, wt-%	7.0	5.6	3.1
MCRT, wt-%	13.5	10.6	8.7

FIGURE 1

CO-PROCESSING PILOT PLANT

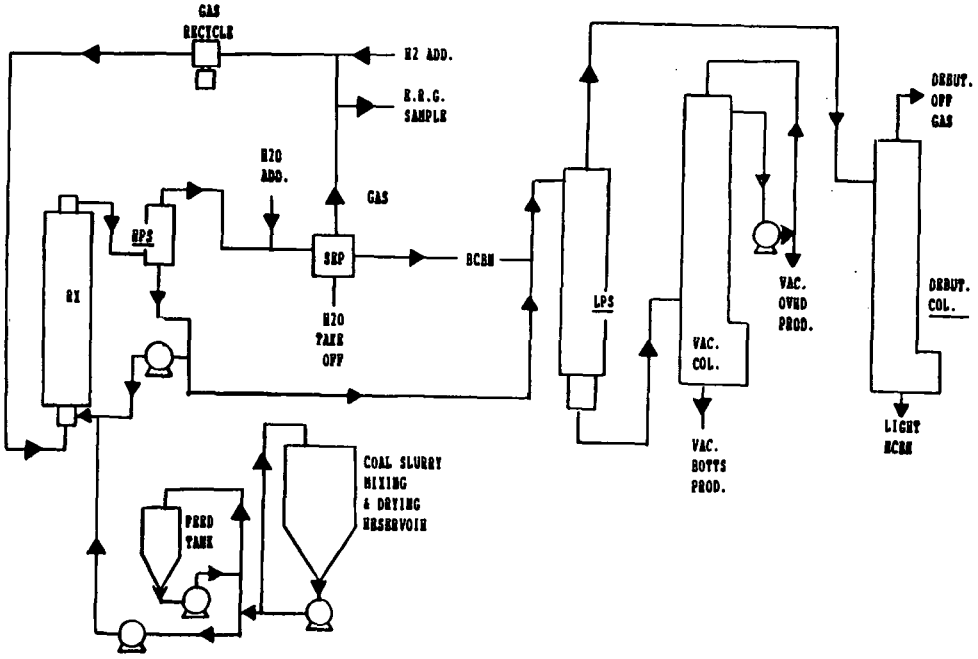

Figure 2

Unconverted Coal Yield
vs. Temperature

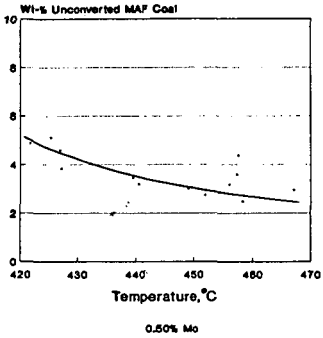

Figure 3

Hept. Insol. Conversion
vs. Temperature

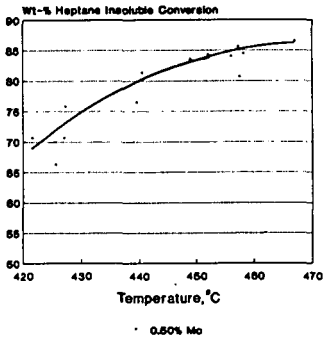

Figure 4

Nondistillable Conversion
vs. Temperature

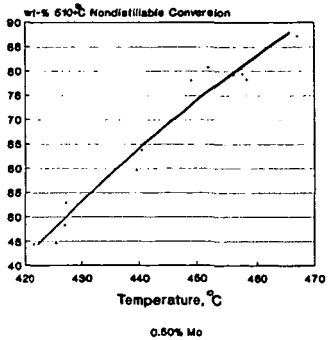

Figure 5

Light Ends Yields
vs. Temperature

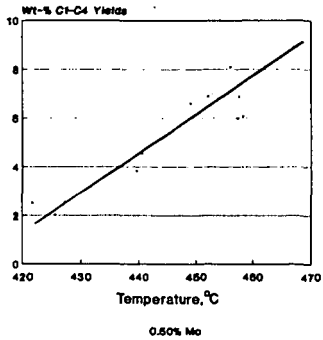

Figure 6

Unconverted Coal Yield
vs. Temperature

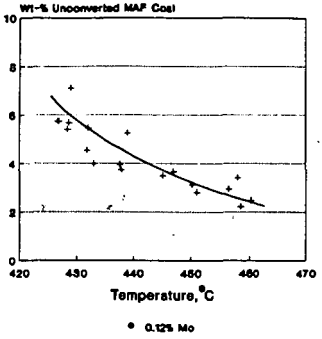

Figure 7

Hept. Insol. Conversion
vs. Temperature

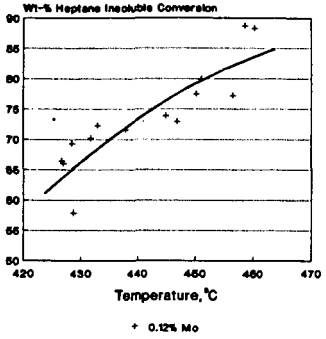

Figure 8

Nondistillable Conversion
vs. Temperature

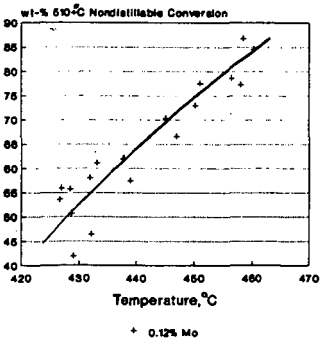

Figure 9

Light Ends Yields
vs. Temperature

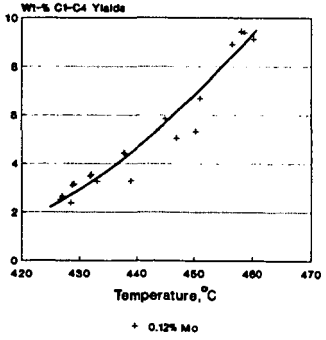

CO-PROCESSING OF NEW MEXICO COAL WITH HONDO RESIDUUM

John E. Duddy and Sudhir V. Panvelker
HRI, Inc., Princeton, NJ 08540

KEYWORDS: coal liquefaction, co-processing, synfuels

INTRODUCTION

Hydrocarbon Research, Inc. (HRI) has developed a process for co-processing coals with heavy petroleum crudes and residua. The process utilizes one or more ebullated bed reactors in series and brings together experience in resid processing (H-Oil process) and coal liquefaction (H-Coal and CTSL processes). Co-processing has been demonstrated with bench-scale and PDU-scale tests.

During last few years, HRI has assessed co-processing performance of several coal and petroleum feedstock combinations. Coals of varying rank including Texas lignite, Black Thunder (Wyoming), Forestburg (Alberta), New Mexico (McKinley mine), and Taiheiyo (Japan) subbituminous coals, Ohio 5/6, Lingan (Nova Scotia) and Westerholt (Germany) bituminous coals were tested. Petroleum residua tested include Maya (Mexico), Orinoco (Venezuela), Cold Lake (Canada), and Hondo (California).

This paper presents results obtained on co-processing of New Mexico coal with a vacuum residuum from Hondo heavy crude. This feedstock combination was found to be particularly reactive in co-processing. Some results on comparative reactivities of Hondo, Maya, and Cold Lake residua, using Texas lignite as a reference coal, are also presented.

EXPERIMENTAL

The bench tests were conducted in a 50 lb/day (nominal size) continuous unit equipped with two close-coupled ebullated bed reactors. Both reactors were charged with commercial NiMo hydroprocessing catalyst which was sulfided during start-up. Unlike commercial operation, each bench test was conducted with a fixed charge of catalyst with no intermediate catalyst additions and withdrawals.

Table 1 shows the analyses of New Mexico (McKinley mine) subbituminous coal and Texas lignite (cleaned, from Homer city). Analyses of Hondo, Cold Lake, and Maya vacuum resids are also shown in Table 1.

RESULTS AND DISCUSSION

New Mexico coal was co-processed with Hondo vacuum resid according to the run plan indicated in Table 2. Condition 1 was the baseline condition at the base space velocity, base reference (internal reactor) temperature of 810°F in both reactors, 33 W % coal concentration in feed, and once-through operation. Coal concentration, space velocity and reactor temperatures were varied over conditions 2 through 4. In condition 2, with coal concentration at 50 W % of fresh feed, atmospheric bottoms were used as recycle (to reduce the feed viscosity) at recycle-to- fresh-feed ratio of 0.5. Condition 5 was identical to condition 1 and was used to assess the extent of catalyst deactivation.

The process performance obtained in co-processing of New Mexico coal with Hondo vacuum resid is shown in Table 2 and in Figures 1 and 2. The product yields are based on ASTM distillations. Coal conversion was calculated based on solubility in quinoline. Residuum (975°F+) conversion was calculated from D-1160 distillation on product vacuum-still-bottoms. Hydrodesulfurization (HDS) and Hydrodenitrogenation (HDN) were calculated from heteroatom contents of the products and the total feed (including ash). Demetallization was based on the metals (Ni + V) content of the liquid product. Net C_4-975°F yield was calculated by subtracting the gas oil content of the feed from the C_4-975°F content of the product and expressing it as a percentage of the feed 975°F+ (MAF) content. Hydrogen efficiency is defined as the ratio of net distillate produced to hydrogen consumption.

Coal conversion for New Mexico coal ranged from 91.0 to 93.1 W % (MAF). There was virtually no effect of catalyst deactivation on coal conversion. Coal conversion dropped from 93.1 W % in condition 1 to 92.5 W % in condition 5. The lowest coal conversion (91.0 W %) was obtained in condition 3 (at high space velocity), however, the decrease was small. Residuum (975°F+) conversion ranged from 85.9 to 93.2 (MAF) W %. There was a small effect of catalyst deactivation, 975°F+ conversion dropped from

93.2 W % in condition 1 to 91.1 W % in condition 5. Again, the lowest conversion was obtained in condition 3. The effect of high space velocity was more pronounced on 975°F+ conversion than on coal conversion, with 975°F+ conversion dropping to 85.9 W % in condition 3.

Hydrodesulfurization (HDS) level was very high throughout the run, ranging from 96.7 W % to 97.7 W %. In conditions using oil-to-coal ratio of 2, more than 95% of the sulfur content of the feed was associated with Hondo. The extremely high level of HDS is an indication of the high reactivity of Hondo. Hydrodenitrogenation (HDN), unlike HDS, was very dependent upon catalyst age, decreasing from 87.4 W % in condition 1 to 67.3 W % in condition 5. High level of demetallization, over 96 W %, was obtained throughout the run.

The net yield of C_4-975°F product was high and ranged from 72.6 W % to 77.9 W % (expressed as percentage of 975°F+ MAF content of feed). The lowest yield was obtained in low-severity (high space velocity) condition. Excluding this condition, the yield range was quite small with very low effect of catalyst deactivation.

The effect of coal concentration on process performance can be assessed by interpolating the performance at condition 1 and condition 5 to condition 2 and comparing it with that observed in condition 2. It is, however, difficult to use this method to assess the effect on HDN due to high, non-linear deactivation effect on HDN performance. The effect of coal concentration on coal and 975°F+ conversions was slightly negative, with that on 975°F+ conversion a little more pronounced. Higher coal concentration also gave a lower net yield of C_4-975°F distillate and showed lower hydrogen efficiency. The latter was caused due to lower hydrogen content of the feed and higher gas (C_1-C_3) and water yields obtained using higher coal concentration. As shown in Table 2, the yield of vacuum gas oil (VGO) (650-975°F) fraction in the product slate was lower in condition 2. However, when yields are calculated on a net basis (by subtracting VGO portion of the feed), the distillate selectivity for condition 2 is not much different from that in condition 1. In both cases, the net yield of VGO was quite small indicating the reactive nature of New Mexico coal *and* Hondo vacuum resid.

In condition 3, low severity was employed by increasing the space velocity from the base value by 60%. Consequently, lower process performance was obtained. As mentioned earlier, coal conversion decreased by a small amount and the 975°F+ conversion and net C_4-975°F yield decreased by a greater amount. The hydrogen consumption fell considerably.

The reference reactor temperature was increased by 15°F in condition 4 maintaining the high space velocity. The increased severity increased process performance to the high levels obtained in the baseline condition. Hydrogen efficiency in condition 4, although lower than that in condition 3 due to higher gas yield, was still quite high. The effect of temperature and space velocity on net distillate selectivity is shown in Figure 3. In condition 3 (base temperature, high space velocity), the net selectivity of VGO was quite high - 14.5 W % (of C_4-975°F product) versus less than 2 W % in condition 5 (base temperature, base space velocity). When the temperature was increased in condition 4 by 15 F, the net selectivity of VGO dropped to 3.1 W % giving a very light product slate. The selectivity in condition 4 was very similar to that in condition 5. The results indicate that the operating variables used in condition 4 would produce a more economical product as compared to the baseline conditions (1/5) due to lower capital cost arising from higher space velocity. Higher temperature operation usually results in higher gas make-up and higher catalyst deactivation. However, the above results suggest that these factors are of small consequence for New Mexico/Hondo feedstock combination.

A noteworthy feature of this test was the effect of catalyst deactivation on performance. The effect of deactivation on coal conversion and HDS was negligibly small. It affected 975°F+ residuum conversion, however, the magnitude was quite small. HDN and hydrogen consumption, especially the former, were markedly affected by catalyst deactivation. Table 3 shows the analyses of the product TBP cuts. All distillate products had very low sulfur contents. There is a significant effect of deactivation on the product quality of heavier cuts. For instance, the 975°F+ liquid portion obtained on day 21 had very low hydrogen content and higher sulfur, nitrogen, and metals contents as compared to that obtained on day 5. It is very interesting to note that there is a large effect on the sulfur content (0.07 W % on day 5 versus 0.48 W % on day 21) although the effect on HDS level is very small (97.7 W % on day 1 versus 96.7 W % on day 21). This is due to very low yields of 975°F+ liquid product.

The small effect on catalyst deactivation on coal and residuum conversions and HDS might be hypothesized as due to predominantly thermal character of these reactions. This is quite true for coal conversion and partly true for residuum conversion. It is quite unlikely that the desulfurization of the thiophenic components typically found in heavy oils would occur by a thermal path. A possible explanation of the behavior observed here might be the non-uniform deactivation of catalyst sites. It is known that hydrotreating catalysts such as the one used here have distinct hydrogenation and hydrogenolysis sites. The former type of sites might have deactivated while the latter type relatively unaffected. HDS rate is dependent upon hydrogenolysis and does not require hydrogenation. HDN reactions require hydrogenation prior to hydrogenolysis and could get affected by deactivation of hydrogenation sites depending upon the limiting step in the reaction network.

Co-processing of New Mexico coal with Hondo vacuum resid gave very high level of demetallization (based on metals (Ni + V) content of the liquid product). Figure 4 shows the mode of demetallization. In all conditions, the total demetallization was in high 90's (W %). In condition 1, catalytic demetallization accounted for more than 80%. The balance was achieved through deposition on coal solids. During the course of the run, as the catalyst deactivated, the relative amount of catalytic demetallization dropped. In condition 5, it accounted for just over 55 W %, the balance was achieved by coal solids. Although this decline in catalytic activity towards demetallization is significant, it is our experience that the above retained activity is higher than that typically observed for a similarly aged catalyst.

The recovered first-stage catalyst had lower carbon content and higher contaminant metals than the second-stage catalyst. This is the usual behavior, however, the first-stage carbon content was lower than that usually found. This perhaps is the cause for higher retained activity towards 975°F+ conversion, HDS and demetallization.

The extremely high HDS level indicated that Hondo vacuum resid was very reactive. In order to compare its reactivity with other residua tested in this program, Texas lignite was co-processed with Maya, Hondo, and Cold Lake. Texas lignite was the reference coal for the program. The run plan and the results are shown Table 4 and in Figure 5. The residuum conversion with Hondo was 92.7 W % versus 90.3 W % with Maya and 88.1 W % with Cold Lake. Similarly, HDS level was higher with Hondo. The product distribution as reported in Table 4 did not show much variation, however, considering Hondo contained substantial amount of VGO, the net distillate product slate with Texas lignite - Hondo combination was more selective towards lighter products.

The reactivity of various coal/residuum combinations towards 975°F+ residuum conversion were modelled by the equation:

$$k = k_o * \exp(-E/RT) * (1+C)^a * \exp(-d*A)$$

where,

- k = first-order rate constant calculated assuming two CSTRs in series,
- k_o = constant representing initial reactivity at 0 W % coal
- E = activation energy
- R = gas constant
- T = temperature
- C = fractional coal concentration
- a = exponent indicating effect of coal concentration
- d = deactivation parameter
- A = catalyst age

This model fits the experimental data obtained under the entire program very well. Table 5 shows a comparison of the model parameters obtained for various feedstock combinations. New Mexico - Hondo combination was the most reactive feedstock and had very low deactivation rate.

CONCLUSION

New Mexico subbituminous coal was co-processed with Hondo vacuum resid in a continuous bench unit employing HRI's Coal/Oil Co-processing Technology. This feedstock was very reactive and gave high yield of distillate product. The hydrodesulfurization was extremely high. The effect of catalyst deactivation on residuum conversion, HDS, and net distillate yield was quite small, however, the effect on HDN was more pronounced. A separate test done on co-processing of Texas lignite with Maya, Hondo, and Cold Lake VSB showed that Hondo was the most reactive residuum.

ACKNOWLEDGEMENTS

The above work was sponsored by U.S. Department of Energy, Alberta Research Council, Mitsui SRC Company and Ruhrkohle Oel und Gas, Electric Power Research Institute and Ontario-Ohio Synthetic Fuels, Ltd.

TABLE 1
ANALYSES OF FEEDSTOCKS

COALS	New Mexico	Texas Lignite
Moisture, W %	7.6	9.4
Ultimate Analysis, W % (Dry)		
Carbon	69.3	64.7
Hydrogen	5.2	4.4
Nitrogen	1.3	1.3
Sulfur	0.5	1.3
Ash	9.8	12.6
Oxygen (Difference)	13.9	15.7

PETROLEUM VACUUM RESIDUA	Hondo	Cold Lake	Maya
API Gravity	7.8	2.6	3.1
Elemental Analysis, W %			
Carbon	82.8	83.5	83.4
Hydrogen	10.6	9.9	9.9
Nitrogen	0.8	0.7	0.7
Sulfur	5.4	5.7	5.1
Metals, WPPM			
Nickel	108	137	105
Vanadium	277	348	562
IBP,°F	750	882	835
IBP-975°F, W %	31.9	9.1	9.6
975°F+, W %	68.1	90.9	90.4

TABLE 2

CO-PROCESSING OF NEW MEXICO COAL WITH HONDO VACUUM RESIDUUM

Condition No.	1	2	3	4	5
Days	1-5	6-9	10-13	14-17	18-21
Relative Space Velocity	1.0	1.0	1.6	1.6	1.0
Reactor Temperature, °F	810	810	810	825	810
Coal Concentration in Fresh Feed, W %	33	50*	33	33	33
Yields (W % Fresh Feed)					
C_1-C_3	6.1	6.3	4.6	6.3	6.4
C_4-350°F	16.0	17.2	13.7	18.4	18.0
350-650°F	40.9	38.2	33.0	38.2	38.5
650-975°F	23.2	19.7	29.2	23.1	22.2
975°F+ Liquid	3.0	4.1	7.9	3.5	4.4
Coal (IOM) + Ash	5.3	8.7	6.3	5.7	5.8
$CO + CO_2$	0.3	0.4	0.5	0.6	0.2
$NH_3 + H_2S + H_20$	9.7	10.3	8.4	8.4	8.7
Total (100 + H_2 Consumption)	104.5	104.9	103.5	104.1	104.0
Coal Conversion (W % MAF)	93.1	92.3	91.0	92.9	92.5
975°F+ Conversion (W % MAF)	93.2	90.3	85.9	92.5	91.1
HDS, W %	97.7	97.1	97.1	97.1	96.7
HDN, W %	87.4	77.4	66.5	67.6	67.3
DEMET, W %	99.1	98.4	99.9	97.6	96.6
C_4-975°F Yield (W % Dry Fresh Feed)	80.2	75.1	75.9	79.7	78.7
Net C_4-975°F Yield (W % 975°F+ MAF)	77.9	74.9	72.6	77.6	76.2
Hydrogen Efficiency (Net C_4-975/H_2 Consumed)	13.0	12.2	15.4	14.3	14.3

* Atmospheric Bottoms were used as recycle (50 W % Fresh Feed) to facilitate pumping

TABLE 3

PRODUCT PROPERTIES
CO-PROCESSING OF NEW MEXICO COAL WITH HONDO VACUUM RESIDUUM

Condition No.	1	2	3	4	5
Day	5	9	13	17	21
IBP-350°F					
API Gravity	51.4	54.8	54.8	54.3	54.8
Carbon, W %	86.5	85.5	86.1	85.5	85.1
Hydrogen, W %	13.9	14.7	14.6	14.5	14.5
Sulfur, W %	0.01	0.01	0.01	0.01	0.01
Nitrogen, W %	0.02	0.11	0.12	0.12	0.11
350-650°F					
API Gravity	32.3	31.0	31.8	31.0	31.8
Carbon, W %	87.6	87.1	87.0	87.5	87.6
Hydrogen, W %	12.8	12.9	12.9	12.6	12.4
Sulfur, W %	0.01	0.01	0.01	0.03	0.02
Nitrogen, W %	0.14	0.22	0.31	0.35	0.24
650-975°F					
API Gravity	22.8	20.1	19.3	20.2	20.3
Carbon, W %	87.4	87.9	87.6	88.0	88.1
Hydrogen, W %	12.0	11.7	12.2	11.8	11.8
Sulfur, W %	0.03	0.02	0.10	0.08	0.11
Nitrogen, W %		0.55	0.45	0.50	0.49
975°F+ Liquid					
API Gravity	4.0	-1.3	-2.2	-8.2	-6.8
Carbon, W %	88.0	89.3	88.7	90.4	89.8
Hydrogen, W %	11.1	9.1	9.0	7.8	7.9
Sulfur, W %	0.07	0.17	0.42	0.30	0.48
Nitrogen, W %	0.51	0.91	1.05	1.27	1.31
Ni, WPPM	0.2	9	25	30	32
V, WPPM	2	5	4	12	4

TABLE 4

CO-PROCESSING OF TEXAS LIGNITE WITH MAYA, HONDO, AND COLD LAKE VACUUM RESIDUUM

Condition No.	1	2	3
Days	1-5	6-8	9-11
Oil	Maya	Hondo	Cold Lake
Relative Space Velocity	1.0		
Reactor Temperature, °F	810		
Coal Concentration in Fresh Feed, W %	33		
Yields (W % Fresh Feed)			
C_1-C_3	6.4	5.9	6.3
C_4-350°F	15.8	16.5	16.4
350-650°F	35.8	38.6	32.1
650-975°F	23.8	23.7	25.0
975°F+ Liquid	6.5	2.6	8.1
Coal (IOM) + Ash	5.8	6.5	6.1
$CO + CO_2$	0.1	0.1	0.1
$NH_3 + H_2S + H_2O$	10.6	10.8	10.5
Total (100 + H_2 Consumption)	104.8	104.6	104.6
Coal Conversion (W % MAF)	92.5	90.6	91.4
975°F+ Conversion (W % MAF)	90.3	92.7	88.1
HDS, W %	95.2	96.7	95.0
HDN, W %	77.9	76.2	67.7
Net C_4-975°F Yield (W % 975°F+ MAF)	76.6	76.5	73.4

TABLE 5

COMPARISON OF FEEDSTOCK REACTIVITY

Feedstock Combination	Initial Reactivity* at 33 W % Coal	Deactivation* Parameter
Texas Lignite + Maya	1.00	1.00
Texas Lignite + Cold Lake	1.00	-
Texas Lignite + Hondo	1.33	-
Taiheiyo + Maya	0.78	0.42
Westerholt + Cold Lake	0.59	0.75
Forestburg + Cold Lake	0.78	0.71
New Mexico + Hondo	1.29	0.51

* Relative to Texas lignite + Maya combination

FIGURE 1

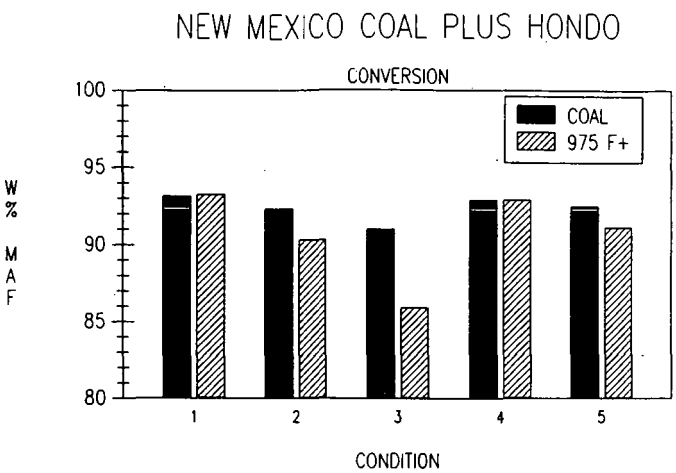

FIGURE 2

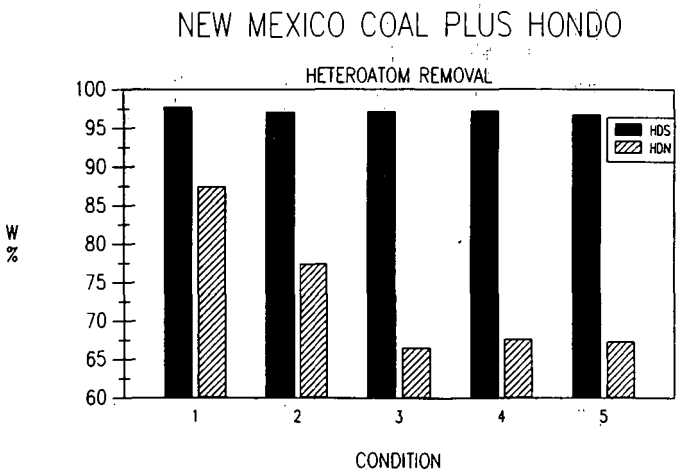

FIGURE 3

NET C4-975 F DISTILLATE PRODUCT

EFFECT OF TEMP / SPACE VELOCITY

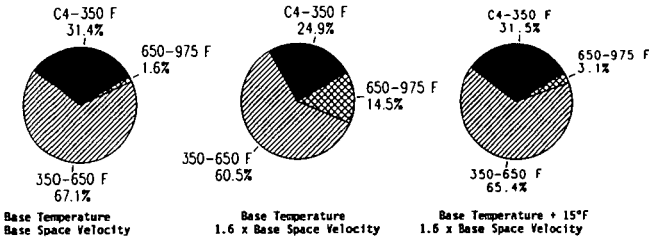

FIGURE 4

NEW MEXICO COAL PLUS HONDO

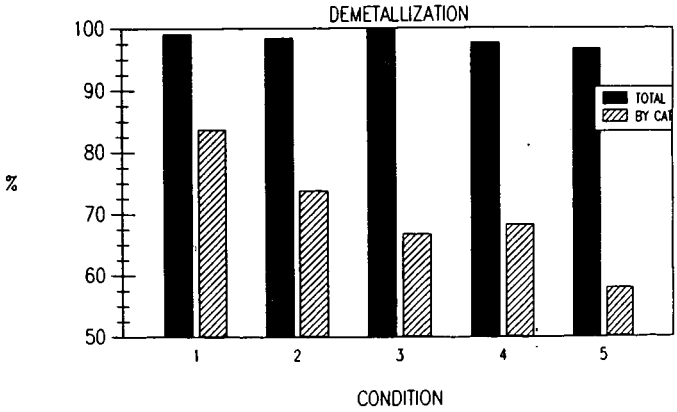

FIGURE 5

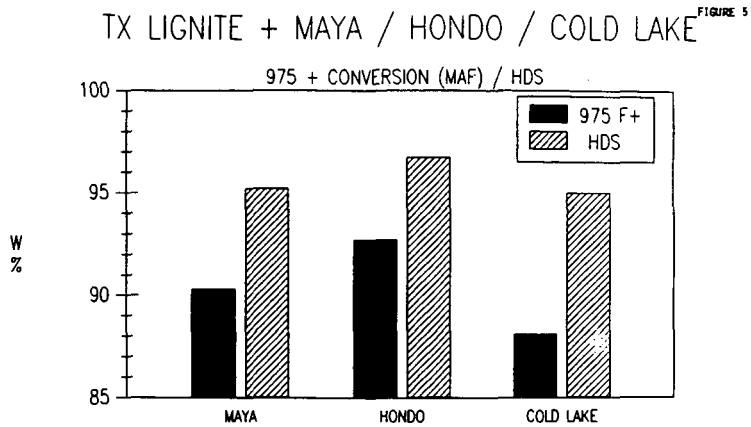
TX LIGNITE + MAYA / HONDO / COLD LAKE
975 + CONVERSION (MAF) / HDS
100
95
90
85
W
%
975 F+
HDS
MAYA
HONDO
COLD LAKE

COUNTERFLOW REACTOR (CFR) FOR COPROCESSING OF COAL AND PETROLEUM FEEDSTOCKS

Dr. Dietmar J. Berger,	Canadian Energy Developments Inc. (CED), 4222 - 97 Street, Edmonton, Alberta, Canada;
Dr. H. Würfel	Gesellschaft für Kohleverflüssigung mbH (GfK), Kokereistrasse, 6620 Völklingen-Fürstenhausen, West Germany;
Dr. Norman Anderson	Kilborn Inc., 2200 Lakeshore Boulevard, Toronto, Ontario, Canada

Keywords: Coprocessing, Counterflow Reactor, Commercial Facility

ABSTRACT

CED/GfK evaluated different processes for the simultaneous upgrading of coal and heavy oil/bitumen during the past five years. The development work on the BSU (I.D. 1.2") and PDU (I.D. 3.5") scale led to a new Counterflow Reactor concept characterized by the counterflow of the liquid or slurry feed and the hydrogen recycle gas stream.

Among others, this counterflow reactor (CFR) has the following advantages over the co-current reactor:

1. Optimum internal recovery of the exothermic heat of reaction and thus less severe feed preheating;
2. No concern of solid settling as liquids and solids are removed from the bottom of the reactor;
3. Lower recycle gas rates determined by reaction kinetics only; and
4. Favorable profile of the hydrogen partial vapor pressure.

During the past years, over 10,000 hours of tests have been performed successfully with different heavy oils and heavy oil/coal slurry feeds with distillable oil yields of up to 85 wt% for heavy oil upgrading and up to 74 wt% for coprocessing. The results have been used as a basis for a technical and economical screening study for a commercial size upgrader in Canada. In the paper, results of the test work and the screening study will be presented.

INTRODUCTION

In 1984, Canadian Energy Developments Inc. (CED) had an extensive feasibility study performed to evaluate upgrading options for the vast energy resource (heavy oil and coal) of Alberta. Upgrading options considered were: heavy oil upgrading, coal liquefaction and coprocessing. At a certain price for heavy oil and at the same production capacity of synthetic crude oil, the feasibility study concluded that 1) coprocessing is economically slightly more attractive than heavy oil upgrading, 2) a heavy oil upgrading facility requires approximately 10% less capital than a coprocessing facility, and 3) coal liquefaction has the lowest return on investment and requires about 75% more capital to be built. Based on these conclusions the feasibility study recommended that for the overall development of the energy resources of Alberta, coprocessing would be the more favored option for a commercial facility.

Up until 1984, process development for coprocessing had not reached a point for commercialization. CED therefore decided to embark on a R & D program to develop its own coprocessing technology. During the past four years, CED performed extensive experimental work on both the Bench Scale Unit (BSU) and the Process Development Unit (PDU) scale and the following coprocessing technologies were evaluated:

1) PYROSOL Technology - i.e. hydrogenation plus coking process,
2) Co-Current Upflow Bubble Reactor Technology - as a one or two stage hydrogenation technology, and
3) Counterflow Reactor (CFR) Technology.

Based on the experimental results and the operation of the PDU for these three technologies, CED has selected the CFR technology for scale up to a commercial coprocessing facility.

COUNTERFLOW REACTOR (CFR) TECHNOLOGY

Process Description and Experimental Results

The CFR technology is a single stage hydrogenation process operating at conditions which promote coal solubilization, solubilized coal and heavy oil hydrogenation and hydrocracking in a single reactor. As the name implies, the CFR features a downward flowing coal/heavy oil slurry in contact with a counter-current make-up plus recycle hydrogen stream. CED's German partner, Gesellschaft für Kohleverflüssigung (GfK) mbH has operated a continuous PDU (8 kg/hr coal/heavy oil feed slurry) using the CFR technology for more than 10,000 hours since the second half of 1987. Individual runs lasted for up to about 700 to 800 hours.

In the CFR technology (Figure 1), the coal and heavy oil are slurried, pumped to reactor pressure and preheated to 150-250°C prior to being charged to the top of the reactor. Recycle and make-up hydrogen is preheated to 400-450°C and injected into the bottom of the reactor. The exothermic heat of reaction is used to raise the incoming feed slurry to reaction temperature. Solubilization of the coal occurs in the top portion of the reactor at a temperature of approximately 400°C, and hydrogenation/hydrocracking takes place in the main reactor zone at temperatures of 445-455°C. Reactor pressure is 18-20 MPa (2,600-2,900 psig).

Hydrogenation products are vaporized as they are formed and are withdrawn from the top of reactor, cooled, condensed and separated in a cold separator. The condensed liquid product, a full range distillate hydrocarbon product is transferred to the secondary upgrading. The hydrogen rich gas stream is scrubbed and recycled.

Unconverted heavy oil/solubilized coal and unreacted coal flow downward in the reactor, counter-current to the upward flowing hydrogen to promote solubilization of the coal and hydrogenation of the coal and heavy oil. The highest hydrogen partial vapor pressure exists at the bottom zone of the reactor where needed to promote conversion of coal and heavy oil fractions that are the most resistant to hydrogenation/hydrocracking. A slurry stream containing unconverted residuum and unreacted coal and ash is withdrawn from the bottom of the reactor, depressurized in the let-down system and charged to a vacuum flash unit.

When processing typical Cold Lake vacuum residue and Alberta subbituminous coal (Table 1) total distillable oil yields of 70-74 wt% are consistently achieved (Table 2) with a hydrogen consumption of 2.9 wt%. The distillate product (Table 3) is a full range product containing, on average, 30% naphtha, 40% middle distillate and about 30% VGO. (Typical operating conditions are shown in Table 4).

Advantages of the CFR

Most reactor technologies produce about the same total distillable oil yield and the same product distribution. The CFR, however, has significant advantages with regard to its operation and reliability which are the direct consequence of the counterflow concept used in the process.

1. No Settling Problem

Since the unconverted feed material, ash and other solid particles are allowed to settle naturally in the reactor, the settling problem associated with co-current reactors does not occur in the CFR. High superficial gas velocities typically in excess of 6 cm/sec. in co-current flow reactors are not required in the CFR as only vaporized and gaseous products leave the reactor overhead and "solids" are withdrawn at the bottom together with the liquid hydrocarbons as a slurry.

2. Low Superficial Gas Velocity

In the CFR technology, superficial gas rates are determined by reaction kinetics only and are not defined by the requirement to keep "solids" in suspension and to carry them overhead in the reactor. All PDU runs with the CFR were performed with superficial gas velocities of 0.5 to 1.9 cm/sec. Maximum duration was about 800 hours of continuous operation.

3. Low Scale-Up Risk

For a commercial size CFR the superficial gas velocities are estimated at around 3cm/sec., i.e. a commercial CFR will operate in the bubble flow regime. Since the PDU also operates in the bubble flow regime the scale up from the PDU to commercial size reactors does not pose a major problem as the reactor scale up parameters are essentially known.

4. Recovery of Exothermic Heat of Reaction

As the vaporized reaction products and hydrogen gas stream rises through the downward flowing feed slurry the exothermic heat of reaction is recovered internally within the CFR. As a result, the preheat duty for the feed slurry is reduced and lower feed slurry preheat temperatures are possible.

5. No External Hot Separator

Because of the counterflow concept, the CFR combines the reactor and the hot separator. An external hot separator is not required to separate the slurry from the distillable oil.

6. Capital and Operating Costs

With the above "technical" advantages, the capital and operating costs for a commercial coprocessing facility will be lower when CFR technology is used as compared to co-current flow reactor technology. For example, as the CFR technology operates at lower superficial gas velocities, recycle gas rates will be reduced significantly which decreases the equipment size for the recycle gas system. Because the slurry preheating requirements are lower, operating costs are decreased as fuel consumption is decreased.

Feasibility Study for Commercial Coprocessing Facility

On behalf of CED, Kilborn Inc. performed a technical and economic feasibility study for a grass-roots commercial coprocessing facility for a suitable location in Alberta. The facility (Figure 2) was designed to process Cold Lake heavy oil and Vesta Mine subbituminous coal and to produce 4,450 cubic metres per day (28,000 BPD) of synthetic crude oil (Table 5).

Capital costs, product revenue and operating cost estimates (Table 6) were prepared and formed the basis for a financial and sensitivity analysis to evaluate the economic potential of a commercial coprocessing facility.

Total Estimated Capital Costs of $671,100K (1989) is composed of:

Direct costs were estimated from actual cost data wherever possible. For licenced processes (secondary upgrading for example) information from potential licensors was used.

Indirect costs (home office engineering construction management, construction indirects, special winterization costs) were estimated as percent of total direct cost. Project contingency was applied at 20% of total direct costs plus home office engineering, construction management and construction indirect costs.

Other costs include allowances for initial catalyst charge, initial chemicals inventory and paid up licence and royalty fees.

Owner's costs include allowances for owner's engineering, project management, environmental application costs, permit costs, spare parts inventory and start-up costs.

Total estimated annual revenue of $206,720K per year (1989) is based on 320 operating days per year. Unit product prices were provided by the Alberta Energy Department, Government of Alberta. It should be pointed out that about $6.8M per year of revenue is created from 22MW excess electricity generated in the commercial facility.

Total estimated operating cost of $129,670K per year (1989) includes the costs of feedstocks, operating and maintenance labor, maintenance parts, utilities, catalysts and chemicals, local taxes and insurance. The unit prices for the feedstocks are based on forecasts from the Alberta Energy Department. The heavy oil price excludes the cost of diluent as the diluent is recovered and returned to the heavy oil production field for use as additional diluent. Plant labor and overhead costs are based on an estimated operating supervision, maintenance and plant overhead staff of 270 personnel. In addition, a contract maintenance labor allowance has been applied for major process unit turn around equivalent to 25 maintenance personnel over the entire year or 150 personnel for two month. A pipeline tariff of $2.00 per cubic metre of heavy oil feedstock, recovered diluent and synthetic crude oil product has been allowed to cover the construction and operating costs of heavy oil diluent and production pipelines amortized over a 20 year period.

Financial and Sensitivity Analysis

A financial and sensitivity analysis was prepared on the basis of a 32 year project life including a 7 year demonstration, engineering and construction period plus a 25 year operating period. The financial analysis uses a cash flow generator model for before and after tax calculations. Cash flow simulations were used to calculate discounted cash flow return on investment/equity (DCF/ROE) for 100% equity or a given debt/equity ratio. The sensitivity analysis considered variations in the type of financing, in capital cost, in price forecasts, in the oil yield and in interest rates. The result of this sensitivity analysis is shown in Figure 3. For each of the financing options (100% equity or 60/40 debt/equity) the upper line refers to a constant percent price differential and the lower line refers to a constant dollar price differential between heavy oil and synthetic crude oil. In any case, the after tax DCF/ROE indicate that a commercial coprocessing facility is economically attractive with normal debt/equity financing methods at synthetic crude oil and bitumen price differentials that are only marginally above current differentials. Furthermore, rates of return of 20 to 22% are realized at current differentials, with project financing methods based on cost and revenue sharing and fiscal structure similar to those recently applied to major energy projects in Canada.

CONCLUSION

The Counterflow Reactor (CFR) technology for the simultaneous upgrading of coal and petroleum feedstocks has been successfully demonstrated at the PDU scale. During 10,000 operating hours, distillable oil yields and product distributions are obtained which are similar to those from a conventional co-current upflow bubble column. The counterflow regime of the CFR, however, brings advantages in operation and reliability which ultimately translates into lower capital and operating costs for a commercial facility. Superficial gas velocities which are only half or possibly one third of those in the co-current mode and the recovery of the exothermic heat of reaction inside the CFR are the main unique features of the CFR technology.

A technical and economic feasibility study suggests that a commercial coprocessing facility with the CFR technology yields attractive return on investments at present price differentials. DCF-ROE of 20-22% can be realized with proper structuring of the financial terms.

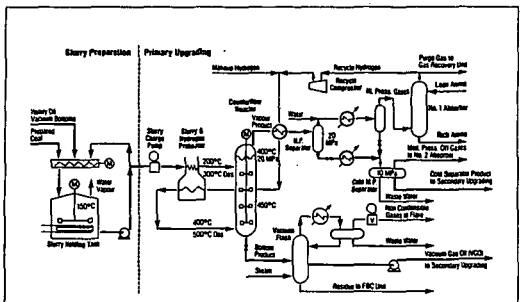

Canadian Energy — Simplified Process Flow Diagram – Primary Upgrading Area — Figure 1

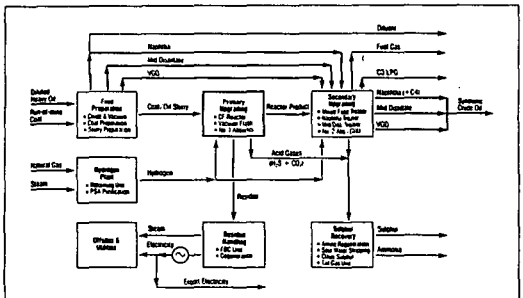

Canadian Energy — Simplified Block Flow Diagram — Figure 2

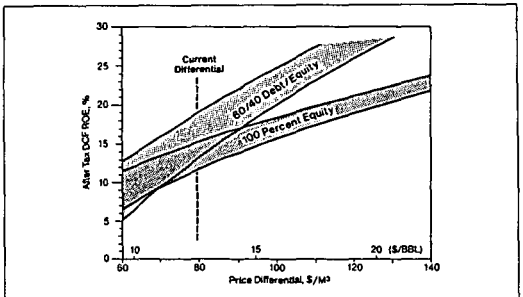

Canadian Energy — Effect of Price Differential on Rate of Return — Figure 3

Heavy Oil - Cold Lake Vacuum Residuum

- Distillation:

IBP	370°C	
5 WT%	423°C	
10 WT%	443°C	
20 WT%	471°C	
FBP	480°C	
(23.6 WT%)		

- Density 1.026 G/ML
- Asphaltenes 13.63 WT%
- Viscosity 80°C 80 Poise
  120°C 2.5 Poise

Coal - Alberta Subbituminous
Battle River Coal Field
Vesta Coal Mine

- Moisture 4.4 WT%
- Ash 13.8 WT% Dry Basis
- Volatiles 43.9 WT% (DAF)

Elemental Analysis WT% (DAF)

C	83.57
H	10.20
N	0.55
S	5.30
O (By Diff)	0.38
C	72.25
H	5.00
N	1.36
S	0.62
O	20.77

Canadian Energy

Feedstock Properties Table 1

	Heavy Oil Hydrogenation	Coal/Heavy Oil Coprocessing
Feeds, WT%		
Vac. Resid.	96.1	67.3
Coal (DAF)	3.9	32.7
H_2 Consumption	1.9	2.9
Products, WT%		
Oil Yield <480°C	83.5	73.7
C_1-C_4 Gas	7.6	10.2
Prod. Water	0.4	4.0
CO, CO_2, H_2S	3.8	4.1
Bitumen >480°C	6.4	9.4
Unconverted Coal	0.2	1.5
WT% Conversion (+480°C)	91.5	87.0

Canadian Energy

Overall Material Balance CFR-PDU Table 2

	Heavy Oil Hyorogenation	Coal/Heavy Oil Coprocessing
Density, KG/Litre	0.898	0.894
Elemental Analysis, WT%		
Carbon	85.81	84.8
Hydrogen	11.64	11.4
Nitrogen	0.40	0.58
Sulphur	1.97	1.47
Oxygen (Diff)	0.18	1.72
C/H	7.37	7.44
Liquid Product Yield (% of oil yield)		
C_1 - 200°C	20.0	30.0
200 - 350°C	50.0	40.0
>350°C	30.0	30.0
C_1 - 480°C	100.0	100.0

Canadian Energy

Hydrogenation Product Quality CFR-PDU Table 3

	Heavy Oil Hydrogenation	Coal/Heavy Oil Coprocessing
Pressure, Bars	200.0	190.0
Temperature, °C		
Top	450.0	451.0
Middle	454.0	457.0
Bottom	446.0	450.0
Hourly Space Velocity KG/HR/LITRE	0.76	0.84
Hydrogen Feed, NM^3/KG	2.9	2.77
Superp. Gas Velocity CM/SEC.	1.4	1.7
Throughput, KG/HR	7.2	8.6
Feed - Vac Resid, WT%	96.1	67.3
- Coal (DAF), WT%	3.9	32.7
- Catalyst	None	None

Canadian Energy

Typical Operating Conditions CFR-PDU Table 4

Feedstocks	• Heavy Oil (Diluted)	5000 m³/d
	• Heavy Oil (Diluent Free)	3500 m³/d
	• Coal	2200 t/d
	• Natural Gas	972 000 Nm³/d
Products	• Synthetic Crude Oil	4450 m³/d
	• Electricity	22 MW
	• Propane	200 m³/d
	• Sulphur	138 t/d
	• Ammonia	30 t/d
	• Diluent (Recycled)	1500 m³/d

Canadian Energy — Feedstock and Product Quantities — Table 5

Direct Costs	413,800
Indirect Costs	214,300
Other Costs	14,000
Owner's Costs	29,000
Total Estimated Capital Cost	**671,100**

Canadian Energy — Capital Cost, $K(1989) — Table 6

	Quantity	*Price*	Operating Cost *$K/Yr (1989)*
Feedstocks			
• Heavy Oil	3500 m³/d	$53.90/m³	60,370
• Coal	2200 t/d	$15.00/t	10,560
• Natural Gas	970 000 Nm³/d	$ 0.05/Nm³	15,550
Other Operating Costs			36,180
Pipeline Tariffs			7,010
Total Estimated Operating Cost*			129,670

*Based on 320 operating days per year

Canadian Energy — Annual Operating Cost — Table 6 con't

	Quantity	*Price*	Revenue *$K/Yr (1989)*
Syncrude	4450 m³/d	$133.65/m³	190,320
Electricity	22 MW	$ 0.04/KWH	6,760
Propane	200 m³/d	$ 55.00/m³	3,520
Sulphur	138 t/d	$ 95.00/t	4,200
Ammonia	30 t/d	$200.00/t	1,920
Total Estimated Revenue*			**206,720**

*Based on 320 operating days per year

Canadian Energy — Annual Product Revenue — Table 6 con't

COAL/RESID COPROCESSING OVER EQUILIBRIUM HYDROTREATING CATALYST

R. J. Torres-Ordonez
S. G. Kukes
Amoco Oil Company
Amoco Research Center
P. O. Box 3011
Naperville, Illinois 60566

W. A. Leet
Amoco Oil Company
P. O. Box 160
Casper, Wyoming 82601

Keywords: Coprocessing, coal, resid.

ABSTRACT

Resid and a 10% coal/resid mixture were hydroprocessed in a flow unit at 760-790°F over an equilibrium commercial hydrotreating catalyst. Coal addition resulted in improvements in both hydrodemetallization activity and Ramscarbon conversion; however, hydrodesulfurization activity remained the same. The addition of 10% decanted oil to the coal/resid feed considerably improved coal conversion.

INTRODUCTION

Extensive information on coal/petroleum resid coprocessing is available in the open literature, both for experiments in batch units and in continuous bench scale units. Oelert (1) provides a review of the background technology and discusses research and development in various coprocessing schemes. Many of these coprocessing studies claim synergisms, or benefits relative to resid hydroprocessing or coal liquefaction. Among these synergisms are:

a) Improved unit operability due to the formation of less solids or coke (2). This benefit may also allow unit operation at higher temperatures than those possible with just resid hydroprocessing.
b) Enhanced metals removal (3-6), which has been attributed to the preferential deposition of the metals on the coal solids instead of on the catalyst (7). This benefit may allow the processing of resids with high metal contents (8).
c) Improved heteroatom removal (4,5,9) (i.e., sulfur, nitrogen and oxygen).
d) Increased distillate yields (4,9,10).
e) Reduction of overall hydrogen requirement (relative to coal liquefaction) with the use of higher H-content resid.

The goal of the current work is to verify and quantify synergisms for the coprocessing of coal and resid over commercial equilibrium hydrotreating catalyst in a continuous bench scale flow unit. The specific objectives are (a) to evaluate the effects of process variables, such as temperature and solvent addition, on coal/resid conversion and product properties, and (b) to determine the impact (if any) of coprocessing on catalyst activity maintenance and catalyst life.

EXPERIMENTAL

Feed Properties

Hydroprocessing experiments were performed on a resid and a blend of this resid with Illinois No. 6 coal, with or without decanted oil. The properties of the above feeds are shown in Table 1.

Reaction Conditions

The hydroprocessing experiments were conducted in an upflow high-pressure unit which contains two 1-liter Autoclave reactors in series. Catalyst baskets, each filled with 60 cc of equilibrium hydrotreating catalyst, were placed in

both reactors. To prevent elutriation, the catalyst was covered with 10 cc of 3 mm glass balls and 1/4 inch of glass wool. Table II gives the experimental conditions for the following four tests:

Test No. 1	Hydroprocessing of Resid
Test No. 2	Coprocessing of 10% Coal + 90% Resid
Test No. 3	Hydroprocessing of 10% DCO + 90% Resid
Test No. 4	Coprocessing of 10% Coal + 9% DCO + 81% Resid

Product Analysis

Products from the hydroprocessing runs were analyzed for tetrahydrofuran (THF) and hexane insolubles. Samples were also subjected to Shell hot filtration tests (SHFT) to determine "solids" concentration. In this test, the sample is filtered through Whatman 50 paper at about 200°F; if the sample does not filter after one hour, 10-20 psi nitrogen is applied. The solids are then washed with hexane (four 50 ml washes for 10 g sample) before final filtration; the recovered solids are termed the SHFT solids. The resulting SHFT filtrate was then analyzed for elemental composition (C, H, N, S, O), metals (Ni, V) and Ramscarbon contents (Tables III and IV). Product gas samples from selected runs were also analyzed by gas chromatography to determine the total material balance closure, which averaged 93% due to plugging problems.

RESULTS AND DISCUSSION

Resid and Coal/Resid Coprocessing Without DCO (Tests No. 1 and No. 2)

Coal addition considerably improved the hydrodemetallization (HDM, calculated as shown in the appendix) of resid at 760-790°F (Figure 1). The HDM benefit from coal addition became smaller at higher temperatures.

The Ramscarbon conversion (HDC, calculated as shown in the appendix) also increased with coal addition, as shown in Figure 2. It is possible that adsorption of asphaltenes (or Ramscarbon to some degree) by unconverted coal resulted in this apparent increase in Ramscarbon conversion. As with HDM, the HDC benefit with coal addition became smaller at higher temperatures.

The hydrodesulfurization (HDS, calculated as shown in the appendix) was not affected by coal addition, as shown in Figure 3. Nitrogen and oxygen removal were low due to the high space velocity and low hydrogenation activity of the equilibrium catalyst.

The THF insolubles (See Table III) were used to estimate coal conversion (see appendix). Within experimental error, the coal conversion remained relatively constant from 760 to 780°F at a minimum of 46-48% to a maximum of 60-62% (see Table V). These conversions were lower than those obtained in the liquefaction of Illinois No. 6 (with coal liquids as solvent) under comparable coal liquefaction conditions (11). The lower coal conversion during coal/resid coprocessing may be due to the poor solvent quality of the petroleum resid.

Resid and Coal/Resid Coprocessing With DCO (Tests No. 3 and No. 4)

Initially a mixture of 90% resid and 10% decanted oil was hydroprocessed for about 120 hours. Then 10% coal was added to the feed and the coal/resid/DCO mixture was hydrotreated for 180 hours. At the end of this run, the coal was removed and the (resid+DCO) was processed for 120 hours to check the baseline. Figures 4-6 show HDM, HDC, and HDS of liquid products as a function of the time on stream. As in the coprocessing without decanted oil, the addition of coal resulted in increases in HDM and HDC (Figures 4 and 5); HDS was only

slightly improved (Figure 6). Regression lines (the solid lines in Figures 4-6) indicated that the equilibrium catalyst was undergoing further deactivation. The addition of coal did not affect this deactivation rate. Catalyst activity for HDM drastically decreased two days after coal was removed from the feed. We do not have an explanation for this unusual observation.

The addition of DCO improved coal conversion, as seen in Table VI. For hydroprocessing at 780°F, coal conversion increased from a minimum of 46% (maximum of 60%) without DCO to a minimum of 66% (maximum of 80%) with DCO addition to the coal/resid mixture.

CONCLUSIONS

The addition of decanted oil to a coal/resid mixture resulted in improved coal conversion. When 10% Illinois No. 6 coal was coprocessed with resid, both metals and Ramscarbon removal from resid were increased, with or without decanted oil. Increases in apparent resid Ramscarbon removal with coal present can be due to heavy molecule adsorption by unconverted coal. Sulfur removal, however, was not affected by coal addition.

ACKNOWLEDGMENTS

The authors acknowledge M. G. Davidson, R. E. Lumpkin and A. J. Swanson for useful discussions.

REFERENCES

1. Oelert, H. M., Coprocessing (Coprocessing with Oil) in Synthetic Fuels from Coal: Status of the Technology, eds. Oelert, H.; Romey I.; Paul, P. F. M.; Imarisio, G., Commission of the European Communities, Luxembourg, 1987 Report No. EUR-11191, pp. 259-338.
2. Hydrocarbon Research, Inc., Ohio Clean Fuels, Inc. Prototype Commercial Coal/Oil Co-processing Plant Project Process Development Demonstration Program, Final (Publishable) Report, October 1989, DOE Cooperative Agreement No. DE-FC22-87PC-79797, Ohio Coal Development Office Contract No. CDO/D-86-59B.
3. Aulich, T. R.; Holm, P. L.; Knudson, C. L.; Rindt, J. R., Coprocessing with Petroleum Resid and Martin Lake Lignite, *ACS Div. Fuel Chem. Preprints*, 1988, vol. 33, pp. 102-113.
4. Hydrocarbon Research, Inc., Coal-Oil Coprocessing: Phase 1, Interim Report, March 1987, EPRI-AP-5101.
5. Hydrocarbon Research, Inc., Coal/Oil Co-processing Program: Phase 2, Interim Report, Publishable Report, April 1988, L-88-1B(600)-1.
6. Rhodes, D. E., Comparison of Coal and Bitumen-Coal Process Configurations, *Proceedings of the Tenth Annual EPRI Contractors' Conference on Coal Liquefaction*, Palo Alto, California, April 23-25, 1985.
7. Cugini, A. V.; Lett, R. G.; Wender, I., Coal/Oil Coprocessing Mechanism Studies, *ACS Div. Fuel Chem. Preprints*, 1988, vol. 33, pp. 71-88.
8. Audeh, C. A.; Yan, T.-Y., Coprocessing of Petroleum Residue and Coal, *Ind. Eng. Chem. Res.* 1987, 26, 2419-2423.
9. Rahimi, P. M.; Fouda, S. A.; Kelly, J. F.; Malhotra, R.; McMillen, D. F., Characteristics of CANMET coprocessing distillates at different coal concentrations, *Fuel* 1989, 68, 422-429.
10. Lenz, U.; Wawrzinek, J., Coprocessing - The Hydrogenation of Lignite Together with Residual Oils, *ACS Div. Fuel Chem. Preprints*, 1988, vol. 33, pp. 27-41.
11. Evans, A. J., Amoco Oil Company, Naperville, IL, Personal communication.

Table I. Hydroprocessing Feed Properties

Feed No.	Composition, % MAF Resid	Coal	DCO	%THF Solids	%SHFT Insol	% C	% H	% N	% S	% O	% Rams-carbon	ppm Ni	ppm V	ppm Fe
1	100	0	0	N.D.[1]	1.6	84.65	10.35	0.45	4.70	0.40	17.7	54	215	21
2	0	0	100	N.D.	N.D.	90.75	7.22	0.17	1.68	1.48	9.4	0	0	0
3	0	100	0	91.06[2]	N.D.	77.31[3]	5.13[3]	1.43[3]	3.93[3]	12.20[3]	N.D.	15	32	15,300
4	90	0	10	N.D.	1.43	85.26	10.04	0.42	4.40	0.51	16.9	49	194	19
5	90	10	0	9.11[4]	11.4	83.92	9.83	0.55	4.62	1.58	25.0	50	197	1549
6	81	10	9	9.11[4]	11.3	84.47	9.55	0.52	4.35	1.68	20.3	45	177	1547

[1] N.D. = not determined
[2] 98.0% MF coal
[3] Wt% MAF (coal contained 1.14 wt% ash and 7.1 wt% moisture)
[4] 9.8% MF coal

Table II. Hydroprocessing Conditions

	1st Stage Reactor	2nd Stage Reactor	Reactor Train
Average Feed Rate, g/hr	206	206	206
Equilibrium Catalyst			
Catalyst Volume, cc	60	60	120
Catalyst Weight, g	65	65	130
WHSV, 1/hr (based on fresh catalyst)	7.4	7.4	3.7
WHSV, 1/hr (based on equil. catalyst)	3.2	3.2	1.6
Effective Reactor Volume*, cc	282	282	564
Residence Time, hr	1.37	1.37	2.74
LHSV, 1/hr	3.4	3.4	1.7
Pressure, psig	2500	2500	2500
Hydrogen Flow Rate			
SCFH	10	10	10
SCFB	7700	7700	7700
Agitator Speed, rpm	1650	1000	

*Effective reactor volume calculated assuming 10% gas holdup and 0.2 cc/g spent catalyst pore volume, i.e.,
Effective Volume = Total Liquid Volume Outside Catalyst Pores x (1-gas holdup fraction) + Catalyst Pore Volume
= 300 (1 - 0.1) + 60 (0.2) = 282

TABLE III: Analysis of Products from Resid and Coal Resid Hydroprocessing

Test No.	Feed Comp[1] %Coal	Feed Comp[1] % DCO	Temp (°F)	Time (hr)	%THF Insol.	% SHFT Solids	% C	% H	% N	% S	% O	% Rams-carbon	ppm Ni	ppm V	ppm Fe
1	0	0	780	63	0.14[2]	5.60	85.86	11.14	0.41	2.31	1.06	10.6	14	53	2
1	0	0	770	136	0.33[2]	3.67	85.63	10.90	0.44	2.57	1.06	12.5	22	78	2
1	0	0	760	155	0.21[2]	4.07[4]	85.63	10.77	0.47	2.83	1.29	13.4	29	105	2
1	0	0	790	179	0.17[2]	5.47	86.07	11.26	0.37	1.97	1.10	9.3	8	31	2
2	10	0	780	255	4.44[3]	13.96[5]	85.65	10.67	0.49	2.54	1.48	13.0	15	38	2
2	10	0	770	283	2.92	17.05	85.42	10.69	0.48	2.71	N.D.	13.8	19	53	2
2	10	0	770	297	5.93	N.D.	85.10	10.43	0.51	3.05	1.41	14.9	24	74	2
2	10	0	760	309	5.13	N.D.	85.31	10.68	0.46	2.95	1.63	13.0	20	62	2
2	10	0	760	325	3.76	14.87	85.04	10.61	0.48	3.06	1.09	14.4	24	74	2

[1] %Coal + %DCO + %Resid = 100%
[2] Average THF insolubles for entire time on stream at the given temperature.
[3] Average of THF insolubles at 255 and 270 hours.
[4] SHFT solids at 165 hours.
[5] SHFT solids at 270 hours.
N.D. = not determined.

TABLE IV. Analysis of Products from Resid and Coal/Resid Hydroprocessing with Decanted Oil[1]

Test No.	Feed Comp[2] % Coal	% DCO	Temp. (°F)	Time (hr)	%THF Insol.	%SHFT Solids	%Hexane Insol.	Filtered Product Quality % C	% H	% N	% S	% Rams-carbon	ppm Ni	ppm V	ppm Fe
3	0	10	780	38	N.D.	2.39	4.93	86.18	10.67	0.45	2.37	12.5	24	73	2
3	0	10	780	62	N.D.	2.45	6.85	86.07	10.68	0.42	2.22	11.4	21	64	2
3	0	10	780	73	0.62	2.24	9.75	85.84	10.71	0.42	2.32	11.4	21	65	2
3	0	10	780	84	N.D.	2.42	9.85	85.34	10.67	0.40	2.39	11.6	23	74	2
3	0	10	780	106	0.50	2.04	9.41	86.46	10.70	0.42	2.38	11.5	22	70	2
4	10	9	780	128	N.D.	6.90	N.D.	86.35	10.56	0.45	2.18	12.0	15	42	2
4	10	9	780	152	3.77	10.61	N.D.	86.33	10.47	0.42	2.35	11.9	15	34	1
4	10	9	780	175	3.36	8.58	14.11	85.99	10.33	0.43	2.42	12.0	17	35	1
4	10	9	780	196	N.D.	10.21	14.92	86.16	10.45	0.49	2.57	13.2	18	42	1
4	10	9	780	216	2.57	10.08	15.43	86.18	10.35	0.43	2.49	12.6	20	44	1
4	10	9	780	239	N.D.	9.72	14.71	86.13	10.43	0.46	2.54	13.7	22	44	15
4	10	9	780	263	3.29	9.49	14.15	85.48	10.43	0.40	2.45	12.8	16	34	1
4	10	9	780	287	N.D.	11.00	15.72	86.03	10.36	0.41	2.65	13.6	22	48	1
3	0	10	780	310	N.D.	3.19	N.D.	85.89	10.39	0.44	3.08	13.3	27	83	1
3	0	10	780	333	N.D.	2.45	N.D.	86.06	10.55	0.42	2.89	13.0	24	74	0
3	0	10	780	357	0.59	2.03	11.51	85.96	10.52	0.43	3.07	13.4	34	126	2
3	0	10	780	381	N.D.	1.89	11.40	86.02	10.45	0.42	3.09	13.3	35	126	2
3	0	10	780	405	0.60	2.08	11.29	86.00	10.30	0.41	3.13	13.5	35	127	2
3	0	10	780	429	N.D.	1.74	N.D.	85.74	10.34	0.41	3.11	13.4	34	127	2

[1] No oxygen analyses were performed for this set of runs.
[2] %Coal + %DCO + %Resid = 100%

Table V. Conversion of THF Insolubles

Temperature, °F	%THF Insolubles in Product Resid	Resid + Coal	% Coal Conversion Minimum	Maximum
760	0.2	4.4	47	61
770	0.3	4.4	48	62
780	0.1	4.4	46	60

*THF insolubles in coal/resid feed = 9.1%
Ash in coal/resid feed = 1.1%

TABLE VI. Hydroprocessing at 780°F

Test	Feed	Time (hr)	%HDM	%HDC	%HDS	% SHFT Solids	% Coal Conversion Minimum	Maximum
1	Resid	63	77	44	54	6	--	--
2	Resid+Coal	255	82	56	53	14	46	60
3	Resid+DCO	62	66	35	51	2	--	--
4	Resid+DCO+Coal	263	80	44	50	9	66	80

FIGURE 1.
COAL/RESID COPROCESSING – HYDRODEMETALLIZATION

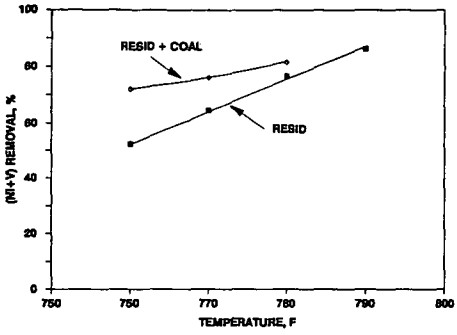

FIGURE 2.
COAL/RESID COPROCESSING – RAMSCARBON CONVERSION

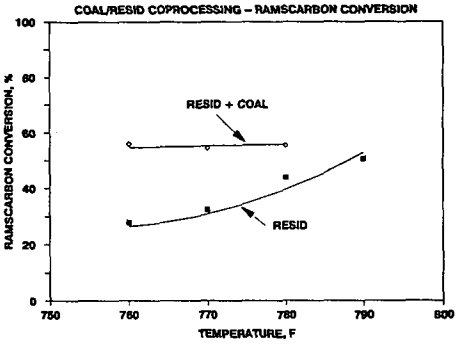

FIGURE 3.
COAL/RESID COPROCESSING – HYDRODESULFURIZATION

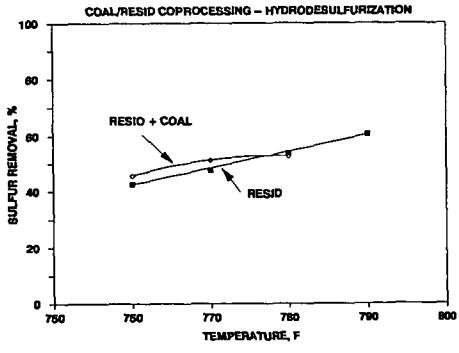

FIGURE 4.

COAL/RESID COPROCESSING WITH DCO AT 780 F – HYDRODEMETALLIZATION

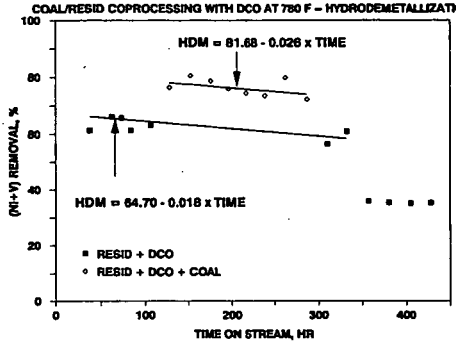

FIGURE 5.

COAL/RESID COPROCESSING WITH DCO AT 780 F – RAMSCARBON CONVERSION

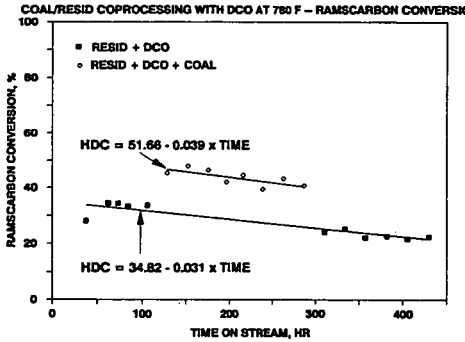

FIGURE 6.

COAL/RESID COPROCESSING WITH DCO AT 780 F – HYDRODESULFURIZATION

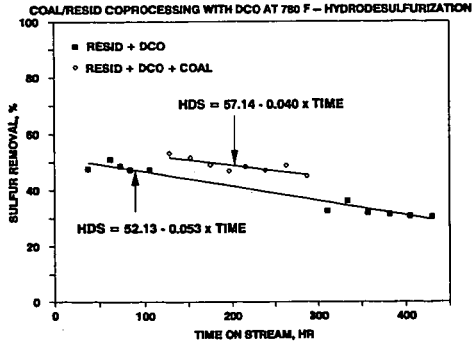

APPENDIX

Conversion Calculations

Figure A-1 shows the block diagram for the reactor system, along with the feed and product streams, and their analysis. The analytical results reported in Tables III and IV were used to calculate the following levels of conversion or removal in the liquid product (assuming no product loss on filtration):

% Conversion or Removal of Component I (HDI):

$$\{[F_{in}I_{feed} - F_{out}(1 - \text{SHFT solids fraction})I_{liquid}]/[F_{in}I_{feed}]\} \times 100$$

where for hydrodemetallization (HDM), I = ppm (Ni+V); for Ramscarbon conversion (HDC), I = % Ramscarbon; and for hydrodesulfurization (HDS), I = % Sulfur. F_{out}/F_{in} represents the material balance which may be calculated based on the total material (0.93), or based on a forced carbon balance (0.99). In Figures 1-6, F_{out}/F_{in} = 0.99 is used; the use of F_{out}/F_{in} = 0.93 gives values that are at most 10% higher.

Figure A-1.
Material Balance Block Diagram for Flow Unit

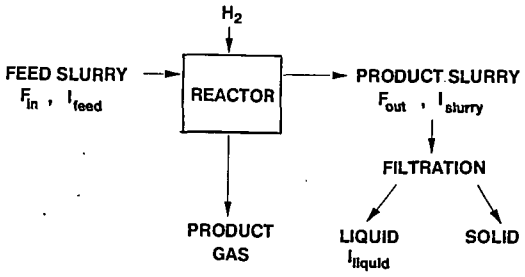

Coal conversion was estimated by conversion to THF solubles. It was assumed that the coal-derived THF insolubles (THF) is given by the difference between the THFI in the coprocessing product and the THFI in the resid hydroprocessing product (weighted by its fraction in the coprocessing feed), i.e.,

Coal Conversion to THF Solubles:

$$1 - \{[\text{THFI-Ash})_{\text{coproc product}} - 0.9\text{THFI}_{\text{resid run}}]/(\text{THFI-Ash})_{\text{coproc feed}}\}$$

The ash deposition on the catalyst could not be evaluated because the catalyst was severely coked and could not be recovered for analysis. Two approaches were used to estimate the ash levels in the coprocessing product. In the first, it was assumed that all of the ash deposited in the catalyst so that $\text{Ash}_{\text{coproc product}} = 0$; the calculated coal conversion is then a minimum. In the second, it was assumed that no ash deposited in the catalyst so that $\text{Ash}_{\text{coproc product}} = \text{Ash}_{\text{coproc feed}} = 1.14\%$; the calculated conversion is then the maximum possible.

MATHEMATICAL MODELLING OF COPROCESSING KINETICS

A.J. Szladow
Lobbe Technologies Ltd.
Regina, Saskatchewan, Canada

S.A. Fouda and J.F. Kelly
CANMET
Energy Mines and Resources Canada
Ottawa, Ontario, Canada

Keywords: Heavy Oil/Coal Upgrading, Modelling, Optimization

INTRODUCTION

CANMET has played a major role in heavy oil/coal coprocessing since the late 1970's. CANMET has conducted studies on determining characteristics of the products and residues from the coprocessing of heavy oil and coal, development of high performance catalysts for the coprocessing of heavy oils and coal, and demonstrating the feasibility of coprocessing Canadian feedstocks. An ongoing experimental program using a continuous bench-scale reactor system has generated a significant amount of scientific and engineering information on process performance and operation. These data were previously reviewed and analyzed for reaction engineering models (1). As a continuation of that study, CANMET and Lobbe undertook a program on computer simulation of coprocessing with special emphasis on studying the effects of coal and additives on the yield and selectivity of coprocessing products, and development of a Coprocessing Simulator as a tool for further work (2).

EXPERIMENTAL

The experiments were conducted in a continuous-flow unit. A detailed description of the unit is given elsewhere (3). Forestburg subbituminous coal from Alberta and Cold Lake + 454°C cut vacuum bottoms were used in the experiments. The coal was ground to -200 mesh and slurried with heavy oil at concentrations of 5 to 30 percent, daf slurry basis. A disposable iron sulphide catalyst was added in amounts from 0.5 to 1.0 percent (w/w Fe on daf slurry). Methods used for catalyst preparation were described previously by Fouda and Kelly (4).

The coprocessing runs were conducted over a temperature range of 400 to 450°C, nominal slurry space velocity 0.5 to 1.5 kg/l/hr, reactor pressure 2000 to 3000 psig, and run duration of 80 to 120 minutes each. The coprocessing workup procedures and product analysis are depicted in Figure 1. The relationships between pitch and distillate yields, and product selectivity are shown in Figures 2 and 3.

MODELLING COPROCESSING KINETICS

Previous publications and reports (1) (2) (5) have shown that despite the limitations of lumping procedures (grouping of the product components) in describing kinetics of complex reaction mixtures like heavy oil/coal , the lumping approach can provide a good approximation of the behavior of various product groups in coprocessing. The performed analyses showed that the characteristics of the model components in Figure 4 are independent of the severity of coprocessing and, therefore, they can be used as a definition of pseudo-components in kinetic analysis. Typical predictive capabilities for low and high severity runs of the developed kinetic models (1) (2) are shown in Table 1. The differences between Model A and Model B pertain to the difference in kinetic rate constants only and not the model structure. This was due to the fact that rate constants for formation of Naphtha and other lighter components were weak functions of temperature and required small adjustments for coprocessing experiments conducted over a wide temperature range as shown in Table 1.

In the current work, a simulator capable of optimizing coprocessing parameters was developed. The simulator included lumped kinetic models for coprocessing reactants and product, coke formation models and hydrogen consumption models as a function of feed composition, additive concentration and reactor operating parameters. Selected examples of product yield simulation over a range of temperatures, for three space velocities, are depicted in Figures 5 to 8. The data shows strong interdependence of temperature and space velocity, over the range studied, and the presence of localized maxima and minima product yield and selectivity, over the reactor operating parameters studied.

Interesting features of coprocessing results are presented in Figure 9, depicting simulation of distillate yield over a range of coal concentration, with and without adjustment of the process model for relative volatility of coprocessing feed and product components. It is shown that the extent of product/feed flashing (adjusted ϕ constants) affects the residence time distribution (RTD) of the heavy components and results in apparent synergistic effects between heavy oil and coal. These effects are particularly strong at low coal concentration and low process severity.

An interesting effect was also shown by optimization studies using derived coke formation and hydrogen consumption models for coprocessing. Table 2 gives optimized results for two different constraints (limits) on coke formation. The data show relatively similar product slate composition despite significant differences (by an order of about 20) in the amount of coke being formed.

SUMMARY

Detailed modelling of the coprocessing of heavy oil bottoms and subbituminous coal, and an evaluation of the effects of coal and additive concentration on product yields and selectivity were completed for the CANMET process. Also, a computer simulation package was developed for simulating and optimizing heavy oil and coal coprocessing kinetics, refining kinetic models and assisting reaction engineering studies for various feedstocks.

Simulation studies revealed: 1) the synergistic effects between heavy oil and coal could be explained, in part, by simulating variant mean residence time distribution (RTD) for the feed and product components; 2) the maximum in the yield of preasphaltenes was shown to shift to lower temperature with increasing residence time; and 3) the extent of product/feed flashing strongly affected the RTD of the heavy components with the RTD effects being most pronounced at low coal concentration and low process severity.

Optimization studies showed that hydrogen consumption was not the key optimization variable at the process conditions studied, i.e., at relatively high heavy gas/oil yield. Also, the studies showed that coke formation and its sensitivity to temperature made optimization of the product slate difficult, i.e., coke formation was a monotonic function of the initial coal and additive concentration, while temperature acted like a threshold variable above which coke was formed rapidly.

REFERENCES

1. Lobbe Technologies Ltd., "Mathematical Modelling of Coprocessing Kinetics," Report prepared for CANMET, September, 1987.

2. Lobbe Technologies Ltd., "Mathematical Modelling of CANMET Coprocessing," Report prepared for CANMET, April, 1989.

3. Kelly, J.F., Fouda, S.A., Rahimi, P.M., and Ikura, M., Paper presented at the CANMET Coal Conversion Contractors Review Meeting, Calgary, November, 1984.

4. Fouda, S.A. and Kelly, J.F., "Coprocessing of High-Volatile Bituminous Coals," Proceedings of the 1987 International Conference on Coal Science, Elsevier, Amsterdam, 1987.

5. Szladow, A.J., Chan, R.K., Fouda, S.A., and Kelly, J.F., "Kinetics of Heavy Oil/Coal Coprocessing," Energy and Fuels, 3, 136 (1989).

Table 1. COPROCESSING PRODUCT YIELD FOR MODEL A AND MODEL B RATE CONSTANTS

	MODEL A	MODEL B	EXPERIMENT
LOW SEVERITY RUN			
THFI	15.7	15.2	14.7
Preasphaltenes	5.1	5.0	1.8
Asphaltenes	14.1	15.3	13.7
Oil	40.1	39.7	37.9
HGO 1&2	13.6	15.2	13.7
LGO	7.3	7.7	6.3
Naphtha	3.5	1.7	4.0
C_1-C_4	0.3	0.3	---
HIGH SEVERITY RUN			
THFI	2.5	1.3	4.3
Preasphaltenes	5.2	2.7	1.8
Asphaltenes	8.3	8.7	1.5
Oil	6.8	5.6	6.7
HGO 1&2	22.4	31.3	32.6
LGO	18.3	26.1	25.7
Naphtha	28.0	18.1	15.3
C_1-C_4	8.6	6.1	6.4

Table 2. OPTIMIZATION RESULTS FOR FORESTBURG AND COLD LAKE FEED

	SPECIFIED CONCENTRATIONS FOR COKE	
	< 2%	< 5%
Product Slate Optimized		
THFI	0.9	0.8
PA	2.9	2.8
A	6.5	6.3
O	4.0	3.8
HGO	28.4	28.3
LGO	25.5	25.1
NAPHTHA	24.9	25.7
C1-C4	6.9	7.1
Hydrogen Consumption	3.52	3.59
Estimated Coke	0.19	3.55

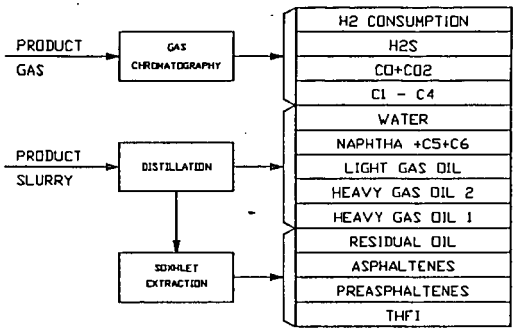

Figure 1. SUMMARY OF PRODUCT ANALYSES

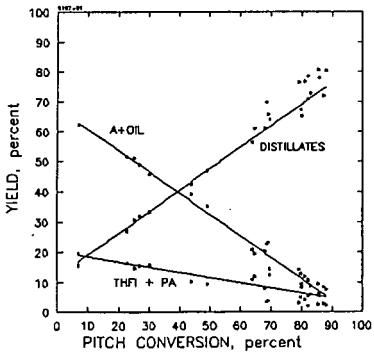

Figure 2. SELECTIVITY OF COPROCESSING PRODUCTS

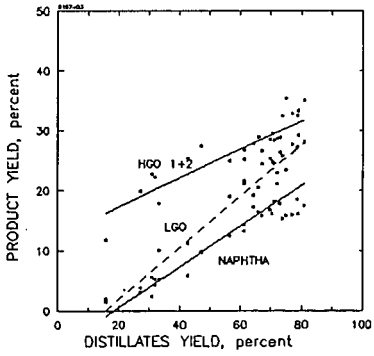

Figure 3. SELECTIVITY OF DISTILLATE FRACTIONS

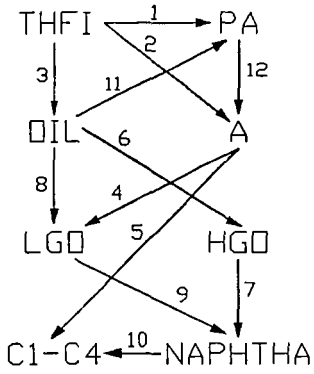

Figure 4. CANMET COPROCESSING MODEL INCORPORATING ADDUCT FORMATION

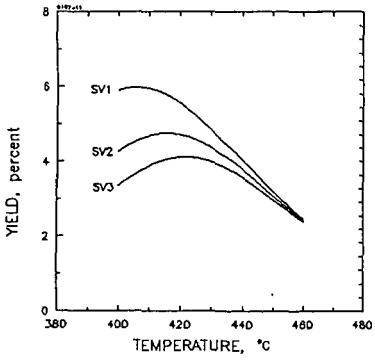

Figure 5. EFFECT OF TEMPERATURE ON PREASPHALTENES YIELD AT THREE SPACE VELOCITIES

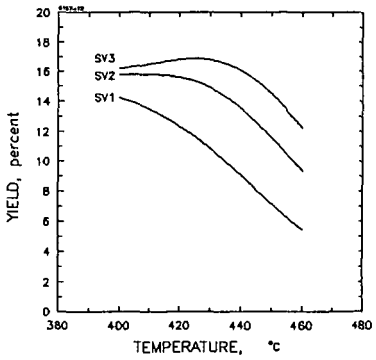

Figure 6. EFFECT OF TEMPERATURE ON ASPHALTENES YIELD AT THREE SPACE VELOCITIES

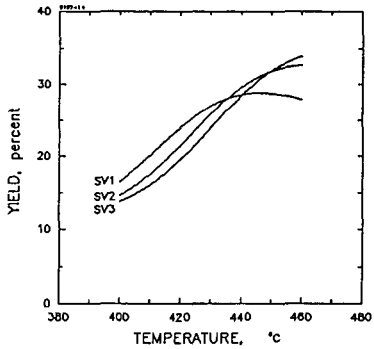

Figure 7. EFFECT OF TEMPERATURE ON HEAVY GAS OIL (1&2) YIELD AT THREE SPACE VELOCITIES

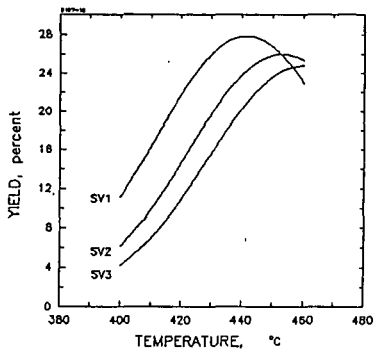

Figure 8. EFFECT OF TEMPERATURE ON LIGHT GAS OIL YIELD AT THREE SPACE VELOCITIES

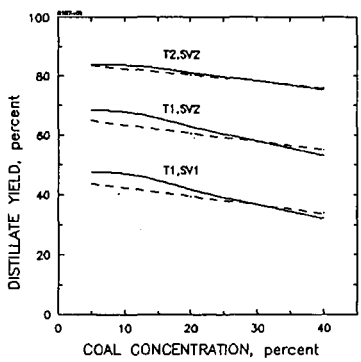

Figure 9. SIMULATED EFFECT OF COAL CONCENTRATION ON TOTAL DISTILLATE YIELD (solid lines for adjusted ϕ constants)

HYDROTREATING AND PRODUCTION OF TRANSPORTATION FUEL FROM COPROCESSED DISTILLATES

T. Ohuchi, M. Carmichael, A. Chambers and K. Muehlenbachs*

Coal and Hydrocarbon Processing Department
Alberta Research Council
1 Oilpatch Drive, Bag # 1310
Devon, Alberta, Canada, TOC IEO

*Geology Department, University of Alberta
Edmonton, Alberta, Canada, T6G 2E3

Keywords: Coprocessing, hydrotreating, isotope

INTRODUCTION

Production of refinery feedstocks and transportation fuels from coprocessing liquids were the objectives of this study. Coal-heavy oil coprocessed products are significantly different from conventional petroleum. In most coprocessing schemes, the first stage coprocessed products contain high concentrations of nitrogen and sulfur, directly inherited from the feed coal and the feed heavy oil. Nitrogen and sulfur must be removed from these first stage products by further catalytic hydrotreating to produce a synthetic crude to be marketed directly to existing refineries for further upgrading. The investigation of nitrogen and sulfur removal focused on producing refinery acceptable products with reference to existing refinery specifications.

An initial study of transportation fuels from coprocessing liquids resulted in production of one gasoline and two diesel products from distillate and gas oil fractions. They were engine tested to evaluate octane and cetane number and other properties which were then compared to the Canadian Standard Specifications.

The isotopic analysis of 13C/12C ratio provides information for quantifying amounts of coal derived matter incorporated into product slates. In the coprocessing of coal and heavy oil, both components of feed are upgraded simultaneously. Quantitative assessment of coal transformation into product fractions would give kinetic and engineering data for efficient development of coprocessing schemes. Using isotopic mass balance techniques, coal incorporation into the first stage coprocessed products (experimental feeds) and secondary upgraded products were calculated [1]

Consequently, this study consisted of (a) investigation of nitrogen and sulfur removal from coprocessed liquids, (b) preliminary production of transportation fuels, and (c) quantitative assessment of coal derived material incorporated into both first stage and secondary upgraded products.

EXPERIMENTAL

Feedstock. Coprocessed slurry was obtained from a process development unit operated by Canadian Energy Developments Inc. (CED). Feed to the unit consisted of an Alberta subbituminous coal (Vesta) and an iron based catalyst

slurried with Cold Lake vacuum bottoms. This slurry was then processed at temperature above 400°C and pressure above 17 MPa. The coprocessed slurry was separated by distillation into naphtha (below 177°C), distillate (178 to 343°C) and gas oil (344 to 508°C) fractions. Table 1 gives the analyses of starting feeds and nitrogen and sulfur concentration of distillables compared to refinery specifications. These fractions were secondary upgraded separately; the ratio of hydrogen flow to feed (vol./vol. ratio) was 1000 unless otherwise provided.

Catalysts. Three commercial catalysts were used: a Ni/Mo for hydrotreating, a different Ni/Mo for hydrocracking and platinum catalyst for reforming. Following presulfidation of the catalyst, and prior to hydrotreating/hydrocracking experiments, the catalysts were conditioned for a minimum 30 hours using a bitumen derived distillate feed. The platinum catalyst was used as received.

Hydrotreating. A continuous flow trickle bed reactor system was used, having a volume of 100 ml. For hydrotreating experiments of the naphtha fraction, a two level fractorial experimental design was used. The two levels of three variables were selected as follows: 390 and 420°C, 8.3 and 12.4 MPa, 1.0 and 3.0 h^{-1}. For the distillate and gas oil fractions, a Box-Behnken statistical experimental design approach was used to study the simultaneous effect of varying reaction temperature (400 to 440°C), pressure (6.9 to 11.0 MPa) and WHSV (1.0 to 4.0 h^{-1})[2]

Preliminary Production of Transportation Fuels. For gasoline production, the feed naphtha was hydrotreated at 420°, 12.4 MPa, WHSV of 3.0 h^{-1} followed by reforming at 500°C, 3.5 MPa, 1.0 h^{-1} and H_2/feed (vol./vol.) of 300. Two diesel products were obtained. One diesel product was produced by hydrotreating of the first stage distillate fraction at 440°C, 6.9 MPa and 2.5 h^{-1}. The other was obtained from the gas oil fraction by hydrotreating at the same conditions used for the distillate followed by further hydrocracking of the hydrotreated gas oil (which was separated by distillation) at 420°, 6.9 MPa and 1.0 h^{-1}

Distribution Of Coal In Product Slates. In order to quantify the amounts of coal derived matter incorporated into product fractions, an istopic analysis of 13C/12C ratio was carried out. The procedure is described elsewhere[3].

RESULTS AND DISCUSSION

(a) Nitrogen and Sulfur Removal From First Stage Coprocessed Products.

Naphtha. Table 2 summarizes the results of hydrotreating of the naphtha fractions and whether the resulting products met refinery specifications (Table 1). Even though the experimental conditions were varied for a two level statistical analysis, the small differences between concentrations of heteroatoms in the products of different experiments did not allow a meaningful analysis of the effect of hydrotreating conditions on nitrogen and sulfur removal. Product specifications for nitrogen were met under all operating conditions; however, those for sulfur were not.

Distillate. The experimental results of the three level test matrix for hydrotreating of the distillate fraction were fit using a quadratic fraction.

Figure 1 illustrates calculated response surfaces of change in concentration of nitrogen in the total liquid product against both reactor temperature and WHSV for hydrotreating of the distillate fraction. These figures show the relative order of effects on nitrogen removal for this range of conditions to be: WHSV > temperature > pressure. Also, some interaction of the three parameters was noted; decreasing WHSV at 400°C dramatically decreased nitrogen content of products but had a lesser effect at 440°C. For all of the conditions studied, the nitrogen concentration of products was below 200 ppm, meeting the specifications of nitrogen content. In terms of sulfur removal, the pressure required to produce acceptable refinery feeds was 6.9 MPa, the lowest in the entire experiments studied. Figure 2 shows the relationship between sulfur concentration in the products and hydrotreatment temperature with varying WHSV at a pressure of 6.9 MPa. This figure illustrates the sensitivity of sulfur content to reaction temperature, especially above 410°C. Decreasing WHSV from 4.0 to 3.0 h^{-1} also reduced sulfur content but further reduction had little effect.

Gas Oil. Figure 3 gives the response surfaces of nitrogen content in products of hydrotreating of the gas oil. Increasing temperature, decreasing WHSV and increasing pressure maximized nitrogen removal. Little interaction of three parameters was observed. The effect of pressure on sulfur removal from the gas oil was negligible. Figure 4 gives contours of sulfur concentration in products with varying WHSV at 6.9 MPa. It provides a range of operating temperature and WHSV that would be available to produce refinery acceptable feeds at 6.9 MPa. Also, using the estimated values from these curves, the activation energy with respect to sulfur removal was calculated using a first order model giving an activation energy of 56.3 kJ/mole.

(b) Preliminary Study of Transportation Fuel Production From Coprocessed Liquids.

In order to maximize the yield of value-added product such as diesel, the conversion of gas oil to distillate should be high. The response surface in Figure 5 shows the yield of distillate from gas oil hydrotreating. The relative order of parameter effects on the yield was temperature > WHSV with pressure having negligible effect. Generally, increasing temperature improved distillate yield. At high temperatures, decreasing WHSV increased distillate yield, while at low temperature, the change in yield from a change in WHSV was negligible.

Selected fractions from the products of secondary upgrading were further processed and tested for their properties as transportation fuels. Table 3 shows the results of an overall mass balance in the secondary upgrading experiments of first stage coprocessed liquids. The difference of 2.0% between amounts of feed and those of upgraded products represents amounts of gaseous products and some experimental errors involved.

Gasoline Product. The hydrotreated naphtha and the naphtha obtained from the product of hydrotreated distillate were combined and then reformed for engine testing as a gasoline product. This product had an octane number of 76.6, slightly less than the Canadian Specification minimum of 83.6 (January, Alberta). Either blending or different reforming conditions would be required to produce an unleaded gasoline product to meet the specifications.

Diesel Product. Table 4 gives the properties of diesel fractions obtained from two different sources compared to the Canadian specifications. One diesel was from hydrotreating of distillate fraction of first stage, and the other from hydrocracking of hydrotreated gas oil fraction. Key measures of diesel quality are cetane number and sulfur concentration. The results of engine testing of the first diesel product (produced from the distillate fraction) gave a cetane number of 40.9, slightly exceeding the minimum specification of 40. Sulfur concentration of this diesel was 349 ppm, much less than the 0.5% maximum specification, indicating that this diesel can be sold to market directly. The second diesel product (produced from the gas oil fraction) had a low cetane number of 28.6; however, the sulfur concentration was again well below the specification. In order to increase the cetane number of the second diesel product, more hydrogen must be added into this fraction, suggesting that further process options must be investigated. Most of the other diesel specification parameters can be adjusted by addition of fuel improvers.

(c) Distribution of Coal Incorporated Into Product Slates

Using a combination of isotopic analysis, elemental analysis of carbon and yield data of the feeds and the hydrotreated products, the concentration of coal derived carbon in each product fraction can be calculated. Figure 6 gives the distribution of coal derived carbon incorporated into the first stage coprocessed products. Figures 7 and 8 illustrate those of the hydrotreated products, indicating that the majority of coal derived carbon existed in the heavier fractions. However, significant amounts of coal derived carbon existed in the distillable products. After hydrotreating, the combined results gave the following concentrations of coal derived carbon in the product fractions: 20.3% in naphtha, 9.2% in distillate and 15.8 % in gas oil.

CONCLUSIONS

The following was concluded from this study:

1. Synthetic crude refinery feedstock specifications for nitrogen and sulfur content could be met for the distillate and gas oil fractions of coal-bitumen coprocessing.
2. The relative effectiveness on nitrogen removal during hydrotreating was WHSV ~ temperature > pressure.
3. On sulfur removal during hydrotreating, temperature had the greatest impact and pressure had a negligible effect.
4. Hydrotreating of distillate fraction directly produced a diesel which met several of the Canadian specifications.
5. Hydrotreatment followed by hydrocracking of gas oil produced a diesel fraction which did not meet the cetane number specification.
6. Coal derived carbon concentrations in the naphtha, distillate and gas oil product fractions after secondary upgrading were 20.3, 9.2 and 15.8 % respectively.

ACKNOWLEDGEMENT

This study was funded from the Alberta/Canada Energy Resources Research Fund, a fund jointly established by the Government of Canada and Alberta. The

project was administered by the Alberta Office of Coal Research and Technology. The project staff are indebted to Canadian Energy Developments, Inc. for supplying first stage coprocessing products.

REFERENCES

1. T. Ohuchi, K. Muehlenbachs, M. Bombin, J. Steer, J. Wilson and A. Chambers, "The Use of Stable Isotopic Ratios For Tracer Study: Applications of $^{13}C/^{12}C$ and D/H ratios in Hydrocarbon Processing." 1989 International Conference on Coal Science, Tokyo, October, 1989, Proceedings, P. 771.
2. G.E.P. Box and D. W. Behuken, "Some New Three Level Designs for the Study of Quantitive Variables", Technometrics, Vol. 2, p. 455-475, 1960.
3. J. Steer, T. Ohuchi and K. Muehlenbachs, "Efficacy of Coal-Bitumen Coprocessing As Determined by Isotopic Mass Balance Calculations", Fuel Processing Technology, 15 (1987), P. 429.

Table 1 ELEMENTAL ANALYSES OF FEEDSTOCKS AND REFINERY SPECIFICATIONS

Starting material as received(%)

	C	H	N	S
Vesta Coal	49.7	3.2	0.94	0.36
Cold Lake V.B.	83.1	9.9	0.75	5.77

Heteroatom concentrations of feeds and refinery specifications(ppm)

	Feeds		Specifications	
	N	S	N	S
Naphtha(<177 C)	770	5200	10	15
Distillate(178-343 C)	3120	17500	200	1000
Gas Oil(>344 C)	5200	24500	<2100	-
Total Blend				<3100

Table 2 HDN AND HDS: Hydrotreating of Naphtha from CED #1

Process Temperature, °C			390	420
Pressure (MPa)	WHSV (hr^{-1})			
8.3	1.0	N	0	0
		S	*	*
	3.0	N	0	0
		S	*	*
12.4	1.0	N	0	0
		S	*	*
	3.0	N	0	0
		S	*	*

0: meets refinery specifications
*: does not meet

Table 3

MASS BALANCE
(Based on slurry without water and gas)

% Feed		% Product		
		Naphtha (gasoline)	Distillate (diesel)	GO
Naphtha	4.9	4.9 **		
Distillate	14.7			
Hydrotreating		1.7	12.3 **	
Gas Oil	24.4			
Hydrotreating		1.2	1.8	(20.7*)
*Hydrocracking		(0.4)	(4.3)	(15.4)
(Subtotal)		0.2	10.4**	15.4
Total	44.0		42.0	

** Engine Tested

Table 4

PROPERTIES OF DISTILLATES COMPARED TO DIESEL SPECIFICATIONS

Property	Type of Diesel A	From Distillate	From Gas Oil
Ignition Quality Cetane Number	40	40.9	28.6
Sulfur, % Mass Max.	0.5	0.035	0.019
Flash Point °C, Min.	40	46.0	77.5
Cloud Point °C, Max.	-34	-27	-22
Pour Point °C, Max.	-39	-30	-45
Kinematic Viscosity at 40°C, cST, Min.	1.3	2.04	3.05
Max.	4.1		
Distillation: 90% Recovered °C, Max.	315	314.5	323
Total Acid Number Max.	0.10	0.009	0.01

Figure 1 HYDROTREATING OF DISTILLATE FROM COPROCESSING PRODUCTS: NITROGEN CONCENTRATION IN PRODUCTS

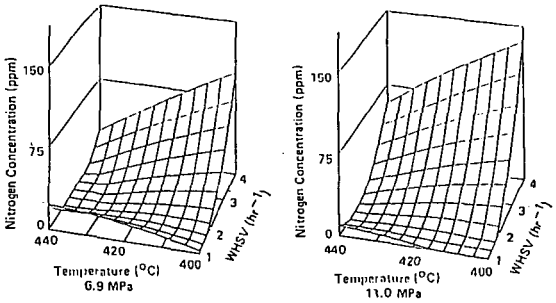

R-square = 0.91

Figure 3 HYDROTREATING OF GAS OIL FROM COPROCESSING PRODUCTS: NITROGEN CONCENTRATION IN PRODUCTS

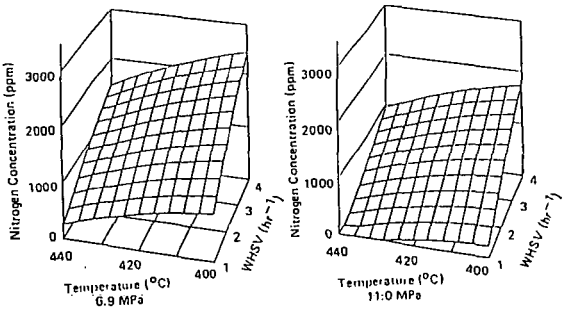

R-square = 0.98

Figure 2
HYDROTREATING OF DISTILLATE FROM COPROCESSING PRODUCTS: EFFECTS OF WHSV AND TEMPERATURE AT 6.9 MPa ON SULFUR REMOVAL

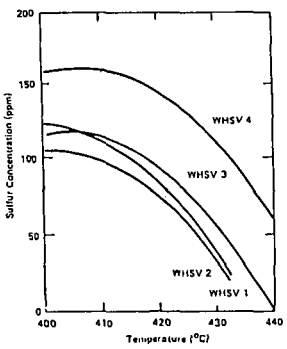

Figure 4
HYDROTREATING OF GAS OIL FROM COPROCESSING PRODUCTS: EFFECTS OF WHSV AND PROCESS TEMPERATURE AT 6.9 MPa ON SULFUR REMOVAL

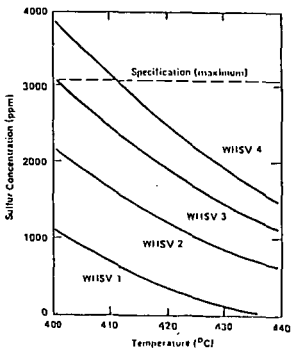

Figure 5

DISTILLATE YIELD PRODUCED FROM GAS OIL OF COPROCESSING PRODUCTS BY HYDROTREATING

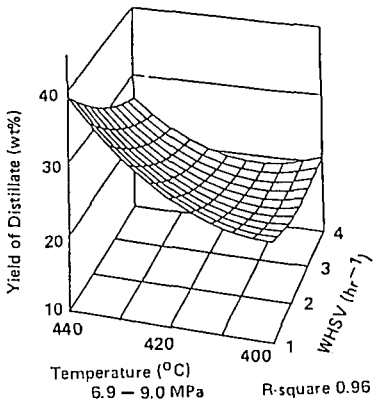

Figure 6

First Stage Coprocessing: Distribution of Coal derived Carbon by Isotopic Analysis

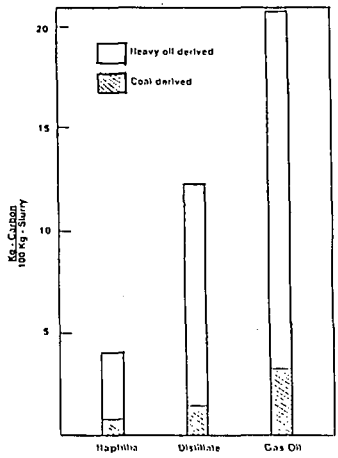

Figure 7

Secondary Upgrading of Distillate from Coprocessing: Distribution of Coal Derived Carbon by Isotopic Analysis

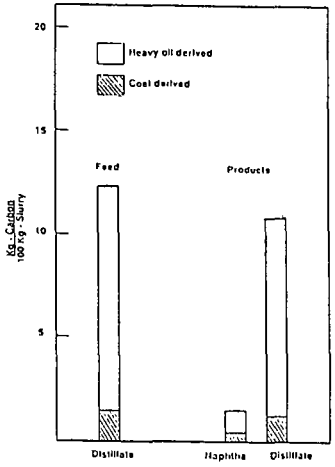

Figure 8

Secondary Upgrading of Gas Oil from Coprocessing: Distribution of Coal Derived Carbon by Isotopic Analysis

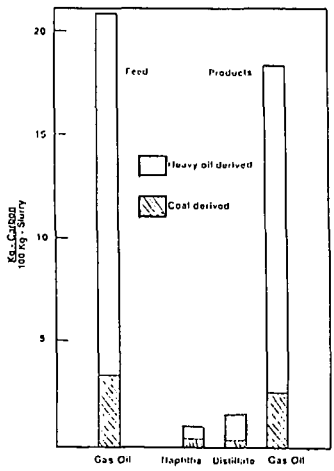

APPLICATION OF STABLE CARBON ISOTOPE ANALYSIS TO CONTINUOUS COAL/OIL COPROCESSING

R. A. Winschel, F. P. Burke and M. S. Lancet

CONSOLIDATION COAL COMPANY
Research & Development
4000 Brownsville Road
Library, PA 15129

INTRODUCTION

Stable carbon isotope analysis is a promising technique for distinguishing and quantifying the individual contributions of the coal and petroleum feedstocks to coprocessing products. Such information is valuable for process modeling and optimization and for discerning reaction pathways and interactions between the two feedstocks. Carbon isotope analysis provides information only on the fate of carbon; however, this is a minor limitation because most products are 85-90% carbon. A potentially significant obstacle to accurate quantitation is selective isotopic fractionation, a phenomenon by which the two stable carbon isotopes from a single feedstock selectively report to different products. Selective isotopic fraction appears to be exacerbated by reaction severity, and it can cause large quantitation errors at high conversion conditions unless some means is employed to correct for it. This paper describes the isotope analysis of samples from a continuous coprocessing bench-unit run performed by Hydrocarbon Research, Inc. (HRI) with Maya vacuum still bottoms (VSB) and Taiheiyo (Japanese) coal at high conversion conditions. A method to correct for selective isotopic fractionation was employed that allowed quantitation of the conversions of the individual feedstocks.

BACKGROUND

Fifteen product oils and two feedstocks were obtained from S. V. Panvelker, of HRI, from HRI continuous coprocessing bench Run 238-2, also known as Bench Run 4. Run 238-2 was a 25-day feedstock reactivity test performed with Maya VSB and Taiheiyo coal. The run was completed in November 1988. Six sets of operating conditions (1,2), each lasting 4 or 5 days, were used during the run, as illustrated in Table 1. The principal variables were oil to MF coal ratio, space velocity, temperature, and catalyst age. Recycle was used only during the 1/1 oil/coal periods. Product yields (2,3) are reported in Table 2. The product samples obtained included five fractions of the net products from each of periods 5, 13, and 25 (conditions 1, 3, and 6, respectively). The fractions included initial boiling point (IBP) by 350°F, 350 by 650°F, and 650 by 975°F distillates, 975°F+ solubles, and unwashed pressure-filter solids. Samples of the two feedstocks also were obtained. Sample size ranged from 10 to 50 g for each sample. Carbon content was determined on each sample with a LECO CHN-600 instrument. Carbon isotope analyses were performed in duplicate on each sample at the Stable Isotope Laboratory of Conoco Inc. in Ponca City, Oklahoma. Carbon isotope ratios and carbon contents of all samples appear in Table 3. The chemical analysis of the coal appears in Table 4.

DISCUSSION

Through use of the isotope ratios and a simple mixing equation, one can calculate the coal carbon/total carbon ratio of each product. Such an approach assumes that there is no selective fractionation of the isotopes, or at least that it is small

enough to be ignored. Uncorrected results, which appear in Table 5, show an over-accounting of coal carbon, presumably from selective fractionation.

Though gas and insoluble organic matter (IOM) samples were not received for analysis, their delta values and carbon contents can be estimated by forcing carbon and carbon isotope balances to 100%. This was done as follows: The pressure-filter solids (PFS) contain entrained oils (lower half of Table 2). The overall yields were adjusted to include the PFS by substituting the PFS for appropriate amounts of each component in the overall yield. Yields and carbon and isotope analyses were thus available on all products except the gas, which was then forced. With the forced gas data so obtained, the IOM data could be forced. The forcing calculation method is detailed elsewhere (4). Several comments on the results from this exercise, which appear in Table 6, are in order. The forced carbon contents of the gases appear reasonable in light of their composition (Table 2). The negative uncorrected coal carbon contents calculated for the gases merely reflect their light (more negative) isotopic composition. This is to be expected and has been observed in those cases for which gas samples actually were analyzed. Of course, the negative values have no physical meaning; they merely reflect isotopic fractionation. The IOM fractions have quite small yields, reflecting the high coal conversions (ca. 95% MAF). The uncorrected calculated carbon contents of the IOM fractions are not fully reasonable; for example, the Condition 1 IOM has more carbon than total mass. This reflects the combination of all errors. The errors in IOM carbon contents are actually quite small on an absolute basis, being less than 1% in all cases. The uncorrected calculated coal carbon contents of the IOMs indicate that their carbon content is virtually all coal-derived.

As noted, the isotope analyses of the product fractions actually analyzed result in an overabundance of coal carbon when not corrected. This overabundance results from the high yields (15-18%) of isotopically light gases (ca. -30.4 per mil from forced balances). Even though the carbon content of the gases is only about 40 to 50%, they still account for 8 to 9% of the total carbon in the feedstocks. A first-order correction to the data can be applied by assuming that the carbon contained in the gases is formed from the petroleum and coal in proportion to the petroleum carbon and coal carbon in the feedstock. The fraction of the petroleum carbon and coal carbon that is not converted to gas then, has an isotope ratio that is heavier (less negative) than the whole petroleum and coal feeds, respectively. The correction method used here relies on three assumptions: 1) the carbon in the gas is formed from the two feedstocks in proportion to the carbon fed to the unit from each feedstock, 2) the difference between the $\delta^{13}C$ of each feedstock and the $\delta^{13}C$ of the gas produced from that feedstock is the same for the coal and the petroleum, and 3) the non-gas-producing carbon undergoes no further selective isotopic fractionation. The calculation method used to make this correction is detailed elsewhere (4). With this correction approach, we calculate delta values of the non-gas-producing petroleum carbon to be -26.88, -26.82, and -26.80 per mil for Conditions 1, 3 and 6, respectively; the average value is -26.84 $\pm$0.04 per mil. The non-gas-producing coal carbon is calculated to have delta values of -23.75, -23.68, and -23.66 per mil, respectively, for the same periods, with an average delta value of -23.69 $\pm$0.05 per mil. The calculated delta values of the petroleum gas and coal gas average -31.46 and -28.32 per mil, respectively.

Carbon sources, selectivities, and conversions of the non-gaseous products are shown in Table 7 on the basis of the corrected delta values. Selectivity is the enrichment of coal carbon/total carbon in a product relative to the whole feedstock. Carbon sources are plotted in Figure I, coal carbon conversions are plotted in Figure 2, and petroleum carbon conversions are plotted in Figure 3. The following observations concern the corrected results from Table 7 and Figures I

through 3. The coal carbon to total carbon ratio in the condensed product fractions increases with boiling point with the one exception of the 975°F+ soluble product. The selectivity data (Table 7) indicate that the IBP x 350°F and 350 x 650°F products are selectively produced from petroleum. The 650 x 975°F and IOM products are selectively produced from coal. The 975°F+ solubles are produced from the two feedstocks without selection. The IOM carbon is close to being entirely coal-derived. In Condition 3, the IOM carbon is calculated to be more than 100% coal-derived; as noted earlier, this error appears to be associated with the need to determine the IOM properties by forced carbon and isotope balances. As expected, all fractions show the greatest coal carbon contributions during Condition 3, which was operated at a 1/1 petroleum/coal ratio. Conditions 1 and 6 were identical (except for catalyst age), including a 2/1 petroleum/coal ratio, and coal carbon contributions are quite similar for their respective products.

The major coal product is the 650 x 975°F distillate (Figure 2); 35 to 42% of the coal carbon reports to that fraction. The coal carbon conversions to IOM (3.4 to 5.8%) indicate that the total conversion of coal carbon to solubles was 94 to 97%. The major petroleum product is the 350 x 650°F distillate (Figure 3); about 38% of the petroleum carbon reports to that fraction. Very little of the petroleum carbon reports to the IOM product.

Interestingly, there is very little difference in conversions of the individual feedstocks between the run periods at petroleum/coal ratios of 2/1 (Conditions 1 and 6) and at 1/1 (Condition 3). Though other operating conditions (T, SV) also were changed, this suggests that within the precision of the data there is no synergy between the feedstocks for conversion, or at least that the degree of synergy is unchanged at ratios of 1/1 and 2/1.

SUMMARY

The analytical results show that selective isotopic fractionation was severe enough during HRI Run 238-2 that accurate carbon source quantitation and individual feedstock conversions cannot be obtained without correcting for isotopic fractionation. A first-order correction was applied that assumes that the feedstocks each fractionate into two "pools" of differing isotopic composition: the gas and the condensed products. The results support the validity of the correction method employed. The petroleum more readily produces light products. Its major product is the 350 x 650°F distillate, whereas that of the coal is the 650 x 975°F distillate. The insoluble organic matter (IOM) is nearly all coal-derived and the naphtha is mostly petroleum-derived. The 975°F+ soluble product is produced in proportion to the feedstock blend. There is no evidence for synergistic interactions between the two feedstocks with respect to conversion to products.

ACKNOWLEDGMENTS

The authors gratefully acknowledge J. E. Duddy and S. V. Panvelker of HRI for supplying the samples and yield data. This work was funded by the U.S. Department of Energy under contract No. DE-AC22-88PC88800.

REFERENCES

1. Panvelker, S. V., Hydrocarbon Research, Inc., letter to R. A. Winschel, March 9, 1989.
2. Duddy, J. E.; Panvelker, S. V. "Bench-Scale Development of Coal/Oil Co-Processing Technology". presented at the DOE Direct Liquefaction Contractors' Review Meeting, Pittsburgh, PA, October 1989.

3. Panvelker, S. V., Hydrocarbon Research, Inc., personal communications to R. A. Winschel, January 19 and 24, 1990.
4. Winschel, R. A.; Burke, F. P.; Lancet, M. S. "Stable Carbon Isotope Analysis of Coprocessing Materials - Monthly Status Report for January 1990". U.S. DOE Report No. DOE/PC 88800-22, February 1990.

TABLE 1
OPERATING CONDITIONS: HRI COPROCESSING RUN 238-2

Condition	1	2	3	4	5	6
Period	1-5	6-9	10-13	14-17	18-21	22-25
Oil to MF Coal Ratio	2	1	1	2	2	2
Recycle-to-Fresh-Feed Ratio	0	0.5	0.5	0	0	0
Relative Space Velocity	1	1	1.6	1.6	1.6	1
Temp., °F (1st and 2nd Stage)	810	810	825	825	810	810

Feedstocks: Taiheiyo coal; Maya VSB
Catalysts: Commercial Ni/Mo on alumina, both stages, batch aged during run.
Source: Reference 1, and for temperatures and catalyst, Reference 2.

TABLE 2
PRODUCT YIELDS: HRI COPROCESSING RUN 238-2

Condition	1	2	3	4	5	6
Period	5	8/9	13	-	-	25
Yields, wt % of dry feed						
H_2O, H_2S, NH_3	8.63		9.32	-	-	8.09
CO	0.05	11.0	0.16	-	-	0.06
CO_2	0.03		0.09	-	-	0.05
C_1 x C_3	4.89	5.5	5.18	-	-	3.97
C_4 x C_7 (in gas)	3.52		3.19	-	-	2.97
IBP x 350°F	12.91		12.72	-	-	13.41
350 x 650°F	32.82	34.7	28.53	-	-	31.05
650 x 975°F	26.57	21.2	24.90	-	-	25.96
975°F+ Solubles	9.59	9.2	11.48	-	-	11.19
IOM	0.88	1.9	1.94	-	-	1.42
Ash	4.27	6.4	6.41	-	-	4.27
H_2 Consumption	-4.16	-4.4	-3.88	-	-	-3.37
Sum(a)	100.00	100.1	100.04	-	-	99.07
Performance, wt % MAF						
Coal Conversion	-	95.6	-	-	-	-
975°F+ Conversion	-	87.5	-	-	-	-
Composition of Unwashed Pressure-Filter Solids, wt % of dry feed						
650°F-	0.10	-	0.41	-	-	0.17
650 x 975°F	1.45	-	3.74	-	-	3.24
975°F+ Solubles	0.63	-	2.11	-	-	1.84
IOM	0.88	1.9	1.94	-	-	1.42
Ash	4.27	6.4	6.41	-	-	4.27
Total	7.33	-	14.62	-	-	10.94

(a) Sums may not equal exactly 100.00% because of slightly different calculation methods used by HRI to arrive at these gas and liquid yields.
Source: Reference 3 and, for Condition 2 data, Reference 2.

TABLE 3
CARBON ISOTOPE RATIOS AND CARBON CONTENTS

	Operating Condition	$\delta^{13}C$, per mil avg.±std. dev.(b)	Carbon wt % (d)
Feedstocks			
Taiheiyo Coal (HRI #5595)	All	-24.12 ±0.02	68.36(d)
Maya VSB (HRI #5567)	All	-27.26 ±0.02(c)	85.75
Products			
IBP x 350°F	1	-26.50 ±0.01	85.41
350 x 650°F		-26.14 ±0.06	87.38
650 x 975°F		-25.75 ±0.04	87.54
975°F+		-25.88 ±0.01	91.11
Pressure Filter Solid(a)		-25.08 ±0.14	47.96
IBP x 350°F	3	-25.70 ±0.03	85.10
350 x 650°F		-25.70 ±0.06	87.76
650 x 975°F		-24.98 ±0.11	88.10
975°F+		-25.54 ±0.01	89.57
Pressure Filter Solid(a)		-24.84 ±0.09	47.06
IBP x 350°F	6	-26.29 ±0.03	85.77
350 x 650°F		-26.19 ±0.07	87.32
650 x 975°F		-25.51 ±0.01	88.01
975°F+		-25.90 ±0.06	91.18
Pressure Filter Solid(a)		-25.42 ±0.01	51.09

(a) Unwashed.
(b) All isotope analyses performed in duplicate at Conoco's Stable Isotope lab.
(c) Original duplicate set of analyses gave -26.20 and -26.86 per mil; however, analyst noted that he could not obtain a representative sample for that pair of analyses. Repeat duplicate analysis are shown.
(d) Reported on an as-determined basis for all samples, except for coal which is reported on a MF basis.

TABLE 4
ANALYSIS OF TAIHEIYO COAL

Moisture, wt % as determined	4.59
Proximate, wt % dry basis	
Volatile Matter	49.26
Fixed Carbon	38.60
Ash	12.14
Ultimate, wt % dry basis	
C	68.36
H	5.69
N	1.02
O (diff)	12.50
S, total	0.27
pyritic	0.07
sulfate	<0.01
organic (diff)	0.20
Cl	0.019
Ash	12.14
Gross Cal. Value, dry, Btu/lb	12,239

TABLE 5

UNCORRECTED COAL CARBON AS PERCENT OF TOTAL CARBON
HRI COPROCESSING RUN 238-2

Product	Operating Condition	Coal Carbon/ Total Carbon, %(b)
IBP x 350°F	1	24.2 ±0.6
350 x 650°F		35.7 ±2.0
650 x 975°F		48.1 ±1.4
975°F+		44.0 ±0.6
Pressure Filter Solid(a)		69.4 ±4.5
IBP x 350°F	3	49.7 ±1.1
350 x 650°F		49.7 ±2.0
650 x 975°F		72.6 ±3.5
975°F+		54.8 ±0.6
Pressure Filter Solid(a)		77.1 ±2.9
IBP x 350°F	6	30.9 ±1.1
350 x 650°F		34.1 ±2.3
650 x 975°F		55.7 ±0.6
975°F+		43.3 ±2.0
Pressure Filter Solid(a)		58.6 ±0.6

(a) Unwashed.
(b) Standard deviation reflects random error but not bias errors.

TABLE 6

PROPERTIES OF GASES AND IOM PRODUCTS BASED ON MASS, CARBON, AND ISOTOPE BALANCES: HRI COPROCESSING RUN 238-2

Run Condition	Yield, lbs Product/ 100 lbs Dry Feed	lbs Carbon in Product/ 100 lbs Dry Feed	lbs Coal Carbon in Product/ 100 lbs Dry Feed (Uncorrected)	Coal Carbon/ Total Carbon Ratio (Uncorrected)	$\delta^{13}C$, per mil
Hypothetical Gases					
1	17.12	6.66	-6.68	-100.25	-30.41
3	17.94	7.64	-6.89	- 90.20	-30.09
6	15.14	7.37	-8.06	-109.36	-30.69
Hypothetical IOM					
1	0.88	1.58	1.55	97.61	-24.20
3	1.94	1.34	1.70	126.98	-23.27
6	1.42	0.91	0.91	99.71	-24.13

TABLE 7

CORRECTED CARBON SOURCES, SELECTIVITIES AND CONVERSIONS HRI COPROCESSING RUN 238-2

Product	Run Condition	Coal Carbon as a % of Total Carbon (a)	Selectivity for Coal Carbon (b)	Conversion of Coal C to Fraction, %	Conversion of Petroleum C to Fraction, %
Hypothetical Gas	1	28.5	1.0	8.3	8.3
IBP x 350°F		10.8	0.4	5.2	17.2
350 x 650°F		22.2	0.8	28.0	39.0
650 x 975°F		34.6	1.2	35.3	26.6
975°F+ Solubles		30.5	1.1	11.7	10.6
Hypothetical IOM		83.8	2.9	5.8	0.4
Total		-	-	94.3	102.1
Hypothetical Gas	3	44.4	1.0	9.9	10.0
IBP x 350°F		36.9	0.8	11.7	15.9
350 x 650°F		36.9	0.8	27.0	36.8
650 x 975°F		60.2	1.4	38.6	20.4
975°F+ Solubles		42.1	0.9	12.7	13.9
Hypothetical IOM		115.8	2.6	4.5	0.5
Total		-	-	104.4	96.5
Hypothetical Gas	6	28.5	1.0	9.2	9.2
IBP x 350°F		17.5	0.6	8.8	16.6
350 x 650°F		20.6	0.7	24.6	37.7
650 x 975°F		42.2	1.5	42.3	23.1
975°F+ Solubles		29.8	1.0	13.4	12.5
Hypothetical IOM		86.0	3.0	3.4	0.2
Total		-	-	101.7	99.3

(a) Petroleum carbon as % of total carbon is 100% minus this value.
(b) Selectivity is calculated as the ratio of coal carbon/total carbon in a product fraction to the coal carbon/total carbon ratio in the whole feedstock.

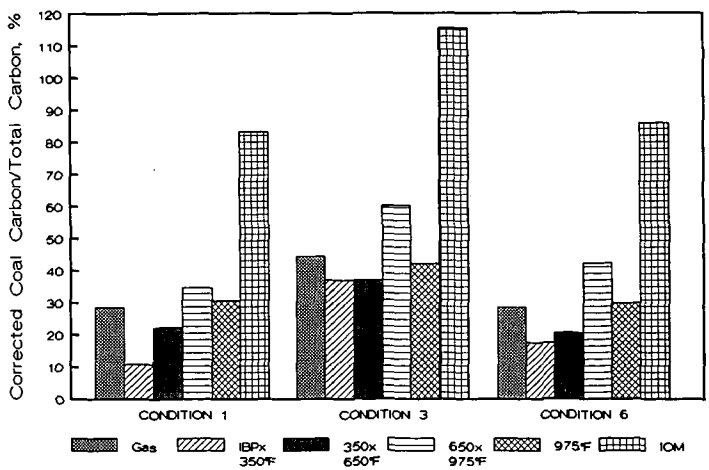

Figure 1. Corrected Coal Carbon to Total Carbon Ratios Plotted vs Run Condition. HRI Run 238-2.

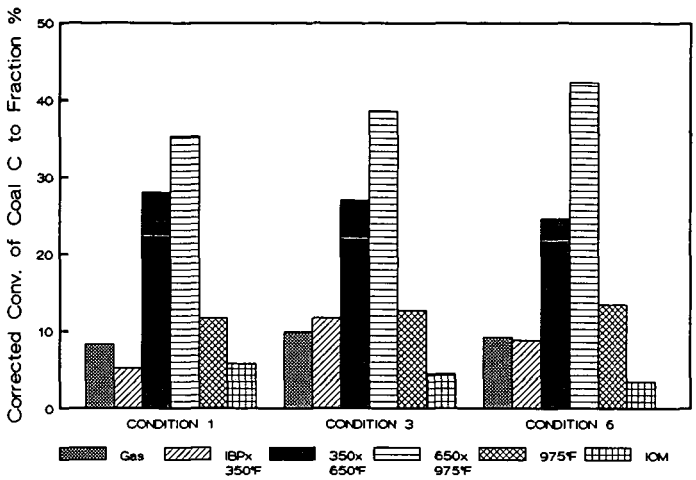

Figure 2. Corrected Conversions of Coal Carbon Plotted vs Run Condition. HRI Run 238-2.

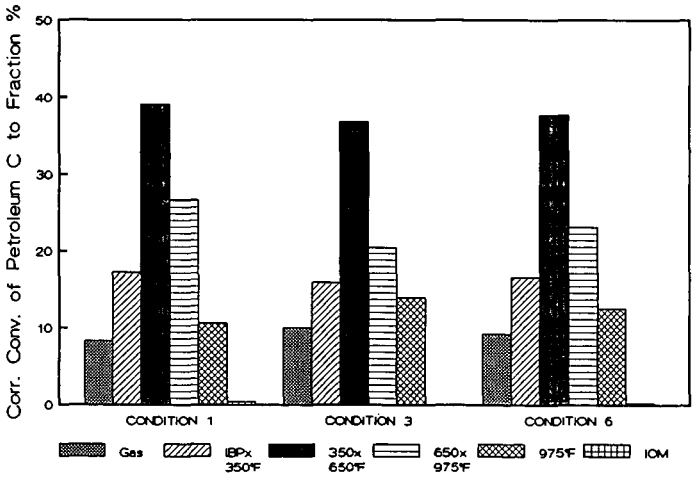

Figure 3. Corrected Conversions of Petroleum Carbon Plotted vs Run Condition. HRI Run 238-2.

PHASE SPLITTING AND SYNERGISM IN COAL OIL COPROCESSING AND COAL LIQUEFACTION

L. Dukhedin-Lalla+, P.M. Rahimi*, and J. M. Shaw+

+Department of Chemical Engineering, University of Toronto, Toronto, Canada, M5S 1A4
*CANMET, Energy Mines and Resources Canada, 555 Booth St., Ottawa, Canada, K1A OG1

ABSTRACT

The phase behaviour of complex hydrocarbon systems relevant to coal-oil coprocessing and direct coal liquefaction was investigated in the temperature range 600 to 700 K, using a batch autoclave apparatus. Bitumen and heavy oil + anthracene mixtures as well as model liquefaction solvents such as pyrene + tetralin are shown to exhibit phase splitting in this region. Gas phase constituents such as H_2, N_2, CH_4, C_2H_6 were found to influence the size and shape of the phase splitting zone but did not alter the phase behaviour per se. Significant fluctuations in the light oil yield obtained from laboratory and pilot scale models of coal/oil coprocessing and direct coal liquefaction processes are frequently attributed to synergism. In this paper, some aspects of synergism are related to phase splitting and the influence of phase splitting on reaction schemes. Preliminary criteria for solvent/diluent selection and operating conditions are proposed.

KEY WORDS: coprocessing, coal liquefaction, synergism

INTRODUCTION

Kinetic studies in heavy oil upgrading, coal/oil coprocessing and direct coal liquefaction are frequently conducted without due consideration for the physical properties of solvents or diluents under the reaction conditions employed (650 to 750 K, 4 to 30 MPa). Consequently, significant fluctuations in light oil yields obtained from laboratory and pilot scale studies, arising from apparently minor perturbations in operating conditions, are frequently attributed to synergistic phenomena [1-6]. As the reaction conditions associated with coprocessing and coal liquefaction typically intersect the critical region of one or more of the principal liquid constituents [7], complex phase behaviour can be anticipated [8, 9]. Phase splitting, for example, is a common phenomenon in the critical and subcritical regions [10]. In addition, hydrogen is a principal reagent in both coal dissolution [11] and oil hydrogenation reactions and hydrogen solubility in liquids is sensitive to composition [12]. Phase splitting and hydrogen solubility can have a direct and significant impact on observed rates for coal dissolution reactions [13, 14], for example, and these phenomena provide a satisfactory explanation for 20 wt % fluctuations in coal conversion arising in pyrene-tetralin mixtures under hydrogen [15] which had previously been attributed to synergism [1]. Results obtained by Rincón and Angulo [3, 4] and Fouda et al. [6] are also consistent with phase splitting [16]. The transition of the diluent or solvent from liquid to supercritical fluid is another phenomenon which can have a significant impact on reaction kinetics.

Many of the model compounds and liquids employed are unstable under the operating conditions investigated and the phase data presented are not equilibrium data per se. Catalysts are ubiquitous actors in these systems and their effect can only be minimized. Glass liners reduce the impact of trace pyrrhotite (a well known dehydrogenation catalyst) on reactor walls, but do not prevent catalytic hydrogenation due to catechol adsorption on stirrer surfaces [17]. Homogeneous isomerization, pyrolysis, and other reactions cannot be neglected at elevated temperatures. The degradation of pyrene [2, 15] and tetralin [18-21], for example, has been reported. Compound degradation cannot be ignored or prevented and phase compositions inevitably exhibit a time dependence.

EXPERIMENTAL

Experiments were conducted in a glass lined PPI autoclave having an inside diameter of 0.095 m and 0.3 m long. The autoclave, equipped with magnetically driven stirrer, internal cooling coil and three heated sample ports, was placed vertically in a 3000 W muffle furnace. All apparatus components were fabricated from type 316 stainless steel. The autoclave temperature was maintained within two degrees of a set point using an Athena temperature controller and a manually actuated internal cooling coil. All model compounds were reagent grade and supplied by Fluka. The anthracene oil was supplied by Allied-Signal and Athabasca bitumen and Venezuela heavy oil vacuum bottoms were supplied by CANMET. Their

properties are listed in Table 1. After loading the autoclave with 150 g of liquid, air was removed by flushing and the autoclave was charged with hydrogen, methane, etc. to a preset pressure and heated at 6 K min^{-1} to the first set point. Once the temperature reached the set point, operating parameters were fixed for 0.5 h. Agitation facilitated the acquisition of phase data. However, it proved necessary to cease agitation 0.5 h before sample retrieval so that emulsions, if present, could break [15]. Samples were collected in ice cold sample vials and immediately diluted in toluene. Species that did not condense at 273 K were not collected. Following sample retrieval the autoclave was heated to subsequent set points and the procedure was repeated.

Samples were analyzed chromatographically and mass spectra were obtained using a Hewlett Packard 5987A radio frequency quadrupole mass spectrometer. Many peaks were not identified unambiguously. Samples (1 μl) were injected directly into a 30 m DB-17 column. Column operating conditions were: carrier gas, helium; temperature program, 373 K for three minutes, 373-548 K at 20 K min^{-1}. Additional GCMS analysis and ASTM standard boiling point data were provided by Shell Canada Ltd. Compositions are repeatable to within 2 to 3 mole %.

RESULTS AND DISCUSSION

Partial phase diagrams for the model systems pyrene + tetralin + (ethane, no gas, nitrogen, or methane) are shown in Figures 1 through 3 respectively. At low gas pressures a liquid-liquid zone appears in all cases at temperatures exceeding 640 K. This zone grows with temperature and at 698 K is quite broad eg. the zone is bounded by 0.25 and 0.60 mole % pyrene when no gas is added. Only ethane causes this zone to shrink at elevated temperatures Figure 1a. Phase splitting can also arise at elevated pressures. For example, with nitrogen (Figure 2), phase splitting arises from splitting of the liquid phase. The high pressure and low pressure zones combines at elevated temperatures. With methane, Figure 3, the vapour phase splits at elevated pressures but these two phases do not coexist with a third phase. Key transitions arising in these systems include: gas-liquid to gas-liquid-liquid at low or high pressure, gas-liquid-liquid to gas-liquid, fluid-fluid or fluid at elevated pressures. These systems are most susceptible to phase splitting at low pyrene contents.

Dukhedin-Lalla et al. [16] reported that the model solvent system indene-decalin did not undergo phase splitting and that the synergism observed by Chiba et al. [2] could not be explained by phase splitting of solvent components. However, decalin is unstable in mixtures with indene, or indene + anthracene oil, as shown in Table 2, and forms naphthalene or naphthalene derivatives at elevated temperatures. The solubility of pyrene like coal liquids in naphthalene at 673 K is 15 to 20 wt % depending on pressure and gas composition as shown in Figures 1 through 4. Chiba et al. [2] reported coal conversions of 53, 65, and 35 wt % in indene, indene (50 wt %) + decalin, and decalin at this temperature and attributed the fluctuation to synergism. The corresponding concentrations of the coal derived liquids in the solvents are 18, 22, and 13 wt %. These concentration values are based on the initial charges of coal (6 g) and solvent (18 g), to a 0.1 litre reactor and the physical properties of naphthalene. The impact of solvent expansion, and evaporation was included in the calculations. While the operating conditions and compositions for the pbase and liquefaction experiments were not identical, the conversion of coal in "decalin", which corresponds to a coal derived liquid concentration in the solvent of 13 wt % compares favourably with the solubility limit for pyrene in naphthalene. The coal conversions reported by Chiba et al. [2] are consistent with phase splitting resulting from exceeding the solubility of coal derived liquids in the solvent where the solubility limit is a function of solvent composition. The decrease in coal conversion in solvents with a high "decalin" content can be explained in a manner analogous to the explanation of synergism in the pyrene-tetralin solvent system [15].

Complex mixtures of aliphatic and aromatic compounds also exhibit phase splitting as shown in Figure 4. Venezuela vacuum bottoms + anthracene oil and Athabasca bitumen + anthracene oil mixtures both exhibit phase splitting above 640 K for compositions in the 30 to 70 wt % range. As many of the species present could not be identified unambiguously or were retained by the column, the compositions shown in figure 4 are incomplete. Simple model systems do not mimic the behaviour of complex systems in this case. Pyrene-hexadecane mixtures, for example, only begin to phase split at 698 K for pyrene contents in excess of 75 wt %. Curtis et al. [5] reported coal conversions for a series of experiments which simulate the transition from coprocessing to coal liquefaction with complex solvents. The solvents comprised mixtures of Maya TLR (petroleum based) and V1067 (a bottoms recycle solvent from the

Wilsonville coal research facility). The authors showed that coal conversion decreased slightly, from 65 to 60 wt %, at 698 K as the V1067 content of the solvent increased from 0 to 35 wt %, with a large coincident increase in insoluble organic matter derived from the solvent. Then coal conversion began to increase rapidly to 75 and 90 wt % conversion at solvent compositions of 50 and 100 wt % V1067. The coal derived liquid content at the end of each of these experiments is 25, 50, 64, and 100 wt % respectively. These results are also consistent with phase splitting. The coal derived liquid content in the experiment where Maya TLR was used as a solvent is 25 wt %. Our results show that at 30 wt % mixtures of coal liquids and petroleum feed stocks phase split. So adding coal liquids to the solvent saturates the solvent with coal liquid thus inhibiting coal dissolution. A separate dispersed liquid phase is is then formed which leads to an increase in the production of insoluble organic matter (IOM) as the dispersed liquid becomes hydrogen starved due to poor liquid-liquid mass transfer and polymerization reactions dominate in this phase. If sufficient coal liquid is added to the solvent it becomes the continuous liquid phase and there is a sharp increase in coal solubility at this point because it is more soluble in coal derived solvent than in petroleum derived solvent. Consequently a greater fraction of the coal is solubilized and hydrogenated, coal conversion increases and the IOM produced by the coal based solvent decreases. In this case the continuous phase appears to change over at a coal liquid content of approximately 50 wt %.

Phase splitting is a fundamental characteristic of the coprocessing and coal liquefaction reaction environment and cannot be neglected in the design or interpretation of experiments, or the design of processes. In coprocessing, for example, care must be taken to ensure that the anticipated coal derived liquid concentration in the diluent does not exceed the solubility limit. Extant data [5, 6] and the present work place the solubility limit in the 25 to 30 wt % range but more dilute systems are preferred. Coal liquids exhibit phase splitting between 2 and 4 ringed compounds. Thus, in direct coal liquefaction, two optima appear to exist from the point of view of solvent selection which lead to different reactor design choices:

1. a heavy recycle solvent operated at a pressure sufficient to ensure adequate hydrogen availability,
2. a middle distillate operated at a pressure high enough to avoid the phase split zone.

The first optimum is best exemplified by the so-called German technologies whereas the second optimum has received little attention [22].

CONCLUSIONS

Phase splitting has been shown to arise in both simple and complex mixtures of aromatic, polynuclear aromatic and aliphatic compounds. This phenomenon is shown to account for fluctuations in coal conversions arising in coal oil coprocessing and coal liquefaction previously attributed to synergism. In particular, liquid yields from coal in coprocessing appear to be limited by the solubility of coal liquids in petroleum based solvents. In coal liquefaction the situation is more complex and a minimum of two solvent optima exist.

ACKNOWLEDGEMENTS

The authors wish to thank Shell Canada Ltd., Allied Signal Corp., and Mr. P. Sacco for their assistance. Funding provided by CANMET through DSS contract 23440-8-9084/01-SS and NSERC is gratefully acknowledged.

REFERENCES

1. Derbyshire, F. J., P. Varghese and D. D. Whitehurst, 1982. "Synergistic Effects Between Light and Heavy Solvent Components During Coal Liquefaction", Fuel, 61, 859-864.
2. Chiba, K., H. Tagaya, S. Sato and K. Ito, 1985. "Coal Liquefaction Using Indene-Tetralin and Indene-Decalin Mixtures as Solvent", Fuel, 64 , 68-73.
3. Rincon, J. E., and R. Angulo, 1986. "Petroleum heavy oil mixtures as a source of hydrogen in the liquefaction of Cerrejon coal", FUEL, 65, 899-902.
4. Rincon, J. E., and R. Angulo, 1987. "Synergism in coal liquefaction using petroleum heavy oil mixtures for the liquefaction of Cerrejon coal", Proc. 1987 Int. Conf. Coal Sci. , 375-8.
5. Curtis, C. W., K. Tsai and J. A. Guin, 1987. "Effects of Solvent Composition on Coprocessing Coal with Petroleum Residua", Fuel Processing Tech., 16, 71-87.

6. Fouda, S. A., J. F. Kelly and P. M. Rahimi, 1988. "The Effect of Coal Concentration on Coprocessing Performance", ACS Fuel Chem. Symp. Series, 33, 178-184.
7. Reid, R., J. Prausnitz, and B. Poling, The Properties of Gases and Liquids, 4th ed., Ch. 8, McGraw-Hill, 1987.
8. Subramaniam, B., and M. A. McHugh, 1986. "Reactions in Supercritical Fluids", Ind. Eng. Chem. Proc. Des. Dev. 25, 1-6.
9. Paulaitis, M. E., J. M. L. Penninger and R. D. Gray, 1983. Chemical Engineering at Supercritical Fluid Conditions Ann Arbor Science, Michigan
10. Adams, R. M., A. H. Knebel and D. E. Rhodes, 1979. "Critical Solvent Deashing", Chem. Eng. Prog. 75 (6), 44-48.
11. Pozzobon, R., S. Yushun and J. M. Shaw, 1990. "The Role of Hydrogen in Coal Particle Disintegration at Elevated Temperatures", CJChE (in press).
12. Shaw, J. M., 1987. "A Correlation for Hydrogen Solubility in Alicyclic and Aromatic Solvents", CJChE, 65, 293-298.
13. Shaw, J. M. and E. Peters, 1989. "The Role of Initial Reaction Conditions in Direct Coal Liquefaction",Ind. Eng. Chem. Res., 28, 976-982.
14. Shaw, J. M. and E. Peters, 1989. "A General Model for Coal Dissolution Reactions", Ind. Eng. Chem. Res., 28, 1795-1801.
15. Shaw, J. M., R. P. Gaikwad and D. A. Stowe, 1988. "Phase Splitting of Pyrene-Tetralin Mixtures Under Coal Liquefaction Conditions", FUEL, 67, 1554-1559.
16. Dukhedin-Lalla, L., P. M. Rahimi and J. M. Shaw, 1989. "Phase Splitting of Complex Hydrocarbon Mixtures", Fluid Phase Equilibria, 53, 415-422.
17. Yoshii, T. R. Yaginuma and H. Yoshikaura,1982. "Unusual Effects of Catechol on the Hydroliquefaction of Coal", FUEL, 61, 865-866.
18. Hooper, R. J., H. A. J. Battaerd and D. G. Evans, 1979. "Thermal Dissociation of Tetralin Between 300 and 450 °C" Fuel, 58, 132-138.
19. Benjamin, B. M., E. W. Hagaman, V. F. Raaen and C. J. Collin, 1979. "Pyrolysis of Tetralin", FUEL, 58, 386-390.
20. McNeill, R. I., D. C. Croanuer and D. C. Young, 1983. "Isomerization of Tetra-hydroaromatic Groups Under Coal Liquefaction Conditions", FUEL, 62, 401.
21. Penninger, J. M. L. and H. W. Slatboom, 1976. "Industrial and Laboratory Pyrolysis", Am. Chem. Soc. Symposium Series, 32, 444-449.
22. Shaw, J. M., and E. Peters. "Toward Optimal Reactor Designs for Direct Coal Liquefaction Processes", Proc. 36th Canadian Chemical Engineering Conf., October 1986.

TABLE 1: Physical Properties and Compositions of Oils (wt %)

		Anthracene Oil	Athabasca Bitumen	Venezuela (blend 24)
Specific gravity		(288.5 K) 1.092	(297 K) 1.046	(294 K) 1.026
Water, %		0.2	-	-
Xylene insoluble, %		0.08	-	-
Pentane insoluble, %		-	38.4	21.4
Distillation, % to	498 K	0.0	-	-
	543 K	7.9	-	-
	588 K	43.7	-	-
	628 K	80.5	-	-
	+628 K	19.0	-	-
	+798 K	-	99.3	95.1
Elemental analysis	C		84.3	84.3
	H		10.9	9.6
	N		0.8	0.7
	O		0.3	0.7
	S		3.5	6.0
Aromatic carbon, %			35.4	30.0
Mean molar mass			983	848

TABLE 2: Sample compositions obtained from ports located at the top (1) middle (2) and bottom (3) of the reactor for the system indene (25 wt %) + decalin (25 wt%) + anthracene oil (50wt %) + hydrogen (5 MPa)

COMPOUND (MOLE FRACTION)	648 K			673 K			698 K		
	PORT 1	PORT 2	PORT 3	PORT 1	PORT 2	PORT 3	PORT 1	PORT 2	PORT 3
INDENE or BENZENE derivative (C_9H_{10})	0.641	0.536	0.533	0.542	0.543	0.269	0.269	0.224	0.205
DECALIN (cis & trans) ($C_{10}H_{18}$)	0.186	0.181	0.171	0.039	0.116	0.031	0.000	0.000	0.000
INDENE or BENZENE derivative ($C_{10}H_{12}$)	0.000	0.014	0.016	0.023	0.013	0.000	0.000	0.000	0.000
SPIRO (4,5) DECANE ($C_{10}H_{18}$)	0.030	0.033	0.033	0.000	0.015	0.000	0.000	0.000	0.000
TETRALIN ($C_{10}H_{12}$)	0.000	0.031	0.012	0.010	0.000	0.000	0.000	0.000	0.000
NAPHTHALENE ($C_{10}H_8$)	0.073	0.091	0.119	0.228	0.171	0.450	0.575	0.584	0.608
NAPHTHALENE derivative ($C_{11}H_{10}$)	0.011	0.013	0.018	0.032	0.021	0.046	0.040	0.050	0.034
NAPHTHALENE derivative ($C_{12}H_{12}$)	0.000	0.000	0.000	0.022	0.000	0.000	0.000	0.000	0.000
ACENAPHTHENE ($C_{12}H_{10}$)	0.017	0.028	0.028	0.016	0.023	0.000	0.000	0.000	0.000
DIBENZOFURAN ($C_{12}H_8O$)	0.009	0.018	0.013	0.019	0.023	0.039	0.000	0.032	0.008
9-H FLUORENE ($C_{13}H_{10}$)	0.011	0.024	0.015	0.030	0.030	0.053	0.036	0.033	0.053
DIBENZOFURAN derivative ($C_{13}H_{10}O$)	0.000	0.002	0.002	0.000	0.000	0.000	0.000	0.000	0.009
ANTHRACENE ($C_{14}H_{10}$)	0.021	0.017	0.031	0.024	0.028	0.061	0.080	0.035	0.058
PYRENE or FLUORANTHENE ($C_{16}H_{10}$)	0.000	0.012	0.008	0.015	0.016	0.051	0.000	0.042	0.018
2 RINGED	0.941	0.899	0.903	0.896	0.879	0.796	0.884	0.858	0.847
3 RINGED	0.058	0.089	0.089	0.089	0.104	0.153	0.116	0.100	0.111
4 RINGED	0.000	0.012	0.008	0.015	0.016	0.051	0.000	0.042	0.041

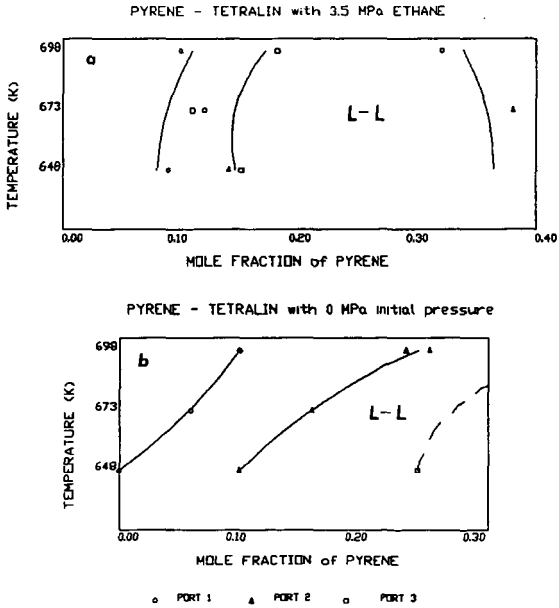

FIGURE 1: Partial phase diagrams for the systems pyrene + tetralin + ethane (a), and pyrene + tetralin (b)

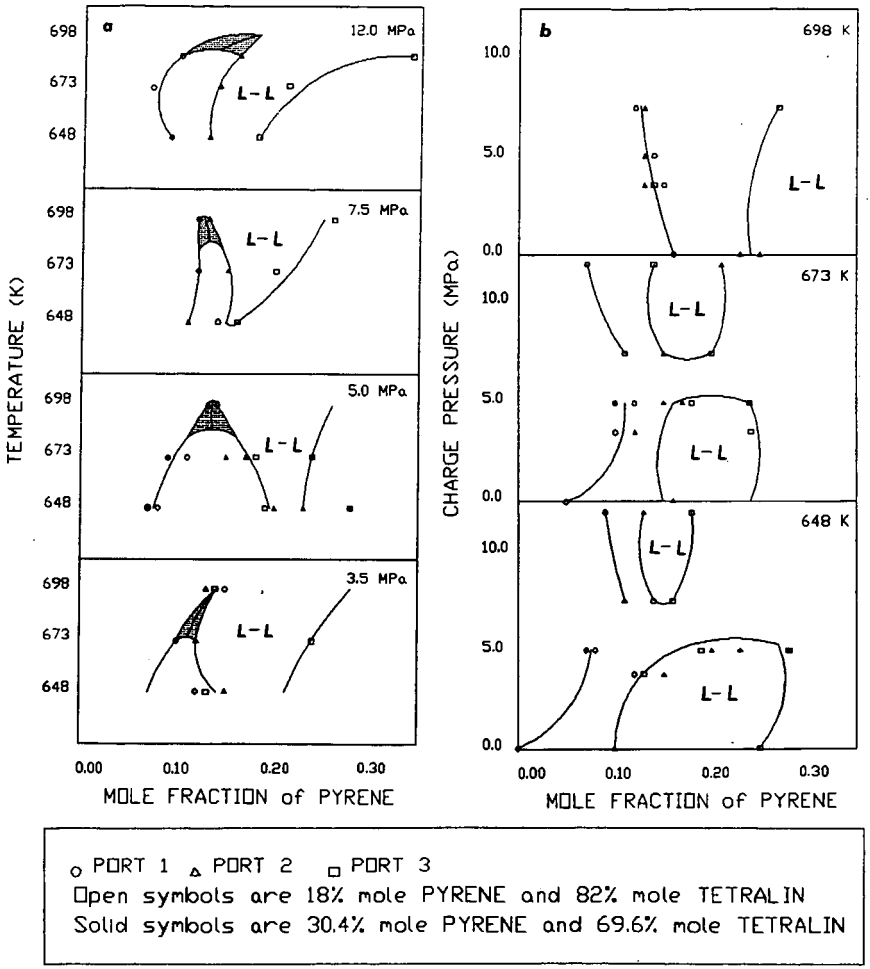

FIGURE 2: Partial phase diagram for the system pyrene + tetralin + nitrogen showing isobars (a) and isotherms (b)

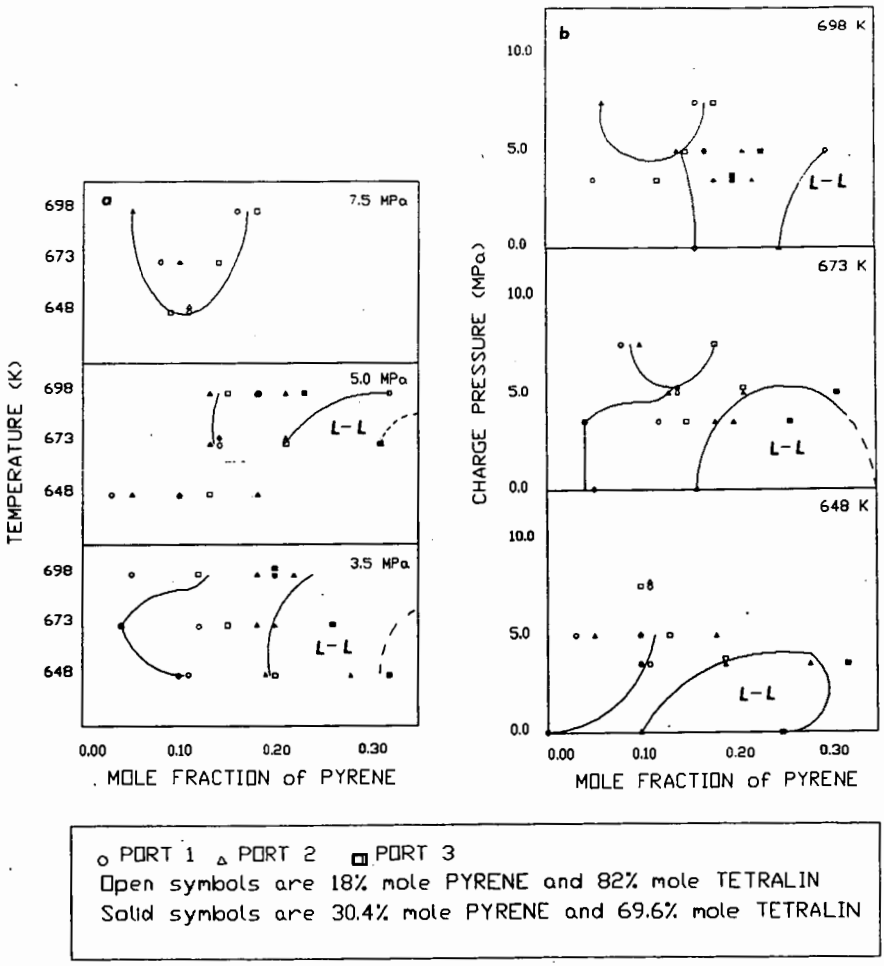

FIGURE 3: Partial phase diagram for the system pyrene + tetralin + methane showing isobars (a) and isotherms (b)

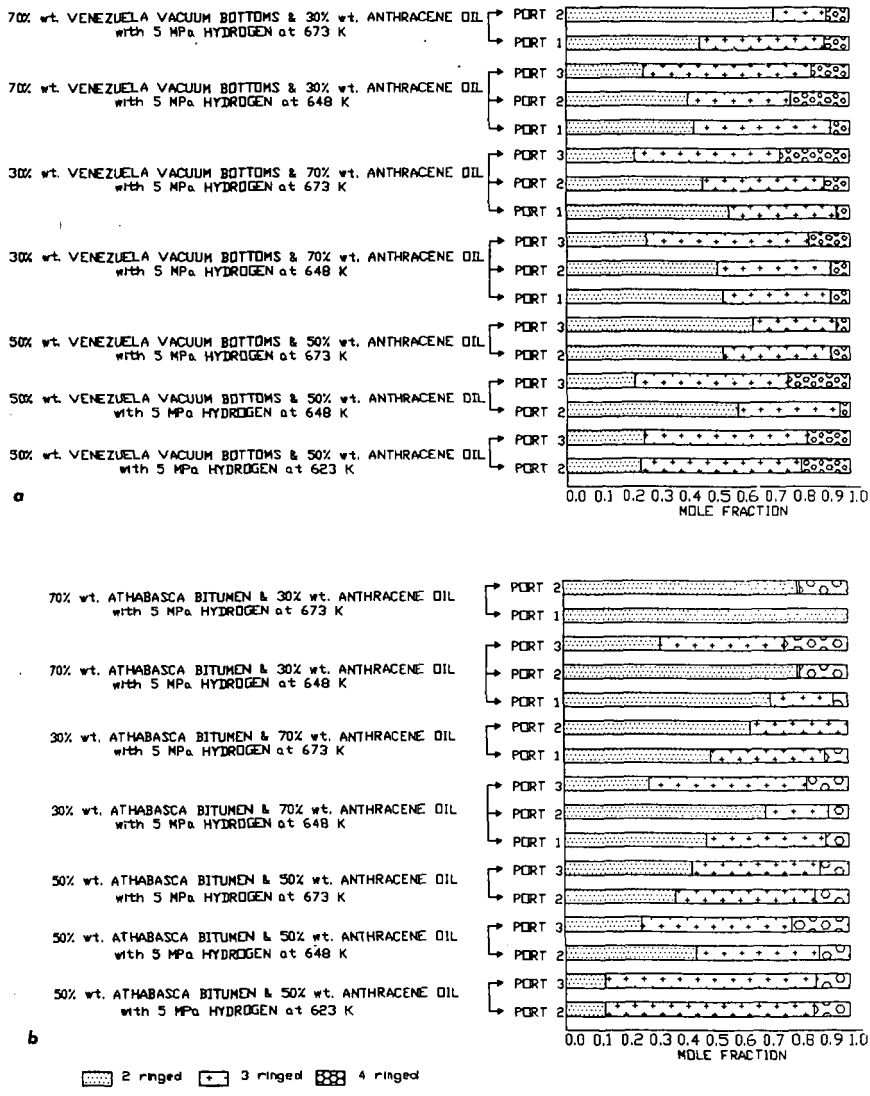

FIGURE 4: Sample compositions obtained from ports located at the top (1) middle (2) and bottom (3) of the reactor for Venezuela vacuum bottoms + anthracene oil + hydrogen mixtures (a), and Athabasca bitumen + anthracene oil + hydrogen mixtures (b)

CHARACTERIZATION OF SOLIDS FROM COAL/RESID COPROCESSING

R. J. Torres-Ordonez, S. G. Kukes, F. S. Lee, D. C. Cronauer,
Amoco Oil Company, Amoco Research Center, P. O. Box 3011,
Naperville, Illinois 60566.

KEYWORDS: Coprocessing solids, coal/resid coprocessing, solids characterization

ABSTRACT

Solids formed from coprocessing of 10% coal/90% resid were characterized by solvent extraction, elemental analyses, C^{13}/C^{12} isotope ratio, ESR, and GPC techniques. The total solids obtained from filtration contained at least 60% adsorbed petroleum-derived material (oil, resin, asphaltene). The THF insolubles in the product contained high oxygen, low vanadium and a higher level of polyaromatic radicals than the soluble fraction, indicating that these insolubles were largely coal-derived material. However, the fraction of the solid product that could be dissolved in either THF or pyridine was mostly petroleum-derived.

INTRODUCTION

The background technology of the coprocessing of coal/petroleum resids has been reviewed by Oelert (1), and additional citations have been discussed in our companion paper (2) being presented at this conference. In summary, such coprocessing is done with the goals of providing the addition of a low cost feedstock, coal; improving unit operability by a reduction in petroleum-derived coke solids; enhancing metals and heteroatom removal; and reducing hydrogen requirements relative to direct coal liquefaction.

Our other paper reported on the coprocessing of 10% Illinois No. 6 coal with 90% resid with decanted oil (DCO) over equilibrium hydrotreating catalyst in a flow unit at 780°F. The addition of coal considerably increased the yield of solids obtained from a Shell hot filtration test, SHFT (2), as seen in Table I.

Normally, in resid hydroprocessing, SHFT solids are free of asphaltenes. The petroleum asphaltene concentration in the product of resid hydroprocessing is calculated as the difference between hexane insolubles and SHFT solids. For the resid/DCO experiment shown in Table I, the asphaltene level is 8.2 wt%. The asphaltene content of the coal/resid/DCO run in Table I calculated in the same manner is lower, 5.2 wt%. If the same levels of petroleum-derived asphaltenes are being formed in both cases, a reasonable assumption (although not certain), the SHFT solids obtained from coal/resid coprocessing must include some petroleum asphaltenes. Therefore, the use of SHFT solids to define asphaltene yield is not valid for the coal/resid case. Moreover, material balance analysis indicated that in addition to asphaltenes, a considerable amount of oil and resin was adsorbed by the unconverted coal.

The objective of this study was to characterize the solids from the coprocessing of coal and resid/DCO. This included verifying the presence of adsorbed petroleum-derived material in the solids; determining the relative distribution of coal-derived and resid-derived fractions; and characterizing the adsorbed petroleum-derived material.

EXPERIMENTAL

Reaction Conditions. The coprocessing of 10% Illinois No. 6 with 90% resid with DCO was conducted in an upflow high-pressure unit which contains two 1-liter Autoclave reactors in series. Catalyst baskets, each filled with 60 cc of equilibrium hydrotreating catalyst, were placed in both reactors. To prevent elutriation, the catalyst was covered with 10 cc of 3 mm glass balls and 1/4 inch

of glass wool. The experiment was conducted at reactor temperatures of 780°F, average feed rate of 206 g/hr and 2500 psig H_2 at 7700 SCFB.

Product Filtration. In addition to the standard SHFT solids determination (2), a modified procedure was used as follows. A composite product was made by blending portions of the daily product samples collected over the 180 hours of coprocessing. This composite product was filtered, the solids were washed with a mixture of 10% toluene and 90% hexane, and then dried in a vacuum oven at 110°C for 16 hours.

Solubility Fractionation. The solids recovered from the above filtration of composite product were sequentially extracted with toluene followed by THF to separate the different solubility fractions. The schematic of the extraction procedure is shown in Figure 1.

Product Analysis. The extracted solubility fractions were analyzed for elemental composition (C,H,N,S,O), metals content (Ni,V) using inductively coupled plasma spectroscopy (ICP), molecular weight distribution using gel permeation chromatography (GPC), and relative levels of polyaromatic radicals and vanadium concentrations using electron spin resonance spectroscopy (ESR). In addition to conventional hexane precipitation, the extracts were separated into oils, resins, asphaltenes and preasphaltenes using a chromatographic technique (3). Oils were eluted from silica gel by hexane; resins were eluted from silica gel by diethyl ether/ethanol (10/1 volume ratio). Asphaltenes and preasphaltenes were insolubles that did not get passed over the silica gel; asphaltenes were toluene soluble (TS), and preasphaltenes were THF soluble and toluene insoluble (THFS/TI). Preasphaltene extraction was also done with pyridine in one case to provide a comparison with THF extraction results.

RESULTS AND DISCUSSION

A mixture of 90% resid and 10% DCO was hydroprocessed for 120 hours, followed by a run period of 180 hours with an added 10% coal. The THF insolubles during the resid/DCO period averaged 0.6 wt%. This value was 3.3 wt% during the coal/resid/DCO period. Therefore, the level of coal conversion to THF solubles was about 80%, assuming no additional THF insolubles were formed from the petroleum-derived feeds during the period of coal addition. This value is lower than the coal conversion results reported by Wilsonville using a similar coal and a coal-derived recycle solvent (4), rather than petroleum liquids. However, due to the low coal feed concentration and the accuracy of the THF insolubles determination, it is not possible to ascertain whether this low conversion is due to solvent effectiveness or to solids being formed from the petroleum feeds.

The SHFT solids during the resid/DCO period averaged 2.3 wt%. This value was 9.6 wt% during the coal/resid/DCO period. The SHFT solids from resid/DCO and coal/resid/DCO hydroprocessing were analyzed for C^{13}/C^{12} concentration ratios using mass spectrometry to determine the relative amounts of coal-derived (or resid-derived) carbon in the SHFT solids. The analyses were performed by Global Geochemistry Corporation in Canoga Park, CA and it was assumed that there was no selective fractionation of the isotopes. The analysis on the SHFT solids indicated that only 28.0% of the solids was coal-derived. Therefore, 6.9% (absolute) was derived from the petroleum fractions, substantially more than the insolubles observed formed without coal present.

The feed coal and the modified SHFT solids from the coal/resid/DCO coprocessing were sequentially extracted with toluene followed by THF to separate different solubility fractions. Table II shows the yields of the solubility fractions from these solids and from the feed coal. The analysis of each of the soluble fractions from the modified SHFT solids for group type is shown in Table III; also shown is the analysis of the resid feed. The relative levels of radical concentrations and vanadium content (paramagnetic VO^{+2}) in selected group types in

each of the solubility fractions were determined from ESR and are shown in Table IV. The elemental composition and metals content (as determined by ICP) of the solubility fractions from the modified SHFT solids are shown in Table V (also shown are the compositions for the coprocessing feed and for the product filtrate). The molecular weight distributions of the toluene soluble fraction (TS) of the coal feed, resid/DCO feed, TS of the modified SHFT solids, and preasphaltenes (THFS/TI) of the modified SHFT solids are shown in Figures 2a,b,c and d, respectively.

Unconverted Coal and THF Insolubles. As shown in Table II, the solids recovered from the filtration of composite product with hexane/toluene (90/10) wash and then THF contained 30 wt% THF insolubles (THFI). If the hexane/toluene wash did not affect the results of the subsequent THF extraction, the THF insolubles (as determined from this sequential extraction) is 2.9 wt% of the product. This value is within the experimental error of 3.3 wt% THF insolubles measured experimentally for the total coal/resid/DCO coprocessing product. Of the 3.3 wt%, 0.6 wt% is resid-derived so that the coal-derived THF insolubles is 2.7 wt%. This value is the same as the 2.7 wt% coal-derived solids inferred from the C^{13}/C^{12} isotope ratio analysis of the SHFT solids.

The high oxygen (Table V) and low vanadium content (Table IV) of the insolubles (THFI fraction) confirm that this is largely coal-derived material. Moreover, these insolubles contain a higher level of free radicals (Table IV) than the asphaltenes in the THF solubles material.

Analysis of the THF Soluble Fractions. The materials retained in the modified SHFT solids were primarily oils and resins, as shown in Table III. The THF solubles of the modified SHFT solids from the coal/resid/DCO run consisted of the toluene solubles and the preasphaltenes; it contained 36 wt% oils, 43% resins and only 21% asphaltenes+preasphaltenes (Table III). The recovered toluene soluble fraction contained 36% oils, 49% resins, and 10% asphaltenes; the remainder of this fraction was made up of preasphaltenes that formed as a result of the extraction and recovery process. The preasphaltene fraction was only about 8% of the modified SHFT solids.

The toluene soluble fraction of these modified SHFT solids was primarily petroleum-derived while the preasphaltenes were a mixture of petroleum- and coal-derived material. The low oxygen content (Table V) and molecular weight distribution (Figure 2b vs. Figure 2c) of the TS confirm that this material is mostly petroleum-derived. In addition, this toluene soluble material had an oil fraction which was very low in radical level (Table IV).

The preasphaltenes retained in the modified SHFT solids definitely had a coal component, as indicated by a high oxygen content (Table V) and the peak in the molecular weight distribution of an estimated value of 250 (Figure 2a vs. Figure 2d). Moreover, the resin fraction of these preasphaltenes contained more radicals than the resin fraction of the TS material (Table IV). These preasphaltenes also had a petroleum contribution, as indicated by its high metals content (Table V). The resin fraction of these preasphaltenes contained six times more vanadium (150 ppm) than the resin fraction of the toluene soluble material (25 ppm). Based on oxygen content, it is estimated that about 24% of the preasphaltenes was coal-derived.

The distribution of free radicals (of polyaromatic nature) among the group types (Table IV) confirms the above observations. Specifically, the free radical level in the asphaltenes is 68% that of the preasphaltenes in the modified SHFT solids. This would be expected if the level of coal-derived material was greater in the preasphaltenes. As a further test, pyridine extraction of the solids was carried out to obtain a pyridine soluble fraction. Pyridine as a more polar solvent extracted twice the level of free radicals than THF; this confirmed that part of the preasphaltenes was coal-derived. The pyridine-extracted preasphaltenes also

contained 20% more vanadium than the THF-extracted preasphaltenes, confirming the petroleum origin of the preasphaltenes.

The characteristics of the toluene soluble material extracted from the modified SHFT solids is shown in Table IV, along with those of the product filtrate and the coprocessing feed. This adsorbed petroleum-derived material had intermediate levels of sulfur, nitrogen and oxygen when compared to the product filtrate and the feed. Metal content was about the same as that of the filtrate and the H/C ratio was comparable to that of the feed. Therefore, this material, 21% of which is 1000°F⁻, is possible additional liquid yield. There is a potential that some of the retained oils and part of the resins could be recovered in a vacuum tower during normal refinery processing.

SUMMARY AND CONCLUSIONS

The THF insolubles and the SHFT solids formed from the coprocessing of 10% Illinois No. 6 coal with a 90/10 resid/DCO feed at 780°F were characterized by solvent extraction, C^{13}/C^{12} isotope ratio, elemental analysis, ESR and GPC. The THF insolubles in these solids contained high oxygen, low vanadium, and a higher level of free radicals than the soluble fraction, indicating that these insolubles were largely coal and coal-derived material. In the characterization of SHFT solids, we found that material containing 36% oils, 43% resins, and 21% asphaltenes and preasphaltenes were retained. The toluene soluble fraction of the SHFT solids was petroleum-derived; and the preasphaltenes were of both coal and petroleum origins. The toluene soluble fraction of the SHFT solids had an intermediate quality between that of the feed and the product filtrate. This represents possible additional liquid yield.

REFERENCES

1. Oelert, H. M., Coprocessing (Coprocessing with Oil) in Synthetic Fuels from Coal: Status of the Technology eds. Oelert, H.; Romey I.; Paul, P. F. M.; Imarisio, G., Commission of the European Communities, Luxembourg, 1987 Report No. EUR-11191, pp. 259-338.

2. Torres-Ordonez, R. J.; Kukes, S. G.; Leet, W. A., Coal/Resid Coprocessing Over Equilibrium Hydrotreating Catalyst, *ACS Div. Fuel Chem. Preprints*, 1990, this volume.

3. Duffy, L. J.; Lee, F. S. C.; Thrash, R. J.; Cannon, C. E., Semi-Automated Liquid Chromatographic Separation of Petroleum Residua and Other Heavy Oils, Presented at the *ACS National Meeting, Petroleum Division Symposium*, September 8-13, 1985, Chicago, IL.

4. Southern Electric International, Inc., Advanced Coal Liquefaction Research and Development Facility, Technical Progress Report, Run 257 with Illinois No. 6 Coal, Doc. No. DOE/50041, 1989.

TABLE I. SOLIDS FROM HYDROPROCESSING AT 780 °F

FEED	YIELD, wt% of feed RESID/DCO	COAL/RESID/DCO
THF Insolubles	0.6	3.3
Hexane Insolubles	10.5	14.8
SHFT Solids	2.3	9.6
Coal-derived SHFT Solids[1]	0.0	2.7

[1] C^{13}/C^{12} isotope analysis on SHFT solids indicated 28.0±5.8% of the solids was coal-derived.

TABLE II. YIELDS OF SOLUBILITY FRACTIONS

FRACTION	EXTRACTION YIELD, wt% MODIFIED SHFT SOLIDS[1]	ILLINOIS NO. 6 (MF BASIS)[2]
Toluene Solubles	62.5	0.6
Preasphaltenes (THF Soluble/ Toluene Insoluble)	7.6	1.8
THF Insolubles (THFI)	29.9	97.6[3]

[1] 9.6 wt% of coprocessing feed (assuming hexane/toluene wash modification to the SHFT test had no effect)
[2] Coal moisture content of 7.1 wt%; coal ash content of 11.5 wt% MF coal.
[3] THF extraction on coal gave 98.0 wt% MF coal.

TABLE III. GROUP TYPE ANALYSIS OF RESID FEED AND LIQUIDS FROM EXTRACTION OF MODIFIED SHFT SOLIDS

FRACTION	DISTRIBUTION, wt% of fraction OIL	RESIN	ASPHALTENE	PRE-ASPHALTENE	LOSSES
Toluene Soluble	35.7	48.6	9.9	3.3	2.5
THF Soluble	36.0	43.1	10.5	10.4	0.0
Resid Feed	8.6	68.1	20.1	3.2	0.0

TABLE IV. RESULTS OF ESR ANALYSIS ON GROUP TYPES EXTRACTED FROM THE MODIFIED SHFT SOLIDS

	Relative Radical Concentration	Vanadium (ppm)
Toluene Soluble Oil	1	<0.1
Toluene Soluble Resin	500	25
Preasphaltene Resin	615	150

	Relative Radical Concentration	Vanadium (ppm)
Asphaltenes	1	680
Preasphaltenes:		
Pyridine-extracted	2.8	940
THF-extracted	1.5	785
THF Insolubles	1.6	230

TABLE V. FEED AND PRODUCT COMPOSITIONS

	ELEMENTAL COMPOSITION, wt%							
	C	H	N	O	S	ppm Ni	ppm V	(H/C)
Coal/Resid/DCO Feed	84.47	9.55	0.52	1.68	4.35	45	177	1.36
Modified SHFT Filtrate	86.24	10.55	0.44	1.11	2.35	24	73	1.47
Modified SHFT Solids:								
Toluene Soluble	85.98	9.52	0.5	0.5	3.26	26	73	1.33
Preasphaltene	83.91	6.03	1.5	4.1	2.90	184	800	0.86
THF Soluble[1]	86.08	9.18	0.62	0.89	3.24	30	106	1.28
THF Insoluble	53.34	3.42	ND[2]	7.1	4.7	ND[2]	ND[2]	0.77

[1] Composition for this fraction determined from compositions of toluene soluble and preasphaltene fractions weighted by the yields of these fractions, as shown in Table II.
[2] ND = not determined

RTO/df/90339
4/23/90

Figure 1. Schematic of Extraction Procedure

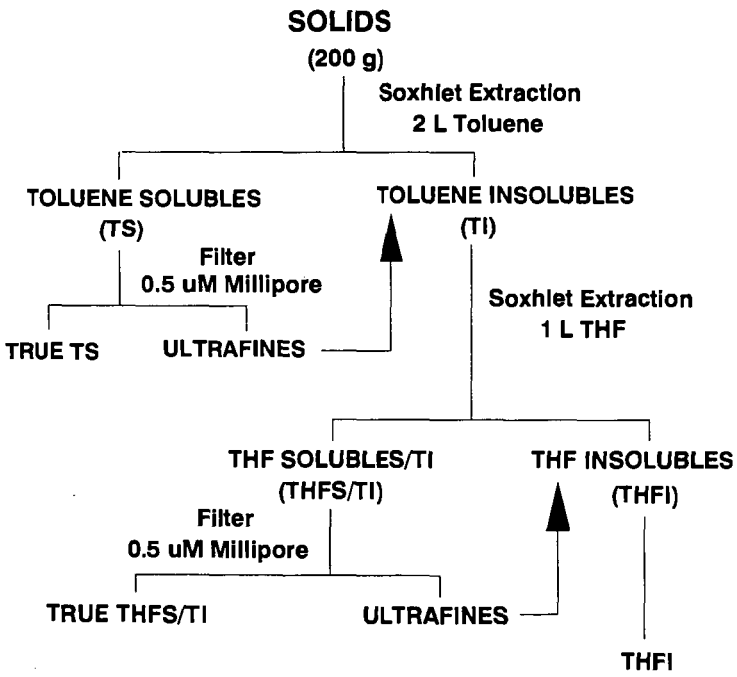

Figure 2. Molecular Weight Distributions from GPC

(Mw = weight-averaged molecular weight)

(a) Toluene Soluble Fraction of Coal Feed

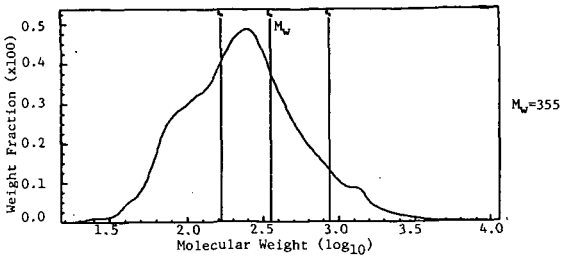

(b) 90% Resid/10% DCO Feed

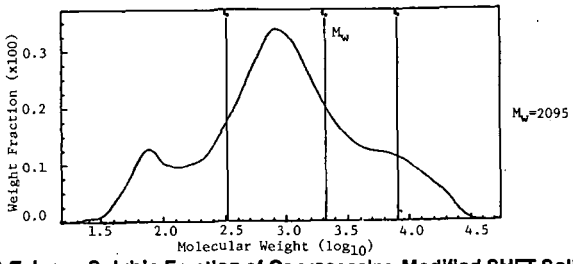

(c) Toluene Soluble Fraction of Coprocessing Modified SHFT Solids

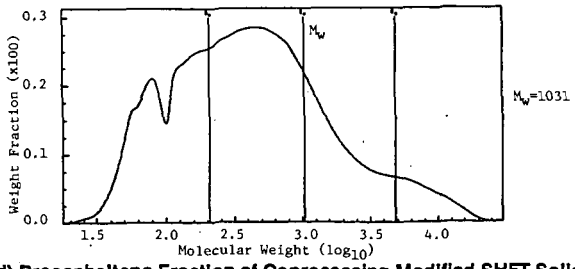

(d) Preasphaltene Fraction of Coprocessing Modified SHFT Solids

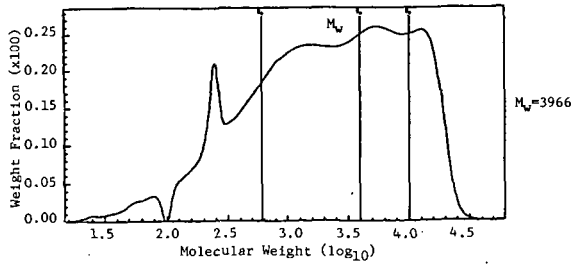

THE SIGNIFICANCE OF HYDROGEN DONOR ABILITY AND THE CHARACTERISTICS OF HEAVY OILS/BITUMENS IN COPROCESSING

P.M. Rahimi, W. H. Dawson and J.F. Kelly

CANMET, Energy Research Laboratories
Energy, Mines and Resources Canada
Ottawa, Ontario K1A OG1

Keywords: coprocessing; hydrogen donor ability; heavy oils/bitumens.

ABSTRACT

The hydrogen donor ability of several heavy oils/bitumens used in CANMET coprocessing and some model compounds was determined using 1,1'-binaphthyl, sulphur and a ^{13}C NMR technique. Using 1,1'-binaphthyl, it was concluded that generally heavy oils/bitumens are better hydrogen donors than model compounds such as tetralin. When sulphur was used as a hydrogen acceptor, tetralin and hydrogenated anthracene oil showed better hydrogen donor ability than any of the oils used. A good correlation was obtained between coal conversion (THF solubles, Forestburg subbituminous coal) and the per cent of transferable hydrogen determined using sulphur. In addition, the ^{13}C NMR method, which was carried out on deasphaltened heavy oils and bitumens gave slightly higher though similar values of transferable hydrogens.

The effect of "solvent" characteristics on coal and pitch conversions and distillate yields was investigated. Generally coal conversions were not affected by the type of vacuum bottoms used or solvent asphaltene content. Although the amount of indigenous saturated compounds in conventional resids was much higher than those in heavy oils/bitumens, coal dissolutions were equally effective in both types of solvents. Pitch conversions and distillate yields were shown to be more sensitive to the types of resid being processed.

Introduction

The role and importance of hydrogen donor solvents in coal liquefaction are well known and have been studied by a number of investigators (1-5). It is also known that the hydrogen donor ability of a solvent is not the only criterion that influences the degree of coal solubilization. The physical properties of the solvent also play an important role (6-7). Irrespective of whether physical and chemical properties of solvents play a significant role, the fact is that in all direct liquefaction processes the "quality" of solvent must be maintained during processing if high coal conversion and distillate yields are desired.

In coprocessing, heavy oils/bitumens which can play the role of "solvent" as in coal liquefaction, are also reactants and their roles as hydrogen donors are less understood. In general it is believed that crude derived petroleum resids and bitumens are not as good hydrogen donors compared with solvents such as tetralin, and consequently they are less effective in coal dissolution (8-9). It has been shown by Curtis et al (9) that the addition of good hydrogen donors such as tetralin and 9,10-dihydrophenanthrene in the coprocessing of Maya topped long resid and Illinois No. 6 coal promoted the production of light products.

In spite of the complexity of the chemistry involved in the recycle solvents used in direct coal liquefaction, there is no doubt that the hydrogen donor ability of the solvent is an important factor for the success of any coal liquefaction process. The question of whether the heavy oils/bitumens in coprocessing play a role as significant as that in coal liquefaction in terms of hydrogen donor ability has received little attention.

To address this question we must first understand the basic differences between the two processes. Ideally, in coprocessing there is no recycle solvent and instead fresh solvent is introduced continuously during the process. Unlike an ideal solvent in coal liquefaction, this coprocessing "solvent" is also a reactant and it is upgraded simultaneously with the coal and its chemical composition changes significantly during processing. In CANMET

coprocessing, a mixture of coal and heavy oils/bitumen is processed in a single-stage once-through operation using iron sulphate as a disposable catalyst. Previous results from our laboratory (10) indicated that the *dissolution* of low-rank Canadian coals was relatively insensitive to the type of bitumen or petroleum resid used. However, *resid conversion* depended on the type of resid employed.

The objectives of the present work were: 1) to determine quantitatively the hydrogen donor abilities of different heavy oils/bitumens and conventional crude derived petroleum resids used as oil feedstocks in CANMET coprocessing and attempt to correlate coal dissolution to the amount of transferable hydrogens available in each and 2) to investigate the effect of "solvent" characteristics on coal and pitch conversions.

Experimental

Materials and Feedstocks

Three crude derived petroleum resids, Boscan, Blend 24 (Venezuela), Maya (Mexico) and Athabasca bitumen and Lloydminster heavy oil vacuum bottoms were obtained from the sample bank of the Primary Upgrading Section, Energy Research Laboratories. IPPL (a vacuum resid from a mixture of sweet crudes from Western Canada) was supplied by the Esso Refinery, Sarnia, Ontario. Cold Lake vacuum bottoms (CLVB) was obtained from the Strathcona refinery of Imperial Oil Ltd, Alberta. Forestburg subbituminous coal from Alberta was supplied by Luscar Limited. Its analysis is shown in Table 1. The 1,1'-binaphthyl from Aldrich was used as received. Raw anthracene oil and hydrogenated anthracene oil were obtained from the Nova Scotia Research Foundation Corporation. The characteristics of the solvents and oils used in this work are shown in Tables 2 and 3.

H-donor measurements using 1,1'-Binaphthyl

For these experiments, the procedure of Kline et al was used (11). The 2-mL reaction vessels were made from 316 SS tubing with end caps. Each sample (0.5 g) was placed in the vessel with 0.5 g 1-1'-binaphthyl and 1.5 g benzene as solvent. The vessels were weighed before the experiment and heated to 430°C for 1 h. A Tecam model IFB 101 fluidized bed sand bath was used as the heating medium. About 2-3 min were required for the reaction vessels to reach the reaction temperature. The vessels were quenched in water, then dried and weighed. Experimental runs having greater than 100 ± 5 wt % material balance were discarded. Each experiment was carried out at least in duplicate.

The contents of the vessels were extracted using THF and analyzed by gas chromatography using a Perkin Elmer Sigma 2000 equipped with 15 m SE-54 capillary column and 3600 data station. The analyses were performed with split mode using an internal standard method. The product analyses were carried out at an initial column temperature of 200°C for 5 min, then temperature programmed at 5°C/minute to 300°C.

H-donor measurements using sulphur

The method used by Aiura et al. for determining transferable hydrogen in coal-derived solvents was modified (H_2S was quantified by a gas chromatography method rather than by titration) and applied for measuring the donatable hydrogen in bitumens/heavy oils (12). Dehydrogenation experiments using sulphur were performed in a 100 mL stainless steel microreactor at 235±3°C and 1 h residence time. The reactor was charged with 5 g solvent to be tested for donatable hydrogen, 4 g sulphur as hydrogen acceptor and 15 g of phenanthrene as diluent. The reactor was shaken vertically and to aid mixing, two stainless steel balls were placed in the reactor which was pressurized to 100 psig with N_2 at room temperature. After the required residence time the reactor was cooled to room temperature and the gases (H_2S and N_2) were collected in a gas bag. The total volume of the gas was measured by water displacement and the composition was determined using a Perkin Elmer Sigma-1B gas chromatograph. From the amount of H_2S formed, the transferable hydrogen was then determined.

Compound type separation and H-donor measurements using ^{13}C NMR

The amount of transferable hydrogen in four heavy oils/bitumens and conventional resids was also measured using ^{13}C NMR according to the method described by Aiura et al. (12). The measurements were carried out on the pentane soluble fractions of the materials (asphaltene free). The pentane soluble fractions were separated on a silica column using a Waters 500 preparative chromatograph into saturates (pentane eluted), aromatics (toluene eluted) and polars (methylene chloride and back flash with methyl-tert-butyl ether eluted). The saturated fractions and the original samples (asphaltene free) were subsequently analyzed by ^{13}C NMR using a Varian XL 300. The amount of transferable hydrogen was calculated from the integrated intensities in the 21-37 ppm range, the carbon contents of the original and the saturated fractions, and the weight per cent of the saturated fractions.

Coprocessing experiments

The coprocessing experiments were carried out in 100 mL stainless steel batch autoclaves equipped with thermowells and pressure transducers. Approximately 20 g of feedstock was placed in the reactor then pressurized with either H_2 or N_2 to 800 psig at room temperature. Using a sand bath, about 3 min were required for the reactor to reach the reaction temperature of 420°C. At the end of a run, the reactor was quenched in a water bath. The reactions were carried out either in the presence or absence of iron sulphate catalyst. The iron concentration was kept constant at 0.6 wt % based on maf slurry charged. The volume of the gaseous products was measured and their compositions were analyzed by a gas chromatograph. The slurry products were extracted using pentane, toluene and THF to determine the amount of oils, asphaltenes, and preasphaltenes respectively. Coal conversions were determined from the amount of THF insolubles. Pitch conversions data shown in Table 6 were obtained using a continuous bench scale coprocessing unit.

Results and Discussion

Using 1,1'-binaphthyl as H-acceptor

The relative hydrogen donor abilities of heavy oils/bitumens and some model compounds measured using 1,1'- binaphthyl are shown in Table 4. At 430°C and in the presence of the hydrogen donors listed in Table 4, 1,1'- binaphthyl is converted to perylene (P) as a major product. Small amounts of rearranged product 2,2'-binaphthyl and a negligible amount of 1,2-binaphthyl were also obtained. The mole ratios of perylene (P) to the sum of 1,1'-binaphthyl plus its rearranged product 2,2'-binaphthyl (B) were taken as measures of the strength of hydrogen donation. The P/B ratios listed in Table 4 are corrected for the amount of perylene formed by heating 1,1'-binaphthyl in the absence of hydrogen donors.

The hydrogen donor abilities for tetralin and 9,10-dihydroanthracene in Table 4 are consistent with those reported by Kline et al (11). The higher values of P/B reported by Kline et al, are attributed to the higher temperature (470°C) employed. For bitumens/heavy oils the P/B ratios remained relatively constant. According to these results using 1,1'-binaphthyl as a hydrogen acceptor, the heavy oils/bitumens tested are better hydrogen donors than tetralin. The mechanism of hydrogen transfer from donor solvents to 1,1'-binaphthyl to form perylene is not well known. It is also unclear why tetralin, which is a good hydrogen donor, does not interact with this reagent as well as heavy oils/bitumens to form perylene. There may be other factors such as physical interactions (favouring heavy oils) that influence the reaction path leading to perylene formation.

In order to correlate the hydrogen donor abilities of bitumens/heavy oils (P/B) for different solvents with coal conversions the dissolution of Forestburg subbituminous coal was studied. In these experiments coal is used as a hydrogen acceptor. Since the objective was to determine the degree of hydrogen transfer from the solvents only to the coal, the experiments were carried out in a nitrogen atmosphere. To prevent coke formation, coal

solubilizations were carried out at a short reaction time of 5 min. The coal conversion results at 5 min in the nitrogen atmosphere and those from 30 min in a-hydrogen atmosphere are also shown in Table 4. For comparison, the results of the liquefaction of the same coal in tetralin under similar conditions are given. For the heavy oils/bitumens, coal conversion into THF solubles remained relatively constant. In the nitrogen atmosphere there is a substantial difference in coal conversion between tetralin and the bitumens/heavy oils. In the hydrogen atmosphere the differences are much smaller. As shown in Table 4 it can be concluded that using 1,1'-binaphthyl as a hydrogen acceptor no general correlation can be obtained between P/B and coal conversions for heavy oils/bitumens and model compounds.

Using sulphur as H-acceptor

Hydrogen donor abilities obtained for heavy oils/bitumens, tetralin, hydrogenated anthracene (HAO) and raw anthracene oils (RAO) using sulphur are shown in Table 5. The amount of transferable hydrogen (TH) for each material was calculated from the amount of H_2S formed in the reaction of sulphur with these materials. Tetralin and HAO showed the highest amount of TH whereas RAO showed the lowest amount of TH. For the heavy oils/bitumens the weight per cent of TH did not change significantly and remained constant at about 1 wt %.

The coal conversion data both in H_2 (30 min) and N_2 (5 min) atmospheres are also shown in Table 5. Using sulphur as a hydrogen acceptor appears to give a better general correlation between coal conversions and hydrogen donor abilities. The exception to this is between HAO and tetralin where coal conversion (in N_2) is significantly higher in HAO (lower TH) than in tetralin.

The results indicate that other factors besides hydrogen donor abilities influence coal dissolution. In a hydrogen atmosphere aromatic hydrocarbons present in the solvents with deficient donatable hydrogens become hydrogen shuttlers transferring hydrogen from the gas phase to the free radicals from coal. Since significant amounts of different aromatic structures are present in the heavy oils/bitumens listed in Table 5, relatively high coal conversions are obtained in a hydrogen atmosphere and the difference in coal conversions between any one of these solvents and a relatively good hydrogen donor such as HAO becomes small.

The results also show that although the amount of transferable hydrogen in RAO is considerably lower than the heavy oils/bitumens listed in Table 5, the coal conversion (in N_2) is similar or higher in this solvent. It can be argued that sulphur may indiscriminately abstract hydrogen from different positions within the molecules of heavy oils/bitumens and that the TH values reported in Table 5 for these materials are not true values for the available hydrogen in hydroaromatic positions. However, as discussed below there is good agreement between dehydrogenation using sulphur and the ^{13}C NMR methods. Again, other properties of the solvents (like physical properties) may play an important role in coal dissolution besides hydrogen donor ability.

The amount of transferable hydrogen of four heavy oils/bitumens as determined by ^{13}C NMR is also shown in Table 5. The weight per cent of TH was obtained using the deasphaltened fraction of these materials. The ^{13}C NMR TH values are comparable (within 0.3 for Blend 24 and Athabasca) with the sulphur dehydrogenation method. Irrespective of the method of TH determination, it appears that heavy oils/bitumens having the same amount of TH are capable of dissolving coal to the same degree.

Effect of heavy oil/bitumen characteristics on coal and pitch conversions

Lett et al (8) in their investigation of the hydrogen donor abilities of heavy oils concluded that heavy oils containing more asphaltenes are better hydrogen donors than those with less asphaltenes. The data presented in Table 5 show that this claim cannot be generalized. Although Athabasca bitumen contains much higher asphaltenes than Blend 24 (Table 3) the amount of transferable hydrogen (measured by ^{13}C and sulphur dehydrogenation methods) and coal conversions is similar. It has also been pointed out by

Curtis et al (13) that the presence of saturated compounds in liquefaction solvents results in lower coal conversions. The data obtained in our laboratory have shown that in coprocessing, the dissolution of coal is not significantly affected by the amount of saturated compounds present in heavy oils/bitumens. Table 6 shows the compositional characteristics of four heavy oils/bitumens. Although the amount of the saturated fraction is more than twice in Maya compared with Athabasca, the coal conversion did not change significantly (Table 6). However, as was shown earlier by Fouda and Kelly (10), distillate production in coprocessing is sensitive to the type of resid processed. In general, under coprocessing conditions, conventional resids containing higher saturated fractions than bitumens usually produce lower distillate yields and pitch conversions.

Conclusions

The degree of hydrogen donor ability of heavy oils/bitumens as determined by three different methods was shown to be very similar at least for the heavy oils/bitumens tested. These coprocessing solvents contain approximately 1 wt % transferable hydrogens and are capable of dissolving about 86 wt % coal in a hydrogen atmosphere and about 20 wt % in a nitrogen atmosphere irrespective of their origin. A relatively good correlation was obtained between coal conversion and transferable hydrogens using sulphur as a hydrogen acceptor. The data presented in this paper also show that the weight per cent of saturated fraction and asphaltenes in the heavy oils/bitumens (under CANMET coprocessing conditions) does not influence the degree of coal conversion. It can also be concluded that the hydrogen donor ability of heavy oil/bitumen is not a determining factor in coal solubilization in catalytic coprocessing and definitely is not as significant as in direct coal liquefaction. It is suggested that under a hydrogen atmosphere the aromatic hydrocarbons can act as hydrogen shuttlers transferring hydrogen from the gas phase to coal derived radicals.

References

1- Mochida, I., Otani, K. and Korai, Y. **Fuel 1985, 64, 906.**
2- Awadalla, A.A., Cookson, D. J. and Smith, B.E. **Fuel 1985, 64, 1097.**
3- Utz, B.R., Appell, H.R. and Blaustein, B.D. **Fuel, 1986, 65, 1085.**
4- Nicole, D., Mayer, A. and Delpuech, J.J. **Fuel Processing Technology, 13, 1986, 311.**
5- Mochida, I., Yufu, A., Sakanishi, K. and Korai, Y. **Fuel, 1988, 67, 114.**
6- Whitehurst, D.D., Mitchel, T.O. and Farcasiu, M. **"Coal Liquefaction, The Chemistry and Technology of Thermal Processes", Academic Press, New York, 1980, Ch.9**
7- Awadalla, A.A. and Smith, B.E. **Fuel 1982, 61, 631.**
8- Lett, R.G. and Cugini, A.V., **Proceedings of DOE Direct Liquefaction Contractors' Review Meeting, Monroeville, PA., October 20-22, 1986, PP. 362-378.**
9- Curtis, C.W., Tsai, K.J. and Guin, J.A. **Fuel Processing Technology , 16 (1987) 71-87.**
10- Fouda, S.A. and Kelly, J.F. **Proceedings of DOE Direct Liquefaction Contractors' Review Meeting, Pittsburgh, PA., November 19-21, 1985, P. V-56**
11- Kline, E.A., Harrison, M.E. and Farnum, B.W., **Am Chem Soc Div Fuel Chem Preprints, (27), 18, 1982.**
12 Aiura,M., Masunaga, T., Moriya, K. and Kageyama, Y. **Fuel 1984, 63, 1138.**
13-Curtis, C.W., Guin, J.A., Hale, M.A. and Smith, N.L. **Fuel 1985, 64, 461.**

Table 1 - Analysis of Forestburg coal

Proximate analysis (wt %, as received)	
Moisture	14.09
Volatile matter	36.37
Fixed carbon	42.67
Ash	6.87
Ultimate analysis (wt % daf)	
C	71.99
H	4.64
N	1.78
O	20.98
S	0.61

Table 2 - Elemental Analyses of Oil Feedstocks (wt %)

Solvents/Oils	C	H	N	O	S
CLVB[a]	82.82	10.57	0.78	0.35	5.66
CLVB(P)[b]	82.62	10.27	0.83	0.26	5.79
Boscan	80.96	10.24	0.90	0.24	5.73
Boscan(P)[b]	81.97	9.83	1.09	0.29	6.40
Maya	84.80	10.10	0.42	< 0.50	4.30
Blend 24[c]	84.31	10.90	0.81	0.33	3.45
Athabasca	82.30	9.60	0.67	0.69	5.96
IPPL[d]	86.40	10.90	0.43	< 0.50	1.71
Lloydminster	83.20	9.84	0.54	0.61	5.73
Raw anthracene oil	91.50	5.74	1.04	0.56	0.58
Hydrogenated anthracene oil	90.60	9.10	0.15	0.26	0.00

[a] Cold Lake vacuum bottoms, [b] +525°C fractions, [c] Venezuela blend vacuum bottoms, [d] vacuum bottoms from a blend of Western Canadian crudes (IBP = 560°C)

Table 3 - Characteristics of Heavy Oil/Bitumen Feedstocks

Solvents/ Oils	Pentane Inso.(wt %)	Toluene Inso.(wt %)	Pitch[a] wt %	CCR wt %	gravity (°API)	Mn[1]	f_a[2]
CLVB[b]	23.5	0.20	83.2	17.1	4.82	788	31
Boscan	22.3	0.09	64.6	16.7	7.77	613	30
Maya	22.3	0.11	86.0	18.4	----	756	34
Blend 24[c]	21.5	<0.10	95.1	18.6	6.95	848	30
Athabasca	38.4	1.21	99.3	23.9	1.49	983	34
IPPL[d]	14.0	0.92	100.0	15.6	9.86	910	30
Lloydminster	37.4	0.22	90.7	22.0	3.39	1081	35

[a] +525°C fraction, [b] Cold Lake vacuum bottoms, [c] Venezuela blend vacuum bottoms,
[d] vacuum bottoms from a blend of Western Canadian crudes (IBP=560°C),
[1] number average molecular weight (VPO),
[2] aromaticity (^{13}C NMR)

Table 4 - Hydrogen donor abilities of model compounds and heavy oils/bitumens measured using 1,1'-binaphthyl and conversion of Forestburg coal

Material	P/B x 100[a]	Coal conversion[b] H_2	Coal conversion[c] N_2
1,1'-Binaphthyl	0.19	----	----
Tetralin	0.51 (1.3)[4]	91.7	59.8
9,10-Dihydroanthracene	10.00 (17.7)[4]	----	----
CLVB[1]	5.50	88.7	22.1
CLVB(P)[2]	6.90	----	----
Boscan	5.40	88.3	20.1
Boscan(P)[2]	7.20	85.1	21.3
Maya	7.00	82.7	19.1
Blend 24[3]	5.70	86.7	21.9

[a]moles of perylene to moles of 1,1'-binaphthyl + moles of byproducts
[b]conversion to THF solubles at 420°C, 30 min and 800 psi H_2
[c]conversion to THF solubles at 420°C, 5 min and 800 psi N_2
[1]Cold Lake vacuum bottoms, [2] +525°C fractions, [3] Venezuela blend vacuum bottoms
[4]values taken from reference 11.

Table 5 - Comparison of hydrogen donor abilities of different solvents/oils and coal conversions.

	Transferable hydrogen (wt %)		Coal conversion (wt %, maf)	
Solvents	Sulphur	^{13}C NMR	H_2, 30 min.	N_2, 5 min
Tetralin	2.01	----	91.7	59.8
CLVB[a]	1.20	1.28	88.7	22.1
Blend 24[b]	1.01	1.32	86.5	21.9
Athabasca	1.02	1.30	86.6	20.8
Maya	1.07	1.13	82.7	19.1
Boscan	1.24	----	88.3	20.1
Boscan (P)[c]	1.17	----	85.1	21.3
IPPL[d]	0.98	----	83.7	19.1
Lloydminster	1.18	----	86.6	20.0
Raw anthracene oil	0.33	----	72.1	26.1
Hydrogenated anthracene oil	1.82	----	94.8	78.2

[a]Cold Lake vacuum bottoms, [b] Venezuela blend vacuum bottoms [c] +525°C fractions, [d]vacuum bottoms from a blend of Western Canadian crudes (IBP=560°C)

Table 6 - Hydrocarbon type separation of heavy oils/bitumens (wt %): Effect of solvent Characteristics on coal and pitch conversions.

Solvent/Oils	Saturates	Aromatics	Polars	Coal conv.	Pitch conv.[c]
CLVB[a]	28.66	58.68	12.66	88.7	34.1 (68.4)
Athabasca	19.50	65.81	14.68	86.6	40.6 (69.0)
Blend 24[b]	36.38	51.13	12.49	86.5	36.0 (62.2)
Maya	41.51	50.82	7.68	82.7	---- (----)

[a]Cold Lake vacuum bottoms, [b] Venezuela blend vacuum bottoms,
[c] results from continuous operation at 425°C and (450°C)

THE CATALYTIC ACTIVITY OF ORGANOMETALLIC COMPLEXES IN COPROCESSING

Honggon Kim and Christine W. Curtis
Department of Chemical Engineering
Auburn University, Alabama 36849-5127

Keywords: coprocessing, organometallic complexes, coal liquefaction

ABSTRACT

The catalytic activity of molybdenum, nickel, and vanadium, generated *in situ* from their organometallic complexes, as well as a presulfided powdered $NiMo/Al_2O_3$ was evaluated in coal-oil coprocessing. The coprocessing reactions were conducted both thermally and catalytically with Illinois No. 6 coal and Khafji or Maya residuum. The activities of molybdenum, nickel, and vanadium present as metal sulfides for converting coal and upgrading petroleum residuum were compared, and the possibility of indigenous nickel and vanadium catalysis in coprocessing was explored.

INTRODUCTION

The coprocessing of coal with petroleum residuum simultaneously upgrades coal, coal liquids and residuum into higher quality products[1-3]. When compared to coal liquefaction, coprocessing is attractive for several reasons[4]. Coprocessing uses a sufficient amount of low-cost petroleum residuum as the processing solvent without the extensive requirement of solvent recycling so that it produces larger volumes of hydrocarbon liquids than does the liquefaction of coal alone. Because coal is partially soluble in asphalt and residuum, less severe reaction conditions are required in coprocessing than in coal liquefaction. Therefore, coke formation is also reduced. In addition, coprocessing can utilize the existing upgrading facilities used for petroleum refining.

Catalytic coprocessing is more desirable than thermal coprocessing[5]. The role of the catalyst in coprocessing is substantial. The amount of coal conversion, the extent of heteroatom removal and saturation of aromatic compounds, and the product distribution in terms of the solubility of fractions, such as oil, asphaltenes, preasphaltenes and insoluble organic matter (IOM), in catalytic coprocessing is influenced by the catalyst used. This experiment evaluated and compared the effects of catalytically active species of Mo, Ni and V generated *in situ* from their organometallic complexes in a sulfur-rich environment on the upgrading of coal and petroleum residuum in coal-oil coprocessing.

Upgrading of coal and petroleum residuum may be achieved by several types of hydrogenation reactions: hydrogenolysis of carbon-carbon bonds or carbon-heteroatom bonds, producing smaller molecular structures, hydrogenation of compounds containing aromatic rings, producing more saturated hydrocyclic compounds, and removal of heteroatoms (S, N, O), producing more environmentally acceptable products with lower sulfur, nitrogen and oxygen contents. From past experience in hydrogenation reactions with model compounds[6,7], each

metal species is expected to show different catalytic activity and selectivity for various types of hydrogenation reactions occurring in coal-oil coprocessing. In this experiment, the catalytic activity and selectivity of different metals in upgrading actual coal and residuum in coprocessing reactions are compared. These experimental results are expected to be useful in evaluating the degree to which the catalytic character of each metal species is attributable to specific types of hydrogenation reactions in coprocessing. The possible catalytic activity of Ni and V indigenous to the residuum used as the solvent in coprocessing is also discussed.

EXPERIMENTAL

Feed Materials. Khafji and Maya petroleum residua and Illinois No.6 coal were selected as feed materials for coprocessing reactions. All of these materials were supplied by Amoco Oil Company. Khafji and Maya were used as received, but Illinois No. 6 coal was pulverized to 100 mesh and kept in a vacuum desiccator before use. The moisture content (6.3 wt%) and ash content (9.8 wt%) of Illinois No. 6 coal were obtained by Auburn University and used in the calculation of experimental results.

Catalyst. Organometallic complexes of transition metals, such as Mo, Ni and V, as well as a supported bimetallic $NiMo/Al_2O_3$, were used as coprocessing catalysts. The precursors of the active metal species of Mo, Ni and V were obtained in the form of an oil-phase naphthenate or octoate, or a solid-phase acetylacetonate and were supplied by Air Products, Shepherd Chemical, Strem Chemical, and Aldrich. The metal contents in the precursors supplied were 3 to 23 wt%. Each catalyst precursor was diluted by n-hexadecane to enhance its fluidity and to keep the metal content consistent in the precursor at 3 wt% of Mo or Ni and 1.5 wt% of V. A solid catalyst, Shell 324 $NiMo/Al_2O_3$, was presulfided in a heated gas stream of 10 vol% H_2S in H_2 and then pulverized to 150 mesh before use.

Thermal and Catalytic Reactions. The coprocessing reactions were performed in 56 cm^3 tubing bomb microreactors which were made of 316 stainless steel and horizontally oriented during reactions. Each coprocessing reaction was conducted with 3g of coal and 6g of Khafji or Maya residuum under reaction conditions of 1250 psig H_2 charged at ambient temperature (about 2820 psig at 400°C and 3000 psig at 425°C), 400°C or 425°C reaction temperature, one hour reaction time, and 550 cpm vertical shaking. In catalytic reactions, each catalyst paste or solid catalyst was introduced at the level of approximately 3000 ppm metal in the feed. In cases of organometallic complexes being used as catalyst precursors, elemental sulfur was added in an amount sufficient to produce metal sulfide *in situ* from each organometallic precursor; 0.038g for thermal reaction, 0.057g for Mo, 0.032g for Ni, and 0.077g for V.

Analysis. The coprocessing products from 3g coal and 6g residuum were fractionated by three different solvents: first, the oil fraction was extracted by hexane; next, the asphaltene fraction was extracted by toluene; finally, the preasphaltene fraction was extracted by tetrahydrofuran. About 9g of the whole product recovered from the coprocessing reaction was dissolved in a total of 450 ml hexane: the recovered product was dissolved in 150 ml hexane, sonicated for 4 minutes, centrifuged to separate hexane solubles and hexane from undissolved product materials, and then all of these procedures were repeated twice. Next, the hexane insolubles were dissolved in 450 ml toluene, and then the toluene insolubles separated from the extraction with toluene were dissolved in 450 ml tetrahydrofuran and extracted using similar procedures as with hexane. The amount of each fraction was compared in terms of gas, oil (hexane soluble), asphaltenes (hexane insoluble but toluene soluble), preasphaltenes

(toluene insoluble but tetrahydrofuran soluble), and insoluble organic matter (IOM - tetrahydrofuran insoluble) on a moisture, ash and catalyst free basis. The amount of gas product produced from the reaction was determined by H_2 analysis using a Varian 3700 gas chromatograph with a 15 m stainless steel column (1/8 inch OD) packed with mixed molecular sieve 13A (75 wt%) and molecular sieve 5A (25 wt%) and with a thermal conductivity detector. Reactions were usually duplicated, and the product distribution and the coal conversion were expressed as the average values. A statement of error is given in the tables.

RESULTS AND DISCUSSION

Efficacy of Coprocessing. The efficacy of coprocessing was evaluated by testing the effect of petroleum residuum on the extent of coal hydrogenation. Three grams of Illinois No. 6 coal were hydrogenated, both thermally and catalytically with Mo naphthenate, with 6g of different solvents: n-hexadecane, which appeared to be nearly nonreactive at the reaction conditions and was soluble in hexane, and Khafji and Maya residua, which were more reactive processing solvents. Each fraction produced from Illinois No. 6 coal was determined by subtracting the amount of that fraction produced from the hydrogenation reaction of 6g of Khafji or Maya alone at equivalent reaction conditions from the overall amount of the same fraction produced from the coprocessing reaction. Khafji and Maya produced more hexane and toluene solubles (oil and asphaltenes) than did n-hexadecane in both thermal and catalytic reactions. In the thermal reactions, the amount of oil and asphaltenes produced from Illinois No. 6 coal was about 7 wt% with n-hexadecane, 24 wt% with Khafji, and 13 wt% with Maya. In the catalytic reactions with Mo naphthenate, the amount of the same fractions produced from Illinois No. 6 coal was about 32 wt% with n-hexadecane, 56 wt% with Khafji, and 53 wt% with Maya. This result indicated that the petroleum residuum enhanced hydrogenation of heavy fractions produced from coal such as preasphaltenes to lighter fractions such as oil and asphaltenes or enhanced the dissolution of the fractions produced from coal in the extracting solvents.

Catalytic Activity of *In Situ* Generated Metal Species in Coprocessing. The activities of Mo, Ni, and V catalysts generated *in situ* from their organometallic complexes in coprocessing were evaluated and compared to each other and that of a presulfided powdered $NiMo/Al_2O_3$ catalyst at equivalent reaction conditions. The organometallic precursors of each metal were in the form of naphthenate, octoate, or acetylacetonate as shown in Table 1. The total active metal loading for each catalyst was about 3000 ppm of the feed materials. Even though sulfur was released from the feed materials during the reaction, a sufficient amount of elemental sulfur was added to generate metal sulfide from each precursor from the beginning of the reaction[8,9]. In the coal-Khafji coprocessing reactions, the Mo and Ni species were the most active for producing toluene solubles (oil and asphaltenes) and for converting coal. The different V species regardless of precursor structure used were the least active (Table 1).

As the reaction temperature was raised from 400°C to 425°C, the recovery of the products decreased from 97 - 100% at 400°C to 85 - 95% at 425°C. This decreased recovery most probably resulted from coking of the coal and residuum materials at the higher reaction temperature in both the thermal and catalytic reactions. In addition, gas production increased from 1 - 2.5 wt% at 400°C to 4 - 5.5 wt% at 425°C. Thermal reaction and catalytic reactions with Mo naphthenate and $NiMo/Al_2O_3$ converted more coal at higher temperature, but reactions with the other catalysts, especially vanadylacetylacetonate, showed reduced coal conversion at 425°C. In thermal and catalytic coprocessing reactions, the actual amount of oil

and asphaltenes produced from coal at 425°C was nearly similar to or sometimes less than that at 400°C. Only Mo naphthenate appreciably enhanced the production of toluene solubles at higher temperature. These results indicated that a high reaction temperature frequently induced the production of more gaseous products and coke as well as other retrogressive reactions producing additional heavier fractions like preasphaltenes and IOM.

The high activity of Mo and Ni species and the low activity of V species were again confirmed in coal-Maya coprocessing reactions (Table 1). The hydrogen consumption in each reaction generally followed the activity of the catalyst used; more hydrogen consumption was observed with Mo, Ni, and $NiMo/Al_2O_3$ catalysts than with V catalysts or no catalyst.

Effect of Sulfur. Even though sulfur species, such as H_2S, were produced from feed materials during the reaction, elemental sulfur was usually added to the catalytic reactions to promote the production of metal sulfides *in situ* from the organometallic complexes. The effect of additional sulfur on the activity of the different catalysts, such as sulfur-sensitive Ni species[7] and sulfur insensitive Mo and V species, was evaluated in coal-Khafji coprocessing (Table 2). Elemental sulfur was added in an amount three times the quantity of sulfur required to produce a metal sulfide from each metal (MoS_2, Ni_3S_2 and V_2S_3). At both reaction temperatures, 400°C and 425°C, additional sulfur usually enhanced the production of oil and asphaltenes and the conversion of coal in both thermal and catalytic reactions except for the reactions with Ni octoate. The reason for the lowered activity of Ni octoate by sulfur has not yet been clearly explained. However, the activity of sulfur-sensitive Ni catalysts in coprocessing was not much affected by additional sulfur: the Ni species was still effective in converting coal and producing fractions of oil and asphaltenes.

Infrared Analysis of Coprocessing Products. Illinois No. 6 coal, residua, and various fractions extracted from coprocessing reactions have been analyzed qualitatively and quantitatively by conventional Fourier transform infrared (FTIR) spectrometry. The relationship between the catalytic activity observed and the infrared spectrum has been examined. The infrared spectrum of the oil fraction from the coprocessing reaction was very similar to that of the residuum used, predominantly showing aliphatic character with only a slight amount of aromatic character. However, the infrared spectrum of asphaltenes from the coprocessing reaction showed more coal character than oil, showing increased aromatic C-H stretch at 3050 cm^{-1}, aromatic ring stretch at 1585 cm^{-1}, and aromatic C-H out-of-plane bending at 860, 815, and 750 cm^{-1}. The infrared spectrum of preasphaltenes was the most similar to that of the coal used; the peaks indicating increased aromatic character and some other peaks indicating C-O stretch, C-C stretch, and O-H bending between 950 and 1300 cm^{-1}, that were not found in the spectrum of oil fraction, resembled the peaks in the spectrum of coal. The relationship between the activity of different catalysts and the infrared spectrum of the product obtained with each catalyst used is under study.

CONCLUSIONS

The activity of *in situ* generated molybdenum, nickel and vanadium catalysts as well as the effect of sulfur on them in upgrading coal and petroleum residuum was evaluated. Petroleum residua enhanced production of toluene solubles from coal compared to the nonreactive solvent, n-hexadecane. Catalytic coprocessing reactions usually produced more oil and asphaltenes than did thermal coprocessing.

In the thermal coprocessing reactions, elemental sulfur introduced at a level of 0.004 g per gram of the mixed reactant of coal and residuum slightly enhanced the extent of oil production and produced less IOM fraction than the thermal reactions without additional sulfur. In the catalytic coprocessing reactions, *in situ* generated Mo and Ni species showed high levels of oil production and coal conversion. But *in situ* generated V species showed low activity similar to that of the additional sulfur in thermal reactions or even lower than the thermal reactions without sulfur depending on organic precursors of V used. A higher reaction temperature of 425°C did not activate V species as much as it did Mo and Ni species. The activities of *in situ* generated metal species (possibly metal sulfides) and a commercial presulfided $NiMo/Al_2O_3$ at the same metal loading of 3000 ppm for converting coal and simultaneously upgrading coal and residuum were observed in the following order.

Mo species ≈ Ni species > $NiMo/Al_2O_3$ > Thermal with sulfur ≥ V species.

Additional sulfur usually enhanced the activity of catalysts in coprocessing except for Ni species from Ni octoate. However, even in the presence of sulfur, the Ni species still showed high activity for coal conversion and oil and asphaltene production. These results indicated that indigenous nickel can be a possible coprocessing catalyst if its precursors in the feed materials are properly concentrated. V, which is usually more abundant in petroleum residuum than is Ni, appeared to have minor catalytic activity for converting coal and residuum to lighter fractions. However, the V sulfide species *in situ* generated showed high activity for heteroatom removal and partially saturating aromatic structures of model chemicals[10]. To understand this discrepancy between the activity of V sulfide species in model and actual coprocessing reactions, a study on the stoichiometry of active V sulfides *in situ* generated in both model and actual coprocessing reactions is required.

ACKNOWLEDGEMENTS

We gratefully acknowledge the support of this work by the U.S. Department of Energy under Grant No. DEFG-2285PC80502 and Contract No. DE-AC22-88PC88801.

LITERATURE CITED

1. Moschopedis, S. E., R. W. Hawkins, J. W. Fryer, and J. G. Speight. 1980. Fuel, 59: 647-53.
2. Mochida I., K. Iwamoto, T. Tahara, Y. Korai, A. Fujitsu, and K. Takeshika. 1982. Fuel, 61: 603-9.
3. Yan, T. Y., and W. F. Espenscheid. 1983. Fuel Processing Technology, 7: 121-33.
4. Monnier, J. 1984. CANMET Report 84-5E. Canada Center for Mineral and Energy Technology.
5. Curtis, C. W., K. J. Tsai, and J. A. Guin. 1987. Ind. Eng. Chem. Res., 26, 12-8.
6. Kim, H., and C. W. Curtis. 1990. Energy Fuels, in press.
7. Kim, H., and C. W. Curtis. 1989. Prepr. Pap.- Am. Chem. Soc., Div. Fuel Chem., 34, 1446-52.
8. Kim, H., C. W. Curtis, D. C. Cronauer, and D. J. Sajkowski. 1989. Prepr. Pap.- Am. Chem. Soc., Div. Fuel Chem., 34, 1432-38.
9. Kottenstette, R. J. 1983. SANDIA Report, SAND82-2495.
10. Sirivejakul, C. 1989. Master's Thesis. Auburn University, Auburn, Alabama.

Table 1. Coprocessing Reactions of Illinois No. 6 Coal and Khafji or Maya Residuum[1]

Reaction Conditions and Catalysts[2]	Product Distribution (wt%)[3] Oil	Asp	Preasp	Toluene Solubles[4]	Coal Conversion(%)
Khafji					
No Reaction	57.5	13.3	2.0	70.8	NA[5]
400°C Reaction					
Thermal Reaction	56.1	17.5	11.4	73.6	56.3 ±2.0[6]
VO Acetylacetonate	55.1	17.9	11.3	73.0	53.2 ±3.4
NiMo/Alumina	58.3	17.4	10.2	75.7	61.9 ±0.6
Ni Acetylacetonate	59.1	18.9	16.6	78.0	86.9 ±2.5
Ni Octoate	61.6	18.4	11.6	80.0	78.0 ±0.4
Mo Naphthenate	61.8	22.3	9.6	84.1	86.4 ±6.7
425°C Reaction					
Thermal Reaction	50.8	17.0	13.4	67.8	60.0
VO Acetylacetonate	48.1	14.0	16.5	62.1	44.6
V Acetylactonate	53.5	17.5	13.6	71.0	69.2
V Naphthenate	55.2	16.9	13.0	72.1	65.0
NiMo/Alumina	60.5	16.0	7.5	76.5	68.5
Ni Octoate	60.2	16.8	9.8	77.0	72.4
Ni Acetylacetonate	60.5	18.7	11.4	79.2	84.8
Ni Naphthenate	62.5	17.3	6.4	79.8	72.4
Mo Octoate	66.7	17.0	3.6	83.7	77.0
Mo Naphthenate	70.3	20.4	3.3	90.5	95.0
Maya					
No Reaction	46.4	23.7	1.6	70.1	NA[5]
400°C Reaction					
Thermal Reaction	49.9	18.7	9.9	68.6	37.4 ±0.2[6]
V Naphthenate	45.6	21.5	13.4	67.1	50.7 ±1.4
Ni Naphthenate	51.1	23.1	17.8	74.2	82.8 ±4.1
NiMo/Alumina	52.2	24.3	11.0	76.5	67.7 ±3.5
Mo Naphthenate	56.7	23.7	7.0	80.4	66.9 ±0.1

[1] Overall product distribution based on the fractions produced from both coal and residuum was compared. The reactions performed at 400°C were duplicated and sometimes repeated more than twice, and the results were expressed as the average values. The standard deviation ($\pm\sigma_n$) of each fraction varied in the range of zero to 1.9 wt% (usually zero to 0.7 wt%) with Khafji residuum and in the range of 0.1 to 3.2 wt% (usually 0.1 to 0.9 wt%) with Maya residuum. The reactions performed at 425°C were conducted once.

[2] Abbreviations: V(vanadium), VO(vanadyl), Ni(nickel), and Mo(molybdenum).
Additional sulfur: 0.037g for thermal reaction, 0.080g for V and VO, 0.031g for Ni, and 0.058g for Mo.

[3] The products were fractionated into gas, oil, asphaltenes(Asp), preasphaltenes(Preasp), and IOM.

[4] Toluene solubles (oil and asphaltenes)

[5] NA: Not available

[6] Standard deviation ($\pm\sigma_n$) of coal conversion (%)

Table 2. Effect of Sulfur on Coal-Khafji Coprocessing[1]

Coprocessing at 400°C \	Thermal	VOAcAc	NiAcAc	NiOct	MoNaph
Without Sulfur					
Oil (wt%)	52.8±1.6	54.4±1.1	58.3±0.1	60.0±0.1	60.0±0.2
Asphaltenes (wt%)	17.2±0.3	17.4±1.5	19.0±0.3	18.1±0.9	20.0±0.4
Coal Conversion (%)	46.9±1.6	42.7±2.8	85.3±1.7	78.7±2.5	76.3±1.3
With Sulfur[2]					
Oil (wt%)	56.1±0.7	55.1±1.0	59.1±0.7	61.6±0.3	61.8±1.2
Asphaltenes (wt%)	17.5±0.2	17.9±1.2	18.9±0.0	18.4±0.0	22.3±1.9
Coal Conversion (%)	56.3±2.0	53.2±3.4	86.9±2.5	78.0±0.4	86.4±6.7

Coprocessing at 425°C \	Thermal	VOAcAc	NiAcAc	NiOct	MoOct	MoNaph
Without Sulfur						
Oil (wt%)	52.5	51.9	55.5	65.6	68.3	69.9
Asphaltenes (wt%)	14.0	12.9	17.7	16.6	15.3	18.0
Coal Conversion (%)	50.3	40.5	80.4	77.1	76.4	92.2
With Sulfur[2]						
Oil (wt%)	55.6	50.8	62.6	62.0	71.2	73.2
Asphaltenes (wt%)	15.4	13.2	17.8	16.0	14.7	18.4
Coal Conversion (%)	60.0	44.6	84.8	72.4	77.0	95.0

[1] The product distribution was expressed as the average values and standard deviations ($X \pm \sigma_n$) based on the fractions of overall products from both coal and residuum in coprocessing. The reactions performed at 400°C were duplicated and sometimes repeated more than twice, and the reactions at 425°C were performed once.
Abbreviations: VOAcAc (vanadium actylacetonate), NiAcAc (nickel acetylacetonate), NiOct (nickel octoate), MoOct (molybdenum octoate), and MoNaph (molybdenum naphthenate).

[2] Additional sulfur amount: 0.038g for thermal reactions, 0.080g for V, 0.031g for Ni, and 0.058g for Mo species.

NATURAL COPROCESSING OF COAL AND TAR

by

Fariborz Goodarzi[1] and Thomas Gentzis[2]

[1] Institute of Sedimentary and Petroleum Geology
Geological Survey of Canada
3303-33rd Street N.W.
Calgary, Alberta T2L 2A7 Canada

[2] Alberta Research Council
Coal Research Centre Devon
One Oil Patch Drive
Devon, Alberta T0C 1E0 Canada

ABSTRACT

This study examines optically the interaction between coal and coal-tar pitch in a self-burning coal setting. Three distinct zones, a thick, lower carbonization, a narrow, middle active combustion and also a narrow, upper oxidation zone were identified. The presence of basic instead of a mosaic anisotropy on the solids is indicative of weathering/oxidation prior to combustion. Air could circulate easily through open fractures within the uncompacted coal fragments, thus facilitating combustion at depth. The coal was carbonized at approximately 500-550°C at a rate of heating of 10°C/min. and subsequently combusted at 550-600°C. The coal has also been thermally altered to produce solid (semi-coke/coke), liquid (tar) and volatile matter. Different types of tar have been observed microscopically, interacting with coal fragments by briquetting them and acting as hydrogen donors to vitrinite.

Because additives such as coal-tar pitch often modify and change the optical texture and nature of residues during laboratory processes such as coal hydrogenation and co-carbonization, useful information can be gained by studying the natural coprocessing of coal with coal-tar pitch using optical microscopy and petrographic techniques.

INTRODUCTION

There have been numerous studies on the interaction between coals of different rank and additives containing oxygen, nitrogen, sulphur, aromatic compounds, petroleum pitches and coal-tar pitches (Marsh, 1973; Marsh et al., 1973a,b,c; Marsh et al., 1974; Marsh et al., 1980; Marsh and Neavel, 1980; Mochida et al., 1979a,b,c), and between coal macerals (Goodarzi, 1984). These additives often modify and change the optical texture and nature of residues during such processes as liquefaction (hydrogenation) and co-carbonization of coal macerals (Shibaoka et al., 1980; Goodarzi, 1984).

It has been shown by Shibaoka et al., (1980) and later by Steller (1981) that during hydrogenation the interaction between a coal and a hydrogen-rich additive results in the formation of reaction rims termed 'hydrogenation rims' These rims are possibly the precursors of vitroplast because they form from the interaction of additive with the vitrinite particles in the coal and are rich in

hydrogen. More recently, Gentzis and Goodarzi (1989) observed reaction rims formed around vitrinite particles due to the influence of carbonization by-products such as tar, in a self-burning coal wastepile in Coleman, Alberta, Canada.

Goodarzi (1984) reported similar reaction rims when highly reactive sporinite was co-carbonized with less reactive vitrinite in coals of the same rank. The reaction rims formed at the boundaries between carbonized vitrinite and sporinite had a distinct optical texture (size and anisotropy of the mosaic units). Goodarzi (1984) used coals from two different ranks (high-volatile bituminous C - % Ro = 0.62, and high-volatile bituminous A - % Ro = 1.04) and observed that the higher the rank of coal, the wider were the reaction rims. When the blend having the lower-reflecting vitrinite was carbonized, two types of optical texture were produced, an isotropic for vitrinite and a granular anisotropic for sporinite.

Three types of interactions may occur between a coal and an additive in a blend during carbonization which may result in the formation of different fluid phases. These are: fluid mixing, solvation and solvolysis (Mochida et al., 1979). During fluid mixing, the two miscible fluids forming from coal and additive create a new fluid with a new molecular composition and properties (Mochida et al., 1979). Solvation is considered to be more of a physical rather than a chemical process and involves the extraction or leaching of the coal by the additive, followed by a subsequent stabilization of the formed molecules in the fluid pitch additive. Solvolysis is a chemical process which involves simultaneous depolymerization and interaction of the coal and additive involving hydrogen transfer mechanism (Mochida et al., 1979).

This study deals with the interaction of organic components such as coal macerals and semicoke/coke fragments with tar generated by the self-burning of coal.

EXPERIMENTAL

A 440 cm deep channel was dug on the top of a self-burning coal wastepile at Coleman Collieries in Alberta and samples were taken from the oxidation (ash), combustion and carbonization zones as well as from unaltered coal. The hot samples were cooled in water immediately to prevent further oxidation and combustion.

The samples were then dried and crushed to pass -20 mesh (<850μm). They were subsequently polished and their maximum and minimum reflectances in oil (n_{oil} = 1.518) were measured using a Zeiss MPM II microscope, fitted with a Zonax microcomputer. Photomicrographs were taken under both plane-polarized light and with partially crossed polars.

RESULTS AND DISCUSSION

Gentzis and Goodarzi (1989) examined the organic petrology of the self-burning coal wastepile in Coleman, Alberta, Canada, (Figure 1a) and reported the reflectance profile of the different zones identified. These zones are: oxidation (ash), combustion and carbonization, all observed from top to base of the wastepile but their boundaries are not well defined (Figure 1b).

Carbonization zone

This zone is thick (~300 cm) and is subdivided into three subzones. The first subzone (B) is approximately 60 cm thick and consists mainly of warm, angular coal fragments. Two types of tar are observed (Figure 1c), an isotropic (% Romax = 1.07) and an anisotropic (% Romax = 2.35).

Subzone C is 180 cm thick and contains loose particles of hot, angular coal and semicoke/coke, becoming increasingly tarry towards the upper part. Three tar types are identified (Figure 1c), one is isotropic (% Romax = 0.72) and the other two are anisotropic (% Romax = 1.25 and 1.52 respectively) showing 'flow' texture.

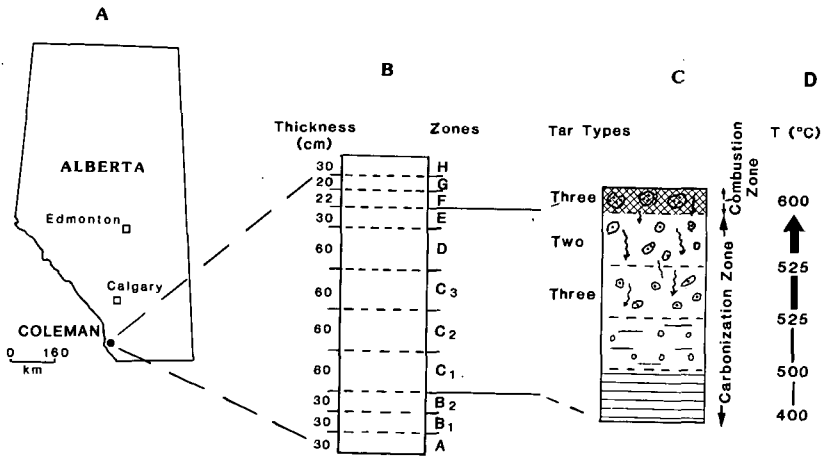

Figure 1 Location map of the coal wastepile in Coleman, Alberta (A), vertical profile of the self-burning coal wastepile showing different zones (B), types of tar (C) and temperature of their formation (D).

Subzone D is 60 cm thick consisting of angular semicoke and two tar types are present (Figure 1c). The isotropic tar has an Romax of 1.10%, while the anisotropic has an Romax of 1.66%.

Combustion zone

This zone is 30 cm thick and consists of a mixture of coke and ash. Both isotropic and anisotropic tars are present. The isotropic ones have an Romax of 0.86 and 1.13%, while the anisotropic ones have Romax values of 1.48, 1.90, 2.62 and 3.65% respectively. The high reflectance tar also shows granularity.

Oxidation (Ash) zone

The ash zone is 22 cm thick and consists of red ash and vents. Four types of tar are present, one isotropic (% Romax = 1.07) and three anisotropic (1.33, 1.53 and 1.77% Ro max respectively).

Heat generated by the combustion of coal alters the coal fragments in the oxidation zone and carbonization zone (Figure 1c) and produces solid residue (semicoke/coke), liquid (tar) and gases. The tar is mainly liquid to gaseous at the temperature of generation (500-550°C) but solidifies upon cooling and forms a pitch-like solid. The presence of the ash zone above the combustion zone in Coleman prevents the complete elimination of volatile by-products and, as a result, volatile matter escapes from vents developed at the side of the wastepile. These vents are impregnated by coal tar-pitch and often heat-affected fragments (semicoke/coke) are briquetted by tar (Gentzis and Goodarzi, 1989). Therefore, tar which formed due to coal devolatilization in the carbonization zone, such as in subzone C, migrates downwards in the wastepile due to force of gravity, penetrates the space among coal fragments and precipitates as isotropic to anisotropic by-products. The downward movement of tar is also due to a heat barrier produced by the combustion zone above (Figure 1b).

Similar observations were made by Goodarzi et al., (1988) on a partially combusted and coked bituminous coal seam from Aldridge Creek, British Columbia, Canada. A pitch-like, viscous material, which was soluble in chloroform-ethanol (87/13) azeotrope (similar to coal tar-pitch) formed from the carbonization of a medium-volatile bituminous coal seam (% Romax = 1.1), had migrated downwards filling the devolatilization vacuoles of the semicoke.

Figure 1c shows the various types of tar and their location in the wastepile and Figure 1d shows the temperature of their formation. Gentzis and Goodarzi, (1989) estimated that the coal was carbonized at a temperature of 500-550°C at a rate of heating of 10°C/min. and subsequently combusted at a higher temperature (550-600°C). The tar which formed in the semicoke subzone C_3 (~525°C) is isotropic, soft, typical of coal tar-pitch (Plate 1a). The coal rank in the Coleman section is medium-volatile bituminous (% Romax = 1.07), similar to the coal rank in Aldridge Creek. In both cases, coal was transformed to coke.

In Aldridge Creek, the coal seam is burning underground and under a sedimentary cover. As a result, the coal seam is directly transformed into carbonized residue. Therefore, no briquetting occurs but only impregnation of semicoke by tar takes place. In Coleman, coal is in fragmented form prior to burning, and is briquetted by tar-pitch as a result of self-burning. Most of the coke fragments in Coleman are subangular showing basic anisotropy, an indication that coal was probably weathered before being combusted (Goodarzi, et al., 1975).

Often, one or two waves of tar are observed filling cavities among semicoke fragments (Plate 1b). These two waves (types) of tar can be recognized on the basis of optical texture, an anisotropic, higher-reflecting tar which was

obviously deposited initially, followed by an isotropic, lower-reflecting secondary tar.

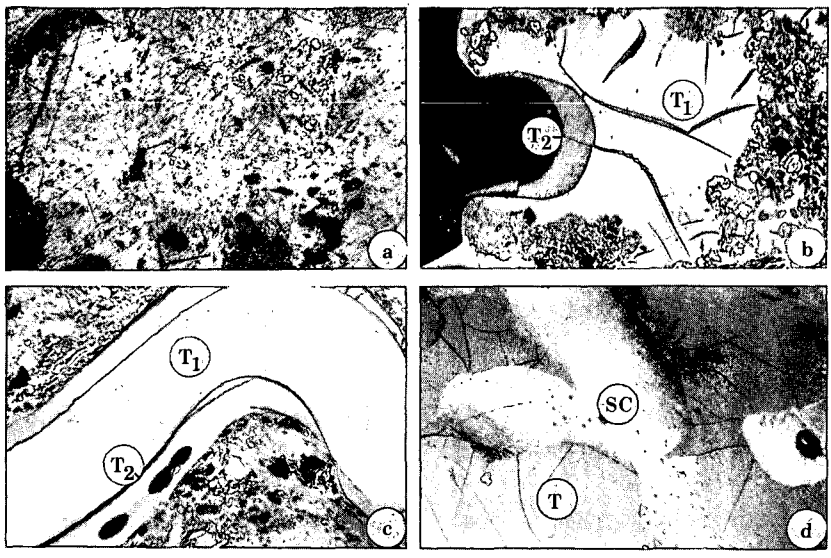

PLATE 1

All photomicrographs taken in black and white, plane-polarized light, under oil immersion. Long axis is 240μm.
a) Isotropic and soft coal tar-pitch, semicoke subzone (C_3); b) Two waves of tar filling cavity in semicoke subzone (C_3). The initial tar (T_1) is higher reflecting, whereas the secondary tar (T_2) is isotropic; c) Two generations of tar showing fluidity; the older one (T_1) has a granular morphology and higher reflectance, the younger one (T_2) shows devolatilization vacuoles and lower reflectance; d) Semicoke fragments (SC) showing devolatilization vacuoles being surrounded by tar (T).

Tar also shows evidence of fluidity, an indication of its mobility. Plate 1c shows two types of tar, a higher-reflecting, slightly granular tar deposited initially and a secondary, lower-reflecting tar exhibiting devolatilization vacuoles. Both tars have infilled the crack between the semicoke fragments and have taken its shape. Occasionally, the subangular fragments of semicoke show devolatilization vacuoles and are completely surrounded by tar (Plate 1d). Within the semicoke subzone (C_3), mixing of semicoke and coal fragments may take place (Plate 2a-b) with tar binding both fragments. The low-reflecting tar is hydrogen-rich and apparently is able to react with the coal particles producing a distinct reaction rim (Plate 2a). This did not occur between the tar and semicoke fragments which show granular mosaic texture but no apparent reaction

rim (Plate 2b).

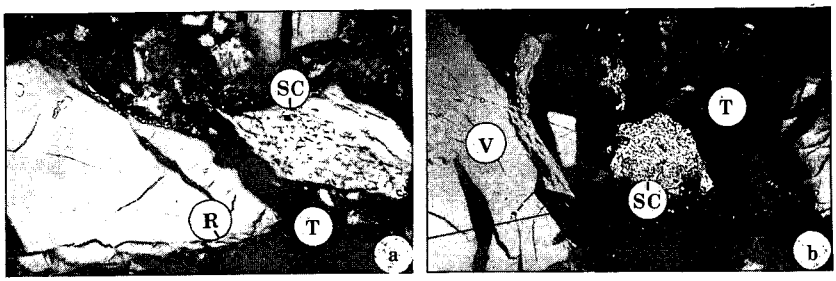

PLATE 2 Conditions same as Plate 1.

a) Low-reflecting, hydrogen-rich tar (T) reacting with coal and semicoke (SC) fragments. Note the presence of a reaction rim (R) between coal and tar; b) Similar to 2a but there is no reaction rim formed due to the interaction of tar (T) and semicoke (SC). Vitrinite (V) also present showing desiccation cracks.

Often the cavities and cracks or surfaces of semicoke and coke fragments are lined by tar, indicating the passage of tar (Plate 3a-b). Tar within the pre-carbonization stage towards the base of the wastepile is often isotropic, soft and appears to have reacted with the coal fragments (Plate 4a). This tar is relatively hot and possibly acted not only as a binder but also as a hydrogen donor to vitrinite particles. The briquetting of angular inertodetrinite fragments by tar is shown in Plate 4b. There is no apparent reaction between tar and inertodetrinite.

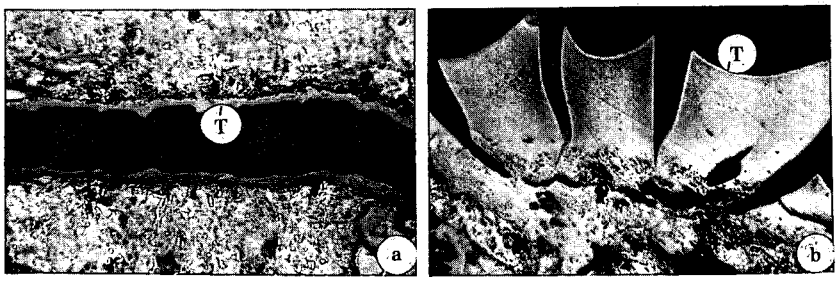

PLATE 3 Conditions same as Plate 1.

a) The presence of thin lining of isotropic tar (T) indicating the passage of liquids and gases through semicoke fragments; b) The deposition of tar (T) in the cavity has lead to the formation of flower-like structures.

The morphology of the vitrinite fragments being briquetted by tar may give an indication as to the temperature of combustion. Usually rounded vitrinite fragments, as shown in Plate 4c, are indicative of higher temperatures as opposed to angular vitrinite fragments (Plate 4d) which indicate lower temperatures.

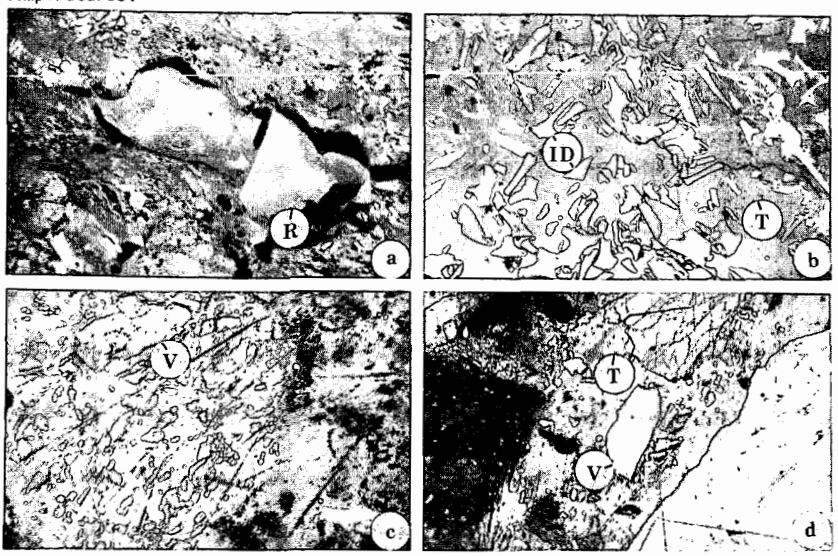

PLATE 4 Conditions same as Plate 1.

a) Tar reacting with coal fragments in pre-carbonization stage to form distinct reaction rims (R). The tar is hot and not only acts as a binder to briquette coal fragments but also as a hydrogen donor; b) Tar (T) is shown here briquetting angular inertodetrinite (ID); c) Tar briquetting rounded to semirounded vitrinite (V); d) Angular vitrinite (V) and inertinite being briquetted by tar (T).

CONCLUSION

The following conclusion can be drawn:

1) Tar generated from the combustion of coal may interact with coal and semicoke/coke fragments. Tar may not only act as a binder but also as a hydrogen donor to coal fragments, thus forming a distinct reaction rim.

2) Different tar types (primary and secondary) can be identified based on morphology, optical texture and reflectance.

3) Tar will briquette loose fragments of coal, as in the case of a wastepile but when coal is present in the form of a coherent seam, briquetting does

not take place but the coal is transformed into carbonized residue impregnated by tar.

ACKNOWLEDGMENTS

The manuscript benefited from critical review by Dr. Alex Cameron, Institute of Sedimentary and Petroleum Geology, Geological Survey of Canada. The authors would also like to thank the staff of Coleman Collieries for access to the area and assistance during sampling and Ms. Joyce Moir, Coal and Hydrocarbon Processing Department, Alberta Research Council for typing the manuscript.

REFERENCES

1) MARSH, H., 1973. Carbonization and liquid crystal (mesophase) development. Part 1 The significance of the mesophase during carbonization of coking coals, Fuel, vol. 52, p. 205-212.

2) MARSH, H., FOSTER, J.M., HERMON, G. and ILEY, M., 1973a. Carbonization and liquid crystal (mesophase) development. Part 2 Co-carbonization of aromatic and organic dye compounds, and influence of inerts, Fuel, vol. 52, p. 234-242.

3) MARSH, H., FOSTER, J.M., HERMON, G., ILEY, M. and MELVIN, J. N., 1973b. Carbonization and liquid crystal (mesophase) development. Part 3 Co-carbonization of aromatic and heterocyclic compounds containing oxygen, nitrogen and sulphur, Fuel, vol. 52, p. 243-252.

4) MARSH, H., DACHILLE, F., ILEY, M., WALKER, P. L. and WHANG, P.W., 1973c. Carbonization and liquid crystal (mesophase) development. Part 4 Carbonization of coal-tar pitches and coal of increasing rank, Fuel, vol. 52, p. 253-261.

5) MARSH, H., CORNFORD, C., and HERMON, G., 1974. Carbonization and liquid crystal (mesophase) development. Part 5 Importance of eutectic zones formed from nematic liquid crystals, Fuel, vol. 53, p. 168-171.

6) MARSH, H., GERUS-PIASECKA, I., and GRINT, A., 1980. Carbonization and liquid crystal (mesophase) development. Part 14 Co-carbonization of coal with A240 ash and petroleum pitch: Effects of conditions of carbonization upon optical heating of resultant cokes, Fuel, vol. 59, p. 343-348.

7) MARSH, H., and NEAVEL, R.C., 1980. Carbonization and liquid crystal (mesophase) development. Part 15 A common stage in mechanisms of coal liquefaction and of coal blends for coke making, Fuel, vol. 59, p. 511-513.

8) MOCHIDA, I., and MARSH, H., 1979a. Carbonization and liquid crystal (mesophase) development. Part 10 The co-carbonization of coals with solvent refined coals and coal extracts, Fuel, vol. 58, p. 790-796.

9) MOCHIDA, I., and MARSH, H., 1979b. Carbonization and liquid crystal (mesophase) development. Part 11 The co-carbonization of low-rank coals with modified petroleum pitches, Fuel, vol. 58, p. 797-802.

10) MOCHIDA, I., and MARSH, H., 1979c. Carbonization and liquid crystal

(mesophase) development. Part 13 Kinetic considerations of the co-carbonizations of coals with organic additives, Fuel, vol. 58, p. 809-814.

11) GOODARZI, F., Fuel, 1984. Optical properties of carbonized sporinite in vitrinite/sporinite blends, Fuel, vol. 63. p. 827-833.

12) SHIBAOKA, M., UEDA, S., and RUSSELL, N.J., 1980 . Some aspects of the behaviour of tin (II) chloride during coal hydrogenation in the absence of a solvent, Fuel, vol. 59, p. 11-18.

13) STELLER, M., 1981. Untersuchungen an Hydrierruckstanden einer Gas flammkohle - Diss. Techn. Hochsch, Aachen, 121 pp.

14) GENTZIS, T. and GOODARZI, F., 1989. Organic petrology of a self-burning coal wastepile from Coleman, Alberta, Canada. International Journal of Coal Geology, vol. 11, p. 257-271.

15) MOCHIDA, I., MARSH, H., and GRINT, A., 1979. Carbonization and liquid crystal (mesophase) development. Part 12 Mechanisms of the co-carbonization of coals with organic additives, Fuel, vol. 58, p. 803-808.

16) GOODARZI, F., GENTZIS, T., and BUSTIN, R.M., 1988. Reflectance and petrology profile of a partially combusted and coked bituminous coal seam from British Columbia, Fuel, vol. 67, p. 1218-1222.

17) GOODARZI, F., HERMON, G., ILEY, M., and MARSH, H., 1975. Carbonization and liquid-crystal (mesophase) development. Part 6 Effect of pre-oxidation upon coking properties, Fuel, vol. 54, p. 105-112.

EUROPEAN DIESEL FUEL - A REVIEW OF CHANGES IN PRODUCT QUALITY 1986-1989

G. M. Wallace
Ethyl Petroleum Additives Limited, London Road, Bracknell
Berkshire, RG12 2UW, England

Introduction

In Europe heavy goods vehicles are effectively 100% diesel engined. This coupled to the significant percentage of diesel powered passenger cars and light duty commercial vehicles results in Europe having the highest penetration of diesel engined vehicles worldwide (Fig 1). Despite the increasingly stringent emission limits and customer performance demands, technological advances by the diesel engine manufacturers are enabling them to keep up with such rapid change. Thus the position of the diesel engine appears secure in Europe, provided consistently high quality road diesel fuel is maintained.

The European refiner is facing a steady increase in demand for road diesel together with a decline in heating/off road gas oil volumes (Fig 2) due to competition from gas and other forms of energy. This is putting pressure on refiners to include greater proportions of cracked gas oils in the road diesel pool with the potential for stability problems - a major area of shortcoming for conversion distillate streams.

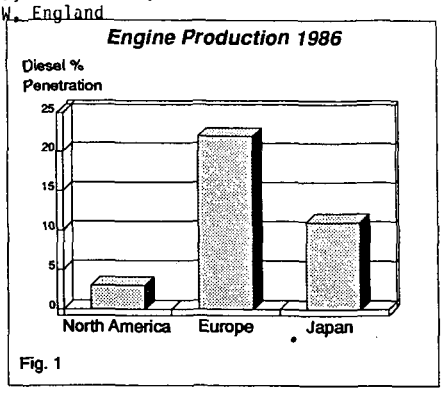

Fig. 1

This paper reviews the results of systematic winter surveys of road diesel fuel in Europe carried out from 1986-89 in which oxidative and thermal stability were evaluated along with other key parameters of diesel fuel quality.

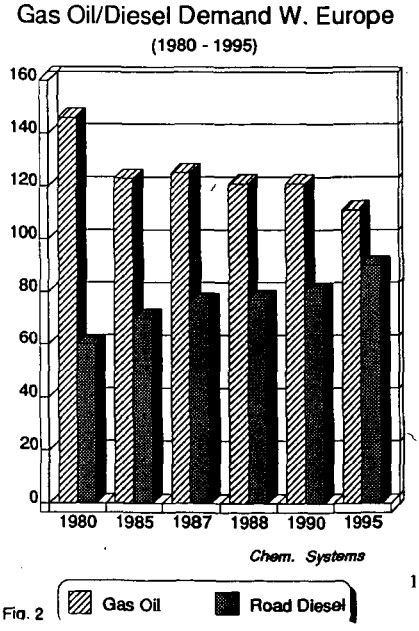

Fig. 2

Diesel Fuel Specifications

In Europe unleaded gasoline is unique in having a common specification from country to country. The national diesel fuel specifications detailed in Appendix 1 follow no set pattern with the exception of low temperature properties. These are consistent with the demands of geography. This lack of commonality of quality is a major concern to trans European operators of diesel vehicles. Likewise only the UK contains any stability standard and that a somewhat relaxed 2.5 mg/100 ml maximum in the ASTM D2274.

From the 1986-89 Ethyl diesel fuel surveys (Refs 1-3 and Appendix 2) consideration will only be given to the following primary diesel fuel properties

1) Density
2) Cetane Number
3) Cetane Index
4) Viscosity
5) Sulphur Content
6) Aromatics Content
7) Olefin Content
8) Oxidative Stability
9) Thermal Stability

Of these cetane number, oxidative stability and thermal stability can be improved by use of a suitable multifunctional diesel fuel additive package. The other primary features are purely influenced by refinery processing.

Density

The density of a diesel fuel affects the mass of fuel entering the combustion chamber and thus impacts on engine power, fuel economy and emissions.

The average density across Europe is essentially unchanged over the 3 years (Table 1). Even when individual countries are considered there is little annual variation. Austria is the only exception where density has risen steadily with time (Fig 3). This is coupled to a 17°C increase in the 50% distillation point and a smaller increase in end-point indicating a change in demand balance (Appendix 2).

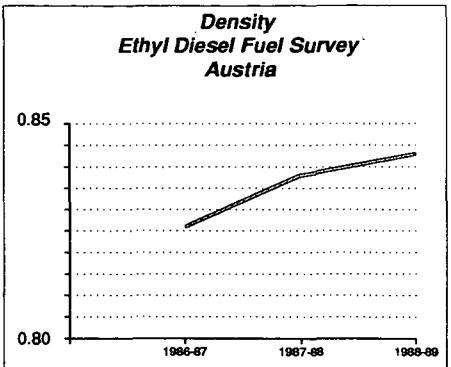

Fig. 3

Ethyl European Diesel Fuel Winter Survey Overall Mean Values

Table 1	1986-87	1987-88	1988-89
Density @ 15°C (g/cm^3) ASTM D4052	0.8380	0.8388	0.8368
Cetane Number, ASTM D613	51.3	51	52.5
Cetane Index, ASTM D976	51.2	50.4	51.3
Viscosity @ 20°C, ASTM D445	4.36	4.22	3.99
Sulphur, % weight, ASTM D4294	0.24	0.27	0.24
Aromatics, % vol ASTM D1319	29.2	32.1	26.9
Olefins, % vol ASTM D1319	0.6	1.6	3.8
Oxid. Stability, mg/100 ml, ASTM D2274	1.3	1.0	0.6
Pad Test, Rating	12*	7.5	5
*only 10 results.			

Cetane Number

Cetane Number is a measure of fuel ignition delay. This we consider to be the time between start of fuel injection and the rapid rise in pressure in the pre-chamber. Many other definitions are sometimes used (Ref 4).

Cetane number defines the ease of auto-ignition of the fuel. Whilst this is generally a reflection of the inherent stability of the molecules in a fuel, ignition improvers are often included to enhance performance.

Despite all the predictions of declining cetane quality due to increasing demand the overall picture in Europe is the reverse (Table 1). This is due to the introduction of premium quality diesel fuels containing multifunctional additives which can include cetane improver. This is most dramatically seen in West Germany (Fig 4) where premium diesel fuel was introduced in 1987 in response to OEM demands for higher quality fuels to reduce environmental emissions. As we discuss the other parameters the impact of this quality enhancement of diesel fuels will be further evidenced.

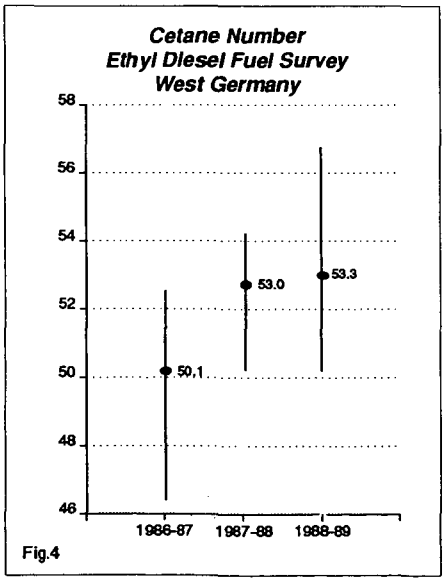

Fig.4

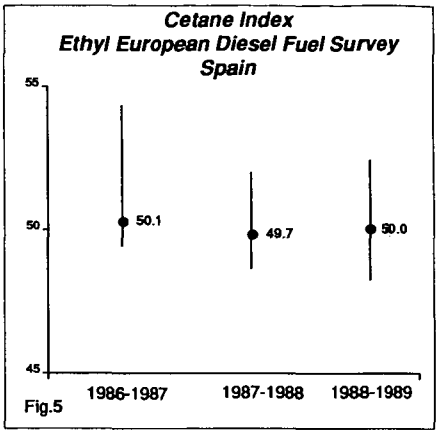

Fig.5

Cetane Index

This is an attempt to empirically predict a fuels ignition quality based on its density and boiling range. As this shows reasonable agreement with a fuels natural cetane it is arguably a better indicator of the European cetane pool than cetane number. And indeed this is unchanged across the 3 year period. However in Spain (Fig 5) both demand and refinery conversion is increasing whilst crude slate has resulted in lower natural indices and numbers. Thus cetane index has fallen steadily despite cetane number remaining high due to legislation of a 50 Cetane Number minimum but a 45 Cetane Index minimum thereby allowing refiners greater flexibility.

Viscosity

Viscosity variations have similar effects to those described for density. Additionally at low viscosities, below about 3 cSt @ 20°C, pumping leakage is increased with hot re-starts becoming difficult under hot ambient conditions, reduced power output and pump lubrication becoming critical. The combination of wide viscosity band variations with wide density variations exacerbates emission levels and vehicle performance.

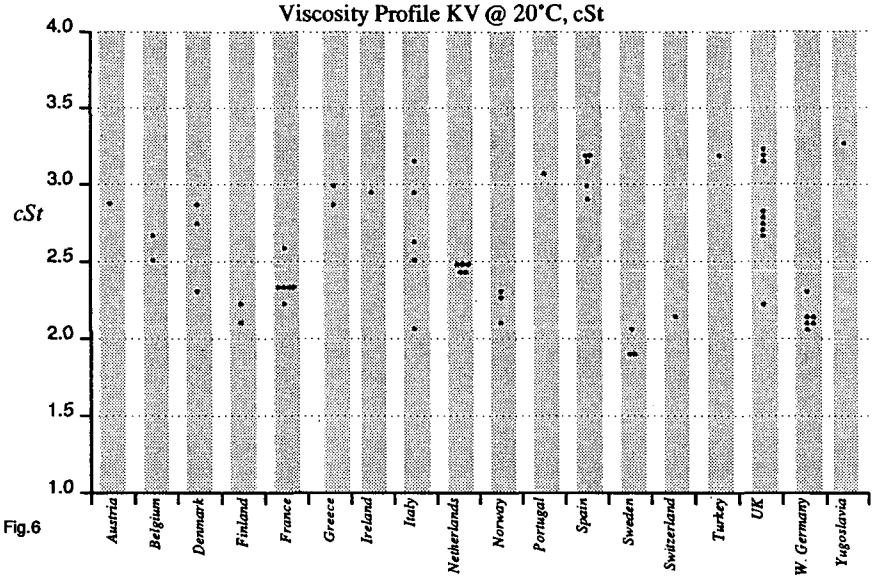

Fig.6

There is some evidence (Table 1) for a general lightening of diesel fuel in Europe as a consequence of lower Cloud points. We do not see wide viscosity variations in Europe (Fig 6) and it is important to note this parameter is not a constraint since it is controlled indirectly by other diesel fuel properties such as Cloud Point, Density and Distillation range.

Sulphur Content

Worldwide concerns about "acid-rain" have resulted in legislation designed to control acidic emissions, most notably oxides of sulphur. Additionally the need for low sulphur fuel for satisfactory operation of low emissions oxidation catalyst equipped diesel vehicles is supporting this drive. The Californian standard of 0.05% max weight is the level that OEM's are requiring. In Europe the typical limit of 0.30% weight has moved down to 0.20% weight in the more environmentally sensitive countries. A good example of this is to contrast the sulphur contents in Italy and West Germany (Fig 7). This is placing increasing pressure on available refinery hydrotreating capacity and penalising higher sulphur crudes.

Aromatics Content

Aromatics, have been considered in certain studies to relate to deleterious emissions, particularly particulates. Several studies (Ref 5) claim to show links between the aromatics content of a diesel fuel and exhaust particulate emissions. Consideration is being

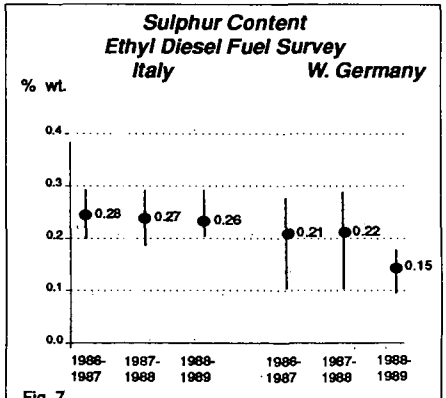

Fig. 7

given within the European Economic Community to follow the US example and limit the aromatics level of road diesel. Also being investigated is the best method for measuring the aromatics as the F.I.A. Method (ASTM D1319) often gives poor separation with heavier boiling European fuels (85% @ 350°C min is the common European limit). Whilst Table 1 would suggest there might be some overall decrease in aromatics levels in Europe it varies significantly country to country. Thus the high degree of conversion stream usage and heavier crude processing/higher distillation range is reflected in the high aromatics levels in Italy versus those of Norway (Fig 8), particularly pre-1988-89.

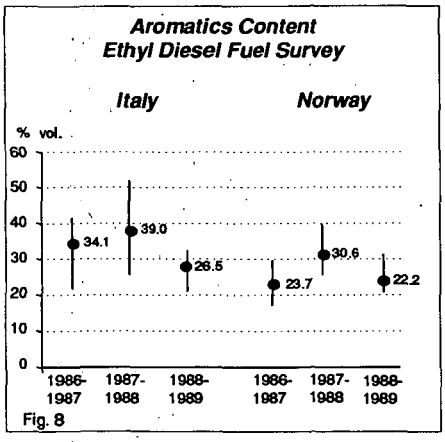

Fig. 8

Olefin Content

Olefin levels in diesel are generally low however in terms of fuel stability they are regularly cited (Ref 6) as significant. It is thus interesting to note that every year from 1986 to 1989 the overall olefin level has doubled in Europe although the total percentage remains very small. Again this reflects the increasing use of conversion streams and level of hydrotreatment.

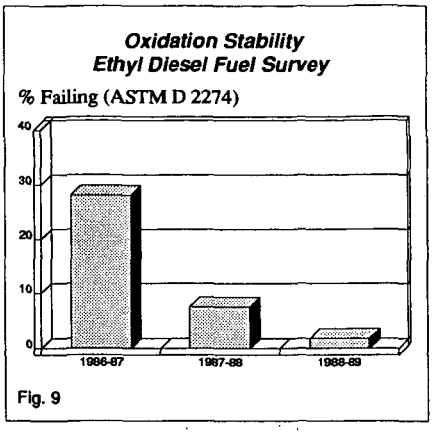

Fig. 9

Oxidation Stability

Oxidation stability is widely considered to be an important parameter in determining the long term storage stability of a fuel. It is typically evaluated using the ASTM D2274 test developed by the US Navy. The limit for satisfactory field performance is usually taken as 1.5 mg/100 ml of insolubles. Figure 9 shows that the percentage of fuels with deposit levels above 1.5 mg/100 ml has fallen to negligible

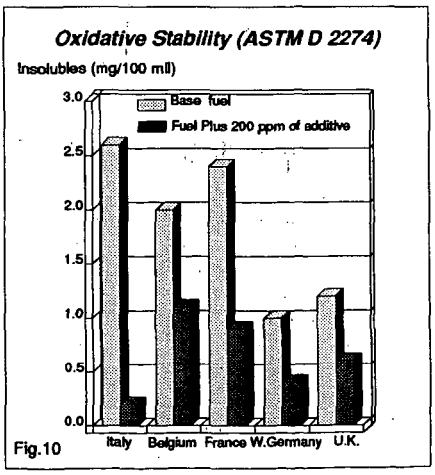

Fig.10

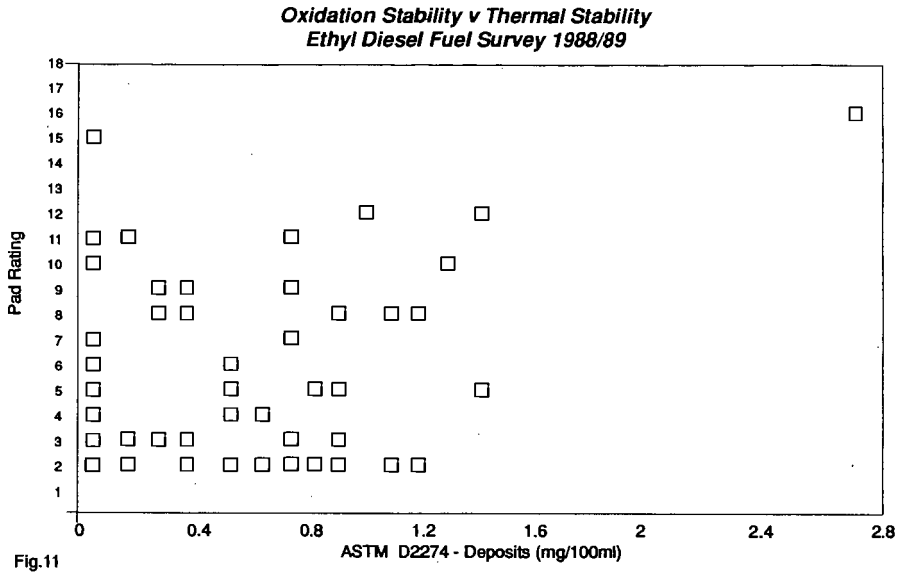

Fig.11

levels. This is thought to be due to the increasing use of multifunctional additive packages offering stability enhancement. An example of their effect is shown in Fig 10. This may also help explain the lack of an obvious relationship between thermal and oxidative stability (Fig 11).

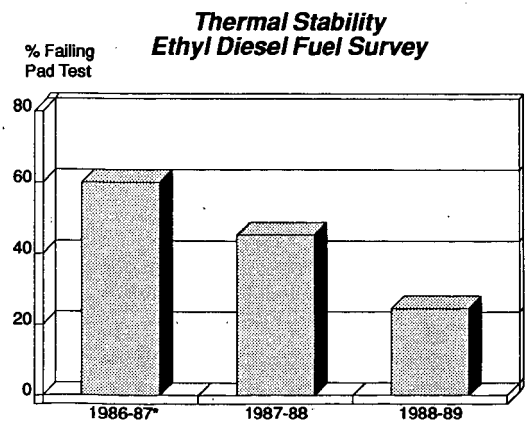

Fig.12 * (limited data-base)

Thermal Stability

Thermal stability whilst important in determining a fuels long term storage stability has also been linked to nozzle coking tendency (Ref 7). It is usually measured by some form of rapid thermal shock test followed by filtration and assessment of the filter deposits. Using the Ethyl Pad Procedure; where a rating of 20 is a black filter, 0 is clean and 7 is the maximum for good field performance we have observed results from 2 to 20 in our surveys. Previous work has suggested possible correlation with nozzle coking tendency, (Ref 8), surveys.

Just as for oxidation stability the percentage of samples with ratings above 7 has declined steadily from 1986-89 (Fig 12). This is also surprising when viewed against the background of increasing olefin levels. Again the use of multifunctional additive packages is improving fuel stability. This also tallies with the poor agreement between olefin content and Pad Rating (Fig 13).

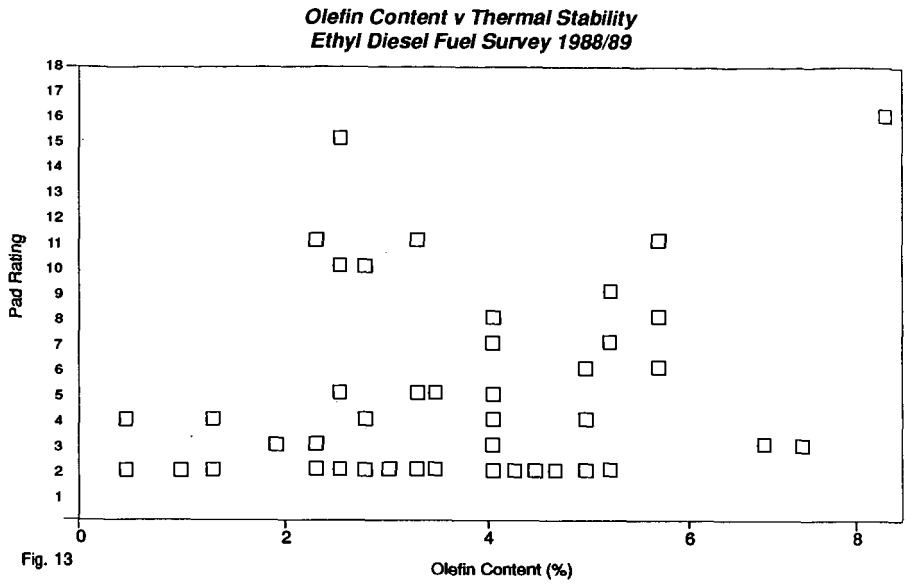

Fig. 13

Conclusions

The data reported in this paper indicate:

1) Diesel fuel quality remains high in Europe due in part to the increasing use of multifunctional diesel fuel additive packages

2) As a result of these marketing factors cetane number is increasing.

3) Sulphur levels are declining throughout Europe.

4) Olefin levels are increasing.

5) Oxidative and thermal stability are improving overall in Europe primarily due to the use of multifunctional diesel fuel additive packages.

References

1) Ethyl European Diesel Fuel Survey Winter 1986-87

2) Ethyl European Diesel Fuel Survey Winter 1987-88

3) Ethyl European Diesel Fuel Survey Winter 1988-89

4) H.A. Henein and J.A. Bolt; SAE 67007

5) E.G. Barry and L.J. McCabe, D.H. Gerke and J.M. Perez; SAE 852078

6) M.W. Schrepfer, R.J. Arnold and C.A. Stansky, Oil and Gas Journal, January 16, 1984

7) M. Fortnagel and B. Herrbrich, API, New Orleans, 1984

8) P.B. Mabley and G.M. Wallace, Third International Stability and Handling of Liquid Fuels Conference, London, 1988

European National Specifications For Diesel Fuel

Country	*Spec. Ref.*	*Density Kg/l*	*Distill, °C*	*KV @ 20°C, cSt*	*Fl. Pt., °C*	*CLPt, °C*	*CFPP, °C*	*Pour Pt, °C*	*Sulphur, % Wt.*	*Cetane Index*	*Cetane Number*
Austria	Ö Norm C1104	0.820-0.860	Min 85% @ 350	3.0 - 8.0	56 min	-	-15/ -22 max (W)	-	0.15 max	-	48 min
Belgium	NBN T52-713	0.820-0.870	Max 65% @ 250 Min 85% @ 350	4.0 max @ 40°C	56 min	-	-15 max (W)	-	0.2 max	-	46 min
France	CSR 09-M	0.810-0.890	Max 65% @ 250 Min 85% @ 350	9.5 max	55-120	-5 max (W) -8 max (W)* *Grand Froid	-15 max (W) -18 max (W)* *Grand Froid	-18 max (W) -21 max (W)* *Grand Froid	0.3 max	-	48 min
Greece	734/AB/86	Report 0.82 - 0.85 Athens	Min 85% @ 350 Max FBP @ 370 Athens	2 - 6 @ 37.8°C	55 min	-	-5 max (W) -2 max Athens (W)	- 9 max (W) - 6 max Athens (W)	0.3 max	47 min Athens 45 min Rest	-
Ireland	I.S.251:1981	0.825 min	Min 85% @ 350 FBP 380 max	2.0 min. @ 40°C	61 min	-2 max (W)	-12 max (W)	-	0.3 max	50 min	50 min
Italy	NC630-01	0.8050.865	Max 65% @ 250 Min 85% @ 350	2.0-5.35 @ 37.8°C	55 min	-	-10 max (W)	- 6 max (W)	0.3 max 0.2 max (cities)	48 min	47 min
Portugal	124/89	0.815-0.865	Max 65% @ 250 Min 85% @ 350	1.8-5.5 @ 40°C	56 min	-	- 6 max (W)	-	0.3 max	45 min	-
Spain	Decree 1485/1987	0.825- 0.860	Max 65% @ 250 Min 90% @ 350 Max FBP @ 380	4.5 max @ 37.8°C (W)	55 min	-1 max (W)	-8 max (W)	-	0.3 max	45 min	50 min
Sweden	SS15 5432	0.800-0.860	Min 10% @ 230 Min 90% @ 360	1.5-4.0 @ 40°C	40 min	-10 max (W)	-20 max (W)	-	0.3 max *0.2 mean*	45 min	45 min
Switzerland	SN181160/1	0.815-0.845	Min 90% @ 360	2.5 - 6.0	55 min	-6 max (W)	-15 max (W)	-15 max (W)	0.2 max	48 min	48 min
Turkey	TSE	0.850 max	Min 90% @ 363 FBP 391 max	1.0-6.0 @ 37.8°C	52 min	-	-	Report	1.0 max	50 * min *Diesel Index	-
U.K.	BS 2869	0.835-0.865	Min 50% @ 310 Min 85% @ 350	2.5-5.0 @ 40°C	56 min	-	-15 max (W)	-	0.3 max	46 min	48 min
W.Germany	DIN 51601	0.820-0.860	Max 65% @ 250 Min 85% @ 350	2.0 - 8.0	56 min	-	-15 max (W)	-	0.2 max	-	45 min
Yugoslavia	JUS B.H2.410	0.810-0.860	Min 90% @ 360	1.8-9.0	55 min	-	-9 max (W)	-	1.0 max	-	45 min

N. B. (W) is Winter

Ethyl Diesel Fuel Survey Winter 1986/87

	ASTM D1298	ASTM D445	ASTM D1319	ASTM D4294	ASTM D1319	ASTM D2274	Pad Test	ASTM D976	ASTM D613
Austria									
Code No.	*Density*	*KV @ 20°C*	*% Aromatics*	*% Olefins*	*% Sulphur*	*Oxidn. Stab*	*Thermal Stab*	*CI*	*CN*
001	0.8260	3.68	19.1	0.2	0.12	1.0	-	52.4	52.0
Belgium									
Code No.	*Density*	*KV @ 20°C*	*% Aromatics*	*% Olefins*	*% Sulphur*	*Oxidn. Stab*	*Thermal Stab*	*CI*	*CN*
002	0.8488	3.89	35.3	0.2	0.24	1.0	-	48.6	49.0
003	0.8466	5.19	42.6	4.7	0.24	1.0	-	51.0	50.2
Denmark									
Code No.	*Density*	*KV @ 20°C*	*% Aromatics*	*% Olefins*	*% Sulphur*	*Oxidn. Stab*	*Thermal Stab*	*CI*	*CN*
004	0.8387	4.05	26.8	0.4	0.22	1.6	-	49.9	53.4
005	0.8530	4.48	32.1	0.4	0.13	1.0	-	46.7	47.5
Finland									
Code No.	*Density*	*KV @ 20°C*	*% Aromatics*	*% Olefins*	*% Sulphur*	*Oxidn. Stab*	*Thermal Stab*	*CI*	*CN*
006	0.8410	3.77	35.3	0.7	0.13	1.0	-	48.4	49.7
051	0.8356	3.42	30.5	0.4	0.17	1.0	-	48.0	48.0
France									
Code No.	*Density*	*KV @ 20°C*	*% Aromatics*	*% Olefins*	*% Sulphur*	*Oxidn. Stab*	*Thermal Stab*	*CI*	*CN*
007	0.8328	3.83	27.8	0.4	0.27	1.0	-	52.4	51.9
008	0.8434	4.36	29.4	0.4	0.30	1.0	-	49.9	50.0
009	0.8372	4.82	30.1	4.2	0.27	1.4	-	54.3	56.2
010	0.8364	4.24	30.7	0.4	0.30	1.0	-	53.2	53.4
011	0.8469	5.28	33.9	0.4	0.28	1.4	7	51.0	52.5
012	0.8380	4.60	30.5	0.4	0.28	2.2	-	52.1	50.0

Greece

Code No.	Density	KV @ 20°C	% Aromatics	% Olefins	% Sulphur	Oxidn. Stab	Thermal Stab	CI	CN
013	0.8423	5.19	32.1	0.4	0.48	2.0	16	52.8	51.2
014	0.8371	4.66	29.6	0.4	0.32	2.0	17	52.8	53.8

Italy

Code No.	Density	KV @ 20°C	% Aromatics	% Olefins	% Sulphur	Oxidn. Stab	Thermal Stab	CI	CN
015	0.8472	5.39	41.5	0.4	0.28	1.8	16	52.3	50.6
016	0.8180	3.03	21.5	0.2	0.26	1.4	-	54.7	53.8
017	0.8493	5.20	41.1	0.4	0.27	2.0	5	50.2	49.4
018	0.8450	5.49	41.9	0.4	0.29	1.8	4	52.9	52.0
019	0.8262	3.98	24.7	0.5	0.30	1.4	-	56.5	55.5

Netherlands

Code No.	Density	KV @ 20°C	% Aromatics	% Olefins	% Sulphur	Oxidn. Stab	Thermal Stab	CI	CN
020	0.8337	3.90	26.5	0.4	0.23	0.8	-	54.4	53.7
021	0.8283	3.75	25.9	0.4	0.17	-	53.1	54.1	
022	0.8264	3.93	23.0	0.4	0.23	0.8	-	55.1	54.4
023	0.8313	3.47	33.1	0.4	0.07	1.2	-	50.8	51.4
024	0.8456	4.22	26.7	0.4	0.18	1.2	-	45.1	45.3

Norway

Code No.	Density	KV @ 20°C	% Aromatics	% Olefins	% Sulphur	Oxidn. Stab	Thermal Stab	CI	CN
025	0.8336	3.34	28.8	0.5	0.29	1.2	-	50.9	49.2
026	0.8247	2.69	19.5	0.5	0.10	1.0	-	47.8	49.0
027	0.8276	3.19	22.9	0.4	0.10	1.0	-	50.5	50.4

Portugal

Code No.	Density	KV @ 20°C	% Aromatics	% Olefins	% Sulphur	Oxidn. Stab	Thermal Stab	CI	CN
028	0.8438	7.02	33.8	0.4	0.46	1.6	-	54.2	54.6

Spain

Code No.	Density	KV @ 20°C	% Aromatics	% Olefins	% Sulphur	Oxidn. Stab	Thermal Stab	CI	CN
029	0.8491	4.80	36.7	0.4	0.31	2.8	18	49.2	49.6
030	0.8290	4.16	25.4	0.4	0.45	3.4	3	54.4	53.9
031	0.8447	5.20	27.9	0.4	0.38	0.8	-	51.6	52.4
032	0.8483	4.94	28.9	0.4	0.35	1.6	-	49.2	50.0

Sweden

Code No.	Density	KV @ 20°C	% Aromatics	% Olefins	% Sulphur	Oxidn. Stab	Thermal Stab	CI	CN
033	0.8338	4.04	27.9	0.4	0.16	1.3	-	53.1	53.8
034	0.8305	3.10	22.0	0.4	0.19	0.8	-	48.5	49.0
035	0.8352	3.47	24.3	0.4	0.23	1.5	-	49.5	49.4

United Kingdom

Code No.	Density	KV @ 20°C	% Aromatics	% Olefins	s% Sulphur	Oxidn. Stab	Thermal Stab	CI	CN
036	0.8438	4.77	27.7	0.4	0.15	2.4	-	50.9	51.9
037	0.8476	4.98	29.2	0.4	0.23	0.8	-	50.1	50.1
038	0.8457	4.74	28.8	0.4	0.09	0.8	-	50.4	50.9
039	0.8484	5.67	31.8	0.4	0.20	0.8	-	52.5	53.6
040	0.8370	4.44	28.2	0.4	0.19	2.3	11	52.2	52.2
041	0.8449	5.00	30.0	1.9	0.18	0.8	-	52.2	52.6
042	0.8412	4.73	28.4	0.4	0.21	1.5	-	52.5	53.6
043	0.8494	5.64	31.0	0.4	0.27	1.0	-	50.9	50.7
044	0.8428	4.51	30.0	0.4	0.22	0.8	-	50.2	50.5

W. Germany

Code No.	Density	KV @ 20°C	% Aromatics	% Olefins	% Sulphur	Oxidn. Stab	Thermal Stab	CI	CN
045	0.8336	3.83	25.5	0.4	0.13	0.8	-	50.8	50.6
046	0.8392	3.84	29.6	0.4	0.24	0.8	-	46.8	46.7
047	0.8292	3.65	21.8	0.4	0.19	1.0	-	54.6	52.7
048	0.8273	3.63	21.3	0.4	0.25	2.0	20	52.8	51.3
049	0.8350	3.44	25.9	0.4	0.28	0.8	-	47.9	46.6
050	0.8259	3.35	21.6	0.4	0.17	0.8	-	51.7	52.9

Ethyl Diesel Fuel Survey Winter 1987/88

	ASTM D1298	ASTM D445	ASTM D1319	ASTM D4294	ASTM D1319	ASTM D2274	Pad Test	ASTM D976	ASTM D613
Austria									
Code No.	Density	KV @ 20°C	% Aromatics	% Olefins	% Sulphur	Oxidn. Stab	Thermal Stab	CI	CN
001	0.8377	4.09	27.8	1.3	0.17	0.9	4	49.7	49.1
Belgium									
Code No.	Density	KV @ 20°C	% Aromatics	% Olefins	% Sulphur	Oxidn. Stab	Thermal Stab	CI	CN
002	0.8390	4.38	36.2	0.9	0.21	0.9	9	51.7	51.7
003	0.8463	4.40	34.1	2.7	0.25	0.9	7	48.7	48.6
Denmark									
Code No.	Density	KV @ 20°C	% Aromatics	% Olefins	% Sulphur	Oxidn. Stab	Thermal Stab	CI	CN
004	0.8392	4.01	28.1	4.3	0.20	0.8	3	50.2	56.7
005	0.8565	5.06	39.3	1.5	0.17	0.8	14	47.2	44.9
Finland									
Code No.	Density	KV @ 20°C	% Aromatics	% Olefins	% Sulphur	Oxidn. Stab	Thermal Stab	CI	CN
006	0.8380	3.33	32.7	2.0	0.11	0.7	14	46.4	49.6
007	0.8397	3.34	34.3	1.8	0.13	12	46.3	49.8	
France									
Code No.	Density	KV @ 20°C	% Aromatics	% Olefins	% Sulphur	Oxidn. Stab	Thermal Stab	CI	CN
008	0.8335	3.48	30.3	0.4	0.28	0.9	7	50.0	48.5
009	0.8374	3.83	30.3	0.5	0.33	0.8	10	50.1	49.0
010	0.8287	3.83	26.5	0.7	0.26	0.9	10	54.3	51.6
011	0.8308	3.58	25.9	0.8	0.23	0.9	2	51.4	52.3
012	0.8395	4.35	32.5	1.3	0.32	0.7	8	51.4	50.4
013	0.8328	3.86	29.0	1.0	0.31	0.9	7	50.7	48.9

Greece

Code No.	Density	KV @ 20°C	% Aromatics	% Olefins	% Sulphur	Oxidn. Stab	Thermal Stab	CI	CN
014	0.8426	4.84	32.8	2.3	0.50	1.2	16	51.9	50.9
015	0.8418	5.87	33.7	0.8	0.29	0.8	3	54.7	53.5

Italy

Code No.	Density	KV @ 20°C	% Aromatics	% Olefins	% Sulphur	Oxidn. Stab	Thermal Stab	CI	CN
016	0.8415	4.82	39.1	1.3	0.25	4.3	14	51.9	49.3
017	0.8272	2.97	27.0	4.8	0.19	0.9	15	49.1	48.1
018	0.8499	5.62	52.1	4.8	0.30	0.9	14	51.7	48.7
019	0.8461	4.45	44.1	1.8	0.30	2.3	14	48.9	50.9
020	0.8362	5.20	32.8	0.8	0.29	2.6	14	55.4	55.7

Netherlands

Code No.	Density	KV @ 20°C	% Aromatics	% Olefins	% Sulphur	Oxidn. Stab	Thermal Stab	CI	CN
021	0.8474	4.32	34.4	1.1	0.27	1.0	2	49.9	51.4
022	0.8365	3.93	28.2	1.0	0.21	0.8	2	51.3	49.9
023	0.8281	4.15	30.1	3.8	0.26	0.8	3	53.4	52.9
024	0.8355	3.77	29.7	2.9	0.21	0.9	2	51.0	49.8
025	0.8403	4.17	32.7	2.2	0.28	0.9	3	50.7	53.1

Norway

Code No.	Density	KV @ 20°C	% Aromatics	% Olefins	% Sulphur	Oxidn. Stab	Thermal Stab	CI	CN
026	0.8454	3.80	31.4	1.6	0.17	0.8	6	46.7	47.0
027	0.8300	3.23	26.5	0.9	0.19	0.9	3	49.4	50.7
028	0.8384	3.56	34.0	0.6	0.13	0.8	7	49.0	48.9

Portugal

Code No.	Density	KV @ 20°C	% Aromatics	% Olefins	% Sulphur	Oxidn. Stab	Thermal Stab	CI	CN
029	0.8411	5.55	34.0	0.6	0.46	0.9	7	53.6	54.6

Spain

Code No.	Density	KV @ 20°C	% Aromatics	% Olefins	% Sulphur	Oxidn. Stab	Thermal Stab	CI	CN
030	0.8555	5.43	38.5	0.7	0.50	0.9	1	47.9	51.2
031	0.8411	4.54	35.8	2.1	0.49	1.2	1	51.2	52.4
032	0.8466	5.21	36.5	1.8	0.42	0.9	-	50.8	50.7
033	0.8590	5.80	49.8	2.1	0.42	0.7	- -	48.8	47.2

Sweden

Code No.	Density	KV @ 20°C	% Aromatics	% Olefins	% Sulphur	Oxidn. Stab	Thermal Stab	CI	CN
034	0.8282	3.22	25.6	1.0	0.19	0.8	8	50.6	52.0
035	0.8285	2.89	24.7	1.0	0.12	0.9	19	46.6	50.9
036	0.8411	3.50	33.6	1.1	0.19	0.8	14	46.9	48.8

Switzerland

Code No.	Density	KV @ 20°C	% Aromatics	% Olefins	% Sulphur	Oxidn. Stab	Thermal Stab	CI	CN
037	0.8297	3.35	26.2	1.0	0.16	0.7	10	51.1	49.9

United Kingdom

Code No.	Density	KV @ 20°C	% Aromatics	% Olefins	% Sulphur	Oxidn. Stab	Thermal Stab	CI	CN
038	0.8467	5.58	39.8	1.1	0.19	0.9	3	51.9	49.1
039	0.8494	4.54	35.9	0.7	0.22	1.8	12	48.3	49.6
040	0.8461	4.38	33.6	1.2	0.05	0.8	5	48.9	48.7
041	0.8510	5.55	38.6	1.5	0.23	0.9	2	51.3	50.9
042	0.8497	4.97	36.8	0.6	0.20	0.9	14	50.9	51.2
043	0.8434	4.82	29.6	1.4	0.23	0.8	3	51.5	51.7
044	0.8483	4.30	34.3	1.3	0.15	0.9	1	49.6	50.8
045	0.8418	4.41	31.3	1.3	0.24	0.8	5	52.0	50.1
046	0.8467	5.58	40.6	3.2	0.20	0.8	8	52.9	54.1

W.Germany

Code No.	Density	KV @ 20°C	% Aromatics	% Olefins	% Sulphur	Oxidn. Stab	Thermal Stab	CI	CN
047	0.8302	3.35	26.5	1.2	0.13	0.8	3	47.4	51.9
048	0.8337	3.54	32.8	1.4	0.26	0.8	3	49.4	50.1
049	0.8215	3.27	23.2	1.0	0.27	0.8	2	52.5	54.4
050	0.8232	3.34	23.7	1.6	0.26	0.9	3	50.8	54.0
051	0.8286	3.11	26.8	0.6	0.29	0.9	10	48.0	54.1
052	0.8287	3.25	26.2	1.9	0.13	0.7	3	49.1	53.5

Yugoslavia

Code No.	Density	KV @ 20°C	% Aromatics	% Olefins	% Sulphur	Oxidn. Stab	Thermal Stab	CI	CN
053	0.8338	4.27	29.1	1.5	0.65	0.9	3	52.7	53.6

Ethyl Diesel Fuel Survey Winter 1988/89

	ASTM D1298	ASTM D445	ASTM D1319	ASTM D4294	ASTM D1319	ASTM D2274	Pad Test	ASTM D976	ASTM D613
Austria									
Code No.	Density	KV @ 20°C	% Aromatics	% Olefins	% Sulphur	Oxidn. Stab	Thermal Stab	CI	CN
001	0.8426	4.42	29.7	4.6	0.14	0.8	2	50.5	53.8
Belgium									
Code No.	Density	KV @ 20°C	% Aromatics	% Olefins	% Sulphur	Oxidn. Stab	Thermal Stab	CI	CN
002	0.8429	4.51	32.5	5.6	0.17	0.5	6	51.4	50.6
003	0.8402	4.22	28.5	4.3	0.23	0.7	7	52.7	49.2
Denmark									
Code No.	Density	KV @ 20°C	% Aromatics	% Olefins	% Sulphur	Oxidn. Stab	Thermal Stab	CI	CN
004	0.8461	4.37	22.6	4.1	0.18	0.5	5	49.1	49.4
005	0.8437	4.21	26.6	1.5	0.17	0.6	4	50.2	48
006	0.8222	3.37	21.8	1.8	0.20	0.8	5	53.6	53.2
Finland									
Code No.	Density	KV @ 20°C	% Aromatics	% Olefins	% Sulphur	Oxidn. Stab	Thermal Stab	CI	CN
007	0.8379	3.30	30.3	0.7	0.07	0.4	2	47.2	50.1
008	0.8384	3.46	31.9	0.9	0.08	0.8	4	48.1	51
France									
Code No.	Density	KV @ 20°C	% Aromatics	% Olefins	% Sulphur	Oxidn. Stab	Thermal Stab	CI	CN
009	0.8365	3.91	28.4	4.4	0.26	0.1	4	53.0	51.7
010	0.8318	3.41	23.0	2.8	0.32	0.1	10	52.0	53.4
011	0.8346	3.80	28.0	3.6	0.19	0.4	3	52.8	51.8
012	0.8289	3.69	26.1	3.6	0.15	0.2	11	52.8	51.8
013	0.8276	3.59	21.0	5.4	0.35	0.6	2	54.7	54.7
014	0.8321	3.47	22.8	5.3	0.30	0.1	7	52.6	51.1

Greece

Code No.	Density	KV @ 20°C	% Aromatics	% Olefins	% Sulphur	Oxidn. Stab	Thermal Stab	CI	CN
015	0.8482	5.35	32.4	4.3	0.48	0.9	8	51.5	56.9
016	0.8278	4.50	17.8	3.8	0.21	1.5	12	57.1	56.9

Ireland

Code No.	Density	KV @ 20°C	% Aromatics	% Olefins	% Sulphur	Oxidn. Stab	Thermal Stab	CI	CN
017	0.8493	4.49	31.7	4.0	0.17	1.3	10	50.3	52.7

Italy

Code No.	Density	KV @ 20°C	% Aromatics	% Olefins	% Sulphur	Oxidn. Stab	Thermal Stab	CI	CN
018	0.8413	4.64	32.4	3.3	0.26	1.1	2	52.2	52.6
019	0.8255	3.64	20.8	8.4	0.25	2.7	16	55.0	53.1
020	0.8358	4.60	27.5	7.0	0.24	0.9	3	54.6	54.7
021	0.8289	3.91	21.7	5.3	0.26	0.7	9	55.7	55.3
022	0.8379	3.92	30.0	3.7	0.30	1.0	12	52.1	54.2

Netherlands

Code No.	Density	KV @ 20°C	% Aromatics	% Olefins	% Sulphur	Oxidn. Stab	Thermal Stab	CI	CN
023	0.8362	3.76	25.1	4.1	0.20	0.7	3	52.1	52.8
024	0.8268	3.63	22.5	3.1	0.16	0.5	2	54.3	52.9
025	0.8234	3.67	22.2	5.1	0.16	0.1	4	56.0	55.4
026	0.8368	3.54	31.0	4.4	0.14	0.9	3	52.3	52.2
027	0.8375	4.18	24.8	4.7	0.19	0.2	2	51.6	52.2

Norway

Code No.	Density	KV @ 20°C	% Aromatics	% Olefins	% Sulphur	Oxidn. Stab	Thermal Stab	CI	CN
028	0.8351	3.45	23.1	2.9	0.12	0.4	2	50.2	51.5
029	0.8283	3.15	20.8	2.6	0.10	0.8	2	47.8	51.6
030	0.8355	3.11	22.8	3.4	0.10	0.1	2	48.0	50.6

Portugal

Code No.	Density	KV @ 20°C	% Aromatics	% Olefins	% Sulphur	Oxidn. Stab	Thermal Stab	CI	CN
031	0.8379	5.51	28.6	4.4	0.49	0.2	2	54.6	56.9

Spain

Code No.	Density	KV @ 20°C	% Aromatics	% Olefins	% Sulphur	Oxidn. Stab	Thermal Stab	CI	CN
032	0.8429	4.77	26.2	2.8	0.41	0.1	2	51.0	54.3
033	0.8509	5.16	36.2	3.6	0.44	0.2	3	50.7	51.6
034	0.8567	4.98	33.5	5.7	0.45	0.7	11	47.5	53.9
035	0.8514	5.01	38.0	3.8	0.52	0.9	5	49.4	51.6
036	0.8463	5.30	35.6	5.0	0.44	1.2	2	51.6	52.8

Sweden

Code No.	Density	KV @ 20°C	% Aromatics	% Olefins	% Sulphur	Oxidn. Stab	Thermal Stab	CI	CN
037	0.8257	2.70	23.2	1.1	0.12	0.7	2	46.0	46.5
038	0.8295	3.15	26.8	1.1	0.09	0.6	2	48.0	48.8
039	0.8239	2.85	22.5	1.5	0.17	0.7	2	48.2	47.9

Switzerland

Code No.	Density	KV @ 20°C	% Aromatics	% Olefins	% Sulphur	Oxidn. Stab	Thermal Stab	CI	CN
040	0.8281	3.18	19.7	5.1	0.11	0.1	6	50.6	52.7

Turkey

Code No.	Density	KV @ 20°C	% Aromatics	% Olefins	% Sulphur	Oxidn. Stab	Thermal Stab	CI	CN
041	0.8391	4.27	26.6	3.7	0.72	0.4	3	53.7	53.7

United Kingdom

Code No.	Density	KV @ 20°C	% Aromatics	% Olefins	% Sulphur	Oxidn. Stab	Thermal Stab	CI	CN
042	0.8462	4.39	28.3	3.5	0.16	0.1	5	51.1	51.8
043	0.8408	4.21	28.1	3.1	0.18	0.5	4	48.7	51
044	0.8506	4.16	32.3	4.0	0.06	0.3	9	47.9	52.2
045	0.8453	4.52	27.7	4.5	0.20	0.1	2	51.6	53.3

United Kingdom (continued)

Code No.	Density	KV @ 20°C	% Aromatics	% Olefins	% Sulphur	Oxidn. Stab	Thermal Stab	CI	CN
046	0.8473	4.42	31.4	3.9	0.17	50.2	49.6		
047	0.8337	4.50	24.6	2.9	0.18	0.1	15	55.4	54.3
048	0.8403	4.18	27.5	3.8	0.16	0.1	3	52.7	55.4
049	0.8455	4.58	33.3	2.6	0.25	0.1	3	51.3	55.3
050	0.8453	4.34	32.4	3.5	0.17	0.1	11	49.4	51.6

West Germany

Code No.	Density	KV @ 20°C	% Aromatics	% Olefins	% Sulphur	Oxidn. Stab	Thermal Stab	CI	CN
051	0.8285	3.24	23.2	4.1	0.12	0.9	2	50.8	56.8
052	0.8238	3.02	19.7	4.4	0.17	0.1	3	49.7	52.4
053	0.8244	3.06	23.3	2.5	0.16	0.3	3	49.2	54.5
054	0.8232	3.01	19.7	6.8	0.16	0.2	3	49.4	53.1
055	0.8371	3.39	31.2	2.9	0.17	1.5	5	47.2	50.2
056	0.8287	3.45	20.3	4.0	0.10	0.3	3	51.4	53.1

Yugoslavia

Code No.	Density	KV @ 20°C	% Aromatics	% Olefins	% Sulphur	Oxidn. Stab	Thermal Stab	CI	CN
057	0.8440	4.64	31.8	5.7	0.90	0.5	8	56.3	53.6

THE CHEMISTRY OF SEDIMENT FORMATION IN AUSTRALIAN MIDDLE DISTILLATE FUELS

Joanna F Pedley , Ludek A Bersnek, Michael G O'Connell and Richard K Solly
Materials Research Laboratory, Defence Science and Technology Organisation PO Box 50, Ascot Vale, Victoria, Australia 3032.
* Visiting Scientist from Directorate of Quality Assurance/Technical Support, Fairmile, Cobham, Surrey KT11 1BJ, UK.

Introduction

In earlier publications it was suggested that the formation of insolubles during storage of an unstable UK middle distillate fuel was caused at least in part by reactions of the chemical species indoles, phenalenes and acids[1,2]. The purpose of this present study was to determine whether reactions involving these species contributed to the storage instability of middle distillate fuels from quite different sources and to investigate the extent of correlation between fuel chemical composition and observed fuel storage stability.

The reaction sequence previously proposed is illustrated schematically in figure 1. The oxidation of phenalene and its alkyl homologues to the corresponding phenalenone species has been shown to occur both in model systems[2] and in middle distillate fuels containing light cycle oils[3]. The formation of indolylphenalenes, indolylphenalenones and 'indolylphenalene/acid salts' by acid promoted reactions of indoles and phenalenones has also been demonstrated by the isolation of these species both from model systems and from unstable fuel containing light cycle oil[2,4,5]. The role of acid in these reactions is not clearly understood. However it is known that at least catalytic amounts of acid are required for indoles to react with phenalenones[4] and there is some evidence to suggest that acids become incorporated into the most polar components of insoluble fuel degradation products[6].

The signficance of this chemistry with respect to the stability of middle distillate fuels produced in Australian refineries has been investigated. The concentrations of phenalenone and alkylindoles were determined before and after storage of fuel samples for 13 weeks at 43C. Insoluble fuel degradation products were analysed by thin layer chromatography and compared with insolubles formed by degradation of fuels from UK sources.

Experimental

Fuel samples were supplied directly from Australian oil refineries and generally consisted of one of five refinery stream types; straight run distillate (SRD), light cycle oil (LCO), hydrotreated light cycle oil (HT-LCO), hydrotreatment unit feed (LCO/SRD) or hydrotreatment unit product (HT-LCO/SRD). The samples from each refinery were combined to produce 12 blends containing 70% straight run distillate and 30% cracked components. The blend compositions are listed in table 1. Aliquots of both blended and unblended components were stored at -12C to minimise degradation before testing and analysis.

The stability of the blends was assessed by storage of 1 litre aliquots of fuel at 43C for 13 weeks, following the method detailed in ASTM D4625. Tests were carried out in duplicate. Filterable insolubles were determined using glass fibre filters (Millipore AP40). Adherent insolubles were determined by hotplate evaporation of gum solvent washings contained in disposable aluminium dishes. The chemical nature of insolubles formed during the storage tests was assessed using thin layer chromatography (silica gel stationary phase, 10% methanol in dichloromethane mobile phase). The concentration of phenalenone was determined using normal phase HPLC with UV detection at 384nm[7]. The

detection limit for phenalenone was 0.5umol/l with repeatability of +/- 10%. The relative concentrations and distributions of alkylindoles were determined by a procedure which involved fractionation of fuel samples over silica gel, followed by addition of an internal standard (1-methylindole) and finally GC analysis with nitrogen specific detection.

GC peaks corresponding to alkylindoles were identified by reference to the published literature[8,9]. The relative concentration of alkylindoles in the fuel blends was calculated by assuming an equal detector response for all isomers and homologues. This method can also be used to determine the distribution and concentration of carbazole and its alkyl homologues.

Results and Discussion

The stability of the 12 fuel blends was assessed by storage at 43C for 13 weeks. This test is widely believed to provide a realistic acceleration of degradation processes which occur at temperatures typically encountered in fuel storage facilities[10]. The relatively mild test conditions are considered to be approximately equivalent to one year of fuel storage at 18C to 24C. The results of this test are given in table 1. The filterable and adherent insolubles, produced during the storage period by all but the most stable fuels (samples 8,10,12,14), were analysed by thin layer chromatography and compared with insolubles produced during storage of unstable UK fuel. The isolation and characterisation of the UK insolubles has been described previously[11,12]. The chromatographic characteristics of the UK and Australian insolubles (both filterable and adherent) were found to be very similar. Subtle differences were noted amongst the most polar sediment components, but the degree of variation was within that previously observed for insolubles from different UK sources. Whilst not conclusive in itself, the similar characteristics of these fuel degradation products provided a positive indication that they may have been formed by common chemical processes.

The effect of chemical composition on observed fuel stability was addressed specifically in terms of the concentration of species highlighted in figure 1. According to this reaction scheme, unstable fuels would be expected to initially contain both phenalenes and indoles, with the concentration of phenalenones, indolylphenalenes and further reaction products (including insolubles) increasing with time. The acidic species required to promote these reactions may be present initially or may be produced during fuel storage. Stable fuels would be characterised by the absence of one or more of these chemical species.

In order to test this line of reasoning, specific chemical analysis was carried out on the fuel blends before and after thermal stress. The initial presence and subsequent reduction in concentration of phenalenes could have been determined in one of two ways; either directly, using reversed phase HPLC with electrochemical detection[7], or indirectly by determination of increasing phenalenone concentration using normal phase HPLC with UV detection. For simplicity of analysis, the latter approach was adopted in this study, with measurements being carried out before storage, after storage for 16 hours at 100C (to provide an initial indication of phenalene/phenalenone content) and after storage for 13 weeks at 43C. The results quoted in table 2 relate only to the concentration of the single species phenalenone. The total concentration of phenalenone species (alkyl- and benz- derivatives) in the fuels samples would of course have been higher. In addition it should be noted that the measured concentration of phenalenone was consistently lower than the initial concentration of phenalene. Previous work has shown that phenalene is not quantitatively converted to phenalenone[2]. The total concentration of alkylindoles was determined in a limited number of the fuel samples before and after the 13 week storage test. The results of these measurements are given in

table 3. The remaining key species highlighted in the reaction scheme, namely acids, were not determined in this study.

The results of the storage tests, given in table 1, showed that the fuels tested covered a wide range of stability.

Four fuels (samples 8,10,12,14) proved to be extremely stable, all producing less than 1mg/l of total insolubles and not darkening in colour beyond 1.5 ASTM D1500 colour units. None of these fuels formed significant quantities of phenalenone during storage, indicating the virtual if not complete absence of phenalene species. The concentrations of alkylindoles in two of these samples were determined. Sample 8 initially contained alkylindoles at a concentration equivalent to 0.19mmols of 1-methylindole, and no significant reduction in concentration was observed during the storage period. The concentration of alkylindoles in sample 10 was an order of magnitude lower than in sample 8, essentially at the detection limit of the method. Again no significant change in concentration was detected during the storage period. The behaviour of these fuels was therefore entirely consistent with the reaction scheme illustrated in figure 1, ie. stable fuels characterised by the absence of one or more of the key reactive species, phenalenes in the case of sample 8 and both phenalenes and indoles in the case of sample 10.

The four very stable fuels (8,10,12,14) all contained hydrotreated light cycle oil blending components. The beneficial effect of hydrotreatment on fuel stability is well known. This improvement in stability on hydrotreatment was clearly shown by the storage test results for the matched fuel pairs 7/8, 9/10, 11/12 and 13/14, where in each case the first sample contained light cycle oil and the second sample contained hydrotreated light cycle oil. The effect of hydrotreatment on the chemical composition of the fuel samples was also consistent with the observed improvement in stability. All the light cycle oil samples produced phenalenone during thermal stress, indicating the initial presence of phenalene species. However these species were removed during hydrotreatment to produce the stable 'phenalene free' fuels discussed previously. The effect of hydrotreatment on the initial alkylindole concentration was found to be variable. The light cycle oil samples all contained alkylindoles. There was no significant reduction in the initial concentration after hydrotreatment for sample pair 7/8, but a 25 fold reduction was noted for sample pair 9/10, indicating the use of much more severe hydrotreatment conditions.

The remaining fuel which contained hydrotreated light cycle oil was sample 16. Despite the hydrotreatment, this fuel was found to be moderately unstable, producing about 8mg/l total insolubles and darkening significantly in colour during the storage period. It produced low but significant levels of phenalenone during storage, thus indicating the initial presence of phenalene species. The alkylindole content of this fuel was not determined. However it is reasonable to asssume that alkylindoles were present, since high levels of alkylindoles were detected in fuel containing light cycle oil from the same refinery (sample 15) and it is unlikely that hydrotreatment conditions which left low levels of phenalene species would significantly reduce the concentration of alkylindoles. In addition, the insolubles produced during degradation of both samples 15 and 16 were clearly shown by TLC to be of the same type as those produced by fuels thought to follow the chemistry outlined in figure 1, which of course requires the presence of alkyindoles.

Other fuels which were found to be of similar stability to sample 16, producing 5 to 12mg/l total insolubles, were samples 6, 7 and 13. All these fuels contained light cycle oil and initially contained alkylindoles and phenalene species. The initial concentration of alkylindoles in sample 13 could not be measured because the fuel contained a high level of 'unidentified' nitrogen compounds which co-eluted and effectively masked the presence of alkylindoles. This was the only sample examined which contained these compounds. Further work is required in order to identify these species and investigate their

significance. The initial presence of phenalene species in samples 6, 7, 13 and 16 was indicated by formation of significant amounts of phenalenone (more than 5μmol/l) after stress of the fuels at 100C for 16 hours with the measured level increasing further during the 13 week storage period. The amount of phenalenone present at the end of the 13 week storage test ranged from 10μmol/l for sample 16 to 230μmol/l for sample 6. This variation, which presumably also reflected differences in initial phenalenes concentration, clearly demonstrated that the degree of fuel instability cannot necessarily be extrapolated simply from the level of phenalene species. Indeed it is also worthwhile noting that the quantity of phenalene species and alkylindole species estimated to be present in fuel insolubles was always small in comparison to amounts potentially available in fuel solution. For example sample 15 produced aproximately 56mg/l of sediment but at the end of the storage period it still contained about 95mg/l alkylindoles and 35mg/l phenalenone (total phenalenones concentration would be several times this level). This observation tended to support previous conclusions that, given the presence of indoles and phenalenes, the amount of insolubles formed during storage is limited by acid concentration[6].

The fuels which proved to be the most unstable during the the 13 week storage period were samples 5, 9, 11 (each producing about 18mg/l total insolubles) and sample 15 (producing about 56mg/l total insolubles). Chemical analysis of these samples indicated the presence of comparatively high levels of phenalene species and alkylindoles, consistent with their observed instability. Examination of the individual SRD and LCO components used in blending of samples 5, 9 and 15 showed as expected that phenalene species and alkylindoles originated entirely from the LCO components.

Significant reductions, >0.05mmol/l, in the overall concentration of alkyindoles were noted for the unstable fuel samples 5, 6, 7, 9 and 15 (concentration changes for the other two unstable fuels, samples 11 and 13 were not determined), thus providing strong evidence for reaction of alkylindoles during fuel storage. These changes represented reductions of between about 20% and 60% of the total initial alkylindoles concentration. The largest proportionate decrease was noted for the most unstable fuel, sample 15, and the smallest decrease for the most stable of these fuels, sample 7. Detailed examination of chromatograms showing the distribution of indoles in these aged fuel samples revealed that in all cases the concentration of certain isomers and homologues had decreased more than others. Figure 2 shows the chromatographic distribution of alkykindoles in sample 15 before and after aging. Very similar profiles were obtained for samples 5, 6, 7 and 9. Dorbon and Bernasconi[9] have also recently noted that the distribution of alkylindoles in light cycle oils changes during aging at 43C. In all cases the decrease in alkylindoles concentration during aging was greater than the quantity of these species estimated to have been incorporated into the insolubles collected at the end of the storage period. The amount of alkylindoles unaccounted for ranged from 3 to 10 times the amount estimated to be contained in the insolubles. The shortfall was probably associated with involatile but soluble fuel degradation products, such as for example the 'sediment precursor' compounds, indolylphenalenes, referred to in previous publications[1,2]. Soluble fuel degradation products of this type almost certainly contribute to 'fuel soluble gum' which may lead to deposits on hot engine and fuel system components.

Summary and Conclusions

The thin layer chromatographic characteristics of insolubles formed during storage of unstable middle distillate fuels from Australian refineries were found to be very similar to those of insolubles produced by the degradation of unstable fuel from UK sources, indicating that they may have been formed by similar chemical processes. All fuels which subsequently proved to be unstable during storage initially contained both alkylindole and phenalene species. Stable fuels were characterised by the absence of one or both of these

compound types. Phenalenes were either removed entirely or their concentration significantly reduced by hydrotreatment, which had the expected effect of improving fuel stability. In one case the initial concentration of alkylindoles was significantly reduced by hydrotreatment, but in all other cases no concentration change was noted. The reactivity of alkylindoles in unstable fuels was demonstrated by reductions in their overall concentration during fuel storage. In line with previous reports[7], the distribution of alkylindole isomers and homologues was observed to change during fuel storage, indicating differences in reactivity amongst the species. Whilst the results of this study show that the absolute amount of insolubles formed during a storage period cannot be correlated directly with the concentration of alkylindole and phenalene species, it is clear that the stable fuels were characterised by the absence of one or both of these species and that both species were present in all the unstable fuels. These results therefore illustrate the potential for application of chemical methods to differentiate between stable and unstable fuels. However other factors clearly need to be considered when assessing the degree of fuel instability. From a chemical viewpoint, fuel acidity and fuel acidity potential are known to be important. Further work is required to identify the nature of acids in middle distillate fuels and to clarify their role in fuel degradation. In addition, physical parameters such as the solubility of fuel degradation products also need to be considered, particularly when fuel stability is assessed simply in terms of the weight of insolubles formed during fuel storage.

References

1. Pedley JF, Hiley RW and Hancock RA; Storage stability of petroleum derived diesel fuel. 3. Identification of compounds involved in sediment formation. FUEL, 1988, Vol 67, p.1124.
2. Pedley JF and Hiley RW; Synthesis of sediment precursor compounds and simulation of sediment formation in cracked gas oil using model systems. Proc. 3rd International Conference on Stability and Handling of Liquid Fuels, London UK 1988 p.510
3. Marshman SJ and David P; Storage stability of distillate diesel fuels: Changes in phenalene and phenalenone concentrations during long term ambient storage. This Conference.
4. Pedley JF; Internal Ministry of Defence report, August 1989.
5. Dolman DM and Hancock RA; Internal Ministry of Defence report, March 1990.
6. Hiley RW and Pedley JF; Storage stability of petroleum derived diesel fuel. 2. The effect of sulphonic acids on the stability of diesel fuels and a diesel fuel extract. FUEL, 1988, Vol 67, p.469.
7. Marshman SJ; Determination of phenalenes in distillate diesel fuels using high pressure liquid chromatography; Liquid chromatographic determination of phenalenones in middle distillate fuels. Submitted for publication in Analytical Chemistry.
8. Pedley JF; The chemistry of sediment formation during the storage of diesel fuel. PhD Thesis, University of London, April 1988.
9. Dorbon M and Bernasconi C; Nitrogen compounds in light cycle oils: Identification and consequences of aging. FUEL, 1989, Vol 68, p.1067.
10. Stavinoha LL and Westbrook SR; Accelerated stability test techniques for middle distillate fuels. ASTM STP 751 (Ed. C Henry) 1981, p.3.
11. Pedley JF and Hiley RW; Formation of insolubles during storage of Naval fuels. Proc. 2nd International Conference on Long-Term Storage Stabilities of Liquid Fuels. San Antonio USA 1986, p.570
12. Pedley JF and Hiley RW; Investigation of sediment precursors present in cracked gas oil. Proc. 3rd International Conference on Stability and Handling of Liquid Fuels, London UK, 1988, p.495.

Copyright
©
Controller HMSO London
1990

Table 1. Results of fuel storage at 43 C for 13 weeks

Sample number	Sample type *	Initial colour	Final colour	Filtered insolubles mg/l	Adherent insolubles mg/l	Total insolubles mg/l
5	A(i)	0.5	4.0	9.9	8.0	17.9
		0.5	4.0	10.7	7.1	17.8
6	B(i)	1.0	4.5	4.7	7.0	11.7
		1.0	4.5	4.6	7.2	11.8
7	B(iii)	1.0	3.0	3.9	1.8	5.7
		1.0	3.0	3.0	1.9	4.9
8	B(iv)	0.5	<1.5	<0.1	0.1	0.1
		0.5	<1.5	0.3	0.4	0.7
9	C(i)a	<1.0	4.5	9.8	8.6	18.4
		<1.0	4.5	9.7	9.9	19.6
10	C(ii)a	0.0	0.5	0.2	0.2	0.4
		0.0	0.5	0.3	0.5	0.8
11	C(i)b	<1.0	<4.0	3.8	14.8	18.6
		<1.0	<4.0	2.5	15.0	17.5
12	C(ii)b	0.0	<0.5	0.8	<0.1	0.8
		0.0	<0.5	0.2	0.6	0.8
13	D(i)	<1.0	<3.0	2.0	7.4	9.4
		<1.0	<3.0	0.8	7.8	8.6
14	D(ii)	1.0	<1.5	1.0	<0.1	1.0
		1.0	<1.5	0.6	<0.1	0.6
15	E(i)	1.5	<7.5	23.4	33.2	56.6
		1.5	<7.5	23.4	32.4	55.8
16	E(ii)	2.5	<4.5	2.5	4.9	7.4
		2.5	<4.5	3.3	5.0	8.3

* X Refinery Code
(i) 30% LCO in SRD
(ii) 30% HT-LCO in SRD
(iii) 30% LCO/SRD in SRD
(iv) 30% HT-LCO/SRD in SRD

Table 2. Results of phenalenone measurements

Sample number	Phenalenone content µmol/l		
	(A) Initial	(B) After 16hrs @ 100 C	(C) After 13wks @ 43 C
5	4.4	42.0	150.1
6	12.7	87.8	230.8
7	6.1	30.7	52.6
8	ND	3.2	2.2
9	8.9	44.2	175.2
10	ND	2.0	ND
11	9.4	37.9	162.3
12	ND	ND	ND
13	ND	6.6	48.8
14	ND	ND	ND
15	15.6	107.2	193.8
16	ND	8.1	10.7

ND = not detected

Table 3. Results of indoles measurements

Sample number	Total indole content (mmol/l equivalent of 1-methylindole)		
	• (A) Initial	(B) After 13wks @ 43 C	$(\bar{A} - \bar{B})$
5	0.32	0.18 +/-0.02	0.14 +/-0.02
6	0.70 +/-0.05	0.39 +/-0.01	0.31 +/-0.06
7	0.23 +/-0.01	0.18 +/-0.00	0.05 +/-0.01
8	0.19 +/-0.05	0.17	insignificant
9	0.50 +/-0.02	0.25 +/-0.01	0.25 +/-0.03
10	0.02 +/-0.01	0.01 +/-0.00	insignificant
13	**	0.06 +/-0.00	
15	1.25 +/- 0.02	0.52 +/-0.03	0.73 +/-0.05

* Average of duplicate results

** Initial alkylindole concentration could not be determined because of interference from 'unidentified' nitrogen compounds

Figure 1. SEQUENCE OF REACTIONS LEADING TO DIESEL FUEL DEGRADATION

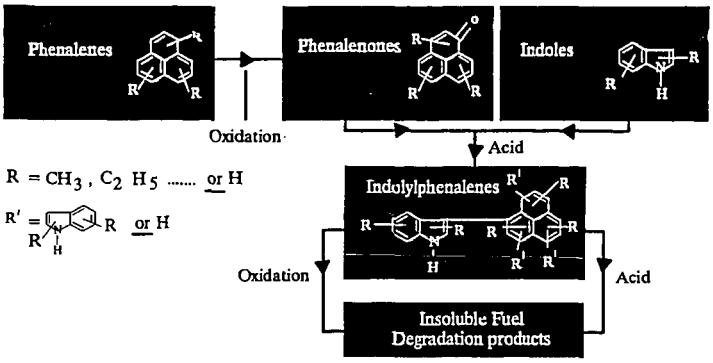

Figure 2. Chromatographic distribution of indoles in fuel sample 15.
GC conditions: 30°C to 280°C at 4°C per minute

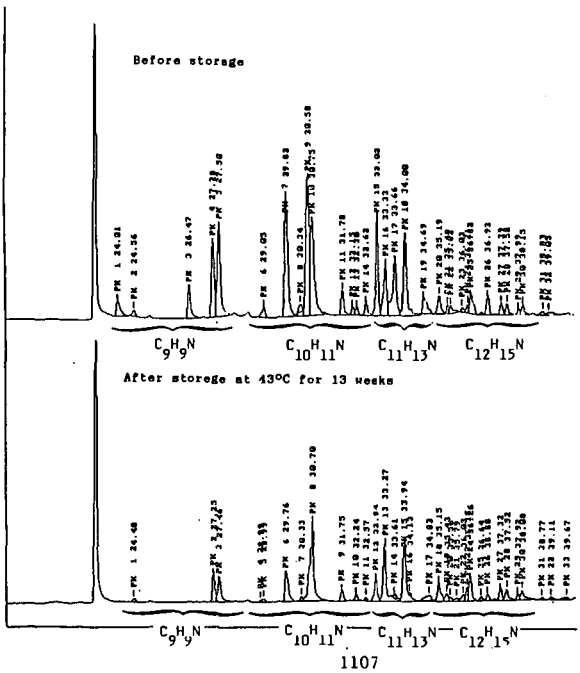

STORAGE STABILITY OF DISTILLATE DIESEL FUELS: CHANGES IN PHENALENE AND PHENALENONE CONCENTRATIONS DURING LONG TERM AMBIENT STORAGE

Sheila J Marshman, Peter David*
DQA/TS, Fairmile, Cobham, Surrey, KT11 1BJ, UK
*BP Research Centre, Chertsey Road, Sunbury-on-Thames, Middx, TW16 7LN, UK

INTRODUCTION

Unstable distillate fuels can degrade during storage forming insoluble sediment and darkening in colour. Pedley, Hiley and Hancock[1,2] have proposed a reaction mechanism to account for the production of the majority of the sediment, in which indoles react with phenalenones to form soluble sediment precursors (indolylphenalenes and indolylphenalenones) which in turn react with acids to form sediment. The chemistry is complex; a simplified mechanism is shown in Figure 1.

Methods of analysis have been developed to quantify phenalenes and phenalenones directly in fuels to low ppm levels[3,4]. Application of these methods to a number of fuels has shown that phenalenes and phenalenones are not present in stable straight run fuels, but are present in a number of cracked fuels. The total concentration of phenalenes and phenalenones may be as high as 0.1%, although blends containing cracked stocks generally exhibit much lower concentrations.

Previous trials[5] have shown that the phenalenes content of an unstable catalytically cracked stock diminished from approximately 0.1% to zero over a period of a year, while the phenalenones content increased. From these trials it became apparent that neither the phenalenes/phenalenones nor indoles contents were necessarily the limiting factors in sediment production. However the trials gave no information on the rate of depletion of the phenalenes, the rate of increase of the phenalenones or the relationship of the concentrations of these species to the production of sediment.

This paper describes the changes in phenalene and phenalenone concentrations of an unstable fuel blend with time, and examines any correlation between these concentrations, sediment levels and colour.

EXPERIMENTAL

A research blend consisting of 50% fresh catalytically cracked gas oil and 50% fresh straight run gas oil (both from North Sea crude stocks) was subjected to long term storage at ambient temperatures in 50 litre vented non-lacquer lined mild steel drums, and sub-sampled for compositional data.
The stability of the blend was assessed initially using ASTM D2274, ASTM D525/D381 modified (16 hours at 100°C in oxygen), an in-house method (3 days at 80°C) and also using ASTM D4625 (storage for 16 weeks at 43°C). The sediment in the latter tests was measured at 4 weekly intervals.
The phenalenes and phenalenones concentrations of the blend were monitored using chromatographic methods[3,4]. The phenalenes were determined using reverse phase HPLC with electrochemical detection to selectively quantify the phenalene species. Phenalenones were measured using normal phase HPLC selectively detecting these compounds by UV absorbance at 400nm. Filterable sediment levels and colour (ASTM D1500) were also monitored at intervals.

RESULTS AND DISCUSSION

Accelerated storage tests.

Results from the ASTM D2274 tests imply that the fuel blend was stable, with <0.1 mg/100ml total insolubles formed during the ageing period (Table 1). Similar results were obtained from the in-house method (3 days at 80°C). Very high levels of gum were predicted by ASTM D525/D381. These tests were therefore considered unsuitable for predicting storage stability. The results of the ASTM D4625 test indicate that the fuel produced <2mg/100ml insolubles during the first four week period but thereafter there was a rapid increase to about 12 mg/100ml after 16 weeks (Fig 2, Table 1).

Ambient storage

Filtered sediment

There appears to have been an induction period of between 16 and 20 weeks during which sediment formation was less than 2mg/100ml. Thereafter there was a rapid increase in sediment in the fuel, rising to about 17mg/100ml after 50 weeks storage (Fig 3, Table 2).

An attempt was made to relate the sediment formed in the ambient drum storage to levels predicted in the ASTM D4625 tests. It has been assumed that 1 week at 43°C is equivalent to 4 weeks storage under ambient conditions. The data show (Table 2) that within the precision of the test procedures, there is some correlation, particularly up to 40 weeks storage. Thereafter, sediment increased at a faster rate in the drum storage and after 50 weeks storage, the level of sediment was greater by a factor of 2 over predicted levels. Although absolute levels of sediment were not predicted accurately, the figures indicated the overall likely stability of the blend.

Phenalenes concentration changes

The initial concentration of phenalenes (phenalene and its alkyl homologues) in the untreated blend was high at 850 mgl^{-1}. The phenalenes concentrations diminished with time and were still present at about 100 mgl^{-1} after one year's storage (Table 3, Figure 4). The results indicate that the oxidation of the phenalenes approximates to a pseudo-first order reaction in the fuel (Figure 5). This conclusion should be treated with caution, however, as the exact mechanism of phenalene oxidation has not yet been established. The phenalenyl radical has been observed in diesel fuels[7,12] and is probably involved in the reaction mechanism in hydrocarbon fuels. It has not yet been established whether phenalenones are produced directly from the radical, or whether further intermediates, such as the hydroxyphenalenes, could also be involved. Phenalenes are also produced as a byproduct of the condensation reaction producing indolylphenalenes and indolylphenalenones[8], thus continually modifying the phenalenes concentration with time. The related compound benzanthracene was initially present at 100mgl^{-1} (the homologues of this compound were not quantified), and although not quantified throughout the storage period, appeared to diminish in a similar way to the phenalenes.

The phenalene homologues exhibited a similar distribution to that seen in other fuels containing 'fresh' catalytically cracked stock, namely that the major constituents were the monomethylphenalenes (about 50% of the initial total phenalene content), followed by the dimethyl or ethyl substituted phenalenes, at about 40%. Phenalene itself comprised only a small proportion of the total phenalene content - approximately 12% (Table 3).

Phenalenones concentration changes

The phenalenones concentrations were initially low at 15mgl^{-1} total phenalenones, with phenalenone itself the major constituent (Table 4). The general pattern of phenalenones distribution previously observed in other fuels was noted in this blend and was consistent throughout the storage period: phenalenone as the major constituent, approximately 40% of the total phenalenones concentration, followed by the 2-, 5-, and 8-methyl derivatives at about 30% to 50% of the phenalenone concentration, and the remaining methyl homologues at low concentrations. The concentration of 9-methylphenalenone remained at trace levels only, 2mgl^{-1} being the highest concentration recorded. The dimethyl or ethylphenalenones and higher homologues were not quantified. However, there are no large peaks in the phenalenone chromatogram unaccounted for. It may therefore be reasonably assumed that unless the dimethyl homologues have considerably lower absorbances at 400nm than phenalenone, these compounds are not a major proportion of the total phenalenones found in fuels. The related benzanthrones were present at all times at considerably lower concentrations than the phenalenones (Table 4), with benzanthrone the major constituent.

There appeared to be an induction period of two to three weeks where the ketones concentrations remained static, after which the concentrations gradually increased. After about 13 weeks the total phenalenones concentrations increased markedly before beginning to plateau out (Figure 6). The benzanthrones acted in a similar fashion. It is interesting to note that the concentration of 2-methylphenalenone was initially very similar to that of the 5- and 8-methyl homologues, but with time the 2-methylphenalenone content increased at a faster rate than its isomers (Figure 7). After a year the concentration of the 2-methylphenalenone was approximately double that of the 5- and 8- substituted isomers. This reflects model compound studies[9] where 2-methylphenalenone was found not to react with indoles in acid conditions.

The concentrations of phenalenone and the methylphenalenones always appeared less than the initial concentrations of phenalene and monomethylphenalenes respectively. As with previous model studies[9], the mass balance for the phenalene species is difficult to reconcile, only approximately 50% of the initial phenalenes being accounted for from the measurement of phenalene, phenalenones and sediment (estimating the contribution from phenalene species in the sediment to be about 35% of the mass). Known products include phenalenones, indolylphenalenes and indolylphenalenones, and salts of these products which comprise a large proportion of the sediment. Phenalanones[11] may also be produced during the reaction with indoles which would in part account for the discrepancy.

Colour and sediment changes

The data indicate a gradual deterioration in colour during the first 20 weeks of storage followed by a period of little change (Table 2, Figure 8). There appears to be a correlation between colour and phenalenones concentrations. The relationship appears to be linear from the available data (Figure 9). The increase in concentration of the coloured ketones with time would contribute to the darkening of fuel during storage and to the formation of the fuel-soluble sediment precursors. The darkening in colour is believed to be more attributable to the formation of the latter and it would be informative to quantify the precursors for this reason.

The relationship between sediment levels and phenalenones concentration is demonstrated in Figure 10. The relationship appears to be linear for this fuel blend, with a sharp change in gradient when the total phenalenones concentration reaches approximately 130mgl^{-1} - equivalent to about thirteen weeks storage. A similar correlation is obtained between sediment levels and the concentration of phenalenones excluding those substituted in the 2-position. The relationship follows the same pattern as for total phenalenones, and there is a sharp change in gradient at about 100mgl^{-1} phenalenones - again, equivalent to about thirteen weeks storage.

Studies of previous trials[5,6] have shown that the strong acid content of fuels starts to increase after similar periods of storage and it is possible that increased production of strong acids such as aromatic sulphonic acids will enhance the rate of sediment production. The initial thiol content of the fuel was low (0.0007%m mercaptan sulphur) and the fuel blend contained negligible strong acid (<0.05mg $KOH.l^{-1}$ by conductometric titration[6]) throughout the storage trial. The concentrations of indoles and phenalenes/phenalenones were very high and it might be expected that the strong acids appeared to be entirely consumed in the production of sediment (Figure 1), indicating that the acidity of the fuel was the limiting factor in the sediment forming process for this fuel.

CONCLUSIONS

There was no correlation between results from accelerated ageing tests at high elevated temperature and levels of sediment produced during natural ageing. Reasonable correlation was obtained with results by ASTM D4625, ageing for 16 weeks at 43°C.

Phenalenes appeared to deplete by a pseudo- first order reaction at ambient temperatures. The reaction possibly proceeds via radical formation but further details of the mechanism are not known ie whether intermediates such as the hydroxyphenalene are produced. The order of reaction obtained should be treated with caution as phenalenes may also be produced as byproducts from the phenalenone/indole condensation reaction. The concentrations of the phenalenones and the benzanthrones increased with time to a plateau. The concentration of 2-methylphenalenone reached higher concentrations than the 5- and 8-methylphenalenones, consistent with model studies showing that this compound does not react with indoles.

Colour and sediment levels appear to follow the same trend as phenalenone concentration. There appear to be direct correlations between the colour and sediment produced and the concentration of phenalenones for this fuel blend. More fuels from different sources should be examined to confirm this. The limiting factor in sediment formation for this fuel appeared to be the acidity of the fuel, in particular the availability of strong acids.

REFERENCES

1. J F Pedley, R W Hiley and R Hancock, FUEL, 67, 1988,
2. J F Pedley, R W Hiley and R Hancock, FUEL, 68, 1989,
3. S Marshman, submitted to Analytical Chemistry for publication, 1990
4. S Marshman, submitted to Analytical Chemistry for publication, 1990
5. S Marshman, Internal Ministry of Defence report, 1989
6. S Marshman, Proc. 3rd International Conference on Stability and Handling of Liquid Fuels, London, 1988
7. J E Bennett,Proc. Chem. Soc.,1961, 144
8. J F Pedley, PhD Thesis, 1988
9. J F Pedley, R W Hiley, Proc. 3rd International Conference on Stability and Handling of Liquid Fuels, London, 1988
10. J F Pedley,Internal Ministry of Defence report, 1989
11. R Hancock, D Dolman, Internal Ministry of Defence report,1990
12. Bernasconi et al, FUEL, 69, 1990

© Controller, Her Majesty's Stationery Office, London, 1990

TABLE 1 - RESULTS OF ACCELERATED AGEING TESTS

Analyisis		Week	Result	Analysis		Week	Result
Filtered Sediment				ASTM D4625			
GFC Paper		0	0.1				
				Filterable Insolubles	mg/100ml	0	<0.1
Colour ASTM D1500		0	<3	Adherent Insolubles	mg/100ml	0	<0.1
				Total Insolubles	mg/100ml	0	<0.1
ASTM D2274							
				Filterable Insolubles	mg/100ml	4	0.7
Filtered Insolubles	mg/100ml	0	<0.1	Adherent Insolubles	mg/100ml	4	0.3
Adherent Insolubles	mg/100ml	0	<0.1	Total Insolubles	mg/100ml	4	1.0
Total Insolubles	mg/100ml	0	<0.1				
				Filterable Insolubles	mg/100ml	8	2.8
ASTM D525 (modified)				Adherent Insolubles	mg/100ml	8	2.1
				Total Insolubles	mg/100ml	8	4.9
Potential gum		0	226				
After heptane wash		0	225	Filterable Insolubles	mg/100ml	12	1.8
Colour after ageing		0	4.5	Adherent Insolubles	mg/100ml	12	6.1
				Total Insolubles	mg/100ml	12	7.9
80°C STORAGE (MOD method)							
				Filterable Insolubles	mg/100ml	16	4.0
Insolubles	mgl^{-1}	0	2	Adherent Insolubles	mg/100ml	16	6.9
				Total Insolubles	mg/100ml	16	10.9

TABLE 2 - FILTERED SEDIMENT AND COLOUR MEASURED DURING AMBIENT STORAGE

Week no	Filtered Sediment mg/100ml Measured	Predicted	Colour ASTM D1500
0	1.1		<3.0
4	0.2		2.5
8	0.7		<4.0
12	1.1		4.0
16	1.1	1.0	5.5
20	2.5		5.5
24	4.7	3.0	5.5
28	7.5		5.5
32	6.6	4.9	6.0
36	10.9		6.0
40	9.2	6.4	6.0
50	16.8	8.3	7.0

TABLE 3 - CHANGES IN PHENALENES CONCENTRATIONS WITH TIME

Time wks	Phenalene mg l^{-1}	C1 Phenalenes mg l^{-1}	C2 Phenalenes mg l^{-1}	Total Phenalenes mg l^{-1}
1.5	115	445	300	860
2	105	395	250	750
8	65	245	140	450
13	70	220	100	390
18	75	350	170	595
24	55	230	135	420
30	35	150	75	260
36	30	115	55	200
40	20	60	30	110
46	20	75	40	135

TABLE 4 - CHANGES IN PHENALENONES CONCENTRATIONS WITH TIME

	Phenalenones concentrations in mg l^{-1}								Total	Total
		Phenalenone Homologues								
Time wks	Phenalenone	2-Me	3 &4-Me	5-Me	6-Me	7-Me	8-Me	9-Me	Phenalenones mg l^{-1}	Benzanthrones mg l^{-1}
1.5	6	2.8	0.9	2.7	ND	ND	2.6	ND	15	0.2
2	6	3.4	0.9	3.2	0.1	0.4	3.0	ND	17	0.2
4	6	5.4	0.4	3.0	0.1	0.1	3.0	ND	19	0.2
6	15	8.5	4.0	6.0	1.6	1.0	4.0	0.3	40.5	4.0
8	15	14	3.0	7.0	1.0	2.0	6.5	0.3	49	8.0
13	34	30	3.0	16	3.6	2.0	15	0.3	104	10
18	49	31	6	21	5	3	19	1.5	135	20
24	64	35	4	14	3	2	25	1.5	149	24
28	64	38	6.5	17	4	5	25	1.5	161	20
36	84	53	9	27	6	4	32	2	217	35
40	70	50	4	23	3	3	25	1	179	22
46	75	60	3	23	1	1	24	1	188	24

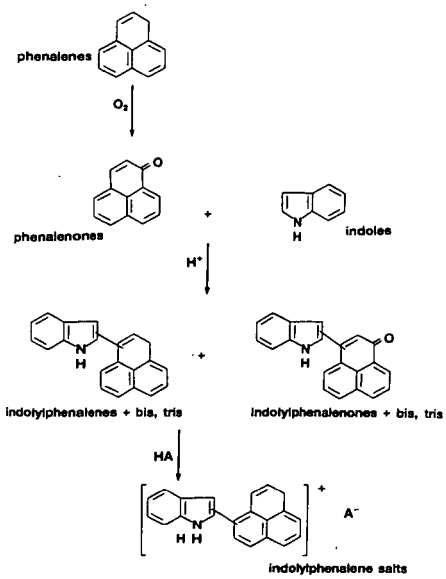

Figure 1. Reaction mechanism for sediment formation.

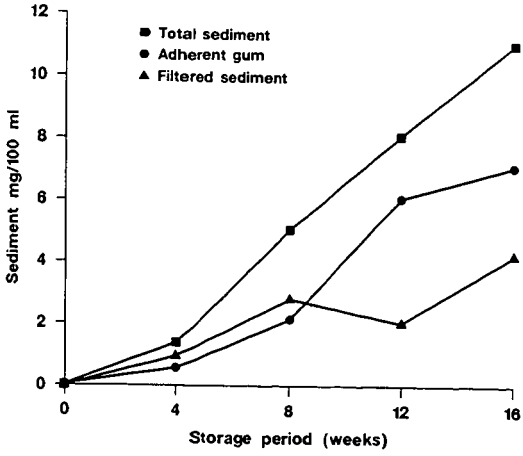

Figure 2. Changes in total sediment with time (bottle storage at 43°C).

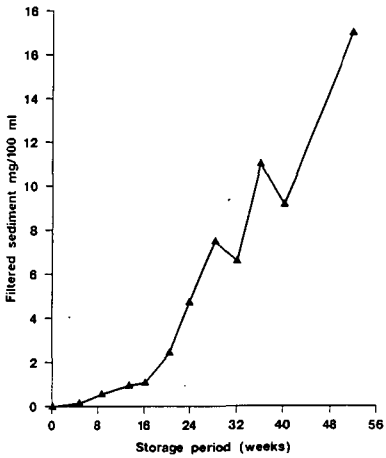

Figura 3. Changes in filtered sediment with time (drum storage).

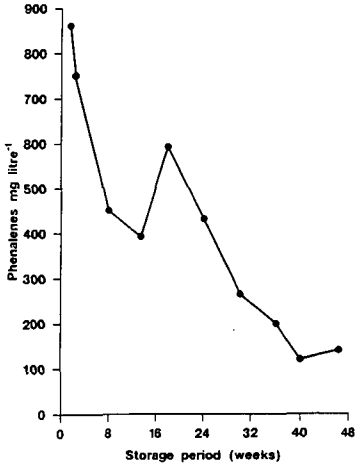

Figure 4. Changes in total phenalenes concentration with time (drum storage).

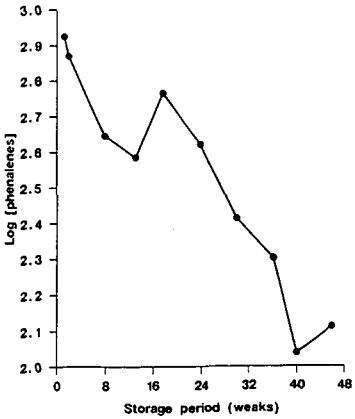

Figure 5. Changes in log [phenalenes] with time (drum storage).

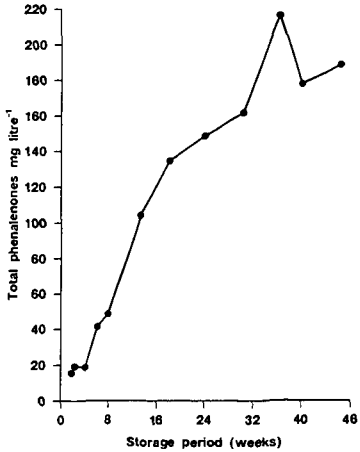

Figure 6. Changes in total phenalenones concentration with time (drum storage).

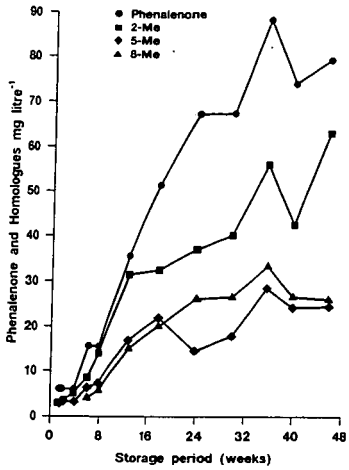

Figure 7. Changes in phenalenone and homologues concentrations with time (drum storage).

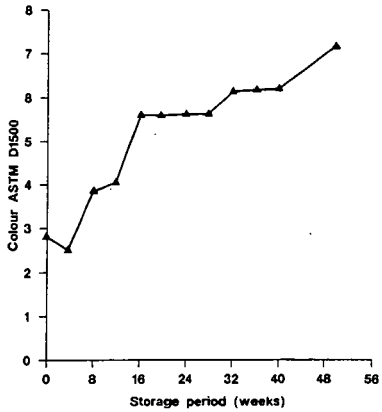

Figure 8. Chenges in colour with time (drum storage).

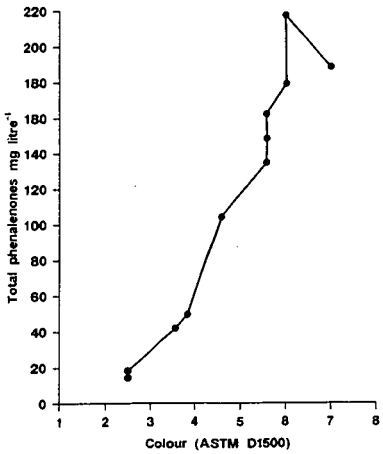

Figure 9. Changes in colour with total phenalenones concentration (drum storage).

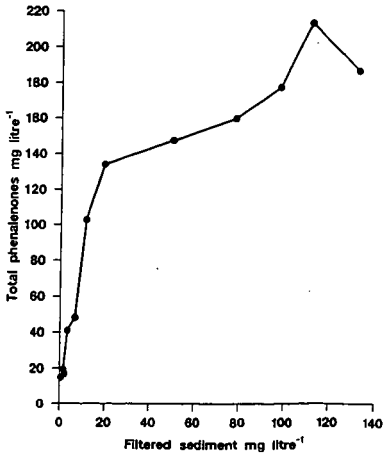

Figure 10. Changes in filtered sediment levels with total phenalenones concentration (drum storage).

Rates of Indole - Phenalenone Reactions in Middle Distillate Fuel

Ludek A. Beranek, Grier G. McVea, Michael G. O'Connell and Richard K. Solly

Materials Research Laboratory, Defence Science and Technology Organisation
PO Box 50, Ascot Vale, Victoria, Australia 3032

ABSTRACT

Although reactions of indole species with phenalene species have been postulated as contributing to sediment formation upon ageing of distillate fuels, no evidence has been found for reaction of phenalenone species in accelerated ageing of fuels by the oxygen overpressure technique or higher temperature ageing. Most indole species, either from chemical sources or from methanol extracts of LCO (MELCO), were found to react under all experimental conditions, even in experiments in which no sediment was produced. Addition of either indole or 2-methylindole to MELCO/straight run distillate mixtures produced considerably more particulate matter on ageing, whereas no additional particulate was formed by addition of 3-methylindole. The results would support formation of indole/phenalene particulate in aged fuels by reaction of phenalene and alkyl substituted phenalenes with the 3-position of alkylindoles.

INTRODUCTION

Reactions between alkylindoles and phenalenones have been postulated to be a significant factor in the formation of sediments in middle distillate fuels.[1] Alkylindoles have also been reported to decrease in concentration during the ageing of fuel containing light cycle oil (LCO).[2] In studies of sediments formed from ageing of distillate fuels from Australian refineries,[3] although species associated with reaction products of alkylindoles with phenalenone were identified in the sediments, in all cases the concentration of phenalenones increased in the ageing fuel mixture. The increases in the concentration of phenalenones is undoubtedly associated with the oxidation of phenalenes present in the LCO.[4] However, as the concentration of phenalenones also increase in the ageing of fuels containing LCO, their specific role in sediment formation remains speculative.

This study was undertaken primarily to investigate the role of phenalenones in the formation of sediments. As a secondary objective, a limited study was also undertaken of the rates of reactions of alkylindoles. Two approaches were used for this investigation. The first was the addition of phenalenone, indole or methylindoles to blends of straight run distillate (SRD) or to 30% LCO/SRD blends followed by accelerated ageing of the mixture. Secondly, polar solvent extraction of LCO was undertaken as a means to separate the polar species containing heteroatoms from the less polar hydrocarbons. The extracts were then added to SRD as means of simulating the presence of LCO in SRD while minimizing the oxidation of phenalenes to phenalenones.

EXPERIMENTAL

Experimental fuel samples were obtained directly from automotive distillate streams of Australian refineries. Experiments in Table 1 were done with SRD from refinery A,[3] while those in Table 3 were done with SRD from refinery G. They were stored at -12°C upon receipt from

the refinery, which was within one week of production. Immediately before being used for the experiments described in this presentation, the samples were thawed, blended and filtered through Millipore AP40 glass fibre filters. Pairs of these filters were used for sediment determination by the method of ASTM D4625. Sediment determination were done in duplicate for model compound additives and the average of the two results shown in the Table 1. Results in Table 3 are for single determinations only.

Commercial samples of indole, 2-methylindole and para-toluenesulphonic acid monohydrate from Fluka Chemika and 3-methylindole and phenalenone (perinaphthenone) from Aldrich Chemicals were used directly as received.

Polar extracts of LCO were obtained by shaking 500 ml of the LCO from refinery F[3] with 5 x 100 ml portions of methanol. The methanol extracts were combined and stored at -12°C. Prior to ageing experiments, measured portions of the methanol extract were evaporated to dryness under vacuum at ambient temperature. The residue was then dissolved in the experimental fuel blend.

Most accelerated ageing studies were carried under oxygen overpressure conditions[5] using the single bomb apparatus of ASTM D942 at a oxygen pressure of 794 kPa and temperature of 95°C as outlined elsewhere.[6] These conditions for an ageing time of 64 hours will be referred to as OP conditions in the remainder of the paper. Studies were also carried out at atmospheric pressure in a thermostated air oven using 700 ml of fuel in loosely capped 1 litre borosilicate flasks.

Phenalenone and indole determinations were performed on the experimental fuel blends prior to and after fixed ageing periods. Determination of phenalenones was performed by high pressure liquid chromatography using a Waters 5 um spherical silica column of 150 mm length and 4.6 mm diameter at ambient temperature. All phenalenones were eluted under isocratic conditions with a 9:1 mixture of heptane with chloroform containing 1.5% propan-2-ol. Following elution of the phenalenones, the column was flushed with propan-2-ol prior to the next run. The phenalenones were detected by serial detectors at wavelengths of 384 nm and 254 nm. Good agreement was obtained between the two wavelengths after standardization with 0-1000 umol/L solutions of phenalenone in the eluent, indicating the minimal co-elution of interfering substance with the phenalenones. Indoles were determined by gas chromatography using a nitrogen specific detector as described elsewhere.[6] Thin layer chromatography (TLC) of sediments were performed on Merck HPTLC Silica Gel 60 F254 plates using a 10% methanol/dichloromethane solvent.[6]

RESULTS AND DISCUSSION

Ageing of samples of SRD alone produces very little sediment, but upon admixture of LCO with the SRD, significant amounts of sediment are produced.[7] Phenols[6], phenalenones[1], alkylindoles[1,2], and acids[7,9] have all been postulated to be precursors for sediment formation. A reference sample of SRD was aged for the equivalent of 3-5 years ambient ageing under the vigorous conditions of the oxygen overpressure test[5] for 64 hours at 95°C with a pressure of 794 kPa oxygen. Both phenalenone and indole then were added to the SRD at concentrations of 588 umol/L and 981 umol/L respectively. These are equivalent to concentrations at the upper end of those measured for phenalenone and alkylindoles in 30% LCO/SRD blends.[3] As may be seen from Table 1, no additional sediment was formed in the fuel containing the additives on ageing.

The results would also suggest that species which catalyse the reactions of indole with phenalenone are not formed from stressing of the SRD under the OP conditions. In particular,

the acid species which would be expected to be formed,[9] do not act as a catalyst. In order to investigate the effect of strong acids further, a saturated solution at 20°C of para-toluenesulphonic acid monohydrate in SRD containing indole and phenalenone as previously was prepared and aged under the OP conditions. This acid is known to be effective in promoting sediment formation in fuel containing LCO.[7] No additional sediment was formed compared to SRD without additives. It may be concluded that the concentration of p-toluenesulphonic acid dissolving at 20°C in combination with acid produced by OP ageing of the SRD is insufficient to promote reaction between the indole and phenalenone in the SRD.

The experiments were then repeated with a fuel mixture of 30% LCO in SRD. This mixture produced 67 mg/L sediment under the OP conditions without the addition of additives. Phenalenone and indole were added and the fuel aged. The amount of sediment increased to 125 mg/L. Phenalenone was then added to the 30% LCO/SRD fuel without any indole. The amount of sediment formed after OP ageing at 63 mg/L was the same within the experimental error as that produced from the reference 30% LCO/SRD blend. Finally, for these series of experiments shown in Table 1, indole without phenalenone was added to the reference fuel. The amount of sediment of 122 mg/L formed after OP ageing was the same as that produced for fuel containing both phenalenone and indole.

The effect of methyl substitution upon the indole nitrogen containing ring was then investigated. The addition of 2-methylindole to the 30% LCO/SRD fuel mixture produced 157 mg/L sediment after OP ageing, whereas the addition of 3-methylindole resulted in only 60 mg/L of sediment. Increased sediment is formed from 2-methylindole compared to indole itself, whereas 3-methylindole does not produce any additional sediment compared to the undoped fuel. These results would suggest that reaction of the indole molecule to form sediments is via the 3-position. The 2-methyl substituent facilitates reaction at the 3-position, whereas the 3-methyl group blocks the reaction.

The results may be compared with the effect upon sediment formation of the presence of both 3-methylindole and tert-butylhydroperoxide in shale derived fuels.[10] Significantly increased sediment formation was observed when both additives were present. It may be concluded that sediment formation from 3-methylindole in the presence of tert-butoxy radicals is predominantly a free radical process. Hindered phenols act as effective free radical traps, but are known to be ineffective in reducing sediment formation in unstable fuels.[11] As no evidence was found for the reaction of the 3-methylindole under the OP conditions of this work, it may be concluded that the OP conditions are more comparable to ambient ageing than those in the presence of free radical promoters.

TLC analyses of the sediments were undertaken to compare sediments produced from the 30% LCO/SRD mixture in the presence and absence of additives. These are shown schematically in Table 2. Thin layer chromatograms of sediments from the reference fuel without additives, and from that containing either phenalenone or 3-methylindole were identical within experimental error, confirming that these additives had not contributed to the sediments. Only sediment from the reference fuel is shown in Table 2. The major feature of the thin layer chromatograms of sediment from the indole additive was the increased prominence of a blue material at approximate R_f 0.25 to 0.35. With the 2-methylindole additive this blue material was very intense. It is postulated to be the acid salts of alkylindolylphenalenes

Direct measurements of indole concentrations were not done for the experiments in Table 1. Indole concentrations that are shown are those which were added to the solution. In a second series of experiments, direct measurements of indole concentrations were made before and after ageing.. For these experiments shown in Table 3, methanol extracts of LCO

from refinery F were also added to SRD from refinery G. This combination was used due to the relatively high indole content of the LCO for refinery F[3] and the water white nature of SRD from refinery G.

Ageing of the SRD under the OP conditions used previously produced 10 mg/L total particulate from the SRD. Similar ageing of the SRD with added indole, both with and without added phenalenone, produced the same amount of sediment as the SRD alone within the experimental error. The indole and phenalenone concentrations were measured in the solution after ageing as shown in Table 3. The final phenalenone concentration was unchanged from that initially and consistent with no additional sediment being formed in the presence of the phenalenone. However, although no additional sediment was formed in either solution in the presence of added indole, in both cases the concentration of indole had decreased to approximate half its original value. These results clearly indicate a non-particulate forming reaction of the indole in the SRD.

Ageing of SRD containing methanol extracts of LCO produced 89 mg/L of sediment. The addition of 490 umol/L of phenalenone to the solution prior to ageing did not produce any change in the amount of sediment formed. The results are comparable with those of Hardy and Welcher,[12] who found that ageing methanol extracts of LCO in hydrocarbons produced sediments of similar mass to that produced from the equivalent volume of unextracted LCO. As with the experiments discussed in the previous paragraph, the total indole concentration (in the case of the extract it is a mixture of many alkyl indoles[3]) decreased considerably in the aged solution, whereas the phenalenone concentration was unchanged after ageing.

The ageing of the methanol extract in SRD was repeated with an air atmosphere in an thermostated oven. Both the initial total alkylindole and phenalenone concentration was low at 270 and 4 umol/L respectively and only 6 mg/L of sediment was formed after 14 days ageing at 80°C. The addition of 780 umol/L of phenalenone to the reference solution resulted in the formation of 7 mg/L of sediment, unchanged within the experimental error. Again there was a significant reduction in the final total indole concentration, but none in the final phenalenone concentration. Finally, a greater concentration of methanol extract in SRD was aged with an air atmosphere for 65 hours at 120°C. After this period, 41 mg/L of sediment had been formed and the total alkylindole concentration had decreased to one fifth of its original value, but the phenalenone concentration was unchanged at 28 umol/L. Not only was the unsubstituted phenalenone concentration unchanged after ageing at the elevated temperature, but so were all other substituted phenalenones as detected in the HPLC chromatogram at a detector wavelength of 384 nm as shown in the chromatograms before and ageing in Figure 1. Although these other species have not been definitively identified as phenalenones, the HPLC retention time and absorption at 384 nm is indicative of the phenalenone chromatophore.

If phenalenone species do not react with indoles in SRD under the severe ageing conditions used in this work, it may be concluded that it is unlikely that they react at ambient temperatures. However, blue and pink materials observed in the thin layer chromatograms of the sediments from this and previous work has been postulated to be acid salts of alkylindolylphenalenes and alkylindolylphenalenones.[1,6] It is proposed that the acids salts arise following reactions between alkylindoles with unoxidized phenalene species to form indolylphenalenes which may subsequently oxidized to indolylphenalenones as shown in Figure 2. Phenalenes have been shown to be present in relatively high concentrations in LCO.[4] The large increase in blue material observed in the thin layer chromatogram of sediment formed upon ageing when 2-methylindole is added to fuel mixture containing LCO follows from coupling with phenalenes at the favoured 3-position of the alkylindoles. This coupling is blocked in the case of 3-methylindole.

CONCLUSIONS

No evidence has been found for reaction of phenalenone species under conditions of oxygen overpressure and elevated temperature ageing of SRD containing either indole and phenalenone as model compounds or these species present from methanol extracts of LCO. Indole species were found to react under all the experimental ageing conditions. Although approximately 50% of indole in SRD aged under OP conditions of 64 hours at 95°C was found to have reacted, no additional particulate matter was formed in the fuel.

Particulate matter was formed on ageing when solid residue from methanol extracts of LCO were added to SRD. The total alkylindole concentration in the SRD/extract mixture decreased by at least 50% during the ageing experiments. However, in none of the experiments was any decrease in phenalenone concentration recorded. No additional particulate matter was formed when phenalenone was added to SRD/extract mixture.

Addition of either indole or 2-methylindole to the extract/SRD mixture resulted in considerably more particulate matter being produced. No increase in particulate was found when the SRD/extract mixture containing 3-methylindole was similarly aged.

REFERENCES

1. Pedley, J.F., Hiley, R.W. Investigation of Sediment Precursors Present in Cracked Gas Oil. *Proc. 3rd Int. Conf. on Stability and Handling of Liquid Fuels.* IP, London, U.K. p.495, 1988.
2. Dorbon, M., Bernasconi, C. Nitrogen Compounds in Light cycle Oils: Identification and Consequences of Ageing. *Fuel*, **68**, 1067, 1989.
3. Pedley, J.F., Beranek, L.A., O'Connell, M.G., Solly, R.K. The Chemistry of Sediment Formation in Australian Middle Distillate Fuels. This conference.
4. Marshman, S.J., David, P. Storage Stability of Distillate Fuels: Changes in Phenalene and Phenalenone Concentrations during Long Term Ambient Storage. This conference.
5. Hardy, D.R., Hazlett, R.N., Beal E.J., Burnett, J.C. Assessing Distillate Fuel Storage Stability by Oxygen Overpressure. *Energy and Fuels*, 1989, **3**, 20.
6. McVea, G.G., Pedley, J.F., Solly, R.K. Assessment of Oxygen Overpressure Test for Prediction of Middle Distillate Fuel Storage Stability. This conference.
7. Hazlett, R.N., Power, A.J., Kelso, A.G., Solly. The Chemistry of Deposit Formation in Distillate Fuels. *Materials Research Laboratory Technical Report 986*. Defence Science and Technology Organization, Melbourne, Australia, 1986.
8. Hazlett, R.N., Power, A.J. Phenolic Compounds in Bass Strait Distillate Fuels: Their Effect On Deposit Formation. *Fuel*, **68**, 1112 (1989).
9. Wechter, M.A., Hardy, D.A. Insoluble Sediment Formation in Middle-Distillate Diesel Fuel: Evidence Concerning the Role of Fuel Acidity. *Energy and Fuels*, **3**, 461 (1989).
10. Mushrush, G.W., Beal, E.J., Hazlett, R.N., Hardy, D.R. Interactive Effects of 2,5-Dimethylpyrrole, 3-Methylindole and tert-Butylhydroperoxide in a Shale Derived Fuel. *Energy and Fuels*, **4**, 16, 1990.
11. Solly, R.K., Arfelli, W. Effect of Stability Additives Upon Distillate Fuel Filterability. *Proc. 2nd Int. Conf. on Stability and Handling of Liquid Fuels.* Southwest Research Institute, San Antonio, Tx, USA, 453, 1986.
12. Hardy D.R., Wechter, M.A. Insoluble Sediment formation in Middle Distillate Diesel Fuel: The Role of Soluble Macromolecular Oxidatively Reactive Species. *Energy and Fuels*, 1990.

FUEL	INDOLE ADDED umol/L	PHENALENONE ADDED umol/L	TOTAL PARTICULATE mg/L
SRD	0	0	17
SRD	981	588	14
30% LCO/SRD	0	0	67
30% LCO/SRD	793	604	125
30% LCO/SRD	0	627	63
30% LCO/SRD	972	0	122
30% LCO/SRD	754[a]	0	157
30% LCO/SRD	792[b]	0	60

a as 2-methylindole
b as 3-methylindole

Table 1. Total sediment formed after oxygen overpressue ageing at 794 kPa for 64 hours at 95°C of fuel from Refinery A.

R_f RANGE	BAND COLOUR	NO ADDITIVES	INDOLE ADDED	2-METHYLINDOLE ADDED
1.00-0.96	green	L	L	L
0.94-0.87	orange	L	M	D
0.74-0.73	green	VL	NO	VL
0.72-0.71	grey	VL	NO	VL
0.55-0.43	pink	M	L	M
0.42-0.26	blue	L	D	VD
0.26-0.22	orange	VL	M	NO
0.21-0.25	yellow	NO	M	NO
0.08-0.04	brown	L	M	M

NO not observed
VL very light
L light
M medium
D dark
VD very dark

Table 2. Thin layer chromatogram schematics of sediment from 30% LCO/SRD fuel from refinery A.

Fuel Ageing	TOTAL ALKYLINDOLE concentration Initial umol/L	Final umol/L	PHENALENONE concentration Initial umol/L	Final umol/L	TOTAL PARTICULATE MATTER mg/L
a	0	0	0	0	10
b	1072	497	0	0	14
c	1072	562	99	95	12
d	1613	921	21	28	89
e	1613	593	511	512	88
f	270	85	4	4	6
g	270	80	786	800	7
h	2555	506	28	29	41

a SRD reference fuel OP aged (64 hr at 95°C with 794 kPa oxygen)
b SRD + added indole OP aged
c SRD + added indole and phenalenone OP aged
d SRD + LCO extract OP aged
e SRD + LCO extract and added phenalenone OP aged
f SRD + LCO extract aged for 336 hr at 80°C
g SRD + LCO extract and added phenalenone aged for 336 hr at 80°C
h SRD + LCO extract aged for 65 hours at 120°C

Table 3. Variation of total alkylindole and phenalenone concentrations and total particulate on ageing SRD containing methanol extracts of LCO with and without added phenalenone.

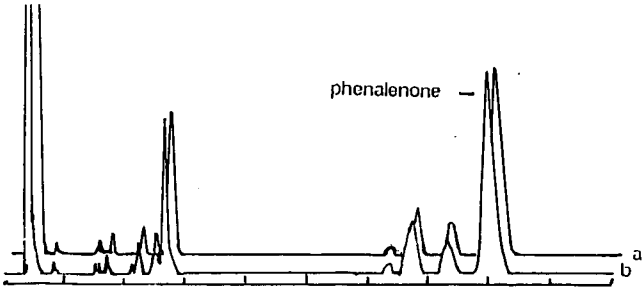

Figure 1. HPLC Chromatogram of absorption at 384 nm for SRD containing methanol extract of LCO, (a) before and (b) after ageing at 120°C for 65 hours.

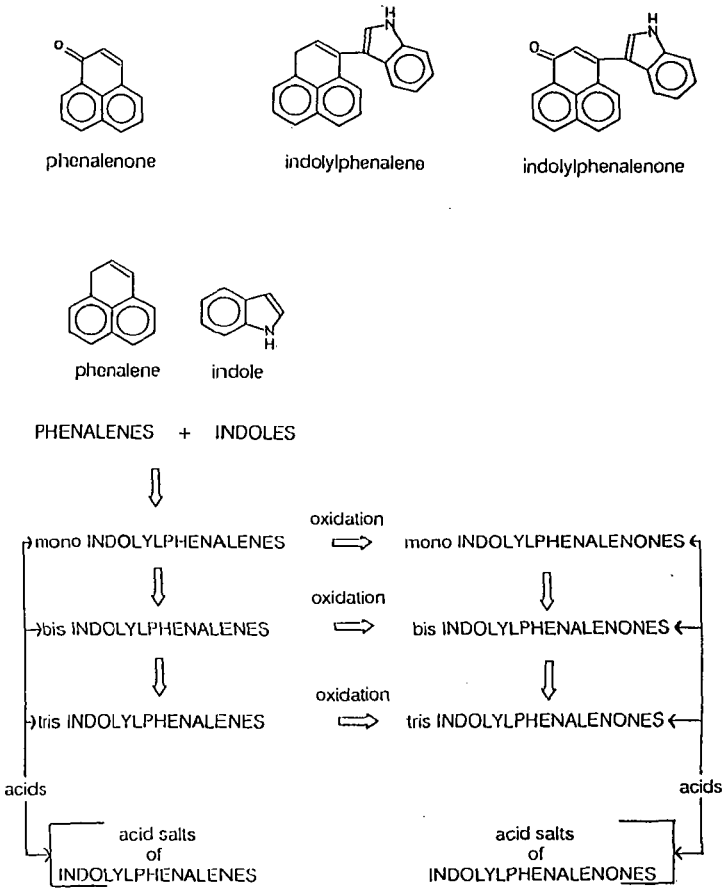

Figure 2. Possible Reaction schematic for formation of particulate from reaction of indole and phenalenone species.

SYMPOSIUM ON STABILITY AND OXIDATION OF MIDDLE-DISTILLATE FUELS
PRESENTED BEFORE THE DIVISION OF PETROLEUM CHEMISTRY, INC.
AND
THE DIVISION OF FUEL CHEMISTRY
AMERICAN CHEMICAL SOCIETY
WASHINGTON, D.C., MEETING, AUGUST 26-31, 1990

COMBINED LIQUID CHROMATOGRAPHY/STABILITY TESTING (LC/ST) APPROACH FOR ISOLATION OF COMPOUNDS RESPONSIBLE FOR FUEL INSTABILITY

By

John B. Green and Kathleen Q. Stirling

IIT Research Institute
National Institute for Petroleum and Energy Research
P. O. Box 2128, Bartlesville, OK 74005
(918/337-4255)

INTRODUCTION

The bulk of prior work on fuel stability problems indicates that the instability of a given fuel usually can be attributed to a relatively small subset of compounds/compound types which are typically present at low abundance in the fuel. For example, recent work has implicated alkylindoles, alkylphenalenes, and sulfonic acids as major contributors to storage instability of diesel fuel (1-12). Phenolic compounds also contribute to diesel sediment formation (13,14), and carboxylic or other acids of similar or greater acidity accelerate the rate of sediment formation (15).

Sediments formed during storage of jet fuels produced by hydrocracking processes largely contained aromatic hydrocarbons and oxygen-containing compounds (16). In the case of thermal instability of jet fuels, compounds that are either easily converted to peroxyl radicals or hydroperoxides, or are important in propagation of the free radical reactions, are of greatest concern (10). Analysis of JFTOT tube deposits and those on filters downstream of the JFTOT tube has indicated contributions from a wider variety of compound types, relative to those formed in storage sediments (17,18).

A common feature of each type of stability problem cited above is the prominent role played by acidic compounds, either as catalysts or direct participants in sediment/deposit formation. Alkylindoles, sulfonic acids, phenolic compounds, carboxylic acids and hydroperoxides all exhibit acidic (hydrogen donor) properties. As a general correlation, Clark and Smith found that total acid content, as determined by yield of acids from nonaqueous ion exchange liquid chromatography, was the best available predictor of thermal stability (19).

Even where the components responsible for stability problems have been identified, there frequently are many unanswered questions concerning the nature of their interaction to form deposits/sediments, which compounds actually initiate or limit the sediment-forming process, and what reactions control the overall rate of sediment formation. Design of cost-effective methods or approaches to resolve a given stability problem normally requires at least some information concerning the sediment-forming process. For example, the effectiveness of tertiary amine additives in storage stabilization of diesel fuels containing light cycle oil may be attributed to their neutralization of acids which catalyze reactions resulting in gums and sediment (11,15).

Chemical separations have been shown to be an effective means for isolation of components that promote instability, as well as aiding in the determination of relevant reactions leading to deposit/sediment formation (e.g., 2,7,13,14). However, the availability of a general scheme for systematic separation of compound classes in jet or diesel fuels, plus a means for rapidly assessing the impact of the resulting fractions on stability, would further improve the applicability of this approach to fuel stability studies. This report describes a series of liquid chromatographic (LC) separations and reblending/stability testing techniques aimed at meeting this need. Representative results are provided to illustrate the merit of this approach as well as problems encountered in its use. In agreement with work cited above, acidic components are frequently implicated as primary promoters of instability from the results reported herein.

EXPERIMENTAL

Figure 1 outlines the complete sequence of available separations. Procedures for each separation step are described in detail elsewhere (20). Typically, stability testing (Figure 2) is performed after each stage of separation, and those results determine the extent and emphasis of additional separations. For example, further separations of neutrals into subtypes indicated in Figure 1 are not performed unless stability tests indicate significant deposit/sediment formation for the whole neutral fraction. Subfractionation of whole acids and bases is more commonly performed since stability tests on acid + neutral or base + neutral blends frequently implicate one or both of those types as promoters/causes of instability. As noted in Figure 2, whole neutrals are typically used as the blend stock for acid/base fractions or subfractions. Fractions are usually reblended according to their proportions in the whole fuel. Comprehensive recomposites (e.g., acids + bases + neutrals) are tested at each stage of the work to check for bias in stability tests and/or contamination/losses during separations. Details of the storage (typically 2 weeks at 80° C) and thermal (modified D 3241) stability test procedures appear elsewhere (17,21,22).

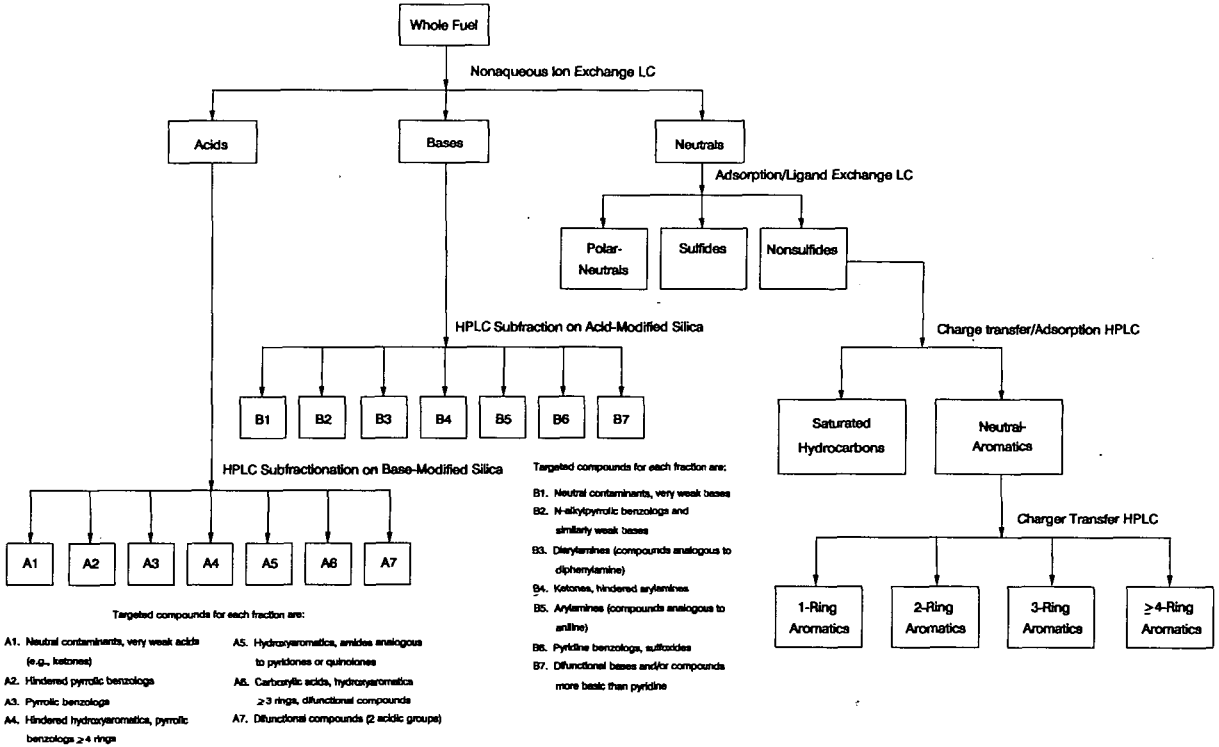

Figure 1. Schematic for LC Separations. Note that sufractionation of neutrals(i.e. into Polar-neutrals, sulfides, etc.) is not normally necessary, since neutrals are usually quite stable.

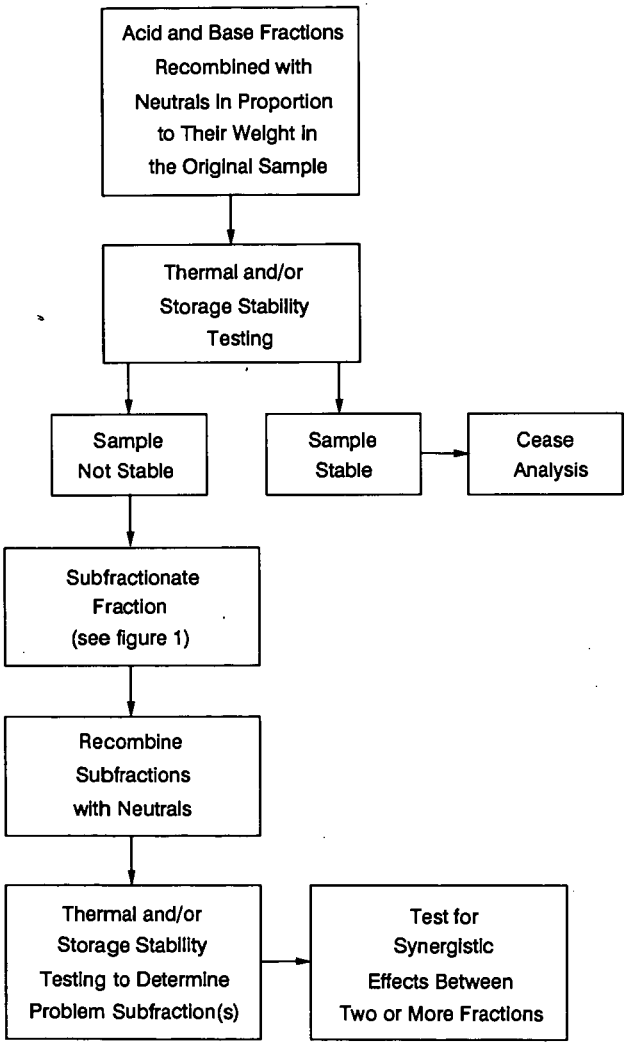

Figure 2. Typical Sequence for Reblending and Stability Testing of Acid and Base Fractions

RESULTS AND DISCUSSION

Tables 1 and 2 show comparisons of thermal stability of two jet fuels (NIPER sample Nos. 2140 and 2302) versus their neutral fractions under mild (Table 1) and moderate (Table 2) thermal stress conditions. The significantly greater thermal stability of neutrals relative to the whole fuel is quite evident from this data. Fraction yields (wt %) from separation of 2140 and 2302 fuels into acids, bases, and neutrals (ABN) were, respectively: 0.17(A), 0.08(B), 98.0(N) (98.2 total); 0.19(A), 0.04(B), 94.5(N) (94.6 total). Thus, removal of a relatively small proportion of acidic/basic material (ca. 0.25 wt %) greatly improved the thermal stability of these two fuels.

TABLE 1
Thermal Stability of Whole Jet Fuels vs. Neutral Fractions, Standard JFTOT (2½ hrs. @ 260° C)

Sample No.	Fraction	Tube Rating	Pressure Drop (psi)
2140	Whole	4	0
2140	Neutral	1	0
2302	Whole	3	0
2302	Neutral	1	0

TABLE 2
Thermal Stability of Whole Jet Fuels vs. Neutral Fractions, Extended JFTOT (277° C)

Sample No.	Fraction	Run Time	Tube Deposit Rating	Filter Pressure Drop (psi)
2140	Whole	12 hours	>>4 (black)	filter plugged
2140	Neutral	12 hours	2	0
2302	Whole	3.5 hours	>4 (brown)	filter plugged
2302	Neutral	3.5 hours	1	0

An earlier report discussed mass spectrometric (MS) analysis of JFTOT tube deposits and sediments from downstream filters from both the 2140 and 2302 fuels (17). Those results indicated a predominance of polar compounds in each case, especially when the MS sample introduction probe was heated above 150° C. Components vaporized at temperatures ≥150° C were probably covalently bonded within the sediment structure (17). Thus, the observed improvement in thermal stability of neutrals versus whole fuels is consistent with the lower thermal stability of acidic and basic components indicated by MS analysis.

Because of the relatively large quantities of sample (ca. 500 mL) required by the JFTOT test, differential scanning calorimetry is currently being explored as an alternate means for evaluating the thermal stability of whole acid and base fractions and subfractions thereof. Those results will be reported in a later paper.

Tables 3 and 4 show separation and storage stability test results for a straight-run middle distillate (450-650° F, 0.5 wt % S, 34 °API). Although as a whole the results clearly show acidic types to be largely responsible for sediment formation in this case, close inspection of the data reveals some inconsistencies. The most significant discrepancy is the difference between total sediment for reblended acids + bases + neutrals versus the original distillate (22 versus 8.7 mg/100 mL). The main reason for the higher apparent sediment yield from the reblended sample was found to be incomplete dissolution of the acid fraction into neutrals during the reblending step. The insoluble material in the acid fraction temporarily suspended into the neutrals (giving the appearance of dissolution), but ultimately added to the weight of insolubles obtained by filtration at the end of the stability test. This error is similarly reflected in the high apparent sediment yield for the acids + neutrals blend (21 mg/100 mL).

TABLE 3
Mass Balances from Separation of a North American Straight-Run Middle Distillate

Fraction[1]	Yield (wt %)
Acids	0.47
A1	0.056
A2	0.019
A3	0.18
A4	0.036
A5	0.047
A6	0.063
A7	0.011
Total, A1-A7	0.412
Bases	0.17
B1	0.082
B2	0.001
B3	0.014
B4	0.013
B5	0.012
B6	0.036
B7	0.018
Total, B1-B7	0.176
Neutrals	98.1
Total, Acids + Bases + Neutrals	98.7

[1]See Figure 1.

TABLE 4

Storage Stability Test Results on Fractions Listed in Table 3[1]

Fraction	Total Sediment (mg/100 mL)	Net Sediment[2] (mg/100 mL)
Acids	21	19
A1	2.7	0.5
A2	8.7	6.5
A3	2.1	-0.1
A4	2.2	0.0
A5	2.2	0.0
A6	7.0	4.8
A7	5.6	3.4
Total, A1-A7	-	15.1
Bases	2.9	0.7
B1	1.9	-0.3
B2	1.4	-0.8
B3	1.5	-0.7
B4	0.7	-1.5
B5	0.5	-1.7
B6	3.4	1.2
B7	5.9	3.7
Total, 81-B7	-	-0.1
Neutrals	2.2	-
Neutrals + Acids + Bases	22	20
Whole Distillate	8.7	-

[1]80° C, 2 weeks, air at ambient pressure. Average of duplicate determinations is shown.

[2]Net sediment = total sediment - sediment from neutrals. (Neutrals were used as diluent for all acid and base fractions).

Because of the unreliability of simple visual inspection of reblended samples for assessment of solubility, they are now routinely prefiltered prior to stability testing. This precaution has significantly improved balances in stability test results for composited fractions versus whole materials over those obtained in early work such as that illustrated in Table 4. The source of the insoluble material is not well defined; contributions from solvent impurities and materials used in the separations (e.g., ion exchange resin artifacts) are suspected. In addition, degraded or otherwise altered fuel components probably make up part of the insoluble material in many cases. It should be emphasized that the overall magnitude of insolubles is quite small. For example, the acid fraction comprises 0.47 wt % (equivalent to ca. 425 mg/100 mL) of the middle distillate; the portion that did not dissolve (ca. 13 mg/100 mL) amounted to only about 3 percent of the acid fraction.

For the purpose of determining sediment directly attributable to a given acid or base fraction, the sediment formed by neutrals alone is typically subtracted from the total sediment for a given acid/base + neutrals blend (see "net sediment" data, Table 4). Although sediment formation may not be strictly an additive property, this or a similar practice is necessary to derive balances for sediment formation of individual fractions for comparison with the whole. Otherwise, the sediment contribution from the neutral fraction would be propagated in proportion to the number of fractions tested, and balances over fractions would invariably exceed that of the whole.

In light of the above discussion, it may be seen that most base subfractions from the middle distillate apparently stabilize the neutral fraction (B1-B5), and only two (B6 and B7) provide a positive net sediment yield. The balance for net sediment yield calculated over the base subfractions (-0.1 mg/100 mL) is within experimental error of that determined for the whole bases (0.7 mg/100 mL). In the case of the acid subfractions, the apparent sediment yield for A2 (6.5 mg/100 mL) is believed to have resulted largely from incomplete solution rather than actual sediment formation. Thus, the dominant sediment-forming acidic compounds are present in A6 and A7, which provide a combined sediment yield (8.2 mg/mL) consistent with that of the whole distillate (8.7 mg/mL). Thus, in the case of both acids and bases, compounds exhibiting the highest polarity/degree of functionality in terms of separation behavior (see the description of subfractions B6, B7, A6, and A7 composition in Figure 1) also show the highest sediment-forming tendency. Their combined concentration in the distillate is extremely low, ca. 0.1 wt %. Effective removal or neutralization of the effects of these compounds should improve the storage stability of the distillate to the level of sediment formation exhibited by the neutral fraction (2.2 mg/100 mL).

CONCLUSIONS

The combination of LC separation and stability testing (LC/ST) is an effective screening tool for identifying components/compound types that promote instability. The LC fractions also constitute a valuable resource for studying sediment formation pathways, synergistic effects between different compound types, and the effectiveness of potential stabilizing additives.

The sensitivity of stability tests to contamination and sample alteration occurring during LC separations places stringent demands on the LC methodology, solvents and materials used, and procedures employed during work-up of fractions and their storage prior to testing. However, the simplicity and direct relevance of stability test results to the issue of fuel stability makes it the method of choice for evaluation of fractions. In contrast, detailed analysis of fresh versus aged fuel fractions proved to be a very laborious approach for estimating their stability (23). Thus, the prudent course of action is to improve separation and reblending techniques where necessary, rather than to look for alternate methods for fraction evaluation.

Although more difficult experimentally, work with actual fuel fractions provides a more realistic assessment of stability problems than possible with simple model systems.

ACKNOWLEDGMENTS

The authors thank J. W. Goetzinger for thermal stability testing, L. Young and S.K.-T. Yu for LC separations, and P. R. Stapp and R. P. Anderson for reviewing the manuscript. The assistance and encouragement provided by D. L. Ripley is also appreciated. Financial support by the U.S. Department of Energy and Naval Air Propulsion Center is gratefully acknowledged.

LITERATURE CITED

1. Pedley, J. F., Hiley, R. W., and Hancock, R. A., Fuel, 66, 1646 (1987).

2. Hiley, R. W., and Pedley, J. F., Fuel, 67, 469 (1988).

3. Pedley, J. F., Hiley, R. W., and Hancock, R. A., Fuel, 67, 1124 (1988).

4. Pedley, J. F., Hiley, R. W., and Hancock, R. A., Fuel, 68, 27 (1989).

5. Pedley, J. F., and Hiley, R. W., Proc. 3rd. Int. Conf. on Stability and Handling of Liq. Fuels, Vol. 2, Inst. Petrol., London, 1988, pp. 495-509 and 510-524.

6. Marshman, S. J., Proc. 3rd. Int. Conf. on Stability and Handling of Liq. Fuels, Vol. 2, Inst. Petrol., London, 1988, pp. 581-595.

7. Hiley, R. W., and Pedley, J. F., Proc. 2nd Int. Conf. on Long-term Storage Stabilities of Liq. Fuels, Vol. 2, Southwest Res. Inst., San Antonio, TX, 1986, pp. 570-584.

8. Malhotra, R., and St. John, G. A., Proc. 2nd Int. Conf. on Long-term Storage Stabilities of Liq. Fuels, Vol. 1, Southwest Res. Inst., San Antonio, TX, 1986, pp. 327-335.

9. Malhotra, R., and St. John, G. A., Proc. 3rd Int. Conf. on Stability and Handling of Liq. Fuels, Vol. 2, Inst. Petrol., London, 1988, pp. 525-537.

10. Taylor, W. F., and Frankenfeld, J. W., Proc. 2nd Int. Conf. on Long-term Storage Stabilities of Liq. Fuels, Vol 2, Southwest Res. Inst., San Antonio, TX, 1986, pp. 496-505.

11. Westbrook, S. R., Stavinoha, L. L., Present, D. L., Hsu, J. P., and Herrera, J. G., Proc. 3rd Int. Conf. on Stability and Handling of Liq. Fuels, Vol. 2, Inst. Petrol., London, 1988, pp. 538-553.

12. Bernasconi, C., Chaffardon, A., Charleux, P., Denis, J., Gaillard, J., and Durand, J. P., Proc. 3rd Int. Conf. on Stability and Handling of Liq. Fuels, Vol. 2, Inst. Petrol., London, 1988, pp. 423-440.

13. Hazlett, R. N., and Power, A. J., Proc. 2nd Int. Conf. on Long-term Storage Stabilities of Liq. Fuels, Vol. 2, Southwest Res. Inst., San Antonio, TX, 1986, pp. 556-569.

14. Hazlett, R. N., and Power, A. J., Fuel, 68, 1112 (1989).

15. Hazlett, R. N., and Kelso, G., Proc. 2nd Int. Conf. on Long-term Storage Stabilities of Liq. Fuels, Vol. 2, Southwest Res. Inst., San Antonio, TX, 1986, pp. 541-555.

16. Sutterfield, F. D., Brinkman, D. W., Bhan, O. K., Green, J. B., Goetzinger, J. W., Sturm, G. P., Jr., Speck, G., and Turner, L., Proc. 3rd Int. Conf. on Stability and Handling of Liq. Fuels, Vol. 1, Inst. Petrol., London, 1988, pp. 321-337.

17. Brinkman, D. W., Bhan, O. K., Green, J. B., Goetzinger, J. W., Grigsby, R. D., and Kamin, R., Proc. 3rd Int. Conf. on Stability and Handling of Liq. Fuels, Vol. 2, Inst. Petrol., London, 1988, pp. 796-807.

18. Grigsby, R. D., Sturm, G. P., Jr., Goetzinger, J. W., Green, J. B., and Anderson, R. P., Preprints, Div. Petrol. Chem., ACS, 35, XXX (1990).

19. Clark, R. H., and Smith, L. Proc. 3rd Int. Conf. on Stability and Handling of Liq. Fuels, Vol. 1, Inst. Petrol., London, 1988, pp. 268-282.

20. Green, J. A., Green, J. B., Grigsby, R. D., Pearson, C. D., Reynolds, J. W., Shay, J. Y., Sturm, G. P., Jr., Thomson, J. S., Vogh, J. W., Vrana, R. P., Yu, S.K.-T., Diehl, B. H., Grizzle, P.L., Hirsch, D. E., Hornung, K. W., Tang, S.-Y., Carbognani, L., Hazo, M., and Sanchez, V., "Analysis of Heavy Oils: Method Development and Application to Cerro Negro Heavy Petroleum," Vols. 1 and 2, NTIS Rept. No. DE9000020, NIPER Rept. No. 452, 1989.

21. Stirling, K. Q., Brinkman, D. W., and Sutterfield, F. D., 3rd Int. Conf. on Stability and Handling of Liq. Fuels, Vol. 2, Inst. Petrol., London, 1988, pp. 808-814.

22. Stirling, K. Q., and Brinkman, D. W., "Stability, Compatibility, and Related Problems of Additives in Naval Distillate Fuels Derived from Lower Quality Feedstocks," NTIS Rept. No. DE89000717, NIPER Rept. No. 352, 1989.

23. Bhan, O. K., Brinkman, D. W., Green, J. B., and Carley, B., Fuel, 66, 1200 (1987).

STORAGE STABILITY OF FUELS - IDENTIFICATION OF NITROGEN COMPOUNDS AND THEIR EVOLUTION DURING AGEING IN ABSENCE AND PRESENCE OF ADDITIVES

by M. Dorbon, C. Bernasconi*, J. Gaillard, J. Denis, Institut Francais du Petrole, FRANCE and *ELF FRANCE, Centre de Recherche de Solaize, FRANCE

INTRODUCTION

The growing need for Diesel fuels and developments in refining processes, particularly the increased use of Fluid Catalytic Cracking (FCC), have led refiners to consider introducing Light Cycle Oils (LCOs) in formulations of distillates for home-heating oils and Diesel fuels.

Unfortunately, the cracking products often undergo changes, and induce darkening and the formation of insolubles liable to cause difficulties in use.

The degradation mechanisms have not yet been clearly identified despite many interesting investigations already conducted. Taylor and Frankenfeld [1] reviewed a number of hypotheses and conclusions drawn from previous studies, and stressed the determining role of oxidation. Many articles have suggested that carboxylic, phenolic and sulfonic acids produced by the oxidation of middle distillates exert a catalytic effect on fuel instability [2, 3, 4] and on the quantity of sediments formed [4]. Bhan *et al* [5] demonstrated that aromatic compounds and non-basic nitrogen compounds, could be the main source of sediment formation. Recently, Pedley *et al* [6,7] found that a major source of strongly-colored sediments was the oxidation of phenalene to phenalenone, followed by the reaction of phenalenone with alkyl indoles, yielding addition products that precipitate under the influence of sulfonic acids, themselves produced by the oxidation of thiols.

In previous work [8] we found that most of the changing compounds were located in the heaviest distillation fraction of LCO (BP > 310 to 315 °C) and that better stability could be achieved by removing this fraction.

Among these compounds, those containing nitrogen were largely identified [9], showing that LCOs always contain three clearly distinct main groups of nitrogen compounds: anilines, alkyl indoles and alkyl carbazoles, and that only the alkyl indoles are subject to change during degradation in storage.

This identification led to the development of a method for determining the changes in alkyl indoles during the storage of several mixtures of straight-run distillates and LCOs in the absence and presence of additives.

EXPERIMENTAL

Several middle distillates were employed and several additives were tested for this investigation.

Middle distillates

•Three straight-run distillates (SR):	B1 and C1, E1
•Three low-sulfur LCOs:	B2 and C2, D2
•Three high-sulfur LCOs:	B3 and C3, D3

The properties of these materials are listed in Table 1. All the ageing tests were performed on LCOs and mixtures in 70/30 proportions of SR distillate and LCO. The sulfur content for some of them was accordingly higher than the present French specification of 0·3% S, but this makes the alteration effect of LCOs more pronounced.

Additives

- AD1 and AD2, mixtures of tertiary amines and metal deactivator.
- AD3, multi-purpose additive containing tertiary amines, metal deactivator and dispersant.

These additives were used mainly at 40 and 200 ppm by weight.

Ageing test methods

Three ageing test methods were employed in the laboratory.

- A highly-accelerated method, in which 350 ml of mixture is subjected for 2 h at 120 °C to a stream of 3 l/h of pure oxygen. The apparatus and bottles used are similar to those of method ASTM D-2274. The insolubles are determined by filtration through a 0·8 µm porosity cellulose acetate filter (Millipore filter AA).

  The amounts of insolubles adhering to the tube walls after only 2 h were too small to be recovered.

- A similar method to ASTM D-4625, in which 300 ml of mixture is placed in contact with atmospheric air in glass bottles at 43 °C for 12 weeks. The filtrable and adhering insolubles are determined as in ASTM D-4625, except that 0·8 µm cellulose acetate filters are used instead of 1·5 µm glass fibers filters.

- A method corresponding to conditions approaching reality, in glass bottles for one year at room temperature in air. Filtrable and adhering insolubles are determined as above.

For these three methods, the color determinations of new and aged samples were performed according to ASTM D-1500.

These three methods can be considered as complementary owing to the different operating temperatures and atmospheres.

Method for analyzing nitrogen compounds

The selective detection of nitrogen compounds by gas-phase chromatography was performed using a Perkin Elmer 8500 chromatograph equipped with a thermo-ionic detector (NPD) and a packed column injector, modified for megabore capillary columns. The column was a 15 m x 530 µm i.d. fused silica capillary column, coated with a non-polar methyl silicon phase. The temperatures were programmed as follows: from 60 to 160 °C at 2·5 °C•min^{-1}, and from 160 to 200 °C at 2 °C•min^{-1}.

RESULTS AND DISCUSSION

Ageing of middle distillates in the absence of additives

Several straight-run middle distillates and low- and high-sulfur LCOs and mixtures of SR distillates and LCOs (70/30) were subjected to the three ageing tests in the laboratory. Table 2 shows the results in colors and weights of insolubles obtained by these tests.

- It appears that the straight-run middle distillates as such are stable, except in color, irrespective of the operating conditions, temperature and duration.

- Pure LCOs, however, are very unstable over long periods at low temperature, particularly high-sulfur LCOs. Most of the insolubles are found in the form of sediments adhering to the bottle walls.

  In short-term tests at high temperature, stability appears to be satisfactory.

- Mixtures of straight-run distillates and LCOs display stability that depends on both of the components. Mixtures based on B1 display greater changes than those based on C1. For B1, the weights of insolubles are higher than anticipated from the results obtained on the two pure components. Filtrable insolubles are present in larger quantities than adhering insolubles. These two remarks do not apply to mixtures based on SR distillate C1. As to the influence of LCOs, as anticipated, mixtures containing low-sulfur LCOs are more stable than those containing high-sulfur LCOs.

If the methods are compared, it appears that the twelve-week method at 43 °C in air is very closely correlated with storage at room temperature. The two-hour method at 120°C in oxygen appears less severe.

Ageing of middle distillates in the presence of additives

Three types of additive, in concentrations of 40 and 200 ppm, were added to the SR distillates/LCOs mixtures B1/B3, C1/C2 and C1/C3, and aged by the three laboratory methods. Table 3 shows the results in color and weight of filtrable and adhering sediments. As a rule, the additives are ineffective against a color change. From the standpoint of sediments, the first two additives AD1 and AD2, based on aliphatic or cyclo-aliphatic tertiary amines combined with a metal deactivator, appear to be more effective according to the accelerated method at 120 °C than with the long-term storage methods at low temperature. The increase in concentration from 40 to 200 ppm does not improve a lot effectiveness according to these tests. Additive AD3, which also contains a dispersant, is more effective in the long-term test, and the concentration effect is significant.

The distribution of the sediments also differs in the long-term tests. With AD1 and AD2, adhering insolubles are higher than filtrable insolubles, and vice versa with AD3. The dispersant component of AD3 tends to keep the insolubles in suspension.

Analysis of ageing as a function of time

To gain a better understanding of the mechanisms of sediment formation and additive action in middle distillates during the different accelerated and long term ageing methods, a kinetic analysis was performed on several SR distillates, LCOs and SR/LCO mixtures (70/30) in the absence and presence of additives.

• Test at 120°C

For this kinetic analysis, two mixtures B1/B2 (70/30) and B1/B3 (70/30) alone and with 40 ppm of AD1 additive were subjected to ageing testing in oxygen for times ranging up to 40 hours (figure 1). A large amount of insolubles is formed during the first few hours, and the increase is then slower. The effectiveness of additive AD1 is substantial, especially during the first hours of rapid change, and then declines but still remains high :

• Tests at 43°C in the absence of additives

Figure 2 shows the curves obtained for constituents and mixtures in 12 weeks tests at 43°C. These curves have various configurations :

- SR distillates C1 and E1 have almost linear increases in insolubles content.

- LCOs give curves with varying configurations. For C2 and C3, a short induction period appears, followed by an abrupt increase in insolubles weight; whereas for D2 and D3, the increase is gradual and stabilization occurs after 8 weeks . Note the difference in scale between low sulfur LCOs and high sulfur LCOs.

- SR distillate / LCO mixtures have highly varying curve configurations as well.

• Tests at 43°C in the presence of additives

Figure 3 shows the curves obtained for SR distillate/LCO mixtures (70/30) in the absence and presence of additives. Additives diminish the amounts of insolubles formed without changing the general configuration of the curves, but preventing the formation of insolubles from reaching too high values.

Changes in nitrogen compounds: analytical method

An analytical procedure was previously developed to identify the nitrogen compounds in LCOs [9]. The same nitrogen compounds were found in many LCOs: aniline and alkyl anilines from C1 to C4, indole and alkyl indoles from C1 to C4, carbazole and alkyl carbazoles from C1 to C3 (Figure 4). Very few differences were observed in the relative proportions of each compound.

The principle of the method is the selective extraction of the nitrogen compounds by liquid chromatography and the analysis of the nitrogen extracts by coupling gas-phase chromatography with mass spectrometry (GC/MS), and by gas-phase chromatography with a specific thermo-ionic detector of nitrogen compounds [9].

Due to the similarity of composition of the LCOs, it is unnecessary to extract the nitrogen compounds from each sample analyzed. To monitor the changes, these clearly identified compounds are analyzed by gas-phase chromatography with nitrogen specific thermo-ionic detector.

This analytical method can only be qualitative for the following reasons.

(a) The response of each compound to the detector depends chiefly on the number of nitrogen atoms in the molecule, and also on the type of compound. Owing to the absence of pure compounds, it is impossible to determine the response factor of each compound.

(b) The proportion of each of these compounds is close to the detection limit, leading to difficulties of integration.

However, the method serves to compare the relative amounts of each nitrogen compound, either between different samples, or between the same samples before and after ageing.

It was previously demonstrated that most of the alkyl indole peaks drop sharply during ageing, whereas the alkyl carbazoles are relatively unaffected (Figure 5). Carbazole in particular was found in the LCOs one of the most important and one of the least altered compounds during storage. This was confirmed by an outside calibration: the height of the carbazole peak remains constant within the experimental errors, for new and aged samples. Hence it proved convenient to use the carbazole in the LCOs as an internal standard. To compare the changes in the alkyl indoles, the ratios of the carbazole/alkyl indole peak heights were determined in different ageing tests, for example as a function of storage time.

Among the 24 alkyl indole peaks counted from 15 to 38 in Figure 4, the eight highest were selected to monitor the changes in these carbazole/alkyl indole peak height ratios. These peaks were:

- 15 and 17 methyl indoles or C1 indoles,
- 19 and 21 C2 indoles,
- 26, 27, 28, 29 C3 indoles.

To assess the significance of this method, a number of repeatability tests were performed on three new and aged C1/C3 samples by successive injections or at intervals of a few days.

Table 4 gives the results of this study.

Changes in the nitrogen compounds observed by gas-phase chromatography analyses were monitored in the following two studies:

- degradation kinetics in ageing tests for LCOs, and for straight-run distillate/LCO mixtures,

- the influence of multi-purpose additives on the ageing degradation of mixtures of straight-run distillates and LCOs.

Effect of test duration on changes in nitrogen compounds

The following products were subjected to ageing:

- LCOs: low-sulfur B2 and high-sulfur C3,

- SR distillate B1/LCO B2 mixture (70/30), and SR distillate B1/LCO C3 mixture (70/30).

The following ageings were carried out:

- at 120 °C in oxygen up to 8 h,
- at 43 °C in air up to 12 weeks.

The results in carbazole/alkyl indole ratios as a function of time are given in Figures 6a, 6b, 6c and 6d for the four products aged at 120 °C. An increase in this ratio can be observed, namely a progressive decrease in the alkyl indole peaks, particularly the C1 and C2 indoles and two of the C3 indoles (26 and 28). This tendency is similar for the four products. As an example, Figure 5 shows a comparison between the NPD chromatograms of LCO B2 before and after ageings. The indole itself (peak 11) also decreases very substantially, but the height of this peak is very difficult to measure in most of the chromatograms, and the corresponding values could not be plotted on the diagrams.

At 43 °C in air, for the same four products, the changes in the nitrogen compounds shown in Figures 7a, 7b, 7c and 7d are similar to those observed at high temperature.

It is interesting to observe that a comparison of these results relative to the decrease in alkyl indoles shows that substantially equivalent values in weights of insolubles are obtained in three months at 43 °C and in 5 to 10 h at 120 °C. This confirms the relationship that may exist between the reactivity of the alkyl indoles and the storage instability of LCOs alone and in mixtures.

Effect of multi-purpose additives on the reactivity of alkyl indoles

Multi-purpose additives AD1, AD2 and AD3 were added at the rate of 40 and/or 200 ppm to the three distillate/LCO mixtures:

- SR distillate B1/ high-sulfur LCO B3 (70/30),
- SR distillate C1/ high-sulfur LCO C3 (70/30),
- SR distillate C1/ low-sulfur LCO C2 (70/30).

These mixtures were subjected to the following ageing tests :

- at 120 °C in oxygen for 2 h,
- at room temperature in air for 12 months.

In addition to the gravimetric determinations performed after filtration of the insolubles (Table 3), the nitrogen compounds were analyzed to monitor their changes.

For the comparative tests performed at 43 °C in 12 weeks, the weights of insolubles are shown in Table 3, but the nitrogen compounds were not analyzed.

Effect on B1/B3 mixtures:

The results are shown in Figures 8a and 8b in the form of the same diagrams as for the previous study, in ratios of carbazole/alkyl indole peak heights for the eight highest peaks.

In the absence of additive, the variation in these ratios or the decrease in alkyl indoles are more pronounced at 120 °C than at room temperature, whereas the weights of insolubles are higher at room temperature than at 120 °C.

Additives AD1, AD2 and AD3 are effective in preventing the reaction of alkyl indoles, because, for all the peaks, they return the carbazole/alkyl indole ratios to values close to the initial values before ageing. This is especially valid for AD1 at 120 °C and at room temperature, and for AD3 at room temperature, whereas the weights of insolubles remain relatively high despite the presence of these additives at room temperature particularly.

Effect on C1/C3 mixtures:

Similar results are shown in Figures 9a and 9b for these mixtures.

The diagrams have the same pattern as the foregoing: increase in the peak ratios, hence decrease in alkyl indoles when ageing without additive, but maintenance of peak ratios at intermediate values or close to the initial values for ageings in the presence of additives. Additive AD1 is more effective for the test at 120 °C than for the test at room temperature, while additive AD3 is highly effective in both types of test. At 40 ppm, and, above all, at 200 ppm, the alkyl indole peaks practically return to their initial value.

For all these C1/C3 mixtures, the weights of insolubles are too low at 120 °C to compare the effect of the additives from this standpoint. At room temperature, however, the weights of insolubles still remain high in the presence of additives, as for the B1/B3 mixtures.

Effect on C1/C2 mixtures:

For C1/C2 mixtures, the weights of insolubles are very low, and demonstrate the good storage stability of these products in mixtures. Tests with additives were not performed at 120 °C. The chromatographic analyses show in Figure 10 that the alkyl indoles preserve their initial content in the ageing test in the absence or presence of additives, which agrees with the relationship between the reactivity of the alkyl indoles and the storage stability.

The investigation of the influence of storage time on the behavior of LCOs and distillates containing a certain proportion of LCO revealed a close correlation between the formation of insolubles and the progressive disappearance of alkyl indoles, providing confirmation of the degradation mechanism proposed by Pedley *et al* [6].

According to this mechanism, moreover, the alkyl indoles only react in the presence of other oxidizable compounds. The products that react with alkyl indoles are perhaps absent in this case. This could explain the fact that in C1/C2 the alkyl indoles are present and not reactive.

The influence of additives on this variation in alkyl indole content during ageing is highly significant. On the one hand, they display great effectiveness in preventing the progressive disappearance of alkyl indoles, because chromatography shows that the alkyl indole peaks retain their initial value. On the other, they are less effective in preventing the formation of insolubles. Hence it appears that other products and other mechanisms are also involved in the degradation of LCOs, independent of the alkyl indoles, and that the additives are poorly effective in combating the detrimental effect of these other products.

CONCLUSIONS

This research project follows an analytical study concerning the identification of nitrogen compounds in middle distillates from fluid catalytic cracking (LCOs) [9].

The development of a method for monitoring the changes in nitrogen compounds served to observe the progressive decrease in the indole and alkyl indole contents during actual and laboratory storage tests on LCOs and mixtures of uncracked distillates and LCOs.

A comparison between the weights of insolubles determined during storage and the decrease in alkyl indoles confirms the degradation mechanism proposed by Pedley *et al* [6], namely the oxidation of phenalene to phenalenone, followed by the reaction of phenalenone with alkyl indoles, yielding precipitates under the influence of sulfonic acids resulting from the oxidation of thiols.

The analyses performed after the ageing tests conducted in the presence of additives showed that the alkyl indoles retain their initial value, while insolubles are still being formed. This would tend to show that some insolubles could be formed by mechanisms different from the one involving alkyl indoles.

REFERENCES :

(1) TAYLOR W.F., FRANKENFELD J.W., 2nd. International Conference on Long Term Storage Stabilities of Liquid Fuels, 1986, San Antonio (TEXAS, USA) pp. 456-511.

(2) HAZLETT R.N., KELSO G., 2nd International Conference on Long Term Storage Stabilities of Liquid Fuels, pp. 541-555

(3) HILEY R.W. , PEDLEY J.F., Fuel, 1988, vol 67, pp. 469-473.

(4) HAZLETT R.N., POWER A.J., 2nd International Conference on Long Term Storage Stabilities of Liquid Fuels, 1986, San Antonio (TEXAS, USA), pp. 556-569.

(5) BAHN O.K., BRINKMAN D.W., GREEN J. B., CARLEY B., Fuel, 1987, vol 66, pp. 1200-1214.

(6) PEDLEY J.F., HILEY R.W., HANCOCK R.A., Fuel, 1988, vol 67 pp. 1124-1130.

(7) PEDLEY J.F., HILEY R.W., HANCOCK R.A., Fuel, 1989, vol 68 pp. 27-31.

(8) BERNASCONI C., CHAFFARDON A., CHARLEUX P., DENIS J., GAILLARD J., DURAND J.P., 3 rd International Conference on Stability and Handling of Liquid Fuels", 1988, London (UK), pp. 423-440.

(9) DORBON M., BERNASCONI C., Fuel, 1989, vol 68 pp. 1067-1074.

TABLE 1

CHARACTERISTICS OF MIDDLE DISTILLATES

Characteristics		SR distillates			Low-sulfur LCOs			High-sulfur LCOs		
		B1	C1	E1	B2	C2	D2	B3	C3	D3
Flash point	°C	111	106	102	85	92	71	81	70	72
Cloud point	°C	7	-8	-1	-10	-9	-37	-10	-15	-10
Cold filter plugging point	°C	6	-9	0	-15	-11	-37	-23	-17	-19
Pour point	°C	3	-12	-3	-27	-21	<-42	-43	-24	-36
Sulfur	%	0.14	0.04	0.11	0.84	0.51	0.59	2.54	1.31	1.69
Total nitrogen	ppm	265	10	230	630	670	510	440	590	685
Basic nitrogen	ppm	170	7	58	100	75	106	90	99	115
Viscosity at 20°C	mm2/s	9.4	5.41	6.53	3.79	4.56	2.94	3.53	3.59	3.89
Density at 15°C	kg/l	0.8639	0.8276	0.8438	0.9355	0.9106	0.8996	0.9382	0.9118	0.9262
DISTILLATION										
Initial boiling point	°C	232	220	200	148	191	150	120	132	138
Final boiling point	°C	402	355	358	339	354	311	334	342	344
MASS SPECTROMETRY										
Paraffins	%	27.4	41.8		14	12.2		10.8	11.7	
Naphthenes	%	43.2	40.5		9.2	16.8		7.8	9.8	
Monoaromatics	%	7	3.7		10.9	10.6		11	12.1	
Diaromatics	%	13.9	8.2		38.3	34.3		38.1	37.7	
Triaromatics	%	6.6	4.4		18	17.5		13.4	14.7	
Benzothiophenes	%	1.5	0.6		6.7	5.7		15.8	10.7	
Dibenzothiophenes	%	0.4	0.8		2.9	2.9		3.1	3.3	

TABLE 2

STABILITY TESTS OF DISTILLATES PURE AND IN MIXTURES

Distillates	Initial color (ASTM D1500)	Insolubles before test mg/100 ml	After 2h. 120°C in O2		After 12 weeks. 43 °C in air				After 1 year at room temperature in air			
			Color	total insolub.*	Color	Filterable insolub.	Adhering insolub.	Total insolub.	Color	Filterable insolub.	Adhering insolub.	Total insolub.
SR middle distillates												
B1	1	0.2	1.5	0.4	3.5	0.5	0	0.5	2.5	0.3	0.5	0.8
C1	0	nd	0	0.1	0.5	0	0.3	0.3	0.5	0.1	1.5	1.6
Low-sulfur LCOs												
B2	2.5	nd	3.5	0.5	H8	2.5	20.9	23.4				
C2	1.5	nd	2.5	0.1	7	6.4	10	16.4	6	6.9	4.7	11.6
High-sulfur LCOs												
B3	2	0.2	<3.5	0.2	7.5	0.8	37.1	37.9				
C3	1.5	nd	3	0.2	7.5	34.7	10.7	45.4	7.5	42.3	17.1	59.4
70/30 mixtures												
B1/B2	2	0.1	6	1.6	6	7.9	4.1	12				
B1/C2	2	nd	<3.5	0.7	5.5	6.5	2.8	9.3				
C1/C2	1	0.1	1.5	0.1	2.5	0.4	1.4	1.8	2.5	0.2	1.7	1.9
B1/B3	2	0.1	6.5	13.8	5.5	11.6	5.4	17	5.5	12.6	4.7	17.3
B1/C3	2	0.2	5	5	5.5	3.8	5.9	9.7				
C1/C3	1	0.1	1.5	0.3	2.5	0.4	6.6	7	3	5.8	3.7	9.5

* No adhering insoluble by this method

TABLE 3

STABILITY TESTS OF MIDDLE DISTILLATES IN MIXTURES WITH ADDITIVES

Distillates + additives	Initial color (ASTM D1500)	Insolubles before test mg/100 ml	After 2h. 120°C in O2		After 12 weeks. 43 °C in air				After 1 year at room temperature in air			
			Color	total insolub.*	Color	Filterable insolub.	Adhering insolub.	Total insolub.	Color	Filterable insolub.	Adhering insolub.	Total insolub.
B1/B3 (70/30)	2	0.1	6.5	13.8	5.5	11.6	5.4	17	5.5	12.6	4.7	17.3
+ AD1 40 ppm	"	"	5	3.1	5.5	3.8	4.2	8	5.5	6.6	4.1	10.7
+ ADI 200 ppm	"	"	nd	nd	5.5	1.6	5.4	7	5.5	5.3	5.9	11.2
+ AD2 40 ppm	"	"	6	3.1	5.5	2.9	6.3	9.2				
+ AD3 40 ppm	"	"		nd	7	3.8	0.7	4.5				
+ AD3 200 ppm	"	"			7	3.8	0.7	4.5	6.5	5.1	2.5	7.6
C1/C2 (70/30)	1	0.1	1.5	0.1	2.5	0.4	1.4	1.8	2.5	0.2	1.7	1.9
+ AD1 40 ppm	"	"		nd	3	0.6	1.8	2.4	3	0.3	2.7	3
+ AD1 200 ppm									3	0.5	2.1	2.6
+ AD3 40 ppm	"	"		nd	3	0.8	0.6	1.4	3	0.8	0.4	1.2
+AD3 200 ppm									3	0.2	1	1.2
C1/C3 (70/30)	1	0.1	1.5	0.3	2.5	0.4	6.6	7	3	5.8	3.7	9.5
+ AD1 40 ppm	"	"	1.5	0.1	2.5	1.3	4.2	5.5	3	0.8	7.8	8.6
+ AD2 40 ppm	"	"	1.5	0.1	3	3	4.9	7.9				
+ AD3 40 ppm	"	"	1.5	0.2	2.5	4.9	0.8	5.7	3	4.8	2.4	7.2
+ AD3 200 ppm	"	"	1.5	0.2					3	2.6	1.6	4.2

*No adhering insoluble by this method

TABLE 4

REPEATABILITY OF DETERMINATIONS OF CARBAZOLE/ALKYL INDOLE PEAK HEIGHT RATIOS BY GAS-PHASE CHROMATOGRAPHY

Sample	Date	Peak 15	Peak 17	Peak 19	Peak 21	Peak 26	Peak 27	Peak 28	Peak 29
C1/C3 no aged	4/14/89	0.9	0.5	0.33	0.33	0.8	0.9	0.75	0.7
	4/17/89	1.1	0.55	0.31	0.34	0.7	0.9	0.9	0.7
C1/C3 aged at 120°C	4/14/89	1.3	0.7	0.55	0.53	1	0.96	1	0.85
	4/17/89	1.4	0.8	0.6	0.53	0.9	0.92	1.05	0.9
C1/C3 aged with AD2 at 120°C	4/14/89	1.3	0.55	0.4	0.4	0.8	1.1	1.1	0.8
	4/18/89	0.95	0.55	0.35	0.35	0.75	0.9	0.8	0.7
	4/18/89	0.95	0.5	0.3	0.35	0.7	0.85	0.75	0.7

F I G U R E 1

AGEING KINETICS AT 120°C IN OXYGEN

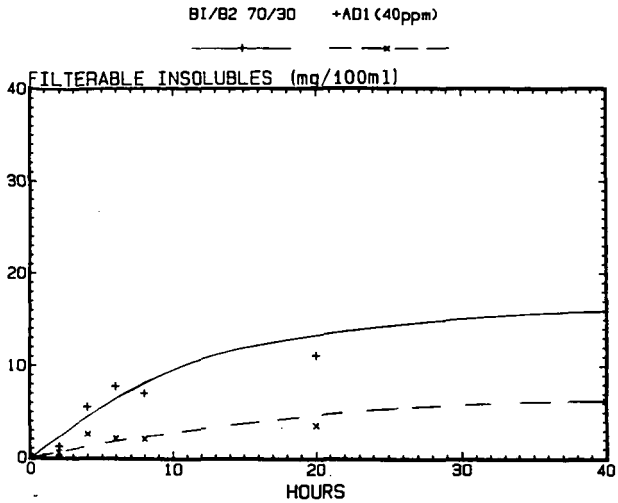

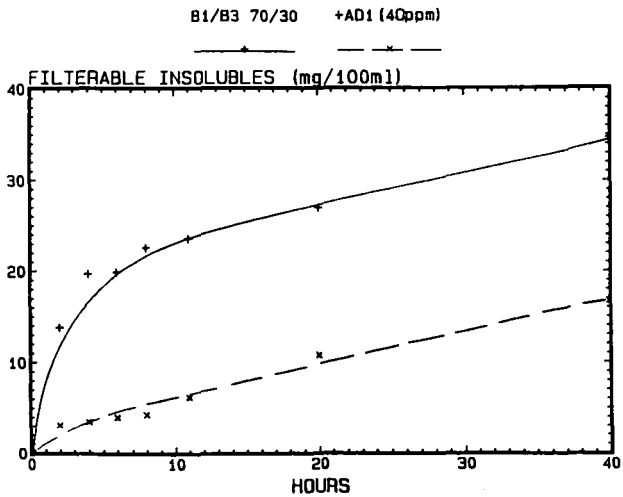

F I G U R E 2

AGEING KINETICS AT 43°C IN AIR (WITHOUT ADDITIVES)

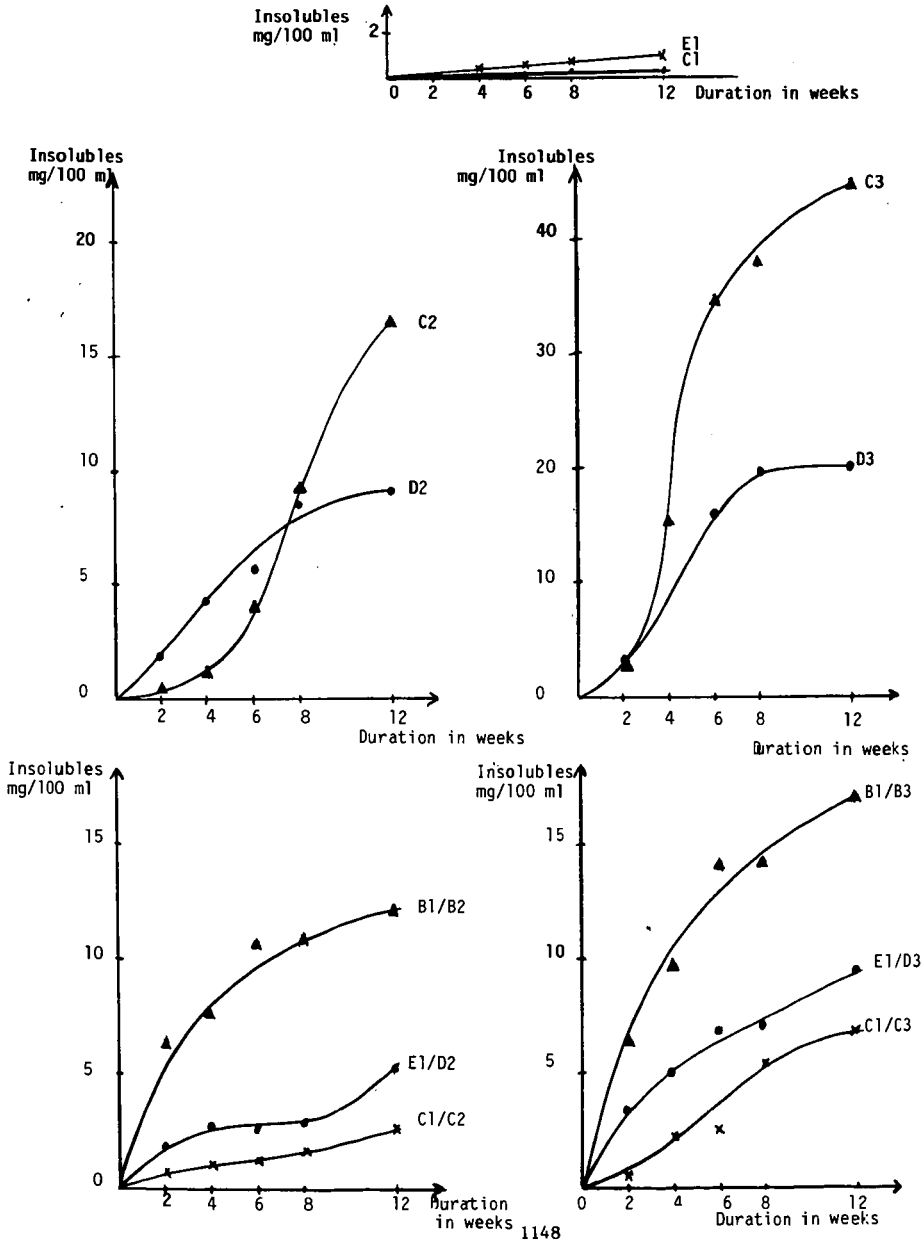

F I G U R E 3

AGEING KINETICS AT 43°C IN AIR (WITH ADDITIVES)

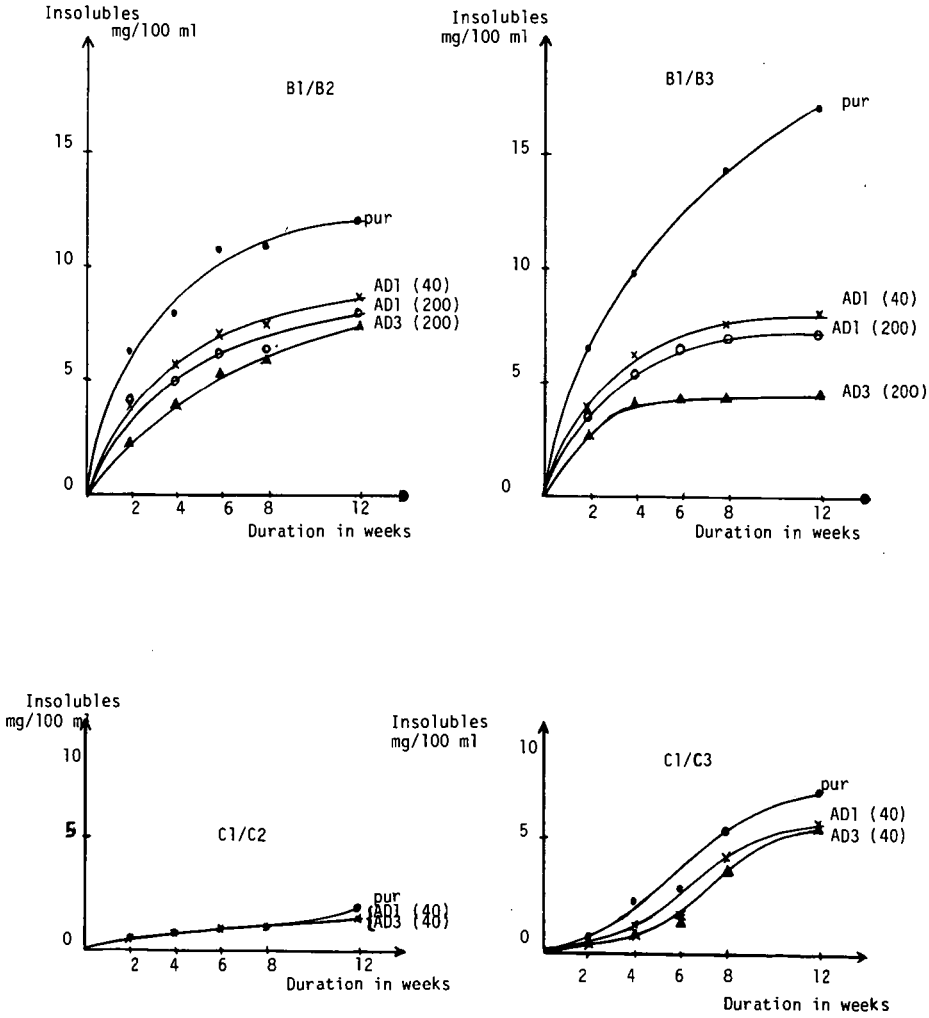

FIGURE 4

NPD CHROMATOGRAM OF NITROGEN COMPOUNDS IDENTIFIED IN A LCO

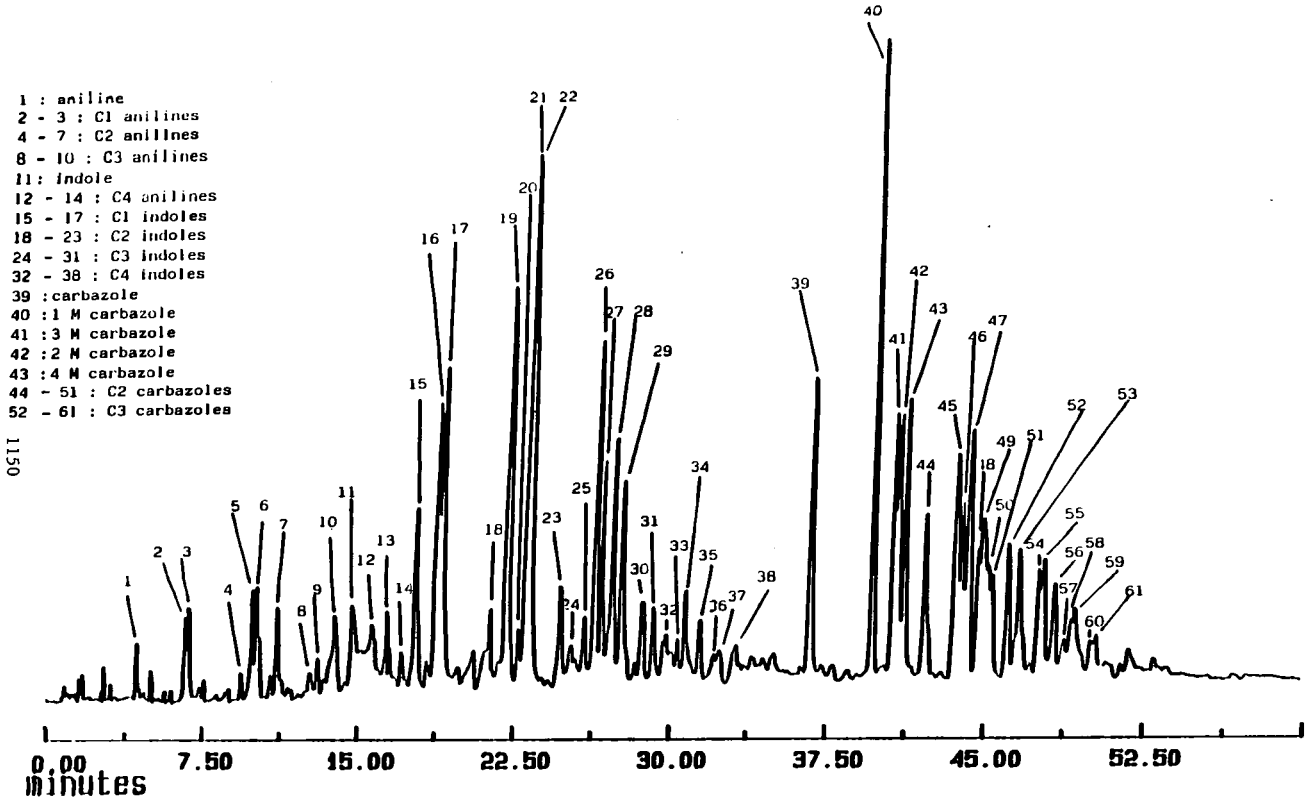

F I G U R E 5
NPD CHROMATOGRAMS OF LCO B2, BEFORE AGEING, AFTER AGEING AT 43°C, AND AFTER AGEING AT 120°C

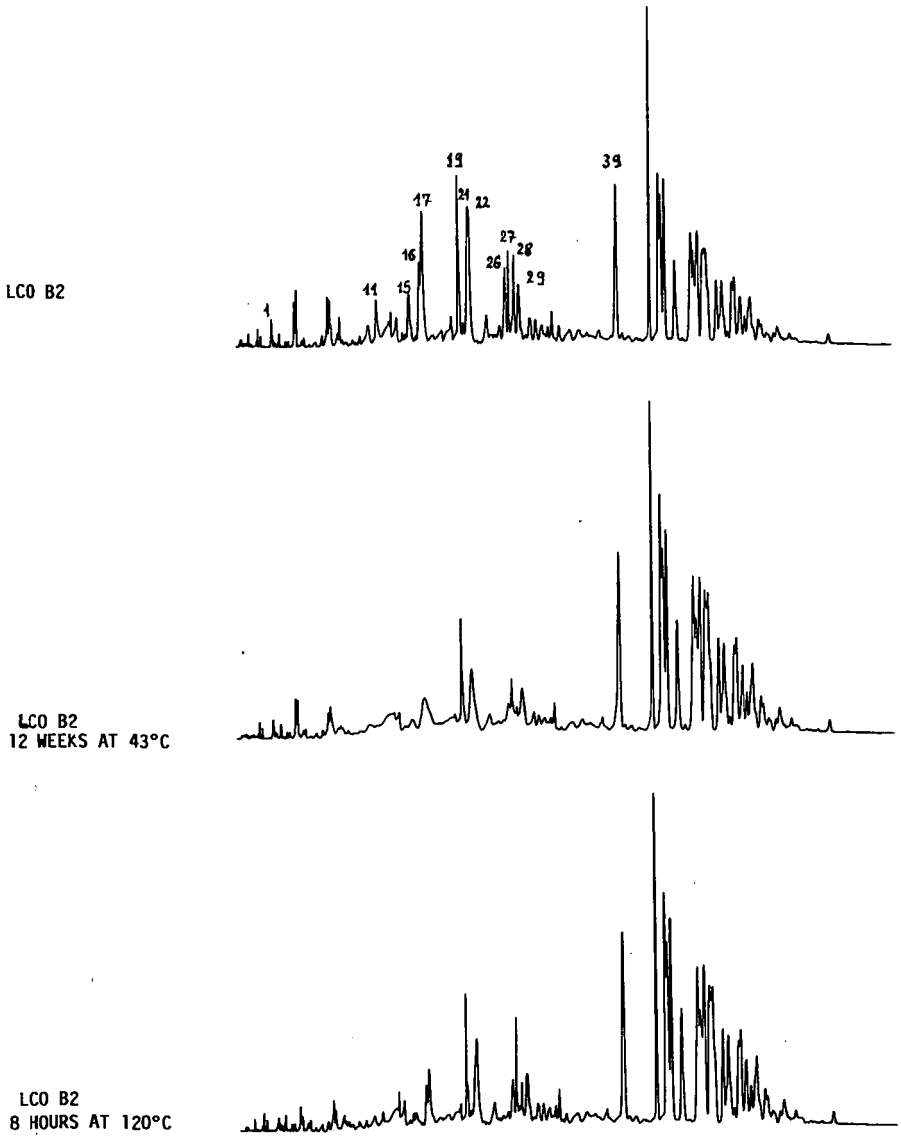

F I G U R E 6

NITROGEN COMPOUNDS AS A FUNCTION OF TIME AT 120°C

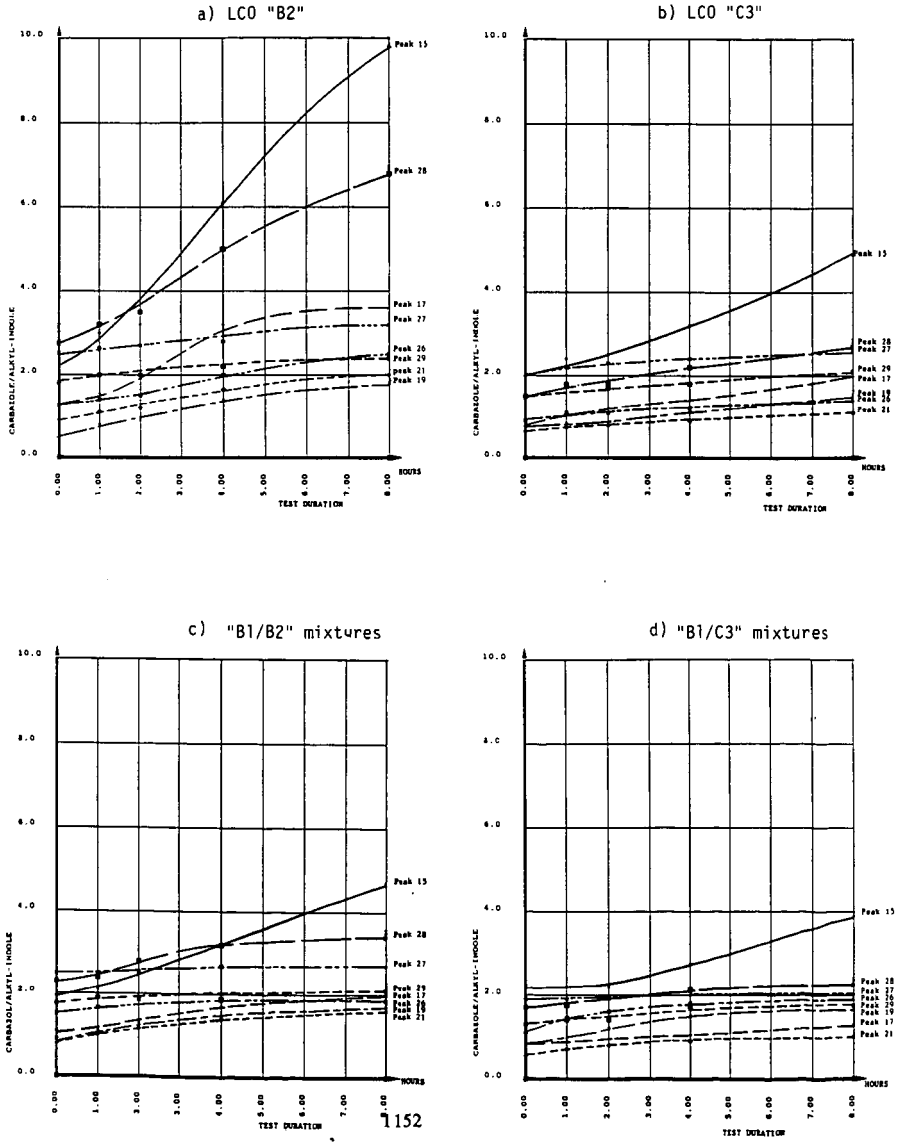

F I G U R E 7

NITROGEN COMPOUNDS AS A FUNCTION OF TIME AT 43°C

a) LCO "B2"

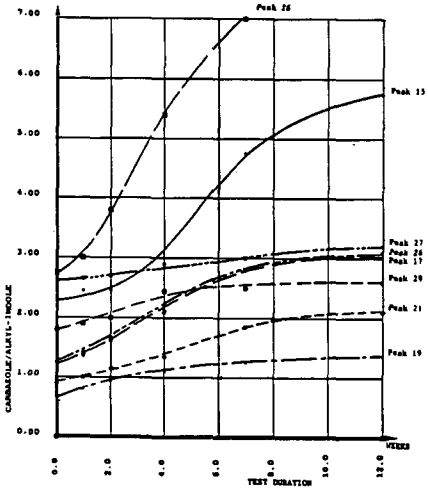

b) LCO "C3"

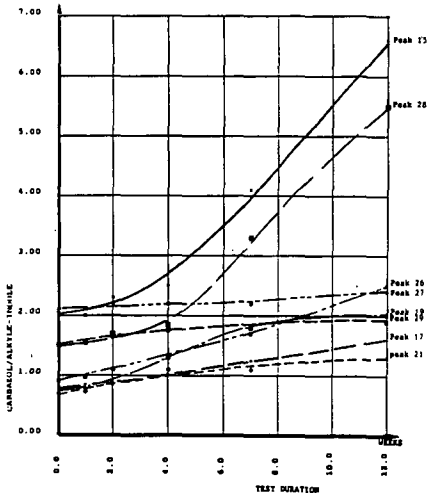

c) "B1/B2" mixtures

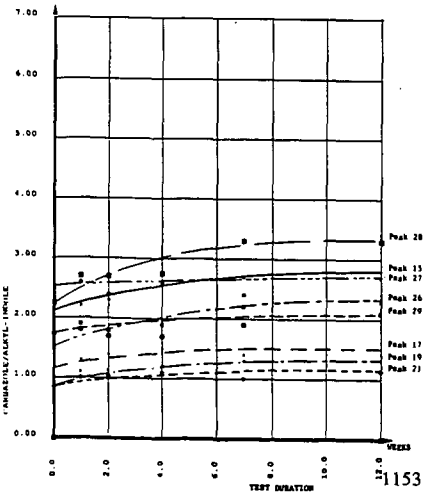

d) "B1/C3" mixtures

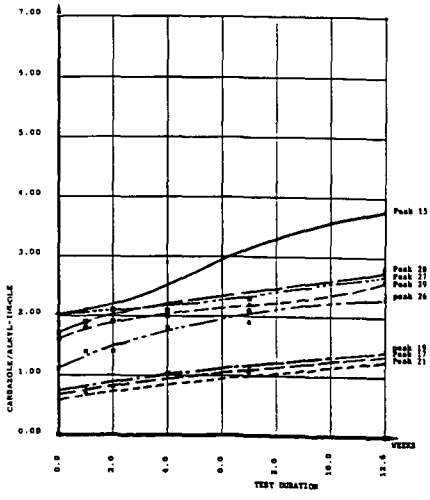

F I G U R E 8

INFLUENCE OF ADDITIVES ON CHANGES IN NITROGEN COMPOUNDS IN B1/B3 70/30 MIXTURES SUBJECTED TO AGEINGS

a) two hours at 120°C in oxygen

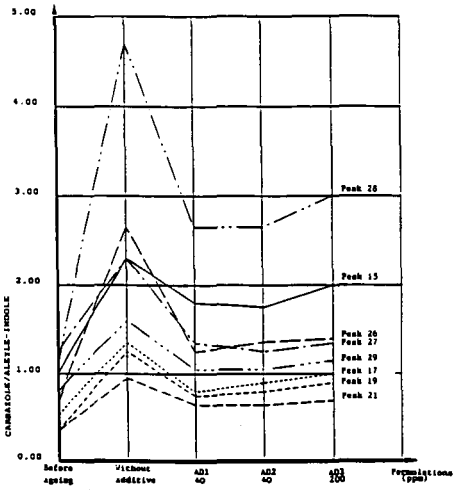

b) one year at ambient temperature in air

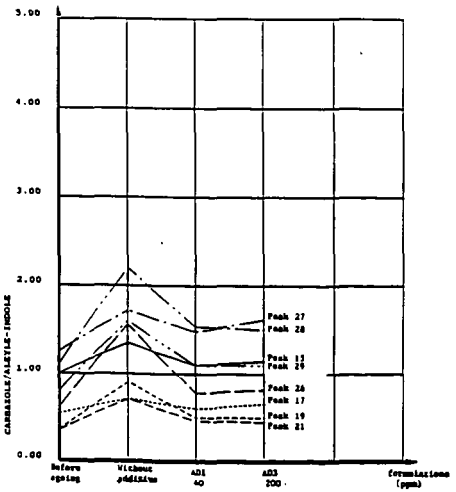

F I G U R E 9

INFLUENCE OF ADDITIVES ON CHANGES IN NITROGEN COMPOUNDS IN C1/C3 70/30 MIXTURES SUBJECTED TO AGEINGS

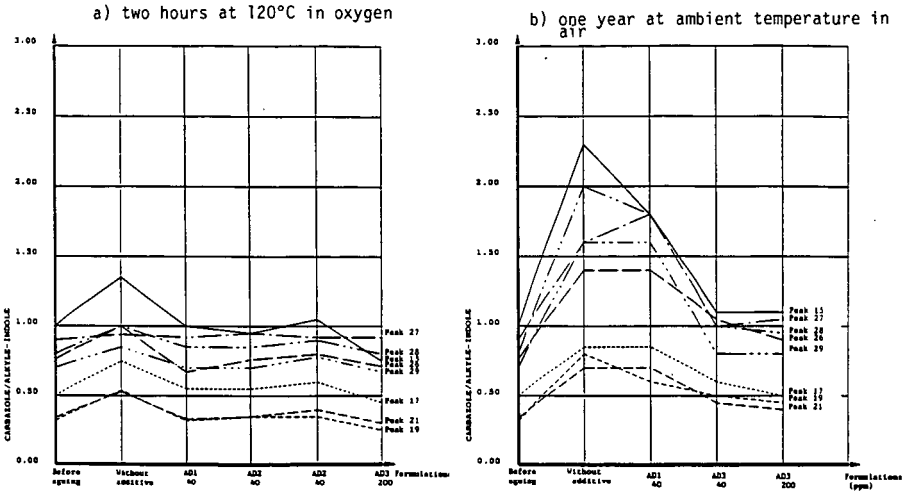

F I G U R E 10

INFLUENCE OF ADDITIVES ON CHANGES IN NITROGEN COMPOUNDS IN C1/C2 70/30 MIXTURES SUBJECTED TO AGEINGS

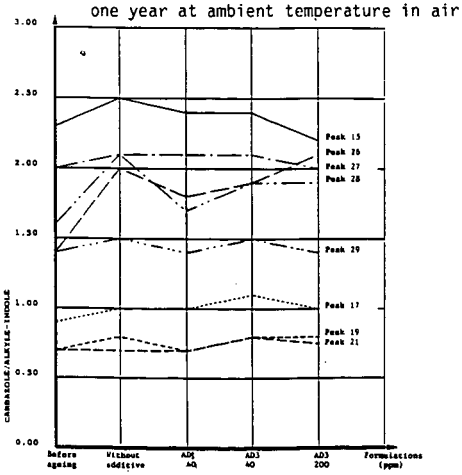

CHEMICAL EXAMINATION OF DISTILLATE FUEL DEPOSITS FORMED DURING STORAGE

Robert N. Hazlett
Hughes Associates, Inc.
5205 Chippewa Pl., Alexandria, VA 22312
and
John A. Schreifels
George Mason University, Chemistry Dept.
Fairfax, VA 22030

INTRODUCTION

Storage stability of distillate fuels has been of modest concern for fuels made by refining processes based on straight run distillation. However, increasing quantities of heavy crudes are being run in refineries using catalytic cracking processes to increase the yield of middle distillate fuels. The cracked products, which contain chemically unstable species, are blended into straight run streams. The unstable components, although diluted by the blending, still exert a strong influence on deposit formation, particularly for long storage periods. The fuel instability is manifested by the formation of insoluble products which play havoc with filters and nozzles of engines.

Oxidation is involved in the undesirable reactions as are fuel components containing hetero-atoms such as sulfur, nitrogen, and oxygen. More than free-radical autoxidation is involved, however, since typical free-radical antioxidants are ineffective in controlling this instablity and can be deleterious (1). Further, degradation is increased by the presence of organic acids with the stronger acids exerting significant effects (2).

In this paper, we utilize several experimental techniques to characterize the insolubles as an aid in understanding the chemical processes which control the undesirable instability. The deposits examined include ones formed in stressed, undoped straight run/light cycle oil (SR/LCO) blends and in similar blends to which acids were added.

EXPERIMENTAL TECHNIQUES AND PROCEDURES

LCO and SR from a US Gulf Coast refinery were blended in a 20/80 ratio. The samples were stressed under accelerated conditions of 80 degC for 7 or 14 days, equivalent to 1 to 2 yrs at ambient conditions. Suspended products of instability were removed by filtration and products adhering to the stressing flask were removed with gum solvent. After evaporation of the solvent, the filterable and adherent insolubles were dried in a vacuum oven at 75 degC. The acids used as dopants were dodecylbenzene sulfonic acid (DBSA), chloroacetic acid (CA), and p-t-butyl thiophenol (PBTP).

Elemental analyses of the insolubles were done by Galbraith Laboratories, Knoxville, TN. Stressed and unstressed fuel blends and deposits were titrated in a non-aqueous solvent with approximately 0.04 N alcoholic KOH. X-Ray Photoelectron

Spectroscopy (XPS) analysis was conducted at the Naval Research Laboratory, Washington, DC and Field Ionization Mass Spectrometry (FIMS) was performed at SRI International, Menlo Park, CA.

EXPERIMENTAL RESULTS

Elemental Analysis. Table I lists the results of elemental analysis of various deposits from the stress tests. The carbon, hydrogen, and oxygen contents were similar for the insolubles from all samples. Nitrogen was lower for the sample derived from the fuel doped with p-t-butyl thiophenol. Sulfur was significantly higher for the blends doped with sulfur compounds, both the DBSA and the PBTP. All of these concentrations fall within the range observed for insoluble material derived from other storage stability experiments. The low H/C ratio (0.9 - 1.0) along with the high nitrogen, sulfur, and oxygen values support the view that hetero-aromatic compounds are major participants in insolubles formation. Chlorine was found in the insoluble sample derived from the fuel blend containing 0.01 M chloroacetic acid. Insufficient sample was available to do the other elements for this sample.

Titration Curves. Non-aqueous titrations of the stressed and unstressed liquid fuels gives useful information on the disposition of the added acids. Typical curves are shown for the sulfonic acid in Figure 1 and for thiophenol in Figure 2. The fuel blends for these titrations were not the same as the stress test samples but the same observations apply. The titrations in Figures 1 and 2 were done on different instruments which used opposite polarity conventions. The titration curve for unstressed DBSA exhibits a very high initial emf compared to the fuel blank. This is characteristic of strong acids such as sulfonic acids. The inflection point for neutralization of the strong acid is about +100 mv. The initial emf for the stressed DBSA is still high but the curve demonstrates that much of the DBSA is not available in the fuel after stress.

The titration curve for thiophenol shows that most of this weak acid has reacted during the stress period. Further, the initial emf has shifted from +120 mv to -220 mv. This is indicative of the presence of a very strong acid, sulfonic acid. Although the titer for strong acid is low, a definite quantity is present.

In addition to titration of the stressed and unstressed fuel blends, the solid sediments formed during the stress were subjected to non-aqueous titration. Strong acid was found in the sediments from the DBSA and PBTP doped samples.

XPS Analysis. This spectroscopic analysis was applied to the solids, both filterable and adherent, formed in the 80 degC stress. This technique affords good qualitative information but is not completely quantatative at low (<1%) levels of atomic %. This is due to electrical charging of the specimen in the high vacuum. Data for a typical analysis of insolubles is shown in Table II. The information is tabulated as atom % as opposed to weight % for Table I. This fact plus the fact that hydrogen is not determined

by XPS explains most of the differences between the results in Tables I and II.

Chlorine was detected only in the CA doped sample but just above the noise level. Sulfur is enhanced in the sulfur doped samples. XPS can distinguish between different valence states of atoms. This was particularly helpful in examining the sulfur composition. As Table III shows, reduced and oxidized forms of sulfur were found in these insoluble sediments. It is noteworthy, however, that the oxidized form predominates in the samples doped with the sulfonic acid and the thiophenol.

FIMS Analysis. This mass spectroscopic method affords a molecular weight pattern for a sample. The solids were pyrolyzed on a temperature-programmed probe in the inlet of the instrument. Further description and use of this technique will be detailed in another paper of this symposium. The highlights of FIMS application to the doped samples are as follows:

(a) Major peak at 326 mass units for DBSA doped fuel; - DBSA mol. wt. is 326
(b) Major peaks at 166, 214, and 330 for PBTP doped fuel; - PBTP mol. wt. is 166, PBTP dimer mol. wt. is 330, and p-t-butyl benzene sulfonic acid mol. wt. is 214
(c) No peaks specific to CA were found in the insolubles from fuel doped with this acid

DISCUSSION

A test for material balance was made for the added acids. This was accomplished by non-aqueous titrations of the unstressed liquid fuel, the stressed liquid fuel, the filtration rinses, and the insolubles dissolved in titration solvent (1 part toluene to 1 part isopropyl alcohol). The petroleum ether rinses contained minute amounts of acid, only slightly more than the solvent blank. Table IV itemizes the balance for DBSA. A significant amount of strong acid was found in the insolubles, at least for the samples to which 1.0 mmol/L of DBSA was added. The acid concentration in the liquid fuel after stress and filtration was definitely lower than in the unstressed fuel. In fact, the amount of insolubles formed increases linearly with the decrease in DBSA concentration. Some of the DBSA could not be accounted for.

Added p-t-butyl thiophenol reacts rapidly at 80 degC and is 90% gone in two weeks. Most of this is probably oxidized to the disulfide.(3) Thus, PBTP and its products cannot be tracked by acid titration. However, a small amount of strong acid is found in the stressed fuel and in the insolubles. Two % of the thiol is found as strong acid in the stressed fuel and one % is found in the insolubles. Thus about 3 % of the thiol is oxidized all the way to a sulfonic acid.

The results on the material balance for chloroacetic acid were mixed. In one fuel the titer on the stressed, filtered fuel was similar to that for the unstressed material. In another fuel, 75 to 95 % of the titratable CA was lost from the liquid fuel after stress. Less than one % of this loss could be accounted for as titratable CA in the insolubles. Bound

(non-titratable) chloride could account for less than one % of the loss (1.2 % Cl in the insolubles x 8 mg/100 mL total insolubles for a fuel blend doped with 6.0 mmol/L of CA).

The overall thrust of the data on DBSA demonstrates that it is an active participant in insolubles formation for the SR/LCO distillate fuel blend. The fact that DBSA is present in the insolubles as titratable strong acid and the fact that the reaction occurs fairly quickly (2 to 5 days at 80 degC to attain a plateau for total insolubles (4)) indicates that the sulfonic acid is involved in salt formation. Corroborating evidence for this viewpoint comes from XPS, which found significant concentrations of sulfur in the oxidized form in the sediment from a DBSA doped fuel blend. The FIMS mol. wt. profile exhibited a large peak at 326, the mass of DBSA, another finding that supports the presence of DBSA in the solid formed during stress.

The earlier theory that acids act as catalysts for forming deposits in SR/LCO blends on the basis of their hydrogen ion concentration (2) must be modified, at least for DBSA. It would appear that DBSA operates in a dual role: (a) acid catalyst for deposit forming reactions and (b) direct participation in insolubles formation by salt formation.

PBTP participates in deposit formation by first oxidizing to p-t-butylbenzene sulfonic acid. This acid can then behave like DBSA, acting in the dual role of acid catalyst and active participant in forming insoluble salts. Only a small fraction of the PBTP converts to acid but the high reactivity of the acid makes it effective at low concentrations. The XPS and FIMS data support the incorporation of the acid in the deposits but direct addition of the thiol to olefins cannot be excluded.

The role of chloroacetic acid in deposit formation cannot be clearly defined on the basis of current knowledge. A theory from earlier work (2), which suggested that CA was acting as an acidic catalyst for deposit formation, may have to be modified.

REFERENCES

(1) R.N. Hazlett, D.R. Hardy, E.W. White and L. Jones-Baer, "Assessment of Storage Stability Additives for Naval Distillate Fuel", SAE Tech. Paper 851231, May 20-23, 1985.

(2) R. N. Hazlett, Fuel Science & Tech. Int'l., 6, 185 (1988).

(3) G.W. Mushrush, J.W. Watkins, R.N. Hazlett, D.R. Hardy and H.G. Eaton, Am. Chem. Soc., Fuel Chem. Div. Preprints, 32, 522 (1987).

(4) R. N. Hazlett and W. Stalick, unpublished data.

TABLE I

Elemental Analysis of Fuel Deposits

Dopant and Conc.	Percent Element							
	C	H	N	S	O	Cl	Ash	Total
None*	77.75	6.08	2.59	1.93	9.38	--	2.24	99.97
DBSA 0.001 M	76.99	6.44	2.53	3.84	9.26	--	0.98	100.04
PBTP 0.03 M	76.86	6.48	1.61	4.42	10.03	--	0.41	99.81
CA 0.01 M	--	--	--	--	--	1.22	--	--

*Deposit formed at ambient temperature. Other deposits formed at 80 degC, two weeks stress.

TABLE II

Percent Atomic Composition of Insolubles by XPS*

Dopant and Conc.	C	O	N	S	Cl
None	79.5	16.5	2.6	1.4	--
DBSA 0.001 M	75.5	18.7	2.9	2.8	--
PBTP 0.03 M	80.5	15.2	1.7	2.5	--
CA	77.0	18.9	2.1	1.3	0.3

*Insolubles formed in 80 degC stress for two weeks
Gulf Coast blend: 20% LCO in SR

TABLE III

Percent Atomic Concentrations of Two Different Types of Sulfur by XPS

Dopant and Conc.	Reduced Sulfur	Oxidized Sulfur	Total Sulfur
None	0.5	0.9	1.4
DBSA 0.001 M	0.9	1.8	2.8
PBTP 0.03 M	0.6	1.9	2.5
CA 0.01 M	0.6	0.7	1.3

TABLE IV

DBSA Material Balance

		DBSA in Fuel			
Stress	DBSA Added	Before Stress	After Stress	DBSA in Insolubles	DBSA Deficit
80 degC 7 days	-0-	0.00	0.08	0.003	--
80 degC 7 days	1.00	0.96	0.71	0.12	0.13
80 degC 7 days	0.30	0.32	0.17	0.02	0.12
80 degC 14 days	1.00	0.84	0.68	0.15	0.01

DBSA Concentration in mmol/L

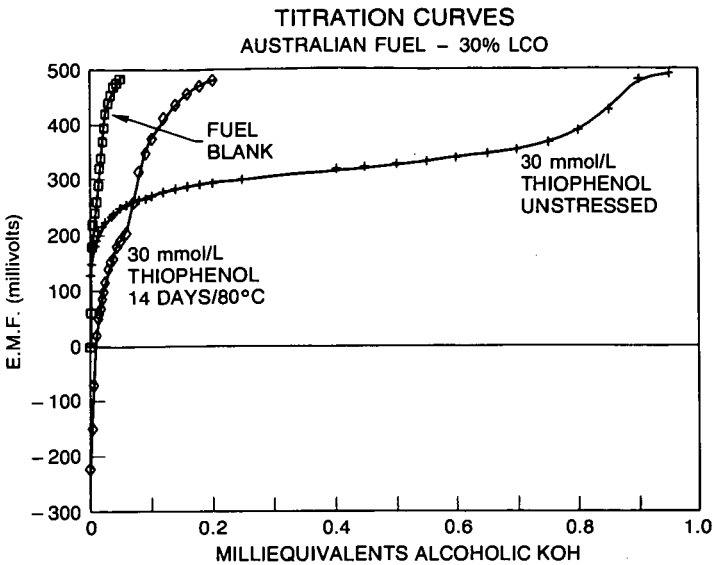

FIGURE 1.

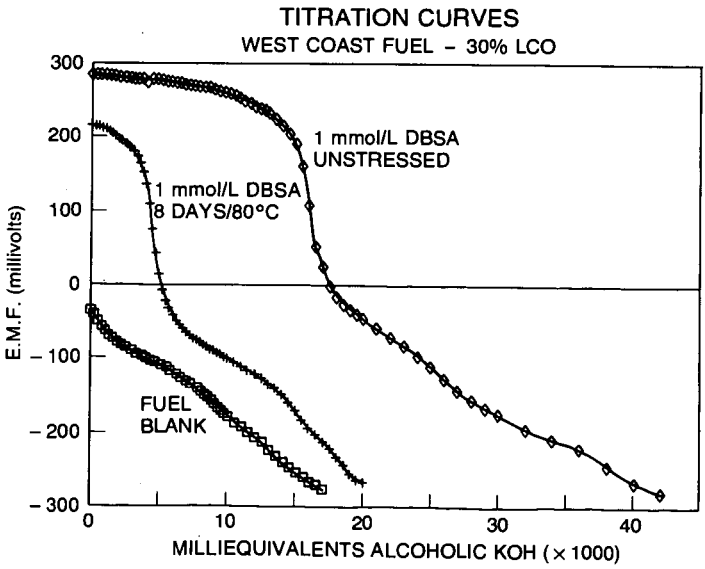

FIGURE 2.

FIELD IONIZATION MASS SPECTROMETRIC ANALYSIS OF SEDIMENTS FROM DIESELS DOPED WITH STRONG ACIDS

Ripudaman Malhotra
Department of Chemical Kinetics
SRI International, Menlo Park, CA 94025

and

Robert N. Hazlett
Hughes Associates, Inc., Wheaton, MD 20902

KEYWORDS: Storage Stability, Adherent Gums, Deposits, FIMS, Sulfonic acids.

ABSTRACT

Filtered sediments formed in Texas diesel containing light cycle oil under ambient conditions and upon accelerated ageing at 80 °C for two weeks with added dodecylbenzenesulfonic acid (DBSA) or chloroacetic acid were examined by pyrolysis-field ionization mass spectrometry (Py-FIMS). During the analysis over 50% of the sediment was devolatilized. The spectra showed very similar profiles and correspondence between most prominent peaks indicating that doping with these acids does not drastically alter the chemistry of sediment formation, but merely accelerates the natural ageing. Sediments formed under accelerated ageing of the diesel doped with *p*-t-butylthiophenol again showed a similar spectrum as well as peaks for the oxidized products of the dopant, namely di-*p*-t-butylphenyl disulfide and *p*-t-butylbenzenesulfonic acid, thereby supporting the suggestion that sediment formation is an acid-catalyzed process and that sulfonic acids or other acids are formed by autoxidation of the fuel. Py-FIMS analysis of the adherent gum formed in the thiol-doped fuel gave a spectrum almost identical to that of the filtered sediment confirming their similar chemical nature.

INTRODUCTION

Storage of fuels often results in the formation of deposits that cause problems with filtration and pumping of the fuels. Furthermore, some soluble gum is also formed that subsequently forms deposits on the hot engine parts causing additional problems. Numerous tests have been developed to predict the tendency of a fuel to form deposits.(1) Often, these tests require stressing the fuel at elevated temperatures, and the relevancy of such tests to storage conditions is not clear. Studies have also been conducted with dopants (2, 3), but again it is unclear whether the deposits formed in the presence of the dopant are the same as those formed under storage. An improved chemical understanding of the nature and causes of deposit formation is clearly needed. Chemical characterization of the sediments is valuable, because the agents reponsible for their formation may be present at extremely low concentration in the fuel, but will necessarily be concentrated in the sediments.

We have previously shown that pyrolysis–field ionization mass spectrometry (Py–FIMS) is very useful in characterizing the deposits formed during storage of fuels.(4,5) We have found that there are a few patterns that repeat in the spectra for sediments from a variety of sources and that the filtered sediments and adherent insoluble gums are very similar in chemical nature with the sediments being enriched in the benzologs of the components in the gum. We also showed that sediments from fuels with dopants such as 2,5-dimethylpyrrole (DMP) are completely different from that observed for undoped fuels; the sediment was largely comprised of DMP-derived materials. This result illustrates the possible dangers associated with studying accelerated aging using dopants and the need to characterize the sediments to ensure that the chemistry being examined is relevant to the native system.

We now wish to report results obtained from a variety of deposits obtained with fuels doped with strong acids or their precursors. The accompanying paper by Hazlett and Schreifels

(6) describes the aging experiments and the analysis of sediments by other techniques, such as titration with alkali and XPS, while this paper focuses on the analysis of the deposits by Py–FIMS.

EXPERIMENTAL

Accelerated Aging. A 20/80 blend of a light cycle oil with straight run diesel was aged at 80°C for 7 (or 14) days. Insoluble sediment formed in the fuel under ambient storage was also examined as an appropriate control. The dopants used in this study were: (1) a sample of dodecylbenzenesulfonic acid (DBSA), (2) *p*-t-butylthiophenol (PBTP), and (3) chloroacetic acid. The sediments were collected by filtration through glass fiber filters and the adherent gums were dissolved in a 1:1:1 (vol) mixture of toluene, acetone, and methanol, transferred to a small vial and the solvent evaporated.

Pyrolysis/Field Ionization Mass Spectrometry (Py/FIMS). The technique of field ionization (FI) consists of passing vapors of the material to be analyzed through a region of intense electric field.(7) This mild technique for ionization results in the formation of only the molecular ions for most compounds, and its nonfragmenting nature makes it particularly useful for analyzing complex mixtures. The FIMS system used in this study has been described elsewhere.(8) It consists of an activated tantalum foil field ionizer interfaced with a 60° magnetic sector mass analyzer and a PDP 11/23 computer for data acquisition and processing. Approximately 50 μg of the sample is introduced via a heatable direct insertion probe. Mass spectral data of the evolving volatiles are collected by repeatedly scanning the magnet over a preset range while the sample is gradually heated from the initial temperature (sometimes as low as -78°C) to approximately 500°C. At the end of the run, the sample holder is retrieved and weighed to determine the fraction that was devolatilized during the analysis. All the samples examined in this study were devolatilized to about 60% during analysis. For a given sample, many spectra are collected, each representing a certain range of temperature. The individual spectra are added to obtain a spectrum of the total volatiles and produce a thermal evolution profile of total volatiles as well as of any given mass peak.

RESULTS AND DISCUSSION

The Py-FIMS analysis of the adherent gum from ambient aging of the fuel gave the spectrum shown in Figure 1. It shows the characteristic groups of peaks corresponding to monomers, dimers, and trimers extending over the mass range 100 to 700 amu. The spectrum contains major peaks at m/z 131, 145, and 159. These features are in accord with those found in our previous investigations.(4,5) The peaks at m/z 131, 145, and 159 have been assigned to methylindole and its homologs (9-11).

Effect of Dodecylbenzenesulfonic Acid. Figure 2 shows the Py–FIMS of the filtered sediment formed upon stressing the fuel at 80°C for 7 days with DBSA as a dopant. The most intense peaks are seen at m/z 298, 312, and 326. Parent ion due to DBSA would appear at m/z 326, and we were puzzled to see the peaks at 312 and 298, which correspond to successive loss of methylene. The FI-mass spectrum of the DBSA sample also gave the peaks at m/z 312 and 298 in addition to the peak at m/z 326 and it appears that the particular sample of dodecylbenzenesulfonic is actually a mixture decyl-, undecyl-, and dodecyl- benzenesulfonic acids. The Py–FIMS of the deposit gave peaks at m/z 131, 145, and 159 and shows the general features of filtered sediments from undoped fuels (5) including relatively prominent peaks at m/z 181, 195, and 209 corresponding to the benzologs of methylindole and its homologs. On the basis of this information, we can surmise that DBSA does not drastically alter the chemistry of sediment formation but promotes the reactions that occur in undoped sediments. To the extent that DBSA is seen in the sediments as a prominent constituent, it must also contribute to insolubles formation. Whether this DBSA is present in the insolubles merely due to adduction or due to the formation of insoluble salts cannot be discerned at present.

Effect of *p*-t-butylthiophenol. Py–FIMS of the sediment obtained from doping the fuel with PBTP is shown in Figure 3. The spectrum is similar to the one for the sediment from the DBSA-doped fuel except that instead of the peaks due to the DBSA sample there are prominent peaks at m/z 166, 214, and 330. The peak at m/z 166 corresponds to PBTP itself and that at 330 to the corresponding disulfide, an expected product of oxidation. The peak at m/z 214 corresponds to *p*-t-butylbenzenesulfonic acid, and this observation lends support to the hypothesis that insolubles formed during storage are a result of acid-catalyzed chemistry, and that the acids are

themselves a product of autoxidation.(6) There is an additional prominent peak at m/z 185, which remains a mystery.

Effect of Chloroacetic Acid. Once again, the Py–FIMS of the sediment from the fuel doped with chloroacetic acid displays general features similar to those for the other sediments. Peaks due to chloroacetic acid (m/z 94 and 96) are absent and it appears that this acid is not adducted into the insoluble sediment. The absence of chloroacetic acid in the sediment would also suggest that salt formation is probably not the reason for the presence of other acids in the sediments, however, Cl was detected in the sediment by XPS (6) and we cannot draw any firm conclusions regarding the mechanism of dopant adduction at the present moment.

CONCLUSION

Pyrolysis–FIMS is a useful technique for characterizing fuel deposits. In this study, we showed that the nature of the deposits formed by doping the fuel with DBSA or chloroacetic acid is similar to that formed in undoped sediments. Substantial amounts of the deposits were devolatilized during the analysis ensuring that the data do not result from an insignificant part of the deposit. Oxidation of *p*-t-butylthiophenol results in the formation of *p*-t-butylbenzenesulfonic acid in addition to the disulfide. The sulfonic acid then catalyzes formation of insolubles.

REFERENCES

1. See, for example, **2nd International Conference on Long Term Storage Stabilities of Liquid Fuels, Conference Proceedings**, Southwest Research Institute, October 1986.
2. F. R. Mayo and B. Y. Lan, *I & E. C. Prod. Res. & Dev.* **1986**, *25*, 333.
3. (a) J. V. Cooney, E. J. Beal, and R. N. Hazlett, *Preprints, Am. Chem. Soc., Div. Petro. Chem.* **1983**, *28*, 1139.

   (b) J. V. Cooney, E. J. Beal, and B. D. Beaver, *Preprints, Am. Chem Soc., Div. Fuel Chem.* **1985**, *30*(2), 303.
4. R. Malhotra and G. A. St.John, **2nd International Conference on Long Term Storage Stabilities of Liquid Fuels, Conference Proceedings**, Southwest Research Institute, October 1986, p. 327.
5. R. Malhotra and G. A. St.John, **3rd International Conference on Stability and Handling of Liquid Fuels, Conference Proceedings**, The Institute of Petroleum, London, September 1988, p. 525.
6. R. N. Hazlett and J. A. Schreifels, *Preprints Am. Chem. Soc. Div. Fuel Chem.* **1990**, *35*, adjoining paper in this volume.
7. H. D. Beckey, **Field Ionization Mass Spectrometry**, Pergamon Press, Elmsford, N.Y., 1971.
8. G. A. St.John. S. E. Buttrill, Jr., and M. Anbar, in **Organic Chemistry of Coal**, J. Larsen, Editor, A.C.S. Symposium Series 71, Washington, DC, 1978, p. 223.
9. R. D. Smith, H. R. Udseth, and R. N. Hazlett, *Fuel* **1985**, *64*, 810.
10. J. F. Pedley and R. W. Hiley, **3rd International Conference on Stability and Handling of Liquid Fuels, Conference Proceedings**, The Institute of Petroleum, London, September 1988, p. 510.
11. O. K. Bhan, S. Y. Tang, D. W. Brinkman, and B. Carley, *Fuel* **1988**, *67*, 227.

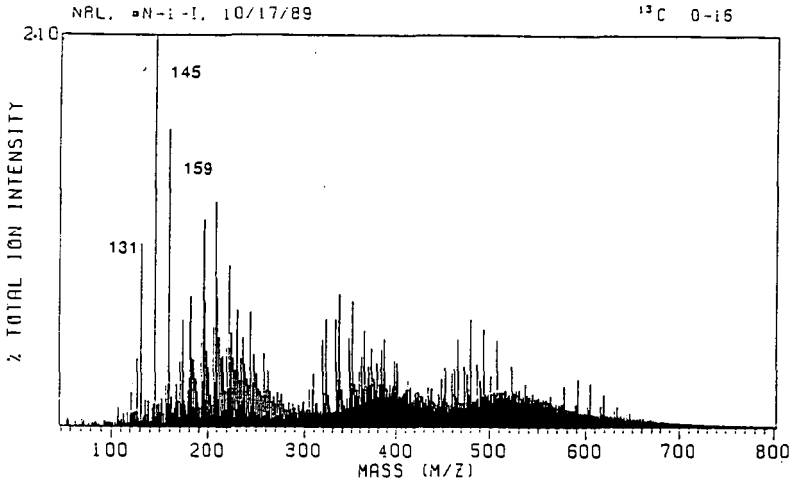

Figure 1. Py-FIMS of insoluble adherent gum from ambient aging of a 20/80 blend of light cycle oil and straight-run diesel.

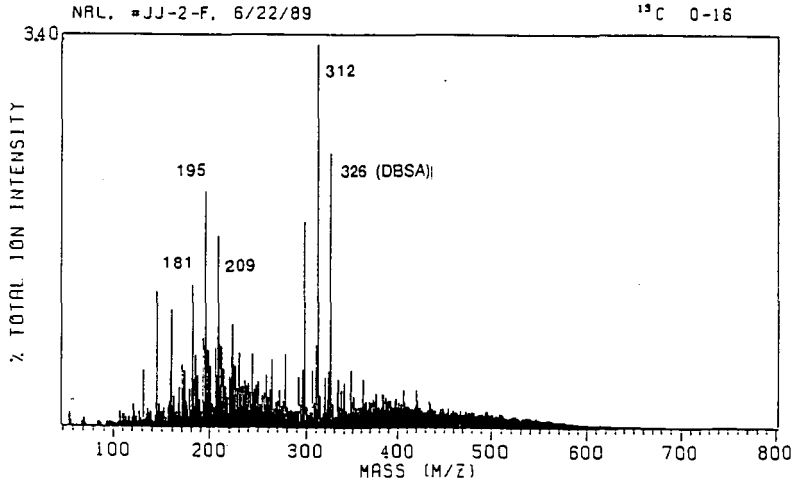

Figure 2. Py-FIMS of filtered sediment from accelerated aging at 80°C for 7 days of a 20/80 blend of light cycle oil and straight-run diesel doped with dodecylbenzesulfonic acid..

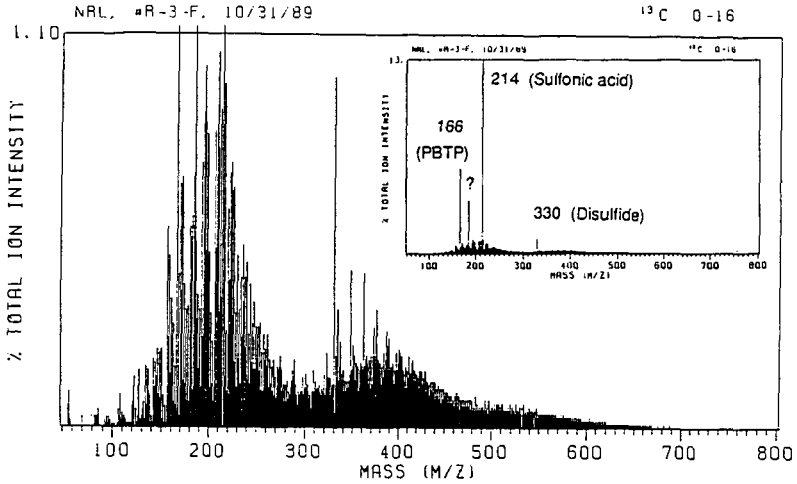

Figure 3. Py-FIMS of filtered sediment from accelerated aging at 80°C for 7 days of a 20/80 blend of light cycle oil and straight-run diesel doped with *p*-t-butylthiophenol. (Inset: Same spectrum with increased vertical scale.)

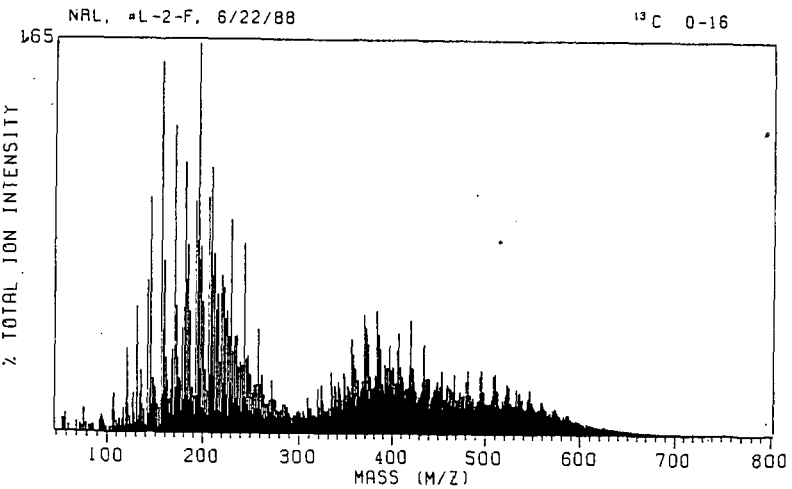

Figure 4. Py-FIMS of filtered sediment from accelerated aging at 80°C for 7 days of a 20/80 blend of light cycle oil and straight-run diesel doped with chloroacetic acid.

THE MECHANISMS OF $Fe(acac)_3$ AND $Cu(O_2CCH_2CH_2CH_2C_6H_{11})_2$ CATALYZED OXIDATION OF TETRAHYDROCARBAZOLE. IMPLICATIONS FOR THE LONG TERM STORAGE STABILITY OF MIDDLE DISTILLATE FUELS.

By

Garret Veloski, Cristen Gilmore, Rajeswari Sridharan, Joanne Kehlbeck and Bruce Beaver

Department of Chemistry
Duquesne University
Pittsburgh, PA 15282

INTRODUCTION

Pedley et al.[1,2] have recently implicated alkylindoles in the chemical reactions which are responsible for the promotion of sediment and color body formation in an unstable diesel fuel (90% North Sea derived straight run/ 10% catalytically cracked) during sixteen months of ambient storage. In addition, Dorbon and Bernasconi[3] have monitored the change in relative concentration of nitrogen compounds (indoles, carbazoles, and anilines) in four different LCO's upon aging (ASTM D4625: 43°C/12wks) and have reported the relative concentration of alkylindoles decreases to the greatest extent during aging.

Control of sediment and color body formation in unstable middle distillates during ambient storage has become an intractable problem. For example, it has been reported that two different commercial additive packages (composed of antioxidant, dispersant and metal deactivator) were ineffective in stabilizing two different unstable diesel fuels during ambient storage[1]. The stabilization of middle distillates by catalytic hydrogenation to remove problematic indole nitrogen compounds is generally expensive owing to the high temperature and hydrogen pressure needed to effect denitrogenation[4].

It is our belief that the ineffectiveness of commercial additive packages to sufficiently stabilize unstable diesel fuels during ambient storage is due to lack of understanding of the complex and fundamental chemistry involved in fuel oxidation. Consequently, we have initiated a research program directed at providing a greater understanding of the chemistry involved in low temperature middle distillate oxidation[5]. Herein, we report results of a model study of the $Fe(acac)_3$ and $Cu(O_2R)_2$ catalyzed oxidation of tetrahydrocarbazole (I, Figure 1), a representative alkylindole.

RESULTS AND DISCUSSIONS

In 1939, Beer et al.[6] reported that while trying to recrystallize various tetrahydrocarbazole derivatives, good yields of tetrahydrocarbazole hydroperoxide derivatives were isolated. In 1950, Beer et al.[7] reported that the structure of these hydroperoxides were that of the corresponding 1,2,3,4-tetrahydro-11-hydroperoxycarbazolenines (II,Figure 1). Subsequent studies revealed that the facile autoxidation of tetrahydrocarbazole derivatives is a general phenomenon and that the mechanism of this process involves a classical peroxyl radical chain[7,8]. Beer et al.[7] and Witkop[9], have also reported that in the presence of reducing agents or alkoxide, tetrahydrocarbazole hydroperoxides (THCHP) (II, Figure 1) are converted into the corresponding 1,2,3,4-tetrahydro-11-hydrocarbazolenine which can rearrange to the corresponding spiro-[cyclopentane-1,2'-ψ- indoxyl] (compound III,IV, respectively, Figure 1). In addition, Witkop and Patrick[9] have reported that in the presence of polar solvents or acids, THCHP rearranges to 8,9-benzcyclononadi-2,7-one (V, Figure 1).

We have confirmed all of the above mentioned results and wish to emphasize that in the presence of a suitable chain breaking-donor (CB-D) antioxidant (BHT, Vitamin E, etc.) solutions of tetrahydrocarbazole are oxidatively stable. However, when trace amounts of either $Cu(O_2CCH_2CH_2CH_2C_6H_{11})$ or $Fe(acac)_3$ are added, THC is slowly oxidized (in the presence of CB-D antioxidants).

Based upon TLC analysis after the metal catalyzed THC oxidation, THCHP and all of the THCHP degradation products previously mentioned are present. Apparently the presence of the Cu and Fe complexes catalyze the formation of THCHP via a nonperoxyl radical chain mechanism.

In Table 1 is reported the effect of addition of two copper deactivators upon the rate of the copper catalyzed THC oxidation. Both deactivators result in a suppression in the rate of oxidation. For instance, in the presence of the better deactivator, N,N'-bis(salicylidene)1,2-diaminopropane, the rate of THC oxidation is about 1/3 of rate in the absence of this deactivator.

We wish to report the following additional observations on the $Fe(acac)_3$ and $Cu(O_2CCH_2CH_2CH_2C_6H_{11})$ catalyzed THC oxidation:

i) Table 2 and 3 reveal the metal catalyzed THC oxidation can occur even when a large concentration of a CB-D antioxidant is present. This observation suggests the mechanisms for these reactions doesn't involve a classical peroxyl radical chain.

ii) In addition, Table 2 and 3 reveal a different rate response in the presence of different concentrations of a CB-D antioxidant. This suggests that the mechanisms for the iron and copper catalyzed oxidations are different.

iii) In Table 4 the rate of a typical copper catalyzed THC oxidation is compared with the rate of an identical reaction in which some tetrahydrocarbazole hydroperoxide (THCHP) was added at the start of the reaction. The observation of similar rates for these reactions additionally suggests that the mechanisms for this reaction is not a classical peroxyl radical chain (lack of chain-branching).

iv) In Table 5 is reported rate data for THC oxidation, as function of THC concentration and metal complex concentration. This data suggests the iron catalyzed reaction is first order in THC and .1 order in iron while the copper oxidation is 1/2 order in THC while .3 order in copper.

CONCLUSION

Pedley et al.[2] have proposed a mechanism which accounts for the involvement of indoles in the formation of sediment and color bodies during ambient aging of an unstable North Sea derived diesel fuel containing catalytically cracked stock. In this mechanism, indoles in the presence of conjugated ketones and acid, result in electrophilic aromatic substitution of the indole with concomitant increase in indole molecular weight and color body formation owing to formation of indolic chromophore. Protonation of the resultant indole results in sediment formation.

The results of this work suggest that alkylindoles can promote fuel degradation in a capacity other than that observed by Pedley et al.[1,2]. In the presence of trace amounts of $Fe(acac)_3$ and $Cu(O_2CCH_2CH_2CH_2C_6H_{11})$, tetrahydrocarbazole is oxidized, initially forming tetrahydrocarbazole hydroperoxide (THCHP). A very high concentration of Vitamin E was necessary to completely inhibit the Cu catalyzed reaction while the Fe catalyzed reaction was not totally inhibited.

We have shown that in the absence of catalytically active metal ions and in the presence of CB-D antioxidant THC is oxidatively stable. This observation suggests that more efficient metal deactivators need to be developed in order to counter the effect of alkylindole oxidation upon middle distillate degradation.

LITERATURE CITED

1. Pedley, J., Hiley, R.W. and Hancock, R.A., Fuel, 66, 1646-1651 (1987).

2. Pedley, J., Hiley, R.W. and Hancock, R.A., Fuel, 68, 27-31 (1989).

3. Dorbon, M. and Bernasconi, Fuel, 68, 1967-1074, (1989).

4. Dorbon, M., Ignatiadis, Schmitter, J., Arpino, P., Guiochon, G., Toulhoat, H. and Huc, A., Fuel, 63, 565-57, (1984).

5. Beaver, B.D., Hazlett, R.N., Cooney, J.V., Watkins, J.M., Fuel Science and Technology Intl, 6(2), 131-150, (1988).

6. Beer, R.J.S., McGrath, L., Robertson, A., Woodier, A.B., Nature, 164, 362-363, (1949).

7. Beer. R.J.S., McGrath, L., Robertson, A., J. Chem. Soc, 2118-2126, (1950).

8. Beer, R.J.S., Broadhurst, T., Robertson, J. Chem. Soc, 4946-4951.

9. Witkop, B. and Patrick, J.B., J. Am. Chem. Soc., 73, 2196-2200, (1951).

ACKNOWLEDGMENT

The partial financial support of the Naval Research Laboratory is gratefully acknowledged.

FIGURE 1

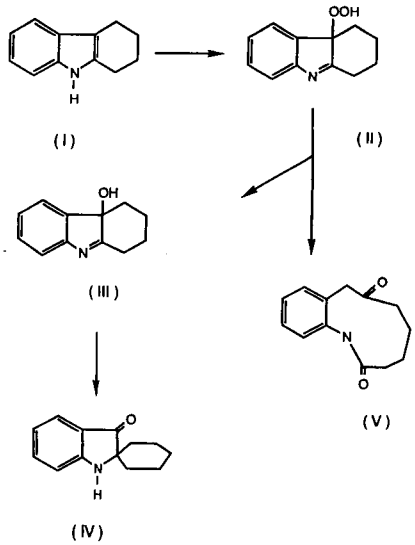

Table 1*

Effect of N,N bis[salicylidene]1,3-propanediamine and N,N'-disalicylidene-1,2-propanediamine on the Rate of THC Oxidation

Conditions: 2.34×10^{-2} M THC; 2.34×10^{-2} M vitamin E; 50°C; 9.95×10^{-5} Cu2+ cyclohexane butyrate; 50mls 3:1 Heptane-Toluene

MDA	Equivalents of Salicylidene (wrt Cu2+)	rate (moles/l min) (E^{-6})
1,3	0	10.4
1,3	1.0	5.6
1,3	1.5	5.5
1,2	0	10.4
1,2	1.5	2.8

*Solutions of purified THC, vitamin E, metal and tridecane (GLC internal standard) were prepared in the appropriate solvent mixtures. The solutions were placed in a constant temperature water bath and bubbled with O_2. Aliquots were taken prior to O_2 bubbling and approximately two hours after bubbling. The aliquots were analyzed for THC decomposition using GLC.

Table 2

Relationship between Vitamin E Concentration and the Rate of THC Oxidation

conditions:
2.23×10^{-2} M THC/ 1.42×10^{-4} M Fe3+acac/ 50°C/ 50mls 3:1 Heptane-Toluene

Vitamin E (moles/l)	rate (moles/l min) (10^{-6})
0.58×10^{-2}	17.0
1.16×10^{-2}	10.9
2.34×10^{-2}	7.1
4.67×10^{-2}	5.9
9.34×10^{-2}	4.8
14.01×10^{-2}	4.0

Table 3

Relationship between Vitamin E Concentration and the Rate of THC Oxidation

conditions:
2.34×10^{-2} M THC/ 1.99×10^{-5} M Cu2+(cyclohexane butyrate)/40°C/ 50mls 3:1 Heptane-Toluene

Vitamin E (moles/l)	rate (moles/l min) (10^{-6})
1.16×10^{-2}	121.0
2.34×10^{-2}	8.34
4.67×10^{-2}	9.55
7.00×10^{-2}	9.23
9.34×10^{-2}	NR
11.67×10^{-2}	NR
16.35×10^{-2}	NR

Table 4

Effect of the addition of THCHP on the rate of THC oxidation

conditions:
2.34×10^{-2} M THC/ 1.99×10^{-5} M Cu2+(cyclohexane butyrate)/ 40°C / 50mls 3:1 Heptane-Toluene/ 2.34×10^{-2} M vitamin E

THCHP (mg)	rate (moles/l min) (10^{-6})
0 (control)	8.34
10	8.42

Table 5

Determination of Order in THC and Metal

Determination of order in THC with Fe3+acac

Conditions: 1.0 eq. Vitamin E (wrt THC) ; 1.41×10^{-4} M Fe3+acac ; 50°C ; 50mls 3:1 heptane -toluene

THC (moles/l)	rate (moles/l min) (E-6)
0.58×10^{-2}	1.55
1.16×10^{-2}	4.1
1.75×10^{-2}	5.5
2.34×10^{-2}	7.1
4.68×10^{-2}	12.6
7.01×10^{-2}	15.4

Table 5

Determination of order in Fe3+acac

Conditions: 2.34×10^{-2} M THC; 2.34×10^{-2} M Vitamin E ; 50°C ; 50mls 3:1 heptane -toluene

Fe3+acac (moles/l)	rate (moles/l min) (E-6)
2.83×10^{-5}	5.9
1.41×10^{-4}	7.1

Determination of order in THC with Cu2+ cyclohexane butyrate

Conditions: 1.0 eq. Vitamin E (wrt THC) ; 9.95×10^{-5} M Cu2+ cyclohexane butyrate; 50°C ; 50mls 3:1 heptane - toluene

THC (moles/l)	rate (moles/l min) (E-6)
1.16×10^{-2}	6.75
2.34×10^{-2}	9.65

Determination of order in Cu2+ cyclohexane butyrate

Conditions: 2.34×10^{-2} M THC; 2.34×10^{-2} M Vitamin E ; 50°C ; 50mls 3:1 heptane -toluene

Cu2+ (moles/l)	rate (moles/l min) (E-6)
1.99×10^{-5}	6.9
4.97×10^{-5}	9.7
9.95×10^{-5}	10.6
19.89×10^{-5}	14.0

WHAT ARE SOLUBLE MACROMOLECULAR OXIDATIVELY REACTIVE SPECIES (SMORS)?

Dennis R. Hardy and Margaret A. Wechter
Naval Research Laboratory
Code 6180, Washington, D.C. 20375-5000

INTRODUCTION

The search for diesel fuel components which can be linked to insolubles or sludge formation as a product of oxidative aging has led to some interesting new findings recently. Pre-filtered fuel which is oxidatively aged under accelerated conditions which simulate one to two years of ambient storage is filtered to determine the product insolubles formed. If the filtrate is then subjected to size exclusion chromatography (SEC), no intermediate molecular weight or size components are observed. If the fuel-insoluble product which has been removed by filtration is solubilized and subjected to identical SEC analysis, a broad peak centered on 600 to 800 daltons is the principle chomatographic feature. If the aged fuel is not filtered and simply dissolved in SEC mobile phase, numerous species of varying molecular size can be detected in the range of 150-1000 daltons. The higher molecular weight features of these chromatograms are very similar to the fuel-insoluble product after aging; the lower molecular weight features are what one would expect if oxidation and condensation reactions of fuel monomeric species were consecutively reacting to form the ultimate fuel-insoluble high molecular weight product. However, the absence of these intermediate molecular weight species in the filtered fuel leads to the unconventional conclusion that oxidation of fuel monomeric species is not responsible for sludge formation.

A second related finding is that after extraction of unstable diesel fuels and light cycle oils (LCOs) with methanol, the tendency of these stocks to form insoluble sediment upon oxidative aging is greatly reduced (1). This finding is illustrated in Table I, where four blends of 30% LCO in straight run from four separate refineries are subjected to aging in the low pressure reactor at 90° C for 24 hours at 100 psig oxygen. The pass/fail criterion is about 6 mg/100 ml. The samples were extracted with strong aqueous base and with methanol (described in experimental section below). The methanol extracted fuels are greatly stabilized in all cases regardless of the relative stabilities of the unextracted control samples.

Table II illustrates the effect of methanol extraction on either the straight run distillate or LCO portion used to make up the blend. It is readily apparent that the insolubles precursors are primarily associated with the LCO portion. More remarkable is the fact that the isolated methanol extract can be dissolved in a hydrocarbon solvent (which by itself does not form insolubles under the LPR aging conditions) and after aging an insoluble sediment can

be isolated. In two of the three blends (B-3 and B-4) a remarkable mass balance is achieved in that the sediment from the extracted blend plus the sediment from the methanol extract in solvent equals the sediment in the unextracted blend. For B-5 the methanol extract in the solvent formed even more sediment than the original fuel blend. These results indicate clearly that the precursors to fuel-insoluble sediment are very efficiently extracted into the methanol.

Attempts were made to analyze the methanol extract from a range of unstable LCOs in order to determine the gas chromatographable monomeric fuel components responsible for insoluble sediment formation. It was not possible to correlate any particular compound or compound class present in the relatively easily analyzed methanol extract as being responsible for the product insoluble sediment.

Evaporating the methanol extracts to dryness led to an intractable tar. Attempts to weigh the tar were abandoned due to the impossibility of achieving constant weights. If this tar is carefully precipitated with hexane, it is possible to isolate a dark solid material which is filterable on a 1.2 micron glass fiber filter. This solid material may be washed with hexane, dried and weighed. The material has been named soluble macromolecular oxidatively reactive species (SMORS) (2). Typical values for SMORS from a variety of straight runs and LCOs are given in Tables III and IV. Again it is apparent that the reactive LCO generally contains SMORS at varying levels, as determined by a simple methanol extraction and hexane precipitation. This led to the observation illustrated in Figure 1 that the weight of SMORS in any catalytically cracked LCO was linearly related to that LCOs tendency to form fuel-insoluble sludge after oxidative aging.

This paper presents additional information about the physical and chemical nature of the SMORS and the nature of their role in blends with straight run distillate streams. The possible use of the simple SMORS determination as a substitute for traditional accelerated storage stability tests in certain cases will also be discussed.

EXPERIMENTAL

All of the fuels and blend stocks fell within ASTM D975 diesel fuel number 2 specification requirements. Most of the much more stringent U.S. Navy Distillate Diesel Fuel specifications (MIL F 16884) were also met by almost all of the fuels and blend stocks. The fuel code used throughout the tables is: SR = straight run distillate, LCO = catalytically cracked light cycle oil, B = a blend of SR + LCO, a number following any of the letter codes refers to a different refinery source. Fuel sources were primarily US in origin but several European samples are included.

The storage stability test utilized is described in detail elsewhere (3) and utilized the so-called low pressure reactor (LPR) at 90° C and 100 psig oxygen for various periods of time.

All fuel samples are first pre-filtered using Gelman Type A/E glass fiber filters before either extraction or aging. The methanol extraction procedure uses fuel/methanol volumes of 100 ml/40 ml in a 250 ml separatory funnel. The two phases are vigorously shaken for about 90 seconds and the system allowed to settle until good separation occurs, typically 2-5 minutes. The fuel layer is then drawn off and discarded and the methanol phase is decanted into a 125 ml brown borosilicate bottle which is immersed to the neck in a boiling water bath to evaporate the methanol. In order to achieve good repeatable quantitation, it is absolutely essential that all the methanol is driven off because of the very high solubility of the hexane insoluble fraction of interest in methanol. After evaporation the sample is allowed to cool to room temperature. About 50 ml of filtered ACS reagent grade hexanes are then added to the bottle and any hexane insoluble material is precipitated. The sample is then vacuum filtered through a pre-weighed 47 mm Gelman type A/E glass fiber filter in a Buchner funnel, rinsed well with hexane and allowed to dry thoroughly before weighing again. If constant weights are not achieved with ambient air drying the samples may be oven dried at about 60° C for an hour. When it is desirable to recover the solid material from the filter for subsequent analysis a 0.8 micron Millipore type AA or a Nylon 66 filter may be substituted for the glass fiber filter, and a Millipore filtering apparatus for the funnel.

RESULTS AND DISCUSSION

The SMORS can be quantitatively isolated either before or after an accelerated aging test (on a separate aliquot if before the aging test). It is important to note that the SMORS solids should not be confused with the product insoluble sediment solids. The product insoluble sediment is removed from the post aged fuel by filtration and then the post aged filtered fuel may be extracted to determine the SMORS solids after aging.

Size exclusion chromatograms of representative samples of the SMORS solids both before and after stress tests were obtained. The chief characteristic was a molecular weight peak of about 700 to 900 daltons. Qualitatively and quantitatively the chromatograms of the SMORS were similar for all LCOs both before and after aging. In addition, the physical appearance and solubility characteristics of the SMORS was similar for all of the LCOs.

The nature of the SMORS led to their descriptive acronym. They are <u>soluble</u> in diesel fuels. They are <u>macromolecular</u>, that is, they are much greater average molecular weight than the diesel fuel range. They are <u>oxidatively reactive species</u>, that is, they are apparently primarily responsible for the oxidative formation of sludge products in the fuel.

The SMORS are not just precursors to sludge formation in catalytically cracked LCOs but are apparently prerequisites in a necessary but not sufficient regard. The examination of SMORS in many diesel fuels has led us to propose the values in Table V as a possible compositional requirement governing storage stability. If a fuel contains a high (>30 mg/100 ml) concentration of SMORS, problem levels of sludge formation are inevitable at ambient conditions in less than 6 months. If the concentration of SMORS is very low (<1 mg/100 ml), irregardless of fuel source, composition and refining process no fuel related sludge formation will take place even after very long storage at ambient. At intermediate levels (1 to 30 mg/100 ml) it would be advisable to further scrutinize the fuel by running a realistic accelerated stability test.

The physical appearance and nature of SMORS is very intriguing. The fact that they are particulate and filterable on a 0.8 to 1.2 micron filter indicate that they are physically similar to the product insoluble sediment. It has been suggested by Chertkov, et al (4) that the product solid phase is not formed by the oxidation of fuel components but is present in the fuel in the form of a colloidal system. Oxidation of the fuel leads to the destruction of this colloidal system and precipitation of the solid phase. They believe that this higher molecular weight material already existent in the fuel is responsible for sludge formation in both diesel and jet fuel. Further they claim that this material should be similar to petroleum asphaltenes except in their much higher oxygen incorporation.

In an effort to extend our understanding of the chemical nature of the SMORS, we investigated the effect of several straight run streams on several LCOs. A high acid (SR-5A) and a low acid (SR-11) fuel was blended into various LCOs and the SMORS yields determined before and after a 24 hour LPR test. The product insoluble sediment was also determined. Table VI illustrates two representative LCOs. The effect of the straight runs regardless of their acid content is not simply that of diluent to the SMORS. For either LCO we would calculate about 14 mg on the basis of dilution for the 40% v/v case and 7 mg for the 20% v/v LCO case. In both cases (pre-stressed) we obtain about double the calculated weight of SMORS. As usual, with either LCO the straight run blends give higher amounts of insolubles than the starting LCO itself. It is quite interesting that the low acid SR yields almost double the high acid SR blend for either LCO. Yet the effect on SMORS is invariant regardless of acid level before or after aging.

Since the addition of the straight run seems to favor the partition of SMORS into the initial methanol extract, we next investigated the effect of a pure hydrocarbon model for the SR on the effect of SMORS yields. Hexadecane was chosen as the diluent and the effect on LCO-5 is given in Table VII. The effect of the pure hydrocarbon diluent is to drive the partition coefficient even more into the initial methanol extract. It is interesting to note that even when the dilute blends are aged about twice the insoluble

sediment is formed over the neat LCO case. The pre-stressed SMORS expressed on a 100 ml LCO basis are 30 to 50% increased in the dilution range of 20 to 80% v/v hexadecane.

This leads us to consider not so much the nature of the SR or diluent phase as controlling the various amounts of product insoluble sediment as the nature of our original determination of SMORS in the blends. In blends, it becomes of greatest importance to maximize the partition coefficient of the initial extraction into methanol. This, then, would allow us to determine if the SMORS (however isolated) are the primary controlling reagents in product insolubles formation.

Since the effect of strong acid addition to blends of catalytically cracked LCO in SR exerts such a pronounced effect on the insoluble sediment production of these fuels (5), we examined the effect of such acid addition on the yields of pre-aged SMORS. Table VIII illustrates our results for LCO-14 with and without the addition of 0.010 M chloroacetic acid. Remarkably the SMORS yields were increased about four fold. This concentration of this acid addition to LCO/SR blends generally has the effect of increasing the product sediment yields by about somewhat less than ten fold. Since Tables VI and VII show the effect of increasing the SMORS yields simply by adding an SR diluent, the effect of adding acids to SR/LCO blends would be predicted to increase the SMORS yields somewhat more than the four fold increase of added acids to the neat LCO. The effect of added acid to the LCO may indeed be nothing more than the destruction of an already existent colloidal dispersion in the cracked LCO material, leading to the production of greater amounts of insoluble sediment.

CONCLUSIONS

The original scheme for isolating this new class of material from fuel (the SMORS), has been extended in the current work. The effect of SR or pure hydrocarbon dilution of the LCO on SMORS yields reveals that the original levels determined in the neat LCOs themselves is probably on the low end. This leads to a desire to maximize the partition coefficient into the initial extractant phase. The addition of an organic acid at low concentration has been shown to have the desired effect and will be pursued using additional acids and blends of LCO/SR in addition to other LCOs.

SMORS are important pre-requisites and precursors of sludge formation in aged diesel fuels. This makes the further refinement of the physical isolation method of SMORS an important area of study. In addition, the further detailed characterization of the SMORS may aid fuel producers and users in minimizing the deleterious impact of this material by selectively controlling and realistically predicting its effects.

REFERENCES

1. Wechter, M. A. and Hardy, D. R., Fuel Sci. Technol. Int. 1989, 7(4), 423-441.
2. Hardy, D. R. and Wechter, M. A., Energy and Fuels 1990 (in press).
3. Hardy, D. R., Hazlett, R. N., Beal, E. J., and Burnett, J. C., Energy and Fuels 1989, 3, 20-24.
4. Chertkov, Ya. B., Likhterova, N. M., and Gorenkov, A. F., Khimiya i Tekhnologiya Topliv i Masel, No. 8, pp. 26-29, August 1989.
5. Hazlett, R. N., Fuel Sc. Technol. Int. 1988, 6(2), 185.

TABLE I. Results of KOH and Methanol Extraction on Insolubles Formation. Aging test is LPR at 90°C, 24 hours, 100 psig oxygen. Pass/Fail criterion is 6 mg/100 ml.

	Mg insolubles/100 ml		
Fuel Blend	Control	KOH Ext.	MeOH Ext.
B-2	1.4	2.0	0.8
B-3	9.4	9.2	2.2
B-4	6.8	3.8	2.4
B-5	11.4	10.6	2.0

TABLE II. Effect of Methanol Extraction on 3 Reactive Fuels. Aging as in Table I. Series 1 = unextracted 70/30 blends. Series 2 = 35 ml extracted SR blended with 15 ml LCO. Series 3 = extracted 70/30 blends (MeOH). Series 4 = 35 ml SR blended with 15 ml extracted LCO. Series 5 = MeOH fraction from series 3 suspended in 25/75 butylbenzene/dodecane.

	Mg insolubles/100 ml		
Fuel Blend	B-3	B-4	B-5
Series 1	10.2	8.2	12.6
Series 2	10.8	7.2	14.6
Series 3	4.0	3.2	2.2
Series 4	5.0	3.2	4.4
Series 5	6.6	5.0	19.6

TABLE III. Weight of Solids Isolated from the Hexane-insoluble Fraction of the Methanol Extract of 7 SR Fuel Stocks. Aging as in Table I.

Fuel Code	Hexane Insolubles (mg/100 ml) Pre-stress	Post-stress	Insol. Sed. (mg/100 ml)
SR-3	0.0	ND	0.0
SR-4	0.1	0.1	0.0
SR-5A	0.7	2.0	0.6
SR-5B	0.0	0.6	0.4
SR-11	0.0	0.1	0.1
SR-12	0.2	ND	0.0
SR-13	0.1	0.1	0.3

TABLE IV. Weight of Solids Isolated from the Hexane-insoluble Fraction of the Methanol Extract of 8 Cracked LCOs and 1 Blended Diesel Fuel. Aging as in Table I.

Fuel Code	Hexane Insolubles (mg/100 ml) Pre-stress	Post-stress	Insol. Sed. (mg/100 ml)
LCO-1	112	116	27.0
LCO-2	14	17	3.3
LCO-3	53	63	13.0
LCO-4	27	40	3.4
LCO-5	92	114	20.0
LCO-12	1	14	4.7
LCO-13	2	101	33.0
LCO-14	2	58	4.0
B-3	14	18	8.2

TABLE V. Use of SMORS (mg/100 ml) as Simple Compositional Test for Predicting Storage Stability of any Mid-distillate Fuel.

Weight of SMORS (mg/100 ml)	Insoluble Forming Tendency	Action
<1	Fuel has indefinite storage life	No accelerated stability test needed
<30 and >1	Fuel stability generally worse at higher SMORS levels	Accelerated stability test required
>30	Fuel will degrade significantly in less than 6 months	No accelerated stability test needed

TABLE VI. The effect of various Straight Run (SR) Distillate Blends in LCOs on SMORS yields. All values in mg/100 ml of fuel.

Volume Ratio SR/LCO	LCO ID	Pre-Stress SMORS Hi Acid SR-5A	Pre-Stress SMORS Lo Acid SR-11	Post-Stress SMORS Hi Acid SR-5A	Post-Stress SMORS Lo Acid SR-11	Insol. Sed. Post Stress High Acid	Insol. Sed. Post Stress Low Acid
0/100	LCO-14	34	34	60	60	3	3
60/40	LCO-14	25	27	35	35	6	10
80/20	LCO-14	15	15	23	19	5	8
0/100	LCO-4	34	34	57	57	2	2
60/40	LCO-4	31	30	35	37	5	10
80/20	LCO-4	17	15	12	19	4	7

TABLE VII. Effect of Hexadecane as Diluent on SMORS Yields of an LCO. Aging conditions as in Table I.

Volume Ratio LCO-5/Hexadec.	mg SMORS per 100 ml LCO	Insol. Sed. (mg/100 ml)
100/0	96	11
80/20	129	23
50/50	148	20
20/80	147	23
0/100	0	0

TABLE VIII. Effect of 0.010 M Chloroacetic Acid on Pre-stressed SMORS Yields.

Sample	SMORS (mg/100 ml)
LCO-14	6
LCO-14 + Acid	23

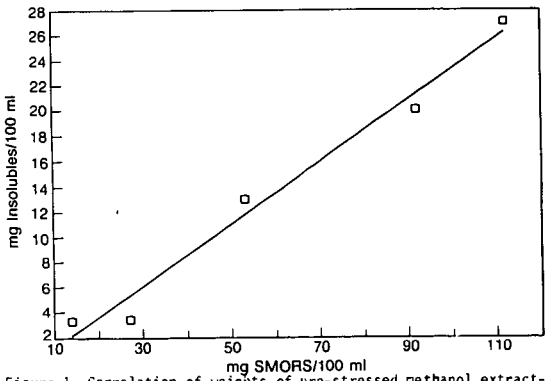

Figure 1. Correlation of weights of pre-stressed methanol extractable/hexane insolubles (SMORS) for 5 LCO samples with corresponding weight of product insolubles. See Table I for aging conditions. Standard error for each axis=±15%.

SYMPOSIUM ON THE
STABILITY AND OXIDATION CHEMISTRY OF MIDDLE DISTILLATE FUELS
PRESENTED BEFORE THE DIVISIONS OF FUELS AND PETROLEUM CHEMISTRY
AMERICAN CHEMICAL SOCIETY
WASHINGTON, DC, MEETING, AUGUST 26-31, 1990

A FUEL STABILITY STUDY: TOTAL INSOLUBLES AS A FUNCTION OF TIME

By

E. W. White, David Taylor Research Center, Annapolis, MD 21402

INTRODUCTION

The David Taylor Research Center, in cooperation with the Naval Research Laboratory (NRL) plus contract laboratories, has been studying the effectiveness of stability additives in Naval Distillate fuels since 1983. Initial studies of the antioxidants permitted in Naval Distillate showed that not all the antioxidants are equally effective and that some might even be detrimental.[1] Later work with nine commercial additives in a number of fuel stocks showed that two of the additives were consistently more effective than any of the other seven additives.[2]

The first test of commercial additives was run on a fuel stock containing 40% light cycle oil. When a low level of insolubles (about 0.6 mg/100 mL of fuel) was obtained, it was considered too low to obtain a good evaluation of the effectiveness of additives. We therefore investigated the effect of stress times greater than the 16 hours prescribed in the ASTM D2274 procedure. Subsequently, we conducted such time studies on a total of 21 fuel stocks. This paper summarizes the results of those studies and discusses the implications of our findings.

MATERIALS AND PROCEDURES

Materials - The 21 fuel stocks used in the study included one straight run (SR) stock, 4 light cycle oils (LCO), 10 SR/LCO blends containing 30%(vol) LCO, 3 containing 40%, 2 containing 15%, and a blend of high sulfur, heavy diesel fuel in a CAT 1H fuel. The stocks were obtained by NIPER (National Institute for Petroleum and Energy Research) from Gulf coast, west coast, east coast, and mid-continent refineries. Table 1 shows available ranges of properties measured on the stocks (not all stocks).

Procedures - The ASTM D2274 test for the oxidation stability of distillate fuel by the accelerated method was used, with modifications.[3] The primary modification was the use of residence times both less than and greater than the 16 hours at 95°C specified by the test method. The maximum time used was 96 hours. In a second modification, we cleaned the apparatus without using chromic acid solution. In a third modification, we evaporated adherent gum solvent by other than the jet gum procedure.

RESULTS AND DISCUSSION

The 21 time response curves of total insolubles as a function of residence, or stress time, are shown in Figures 1 through 5. They exhibit a tendency toward an S-shaped curve consisting of an induction period, followed by a period of rapid formation of total insolubles, and finally a leveling off to some final value. The curve obtained with Fuel 30-10 (Figure 2) is the best example of this tendency. Sauer and coworkers [4], using a somewhat different test procedure, published similar curves as long ago as 1958. Cooney and coworkers[5], Hazlett and coworkers[1], and Westbrook and coworkers[6] also obtained similar curves in 80°C bottle tests.

Various mechanisms have been proposed for the formation of insolubles in fuels. Sauer and coworkers[4] suggested the side-chain oxidation of reactive compounds in a fuel to form hydroperoxides which then decomposed to form aldehydes; the aldehydes were postulated to react with other peroxides to form peroxyhemiacetals, which in turn decomposed to form condensed, esterified higher molecular weight products. They suggested a typical sediment molecule containing a pyrrolic structure.

Frankenfeld and coworkers[7], from a study of dimethylpyrrole (DMP) in jet fuel, concluded that sedimentation appeared to be a free radical, autoxidative reaction involving a mechanism similar to that proposed by Sauer. They also concluded from a study of shale liquids that nitrogenous sediment formation in such liquids involves oxidative oligomerization of nitrogen compounds and that the neutral, heterocyclic compounds such as alkyl pyrroles and indoles appear to be especially reactive.

Hazlett and coworkers,[8] in a study of diesel fuels doped with DMP and stressed at 80°C, conducted elemental analyses, gas chromatographic analyses, and infrared spectroscopic examinations of the sediment. They remarked on the consistency of the elemental analyses on sediments from tests conducted under a wide variety of conditions. They found the atomic ratio of carbon to nitrogen was about 6:1 indicating the sediment was derived from the DMP.

The shape of the curves found in the current study is consistent with such past work. An induction period is consistent with the theory of consecutive reactions and the approach to a final value of total insolubles is consistent with the findings of an oligomerization with a specific chemical composition. We suggest that a few reactive species present in a fuel, primarily the reactive nitrogen compounds identified by Frankenfeld are involved in sediment formation. The rate at which such formation takes place, however, may be a function of the acidity and solvency of the system, of the presence of catalytic substances such as copper compounds, and of the presence of inhibitors, either naturally present or added.

Figures 1 - 5 also show the normal 16 hours of residence is frequently too early to catch the part of the curve where total insolubles increase at a fast rate. In most cases, the breakpoint has occurred by 20-24 hours. See, for example, the curves for Fuel 30-10 in Figure 2 and for LC-2 in Figure 3. The total insolubles produced in LC-2 by the end of 32 hours of residence time is 20-times the total insolubles produced in 16 hours.

Thus, the curves make us realize that no single-time test of short duration can be adequate for defining the behavior of a fuel in ambient storage. Rather, we need a test method that determines the induction period (the breakpoint time), the rate of increase of insolubles formation following the breakpoint, and the ultimate total insolubles formed after a long period of oxidative stability testing.

As a by-product of our time response program, we obtained some interesting data on the effect of light cycle oils (LCO) on the stability of straight run stocks. In two cases, we had available both the straight run stock and the LCO in addition to blends of 15%, 30%, and 40% LCO in the straight run. In the one case, we ran time response curves for the entire gamut of concentrations. The total insolubles obtained after 16 hours, 32 hours, and 40 hours of residence time are shown in Figure 6 as a function of the LCO concentration.

The lack of linearity of the curves in Figure 6 indicate that total insolubles obtained with the straight run stock and with the LCO are not additive. Addition of the more stable straight run stock to LCO does not provide a simple diluent effect. The chemistry responsible for this effect is not known, but it may be related to the acidity of the system, which some investigators, such as Hazlett[9], postulate as having a catalytic effect on the reactions involved in insolubles formation.

We have one additional figure, a figure which shows the effect of pre-aging. Pre-aging was accomplished by sparging a fuel with air and then allowing the sample to sit for a month at ambient laboratory temperatures before running D2274-type tests. Figure 7 compares the time responses of the pre-aged fuel and of the same fuel prior to pre-aging. The pre-aged fuel started rapid formation of insolubles at a much earlier point in time than the unaged fuel. Beyond the point at which 1.5 mg of total insolubles per 100 mL of fuel have been formed, the two curves are essentially parallel. This indicates the rate of formation of new insolubles is the same for the pre-aged and unaged fuel.

We postulate that the pre-aging permitted the formation of intermediates which would normally be produced during the early stages of the D2274 test. Then, when the pre-aged fuel was tested by the D2274 procedure, the formation of the insolubles could start immediately. We further postulate that, once the intermediates have been formed, the further reaction to form total insolubles is the same in the two cases.

FINDINGS AND CONCLUSIONS

1. Time response curves of total insolubles vs. residence time have an S-shape if carried for a sufficient period, and the total insolubles level approaches an asymptotic value.

2. Single time stability tests are incapable of fully defining the stability characteristics of a fuel.

3. The blending of two fuel stocks may not result in sediment formation that is a linear function of the sediments produced by each fuel stock alone.

4. Pre-aging a fuel stock prior to determining its time response curve affected only the length of the induction period.

LITERATURE CITED

(1) Hazlett, R.N.; Hardy, D.R.; White, E.W.; and Jones-Baer, L., SAE Paper 851231 (1985)

(2) Hardy, D.R.; Beal, E.J.; and Hazlett, R.N., Conference Proceedings, Third International Conference on Stability and Handling of Liquid Fuels, London, U.K., pp. 399-411 (1988)

(3) Test Method D2274, Oxidation Stability of Distillate Fuel Oil (Accelerated Method), Annual Book of ASTM Standards, Vol. 05.02

(4) Sauer, R.W.; Weed, A.F.; and Headington, C.E., PREPRINTS, Div. of Petrol. Chem., ACS, Vol.3 (No.3), 95 (1958)

(5) Cooney, J.V.; Beal, E.J.; and Hazlett, R.N., PREPRINTS, Div. of Petrol. Chem., ACS, Vol. 28 (No. 5), 1139 (1983)

(6) Westbrook, S.R.; Stavinoha, L.L.; Present, D.L.; Hsu, J.P.; and Herrera, J.G., Proceedings, Third International Conference on Stability and Handling of Liquid Fuels, London, U.K., pp. 538-553 (1988)

(7) Frankenfeld, J.W., Taylor, W.F., and Brinkman, D.W., U.S. Dept. of Energy Contract Report No. DOE/BC/10045-23 (1982)

(8) Hazlett, R.N., Cooney, J.V., and Beal, E.J., Proceedings, Conference on Long-Term Storage Stabilities of Liquid Fuels, Tel Aviv, Is., pp. C18 - C39 (1983)

(9) Hazlett, R.N. and Kelso, G., Proceedings, Second International Conference on Long-Term Storage Stabilities of Liquid Fuels, London, U.K., pp. 541-555 (1986)

TABLE 1
RANGES OF PROPERTIES OF STOCKS USED IN TIME STUDY

Property	30% Blends	40% Blends	LC Oils	Other Stocks
Density, kg/m^3	840 - 895	859 - 901	896 - 953	836 - 869
Viscosity, cSt	2.0 - 3.8	2.6 - 3.2	2.6 - 3.3	2.9 - 3.2
Distillation, ^oC				
IBP	144 - 223	180 - 221	213 - 224	198 - 217
10% Point	207 - 258	234 - 244	243 - 254	232 - 243
50% Point	232 - 292	270 - 283	269 - 283	267 - 283
90% Point	290 - 332	313 - 335	306 - 326	319 - 335
End Point	324 - 349	345 - 349	323 - 329	338 - 349
Cetane Index	38 - 49	36 - 48	23 - 37	44 - 54
Sulfur, %	0.2 - 0.8	0.2 - 0.9	0.3 - 1.0	0.3 - 0.6
Nitrogen, mg/L	43 - 266	44 - 246	61 - 428	25 - 151
TAN, mg KOH/g	.02 - .23	.02 - .15	.02 - .06	.04 - 0.25
Bromine No.	.23 - .43	.51 -1.13	0.47	.12 - .47

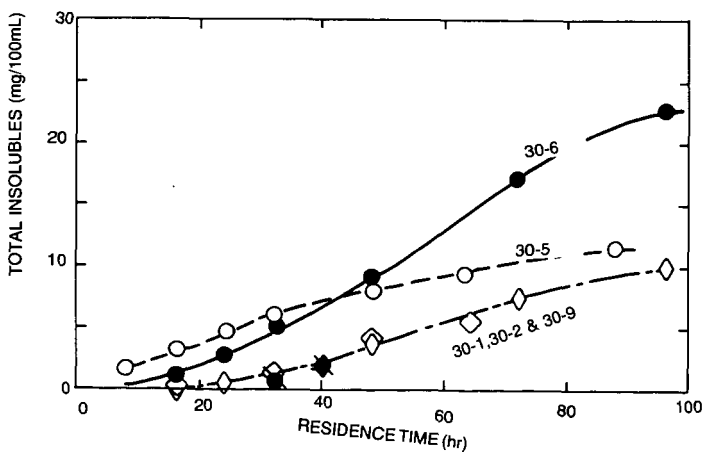

Fig. 1 - Time response curves for five fuels containing 30% LCO and 70% SR (Fuels 30-1, 30-2, 30-5, 30-6, and 30-9).

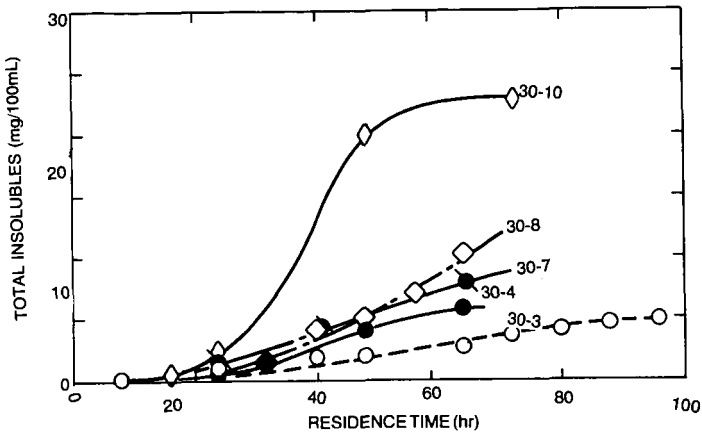

Fig. 2 - Time response curves for five fuels containing 30% LCO and 70% SR (Fuels 30-3, 30-4, 30-7, 30-8, and 30-10)

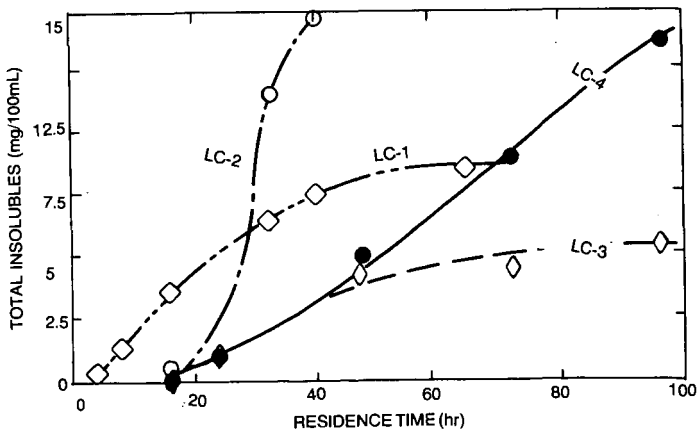

Fig. 3 - Time response curves for four light cycle oils

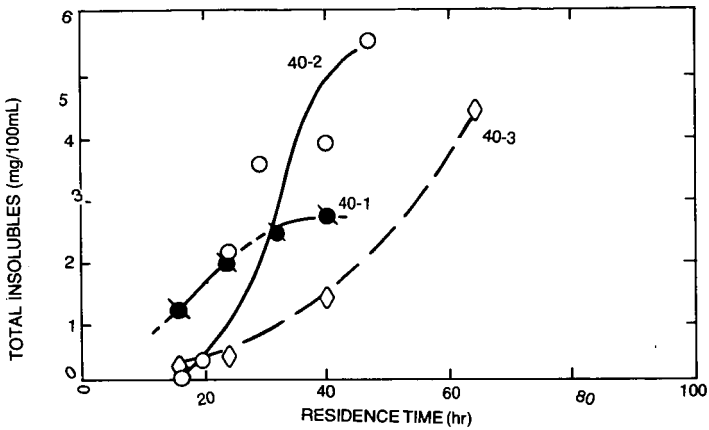

Fig 4 - Time response curves for three fuels containing 40% LCO and 60% SR.

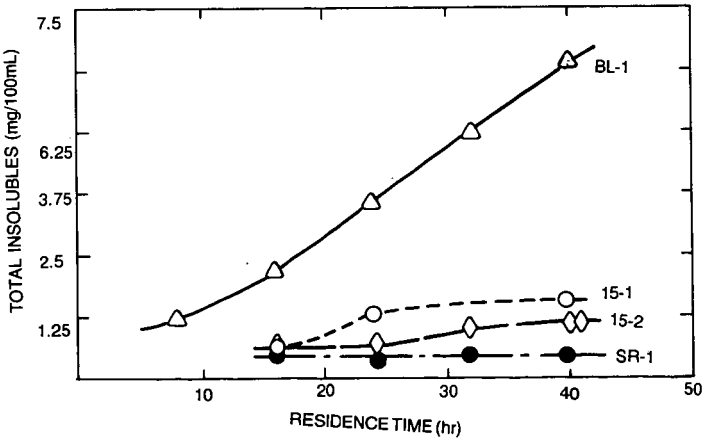

Fig. 5 - Time response curves for four miscellaneous fuels (Fuels 15-1 and 15-2 containing 15% LCO; straight run Fuel SR-1; and Fuel Blend BL-1, a high sulfur diesel fuel in CAT 1H fuel).

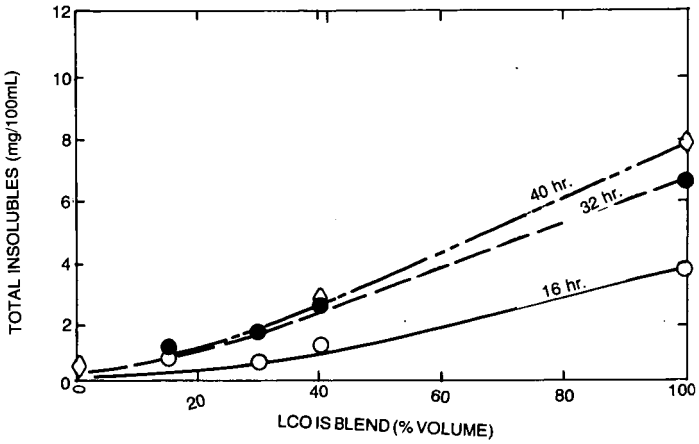

Fig. 6 - Curves showing effect of LCO concentration in straight run/light cycle oil blends on the total insolubles formed in 16 hours, in 32 hours, and in 40 hours of D2274-type stressing.

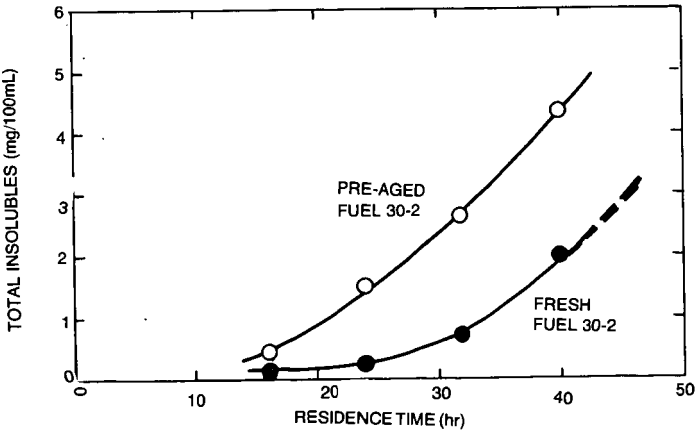

Fig. 7 - Time response curves for pre-aged and unaged Fuel 30-2; the effect of pre-aging on the formation of total insolubles.

STABILITY OF AUSTRALIAN AUTOMOTIVE DIESEL FUELS

L.D. Palmer and I.A. Davis
Ampol Research & Development Department, Lytton, Brisbane Qld 4178

E.J. Beal and D.R. Hardy
Navy Technology Center for Safety and Survivability, Code 6181
Naval Research Laboratory, Washington, DC, 20375-5000

INTRODUCTION

The storage stability of automotive diesel (ADF) fuel can vary across a wide spectrum, depending principally on the properties of its parent crude oil and the refining processes employed in its production. Fuels with inadequate storage stability produce insoluble gums and organic particulates which result in engine operability problems due to blocked fuel filters. There is currently no precise definition of just what constitutes acceptable storage stability for automotive diesel fuel. As an approximate guide, a rate of formation of insolubles of 20 mg/L per year of ambient storage has been proposed as the maximum rate for 'stable' ADF.[1-3] The absence of an accelerated test which can reliably predict the storage stability of diesel fuels has contributed to the current unsatisfactory situation. However, a test developed by the US Naval Research Laboratory is showing considerable promise for satisfying this long-standing need.

RESULTS AND DISCUSSION

Stability of Australian ADFs The results of stability tests on 76 ADFs from the eight major Australian refineries are shown in Figure 1. These fuels were produced during the 15 month period from October 1987 to the end of December 1988. Most fuels were obtained during transfers of ADF from the refineries to terminal distribution tanks, so the fuels can be assumed to be less than one month old prior to being subjected to stability tests. The survey results in Figures 1 and 2 were obtained using the 43°C/13 week test, which simulates one year of storage at typical ambient temperatures. As discussed in the following section, this test is regarded as a reliable indicator of storage stability, and has recently been adopted as an ASTM Standard test method.

Figure 1 shows that the stabilities of Australian ADFs span a wide range. Of the 76 fuels tested, a majority (76%) yielded less than 10 mg/L of insolubles. A majority (67%) of those fuels which yielded insolubles >10 mg/L emanated from a single refinery, and all of the fuels with inadequate stability (>20 mg/L) came from that refinery. Figure 1 shows, however, that the same refinery produced batches of high stability ADF in addition to the low quality batches, resulting in average insolubles of 12 mg/L. This average level of insolubles is by far the highest of any of the eight refineries (see Figure 2). Three refineries consistently produced very high stability ADF, with average total insolubles <4 mg/L. The remaining four refineries produced ADF with average total insolubles of 6-7 mg/L, indicative of ADF with good storage stability quality.

From a similar though less extensive survey of Australian ADFs covering

the period 1982-86, it was concluded that Australian ADFs were exceptionally stable, and that ADF yielding more than 5 mg/L insolubles in the 43°C/13 week test was rarely produced by Australian refineries.[4] The current survey shows a very different picture with approximately half of Australian ADF production yielding more than 5 mg/L of insolubles. However, judged by the <20 mg/L criterion for stable ADF, current Australian-produced ADFs (apart from refinery C) generally have high storage stability quality.

The very high stability observed in the 1982-86 period was attributed to the low heteroatom content of Gippsland Light (the principal crude feedstock for Australian refineries), and to the widespread use of diesel hydrotreating process or stabilizing additives. There have been many publications[2] warning that the stability of automotive diesel fuel must decline as refiners meet increasing ADF demands by inclusion of higher proportions of cracked blendstock (light cycle oil), and as refiners are forced to process crudes containing greater proportions of certain destabilizing heteroatom compounds. Furthermore, the stability of (untreated) cracked blendstock may have decreased as refiners direct heavier feedstocks to their cracking units. These trends are probably contributing to the lower storage stability revealed in the 1987-88 survey. Other factors may also have contributed. Some refiners may be seeking to reduce refining costs by reducing use of their highly effective but expensive hydrotreating units. This cost-saving approach is attractive because it has been demonstrated that storage stability can be achieved without hydrotreating, by careful selection of a stabilizing additive package.[4,5] From results of the current survey of Australian ADFs, it is apparent that at least one refiner is either underdosing or making a poor selection from the range of commercially available stabilizing additives. Furthermore, an underlying cause for this situation may be the use of unreliable accelerated stability tests to assess the performance of commercially available additives.

Accelerated Stability Tests The formation of insoluble organic matter in diesel fuels during storage is the result of complex interactions among a range of reactive species in the fuel, and molecular oxygen. At least three classes of chemical reaction (eg oxidative gum formation, acid-base reactions and esterification) can occur.[2,6,7] The more reactive compound classes include heteroatom compounds and olefins. Certain compounds eg alkyl pyrroles, indoles[8,9] and thiophenols[10] are known to be particularly potent destabilizers of diesel fuel. Recent years have seen a renewed interest in achieving a better understanding of the complex chemistry of diesel fuel degradation, leading to an improved understanding of the complex chemistry involved.[11,12]

The complexity of the chemistry of diesel fuel degradation has been the principal barrier to the development of a reliable accelerated storage stability test. The methods used to accelerate the insoluble-forming reactions include higher temperature, higher oxygen concentration and copper catalysts. Certain insoluble-forming reactions, however, may be more sensitive to the accelerated reaction conditions. Hence, the overall chemistry occurring under the accelerated conditions may be quite different from that occurring under non-accelerated conditions viz. normal storage of ADF. Consequently, highly accelerated tests are likely to be the least reliable indicators of storage stability, unless they have been thoughtfully devised and carefully evaluated.

Based on American and European experience, there is general agreement that the mild acceleration involved in the 43°C/13 week storage stability test results in reliable assessment of storage stability at normal storage temperatures. Consequently, the American Society for Testing and Materials introduced the new standard test method ASTM D4625 "Distillate Fuel Storage Stability at 43°C" in 1988. For Australian ADFs, Figure 3 compares results from the 43°C/13 week ASTM test and one year storage of 700 mL samples in metal cans in a non-air conditioned shed in Brisbane, Australia (average temperature ≈25°C). While the experimental data show some scatter, it can be concluded that the quantity of insolubles formed during storage at ambient temperatures for one year is approximately equal to the quantity formed during 13 weeks at 43°C. Thus the 43°C/13 week test can be confidently employed for assessing the ambient storage stabilities of Australian ADFs.

Figure 4 shows the correlation between total insolubles formed in the more accelerated 80°C/7 day test and insolubles formed in the 43°C/13 week test, for a selection of Australian ADFs. The figure shows that the 80°C/7 day test can serve a useful predictive function for the more stable fuels, even though results do not correlate particularly well with results from the 43°C test. Those fuels which yielded less than 3 mg/L in the 80°C test also performed well in the 43°C test. However, fuels yielding 4-8 mg/L in the 80°C test yielded a very wide range of insolubles (3-32 mg/L) in the 43°C test. Hence, as a potential quality control test, the 80°C/7 day test shows inadequate correlation with the 43°C/13 week test if it is to be applied to fuels with a wide range of storage stabilities. Thus the acceleration of the processes of formation of filter-blocking insolubles has reduced the reliability of the accelerated test, even before the time required for the test has been shortened to the <24 hr period desirable for a refinery quality control test method.

Other studies involving attempts to accelerate ambient storage conditions by raising the temperature and shortening the test time suggest that 80°C/7 days may be much too severe to attempt a reasonable correlation to 43°C/13 week tests (Hardy et al, 1986). That work suggests that 80°C/4 to 5 day bottle tests should correlate much better with the 43°C/13 week tests for any given fuel. Unfortunately the precision of the test results obtained at 80°C/4 to 5 days is very poor and hence those conditions are not acceptable as a refinery quality control test for accelerated stability. Shortening the test time at 80°C below 4 days results in increasingly poor test precision or repeatability thus effectively barring the use of this test at the refinery.

One Australian refiner adopted an accelerated test based on a temperature of 100°C and the accelerating effect of soluble copper at a concentration of 10 mg/L. The test period of 2 h was short enough for the test to be used for quality control, and the test was used for acceptance/rejection purposes for ADF exchange between some Australian oil companies. Figure 5 shows that the test is clearly unsuitable for this application, even though there is a degree of correlation with the 43°C/13 week test. The problem is that some fuels which are stable (according to the <20 mg/L criterion for the 43°C/13 week test) are classed as unstable by the highly accelerated copper naphthenate test. Such a test is clearly unsuitable for quality control of large production batches of ADF, and in the light of evidence such as

presented in Figure 5, the test was abandoned in 1988. The possibility that similar situations may reoccur again highlights the need for a reliable short-term test for quality control of ADF storage stability.

While Figures 4 and 5 show that attempts to accelerate the formation of insolubles can result in unreliable storage stability tests, the combination of increased temperature and oxygen pressure may be more reliable. Figure 6 shows results for five US middle-distillate fuels, spanning a broad range of stability, when tested at 43°C for 18 weeks in atmospheric bottle tests and 43°C for 4 weeks at 100 psia oxygen. A linear least squares correlation gives $R^2 = 0.98$ for these two tests. The correlation between 43°C/4 weeks/100 psia and 80°C/64 hr/100 psia of oxygen is 0.97 for these same five fuels. This is a clear indication that a combination of increased temperature and increased oxygen pressure together should be quite useful for predicting ambient storage stability for most middle-distillate fuels.

<u>The Oxygen Overpressure Stability Test</u> A new oxygen overpressure method for predicting distillate fuel's tendency for forming deleterious fuel insolubles during ambient storage is rapid and precise and is predictive for up to 3 years of ambient conditions. For this test 100 mL samples of filtered fuel in 125 mL borosilicate bottles were placed in a low pressure reactor (LPR). The reactor was sealed and pressurized with 99.5% pure oxygen to 100 psig. The samples were stressed, while maintaining the oxygen pressure, under accelerated storage conditions for set temperatures and times. At the end of the stress period, the amount of filterable sediment and adherent sediment were determined gravimetrically and reported as total insoluble sediment weight. Samples were run in triplicate and the average values are reported in mg/100 mL.[13]

Work at 43°C for up to 4 weeks at 100 psig (see Figure 6) and at 80°C for up to 64 hours at psia shows very good correlation with bottle tests done at 43°C (slight variation of ASTM D4625). In an attempt to make the test shorter, recent work has been done at 90°C for 16 hours at 100 psig for possible use as a new ASTM method.

Table 1 shows comparison gravimetric results for two accelerated storage stability tests using a variety of diesel fuels. Two of the fuels are blends of 30% cracked stock (LCO) and 70% straight run. One fuel is a blend of 30% diesel fuel containing 2% sulfur (HSD) and 70% straight run. The remaining fuels were US Naval Distillate fuels (NATO F-76). Very good correlation between the results of the lower temperature bottle tests and the oxygen overpressure tests is shown. When the pass/fail criteria at the bottom of the table is applied, it can be seen that, with the exception of one sample, the oxygen overpressure method correctly assessed the stability of these fuels when compared with the longer bottle tests. This fuel would be considered marginal by both methods.

This method has also been useful in assessing the relative effectiveness of middle-distillate fuel stabilizer (antioxidant) additives. Table 2 shows typical results for a slightly unstable fuel. The oxygen overpressure method correctly assessed the additive-free fuel in addition to evaluating the additives when compared to the lower temperature test. Additive 7 is a noteworthy exception when comparing the two test methods. This indicates the need to possibly extend the

test times of the 16 hour 100 psig test to exceed reaction induction times. Also, in two cases, additives 3 and 4, the 90°C test appears to be more severe than the 43°C test.

Figure 7 shows the gravimetric results obtained when the same six fuels, of various stabilities, were analyzed at NRL and at AMPOL using the oxygen overpressure method. Very good correlation between the results is shown, especially when it is considered that the samples were analyzed using reactors constructed separately at each of the labs. These results also show that the method has good reproducibility.

CONCLUSIONS

The storage stability of Australian automotive diesel fuels has decreased from the extremely high quality which existed five years ago. With the exception of one refinery, however, Australian refineries still produce ADF with good storage stability. Assessment of long-term storage stability by means of highly accelerated laboratory tests remains a challenge. Most highly accelerated tests have limited reliability when compared with the mildly accelerated 43°C/13 week test. The oxygen overpressure method, however, is showing promise of filling the long-standing need for a rapid, reliable test.

REFERENCES

1. Hardy, D.R., Hazlett, R.N.,Giannini, R. and Strucko, R., SAE Technical Paper Series No. 860895, 1986.
2. Schrepfer, M.W., Arnold, R.J. and Stansky, G.A., **Oil and Gas Journal**, 16 January 1984, p.79.
3. Stavinoha, L.L. and Westbrook, S.R., ASTM Special Technical Publication 751, 1981, pp.3-21.
4. Smith, R.J. and Palmer, Proc. 2nd International Conference on Long Term Storage Stabilities of Liquid Fuels, 1986, p.875.
5. Mabley, P.B. and Wallace, G.M., Proc. 3rd International Conference on Stability and Handling of Liquid Fuels, 1988, p.412.
6. Hazlett, R.N., Power, A.J., Kelso, A.G. and Solly,R.K., Materials Research Laboratories, Report No. MRL-R-986 Melbourne, Australia, 1986.
7. Taylor, W.F. and Frankenfeld, J.W., Proc. 2nd International Conference on Long Term Storage Stabilities of Liquid Fuels, 1986, p.496.
8. Pedley, J.F., Hiley, R.W. and Hancock, R.A., **Fuel**, 1989, 68, P.27.
9. Oswald, A.A. and Noel, F., **J. Chem. Eng. Data**, 1961, 6, p.294.
10. Offenhauer, R.D., Brennan, J.A. and Miller, R.C., **Ind. Eng. Chem.**, 1957, 49, p.1265.
11. Stavinoha, L.L., Ed., Proc 2nd International Conference on Long Term Storage Stabilities of Liquid Fuels, Southwest Research Institute, San Antonio, Texas, 1986.
12. Hiley, R.W., Forward, Proc. 3rd International Conference on Stability and Handling of Liquid Fuels, The Institute of Petroleum, London, 1988.
13. Hardy, D.R., Hazlett, R.N., Beal, E.J. and Burnett, J.C., **Energy and Fuels**, 1989, 3, p.20.

TABLE 1. TOTAL INSOLUBLES (mg/L) FROM ACCELERATED STABILITY TESTS

Sample Description	43°C/18 wk Bottle Test	90°C/16 hr/100 psig LPR Test
30%LCO/70%SR (Refinery 1)	89	46
30%LCO/70%SR (Refinery 2)	60	38
30%HSD/70%SR (Refinery 3)	44	62
NATO F-76 (1)	39	39
(2)	5	7
(3)	7	13
(4)	11	7
(5)	12	14
Pass/Fail	40	30

TABLE 2. TOTAL INSOLUBLES (mg/L) FOR (30%LCO/70%SR) DIESEL FUEL FROM A U.S. GULF COAST REFINERY TREATED WITH VARIOUS STABILIZING ADDITIVES

Sample Description	43°C/18 wk Bottle Test	90°C/16 hr/100 psig LPR Test
2	19	7
3	28	38
4	39	52
9	43	31
6	45	28
8	47	24
1	52	34
5	56	31
7	56	14
Neat	62	45
Pass/Fail	40	30

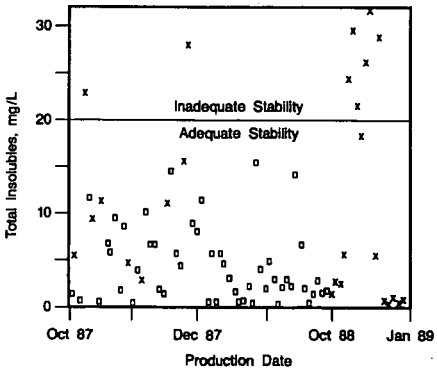

Figure 1. Total Insolubles Formed During Oven Storage at 43°C for 13 Weeks. Cross-Symbols – Refinery C; Square Symbols – Other Australian Refineries.

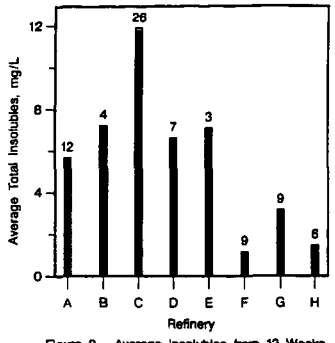

Figure 2. Average Insolubles from 13 Weeks at 43°C for ADF from Australian Refineries. The Numbers of Samples Tested Are Indicated.

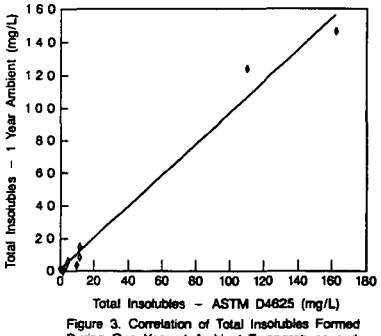

Figure 3. Correlation of Total Insolubles Formed During One Year at Ambient Temperatures and During 13 Weeks at 43°C (ASTM D4625).

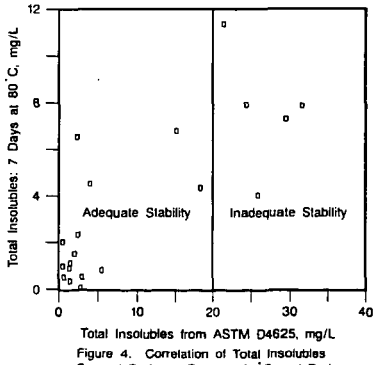

Figure 4. Correlation of Total Insolubles Formed During 7 Days at 80°C and During 13 Weeks at 43°C (ASTM D4625).

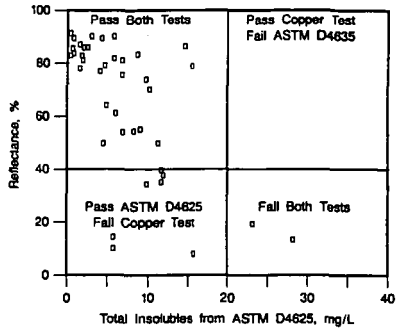

Figure 5. Correlation of a Stability Test Employing Copper as an Accelerating Agent with Insolubles Formed During 13 Weeks at 43°C.

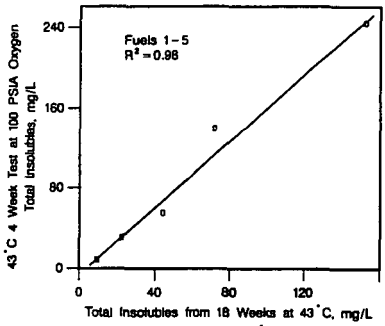

Figure 6. Comparison of 43°C/4 Week/100 PSIA O_2 Test Results with 43°C/18 Week Data.

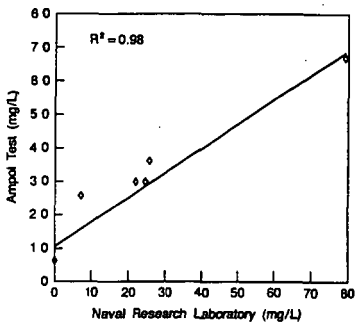

Figure 7. ASTM Round Robin Results for Oxygen Overpressure Stability Test (90°C/16 Hr/100 PSIG)

Assessment of the Oxygen Overpressure Test for Prediction of Middle Distillate Fuel Storage Stability

Grier G. McVea, Joanna F. Pedley* and Richard K. Solly

Materials Research Laboratory, Defence Science and Technology Organisation
PO Box 50, Ascot Vale, Victoria, Australia 3032

* Visiting Scientist from Directorate of Quality Assurance/Technical Support
Fairmile, Cobham, Surrey KT11 1BJ, UK

ABSTRACT Gravimetric amounts of sediment produced by the oxygen overpressure test for ageing middle distillate fuels for 16 hours at 90°C with a pressure of oxygen of 794 kPa (100 psig) have been compared with that produced by ASTM D4625 conditions at 43°C for 13 weeks. Fifteen fuel blends comprising 30% light cycle oil or 30% hydrotreated light cycle oil were included in this study. Whereas approximately half of the fuel blends produced comparable amounts of sediments by the two procedures, there was no correlation overall for ranking fuels based on sediment produced. Comparison of gravimetric amounts of sediments produced by 12 months ambient ageing with that produced in the oxygen overpressure test of the ambient aged fuels again produced no correlation between the two procedures. The species separated by thin layer chromatography of the sediment produced in the oxygen overpressure test were compared with those produced under ASTM D4625 conditions. There was much similarity in the species observed for the standard oxygen overpressure conditions, but significant differences were noted as the temperature of stress used in the oxygen overpressure test was raised above 90°C. At the higher temperatures, brown species extending over all R_f values began to predominate in the thin layer chromatograms.

INTRODUCTION

World wide demand for middle distillate fuel continues to increase as at a greater rate than other fractions of the oil refinery barrel. This demand is being partly met by the greater use of cracking of the heavier distillation products and incorporation of this cracked stock in the form of light cycle oil (LCO) into automotive diesel fuel. The direct incorporation of LCO into automotive diesel fuel is one of the major, if not the most significant contributing factor, to the formation of insoluble particulate and gums on storage of the fuel.[1]

With the decrease in fuel stability, the necessity for an accurate test to predict the storage stability of a distillate fuel is increased. Lower temperature bottle tests are generally the best indicators of storage stability and recently a 43°C test has been standardized as ASTM D4625. The length of time required to obtain significant amounts of sediment for reliable results by ASTM D4625 is a major drawback for quality control. The method of ASTM D2274 has been the most widely used rapid method for assessment of the fuel storage oxidative stability of a fuel.[2] However, it has been found that this test is a poor predictor for the storage stability of freshly refined fuel containing catalytically cracked stock.[3] For many fuels, the amount of sediment produced in the 16 hour period at 95°C is too small to be measured accurately.[4] Recently an oxygen overpressure technique has been proposed in which fuel is stressed for 16 hours at 90°C in an atmosphere of 794 kPa (100 psig) oxygen.[3] This test has

the advantage that significant amounts of sediment were produced in a relatively short time period and good precision was obtained in replicates of gravimetric amounts of sediment.

For this oxygen overpressure technique to find widespread use as a predictive tool, it is necessary that it predicts the relative ambient storage stability of distillate fuels. This study was undertaken to correlate gravimetric amounts of sediment produced under both ambient and ASTM D4625 conditions with that of the oxygen overpressure technique. Reference fuels were chosen so as to include both freshly refined diesel fuel containing either thermally or catalytically cracked stock and aged commercial diesel fuels. Opportunity was taken of an associated study[5] to compare the species present in sediments from oxygen overpressure conditions with those produced from the ASTM D4625 procedure. Correlation of both gravimetric amounts of sediment and chemical species present in the sediment would add to the confidence with which the oxygen overpressure technique could be used for predicting the relative storage stability of distillate fuels.

The role of reactions between alkylindoles and phenalene species to sediment formation in the reference distillate fuels is presented elsewhere.[5] In this presentation, the initial concentration of alkylindoles in the reference fuels is considered in relation to the species observed in thin layer chromatograms of sediments produced by the oxygen overpressure technique and in correlations between total amounts of sediment produced by oxygen overpressure conditions and the ASTM D4625 procedure.

EXPERIMENTAL

Samples from automotive distillate refinery streams of straight run distillate (SRD), light cycle oil (LCO) and hydrotreated light cycle oil (HTLCO) were obtained directly from Australian refineries. All samples were reported to have being produced in less than one week of receipt. LCO was from catalytic crackers for all refineries except one, which has a thermal cracking unit. Samples were either blended upon receipt for immediate commencement of the ageing trial or stored as unblended components at -12°C. Experimental fuels were prepared by mixing 30% (volume/volume) LCO or HTLCO with SRD and filtering the mixture through glass fibre membranes (Millipore AP40) immediately prior to use. For all experimental samples, except FG1 and FG2 of Table 3, the sample components originated in the same refinery. Samples FG1 and FG2 were mixtures of 30% LCO and 30% HTLCO respectively from refinery F with SRD from refinery G.

Oxygen overpressure measurements were determined in the single bomb apparatus of ASTM D942 using 75 ml of fuel in 100 ml lipless borosilicate containers. The bomb containing the fuel sample was purged three times with 99.5% purity oxygen prior to being placed in a thermostated liquid bath which maintained the temperature to within 0.1°C. After being immersed in the bath for 15 minutes, the pressure was adjusted to 794 kPa (100 psig). During most runs the oxygen pressure decreased by 40-50 kPa. Upon completion of a run, the bomb was removed from the liquid bath and allowed to cool to ambient temperature prior to sediment determinations.

Suspended particulate matter in the samples was determined by filtration of the fuel through duplicate pre-tared glass fibre membranes (Millipore AP40). Adhered insolubles were determined by rinsing the containers with triple solvent (equal amounts of toluene, acetone and methanol) and hot plate evaporation of the solvent in disposable aluminium dishes and algebraic subtraction of a blank evaporation of equivalent amounts of solvent. Total sediment was the sum of the suspended particulate matter and the adhered insolubles. Data shown in the tables is the average of two duplicate fuel sample determinations.

The 13 week 43°C ageing was carried out according to the method of ASTM D4625 using 1 litre borosilicate containers thermostated in an air oven. The automotive diesel fuel samples listed in Table 4 were obtained directly from retail commercial outlets or sampled directly from user storage tanks in Northern Australia. Although the specific origin of this fuel is unknown, it is most likely that a significant proportion originated from refineries in Singapore. The fuel was stored in 1 litre plastic containers at ambient temperatures for 12 months after collection of the samples prior to the measurements. Total sediment measurements as described above were determined for the fuel prior to its use for the oxygen overpressure measurements.

Thin layer chromatograms of the sediments were obtained by dissolving the sediment directly from the glass fibre membranes with 10% methanol in dichloromethane. This solvent was then used as the mobile phase with a silica gel stationary phase. Alkylindoles were determined in the fuel samples after concentration of the polar species on a small column of silica followed by elution with dichloromethane. This solvent was evaporated with a gentle stream of nitrogen and the residue dissolved in toluene containing 1-methylindole as an internal standard. Separation of the constituents was achieved by injection into a gas chromatograph equipped with a BP1 capillary column (25 m x 0.5mm), a nitrogen specific detector and temperature programmed oven from 30°C to 280°C at 4°C per minute. Peaks from the nitrogen specific detector with a retention time between that for 1-methylindole and carbazole were considered to be alkylindoles with reference to previously published chromatograms[6]. All peaks in this range were summed and converted to a mole concentration by assuming an equal molar response on the nitrogen specific detector to that for 1-methylindole.

RESULTS AND DISCUSSION

The effect of oxygen pressure, temperature and time has previously been reported for the oxygen overpressure (OP) technique.[3] Little variation was found when the oxygen pressure exceeded 350 kPa, so all measurements in this study were carried out with an oxygen pressure of 794 kPa (100 psig). With one of the refinery fuel blends in this study (A1), comparative measurements were made between a number of OP conditions and the ASTM D2274 and ASTM D4625 procedures. As may be seen from Table 1, sediment corresponding to medium instability was obtained for the ASTM D2274 and ASTM D4625 procedures for fuel A1. Similar amounts of sediment were obtained from 26 hr/80C and 16 hr/95C OP conditions.

FUEL	ASTM D2274 16 hr 95C mg/L	ASTM D4625 13 weeks 43C mg/L	OXYGEN OVERPRESSURE 794 kPa O_2 26 hr 80C mg/L	16 hr 90C mg/L	16 hr 95C mg/L	64 hr 95C mg/L	16 hr 120C mg/L
A1	13	18	16	8	18	70	88
F1		15		33		119	

Table 1. Comparison of Total Sediment from ASTM D2274 and ASTM D4625 ageing with oxygen overpressure ageing for fuel A1 and F1.

Less sediment was obtained from 16 hr/90C OP conditions. A smaller number of comparative measurements was made for fuel F1. However, comparing only ASTM D4625 conditions with those for OP at 16 hr/90C, it may be noted that OP conditions produced 2.2 times as much sediment, whereas for fuel A1, the equivalent ratio was 0.4.

The total amount of sediment increased significantly as the temperature or time of ageing increased for OP conditions. The sediments produced by the experiments shown in Table 1 were separated into constituents by thin layer chromatography on silica gel. The results are shown schematically in Table 2.

A high degree of similarity in the species was observed in the sediment produced under ASTM D4625 conditions and OP conditions of 16 hr/90C. There was a higher degree of similarity in these chromatograms than those only for ASTM D4625 conditions from ageing the low and high alkylindole content blends of Table 3. Details of the ASTM D4625 sediments will be discussed elsewhere at this conference[5] with rate process associated with the formation of the species.[7]

A major feature of the thin layer chromatograms was the increased intensity in the OP 16 hr/90C sediments of the pink material at an R_f value of approximately 0.45 and the orange material at approximate R_f 0.25. The intensity of this orange material was less on freshly chromatographed plates, but increased with age. If the orange band at R_f 0.25 was rechromatographed, an orange band at approximate R_f 0.90 was formed. Rechromatography of the pink material at R_f 0.45 again produced an equivalent pink band, but also an orange material at R_f 0.25. It is postulated that the pink material is the acid salts of indolylphenalenones, which partly disassociate on the thin layer plates to form orange indolylphenalenones.[8] The increased formation of indolylphenalenone products under OP conditions is consistent with the increased oxidation environment.

The blue material at approximate R_f 0.30 is believed to be acid salts of indolylphenalenes.[9] These salts are very pronounced in the high alkylindole fuel sediment under ASTM D4625 conditions. The proportion of the blue material decreased as the temperature and time of the OP conditions increased. At the longer OP times (64 hours) and temperatures (120°C), the proportion of brown streaking material on the thin layer chromatograms increased. This material extended over all R_f values and was the predominate material in the chromatogram of the OP 120°C sediments. As the formation of the brown material is accompanied by a decrease in the pink and blue materials on the thin layer chromatograms, it is postulated to be a polymeric material produced by further reaction of the indolylphenalene and indolylphenalenone salts. The formation of the brown material places an upper limit on the temperature of the oxygen overpressure test.

Comparison of the amount of sediment produced by ASTM D4625 conditions and the OP test at 16 hr/90C was extended to 15 fuels blends shown in Table 3. Whereas the ratio of sediment produced by the two procedures is within 1.0 ± 0.2 for a number of fuels, many fuels show a significant deviation from this ratio. No definite trend is obvious from the data in the table. The number of fuels in which significantly more sediment is produced by OP conditions is greater than the number of fuels in which significantly less sediment is produced. This may be the reason that these OP conditions have been postulated to be equivalent to three years ambient storage.[3] However, this extrapolation would be very favourable to fuels such as A1 and E2 which produce significantly less sediment under the OP conditions. Attempts to correlate the total amount of alkylindoles in the fuels with agreement of the total amount of sediments by the two procedures did not yield any obvious relationship.

The comparative study was extended to some commercial automotive diesel fuels collected from Northern Australia which had been in storage for 12 months at ambient

temperatures. It may be noted that oxygen overpressure determinations and measurement of alkylindole concentrations were carried out on fuel which had been aged for at least 12 months and from which sediment produced by the ambient ageing had been removed. As may be seen from the data in Table 4, there does not appear to be any relationship between the gravimetric amount of sediment produced by the two procedures. The ratio of sediment produced by one year ambient ageing compared to OP conditions ranged from 0.3 to 2.8.

CONCLUSIONS

The oxygen overpressure test at a temperature of 90°C for 16 hours at 794 kPa pressure oxygen will produce comparable amounts of sediment for many fuels to that formed by ageing the fuel for 13 weeks at 43°C. However, there are a significant number of fuels which either produce greater or smaller amounts of sediment under oxygen overpressure conditions compared to lower temperature air environment ageing. As the difference in the relative amount of sediment is in both directions, it is unlikely that variation of the oxygen overpressure conditions will produce good correlation for all fuels. In this study, an attempt was also made to correlate the variation in relative amount of sediment with the total amount of alkylindoles in the fuel, but no relationship could be found.

Conclusions reached from the use of relative amounts of total sediment produced by oxygen overpressure conditions as the sole reference criteria for mechanistic studies of distillate fuel ageing processes should be interpreted with much caution.

ACKNOWLEDGEMENTS

The contribution of all major Australian oil companies in making fuel samples from refinery streams available to this study is gratefully acknowledged towards maintaining the generally high standards of Australian Defence and commercial automotive diesel fuels.

REFERENCES

1. Arfelli, W., Power, A.J., Solly, R.K. The Storage Stability of Automotive Diesel Fuel. *Proc. 4th Int. Conf. Automotive Engineering*. SAE Australasia, Melbourne, 1987, Paper No. 871269.
2. Oxidative Stability of Distillate Fuel Oil; ASTM D2274-74; American Society for Testing and Materials.
3. Hardy, D.R., Hazlett, R.N., Beal E.J., Burnett, J.C. Assessing Distillate Fuel Storage Stability by Oxygen Overpressure. *Energy and Fuels*, 1989, **3**, 20.
4. Stirling, K.Q., Brinkman, D.W. NIPER-352; National Institute for Petroleum and Energy Research, Bartlesville, OK, 1988.
5. Pedley, J.F., Beranek, L.A., O'Connell, M.G., Solly, R.K. The Chemistry of Sediment Formation in Australian Middle Distillate Fuels. This conference.
6. Dorbon, M., Bernasconi, C. Nitrogen Compounds in Light cycle Oils: Identification and Consequences of Ageing. *Fuel*, **68**, 1067, 1989.
7. Beranek, L.A., McVea, G.G., O'Connell, M.G., Solly, R.K. Rate of Indole Phenalenone Reactions in Middle Distillate Fuel. This conference.
8. Pedley, J.F., Mathys, G.I. To be published.
9. Pedley, J.F., Hiley, R.W. Investigation of Sediment Precursors Present in Cracked Gas Oil. *Proc. 3rd Int. Conf. on Stability and Handling of Liquid Fuels*. IP, London, U.K. p.495, 1988.

FUEL A1

R_f RANGE	BAND COLOUR	ASTM D4625 13 weeks 43C	794 kPa O_2 16 hr 90C	64 hr 95C	16 hr 120C
1.00-0.95	green	L	VL	VL	VL
0.92-0.84	orange	L	L	L	M
0.73-0.71	green	VL	VL	VL	VL
0.64-0.62	grey	VL	VL	VL	VL
0.56-0.55	grey	VL	VL	VL	VL
0.49-0.33	pink	M	L	L	NO
0.33-0.25	blue	M	M	VL	VL
0.25-0.19	orange	NO	M	L	NO
0.25-0.19	pink	M	NO	NO	NO
0.09-0.06	brown	M	M	M	D
0.05-0.02	yellow	M	M	M	NO

FUEL F1

R_f RANGE	BAND COLOUR	ASTM D4625 13 weeks 43C	794 kPa O_2 16 hr 90C	64 hr 95C
1.00-0.96	green	L	L	L
0.94-0.87	orange	M	M	M
0.55-0.49	violet	L	L	L
0.49-0.46	pink	L	M	M
0.46-0.27	blue	D	M	L
0.27-0.22	orange	L	M	NO
0.10-0.08	brown	NO	M	D
0.05-0.03	yellow	L	M	VL

NO	not observed
VL	very light
L	light
M	medium
D	dark

Table 2. Thin layer chromatogram schematics of sediment from fuel A1 (low alkylindoles) and F1 (high alkylindoles).

FUEL SAMPLE	ASTM D4625 mg/L	OXYGEN OVERPRESSURE mg/L	RATIO	TOTAL ALKYLINDOLES* umol/L
A1	17.8	8.0	2.2	384
B1	11.8	19.5	0.6	632
B2	0.4	4.0	0.1	193
C1	19.0	19.9	1.0	506
C2	0.6	<0.1	>6.0	54
D1	9.0	10.0	0.9	nd
D2	0.8	1.0	0.8	nd
E1	56.2	47.0	1.2	1204
E2	7.9	1.0	7.9	nd
F1	14.6	33.2	0.4	1089
F2	18.6	21.3	0.9	904
G1	12.3	11.4	1.1	707
G2	0.2	2.0	0.1	49
FG1	12.4	24.5	0.5	nd
FG2	18.1	19.0	1.0	nd

* Assuming equal molar detector response to 1-methylindole
X1 30% LCO/SRD fuel blends
X2 30% HTLCO/SRD fuel blends
nd not determined

Table 3. Comparison of Total Sediment from ASTM D4625 (13 weeks at 43°C) with oxygen overpressure ageing (16 hours at 90°C with 794 kPa pressure oxygen) for 30% LCO/SRD and 30% HTLCO/SRD fuel blends.

FUEL SAMPLE	COLOUR ASTM D1500	AMBIENT mg/L	OXYGEN OVERPRESSURE mg/L	RATIO	TOTAL ALKYLINDOLES* umol/L
1	2.5	14	43	0.3	355
2	4.0	39	30	0.8	nd
3	1.5	14	16	0.9	44
4	2.0	11	4	2.8	129
5	1.5	11	24	0.5	17
6	1.5	5	5	1.0	<10
7	nd	11	<1	>11	223

* Assuming equal molar response to 1-methylindole
nd not determined

Table 4. Comparison of Total Sediment from one year ageing at ambient temperature with oxygen overpressure ageing (16 hours at 90°C with 794 kPa pressure oxygen) for commercial fuels from Northern Australia.

DEVELOPMENTS IN DIESEL FUEL STABILITY FORECAST METHODS

Nahum Por and Dr. J. Ben Asher

The Israel Institute of Petroleum and Energy
P.O.B. 17081, Tel Aviv 69975, Israel

ABSTRACT

A rapid oven test was designed and used for estimation of diesel fuel stability forecasts as well as for establishing mechanisms of diesel fuel degradation processes. The 17 hours test at 110°C in specially designed bottles allows withdrawal of a vapour phase sample, enabling determination of the oxygen depletion rate, which, in conjunction with the gum formation rate, indicates whether the degradation process is of an oxidative or a polymerization type. In order to enable determination of gum formation rate in diesel fuels of a final boiling point above 300°C, a special procedure had to be devised. The gum content of any diesel fuel is of a large importance, since it indicates not only the rate of degradation products formation, but also allows its physical examination. The estimates for diesel fuel storage stability properties as used in the Rapid Oven Test (ROT) are existent gum (determined by the modified procedure), oxygen depletion in the vapour phase, acidity and colour, - all before and after exposure to the oven test. The rate of change of these properties indicates the resistivity of the diesel fuel to environmental influences during storage.

THE BACKGROUND

Difficulties have been experienced when diesel fuels had to be evaluated in respect of their behaviour in medium and in long term storage, especially in case of their operational stabilities. Operational stabilities, as referred to in this paper, are associated with the behaviour of diesel fuels in fuel tanks of vehicles or equipment, which have to be ready for immediate use, even when not operated constantly. Such vehicles or equipment are put into operation from time to time in order to ensure their proper functioning. The diesel fuel is thus circulated in the fuel system and exposed to high temperatures and contact with metals before it is returned to the fuel tank. Such conditions are extremely unfavourable to the diesel fuel properties, especially if their chemical composition makes them susceptible to changes in their original properties and to formation of degradation products.

The growing use of catalytic crackers and visbreakers, necessary for production of increased proportions of distillates in general and of motor gasolines in particular, yield correspondingly larger

amounts of cracked (unstable) middle distillates. These can be hydrotreated in order to saturate some of the unsaturated components, thus improving their stabilities, - or they can be used as diluents for back-blending heavy residues for obtaining specification grade residual fuel oils. Stability improving additives can be also used for obtaining satisfactorily stable products. Nevertheless, some of the cracked middle distillates find their way into the diesel fuels, impairing so their stability properties.

The situation described in the foregoing makes it necessary to:

a. Employ efficient means for estimating stability properties of diesel fuels in short, medium and long term storage, as well as their operational stabilities;

b. Have at disposal suitable testing procedures for evaluation of stability improving additives, in respect of types as well as of concentrations.

DIESEL FUEL STABILITY ESTIMATING PROCEDURES

Good diesel fuel stability estimates should fulfil the following requirements:

a. They should be reliably indicative of the diesel fuel stability properties;

b. The obtained results should be well reproducible;

c. Testing procedures should be easily and fastly carried out and results should be obtainable after an as short a time as possible.

Most of the the presently used oven tests respond well to the first two conditions, but not to the third, which in itself is of a large importance in routine stability monitoring. An effort was therefore made to devise an accelerated oven test, which would respond to all the above mentioned requirements.

The oven test procedure suggested in this respect is the Rapid Oven Test (ROT), in which fuel samples are are kept for 17 hours at a temperature of 110°C in half liter glass bottles, sealed with crimp type caps enabling puncture and withdrawal of vapour samples from the outage with a hypodermic syringe. The main parameters serving as stability estimates are total gums (composed of filterable sediment, adherent insolubles and existent gum), and oxygen depletion in the vapour phase above the tested fuel.

EXISTENT GUM OF WIDE BOILING POINT RANGE DIESEL FUELS

Values of existent gum are indicating the rate of degradation products formation and are therefore of a great importance. Moreover, the physical formation of gums allows the determination of their chemical composition, which in itself is also a valuable tool in the study of degradation products formation in diesel fuels.

The problem in this respect is that the current method for existent gum determination (ASTM D 381) is suitable only for diesel fuels the final boiling point of which does not exceed 320°C. A modified method allowing existent gum determinations of diesel fuels of a final boiling point of up to 400°C had to be therefore devised. The proposed procedure is based on evaporating a blend consisting of 25% volume of the full range diesel fuel and 75% volume of a kerosine, the existent gum of which had been previously determined and is used as a blank. 50 ml of the blend are evaporated under conditions prescribed by the ASTM D 381 procedure, The residue is weighed and the result is reported as mg gum per 100 ml of the diesel fuel, after the contribution of the kerosine gum (blank) had been deducted.

DETERMINATION OF BREAKDOWN MECHANISMS BY THE RAPID OVEN TEST

The oxygen depletion rates indicate not only the degradation products formation rate but also the nature of the particular degradation process: In case of gum formation without an appreciable drop in the oxygen content of the gaseous phase, the degradation process can be assumed to be of a polymerization nature:

$$R\cdot + M \longrightarrow RM\cdot$$
$$RM\cdot + M \longrightarrow RMM\cdot \quad \text{etc.}$$

In case the degradation process is accompanied by a significant drop in the oxygen content of the gaseous phase, it can be assumed to be of an oxidative nature. This can be also seen by the peroxides content of the tested fuel or the chemical composition of the gums:

$$R\cdot + O_2 \longrightarrow ROO\cdot$$
$$ROO\cdot + RH \longrightarrow ROOH + R\cdot \quad \text{etc}$$

Since these polymerization chain reaction mechanisms are well known, they are not discussed in detail in the framework of this paper.

DISCUSSION OF RESULTS

Table 1 summarizes properties of the four diesel fuel types used in the experimental sets described in this paper:

Type A is a straight run product of a relatively low final boiling point and is assumed to be relatively stable. Types B an C are diesel fuels of wider boiling point ranges, the final boiling point being

about 370°C. Type B is an aged product a sample of which had been drawn from an experimental long term field storage tank, while Type C is a corresponding freshly produced product.

Type D is a blend of the Type C commercial product and a cracked gas oil sample in a ratio of 2 to 1. This diesel fuel sample is assumed to be unstable. The analysis of the cracked gas oil component is given in the last column of Table 1.

Comparative results of long term storage stability tests of the four diesel fuel types, using several testing procedures, are given in Table 2 and Table 3:

Samples were drawn and analysed at the beginning of the storage period and after 14, 25 and 45 weeks of storage at ambient temperature in vented steel drums. Stability tests of each of the samples were carried out according to the particular procedure of each of the test methods and observations as to the following items were recorded:

a. Comparison of results obtained by the various testing procedures, especially in respect of their correlation with results obtained by the Rapid Oven Test (Table 2);

b. Effect of the long term storage period on the results obtained by the various testing procedures (Table 2);

c. Effect of the diesel fuel characteristics on results obtained by the various testing procedures (Table 2);

d. Evaluation of stability improving additives added to the various diesel fuel types, before, during and after long term storage, - using several stability test methods (Table 3).

a. Comparison of results obtained by the various testing procedures:

It is not always possible to compare absolute results obtained by the various stability tests: For example peroxide contents or gum formation rates in samples subjected to accelerated oxidations or to U.V. irradiations are higher than those obtained by the Rapid Oven Test, but peroxide contents and gums obtained by the Rapid Oven Test are higher than those obtained by other oven tests, in which contact with air is limited. Trends, rather than absolute results, should be therefore taken into consideration. Examination of these trends indicates a satisfactory correlation between the stability testing procedures used in this context.

It was observed that for diesel fuels containing stability improving additives, some of the obtained results were rather erratic. This is especially true in cases where unsuitable additives had been used or when their concentrations were either insufficient or excessive. This

phenomena can be explained by the susceptibility of some of the additives to the severity of some of the testing procedures, affecting the obtained results correspondingly. In this case oven storage tests, rather than accelerated oxidations or U.V. irradiations, should be used preferably. The Rapid Oven Test, being less time consuming, is especially suitable in this case.

b. Effect of long term storage:
Degradation formation rates are affected by exposure of diesel fuel samples to long term storage. It is interesting to note that Type B diesel fuel (taken from an experimental field storage tank, i.e. an aged sample) exhibits much higher degradation product formation rates than a corresponding fresh product (Type C); this is true before, as well as during the laboratory storage. All the stability testing procedures used show the same trend.

c. Effect of diesel fuel characteristics:
Fresh straight run diesel fuel samples (Type A and Type C) are less affected by long term storage as compared to the aged diesel fuel sample (Type B); the most affected sample during storage is the diesel fuel containing a cracked gas oil component (Type D). This trend can be seen by all the procedures used in this respect.

d. Evaluation of stability improving additives:
From the many data obtained in several experimental sets carried out in this respect, it can be seen that the type as well as the concentration of the stability improving additives has to be determined in each case. Some additives are suitable for one type of diesel fuels, while not improving the situation in case of another type. Concentrations of stability improving additives have also to be adjusted according to the diesel fuel type. Unsuitable additives, or insufficient or excessive concentrations, might affect the degradation product formation rate adversely.

It should be remarked that for brevity sake not all the results discussed in the foregoing are reported in this paper; however, the foregoing discussion is based on numerous data obtained in several experimental sets.

CONCLUSIONS

The proposed Rapid Oven Test has been described and compared to other diesel fuel stability testing procedures and satisfactory correlation has been established. The merits of this test have been discussed as follows: Results obtained by the ROT are usually well reproducible and indicative as to the stability properties of diesel fuels; as an oven test the ROT is not excessively time consuming and yields results in an acceptable period of time; the ROT enables drawing of conclusions as to breakdown mechanism for each particular case and finally, results obtained by the ROT are less erratic in case of diesel fuels containing less suitable additives especially if those are added at insufficient or excessive concentrations.

TABLE 1: Analyses of diesel fuel types used for evaluation of stability testing procedures

Test Method	Unit	Results				
		Light Atmospheric Gas Oil (TYPE A)	Gas Oil from Field Storage (TYPE B)	Commercial Gas Oil (TYPE C)	Comm. G. Oil.-Cracked G. Oil Blend 2:1 (TYPE D)	Cracked Gas Oil
Density, 15°C ASTM D-1298	gr/cm^3	0.8442	0.8544	0.8512	0.8696	0.9058
Boiling Range ASTM D-2887	°C	218-327	208->370	220-368	198-362	197-298
Refractivity Index ASTM D-1218		1.46805	1.4730	1.47205	1.48605	-
Pour Point ASTM D-97	°C	-15	0	0	-6	<-30
Cloud Point ASTM D-2500	°C	-14	+3	+3	-4	<-30
Cold Filter Plugging Point IP-309	°C	-15	+2	0	-5	<-30
ndM Analysis						
Aromatic Rings		0.28	0.53	0.53	0.8	-
Naphtenic Rings		0.93	0.56	0.56	0.31	-
C in Aromatic Structure	%	11.4	19	19	32.9	-
C in Naphtenic Structure	%	37.2	20	20	16.7	-
C in Parafinic Structure	%	51.2	61	61	50.3	-
Aniline Point IP-2	°C	70.1	72.4	72.4	55.2	<30
Bromine Number IP-129		0.6	0.6	0.7	3.9	10
Carbon Residue (Conradson) ASTM D-189	% mass	0.04	0.01	0.03	0.05	0.55
Total Sulphur Content ASTM D-129	% mass	0.42	0.52	0.53	1.05	-
Total Nitrogen Content UOP-384	ppm	770	770	250	210	-
Basic Nitrogen UOP-269	ppm	67	120	59	69	93
Pyrroles UOP-276	ppm	1.5	1	1.5	1	-
Filterable Insolubles ASTM D-2276 (mod.)	mg/liter	0.4	1	2	2	-
Existent Gum ASTM D-381 (mod.)	mg/100 ml	<1	<1	<1	3	17
Peroxides ASTM D-3703 (mod.)	meq/liter	0.7	1.8	0.4	0.9	-
Acidity ASTM D-974	mg KOH/gr	0.03	0.008	0.03	0.03	0.01
Color ASTM D-1500		0.5	2	1	2.5	4

TABLE 2: Long term storage stabilities of diesel fuels without additives

	TYPE A				TYPE B				TYPE C				TYPE D		
	Gas oil before storage	After 14 weeks storage	After 25 weeks storage	After 45 weeks storage	Gas oil before storage	After 14 weeks storage	After 25 weeks storage	After 45 weeks storage	Gas oil before storage	After 14 weeks storage	After 25 weeks storage	After 45 weeks storage	Gas oil before storage	After 14 weeks storage	After 25 weeks storage
Carbon Residue, % mass	0.05	0.06	0.04	0.05	0.01	0.05	0.02	0.09	0.03	0.03	0.01	0.06	0.05	0.1	0.06
Filterable Insolubles, mg/100 ml	0.04	0.26	0.5	8.6*	0.1	0.4	0.2	22.3*	0.2	0.2	0.3	4.2*	0.2	1.2	2.7
Existent Gum, mg/100 ml	0	1.2	1.6	1.8	1	2.6	1.4	7.6	<1	0.4	0	3.8	3.2	6.2	2.6
Peroxides Content, meq/l	0.73	0.12	0.14	0.7	1.8	0.8	1.4	3.9	0.41	0.16	0	0.23	0.9	1.8	0.46
Acidity, mg KOH/gr	0.03	0.03	0.03	0.27	0.01	0.1	0.006	0.13	0.033	0.04	0.03	0.29	0.03	0.03	0.003
Colour Union	<0.5	<0.5	1	1.5	<2	<3	4	4	<1	<1.5	1.5	1.5	<2.5	<3.5	4
ACCELERATED OXIDATION ASTM D-2274															
Peroxide Content, meq/l	-	0.63	2.9	2.1	-	1.7	1.3	2.3	-	0.4	1.5	0.5	-	2.2	1.8
Colour Union	-	-	-	3	-	-	-	5	-	-	-	3	-	-	-
Adherent Insolubles, mg/100 ml (a)	0.1	0.8	0.6	0.6	1.5	0.3	0.8	0.3	0.1	0.2	1	0.1	0.6	0.5	4.7
Filterable Sediment, mg/100 ml (b)	0.3	1.1	0.7	0.7	0.4	0.6	0.2	0.2	0.2	0.4	0.3	0.6	0.8	2	0.7
Total Sediment (a+b), mg/100 ml	0.4	1.9	1.3	1.3	1.9	0.9	1.0	0.5	0.3	0.6	1.3	0.7	1.4	0.7	5.4
Existent Gum, mg/100 ml	-	3.2	6.7	5.8	-	2.8	3.6	4	-	8.1	8.3	2.4	-	8.2	25
UV IRRADIATION															
Peroxide Content, meq/l	0.73	0.53	0.38	2	1.8	1.3	2.7	2.35	0.4	0.8	0.9	0.94	-	2.5	2.8
Colour Union	<0.5	<0.5	1	2	<2	<3	4.5	4.5	<1	<1.5	2.5	2	<3	<3.5	5
Existent Gum, mg/100 ml	1.4	1.2	4.4	4	2.8	6.6	5.4	14.8	4.4	1.2	3.6	5.6	55	14.2	21
RAPID OVEN TEST															
Oxygen Consumption, %	-	10	4.8	8.6	9	8	5	10.5	2	-	1	5.3	4	-	4.8
Peroxides Content, meq/l	-	-	1.4	-	-	-	2.6	-	-	-	1.3	-	-	-	2.4
Colour Union	-	-	-	3	-	-	-	5	-	-	-	2.5	-	-	-
Filterable Sediment, mg/100 ml (a)	0.5	0.92	1	1.3	2.2	0.7	1.5	0.9	0.2	0.8	1.7	0.7	1.0	1.5	1.9
Adherent Insolubles, mg/100 ml (b)	0.2	1.5	0.8	2.2	0.3	0.2	0.6	1.3	0.5	1.0	0.5	0.4	0.2	0.6	0.7
Existent Gum, mg/100 ml (c)	2.7	2.1	5.2	3.9	2.8	6.2	6.3	11.3	2.9	1.9	6.5	4	5.6	10.8	11
Total Gums (a+b+c)	3.4	4.5	7	7.4	5.3	7.1	8.4	13.5	3.6	3.7	8.7	5.1	6.8	13.2	13.6
DUPONT 150°C TEST															
Colour Union (before)	<0.5	<0.5	1	1.5	<2	<3	4	4	<1	-	1.5	1.5	<2.5	<3.5	4
Colour Union (after)	<1	<1	2	2.5	<3	<3.5	4.5	5.5	<1.5	-	2	2	<3.5	<4	4.5
Rate of the Blotter	3	4	3	3	5	7	5	8	2	-	2	4	16	16	9-10
Filterable Sediment, mg/100 ml	-	-	0	-	-	-	1.7	-	-	-	0.4	-	-	-	0.4
Peroxides Content, meq/l	-	-	0.3	1.2	-	-	2.1	1.6	-	-	0.5	0	-	-	1.2

*water

TABLE 3 : Long term storage stabilities of diesel fuels with 80 ppm Additive B

	Type A			Type B			Type C			Type D		
	Gas oil before storage	After 25 weeks storage	After 45 weeks storage	Gas oil before storage	After 25 weeks storage	After 45 weeks storage	Gas oil before storage	After 25 weeks storage	After 45 weeks storage	Gas oil before storage	After 25 weeks storage	After 45 weeks storage
Carbon Residue, % mass	0.02	0.08	0.03	0.03	0.02	0.05	0.02	0.03	0.04	0.06	0.03	0.13
Filterable Insolubles, mg/100 ml	2	0.68	0.43	0.3	0.62	0.56	0.7	0.4	0.56	1.4	0.95	1.9
Existent Gum, mg/100 ml	2.8	1.0	1.6	5.7	12.8	5.8	1.8	1.8	3.8	3.5	7.0	10.6
Peroxides Content, meq/l	0	0.36	0	0	1.6	0	0	0	0	0.05	1.2	0
Acidity, mg KOH/gr	0.03	0.1	0.04	0.02	0.04	0.03	0.03	0.08	0.04	0.05	0.06	0.03
Colour Union	<1	<1.5	1	<3	3.5	3.5	<1.5	1.5	1.5	<3.5	4	4.5
AFTER ACCELERATED OXIDATION ASTM D-2274												
Peroxide Content, meq/l	0.05	0.7	-	2	1.4	-	0.05	0	-	1.4	2.4	-
Colour Union	-	1.5	-	-	4.0	-	-	2.0	-	-	5.0	-
Adherent Insolubles, mg/100 ml a	0.4	0.3	0.46	0.2	0.2	0.30	0.13	0.12	0.2	0.7	0.5	0.62
Filterable Sediment, mg/100 ml b	0.2	0.14	0.16	0.7	0.07	0.28	0.24	0.31	0.2	0.6	1.04	0.90
Total Sediment (a+b), mg/100 ml	0.6	0.44	0.62	0.9	0.27	0.58	0.37	0.43	0.4	1.3	1.6	1.52
Existent Gum, mg/100 ml	4	2.1	-	3	6	-	3.6	5.6		12.3	12.8	-
UV IRRADIATION												
Peroxide Content, meq/l	0.05	1.6	0	1.8	1.6	0	0.005	0.47	0	1.2	2.1	0
Colour Union	<1	1.5	1	<3	3.5	3.5	<1.5	2.0	1.5	<4	4.5	4.5
Existent Gum, mg/100 ml	0.4	0.6	1.6	2.6	14.4	18.4	0.2	4.2	4.2	5.8	8.8	13.8
R.O.T.												
Oxygen Consumption, %	-	1.4	2.1	-	2.6	3.3	-	2	3.8	4.8	6.7	11.9
Peroxides Content, meq/l	0.03	-	0	1.4	-	0	0.2	-	0	1.3	-	traces
Colour Union	-	2	-	-	4.5	-	-	2.5	-	-	5.5	-
Filterable Sediment, mg/100 ml a	0.2	0.2	0.4	0	0.04	0.4	0.2	0.2	8	1.5	3.7	5.2
Adherent Insolubles, mg/100 ml b	0.2	1.8	0.4	0	0.07	0.2	0	0.3	0	0.4	3.6	0
Existent Gum, mg/100 ml c	1.4	4.2	3.4	4	5	7.2	0.6	4	-	7.9	21.8	-
Total Gums (a+b+c)	1.8	6.2	4.2	4	5.1	7.8	0.8	4.5	-	9.8	29.1	-

THE USE OF SIMPLE RAPID COLORIMETRIC TECHNIQUES FOR MEASUREMENT OF LIGHT CYCLE OIL CONTENT AND RELATIVE STORAGE STABILITY OF DISTILLATE FUELS

Richard K. Solly

Materials Research Laboratory, Defence Science and Technology Organisation
PO Box 50, Ascot Vale, Victoria, Australia 3032

ABSTRACT A simple colorimetric technique has been developed which accurately measures the relative amount of unhydrogenated light cycle oil in distillate fuels. Distinctive colours are formed within 10 minutes from the addition of 1 - 2 ml of fuel to a small column of active white powder in clear glass or plastic tubes. Visually, the intensity and colouration of the powder may be immediately correlated with the type and amount of light cycle oil in the fuel. Analytical values with higher degrees of precision for light cycle oil contents in the 0 to 30% range are obtained by washing the coloured material from the tubes with solvent and measuring the absorbance with a colorimeter or spectrophotometer. Results are presented for the correlation between colorimetric values, unhydrogenated light cycle oil content and diesel fuel storage stability.

INTRODUCTION

Many studies have implicated polar compounds of oxygen,[1,2] nitrogen[3] and sulphur[4] in hydrocarbon fuel mixtures for the degradation of hydrocarbon fuels upon storage. However, although many mechanisms have been postulated, none of these processes will fully explain the nature of the sediment formed by degradation of automotive diesel fuel.[5]

Better understanding of the chemistry of diesel fuel degradation will not only allow development of rapid and accurate tests for the measurement of fuel instability, but also modification of refinery processes to minimize the formation of detrimental species. The presence of unhydrogenated middle distillate light cycle oil from cracking of heavier petroleum components plays a significant role in the degradation of automotive diesel fuel.[6]

Rates of possible processes occurring in automotive diesel fuel containing light cycle oil have been investigated towards understanding the chemistry of fuel degradation.[7] Variations in absorbance in both the ultraviolet and visible regions were used to measure rates of reaction.[8] The colour of species which absorb in the visible region of the spectrum can be detected by eye. In this paper, the use of visual and instrumental absorption procedures are presented to illustrate the ease with which light cycle oil can be detected by direct means in as little as 0.5 ml of automotive diesel fuel.

EXPERIMENTAL

Reference fuels used in this study were samples from automotive distillate refinery streams of straight run distillate (SRD), light cycle oil (LCO) and hydrotreated light cycle oil (HTLCO) obtained directly from Australian refineries within one week of production. Samples were either blended immediately for ageing studies or stored as unblended components at -12°C. Experimental blends were prepared by mixing on a volumetric basis freshly thawed

LCO or HTLCO with SRD. Ten commercial automotive diesel fuels purchased directly from retail outlets were also included in this study.

The LCO Colorimetric Tubes were prototype units developed at the Materials Research Laboratory of the Defence Science and Technology Organization. Results obtained in this study were obtained with 4 cm of active white powdered solid material packed in 5 mm diameter glass tubes. It is anticipated that standardized Colorimetric Tubes will be produced commercially in unbreakable clear plastic packs under licence to the Commonwealth of Australia.

Plastic syringes were used to add 2 ml of fuel to the Colorimetric Tubes and apply gentle pressure so that the fuel passed through the column of powdered material in the tubes within 30 seconds. Colour development commenced immediately on the white powder and in most cases full visual development was achieved at ambient temperatures within 10 minutes. Spectral measurements reported in this paper were obtained after washing the column with 1 ml of hexane to remove residual fuel followed by 6 ml of methanol. In each case, gentle pressure was applied from the syringe used to add the liquid so that it passed through the powdered solid within 30 seconds. Spectra were recorded immediately in the methanol wash liquid using 1 cm pathlength cells.

Comparative ageing studies were done at 43°C for 13 weeks by the method of ASTM D4625 or by an oxygen overpressure technique at 90°C.[9] The single bomb apparatus of ASTM D942 was used for the oxygen overpressure measurements as described elsewhere.[10]

RESULTS AND DISCUSSIONS

Results reported in this presentation represent colorimetric development which was the composite of a large number of chemical processes from which possible reactions may be postulated.[8] The active solid powder was a mixture of a number of possible ingredients which may be formulated with a large range of activities and selectivities. The white powder acts both as an active catalyst and solid support for colour development.

Visual colour development was rapid (within 5 minutes) and occured in contact with very small amounts of unhydrogenated LCO. One batch of active powder had to be discarded after being coloured by accidental contact with a stirring rod which was unwashed after being used to stir a blend of LCO. The normal human eye is very sensitive to differentiating comparative shades of colour which are difficult to reproduce in coloured photography and not feasible in a black and white conference proceedings. Maximum selectivity to visual observations for a range of LCO concentrations was obtained by using an active powder with low catalytic activity. Coloured slides of Colorimetric Tubes forming part of the in-session presentation are from tubes with low catalytic activity.

Medium to high catalytic activity promotes more rapid colour development (no further noticeable visual changes after one minute) and a final colour which was black or a very dark blue/green. The visual colour variation was greatly reduced for a range of LCO from 0 to 30%. However, if coloured material was washed from the active powder as described in the experimental section, a variation in the absorbance was readily seen as determined by a simple colorimeter or a spectrophotometer.

The rapidity of the colour development is shown in Figure 1, in which the Colorimetric Tubes of medium catalytic activity were washed after 2 to 1500 minutes following the addition of 2 ml of fuel containing 15% LCO oil from refinery F (refinery designations as in other presentations at this conference[10]). Both the absorbance and the peak maximum were a function of time. However, from 300 to 1400 minutes the absorbance at 650 nm was relatively constant. This follows from the broad band absorbance in the region 600 - 700 nm which is

shown in Figure 2 for the fuel after 300 minutes contact time with the active powder in the Colorimetric Tube.

Following from Figures 1 and 2, it was concluded that the most consistent results would be obtained by allowing fuel material to stand on the Colorimetric Tubes for 16 hours (overnight) at ambient temperatures. After the coloured material was washed from the tubes, the absorbance was recorded at the maximum in the region 600 - 700 nm.

Results obtained with 5 blends of LCO from three refineries are shown in Figure 3. The variation of the absorbance with concentration was approximately linear from 0 to 30% LCO content. Refineries A and G were processing Australian Bass Strait crude at the time the samples were obtained, whereas refinery F was processing Middle Eastern crude. It may be noted that the absorbance for a constant LCO content from refinery F was approximately twice that from refineries A and G. It was of interest to compare the amount of sediment produced both by ASTM D4625 and oxygen overpressure ageing as shown in Table 1.

FUEL SAMPLE	ASTM D4625 mg/L	OXYGEN OVERPRESSURE mg/L
A	18	8
F	15	33
G	12	11

Table 1. Sediment produced by ageing 30% LCO in the SRD for 13 weeks at 43°C under ASTM D4625 conditions or 16 hours at 90°C under 794 kPa oxygen overpressure conditions.

Fuel from refinery F which produces the greatest absorbance from the Colorimetric Tubes, produces the most sediment from the oxygen overpressure ageing, but not from the 43°C ageing. The absorbance produced by the fuel mixtures from refineries A and G was very similar, whereas there was a small variation in the amount of sediments produced by the two ageing procedures.

Whereas approximately linear correlation was obtained between the amount of absorbance from Colorimetric Tubes and light cycle oil content (Figure 3), the amount of insoluble sediment produced by increasing LCO content was not linear as shown in Table 2.

It was most probable that chemical reactions producing soluble precursors to insoluble particulate matter increase with increasing LCO content. LCO has a much higher aromatic content (50-80%) than SRD (10 -20%) and is a much better solvent than SRD for the insoluble particulate matter. Thus less insoluble matter precipitates from solution. However, the particulate precursors remain in solution where they have an increased tendency to form injector and possibly cylinder deposits. Thus for measurement of LCO content and possible injector deposit potential, the Colorimetric Tubes offer higher precision than gravimetric measurements of deposit formation on ageing.

LCO %	TOTAL SEDIMENT mg/L
5	11
10	20
15	28
20	29
30	33

Table 2. Sediment produced by ageing LCO/SRD blends from refinery F under oxygen overpressure conditions of 794 kPa oxygen at 90°C for 16 hours.

A number of Australian retail automotive diesel fuels have been tested with the Colorimetric Tubes. The absorbance produced after passing 10 retail fuels through Colorimetric Tubes of low activity is shown in Figure 4. Reference fuels are 0 and 1% LCO from refinery G and 5% LCO from refineries A and G. Low activity tubes were used so that visual selection of LCO content could be compared with that obtained by absorbance measurements. As may be seen from the coloured slide projection prepared for oral presentation of this paper, visually fuel 2 is readily selected as producing the darkest blue/green colouration, comparable to that produced by the 5% LCO standards. Fuels 3, 7 and 6 follow in colour intensity of the tubes. Fuel 9 was readily selected as having the least blue/green colour development of the Colorimetric Tubes.

Fuels 2 and 9 were subject to oxygen overpressure ageing at 794 kPa pressure for 64 hours at 95°C. Although this accelerated ageing might be compared to 3-5 years ambient ageing,[9] only 12 and 1 mg/L of insoluble sediment was produced, consistent with the low and very low levels of unhydrogenated LCO respectively in the fuels.

Undiluted hydrotreated LCO was also passed through the Colorimetric Tubes. That from refineries C and D (reference 10) produced very little colour development, whereas that from refineries E and F produced medium and intense colour development respectively. These results are comparable with sediment levels from 13 weeks 43°C ageing of 30% hydrotreated LCO/SRD blends of less than 1 mg/L from refineries C and D and 8 and 19 mg/L from refineries E and F. It was concluded that either the hydrotreatment process producing the sample at refinery F was ineffective or the sample was unrepresentative.

CONCLUSIONS

Colorimetric tubes have been shown to be a rapid and simple means of determining the amount of unhydrotreated LCO middle distillate fuels either by direct visual means or more quantitatively by colorimetric or spectrophotometic measurements. They are non-toxic and relatively inexpensive to produce and may be used by non-technical personnel in a field environment to obtain direct measurements of relative unhydrogenated light cycle oil content of hydrocarbon fuels. With 2 ml of fuel or less, measurements may be obtained within 10 minutes.

The colour formation on the tubes has been shown to be proportional to both the type of unhydrogenated LCO and the amount in a fuel. The amount and type of LCO may then be

correlated with the formation of sediments by ambient or accelerated ageing techniques. The rapidity and simplicity of the technique makes it ideal for use as a quality control technique at all points of the distribution system, from the refinery outlet, bulk distribution terminal through to the consumer holding tanks. They may be used with any fuel for which control of unhydrogenated LCO is considered desirable. This is primarily the higher quality diesel fuel market at the moment, but the sensitivity of the technique lends itself to determining the effectiveness of hydrogenation for hydrogenated LCO added to aviation distillate.

The Colorimetric Tubes accelerate the rate of reactions of species associated with LCO in small amounts of fuel and concentrate the products in a form which is readily measured. Their use with a wide range of fuels has much potential to enable comparison of the species present in the fuels and a wider understanding of the chemistry associated with fuel instability.

REFERENCES

1. Hazlett, R.N. Power, A.J. Phenolic Compounds in Bass Strait Distillate Fuels. Their Effect on Deposit formation. *Fuel*, **68**, 1112, 1969
2. Pedley, J.F. and Hiley, R.W. Investigation of Sediment Precursors Present in Cracked Gas Oil, *Proc. Int. Conf. on Stability and Handling of Liquid Fuels.* IP, London, U.K. p495, 1988
3. Dorbon, M., Bernasconi, C. Nitrogen Compounds in Light Cycle Oils: Identification and Consequences of Ageing. Fuel, **68**, 1067 (1989).
4. Hazlett, R.N., Power, A.J., Kelso, A.G. and Solly, R.K. The Chemistry of Deposit Formation in Distillate Fuels. *Materials Research Laboratory Technical Report* No 986, Defence Science and Technology Organization, Melbourne, Australia, 1986.
5. Hardy, D.R., Wechter, M.A. Insoluble Sediment Formation in Middle Distillate Diesel Fuel: The Role of Soluble Macromolecular Oxidatively Reactive Species. *Energy and Fuels*, 1990.
6. Arfelli, W., Power, A.J., Solly, R.K. The Storage Stability of Automotive Diesel Fuel. *Proc. 4th Int. Conf. Automotive Engineering.* SAE Australasia, Melbourne, 1987, Paper No. 871269.
7. Beranek, L.A., McVea, G.G., O'Connell, M.G., Solly, R.K. Rate of Indole Phenalenone Reactions in Middle Distillate Fuel. This conference.
8. DeNola, G., Solly, R.K. To be published.
9. Hardy, D.R., Hazlett, R.N., Beal E.J., Burnett, J.C. Assessing Distillate Fuel Storage Stability by Oxygen Overpressure. *Energy and Fuels*, 1989, **3**, 20.
10. McVea, G.G., Pedley, J.F. and R.K. Solly. Assessment of the Oxygen Overpressure Test for Prediction of Middle Distillate Fuel Storage Stability. This conference.

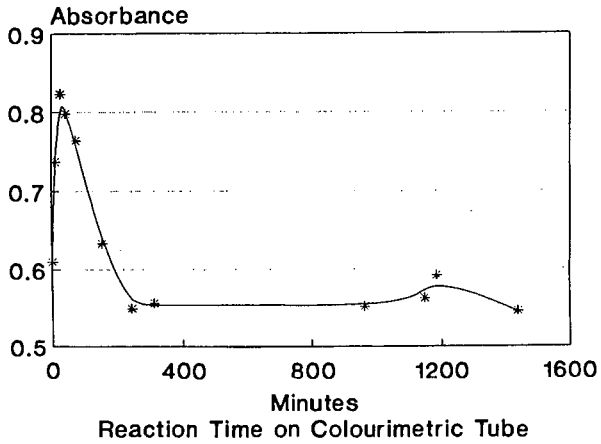

Figure 1. Variation of absorbance at 650 nm of Colorimetric Tube methanol washings for 15% LCO/SRD mixtures of Fuel F.

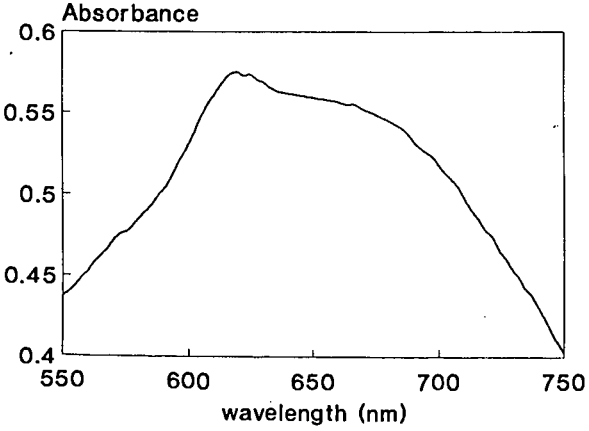

Figure 2. Spectra of Colorimetric Tube methanol washing after 300 minutes reaction time on tube for Fuel F.

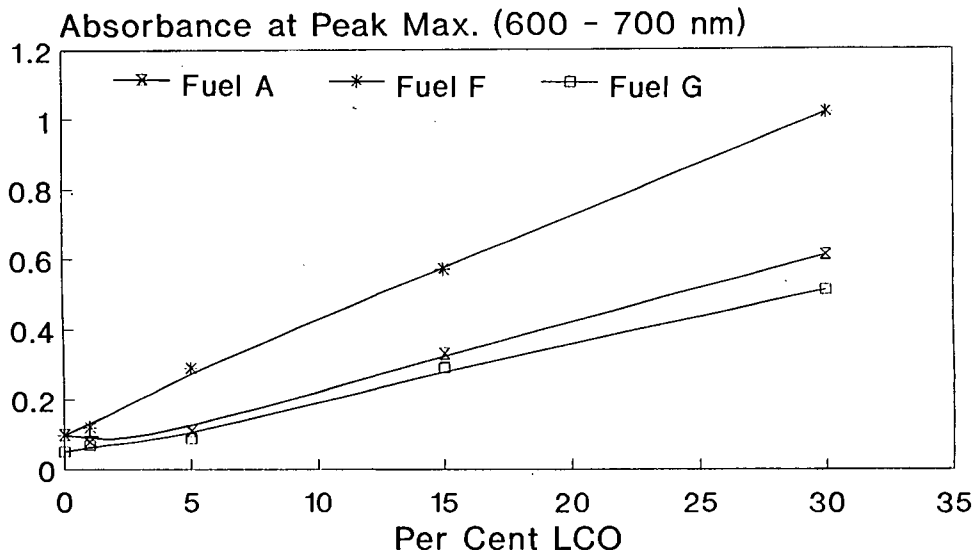

Figure 3. Absorbance of medium activity Colorimetric Tube methanol washings after 16 hours reaction time on the tube at ambient temperatures for Fuels A, F and G.

1221

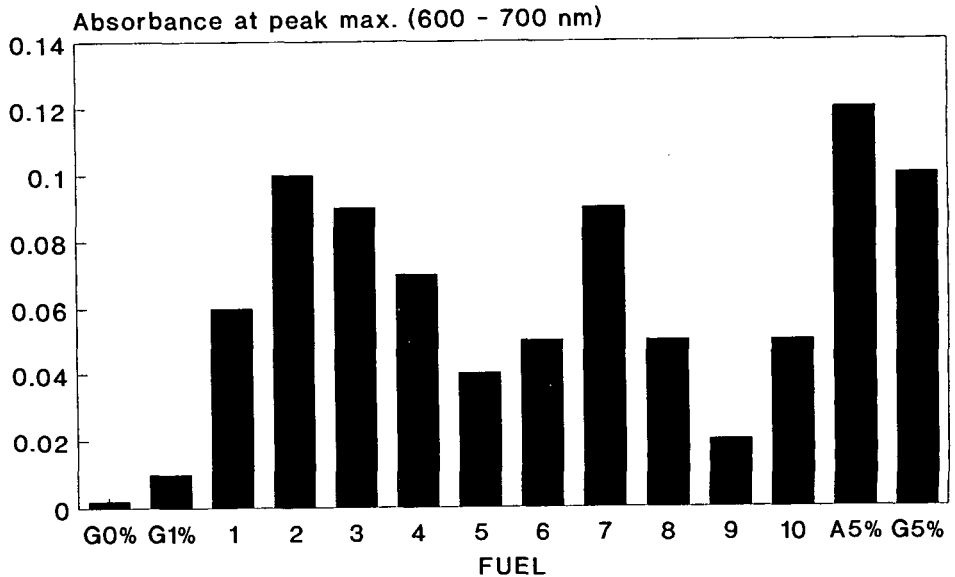

Figure 4. Absorbance of low activity Colorimetric Tube methanol washings after 16 hours reaction time on the tube for 10 commerical automotive diesel fuels compared to 0, 1 and 5% LCO/SRD standards for Fuels A and G.

SYMPOSIUM ON THE STABILITY AND OXIDATION CHEMISTRY OF MIDDLE DISTILLATE FUELS, DIVISION OF FUEL AND PETROLEUM CHEMISTRY, AMERICAN CHEMICAL SOCIETY, WASHINGTON D.C. MEETING, AUGUST 1990

THE ROLE OF A METAL DEACTIVATOR ADDITIVE IN IMPROVING THE THERMAL STABILITY OF AVIATION KEROSINES: ADDITIVE ADSORPTION STUDIES

By

R.H. Clark, K.M. Delargy and R.J. Heins
Shell Research Ltd., Thornton Research Centre, P.O. Box 1, Chester CH1 3SH

INTRODUCTION

SCOPE OF PREVIOUS WORK

In an earlier paper[1], we reported studies that elucidated the mechanisms whereby MDA can affect the stability of jet fuel. The work not only investigated MDA in its claimed role as a metal chelating agent, but, more significantly, assessed the role of this additive within engine fuel system environments and within the thermal stability specification test (JFTOT). Thus the experimental work was on three parallel fronts:

- Realistic-large scale simulations of engine components
- Specification testing - the JFTOT
- Fundamental mechanistic studies

Glassware fuel oxidation studies clearly demonstrated the ability of MDA to act as a metal chelator, resulting in a near-unity chelation ratio. However, in the dynamic stability tests (i.e. fuel system simulators and the JFTOT), where fuel flows over a heated metal surface, the action of MDA was less clearcut. In particular, in spite of eliminating the metal chelation mechanism by using a metal-free fuel, benefits to fuel stability were still evident in our oil-cooler simulation[2] (Single-Tube Heat-Transfer Rig, STHTR) and the JFTOT. This improvement in fuel stability was attributed to MDA acting as a metal passivator and retarding the formation of lacquers on metal surfaces.

The passivation role of MDA was most evident on clean metal surfaces; once sufficient fuel lacquer had coated the metal surface, passivation ceased to be a factor controlling lacquer deposition. This differing response of a clean versus lacquered surface was of great concern for the specification test (JFTOT); given its short duration and low lacquer loadings, the JFTOT responds particularly strongly to the passivating action when compared with a more realistic rig (e.g the STHTR) employing a longer test duration (25 - 100 hours). Thus, any improvement in fuel performance in the JFTOT obtained from the use of MDA may not necessarily be manifest in service. Figure 1, taken from reference 1, illustrates the different benefits of MDA on a low-metal-content fuel in a variety of systems.

CURRENT OBJECTIVE

Our use of a wide range of experimental systems has provided strong empirical evidence for the passivation mechanism of MDA, and, in particular, the overresponse of the JFTOT to MDA. Nevertheless, it was thought desirable to confirm such a mechanism by independent means. It was reasoned that a surface analysis technique would offer the opportunity of directly observing the adsorption of MDA molecules onto a metal surface. The chosen technique should be (i) sensitive enough to resolve a monolayer of MDA, and (ii) sufficiently discriminating to observe MDA in the presence of fuel or fuel lacquers. SIMS (Secondary Ion Mass Spectrometry) appeared a viable option, thus the overall aims became:

- To apply SIMS to observe directly the adsorption of MDA molecules onto aluminium surfaces, in particular JFTOT test specimens.
- To continue SIMS work to elucidate how MDA influences the lacquer patterns on a JFTOT test specimen

EXPERIMENTAL

SIMS

Secondary Ion Mass Spectrometry (SIMS) is a highly surface sensitive analytical technique (sampling depth ≈ 0.5 - 1 nm) which involves the bombardment of a sample surface with a primary beam of energetic particles (normally ions or atoms). This results in the emission of a range of secondary particles, including positively and negatively charged ions. These secondary ions, both atomic and molecular species, are subsequently mass analysed to generate surface mass spectra similar to those obtained in conventional organic mass spectrometry. The technique, therefore, provides elemental analysis in addition to detailed and highly specific chemical structure information.

This study was carried out using a VG IX23S instrument equipped with a Poschenrieder time-of-flight analyser and a pulsed liquid metal ion source (Ga^+, 30 KeV)[3]. For each sample, secondary ion spectra were recorded from an area of 0.5 mm x 0.5 mm. All spectra were generated under static SIMS conditions, where sufficiently low primary ion doses are used such that the samples are effectively undamaged throughout the course of the analysis. Both positive and negative ion spectra were recorded in the mass range 0 - 1500.

JFTOT

In essence, the JFTOT rig[4] provides a system for passing a small sample of fuel (600 cm^3) over a heated metal test section. The JFTOT assesses the stability of a fuel by its propensity to lacquer the test section and from the associated blockage of a downstream filter by decomposition products. For specification purposes, the hottest temperature on the test section (aluminium tube) is controlled to 260°C for 2.5 hours.

To pass the test, the tube lacquer must not be darker than the specified limit, and the filter pressure drop should not exceed 25 mm Hg. This results in a go/no go specification test. For research purposes, various refinements may be made to the procedure to allow fuel ranking.

TEST FUEL AND ADDITVE

The test fuel was chosen so as to represent current refinery production. However, to minimise potential interference from other polar species within the SIMS analysis, the fuel was taken from commercial hydrotreated stock with a low intrinsic sulphur content. The fuel was pre-filtered to 0.45 μm before use. Two sources of the MDA concentrate were used:

(i) 75% w/w MDA in xylene, proprietary name DuPont DMD No. 1.
(ii) 50% w/w MDA in xylene, proprietary name DuPont DMD No. 2.

SAMPLE PREPARATION

Table 1 summarises the various sample preparation procedures. Samples comprised three basic types:

(i) Sections of aluminium foil (approx 0.5 x 0.5 cm) for static/soaking experiments. These were pre-treated by ultrasonic cleaning with a trisolvent solution (an equivolume blend of toluene, isopropyl alcohol and acetone).

(ii) Sections from JFTOT tubes (1.8 cm long) used in static/soaking experiments. The position of the sample along the tube was not critical.

(iii) Sections from JFTOT tubes (1.8 cm long) used in a dynamic experiment, i.e. the uncut tubes had been run in the conventional JFTOT rig. These samples were taken to bracket the position on the test section corresponding to the hot spot (38.7 mm from the fuel inlet).

Except where indicated, all JFTOT tubes were used straight from the pack without any pre-treatment in compliance with the specification test conditions. Similarly, after exposure to the fuel or MDA solutions, the samples were rinsed with Analar grade heptane and allowed to dry (in accordance with the ASTM D3241 method[4]). The 1.8 cm samples were sectioned from the JFTOT tubes using a Beuhler saw. A stream of compressed air was used to remove any metallic debris from the sample surface.

RESULTS AND DISCUSSION

SIMS SPECTRUM - FRAGMENTATION PATTERN

Positive and negative ion spectra were taken in the mass range 0 - 1500; examples of spectra are given in Figures 2 and 3. The molecular weight (M) of MDA is 282, and ions corresponding to $(M+H)^+$, at 283 daltons, and $(M-H)^-$, at 281 daltons, were detected. A number of other ionic species were also observed but only in the presence of MDA; these are listed in

Table 2 together with the most probable assignments for molecular fragments arising from MDA. In addition to these characteristic ion fragments, a number of low-mass species were also detected in the positive and negative ion spectra, e.g. $C_xH_y^+$, Ph^+, $PhCH_2^+$, C_n^-, C_nH^-, CN^- and PhO^-. Of all the fragments, the species at 118^- is considered to be, analytically, the most useful. The signal is of good intensity and is a highly characteristic indicator of MDA. Quasimolecular ions at 283^+ and 281^- are of limited use only: the intensity of the 283^+ signal is likely to be strongly dependent on the surface structure of MDA. Whilst the 281^- species is analytically more useful for assessing intact MDA molecules on a surface, it overlaps with a signal from an oleate-containing species. Consequently, any conclusions based on the 281^- signal alone are subject to some uncertainty. Thus for the purpose of comparison between samples the 118^- peak was used. As this peak lies adjacent to a characteristic reference peak for the substrate, $Al_2O_4H^-$ at 119^-, peak area ratios could be used with confidence to monitor the concentration of adsorbate. The relative surface concentration (C) of MDA was monitored using computed peak areas (A_{118} and A_{119}) in the following manner:

$$\%C = \frac{A_{118}}{A_{118} + A_{119}} \times 100 \qquad \ldots(1)$$

The surface concentrations for each sample are shown diagrammatically in Figures 4 - 7. Interpretation of all results with equation 1 requires care, in that SIMS is considered only semi-quantitative. It is more important to consider trends within a series of specimens rather than absolute values.

PRELIMINARY FINDINGS

Initial experiments made use of simple samples in the form of aluminium foil sections. With these, there was a close similarity between the SIMS spectrum of the foil wetted by an MDA solution (derived from a DMD No 2 concentrate) and that of foil exposed to the same solution and then rinsed in heptane. Those features common to these two spectra were not evident in the third spectrum, which corresponded to a foil sample that had not been in contact with MDA. In addition, differences between the samples could be seen in the surface concentrations of MDA as determined from equation 1.

However, there were various features of the SIMS MDA spectrum which corresponded to mass numbers higher than the molecular weight of the additive, suggesting that this sample of MDA had degraded or polymerised. This potential problem of storage stability accordingly led us to seek a fresh sample of MDA for the main body of experimentation.

JFTOT TUBE SAMPLES - STATIC PREPARATION

These preliminary findings having shown that SIMS had sufficient sensitivity to detect MDA adsorbed onto aluminium surfaces, subsequent samples were prepared to reflect more closely the reality of the

specification test:

- solutions of MDA were made up with commercial jet fuel
- aluminium samples were taken from JFTOT test sections

Whilst it was clearly desirable for all JFTOT tubes to be used without any surface pre-treatment (i.e. as ASTM D3241), there were concerns that residual cutting oils on the aluminium could interfere with the SIMS detection or alternatively reduce the number of surface sites available for additive adsorption. As a precaution, two similar sets of samples were prepared: one untreated and the other pre-cleaned. However, it was recognised that these various preparations suffered from the shortcoming of being static immersion tests at ambient temperature. SIMS spectra were recorded for the following untreated JFTOT tubes:

(i) Fuel wetted and heptane rinsed
(ii) Fuel + 5.7 mg/l MDA wetted and heptane rinsed
(iii) Fuel + 64.8 g/l MDA wetted and heptane rinsed
(iv) Neat MDA cast onto a JFTOT tube as a reference spectrum
(v) Sample (ii) was then repeated using a pre-cleaned JFTOT tube.

The results in terms of MDA surface concentrations are illustrated in Figure 4. SIMS could detect MDA in all samples that had been exposed to the additive. Moreover, the concentration of additive within the original bulk solution had a strong effect on the resultant surface concentration; the 5.7 mg/l MDA solution gave a spectrum in which the additive was only just discernible, whereas the 64.8 g/l solution resulted in an MDA signal comparable to that of the neat additive. This effect of concentration suggests an equilibrium between the MDA in the fuel solution and the molecules adsorbed onto the metal, presumably following a simple adsorption-type mechanism (e.g. Langmuir isotherm). From this, it can be concluded that, at the specification MDA concentration, not all the surface sites will be occupied by the MDA molecule. Comparison of the pre-cleaned tubes and the as-received examples indicated better adsorption of the additive onto a cleaned tube, presumably because more surface sites have become available. However, the cleaned system is less relevant to the specification conditions.

JFTOT TUBE SAMPLES - DYNAMIC PREPARATION

Data from the first two sets of experiments gave the necessary confidence to dispense with the idealised model systems and to use samples actually generated within the JFTOT rig and covering a range of temperature and additive concentration. In particular, it was seen as crucial that at least one condition should reflect the current specification test conditions (260°C maximum tube temperature, 2.5 hours duration, MDA concentration 5.7 mg/l maximum).

(a) Concentration dependence

Figure 5 illustrates the amount of MDA present on the surface as a function of the original additive concentration for tests at ambient temperature. The results agree with those seen in the static experiments where the MDA adsorbed onto the surface increased with bulk additive

concentration. However, more detail can be derived by applying a simple Langmuir-type adsorption model. The surface concentration approaches a limiting value for the two highest bulk additive concentrations (570 mg/l and 57 g/l), indicating that the surface sites are approaching saturation. This further confirms that at the specification concentration (5.7 mg/l) only a small fraction of available sites are occupied by adsorbed MDA molecules.

(b) Effect of temperature

An increase in the surface concentration of MDA is observed with increasing temperature (Figures 6 and 7). A small increment accompanies the change from 25°C to 140°C, but a dramatic one results on further increasing the test temperature to 260°C. This temperature dependence of MDA adsorption is unexpected; one might predict an exothermic heat of adsorption, and thus a decreasing amount of MDA adsorbed with increasing temperature. This anomalous increase in surface MDA concentration coupled with the strong non-Arrhenius temperature response suggests that a simple adsorption mechanism is not occurring. A plausible explanation could be that, in addition to reaching the surface by an adsorption mechanism, the MDA molecules can also add to the surface by polymerising to form an MDA matrix on the surface. Alternatively, fuel lacquer could entrain MDA molecules on the surface.

A MODEL FOR MDA PASSIVATION

In our previous paper[1], we discussed how MDA could modify and passivate a metal surface. This latest work allows us to hypothesise as to the nature of the mechanism by which MDA passivates. It is doubtful that the passivation results solely from MDA molecules adsorbed onto the metal surface. A two-stage mechanism is proposed: firstly, the MDA molecules adsorb onto some of the available surface sites and then subsequently, under the influence of heat, the adsorbed MDA molecules crosslink with each other and those in solution to form an MDA matrix; alternatively, the MDA molecules could be entrapped within a fuel lacquer film. It is proposed that such a polymerised MDA layer presents a less favourable substrate for lacquer formation than a bare Al/Al_2O_3 surface. Since our previous work has shown that this passivation is short-lived, it is assumed that either the fuel lacquer grows thick enough on the surface to hide the passivating layer, or, alternatively, the passivating layer is metastable and is eventually displaced by fuel lacquer. Unfortunately, in its current form the SIMS approach is unable to confirm such a mechanism. If the MDA is undergoing reaction, one would expect a decrease in the parent ion signals at higher temperatures. In the event these signals are rather weak and obscured by other species. However, it has been noted that at higher temperatures there is an increase in the CN^- signal relative to the 118^- signal, which suggests breakdown of the MDA molecule.

CONCLUSIONS

SIMS offers the sensitivity and discrimination required to detect the MDA molecule on an aluminium surface. The surface concentration of adsorbed MDA is a function of the original bulk MDA concentration and

appears to reach a saturation for bulk concentrations of ~ 57 g/l, indicating a simple Langmuir-type adsorption model. A fuel doped with MDA at the specification limit (5.7 mg/l) when run in the JFTOT will result in MDA being adsorbed onto the aluminium test specimen. However, relatively few surface sites will be occupied at this lower concentration.

The strong influence of temperature and the non-Arrhenius behaviour of the MDA surface concentration indicate that more than an adsorption mechanism is in operation at elevated temperatures. This evidence indicates that MDA passivation of the JFTOT test section does not result solely from surface adsorption; the MDA molecule may well be present as a polymer or in a fuel decomposition matrix.

ACKNOWLEDGEMENTS

The authors are indebted to Dr. Alan J. Paul of the Centre for Surface and Materials Analysis, UMIST, Manchester for his experimental expertise, interpretation and helpful discussions. The support of the British Ministry of Defence is gratefully acknowledged.

REFERENCES

1. R.H. Clark, The Role of a Metal Deactivator Additive in improving the Thermal Stability of Aviation Kerosines, presented at the 3rd International Conference on the Stability and Handling of Liquid Fuels, London, September 1988, Paper #47, p. 283, Institute of Petroleum (1989).

2. J.S. Mills and D.R. Kendall, The Quantification and Improvement of the Thermal Stability of Aviation Fuels, presented at the 30th International Gas Turbine Conference, Houston, Tex., March 1985, ASME Paper 85-GT-33.

3. A.J. Eccles and J.C. Vickerman, The Characterisation of an Imaging Time-of-flight Secondary Ion Mass Spectrometry Instrument, J. Vac. Sci. Technol. A7(2), 234 , (Mar/Apr 1989).

4. Manual of ASTM Standards, ASTM D3241, Vol 05.02 (1989).

Table 1

A summary of the sample preparation stages

Sample Group	Pre-treatment of specimen	MDA conc. (mg/l)	Heptane rinse after MDA exposure	Use of JFTOT	JFTOT test Temperature (°C)
(i) Aluminium foil (MDA No. 2)	Ultrasonic clean with trisol	0	✓	x	
		160,000	✓	x	
		160,000	x	x	
(ii) JFTOT test sections (MDA No. 1)	Ultrasonic clean with HPLC grade methanol. In addition duplicate set of uncleaned specimens.	0	✓	x	
		5.7	✓	x	
		64,800	✓	x	
		concentrate	x	x	
(iii) JFTOT test sections (MDA No. 1)	None	5.7	✓	✓	25
		57	✓	✓	25
		570	✓	✓	25
		57,000	✓	✓	25
		5.7	✓	✓	140
		5.7	✓	✓	260
		57	✓	✓	260

Table 2

Fragmentation of MDA in TOF SIMS:

ION MASS	FRAGMENT ION
107^+	$C_6H_4(OH)CH_2^+$
120^+	$C_6H_4(OH)CNH^+$
134^+	$C_6H_4(OH)CHNCH_2^+$
148^+	$C_6H_4(OH)CHNCH(CH_3)^+$
162^+	$C_6H_4(OH)CHNCH(CH_3)^+CH_2^+$
283^+	$(M + H)^+$
118^-	$C_6H_4(CN)O^-$
120^-	$C_6H_4(OH)CNH^-$ OR $C_6H_4(CHNH)O^-$
281^-	$(M - H)^-$

NOTES: (1) M = molecular species (mol. wt. = 282)
= $C_6H_4(OH)CHNCH(CH_3)CH_2NCHC_6H_4(OH)$

(2) ALSO DETECTED WERE: $C_XH_Y^+$, Ph^+, $PhCH_2^+$, C_n^-, C_nH^-, CN^-, PhO^- ETC.

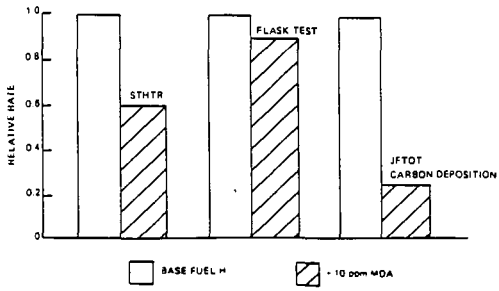

FIG. 1 – The influence of MDA on the behaviour of a sweetened fuel H. STHTR operated at 225°C condition, Flask at 160°C, JFTOT at 350°C to determine carbon deposit weight (Reference 1).

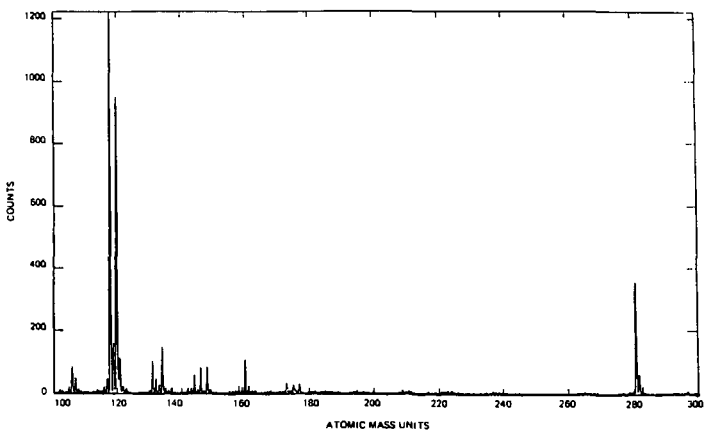

FIG. 2 – Negative ion TOF SIMS spectrum of MDA concentrate cast onto aluminium JFTOT tube.

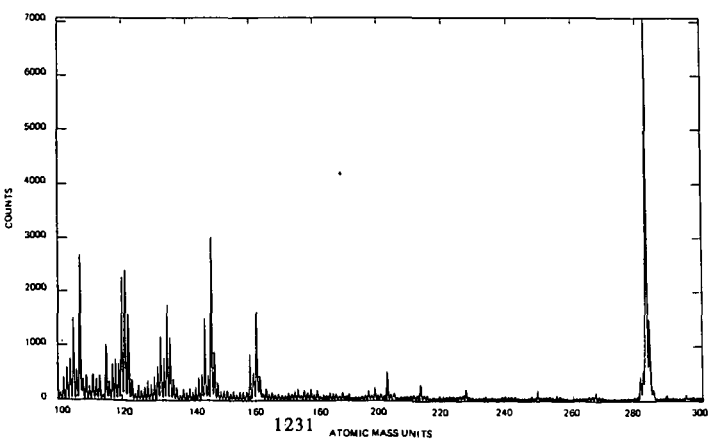

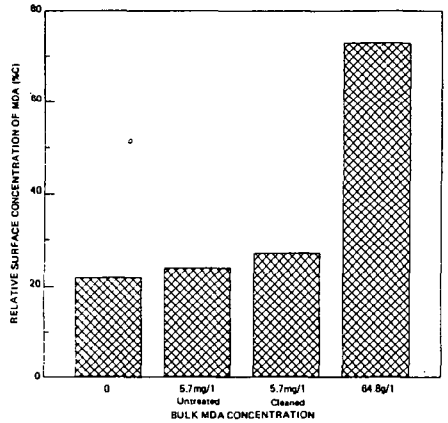

FIG. 4 – The influence of MDA bulk concentration on the resulting MDA surface concentration of JFTOT test specimens. Samples generated within a static experiment.

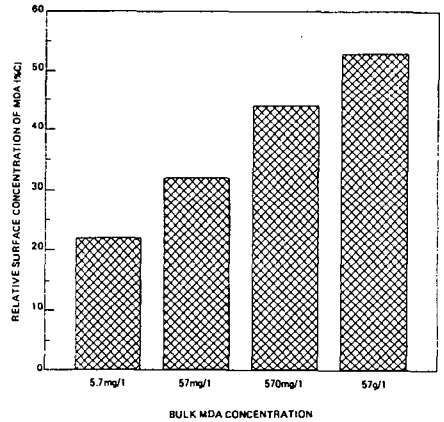

FIG. 5 – The influence of MDA bulk concentration on the resulting MDA surface concentration of JFTOT test specimens. Samples generated within a JFTOT rig at ambient temperature.

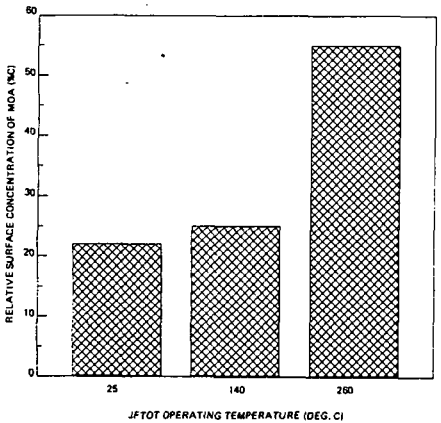

FIG. 6 – The influence of JFTOT operating temperature on the resulting MDA surface concentration of JFTOT test specimens (MDA bulk concentration 5.7mg/1).

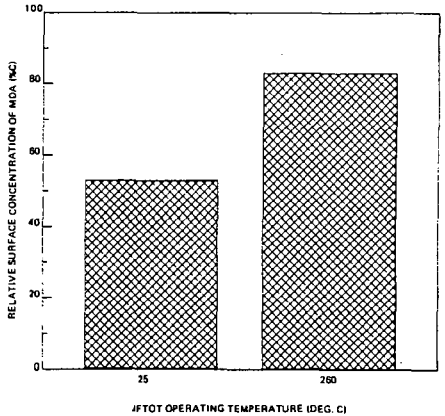

FIG. 7 – The influence of JFTOT operating temperature on the resulting MDA surface concentration of JFTOT test specimens (MDA bulk concentration 57g/1).

CHARACTERISATION AND QUANTIFICATION OF DEPOSITS FROM THERMALLY STRESSED AVIATION FUELS

Clive Baker, Peter David, Robert Finney
Diane Hall, Ray Swatridge
BP Research Centre, Chertsey Road, Sunbury-on-Thames, Middx, TW16 7LN, UK

1. INTRODUCTION

Deposits generated during thermal stressing of jet fuels in the JFTOT (Jet Fuel Thermal Oxidation Tester) hold a great deal of potential information about the mechanism and chemistry of fuel degradation, providing a suitable technique can be found for "unlocking" the data. Previous work at the BP Research Centre at Sunbury-on-Thames (RCS) using Auger Electron Spectroscopy has shown that magnesium (present in the tube alloy) will segregate at the tube surface and inhibit carbon deposition (1). The aims of recent work are to investigate further the causes and mechanisms of deposition, both in terms of chemical species and physical parameters.

JFTOT tube deposits have been examined by Scanning Electron Microscopy/Energy Dispersive Analysis of X-rays (SEM/EDX). This non-destructive technique enables a "profile" of the relative abundance of different elements present in the deposit along the tube length to be drawn. Further chemical characterisation of deposits has been made using Laser Ionisation Mass Analysis (LIMA); again, analysis has been performed along the length and through the depth of the deposit, providing information on deposit profiles in relation to tube temperature. It is now possible to obtain reproducible and reliable information about deposition levels enabling the influence of different factors such as temperature, time and fuel composition to be studied.

Much effort has been devoted during the past decade to characterisation of JFTOT tube deposits with less attention being given to the formation of particulate material during thermal stressing of fuels. It is believed that these could have as equally deleterious effects in aircraft fuel systems as surface layer deposits. Specific fuels are known to produce sufficient particulate material during normal JFTOT tests to give a measurable pressure differential across the standard JFTOT 17μm Dutch weave test filter. To study the formation of filterable deposits, an Alcor HLPS (Hot Liquid Process Simulator) has been modified at RCS to incorporate a 0.45μm Millipore membrane downstream of the heater tube test section, as a direct replacement for the standard filter. Filterable particulate deposits are collected during tests and characterised in terms of total mass and chemical composition.

Use of LIMA and SEM/EDX to characterise deposits generated in the JFTOT and the modified HLPS apparatus is described in this paper, with particular reference to the influence of fuel composition and test operating conditions on tube deposition and filterable deposit formation.

2. APPLICATION OF SEM/EDX TO JFTOT TUBE DEPOSIT ANALYSIS

In SEM/EDX, bombardment of the deposit with a low energy probe (3.0kv) enables X-rays to be generated from the individual elements present at the point of analysis. This energy is sufficient to ensure that an aluminium signal from the tube itself is seen whilst maximising the surface sensitivity. Thus a ratio of the particular element under investigation to the aluminium can be given. As the thickness of the deposit varies, the response due to both carbon and aluminium will alter respectively. It is therefore not possible to give an absolute value to the carbon content, but by quoting it as a ratio to the aluminium, a comparative value is obtained. Repetitive analysis at points along the deposit length enables a profile of C/Al values with tube position to be plotted. Calibration of the peak areas, using

carbon films of known thickness would allow at least semi-quantitative measurement of deposit thickness. Owing to the varying response of the technique to different elements, it is not possible to establish relationships between different elements in one deposit, only to compare the abundance of any one element from deposit to deposit.

Typical profiles are given (Fig 1) with the profile obtained from an unused tube included for comparison. Uniformity of the deposit was checked by determining the profile on two sides of the tube. A small difference was observed, but this was not thought to be significant.

From the profile obtained from a typical JFTOT deposit, the carbon concentration is seen to be symmetrical about a point which occurs downstream of the maximum tube temperature (39mm). There is a substantial increase in the amount of deposition after the maximum tube temperature. Where TDR traces show "splitting" of peaks, SEM/EDX has shown the deposit to consist of a single gaussian distribution envelope mainly of carbon. This throws some doubt on the validity of the TDR for tubes with thicker deposits.

2.1 Relationship between deposition and tube assessment

The relationship between visual ratings, TDR values and SEM/EDX traces is shown (Figs 2,3). There is good agreement, although SEM/EDX can identify trace levels of degradation carbon on a tube that has been given a visual rating of 1 and a TDR rating of zero. It is clear that the sensitivity of any assessment technique must be taken into account when defining the breakpoint of fuel as the temperature at which "onset of deposition" occurs.

2.2 Prediction of fuel breakpoint

The deposit C/Al ratio at any point in the profile can be plotted against the corresponding tube temperature; two values for each temperature are obtained, one upstream and one downstream of the maximum tube temperature (Fig 4). For a given fuel run at different temperatures in JFTOT tests, the C/Al ratios at equivalent tube temperatures on the upstream side of the maximum tube temperature show good agreement (Fig 5). This suggests that the thickness of deposits generated during JFTOT tests may be constant at a specific tube temperature for a given fuel. Thus with knowledge of carbon thickness associated with a visual rating of 3, it may be possible to estimate the breakpoint temperature of a fuel from the SEM/EDX profile generated from a single JFTOT test at a temperature higher than the breakpoint. This procedure may find applications for research purposes.

2.3 Kinetics of deposition

Maximum C/Al ratios obtained for one fuel at a constant temperature are plotted against test duration in Fig 6. The extent to which the non-linear response of the SEM/EDX to deposits of varying thickness affects these results is not known. However, the extended "induction period" observed implies a genuine change in mechanism, with deposition perhaps being governed by either a catalytic reaction with the tube surface or by an adherence effect. Others have also noticed this so-called "induction period" before the onset of deposition (2). The significance of this "induction period" with respect to aircraft fuel system operation needs to be established.

2.4 Role of metals and MDA (Metal Deactivator Additive)

The presence of metals in fuel causes a reduction in thermal stability, although it is not known whether the metal plays an integral part in deposition or acts only in a catalytic capacity. Addition of MDA generally produces an apparent increase in thermal stability as perceived by the JFTOT. The mechanism for this "improvement" is not understood clearly and may be ascribed either to a bulk fuel reaction or to a "passivation" of the tube surface. In order to address some of these aspects, experiments were carried out using one fuel with differing levels of metals, MDA and metal/MDA; results are shown in Table 1.

It is shown (Table 1, Fig 7) that copper had a deleterious effect on the thermal stability of the fuel, with an increase in carbon deposition with increasing levels of copper. Interestingly, copper was observed in the deposit and was also seen to increase as fuel copper levels were increased (Fig 8). When MDA was added, the thermal stability was seen to improve over and above that of the base fuel. This time, however, there was no evidence for copper in the deposit, indicating that the metal chelate plays no part in deposition. This would imply that the free copper reacts with species in the fuel to cause deposition, but will preferentially bind to the MDA. It is apparent that the MDA performs its accepted role well in metal chelation, and also appears to have some other additional effect on JFTOT results as yet not fully understood. Tubes run with dodecane doped with copper showed that in the absence of a deposit no copper was detected on the tube surface.

Addition of iron to the fuel was seen to promote deposition to a much greater extent, but, in contrast to the copper, iron was not found to be present in the deposit. Although MDA was found to negate the effect of the iron, the additive was not as efficient as with the copper at improving JFTOT breakpoint.

Iron appears to play a catalytic role in deposit formation. Although chelation with MDA reduces its activity, it may be that some limited catalysis can still occur even in the chelated form or that the chelate is not thermodynamically stable at higher temperatures.

3. APPLICATION OF LIMA TO JFTOT TUBE DEPOSIT ANALYSIS

LIMA analysis of the deposits has shown variations in the chemical composition with respect to temperature and tube location. The proportion of aromatic to aliphatic hydrocarbons is seen to increase towards the maximum tube temperature and also nearer the tube surface in a deposit, where presumably a temperature gradient exists across the deposit. As such, it may be that chemical changes occur in the deposit after it has been laid down and that therefore characterisation of the deposit in this way may not be a fruitful exercise.

3.1 MDA studies

The presence of MDA on tube surfaces has been shown by LIMA. The negative ion spectrum generated from analysis of MDA on stainless steel or aluminium substrates shows characteristic peaks at 119 and 146 amu (atomic mass units) (Fig 9). These peaks have been observed in spectra from tubes which have been contacted with dodecane or fuel containing MDA, at ambient or at elevated temperatures (Fig 10). They have not been observed during analyses of new JFTOT tubes or deposits generated from fuels which had not been treated with MDA, when peaks characteristic of fuel degradation products only are observed.

Immersion of a new JFTOT tube in fuel containing MDA at ambient temperature results in a layer of MDA on the tube surface, identifiable by LIMA. Variation in contact time does not appear to alter the level of coating, although absolute levels of MDA were not quantifiable. These tests are confirmation of the affinity of MDA for virgin metal of the JFTOT tube surface. The "strength" of the MDA coating can be demonstrated by performing tests on tubes pre-coated with MDA by immersion in treated fuel; the MDA is not removed in subsequent JFTOT tests using untreated fuel. There is however, some evidence for carryover of MDA from previous JFTOT tests although the extent of carryover is insufficient to have a measurable influence on visual rating or TDR assessments.

The passivation role attributed to MDA in the JFTOT test is undoubtedly related to the affinity of the additive for the metal surface. LIMA provides the opportunity to study the phenomenon in detail.

4. FORMATION OF PARTICULATE MATERIAL DURING THERMAL STRESSING

Tests on the modified HLPS have shown that in addition to tube deposition, substantial filterable deposits are formed which are not normally detected in standard JFTOT tests, and at temperatures below the recognised breakpoint of the fuel. These increase exponentially with temperature (Fig 11).

The influence of fuel metal content was demonstrated by addition of copper and iron (as naphthenate) to the fuel, when there was a significant increase in the mass of deposit at a given temperature (Figs 12, 13). With copper, the level of tube and filterable deposits increased with fuel copper content and copper was observed to be inherent in the deposits in increasing amounts. In contrast, while iron had a detrimental effect, there appeared to be a limiting level of iron above which formation of filterable deposits was not increased. Also, iron was not present in the tube deposits, but was observed in the filter deposits. These data coupled with results from other JFTOT studies (Section 2.4) suggest that the deleterious effects of iron and copper are caused by different mechanisms. In particular, iron appears to behave as a catalyst and is not inherently involved in deposit formation on the tube, whereas copper appears to combine with fuel species to promote deposition, in addition to any catalytic role it may have.

Addition of excess MDA to the metal doped fuels restored the quality to that of the base fuel (Figs 12, 13) indicating that the MDA was effective in negating the effect of the metals. To what extent this was caused by passivation of the tube surface and hence reduced reactivity, or by a genuine bulk fuel improvement is at this stage unclear.

The rate of formation of filterable deposits is shown in Fig 14. Initially, there was a linear increase, but thereafter, the rate of formation was reduced. (The fuel flow rate is kept constant throughout the test by adjusting the variable speed pump to compensate for the increase in pressure differential across the test filter.) It is proposed that the rate of formation of filterable deposits is affected by two factors. As deposition occurs on the tube surface, (i) the surface reactivity of the tube is inhibited, leading to reduced overall fuel degradation, and (ii), the tube exhibits enhanced adhesion properties, such that bulk fuel degradation products are retained, leading to an increase in tube deposition and a decrease in filterable deposits. This is shown schematically (Fig 14) where the tube deposits have been calculated as the difference between linearly increasing filterable deposits and actual measured levels. The variation in tube deposits with time is in good agreement with SEM/EDX data generated from JFTOT deposits (Section 2.3). Also, the mass of tube deposits predicted is of the same order of magnitude as measured by others in carbon burn-off assessment of JFTOT tube deposits (3).

Particle size measurements performed using laser diffraction techniques (Fig 15) demonstrate large increases in the number of particulates after thermal stressing, with the majority in the sub-micron size range. The implications for aircraft fuel system operation need to be established.

5. CONCLUSIONS

SEM/EDX and LIMA have been used for reliable characterisation of JFTOT and HLPS tube deposits providing information about deposit formation in relation to operating parameters and fuel composition. Tentative mechanisms for the role of metals and MDA on thermal stability have been proposed.

Tests on a modified HLPS have shown that substantial filterable deposits are formed during thermal stressing of fuels which are not detected in standard JFTOT tests. These have been shown to occur at temperatures below the JFTOT breakpoint of the fuel and to vary with temperature and fuel composition. Models have been proposed to demonstrate the relationship between tube and filterable deposits. These initial investigations will form the basis for more detailed studies on jet fuel thermal stability.

6. REFERENCES

1. An AES Depth Profiling Study of the Deposits formed on Aluminium during Jet Fuel Thermal Oxidation Test.
   Baker C, David P and Hazell L.
   Surface and Interface Analysis Vol 9 507-513 (1986)

2. The Thermal Degradation of Aviation Fuels in Jet Engine Injector Feed-Arms Part 1 - Results from a Full-Scale Rig.
   Kendall D R et al.
   Tokyo International Gas Turbine Congress (1987)

3. The Influence of Polar Compounds on the Stability of Jet Fuel
   Kendall D R et al.
   Presented at 2nd International Conference on Long-Term Storage Stabilities of Liquid Fuels. San Antonio, Texas (1986)

7. ACKNOWLEDGEMENTS

The authors would like to thank Air BP and UK MOD(PE) for their sponsorship of this work.

TABLE 1

JFTOT DATA OBTAINED ON MEROX TREATED KEROSINE SHOWING THE EFFECTS OF METALS AND MDA ON TUBE RATING

FUEL				TDR					
Cu (ppb)	Fe (ppb)	MDA (ppm)	Temp °C	Spun	Spot	Posn	PRESSURE Δ p-mmHg	VISUAL RATING	MAXIMUM C/Al RATIO
-	-	-	260	2.5	3.5	45	0.1	<2	0.08
83	-	-	260	14	15	44	0.2	4	0.74
166	-	-	260	16	17.5	31/49	0.3	4	1.36
83	-	5.70	305	5.5	8.5	44	>25	A	0.38
83	-	0.57	260	0	0	-	0.2	1	0.03
83	-	0.57	305	50	50	38	2.5	>4	2.50(9kv)
-	-	0.57	305	9	11	43	0.7	2A	ND
-	-	1.14	305	0	0	-	0.3	1	ND
-	-	2.28	305	0	0	-	0.4	1	ND
-	78	-	260	44	45	38	>25	4	10.1(5kv)
-	78	5.7	260	0	0	-	3.3	1	ND
-	78	5.7	305	22	25	42	>25	4P	0.64(5kv)

ND - Not Determined

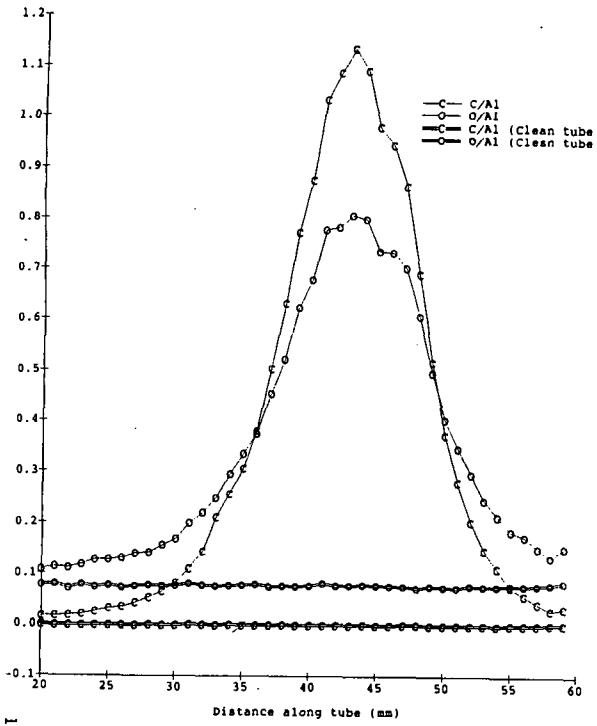

Figure 1. Typical SEM / EDX profile for JFTOT deposit with result from clean tube for comparison.

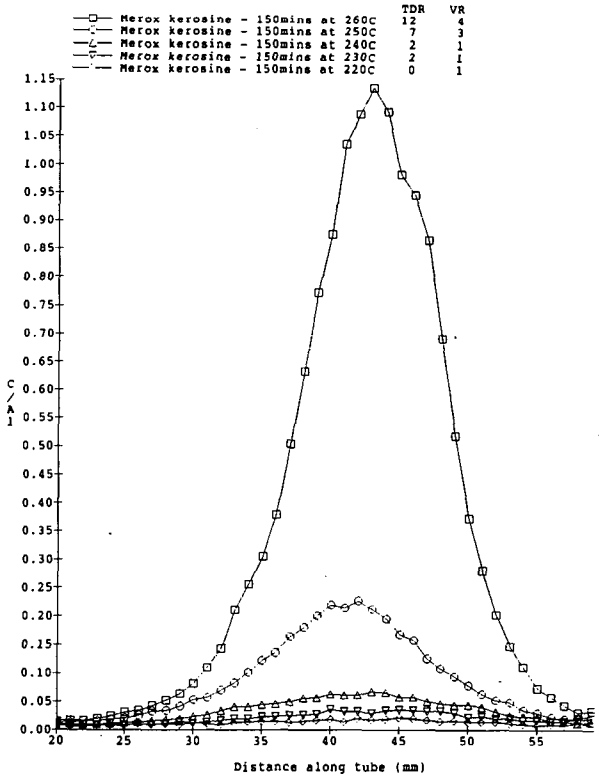

Figure 2. Carbon deposition on JFTOT tubes: Correlation with TDR and VR.

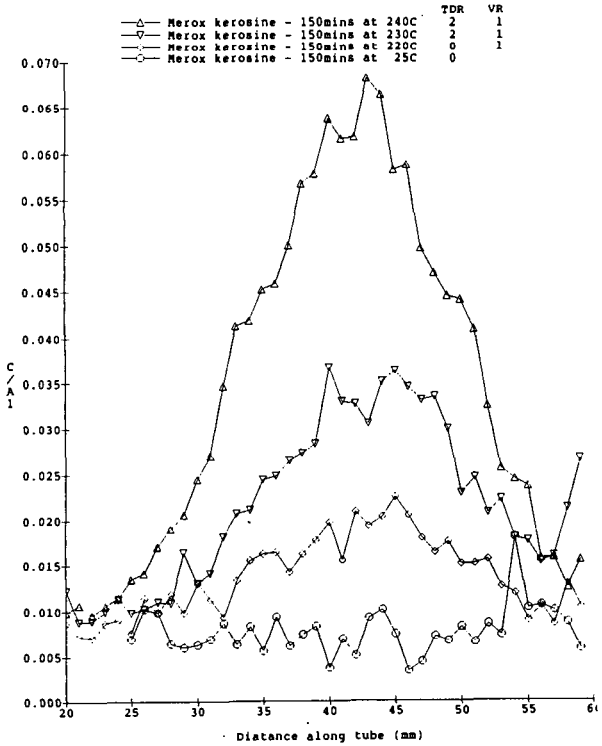

Figure 3. Carbon deposition on JFTOT tubes: Correlation with TDR and VR.

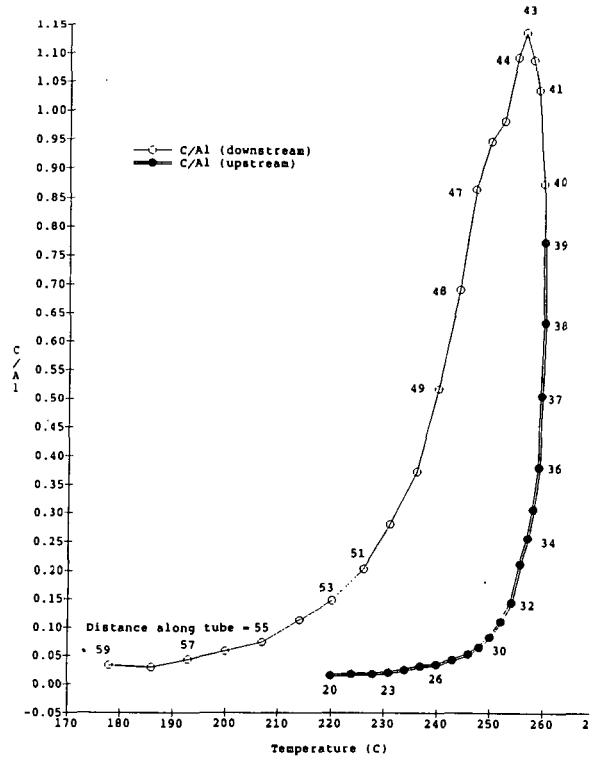

Figure 4. Temperature profile of carbon deposit Merox kerosine at 260°C.

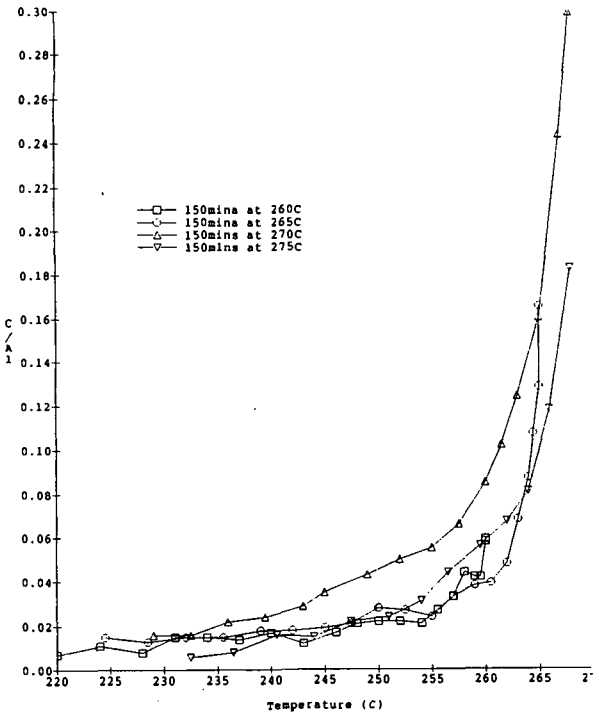

Figure 5. Relationship of upstream C / Al ratios to temperature of deposition (Merox kerosine).

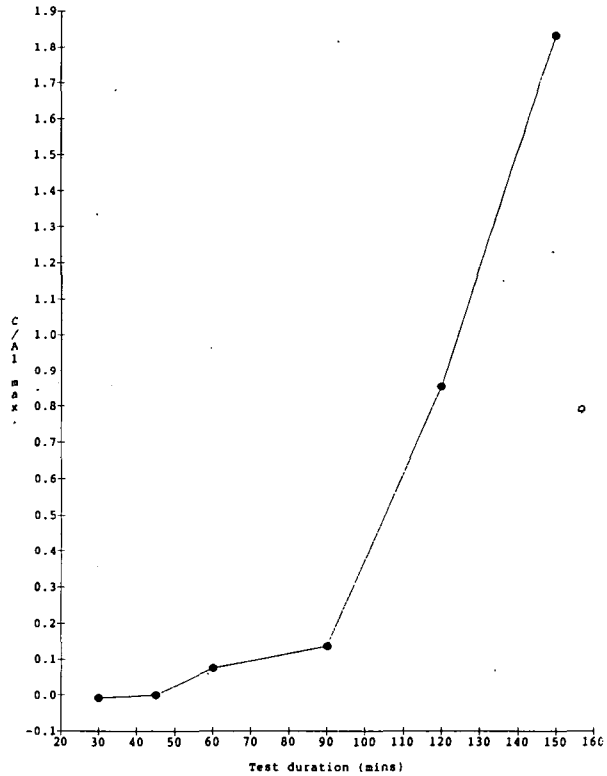

Figure 6. Maximum C / Al ratios against test duration -Merox kerosine at 275°C.

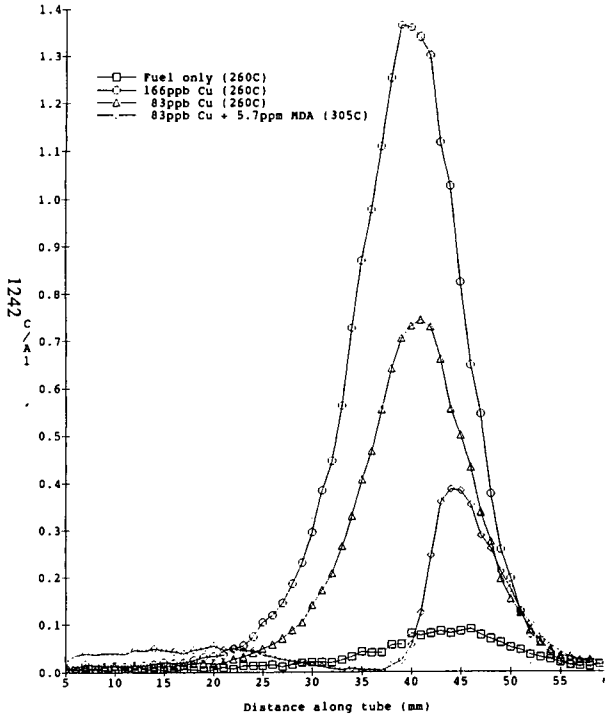

Figure 7. Comparison of C / Al ratios for Merox kerosine blends.

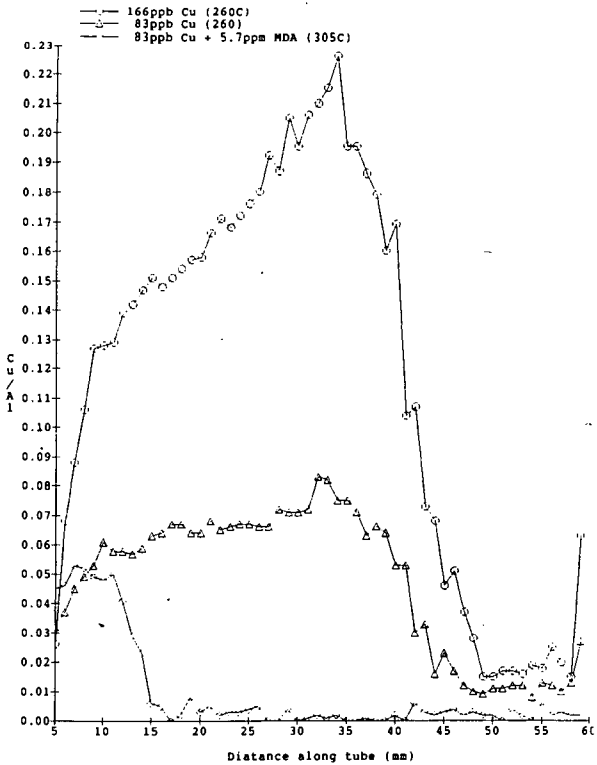

Figure 8. Comparison of Cu / Al ratios for Merox kerosine blends.

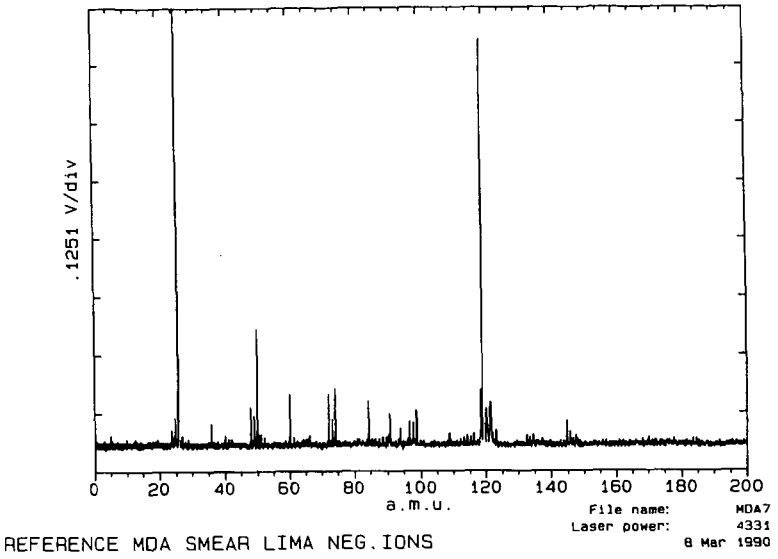

Figure 9. Metal deactivator additive.

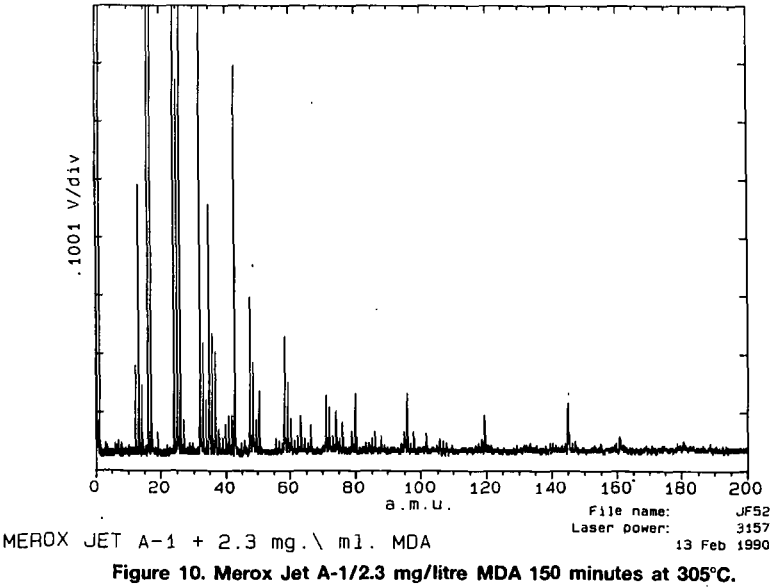

Figure 10. Merox Jet A-1/2.3 mg/litre MDA 150 minutes at 305°C.

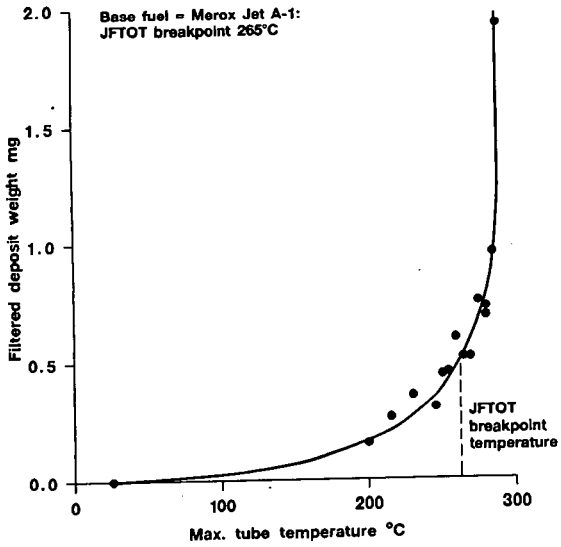

Figure 11. Modified HLPS tests. Influence of temperature on filtered deposit levels.

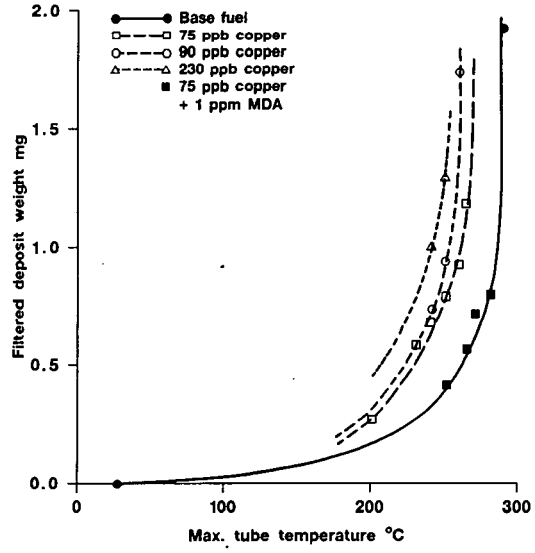

Figure 12. Modified HLPS tests. Influence of soluble copper and MDA on filtered deposit levels.

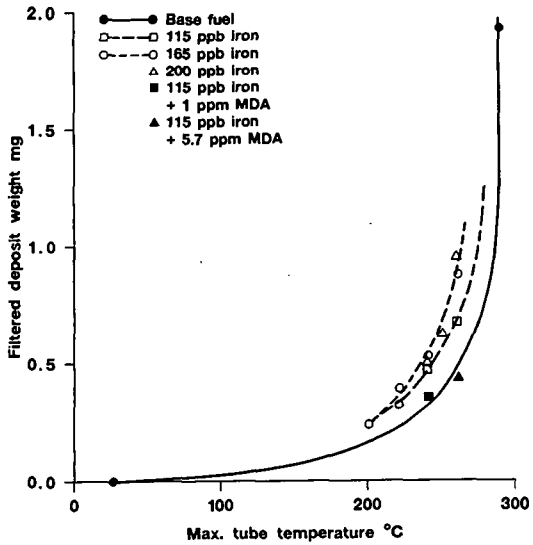

Figure 13. Modified HLPS tests. Influence of soluble iron and MDA on filtered deposit levels.

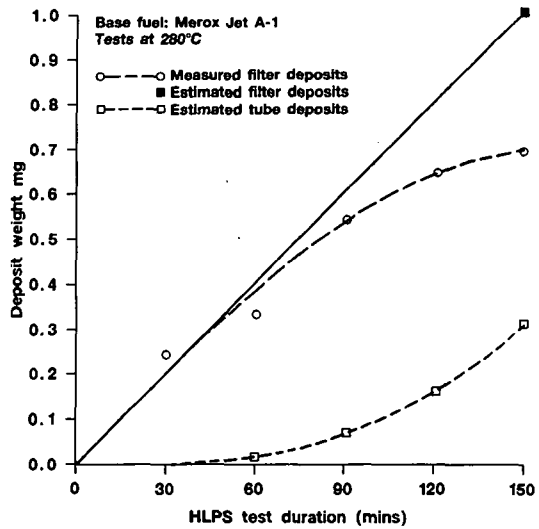

Figure 14. Modified HLPS tests. Relationship between tube and filter deposits.

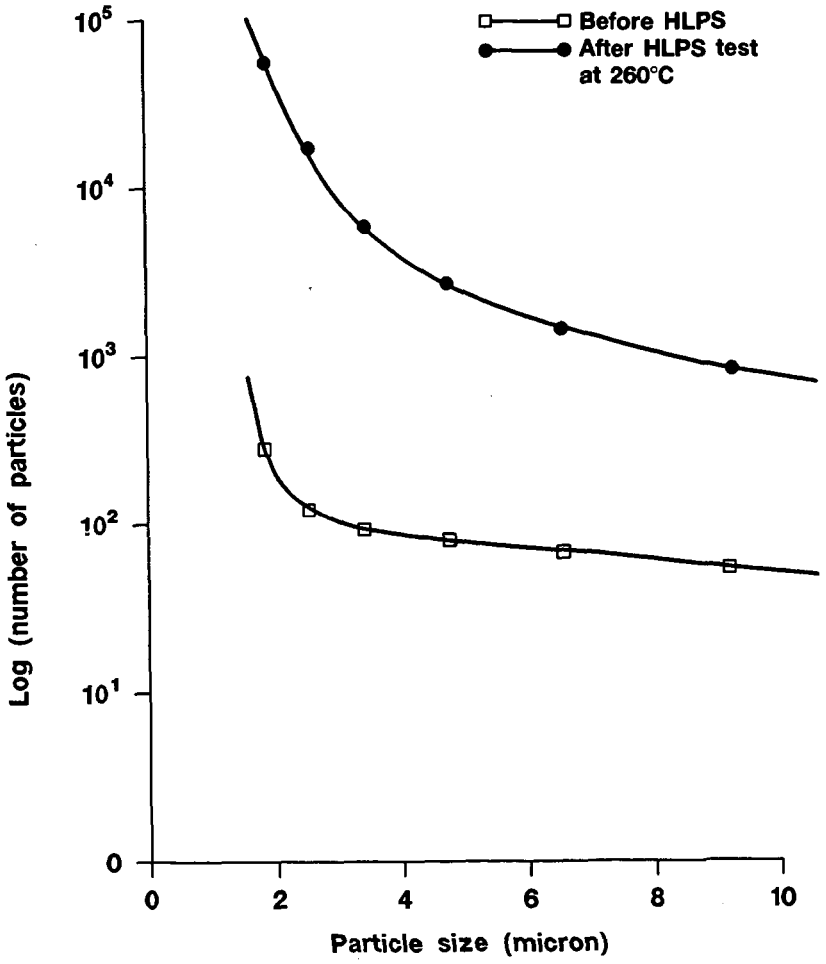

Figure 15. Influence of thermal stressing on particle size (number) distribution. Fuel: Merox Jet A-1 + 75 ppb copper.

The Catalytic Activity of Transition Metal Complexes in Oxidation Reactions Utilizing Hydroperoxides

J. J. Weers and C. E. Thomasson
Petrolite Corporation
Research & Development
369 Marshall Avenue
St. Louis, MO. 63119

INTRODUCTION

Hydroperoxides and oxy-based radicals have often been identified as residue and color formation precursors in hydrocarbon fuels during storage[1]. Typically the peroxides are generated during the propagation step of an air autoxidation mechanism and their formation is continuous as long as initiators and oxygen are present for the reaction to occur. A study performed in jet fuel determined that the square root of peroxide concentration is proportional to fuel storage duration[2]. The peroxide species, once formed in the fuel, have a wide range of possible reactions in which they can participate. For example, the reaction with olefins[3], nitrogen compounds[4] and sulfur compounds[5] present in the hydrocarbon yields epoxides, amine oxides or nitro compounds, and disulfides, sulfoxides, sulfones, etc., respectively. The reactivity of the peroxide species toward the above derivatives can be modified in a number of ways. One of the more common methods is the introduction of a metal catalyst. The metal, when present even in catalytic amounts, may cause rapid degradation of the peroxides into oxy or peroxy radicals[6].

$$M\ (+2) + ROOH \longrightarrow M\ (+3) + RO^{\cdot} + OH^{-} \qquad \text{(Eq. 1)}$$

$$M\ (+3) + ROOH \longrightarrow M\ (+2) + ROO^{\cdot} + H^{+} \qquad \text{(Eq. 2)}$$

The formation of esters, olefins or even alkyl halides is possible depending on the catalyst present, its oxidation state and the counter ion associated with it[7]. Vanadium complexes for example have been shown to be excellent catalysts for the oxidation of tertiary amines to amine oxides[8]. Iron and cobalt were found to be poor catalysts for the same reaction. Phenols have also been shown to be oxidatively unstable in fuels[9] yielding an additional reagent for the peroxides to interact with in these systems.

A factor which has not been as widely studied is the influence of ligands on the catalytic activity of the metal[10]. When the metal is in a mid-distillate, there are a variety of nitrogen and sulfur, etc., species present to act as ligands to complex the metal. The complex may have a much different redox potential than the metal itself as well as having ligands blocking potential coordination sites for the peroxide and thereby preventing its decomposition from occurring.

A study was thus conducted to investigate the influence various ligands have on the oxidation of olefins and phenols by hydroperoxides in the presence of various metal catalysts. The reactions were investigated without added solvent as well as in a No. 2

diesel fuel to determine if the reactivity was similar or if other fuel components present in the hydrocarbon would alter the results. Reactions were conducted under conditions commonly used for mid-distillate fuel stability testing.

EXPERIMENTAL

In the cyclohexene oxidation studies, samples were prepared using 0.1 mole cyclohexene, 0.1 mole 90% tert-butyl hydroperoxide, 1 x 10^{-3} mole metal catalyst and 5 x 10^{-3} mole of the ligand where applicable. The samples were heated at the specified temperature for the desired time period and then analyzed by ^{1}H and ^{13}C NMR (Varian Gemini 300) and by GC mass spectroscopy (DuPont DP-1 mass spectrometer). Product yields were determined by capillary GC (HP-5710A). Fuel studies utilized the above amounts of dopants added to a 300 mL sample. All samples were stirred until homogeneous and then stored in an oven at 43°C until analyzed for residue content as specified in ASTM D-4625.

Experiments for phenol oxidation were performed using 0.1 mole p-cresol, 0.1 mole 90% tert-butyl hydroperoxide, 1 x 10^{-3} mole catalyst and 5 x 10^{-3} mole ligand. Product yield was determined by gas chromatography after conversion of the phenol mixture to their methyl ethers by treatment with Me_4NOH and MeI to increase their volatility. Fuel studies were run using 1000 ppm p-cresol and hydroperoxide, 1 ppm metal catalyst and 5 ppm ligand. The p-cresol, cyclohexene, tert-butyl hydroperoxide and the metal catalysts, cobalt acetate monohydrate ($Co(OAc)_2$), copper acetate tetrahydrate ($Cu(OAc)_2$), nickel acetate tetrahydrate ($Ni(OAc)_2$), vanadium pentoxide, anhydrous ferric chloride and the ligands pyridine and tetrahydrothiophene (THT) were purchased from Aldrich Chemical Co. and used as received. The ligands chelant 1 and chelant 2 are proprietary commercial metal chelants used as mid-distillate fuel stability additives. Fuel utilized in the studies was a No. 2 diesel fuel produced at a Gulf Coast refinery containing a 80/20 mixture of straight run distillate and LCO.

RESULTS

Analysis of the cyclohexene oxidation products present after heating, indicated each contained a complex mixture of tert-butanol, acetone, cyclohexene, 2-cyclohexene-1-ol, 2-cyclohexene-1-one, tert-butoxy-2-cyclohexene and 2-cyclohexenyl-tert-butyl peroxide. The wide variety of products is indicative of the complexity of the reaction and of the many different reaction mechanisms available for the peroxides and radicals. The ether and peroxide products formed by oxidation of cyclohexene most likely resulted from attack of RO• and ROO• radicals on the olefin, followed by hydrogen elimination and double bond formation. Both oxy and peroxy radicals are present in the reaction mixtures from the metal catalyzed decomposition reactions illustrated in equations 1 and 2. The 2-cyclohexene-1-one is probably present as a thermal decomposition product of the 2-cyclohexenyl-tert-butyl peroxide. This peroxide is quite thermally stable and thus the decomposition is likely occurring in the injector of the gas chromatograph during analysis rather than in the experiment itself. The 2-cyclohexene-1-ol could be formed by several mechanisms. Attack of a hydroxyl radical, generated by thermal or radical induced decomposition of the hydroperoxide, is a possible mechanism. Hydrogen abstraction by a cyclohexenyl oxy radical generated by decomposition of the peroxide is also possible. It is not possible from these data to determine which mechanism is occurring under our reaction conditions.

The high yield of 2-cyclohexenyl-tert-butyl peroxide compared to the yield of the ether was surprising as both RO• and ROO• radicals should be present if the cycle shown in equations 1 and 2 was operative. The higher yield of the peroxide suggest a second

process is occurring in which the RO· radicals are converted to ROO· followed by reaction with cyclohexene. A likely mechanism for this reaction is the hydroperoxide oxidation of the oxy radical[11],

$$RO\cdot + ROOH \longrightarrow ROH + ROO\cdot \qquad \text{(Eq. 3)}$$

This reaction apparently is faster than the reaction of the RO· radical with cyclohexene.

In the absence of added ligand, a relative ranking of the activity of the catalyst in the order V (V) >> Co(II) > Fe(III) > Cu(II) > Ni(II) was obtained (Table 1). All of the ligands reduced the activity of the vanadium catalyst and increased the activity of nickel. Apparently the ligands present in the vanadium experiment compete for coordination sites on the metal, either as free ligand or as an oxidized species (amine oxide, sulfoxide, etc.), and thereby decrease the ability of the catalyst to complex the hydroperoxide and initiate oxidation[12]. In the case of the nickel catalyst, the opposite effect is observed. The ligands can modify the catalyst's solubility, redox potential, etc., with a resulting increase in activity. The results with the other metals were mixed with some ligands promoting oxidation while others inhibited it. For copper, the oxidation of cyclohexene by t-BuOOH has been studied in the absence of added ligand[13]. A copper naphthenate catalyst was used and the peroxide and ketone were the only cyclohexene based oxidation products detected. The alcohol and ether were not detected in their study, and indeed, were minor products in our study until pyridine or tetrahydrothiophene ligands were present. The ligands increased the total yield of the alcohol and ether as well as the overall yield of all cyclohexene oxidation products with copper as a catalyst. Both of the metal chelants (chelant 1 and chelant 2) decreased the amount of oxidation product obtained. These materials are used commercially as "metal deactivators" in fuels and thus the lower oxidation product yield would be expected. The total amount of material identified in the mixture containing chelant 1 was low (78%) indicating a lot of unidentified material was present. Pyridine and chelant 1 increased the activity of the iron and cobalt catalyst while tetrahydrothiophene and chelant 2 had the opposite effect. The nature of the ligand is thus important in determining if a metal catalyst is an inhibitor or a pro-oxidant.

The activity of the iron, copper and cobalt catalysts, with and without pyridine or tetrahydrothiophene ligands, in a real diesel fuel was also investigated. In this case sulfur, nitrogen etc., components of the fuel may also influence the oxidation reactions. On monitoring the samples, it was observed that very significant degradation of the samples had occurred after only 1.5 weeks storage at 43°C. The insoluble (filterable + adherent) residue values were thus obtained (Table 2) and compared to the results in Table 1. A high level of sedimentation was assumed to be indicative of a high level of oxidation occurring in the fuel. The results were surprising however, in that the sample doped with only the hydroperoxide was much more unstable than the untreated fuel, while the sample containing both hydroperoxide and cyclohexene was only slightly more unstable. This would suggest the peroxide reacts with the cyclohexene in the fuel to give soluble products, while in its absence, the hydroperoxide reacts with other fuel components to give insoluble products. Addition of the metals to these systems greatly increased the amount of residue obtained. Copper with the pyridine ligand gave particularly high values of residue. The tetrahydrothiophene ligand gave variable results, increasing sediment with iron but decreasing the level of residue with copper and cobalt.

Analysis of the phenolic components present in mid-distillate fuels has indicated a complex mixture of low molecular weight alkyl phenols are present and that these materials can have an influence on the fuels storage stability[14]. Coupling reactions to give biphenyldiols are postulated to be active mechanisms involved in the instability work. Metals are known catalyst for the reaction and thus their influence on the oxidative coupling a model compound, p-cresol under fuel stability test conditions was investigated. The results (Table 3) indicated all metals when mixed with p-cresol even in the absence of added hydroperoxide or ligand gave some coupled product. A relative ranking of the catalyst in the order V(V) = Cu(II) > Fe(III) > Co(II) was obtained. In this case atmospheric oxygen in the sample is the only oxidant present. With the ligands present yields were also relatively low. When the experiment was repeated with added hydroperoxide as oxidant, the yield of coupled products increased dramatically. Copper clearly was the best catalyst for the autoxidation. Not only was the yield of the bis-phenol increased, but large amounts of trimer and even tetramer were measured (Table 4). Copper has been identified previously as an excellent catalyst for this reaction in agreement with our results[15]. The ligands were again influential on product yield but the results were variable. All ligands decreased the yield of oxidation products when used in combination with the copper catalyst. The sample containing pyridine was unusual in that the ligand decreased the yield obtained to that obtained in the absence of catalyst. Pyridine has been found to be a poor ligand in previous studies utilizing copper-amine catalyst to oxidize phenols and the studies indicate a strong dependence of the structure of the metal complex in these systems[16]. Pyridine was a pro-oxidant for the iron catalyst. Higher yields of trimer in particular being obtained when the ligand was present. The commercial metal chelants were good oxidation inhibitors for this metal, however only 78.9% of the material analyzed by the GC could be identified in the sample containing chelant 1. Compounds other than bisphenyldiols etc., were formed. This is not surprising as products resulting from C-O coupling are possible as well as from addition of the ROO· radicals to the phenol ring. The influence of the ligands on the activity of the cobalt catalyst was smaller, with pyridine again acting as an antioxidant and tetrahydrothiophene acting as a pro-oxidant. The percentage of the products identified with the sample containing chelant 1 was again low indicating additional unidentified products were present. Vanadium pentoxide alone was second only to copper in its ability to catalyze the oxidation. The tetrahydrothiophene and chelant 2 did not seem to influence its activity much while chelant 1 and pyridine again lowered the amount of oxidation occurring.

Many of the above observations were not found to correlate with samples of diesel fuel treated with the reagents and stressed at 149°C for 30 min (Table 5). Using residue pad ratings as an indicator of fuel degradation, it was clear pyridine ligand was not a catalyst deactivator as observed in the above reactions. With each of the metal catalyst evaluated, the amount of residue formed on stressing the fuel was higher in the presence of pyridine. With the exception of cobalt, the two chelant ligands were the only ones which did show some improvement in the amount of residue obtained. Apparently components present in the fuel also participate in the reactions occurring to generate the residue. The p-cresol and hydroperoxide by themselves did not influence the pad ratings.

CONCLUSIONS

The presence of ligands in a metal catalyzed oxidation of an olefin or phenol can have a large influence on product yield and distribution. The influence is, however, dependent on the metal and the species being oxidized. For example pyridine increased the yield of cyclohexene oxidation products with the copper catalyst while it decreased the yield observed with vanadium. In the phenol coupling experiment, the addition of

pyridine gave lower yields of products than did copper itself. Many of the results could also not be correlated with residue values obtained in the real fuel. Residue values did not agree well with the product yields obtained. Apparently other components of the fuel also react with the dopants altering the results.

REFERENCES

1. Taylor, W. F., Frankenfeld, J. W., Conference Proceedings, 2nd Int. Conference on Long Term Storage Stability of Liquid Fuels, 1986, 496-511.

2. Fodor, G. E., Naegeli, K. W., Kohl, D. B., Energy and Fuels, 1988, 2, 729-734.

3. Edwards, J. O., "Peroxide Reaction Mechanisms", Interscience Publishers, 1962, 77.

4a. De La Mare, H. E., J. Org. Chem., 1960, 25, 2114-2126.

b. Capp, C. W., Hawkins, E. G. E., J. Chem. Soc. 1953, 4106-4109.

c. Murry, R. W., Rajadhyaksha, S. N., Mohan, L., J. Org. Chem. 1989, 54, 5783-5788.

5. Mushrush, G. W., Hazlett, R. N., Hardy, D. R., Watkins, J. M., Conference Proceedings, 2nd Int. Conference on Long Term Storage of Liquid Fuels, 1986, 512-522.

6. Robertson, A., Waters, W. A., Trans. Faraday Soc., 1946, 42, 201.

7. Cardinate, G., Grimmelkhuysen, J. C., Laan, J. A., Van Lier, F. P., Van der Steen, D., Ward, J. P., Tetrahedron, 1989, 45, 5971-5978.

8. Sheng, M. N., Zajacek, J. G., J. Org. Chem., 1968, 33, 588-590.

9. Hazlett, R. N., Power, A. J., Conference Proceedings, 2nd Int. Conference on Long Term Storage Stability of Liquid Fuels, 1986, 556-559.

10. Li, N. C., Tzou, J. R., Chang, H., Wang, S. M., Chin, J., J. Chem. Soc. 1987, 34, 91-98.

11. Bell, E. R., Raley, J. H., Rust, F. F., Seubold, F. H., Vaughan, W. E., Discussions Faraday Soc., 1951, 10, 242.

12. Carlin, R. L., J. Am. Chem. Soc., 1961, 83, 3773-3775.

13. Kharasch, M. S., Paulson, P., Nudenberg, W., J. Org. Chem. 1953, 18, 322-327.

14. White, C. M., Jones, L., Li, N. C., Fuel. 1983, 62, 1397-1403.

15. Kushioka, K., J. Org. Chem., 1984, 49, 4456-4459.

16. Hewitt, D. G., J. Chem. Soc., 1971, 2967-2973.

TABLE 1

Product Distribution in Cyclohexene Oxidations

Catalyst	% Cyclohexene Oxidation Product Yield after 24 hrs at 43°C* Alcohol	Ketone	Ether	Peroxide	Total	Total Identified**
None	0.4	0.4	0	0.1	0.9	79.9
$Cu(OAc)_2$	0.9	1.4	0	1.0	3.3	90.5
+ Chelant 1	0	1.6	0	0.9	2.5	78.0
+ Chelant 2	0	0.2	0	0.5	0.7	95.5
+ Pyridine	2.9	9.0	0.2	1.8	13.9	76.6
+ THT	1.3	2.0	0	1.1	4.4	89.3
$FeCl_3$	1.7	1.6	0	0.8	4.1	91.5
+ Chelant 1	0.9	6.0	0	0.4	7.3	81.6
+ Chelant 2	0.7	2.4	0	0	3.1	84.8
+ Pyridine	1.8	5.0	0.3	0.5	7.6	87.7
+ THT	1.1	1.8	0	0	2.9	81.7
$Co(OAc)_2$	2.5	2.5	0	0.3	5.3	95.8
+ Chelant 1	1.8	6.3	0	0.3	8.4	83.5
+ Chelant 2	0.8	2.6	0	0	3.4	87.3
+ Pyridine	1.6	5.7	0.1	0	7.4	85.0
+ THT	2.4	2.6	0	0	5.0	92.1
V_2O_5	0	21.4	0	1.5	22.9	96.9
+ Chelant 1	2.0	5.1	0	0.8	7.9	78.9
+ Chelant 2	1.8	3.1	0	2.4	7.3	79.1
Pyridine	0.6	1.4	0	0	1.0	99.6
+ THT	1.1	8.4	0.3	0.8	10.6	95.2
$Ni(OAc)_2$	0.4	0.4	0	0	0.8	99.3
+ Chelant 1	2.1	4.2	0	0.4	6.7	83.8
+ Chelant 2	0.7	3.1	0	0	3.8	79.7
+ Pyridine	0.4	0.5	0	0	0.9	98.7
+ THT	0.7	1.0	0	0	1.7	97.7

* Alcohol = 2-cyclohexene-1-ol; Ketone = 2-cyclohexene-1-one; Ether = t-butoxy-2-cyclohexene; Peroxide = cyclohexenyl-tert-butyl peroxide.

** Sum of acetone, t-butanol, cyclohexene and alcohol, ketone, ether and peroxide cyclohexene derivatives yields.

TABLE 2

Fuels Stability Studies Utilizing Cyclohexene, Hydroperoxide, Metal Catalyst and Various Ligands

Dopant	Insoluble Residue (mg/100 mL)*
None	0.3
Cyclohexene	0.3
t-BuOOH	1.7
Cyclohexene + t-BuOOH	0.5
+ $FeCl_3$	6.1
+ $FeCl_3$ + Pyridine	3.4
+ $FeCl_3$ + THT	19.0
+ $Cu(OAc)_2$	13.0
+ $Cu(OAc)_2$ + Pyridine	32.0
+ Cu $(OAc)_2$ + THT	9.3
+ Co $(OAc)_2$	2.0
+ Co $(OAc)_2$ + Pyridine	2.9
+ Co $(OAc)_2$ + THT	1.9

* After 1.5 weeks at 43°C

TABLE 3

Influence of Hydroperoxide on p-Cresol Oxidation

Catalyst	% p-Cresol Oxidation Product Yield Without t-BuOOH	With t-BuOOH
None	0	2.0
$Cu(OAc)_2$	2.7	37.2
$FeCl_3$	1.4	10.8
$Co(OAc)_2$	0.3	8.6
V_2O_5	2.8	12.8

* After 90 min storage at 149°C. Total of dimer, trimer and tetramer products.

TABLE 4

Product Distribution in p-Cresol Oxidation by Tert-Butyl Hydroperoxide

Catalyst	% Oxidation product Yield * Dimer	Trimer	Tetramer	Total	Total Identified **
None	2.0	0	0	2.0	99.8
$Cu(OAc)_2$	22.9	9.6	4.7	37.2	94.8
+ Chelant 1	8.2	2.2	2.5	12.9	91.4
+ Chelant 2	11.8	4.8	3.5	20.0	99.0
+ Pyridine	3.4	0	0	3.4	96.5
+ THT	6.5	1.9	0	8.4	95.1
$FeCl_3$	10.4	0.4	0	10.8	97.5
+ Chelant 1	1.3	1.0	0	2.3	78.9
+ Chelant 2	5.1	0	0	5.1	95.0
+ Pyridine	12.6	3.1	0	15.7	96.6
+ THT	9.3	1.7	0	11.0	91.5
$Co(OAc)_2$	4.2	4.4	0	8.6	90.4
+ Chelant 1	6.1	0.5	0.1	6.7	82.5
+ Chelant 2	7.6	0.9	0	8.5	95.1
+ Pyridine	4.0	0.4	0	4.4	93.0
+ THT	6.8	4.8	0	11.6	69.6
V_2O_5	10.7	2.1	0	12.8	88.6
+ Chelant 1	6.5	0.9	0	7.4	80.0
+ Chelant 2	11.1	2.0	0	13.1	91.4
+ Pyridine	6.0	0.6	0	6.6	93.0
+ THT	10.9	1.4	0	12.3	87.1

* After 90 min at 149°C.

** Sum of t-butanol, p-cresol, dimer, trimer and tetramer yields.

TABLE 5

Dopant	Residue Pad Rating * Without t-BuOOH	Residue Pad Rating With t-BuOOH
None	4	4
p-Cresol	4	4
+ $Cu(OAc)_2$	5	20
+ Chelant 1	4	3
+ Chelant 2	4	3
+ Pyridine	5	20
+ THT	5	17
+ $FeCl_3$	14	11
+ Chelant 1	7	3
+ Chelant 2	4	4
+ Pyridine	15	16
+ THT	17	15
+ $Co(OAc)_2$	4	3
+ Chelant 1	5	3
+ Chelant 2	3	7
+ Pyridine	4	8
+ THT	3	4
+ V_2O_5	4	4
+ Chelant 1	3	3
+ Chelant 2	3	4
+ Pyridine	4	7
+ THT	3	4

* After 90 min storage at 149°C. Pad rating scale; 1 = clean pad to 20 = heavy residue.

ANALYSIS OF PHENOLIC ANTIOXIDANTS IN JP-5 AVIATION FUELS

Mei-Hsia Alice Huang and Lynda M. Turner
Fluid Sciences Division
Naval Air Propulsion Center, Trenton, NJ 08628

ABSTRACT

The Navy requires the addition of antioxidants to prevent the degradation of JP-5 aviation fuel in storage. Monitoring phenolic compounds commonly used for this purpose is essential to determine the quality of prepositioned aviation fuel supplies. The large number of chemical constituents in JP-5 fuels provides complex chromatograms which, for most approaches, hinder the detection of antioxidants. In this study, however, liquid chromatography with electrochemical detection and a judicious choice of the mobile phase provided good resolution of many antioxidants. Several phenolic antioxidants are evaluated in fuels originating from different crude sources and processing techniques.

INTRODUCTION

The jet fuel supply and distribution system is very complex and unpredictable. The refineries supplying the U.S. Navy with JP-5 fuel change annually depending upon cost, logistics and the political situation in the oil industry. JP-5 properties within a given geographic area, therefore, are becoming more variable.[1]

Trends indicate future crude sources will have higher unsaturated hydrocarbon, heteroatom and metallic contents. All of these properties require increased hydroprocessing to produce an acceptable JP-5 product. Jet fuel is changing from a product made by simple distillation to a variable blend of streams from different processing units.[2]

The Navy is becoming increasingly concerned with the properties of the JP-5 now available for consumption and is relying less on property/performance relationships which existed ten years ago. The Naval Air Propulsion Center (NAPC) has initiated a Fuels Diagnostics Program to facilitate the measurement of JP-5 properties and interpretation of their relationship with aircraft engine performance. An integral part of this program is to collect, modify and/or develop analytical methods which will allow us to make evaluations.

The stability of our current JP-5 supplies must be periodically monitored. This is especially true for fuels placed in strategic storage locations for extended periods. Due to the shortage of pristine, straight distillate fuels, storing fuels with known less-than-desirable stability characteristics is becoming more of a reality. Presently, the Navy does not have regulations to prohibit the storage of fuels processed by techniques other than straight distillation. The Navy must rely heavily upon the addition of antioxidants to

prevent fuel degradation. The additives currently accepted in Specification MIL-T-5624 are phenolic in structure and serve to inhibit the degradation of fuel components by breaking the reaction chain of the peroxy radical which occurs during the hydrocarbon auto-oxidation process.[3]

A study conducted[4] had shown that peroxidation will occur only after the additive has been depleted. Therefore, tracking an additive's depletion pattern would give forewarning of fuel degradation. Having this information prior to degradation could assist the Navy in making decisions regarding when to rotate JP-5 stock. This could reduce the number of potential JP-5 fuels which may have to be downgraded to Diesel Fuel Marine (DFM) due to high peroxide content, thus not meeting military aviation fuel stability requirements.

Gas chromatographic and liquid chromatographic techniques for determining commercial phenolic antioxidants in aviation turbine fuels have been reported.[5-9] Unfortunately, only a few antioxidants were investigated in these papers. Pearson[6] presented an internal standard technique using gas chromatography-mass selective detection for two antioxidants. Cunningham and Hillman[7] reported a liquid chromatographic method with ultraviolet detection that can be applied to measure several hindered phenolic antioxidants. Also in this paper, an extractive procedure was developed to remove part of the "main fuel peak" from the chromatogram. Hayes and Hillman[8] used liquid chromatography with electrochemical detection (LCEC) for determining a single antioxidant in turbine fuel. A modified LCEC procedure to determine the retention time of several antioxidants was presented by Vogh.[9] However, the results were obtained with severely hydroprocessed neat (additive-free) jet fuels. Further modifications to this LCEC method were carried out in our study at NAPC to measure additional commercial phenolic antioxidants in actual refinery-produced JP-5 fuels.

EXPERIMENTAL SECTION

The isocratic liquid chromatographic system consisted of a solvent delivery pump (SSI Model 222B Single-Piston) with the flow rate set at 0.5 ml/min., a pulse damper (SSI Model LP-21 Lo-Pulse Damper), a Rheodyne 7176 injector with 20 microliter sample loop, a Rheodyne 73XX column inlet filter, and a 4.6 mm I.D x 25 cm stainless steel Du Pont Zorbax C_8 reversed phase column of 5 micron particle size.

The detector was a flow-by type electrochemical (EC) detector (EG&G Princeton Applied Research Model 400). The EC detector contained a glassy carbon working electrode and a reference electrode. The reference cell was filled with a solution containing 3 M sodium chloride and saturated silver chloride. The EC detector was operated in the DC mode at 1000 mV, a current of 100 nA, a 1.0 second time constant, and a cathodic output. A Perkin-Elmer LCI-100 integrator was used for peak area measurements.

The mobile phase consisted of a mixture of 30% of 0.02 M potassium acetate buffer, 60% of 2-propanol, and 10% methanol. This solution was vacuum filtered through Millipore HVHP 0.45 micron filter paper and degassed for at least ten minutes (sonicated with vacuum).

The response factor and the retention time for each antioxidant in JP-5 fuel samples varied slightly from day to day. This was probably due to slight variances of conditions of the analytical instrumentation and the composition of the mobile phase. Therefore, it was necessary to run a standard solution every day for calibration prior to the analysis of each fuel sample. If more analyses needed to be run the following day, it was essential to pump the mobile phase continuously overnight at a low flow rate. If this was not done, the system might become clogged and damaged by the deposits that could be formed by the buffer solution in the mobile phase. If the instrument was going to be turned off for long period, distilled water with 10% methanol had to be pumped through the system for few hours, followed by acetone for at least half an hour prior to turning off the pump.

RESULTS AND DISCUSSION

Hindered phenolic type antioxidants are typically added into JP-5 fuel at a concentration of 17 to 24 ppm during the refining process. At this level, analytical methods with commonly used detectors do not provide sufficient sensitivity for identifying and quantifying the antioxidants. An electrochemical (EC) detector was chosen in this study due to its selectivity and sensitivity for phenolic compounds. With EC detection, compounds that contain either electro-oxidizable or electro-reducible organic functional groups will be detected. Thus, many hydrocarbon fuel components can be conveniently eliminated from detection making it easier to isolate antioxidant peaks.

Based on initial testing, it was determined that improvements could be made to the mobile phases that had been used and reported in other papers.[7-9] A variety of solvents and combinations of solvents were evaluated. The mobile phase that was found to be most effective in this study (see Experimental Section) provided much improved resolution of many antioxidants and minimized the miscibility problem between JP-5 fuel and the mobile phase.

Seven antioxidants that are commonly added to JP-5 aviation fuels were studied in this work. The chemical compositions of these antioxidants are listed in Table 1. Most antioxidants that are added to JP-5 fuels at the refinery are phenolic mixtures. Of the antioxidant structures that are or had been used in the military specification, only three antioxidants (AO-A, AO-B, and AO-E) are single component additives.

In the preliminary phase of this study, antioxidants were added at the 17 to 25 ppm level into a "clean" fuel to prepare standards. A hydrocracked JP-5 type additive-free fuel (Fuel X) was used as the "clean" fuel. It was selected

because the high intensity region in its chromatogram (Figure 1) is much narrower than a typical JP-5 fuel (Figure 2, Fuel #1) due to differences in refinery processing (e.g. hydrocracking vs straight run). The antioxidants in the prepared standards were then characterized by their chromatogram retention time (Figures 3 and 4). This "preliminary" information for each antioxidant was then applied to the analyses of "actual" JP-5 fuel samples.

A number of actual JP-5 fuels originating from different crude sources and processing techniques were evaluated. Examples of their typical chromatograms are shown in Figure 5 (Fuel #2) and Figure 6 (Fuel #3). Unfortunately, for most of these fuels, the "main fuel peak" that elutes during the first fifteen minutes retention time completely masks the peaks of a number of the antioxidants in this study. Antioxidants AO-B, AO-C, AO-D, the minor peak for antioxidant AO-F, and the minor peaks for antioxidant AO-G are completely blocked by this "main fuel peak". It is impossible to positively identify antioxidants AO-B, AO-C and AO-D in JP-5 fuel samples unless the "main fuel peak" can be eliminated partially or completely from the chromatogram.

The major component of antioxidant AO-F has the same chemical composition as antioxidant AO-E. Therefore, they will be detected with the same retention time. Thus, when this peak is detected in "real" JP-5 with the large "main fuel peak", it is not known if the minor peak for antioxidant AO-F is being masked. In this case, it is impossible to determine whether antioxidant AO-E or AO-F is present in the JP-5 fuel sample.

Regardless of the difficulty in identifying some antioxidants as mentioned above, antioxidant AO-E (or the major component of antioxidant AO-F), a component of antioxidant AO-G, and antioxidant AO-A in JP-5 fuel samples still can be detected by HPLC analysis. Peak retention times for antioxidant AO-E and antioxidant AO-G are very close to each other (Figure 7, Fuel #4). However, these two antioxidants will never be added simultaneously into JP-5 fuel by the manufacturer. Therefore, the antioxidant which is actually present in the fuel can be identified by spiking one of these antioxidants into the fuel.

Not all fuels contain the large "main fuel peak" in their chromatogram. The intensity of the "main fuel peak" in Figure 7 is much narrower than the one for most typical JP-5 fuel samples as shown in Figure 2. This difference is most likely due to the fact that JP-5 Fuel #4 was produced by different refinery processing. The antioxidant peaks in this chromatogram did not originate from the fuel sample. Antioxidants AO-A, AO-E, and AO-G were added into the fuel before running the chromatogram.

Quantitative analysis of "actual" JP-fuels involved several steps. A chromatogram was run on the as-received JP-5 fuel for a "preliminary" identification of antioxidant peaks. Next, a standard was prepared from a "blank" fuel. Because "actual" JP-5 fuels vary in chemical composition which affects the peak area measurement in the analysis, it is necessary to prepare

a standard for each fuel sample. A "blank" fuel was obtained by filtering the JP-5 fuel through either a silica gel column or an Alumina N Sep-Pak cartridge. This step removed the antioxidant from the fuel and their peaks from the chromatogram. An antioxidant at a concentration of 10 to 25 ppm was added into a "blank" fuel to prepare a standard. The prepared standard was then analyzed to calculate the response factor for each corresponding antioxidant. With the response factor for each antioxidant and the fuel chromatogram that was obtained in the first step, the amount of antioxidant in the JP-5 fuel sample was determined by the external standard technique.

For most fuel samples, there was only a very small peak shown at the chromatogram retention time that corresponds to antioxidant AO-A (Figure 2). It is very difficult to accurately measure such a low concentration directly. However, in this case, the amount of antioxidant AO-A in JP-5 fuels could be more accurately determined by an addition technique than with an external standard technique. The addition method was conducted as follows: A known amount of antioxidant AO-A was added into a "blank" fuel to calculate its response factor. The "blank" fuel was prepared by the same filtration technique described earlier. After spiking a known amount of antioxidant AO-A into an actual JP-5 fuel sample (Figure 8), the total concentration of antioxidant AO-A in the spiked fuel sample was determined. The difference between this measured total amount of antioxidant AO-A and the known amount that was added into the fuel sample was the original concentration of antioxidant AO-A in the JP-5 fuel sample.

The effects of interferents occurring at the location of an antioxidant peak may also be minimized by using the addition technique described in the preceding paragraph. When Fuel #1 was filtered through an Alumina N Sep-Pak cartridge, a small shoulder remained at the prior location of the antioxidant AO-A peak (Figure 9). This demonstrates that care must be taken to account for interferents in quantitative analyses. This process effectively subtracts out baseline interferents since the response factor is determined on a "blank" fuel containing interferents.

CONCLUSIONS

A number of JP-5 aviation fuel samples were examined by liquid chromatography with electrochemical detection. A mobile phase was found which provided good resolution. All antioxidant peak locations were identified and quantitative analysis demonstrated at use levels (17-24 ppm). A detection limit of about 1 ppm was found for all antioxidants. However, many JP-5 fuels have a "main fuel peak" which masks some of the antioxidant peaks. Thus, a complete qualitative/quantitative analysis of actual JP-5 fuel samples was greatly dependent on the location of the antioxidant peaks with respect to the "main fuel peak". A technique for eliminating the "main fuel peak" (partially or completely) from the chromatogram needs to be developed to analyze the antioxidant peaks which are located in that region and will be the objective of subsequent work.

ACKNOWLEDGEMENT

The authors wish to thank Dr. M. N. Sundberg for helpful discussions on this project. Also, the authors would like to express their thanks to Dr. E. Florio for technological assistance.

REFERENCES

1. The Characteristics of Future Fuels Hadallar, O.J., Momentary, A.M., Boeing Commercial Airplanes, August 1984

2. IBID

3. Auto-oxidation and Antioxidants of Petroleum Nixon, Alan C., Interscience Publishers, Shell Development Company, Emeryville, CA

4. Sutterfield, F.D. et al. The Third International Conference on Stability and Handling of Liquid Fuels Conference Proceeding; vol. 1 pg. 321; 13-16 September 1988.

5. Pearson, C.D., J. Chromatogr, 1988, V.449, pp. 440-447

6. Bartl, P., Schaaf, H. Presentius Z. Anal. Chem., 1982, V.310, pp. 250

7. Cunningham, A.F., Hillman, D.E. J. Chromatogr, 1978, V.148, pp. 528-531

8. Hayes, G.E., Hillman, D.E. J. Chromatogr, 1985, V.322, pp. 376-379

9. Vogh, J.W., Unpublished report, National Institute for Petroleum and Energy Research

TABLE I

Antioxidants Commonly Used in JP-5 Aviation Fuels

Antioxidant	Chemical Composition
AO-A	2,6-di-*tert*-butyl-4-methylphenol
AO-B	6-*tert*-butyl-2,4-di-methylphenol
AO-C	72% min 6-*tert*-butyl-2,4-dimethyl-phenol 28% max *tert*-butyl-methylphenols and *tert*-butyl-dimethyl-phenols
AO-D	60% min 2,4-di-*tert*-butylphenol 40% max mixture of *tert*-butylphenols
AO-E	2,6-di-*tert*-butylphenol
AO-F	75% min 2,6-di-*tert*-butylphenol 25% max *tert*-butylphenols and tri-*tert*-butylphenols
AO-G	55% min butylated ethyl phenols 45% max butylated methyl and dimethyl-phenols

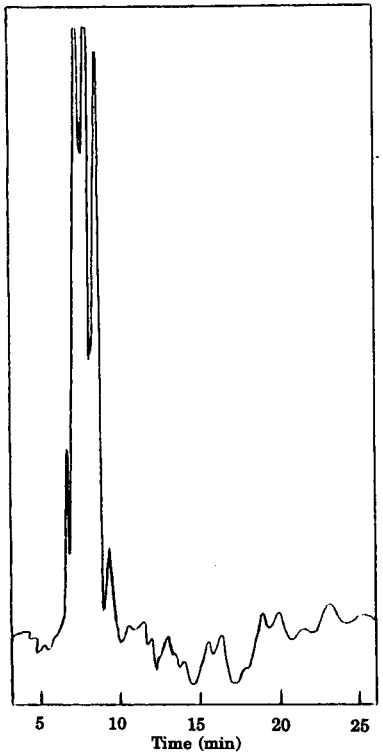

FIGURE 1: Chromatogram of "Clean" Fuel X (with no antioxidants)

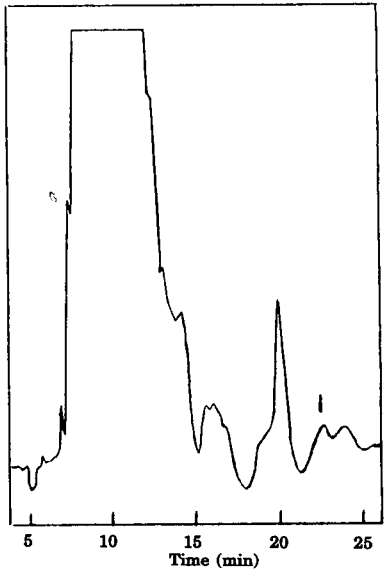

FIGURE 2: Chromatogram of "Typical" JP-5 Fuel #1 containing AO-A (1)

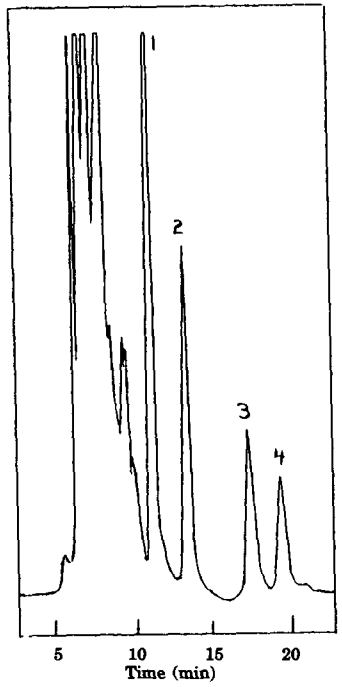

FIGURE 3: Chromatogram of "Clean" Fuel X containing AO-A (4), AO-B (1), AO-C (1), AO-D (2), AO-E (3) and AO-F (3)

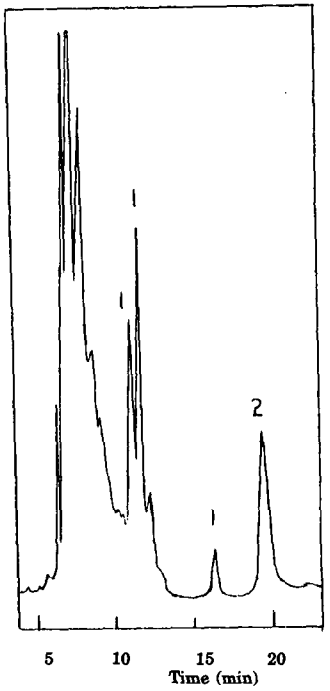

FIGURE 4: Chromatogram of "Clean" Fuel X containing AO-A (2) and AO-G (1)

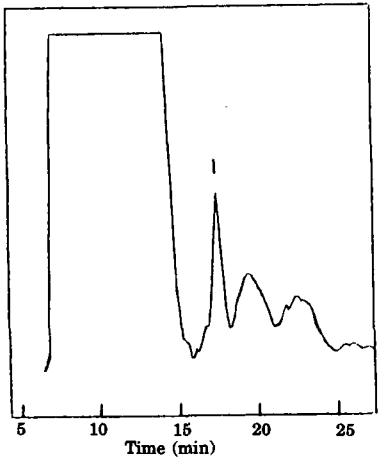

FIGURE 5: Chromatogram of JP-5 Fuel #2 containing AO-E (1) or AO-F (1)

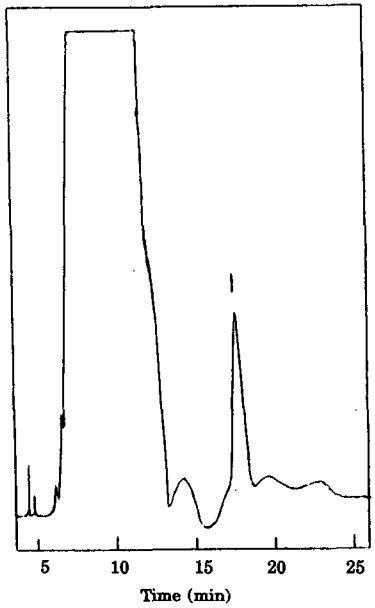

FIGURE 6: Chromatogram of JP-5 Fuel #3 containing AO-E (1) or AO-F (1)

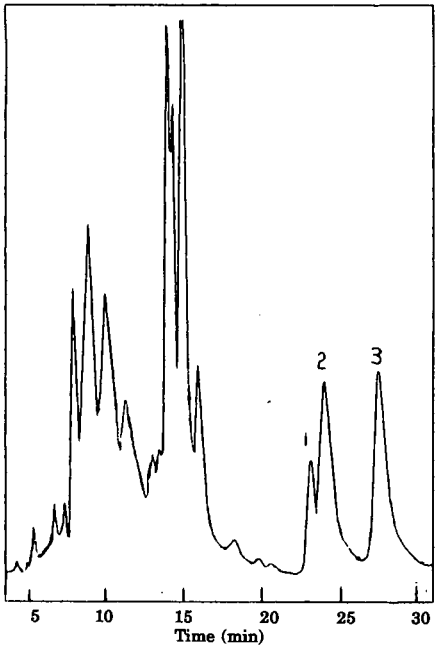

FIGURE 7: Chromatogram of JP-5 Fuel #4 containing AO-A (3), AO-E (2), and AO-G (1)

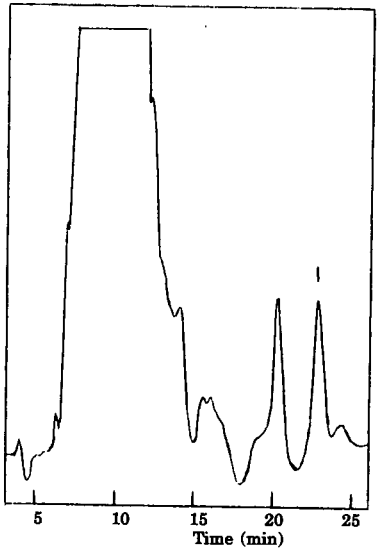

FIGURE 8: Chromatogram of JP-5 Fuel #1 spiked with AO-A (1)

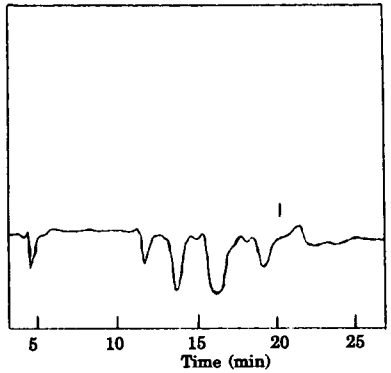

FIGURE 9: Chromatogram of JP-5 Fuel#1 filtered through an Alumina N Sep-Pak cartridge showing interferent (1)

PEROXIDE FORMATION IN JET FUELS

George E. Fodor* and David W. Naegeli
Belvoir Fuels and Lubricants Research Facility, Southwest Research Institute, 6220 Culebra Road, San Antonio, Texas 78228

ABSTRACT

This paper reports recent results from an ongoing study of the kinetics of peroxide formation and the development of a method to measure potential peroxides in jet fuels. In the earlier work, rates of peroxide formation in six jet fuels were measured over a temperature range of 43 to 120 °C with oxygen partial pressures ranging from 10 to 1140 kPa. Global rate constants for the peroxide formation were based on a kinetic model of the autoxidation process, which showed that the peroxide concentration increased as the square of the stress duration. The rate of peroxide formation was strongly dependent on temperature, but independent of the partial pressure of oxygen. Recently, rates of peroxide formation have been measured in four more jet fuels at temperatures of 80, 100 and 120 °C with an oxygen partial pressure of 240 kPa. Global Arrhenius rate constants for peroxide formation were determined for the induction and post-induction periods in the new fuels. These results were found to be in good agreement with the earlier work, which encouraged the development of a test method to predict rates of peroxide formation at ambient conditions from rate measurements at elevated temperatures.

INTRODUCTION

The need for a method of predicting the potential formation of peroxides in jet fuels arose from fuel pump failures in jet aircraft. Shertzer (1), Hazlett, et al. (2), and Love, et al. (3) found that peroxides cause significant deterioration of neoprene, nitrile rubber, and Buna-N diaphragms and O-rings used in aircraft engine fuel pumps.

To avoid future problems, a program was initiated to study the kinetics of peroxide formation and ultimately to develop a timely method of predicting the potential peroxide content of jet fuels.(4-7) Several test methods have been developed to determine the oxidative stability of fuels, e.g., ASTM D 2274; they are carried out at elevated temperatures to reduce the test duration to an acceptable level. An accelerated high-temperature test is also desired for the timely determination of potential peroxide formation in jet fuels.

It is well-known that peroxides form in fuels by an oxidation process that is slow at room temperature, but relatively fast at temperatures ranging from 80 to 120 °C.(7-9) Since the objective was to provide a basis for a practical test method, not exceeding about 48 hours, the foremost goal was to determine if the mechanism of peroxide formation at elevated temperatures was the same as that at ambient temperature. If the mechanism is unchanged over a limited temperature range (e.g., 0 to 150 °C), it is possible to predict ambient temperature behavior from a global Arrhenius rate expression that can be determined by making two or more rate measurements at higher temperatures.

Recent results have shown that the reaction mechanism responsible for peroxide formation is the same from ambient temperature conditions to at least 120 °C.(7) In that work, rates of peroxide formation in six jet fuels were measured over a temperature range of 43 to 120 °C with oxygen partial pressures ranging from 10 to 1140 kPa. Experiments in the 80 to 120 °C range were performed in a pure oxygen atmosphere in a stirred pressure reactor. Long-term experiments at 65 and 43 °C were accomplished by bottle storage with fuels exposed to air. Global rate constants for peroxide formation, derived from a kinetic model of the autoxidation process, were strongly dependent on temperature and independent of the partial pressure of oxygen. In the present study, global rates of peroxide formation were measured in four more jet fuels in the temperature range of 43 to 120 °C. Additionally, limited oxidation experiments were also performed on dodecane, ethyl benzene, and tetralin. These results support the conclusions of the earlier work (7) and agree favorably with other reported rate measurements.

EXPERIMENTAL SECTION

To establish baseline data on the long-term stability, a modified version of the ASTM D 4625 method of bottle storage at 43 °C was used.(10) The modified procedure ensured that the autoxidation reactions will not become oxygen concentration limited. In the revised procedure, each fuel sample was purged with "synthetic" air until the fuel became saturated with oxygen, as determined by gas chromatography. Then the fuel samples were stored at 43 °C in sealed amber borosilicate bottles. The oxygen contents were determined periodically in both the liquid and vapor phases. If the oxygen concentration in the vapor phase dropped below 10.0 vol%, the remaining bottles of the same fuel were again aerated.

Accelerated oxidative stressing of the test fuels was carried out in replicate in two nominally identical 600-mL, 316 stainless-steel pressure reactors. Temperature was regulated to ± 0.5 °C, and the oxygen pressure was continuously monitored. For details of the experimental procedure, see Ref. 7.

The test fuels selected for this study are described in **Table 1**. Since the objective of this paper is to compare the new results with those obtained previously, (7), a description of the fuels 1 through 6 examined in the first study will also be included.

The new test fuels 7 through 10 were hydrocracked kerosenes in the Jet A boiling point range.

All the test fuels were claimed by the suppliers to be free of synthetic antioxidant-type additives. Infrared analysis of the polar fraction of the fuels did not show any substituted phenolic or amine-type compounds in excess of the detection limit, < 5 ppm.

MECHANISM

It is well-known that the autoxidation of hydrocarbons is based on a free-radical mechanism (11), which includes the familiar radical initiation, propagation, and termination reaction steps. While several reaction steps are conceivable in the overall autoxidation of hydrocarbon fuels, the formation of alkyl hydroperoxides, ROOH, water and gums may be described by the mechanism shown in Reactions 1 through 6 in **Table 2**.

In this mechanism, the alkyl peroxide, ROOH, itself initiates the chain mechanism defined by these reactions. For a truly pristine fuel, a chain propagated autoxidation process can not start unless there is a trace of a radical initiator such as ROOH present. In reality, all fuels contain a trace of ROOH even though the concentration is below the detection limits of current analytical methods. In fact, since free radicals are inevitably formed in fuels by exposure to background radiations such as muons, it is highly probable that traces of ROOH will form by Reactions 4 and 5 in **Table 2**.

The remaining mechanistic arguments and derivation of the kinetic relationships were discussed earlier.(7) Basically, it was concluded from both theory and experiment that the formation of peroxides in jet fuels is independent of the oxygen concentration and appears to depend only on the hydrocarbon concentration, which is assumed to be constant during the autoxidation process. The final relationship based on Reactions 1 through 6, which was used in the analysis of the data, is

$$[ROOH]^{1/2} = k_5/(k_1/2k_6)^{1/2}\,[RH]\,t \qquad \text{(Equ. 1)}$$

where the combination of constants $k_5/(k_1/2k_6)^{1/2}$ $[RH]$ is the global rate constant for peroxide formation. It is important to note (9), however, that if the partial pressure of oxygen is too low (< 7 kPa), Reaction 4 may become the rate controlling step in the mechanism, and Reaction 7 below would then take the place of Reaction 6.

$$R^{\bullet} + R^{\bullet} = R_2 \qquad \text{(Reaction 7)}$$

For the oxygen-starved reaction, it may be shown that

$$[ROOH]^{1/2} = k_5/(k_2/2k_7)^{1/2}\ [O_2]\ t \qquad \text{(Equ. 2)}$$

where the peroxide concentration now depends on the oxygen concentration, $[O_2]$, in the fuel.

RESULTS AND DISCUSSION

The basic goal of this study was to develop a method to predict the slow formation of peroxides in jet fuels at ambient conditions from global rate constants obtained at higher temperatures. In the previous work (7) on fuels 1 through 6, the rates of peroxide formation were measured over the temperature range 43 to 120 °C, and the partial pressure of oxygen was varied from 10 to 1140 kPa. In the continuation, global rate constants for the formation of peroxides were measured in fuels 7 through 13.

Existing methods for the evaluation of the storage stability of distillate fuels include "bottle storage" under an atmosphere of air at 43 and 65 °C (10,12) for extended periods ranging from weeks to months. To establish baseline data, bottle storage tests were performed on fuels 1 through 8. Fuels 1 through 4, 7 and 8 were aged at 43 °C, and fuels 5 and 6 were aged at 65 °C. All the test fuels were stressed in the stirred pressure reactors at temperatures ranging from 80 to 120 °C.

Results of the experiments on the new fuels 7 through 10 are shown in **Figures 1 through 7**. **Figure 1** shows the peroxide concentration time curves for fuels 7 and 8 measured in bottle storage experiments at 43 °C. **Figures 2 and 3** show the peroxide concentration versus time curves for fuels 7 and 8 measured in the stirred reactor at 80, 100, and 120 °C. Fuels 7 and 8 each had pronounced induction periods that lengthened as the stress temperature was lowered. The induction periods were substantial considering that synthetic antioxidants were not added to these fuels. Previous studies (13) on the autoxidation of hydrocarbons have shown that similar induction periods appear in autoxidations of hydrocarbons when antioxidants are added.

Figure 4 shows the Arrhenius plots of the global rate constants determined for fuels 7 and 8. **Figures 5 and 6** show the peroxide concentration time curves for fuels 9 and 10 measured in the stirred reactor at 80, 100, and 120 °C. Fuels 9 and 10 also exhibited pronounced induction periods that increased as the stress temperature was lowered. **Figure 7** shows the Arrhenius correlation of the global rate constants measured in the stirred reactors.

The results given in **Table 3** show a favorable correlation of global rate constants over the temperature range of 43 to 120 °C. Except for the induction period of fuel 7, the activation energies were also about the same, ≈ 22 kcal/mol. The activation energy for the induction period for fuel 7 (28.4 kcal/mol) is similar to that (29.4 kcal/mol) obtained earlier for fuel 3. Fuels 3 and 7 represent two instances where the activation energy for the induction period is higher than what has been commonly observed for fuels. It is important to note, however, that an activation energy as high as 29.4 kcal/mol is not unusual for the formation of peroxides in hydrocarbons. Rubio, et al. (14) measured rate constants in basically the same way as the present study and found an activation energy of 31 kcal/mol for peroxide formation in C_{10} to C_{16} normal alkanes. Arrhenius parameters given for fuels 9 and 10, which do not include 43° or 65 °C data, are consistent with those of the other fuels.

Two issues arose from the previous study.(7) First, there was a desire for some confirmation of the results obtained from the stirred reactors. To satisfy that need, rates of peroxide formation were determined in dodecane and compared with data in the literature. A second concern was that there were induction periods observed when the test fuels were known to be free of synthetic antioxidants. The induction periods generally lasted until the peroxide concentration reached about 50 to 100 ppm.

To satisfy the above concerns, some experiments were conducted with model compounds. The global rate constant for dodecane was measured at 120 °C and was found to compare favorably with similar rate constants measured

by Rubio, et al. (14) for peroxide formed in decane, dodecane and hexadecane. The rates of peroxide formation in ethyl benzene and tetralin were measured in the stirred reactor at 80 °C. It is interesting to note that there were no induction periods observed in the oxidations of the model compounds. Because these compounds contained traces of peroxides when procured, they were carefully purified by distillation before they were oxidized. The distillation may have removed trace amounts of antioxidant-type impurities that could have caused an induction period. The fact that the test fuels were reportedly free of antioxidants, but nevertheless exhibited induction periods, suggests that fuels contain natural oxidation inhibitors that appear to be quite alien to synthetic antioxidants.

Table 4 shows that the global rate constants for model compounds decrease in the order tetralin > ethyl benzene >> dodecane. The rate constant for dodecane was calculated using a rate expression developed by Rubio, et al.(14)

If the well-known argument is used, i.e., the rate-controlling step in the autoxidation process is the attack on the C-H bond by the $RO_2\bullet$ radical, then the ease of hydrogen abstraction determines the overall rate of oxidation.(9,13, 15-17) The results in Table 4 agree with the basic order of free-radical attack on the carbon-hydrogen bond, which is benzylic and allylic H >> aliphatic H.

Since the rate of peroxide formation in alkyl-substituted aromatics is about 100 time faster than in normal alkanes, it would seem that it is the aromatic constituents of the fuel that determine the peroxide potential. This belief seems to concur with the observations in that the rate constants of the test fuels, except for fuel 1, are similar to that of ethyl benzene (3.9×10^{-6} $(mol/l)^{1/2}/s$), i.e., they ranged from about 1×10^{-6} to 4×10^{-6} $(mol/L)^{1/2}/s$ at 80 °C. The aromatic contents of the fuels ranged from 8.5 to 44.0 percent and the amounts of alkyl groups bonded to the aromatic rings ranged from 4.3 to 17.7 percent. The aromatic alkyl group content was determined as the difference between the total aromatics by FIA and the total aromatic ring carbon measured by UV absorption spectroscopy. It seems reasonable to conclude that the aromatics play a major role in determining the peroxide potential since the concentration of benzylic type C-H bonds appears to be in plentiful supply in all the test fuels.

The above argument seems reasonable except for fuel 1, which formed peroxides at a much slower rate than the other test fuels. In fact, the measured rate of peroxide formation in fuel 1 at 120 °C was somewhat less than that measured in dodecane. There was nothing unusual about the composition of fuel 1. Its total aromatic content was 18.7 percent and the amount of aromatic alkyl groups was 9.3 percent, so there was no obvious reason why the fuel should have oxidized so slowly. Perhaps, because it was a straight run fuel, i.e., not hydrocracked etc., the natural oxidation inhibitors were preserved in the refinement process. A complicating factor is that a later report by the refiner of fuel 1 indicated that this fuel "may have been" Merox treated. It is interesting that some fuels seem to contain relatively potent natural oxidation inhibitors that are not detectable by the analytical methods used to measure synthetic antioxidants.

CONCLUSION

The new results on fuels 7 through 10 agree with the original observations (7) on fuels 1 through 6. It is evident from the Arrhenius correlations that the mechanism designated by reactions 1 through 6 predominates over the temperature range of 43 to 120 °C.

Potential peroxide formation in jet fuels depends on both the reactivity of the bulk hydrocarbons and the presence of small, possibly undetectable, amounts of (natural) antioxidants.

It is concluded that the peroxide potential of jet fuels at ambient conditions can be predicted from relatively timely measurements at elevated temperatures. However, since the activation energies for peroxide formation in jet fuels range from 19 to 29 kcal/mol, it is concluded that a timely prediction of peroxide potential at ambient conditions would require measurements of global rate constants at two or more elevated temperatures.

ACKNOWLEDGMENT

This work was conducted at the Belvoir Fuels and Lubricants Research Facility, located at Southwest Research Institute (SwRI), for the Naval Research Laboratory (NRL) under Contract No. NOOO14-85-C-2520. For completeness, this paper includes the results of earlier work funded by the Naval Air Propulsion Center (NAPC). NAPC funding was provided by a Military Interdepartmental Purchase Requisition through the U.S. Army Belvoir Research, Development and Engineering Center under Contract DAAK70-85-C-0007. The project monitors for the Navy were Dr. D.R. Hardy of NRL and C.J. Nowack, G.E. Speck, and L.M. Turner of NAPC. We gratefully acknowledge the invaluable participation by J.P. Cuellar, Jr.; K.B. Kohl; and M. Voigt. Editorial assistance provided by J.W. Pryor, Sherry Douvry, and LuAnn Pierce is also acknowledged with appreciation.

REFERENCES

1. Shertzer, R.H., Final Report No. NAPC-433, Naval Air Propulsion Center: Trenton, NJ, 1978.
2. Hazlett, R.N.; Hall, J.M.; Nowack., C.J.; Craig, L.C., Proceedings of the Conference on Long-Term Stabilities of Liquid Fuels, Israel Institute of Petroleum and Energy: Tel Aviv, Israel, 1983, No. B132.
3. Love, B.E.; Hatchett, K.A.; Peat, A.E., "Fuel-Related Problems in Engine Fuel Systems," SAE Trans. 1967, 75, pp. 441-463.
4. Fodor, G.E.; Naegeli, D.W.; Kohl, K.B.; Cuellar, J.P., Jr., Interim Report BFLRF No. 199, AD A163590, Belvoir Fuels and Lubricants Research Facility, Southwest Research Institute, San Antonio, TX, June 1985.
5. Fodor, G.E.; Naegeli, D.W., Proceedings of the 2nd International Conference on Long-Term Storage Stabilities of Liquid Fuels, Southwest Research Institute, San Antonio, TX, 1986, pp. 632-645.
6. Fodor, G.E.; Naegeli, D.W.; Kohl, K.B.; Cuellar, J.P., Jr., Interim Report BFLRF No. 243, AD A189293, Belvoir Fuels and Lubricants Research Facility, Southwest Research Institute, San Antonio, TX, June 1987.
7. Fodor, G.E.; Naegeli, D.W.; Kohl, K.B., "Peroxide Formation in Jet Fuels," Energy & Fuels, 1988, 2, pp. 729-734.
8. Watkins, J.M., Jr.; Mushrush, G.W.; Hazlett, R.N., Prepr. Pap.--Am. Chem. Soc., Div. Fuel Chem. 1967, 32(1), pp. 513-521.
9. Walling, C., Free Radicals in Solution, John Wiley, New York, 1957, Chapter 9.
10. Standard Test Method for Distillate Fuel Storage Stability at 43°C (110°F), ASTM D 4625.
11. Frost, A.A.; Pearson, R.G., Kinetics and Mechanism, Wiley: New York, 1961, pp. 248-251.
12. Hall, J.M.; Hazlett R.N., Results of the Third CRC Cooperative Test Program on Hydroperoxide Potential of Jet Fuels, May 21, 1987.
13. Nixon, A.C., In Autoxidation and Antioxidants, Lundberg, W.O., Ed., Interscience: New York, London, 1962, Chapter 17.
14. Rubio, F.C.; Rodriguez, F.D.; Gonzalez, F.F.; and Jimenez, V.M., Anales de Quimica. Serie A: Quimica Fisica y Quimica Techica., 1980, 76(2), pp. 261-264.
15. Betts, J., Quart. Rev. 1971, 5, pp. 265-288.
16. Szwarc, M.; Buckley, R.P.; Gresser, J., Prepr. Pap.--Am. Chem. Soc., Div. Pet. Chem. 1958, 3(1), pp. 149-159.
17. Korcek, S.; Chenier, J.H.B.; Howard, J.A.; Ingold, K.U., Can. J. Chem. 1972, 50, p. 2285.

Table 1. Model Fuels

Fuel Code	Fuel Type
1	Straight-run, additive-free, salt-dried, clay-treated kerosene
2	Hydrocracked kerosene, alumina treated
3	Hydrocracked kerosene
4	Fuel 3, alumina treated
5	Hydrofined kerosene
6	Hydrocracked kerosene
7	Hydroprocessed kerosene
8	Hydroprocessed kerosene
9	Hydrocracked kerosene
10	Hydrocracked kerosene
11	Dodecane, distilled
12	Ethyl benzene, distilled
13	Tetralin, distilled and alumina treated

Table 2. Mechanism of Hydrocarbon Oxidation

ROOH			=	HO•	+	RO•	(1)
HO•	+	RH	=	R•	+	H_2O	(2)
RO•	+	RH	=	R•	+	ROH	(3)
R•	+	O_2	=	RO_2•			(4)
RO_2•	+	RH	=	R•	+	ROOH	(5)
RO_2•	+	RO_2•	=	Products			(6)

Table 3. Linear Regression Analysis of the Arrhenius Plots Based on $\ln k = \ln A - E_a/RT$

Fuel Code	Period	Range T, °C	E_a kcal/mol	ln A	R^2
1	Unknown	43-120	19.4	23.5	0.963
2	Unknown	43-120	21.6	29.4	0.998
3	Unknown	43-120	29.4	40.3	0.985
4	Unknown	43-120	22.0	30.5	0.998
5	IP	65-120	23.0	30.5	0.999
5	PIP	65-120	21.3	28.8	0.999
6	IP	65-120	21.9	28.2	0.969
6	PIP	65-120	21.5	28.8	0.997
7	IP	43-120	28.4	38.7	0.990
7	PIP	43-120	23.3	32.4	0.988
8	IP	43-120	23.0	30.0	0.994
8	PIP	43-120	23.0	31.9	0.990
9	IP	80-120	22.9	29.3	0.999
9	PIP	80-120	20.7	29.0	0.944
10	IP	80-120	24.4	31.4	0.999
10	PIP	80-120	24.1	32.8	0.984

Notes: IP = Induction Period; PIP = Post-Induction Period.

Table 4. Global Rate Constants for Model Compounds at 80 °C

Compound	Global Rate Constant, $(mol/L)^{1/2}/s \times 10^6$
Dodecane	0.058
Ethyl benzene	3.9
Tetralin	18.3

Figure 1

PEROXIDE FORMATION
DURING 43 °C BOTTLE STORAGE

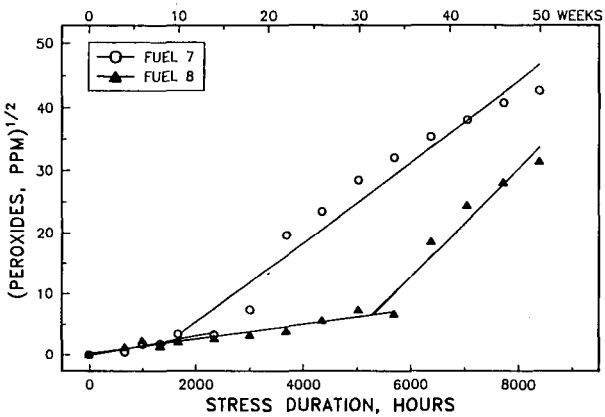

Figure 2

OXIDATION OF FUEL 7
AT 80, 100, AND 120 °C

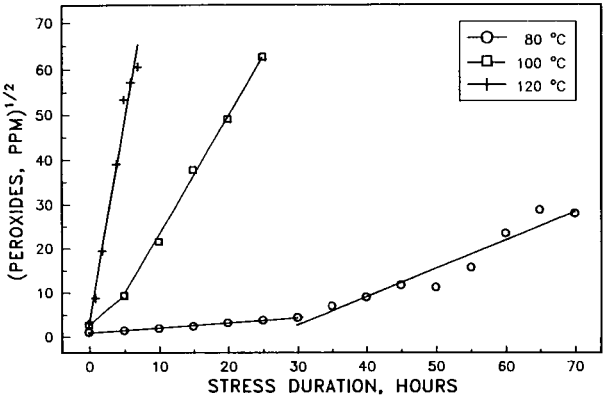

Figure 3

OXIDATION OF FUEL 8
AT 80, 100, AND 120 °C

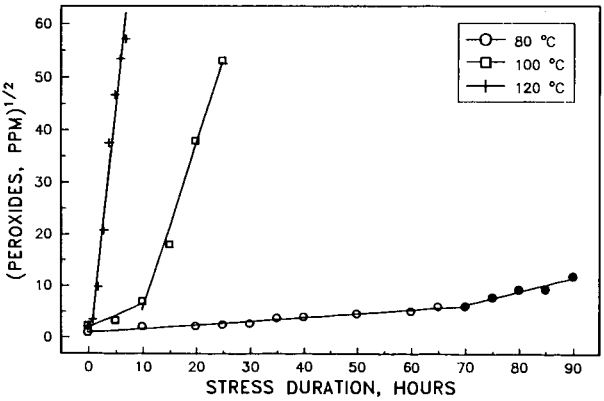

Figure 4

ARRHENIUS PLOT OF OXIDATION
FUELS 7 & 8

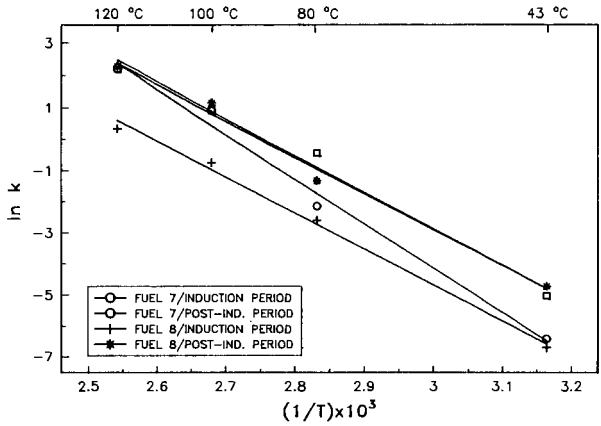

Figure 5

OXIDATION OF FUEL 9
AT 80, 100, AND 120 °C

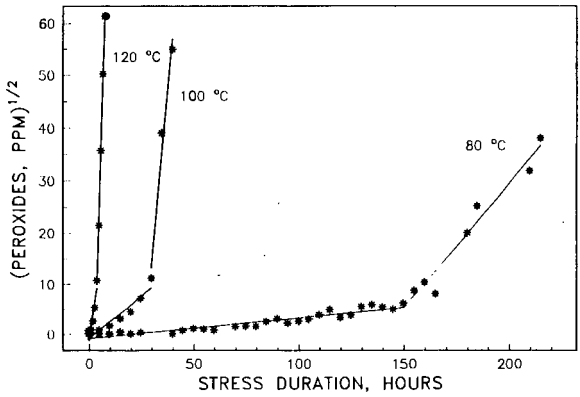

Figure 6

OXIDATION OF FUEL 10
AT 80, 100, AND 120 °C

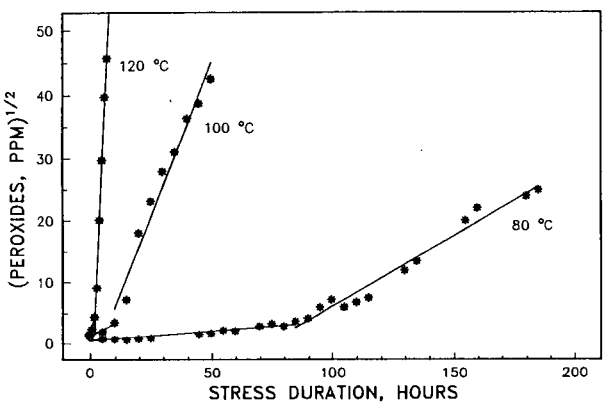

Figure 7

ARRHENIUS PLOT OF OXIDATION
FUELS 9 AND 10

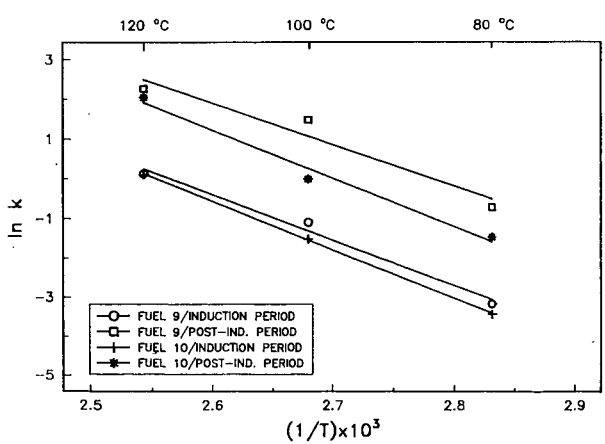

ACCELERATED PEROXIDE FORMATION IN JET FUEL USING CONVENTIONAL AND OXYGEN OVERPRESSURE METHODS

Bruce H. Black
GEO-Centers, Inc., Ft. Washington, MD 20744
Dennis R. Hardy and Erna J. Beal
Navy Technology Center for Safety and Survivability
CODE 6181, Naval Research Laboratory, Washington, DC 20375-5000

INTRODUCTION

In recent years the quality of petroleum feedstocks used by refineries has decreased. This has necessitated the use of more severe refinery processes in order to produce jet fuels of higher thermal stability and cleanliness. Unfortunately, these processes remove species that inhibit the formation of hydroperoxides during storage. As a result the storage stability of some jet fuel products, as measured by hydroperoxide formation, has decreased.

Hydroperoxides in jet fuel have a deleterious effect on elastomers in aircraft fuel systems. (1-3) This problem was first recognized in the early 1960s when an unusually large number of flexible fuel manifold hose failures occurred in aircraft operating in the Far East. (4) To investigate the cause for these failures, a rubber immersion test was developed to distinguish between good and bad fuels. Rubber samples were immersed in jet fuel at 100±1°C and their rate of deterioration, from visual inspection, was recorded. Peroxides, which were known to cause rapid deterioration of elastomers, were monitored during the immersion test. The peroxides in a fuel as received were designated existent peroxides. The peroxides that formed after the fuel was heated to 100°C for 100 hours were designated potential peroxides. In general, as the concentration of potential peroxides in a fuel increased, the failure time for a rubber sample decreased. (4)

During the 1970s and 1980s, additional hydroperoxide induced elastomer failures in aircraft fuel systems occurred. In one instance the failure resulted in the loss of an aircraft. As a result of these failures, a cooperative program was initiated to develop a method to predict a jet fuel's tendency to form hydroperoxides during storage. Six laboratories participated and seven fuels, some of which contained a phenolic antioxidant, were included in the first Coordinating Research Council, Inc., (CRC) cooperative interlaboratory testing (round robin).

A procedure similar to the rubber immersion test was used. Fuel samples were stressed in capped brown borosilicate glass bottles at 100°C for up to 168 hours. The fuel samples were periodically analyzed for hydroperoxide concentration at intermediate intervals by ASTM D3703-78. (5) The results indicated that this procedure had fair repeatability and poor reproducibility. The participants concluded that additional work was needed to achieve better values.

Prior to further developmental work, it was suggested that testing at 100°C may not be indicative of peroxidation at ambient conditions. To verify this possibility, an experiment was performed in which four

fuels from the first round robin were stressed at 43°C, 65°C, and 80°C. Aliquots of the fuels were periodically removed for peroxide analysis. Peroxidation rates at these temperatures were compared to the rates obtained at 100°C in the first interlaboratory round robin.

The fuel samples were, unfortunately, stressed in capped bottles. This limited the amount of oxygen available to the samples. At higher temperatures, 80°C and 100°C for instance, the frequency at which aliquots were removed allowed for more frequent replenishment of atmospheric oxygen. At the lower temperatures where aliquot removal was less frequent, oxygen starvation led to a decrease in the peroxidation rate. This suppression of peroxidation rate in turn led to the erroneous conclusion that peroxidation occurs by a different mechanism at elevated temperatures. In further studies, therefore, the temperature at which fuels were stressed was limited to 65°C.

Two additional interlaboratory round robins were performed. This work culminated in a set of standard test conditions that are useful in research studies. (6) These conditions, however, have serious limitations for fuel quality use. These include the duration, 4 weeks, and the limitation as a Go/No Go (pass/fail) test. The use of a pass/fail criterion does not allow fuels to be ranked relative to each other. Furthermore, under these conditions antioxidant additives cannot be easily or quickly tested for their relative effectiveness. Clearly a more rapid and meaningful test must be developed.

This paper describes experiments that compare fuels stressed at 65°C in capped and vented bottles. Also described is a method for distinguishing between various antioxidant additives using a serial dilution technique.

EXPERIMENTAL

Five fuels were used in this study and included: Three JP-5 blending stocks; coded Fuel #1, #2, and #3; Shale II, a finished JP-5 jet fuel; and n-dodecane. The n-dodecane was treated with silica gel to remove polar species that may have influenced peroxidation rate. This was done by adding 250g of 100-200 mesh activated silica gel to two liters of n-dodecane. The mixture was magnetically stirred for six hours. Two liters of each sample were prefiltered through a pair Gelman type A/E glass fiber filters prior to accelerated aging.

Two sets of each sample were prepared. The first set remained exposed to atmospheric oxygen, and the second set remained tightly capped for the duration of the test. For each anticipated hydroperoxide analysis period, two 125mL brown borosilicate glass bottles each containing a 100mL sample were prepared. The duplicate samples were initially to be analyzed for hydroperoxide concentration in duplicate every two weeks for eight weeks. This was later modified and single samples were analyzed in duplicate for up to twelve weeks. The samples were stressed in an oven at 65°C for the duration of the test.

Phenolic antioxidant experiments were performed using a serial dilution technique. Two pure compounds, 2,6-di-t-butyl-4-methyl phenol (26dtb4mp) and 2,4-di-t-butyl phenol (24dtbp), were used in this study.

Stock solutions were prepared by dissolving 24mg of an additive in 1.0L Fuel #1. This is the maximum concentration allowed in JP-5 jet fuel by MIL-T-5624N. (7) Aliquots of the stock solution were diluted to 100mL, with an appropriate volume of neat Fuel #1, in 125mL brown borosilicate glass bottles. A series of samples for each additive were produced with concentrations between 24.0mg/L and 0.3mg/L.

An entire sample set of either additive, including a 100mL additive-free Fuel #1 aliquot, was simultaneously stressed in a low pressure reactor (LPR) at 100°C and an oxygen overpressure of 793kPa. (8) After 24 hours under these conditions, the samples were removed and analyzed for peroxide concentration.

A Mettler DL20 automatic titrator was used for peroxide determinations. Analyses were performed according to ASTM D3703-85: the Standard Test Method for Peroxide Number of Aviation Turbine Fuels. (5)

RESULTS

The results of accelerated aging at 65°C in capped bottles are shown in Figure 1a. It can be seen that four of the samples approached hydroperoxide concentrations of approximately 90ppm. The fifth sample, Shale II JP-5, continued slow peroxidation for the duration of the test. The results of accelerated aging at 65°C in vented bottles is shown in Figure 1b. It can be seen that three samples, Fuels #1, #2, and #3, produced extremely high concentrations of hydroperoxides under these conditions. In Figure 1c the peroxidation of n-dodecane and Shale II JP-5 in vented bottles is shown with an expanded ordinate.

Comparison of Figures 1a and 1b shows that peroxidation rate in the capped bottles is significantly reduced. This is a result of the limitation of atmospheric oxygen. Although not apparent from these figures, the hydroperoxide concentration in the two sets of fuels significantly differed at two weeks. At four weeks Fuel #3 had the highest hydroperoxide concentration in both sets of fuels. It can be seen, however, that the concentration in the vented sample was nearly eight times that of the capped sample. After four weeks, the hydroperoxide concentration in Fuel #3 continued to increase in the vented bottle. In the capped bottle, however, the concentration of hydroperoxides remained relatively constant. This indicates that oxygen starvation has occurred.

In Figure 1b it can be seen that Fuels #1 and #2 also exhibited a tendency to form high concentrations of hydroperoxides. Both of these fuels undergo a relatively slow rate of peroxidation for six weeks. After six weeks, both fuels rapidly form hydroperoxides. In the vented bottle, Fuel #1 undergoes peroxidation at a linear rate until ten weeks. In the capped bottle, however, Fuel #1 peroxidizes at much slower rate. Unlike Fuel #3, Fuel #1 slowly approaches what appears to be a limit of approximately 100ppm.

Similar characteristics are exhibited by Fuel #2. In the vented bottle this fuel undergoes a rapid rate of peroxidation after six weeks. The peroxide concentration continues to increase for the duration of the test. In the capped bottle, however, Fuel #2

peroxidizes at a much slower rate finally reaching a concentration limit similar to that of Fuels #1 and #3. These results indicate that accelerated aging in capped bottles not only limits the amount of hydroperoxides formed, but reduces the rate at which peroxidation occurs.

Figure 1c shows the rate of peroxidation for n-dodecane and Shale II JP-5 in vented bottles. Both fuels exhibited a relatively slow and linear peroxidation rate. When compared to Figure 1a, it can be seen that Shale II exhibited similar characteristics in capped bottles. The Shale II sample reached a maximum hydroperoxide concentration of 28ppm in the vented bottle. In the capped bottle the maximum concentration formed is approximately 18ppm. In general, the rate of hydroperoxide formation in the capped bottles was approximately 68.6 ± 7.8% of the rate in vented bottles for the Shale fuel. This again shows that accelerated aging in capped bottles reduces peroxidation rate.

The rate of hydroperoxide formation in n-dodecane in capped bottles seemed to exhibit a periodicity. This was much less apparent in the vented samples. The maximum concentration of hydroperoxides formed was similar in both sets of samples. It is expected that after twelve weeks the hydroperoxide concentration in the capped n-dodecane sample would remain constant.

A cursory examination of phenolic antioxidant effects at 100°C and 793kPa oxygen for 24 hours was also performed. It is well known that hindered phenols significantly reduce liquid phase free-radical autoxidation of hydrocarbon fluids. (9-11) The relative effectiveness of these compounds has been shown to be structure dependent. (9) In general, the presence of a t-butyl group in the 2-position or both the 2- and 6-position increases its effectiveness as an antioxidant. The presence of an alkyl group in the 4-position also leads to an increase in its antioxidant properties. If the alkyl group in the 4-position possesses α-branching, such as a t-butyl or an isopropyl group, however, the additive's antioxidant characteristics are diminished. (9)

Figure 2a shows the effect of 26dtb4mp in Fuel #1 using the serial dilution technique. It can be seen that this additive exhibits an antioxidant effect to concentrations as low as 0.3mg/L. Figure 2b shows the effect of 24dtbp in Fuel #1. It can be clearly seen that under these conditions, 24dtbp is a significantly less effective antioxidant than 26dtb4mp as would be expected.

Figure 2c is a side-by-side comparison of the effect of the two additives. This shows that 26dtb4mp is approximately 20 times more effective than 24dtbp at various concentrations, e.g., 0.3mg of 26dtb4mp is as effective as 6.0mg of 24dtbp; 0.6mg of 26dtb4mp is as effective as 12.0mg of 24dtbp, etc. These results show that under these conditions it is possible to evaluate the effect of various antioxidants relative to each other.

SUMMARY

In the past additive-free fuels have been ranked relative to each other by the length of their induction period. This period is

characterized by slow peroxidation until a readily discernible change in rate occurs, i.e., the "breakpoint". Antioxidants have also been compared by their ability to increase the induction period in a particular fuel. Unfortunately at higher temperatures the induction period for additive-free fuels is either minimal or non-existent. This renders its measurement quite subjective. Furthermore, the end of the induction period, or breakpoint, often occurs at hydroperoxide concentrations higher than are allowed by MIL-T-5624N. (7) The use of the breakpoint as a criterion for ranking fuels or additives is, therefore, not appropriate.

The rate at which a fuel approaches the military specification peroxide limit, 8ppm, would be more useful. For example, a fuel with a longer induction period than another fuel is not necessarily better. If the first fuel's induction period rate is greater, it will reach the specification limit sooner. Unfortunately, the use of induction period rate also presents problems. At lower temperatures the induction period for additive-free fuels is long enough to objectively measure an induction period rate. At higher temperatures, 100°C and 120°C for instance, the induction period rate measurement, like its length, is too subjective.

If more objective measurements of induction period rates are desired, it is necessary to remove and titrate samples for hydroperoxide concentration at very frequent intervals. At 100°C and 120°C, it may be necessary to analyze fuel samples every 30 minutes, or less. For additive-free fuels, or fuel samples obtained from field activities, these labor intensive induction period rate measurements are necessary.

For antioxidant evaluations, the use of the serial dilution technique has advantages over induction period rate and length measurements. First, it is not a subjective test. All samples of a particular fuel and additive combination are stressed under exactly the same conditions. The technique is not concerned with either the length or rate of the induction period. It simply compares the concentration effect of various antioxidants on peroxidation in a given fuel. Second, the technique is far less labor intensive. These advantages make this technique useful for further antioxidant evaluations.

REFERENCES

1. Shertzer, R.H.; "Aircraft Systems Fleet Support/Organic Peroxides in JP-5 Investigation," Final Report NAPC-LR-78-20, Naval Air Propulsion Center, Trenton, NJ, 27 September 1978.

2. Hazlett, R.N., Hall, J.M., Nowack, C.J., Turner, L.; "Hydroperoxide Formation in Jet Fuels," Proceedings of the Conference on Long Term Stabilities of Liquid Fuels; Israel Institute of Petroleum and Energy, Tel Aviv, Israel, December 1983, pp. B132-B148.

3. Nadler, C.; "Effect of Oxidizing Fuels on Aircraft Fuel System Elastomers and Sealants," Final Report NADC-80076-60, Naval Air Development Center, Warminster, PA, 20 May 1980.

4. Smith, M.; "Aviation Fuels," G.T. Foulis & Co. Ltd., Henley-on-Thames, Oxfordshire, UK, 1970.

5. Standard Test Method for Peroxide Number of Aviation Turbine Fuels; ASTM D3703-85; American Society for Testing and Materials; Philadelphia, PA, 1989.

6. Hall, J.M., Hazlett, R.N.; "Results of the Third CRC Cooperative Test Program on Hydroperoxide Potential of Jet Fuels," NRL Memorandum Report 5985, Naval Research Laboratory, Washington, DC, 21 May 1987.

7. Military Specification, MIL-T-5624N, "Turbine Fuel, Aviation, Grades JP-4, JP-5 and JP-5/JP-8 ST," ASD/ENES, Wright-Patterson AFB, OH, 10 February 1989.

8. Hardy, D.R., Hazlett, R.N., Beal, E.J., Burnett, J.C.; Energy & Fuels **1989**, 3, 20-24.

9. Scott, G.; "Atmospheric Oxidation and Antioxidants," Elsevier Publishing Company, New York, NY, 1965.

10. Bamford, C.H., Tipper, C.F.H., Eds.; "Chemical Kinetics," Volume 16: Liquid-Phase Oxidation; Elsevier Scientific Publishing Company, New York, NY, 1980.

11. Pospisil, J., Klemchuk, P.P., Eds.; "Oxidation Inhibition in Organic Materials," Volume 2; CRC Press, Inc., Boca Raton, FL, 1990.

ACCELERATED PEROXIDE FORMATION
12 Wks @ 65C & Atm. Air (Capped Bottle)

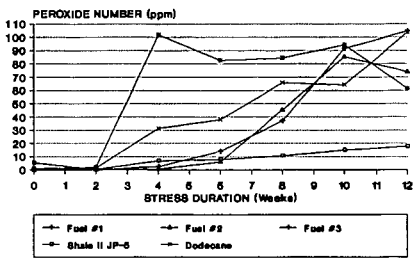

FIGURE 1a

ACCELERATED PEROXIDE FORMATION
12 Wks @ 65C & Atm. Air (Vented Bottle)

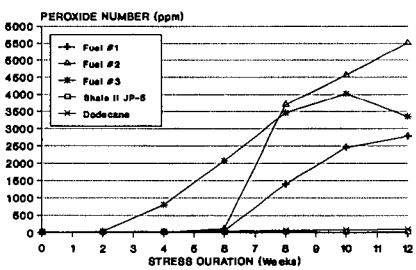

FIGURE 1b

ACCELERATED PEROXIDE FORMATION
12 Wks @ 65C & Atm. Air (Vented Bottle)

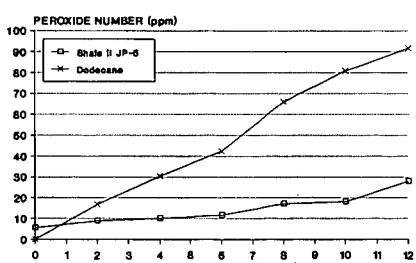

FIGURE 1c

2,6-di-t-Butyl-4-Methyl Phenol
LPR @ 100C & 793kPa Oxygen

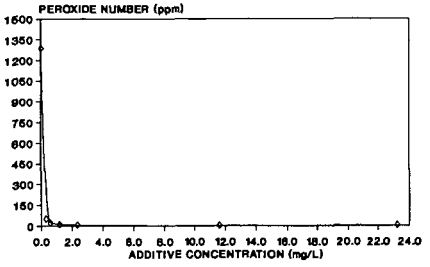

FIGURE 2a

2,4-di-t-Butyl Phenol
LPR @ 100C & 793kPa Oxygen

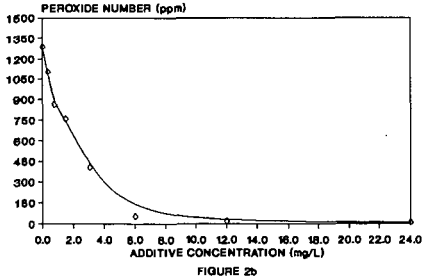

FIGURE 2b

PHENOLIC ANTIOXIDANT EFFECT
LPR @ 100C & 793kPa Oxygen

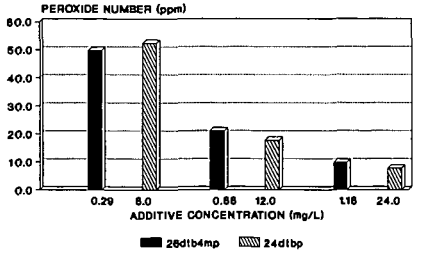

FIGURE 2c

SYMPOSIUM ON STABILITY AND OXIDATION OF MIDDLE-DISTILLATE FUELS
PRESENTED BEFORE THE DIVISION OF PETROLEUM CHEMISTRY, INC.
AND
THE DIVISION OF FUEL CHEMISTRY
AMERICAN CHEMICAL SOCIETY
WASHINGTON, D.C. MEETING, AUGUST 26-31, 1990

ANALYSIS OF SOLIDS FORMED DURING THERMAL- AND STORAGE-STABILITY TESTING OF JET FUELS DERIVED FROM PETROLEUM AND FROM COAL

By

R. D. Grigsby, G. P. Sturm, Jr., J. W. Goetzinger,
J. B. Green, and R. P. Anderson

IIT Research Institute
National Institute for Petroleum and Energy Research,
P.O. Box 2128, Bartlesville, OK 74005

INTRODUCTION

Recently, the Department of Energy and the Air Force began a program to investigate the production of jet fuel and other commercial products from the gasification of lignite at the Great Plains Gasification Plant (GPGP), Beulah, North Dakota. This project was undertaken to increase the economic viability of the plant and, at the same time, to create a reliable source of jet fuel for Air Force bases in the northern great plains area (1). In cooperation with DOE and the Air Force, the National Institute for Petroleum and Energy Research (NIPER), has investigated the thermal and storage stability properties of a JP-8 jet fuel produced from GPGP liquid by-products and compared these properties with those of a conventional JP-8 fuel derived from petroleum.

Several decades of investigations on fuel stability have increased our knowledge of the chemistry involved in fuel degradation. Most of these studies have been focused on trace heteroatomic components in fuels (2-16). In the past, ambient storage stability and high temperature thermal stability have been viewed as two separate issues, especially when trace contaminants have been considered. However, our recent findings on petroleum-derived jet fuels indicate that hydrocarbons in neutral fractions from relatively clean fuels are susceptible to oxidative degradation at high temperatures and under ambient storage conditions (10).

Hydrocarbon types that seem to be emerging as important in fuel degradation are the cycloalkylaromatics, such as indans and tetralins (11). These types are abundant in many coal liquids, including the hydrotreated tar-oil distillates from GPGP. In this respect, determination of the thermal and storage stabilities of jet fuel produced from lignite or coal is significant.

Perhaps the most undesirable consequence of fuel degradation is the formation of solids. Thus, a logical approach in studying degradation is to investigate the compositions of the solids formed under ambient storage conditions and at high temperatures to which the fuel might be subjected in a turbine engine. We have used separation procedures and identification methods, particularly HPLC and mass spectrometry, to analyze solids formed under simulated-storage and high-temperature conditions (11,17-21). Two fuels were studied in the present investigation: a coal-derived fuel and a conventional fuel from petroleum. A comparison of results from these two fuels is reported.

EXPERIMENTAL

The two fuels studied were a JP-8 (NIPER No. 2987) produced from GPGP liquid by-products (No. 89-WEH-157) and a petroleum-derived reference JP-8 (NIPER No. 2955).

The storage stability of both fuels was determined by two different methods. In the first, samples were aged at 80° C under 100 psig oxygen for 1, 2, 3, and 4 weeks. In the second, aging was performed by ASTM method D 2274, in which oxygen was bubbled through the samples for 16 and 40 hours at 95° C.

The sediment produced by aging the coal-derived fuel at 80° C was characterized by separation into six fractions using an HPLC acid-fractionation method developed at NIPER in other investigations (17,18). Compound types were separated into fractions of increasing acidity.

Both fuels were subjected to thermal-stability testing in a jet fuel thermal oxidation tester (ALCOR, Inc., San Antonio, TX) using ASTM method D 3241 (JFTOT test). Breakpoints were also determined for each fuel. The fuels were then stressed for extended periods of time at 10° C above the breakpoint to generate sufficient solids on the heated tube and on a downstream filter to permit mass-spectral analysis (20,21).

For extended runs, the fuel-flow system of the JFTOT apparatus was modified so that the fuel passed from the heated test section through a 25 mm diameter membrane filter to a variable-speed pump and then to a spent-fuel reservoir. A fuel-flow rate of 1 mL/min was used (20,21).

In the first extended test with the 2955 reference fuel, a nylon filter with a pore size of 0.45 μm was used to collect the filterable solids. The tube temperature was 280° C. After seven hours, the filter plugged and the experiment was stopped. For the second extended run with the same fuel, a glass-fiber filter, type GF/F, with a 0.7 μm pore size was used. A ten-hour run gave no detectable plugging. However, when the apparatus was disassembled, the filter was found to be partially disintegrated. In the extended JFTOT run with the coal-derived fuel (2987), the tube temperature was 310° C. A nylon filter with a pore size of 0.45 μm was used, and after 17 hours it became plugged. The JFTOT tubes and filters from the experiments with both fuels were saved for analysis by mass spectrometry.

The mass-spectrometric method used in the analyses of the JFTOT tube deposits and filterable sediments was developed previously as part of a similar investigation on fuel stability (19,20). Probe microdistilllation/mass spectrometry (PMD/MS) was used to provide high resolution mass spectra of the solids, and the data were analyzed to produce curves of ion intensity vs. temperature or time (elimination curves) for ions identified with specific elemental formulas (19).

Deposits on the JFTOT tubes were sampled by machining their surfaces in a lathe using a cleaned tool bit (20). Turnings containing each deposit were then placed in a temperature-programmed quartz probe for introduction under PMD/MS conditions into a Kratos MS-50 high resolution mass spectrometer (Kratos Analytical Instruments, Manchester, U.K.). Probe temperature was increased linearly at 10° C/min. Twenty to thirty spectra were recorded at a resolving power of 10,000 to 20,000 over a temperature range from ambient to greater than 400° C. Seventy eV electron impact was used for ionization to maximize the signal-to-noise ratio on mass-spectral peaks being formed from a limited amount of sample. Mass spectra were not recorded below m/z 70.

Sediments on the filters used with the JFTOT apparatus were sampled by cutting small filter strips for introduction by probe into the mass spectrometer (20). Using this approach, spectra of the filterable sediments were recorded under the same conditions as given for the tube deposits, except that 25 eV electron impact was used for ionization of the sediment from fuel 2955. The lower-energy ionization was selected to suppress intensities of fragment-ion peaks, but this method did not appear to offer any advantage over 70 eV electron impact and was not used with the other samples. To avoid thermal decomposition of the nylon filter used with fuel 2987, the probe temperature was limited to approximately 300° C.

RESULTS AND DISCUSSION

Initial Fuel Characterization. Results from the initial characterization of both fuels are shown in Table I. The coal-derived fuel (No. 2987) showed a very slight color that may have been caused by suspended clay. This also explains the relatively long filtration time for the fuel. Both fuels easily met the viscosity specification, and both passed the simulated distillation test (results not shown), except for slightly exceeding the maximum value for the endpoint temperature. The simulated distillation also showed that the coal-derived fuel contained more low-boiling components than the reference fuel. No peroxides were detected in the reference, but the coal-derived fuel showed a trace (0.5 ppm).

Storage Stability. Table II summarizes results from the storage stability experiments. The coal-derived fuel (2987) showed lower sediment formation through three weeks of storage at 80° C under 100 psig oxygen. However, the peroxide content in 2987 was consistently higher than in the reference fuel (2955) and reached a maximum at approximately three weeks. Between three and four weeks, the coal-derived fuel deteriorated significantly. A large quantity of sediment was formed and the fuel darkened. After three weeks, the peroxide content in 2987 decreased somewhat, as has been observed in storage-stability testing with other fuels.

The oxidation-stability test (ASTM D 2274) on the two fuels gave similar results (not shown) to those obtained from the storage stability test. Through 40 hours, the coal-derived fuel showed less sediment formation and color than the reference fuel. Peroxide values were somewhat higher in the coal-derived fuel.

Fractionation by HPLC of Sediment Formed During Storage-Stability Testing of Coal-derived Fuel. The sediment produced by aging the coal-derived fuel for four weeks at 80° C under 100 psig oxygen was characterized by separation into six fractions using an HPLC acid-fractionation method (17,18). Yields of the fractions, which are separated according to increasing acidity, are given in Table III along with compound types typically present in each fraction. Any neutral or basic compounds would be expected in fraction 1 together with very weak acids. The relatively low recovery of 78.74% is attributed to loss of material in the work-up of fraction 6 and possible retention of very polar substances on the HPLC column. The yield data show that the bulk of the sediment was separated into fractions 5 and 6, which typically contain carboxylic acids and difunctional acids, respectively.

Thermal Stability. Results from the JFTOT test (ASTM D 3241) of the reference fuel (2955) and coal-derived fuel (2987) are given in Table IV. Both fuels easily met the specifications. Fuel 2987 was stable to a higher temperature than fuel 2955, as determined by the breakpoint temperatures of 295° C and 275° C, respectively.

Mass-Spectral Analysis of JFTOT Tube Deposits and Filterable Sediments. To make a reasonable comparison of results obtained from a large amount of mass-spectral data, abbreviation in tabulated form is used to discuss compound types identified in the solids formed during fuel degradation. Each table lists ions detected in homologous series corresponding to a particular elemental formula. For example, ions arising from hydrocarbons are classified as having C_nH_{2n+z} formulas where Z ranges from +2 to -23. Thus, molecular ions for alkylbenzenes (C_nH_{2n-6}) are listed under a Z number of -6. Major fragment ions are given along with molecular ions. These occur in series having a Z number one less than the number for molecular ions. For alkylbenzenes, fragment ions thus occur in the C_nH_{2n-7} series (Z number of -7). No ion intensities are given, but the prominence of homologues in a particular series can be estimated from the number of molecular and fragment ions detected for the series. The molecular mass of the first member of a series is identified with the parent compound, e.g., 78 with benzene in the alkylbenzene series. If the first ion detected in a molecular-ion series has a mass less than the mass listed for the parent compound, the ion may arise by rearrangement or it may belong to a series for another type not identified. In either case, the fact that the ion cannot be a molecular ion in the listed series is mentioned in a footnote to the table.

It is necessary to emphasize that names of compound types given in the first column of the tables are intended to be suggestions only. Undoubtedly, many of the ions having the specified elemental formulas do arise from the type indicated; however, others may originate from types not identified. In the discussion that follows, names are restricted to those given in the tables with the understanding that ions in the series can originate from other compound types, as well.

Analysis of Filterable Sediment and Tube Deposit from Coal-Derived Fuel. Numerous compound types were detected in the solids formed during thermal stressing of the jet fuel from coal, including those containing only carbon and hydrogen as well as heteroatomic types containing oxygen and nitrogen. Only traces of compounds containing sulfur were found.

In Table V identification of hydrocarbons in the filterable sediment and tube deposit is presented for the thermal degradation of fuel 2987. A broad range of aliphatic and alicyclic compound types was found in both solids. No molecular ions for alkanes were identified (nor were they expected), but fragment ions corresponding to alkyl groups were found over a mass range extending to m/z 155 in the spectra from the sediment and to m/z 183 in the spectra from the tube deposit. These fragments may have arisen from alkanes or from other compound types having alkyl side chains. Numerous molecular and fragment ions were recorded for olefins, dienes, cycloalkanes, cycloalkenes, and bicycloalkanes. These compound types were distributed rather uniformly between the tube deposit and the filterable sediment. For example, molecular ions for dienes, cycloalkenes, and bicycloalkanes were detected from m/z 68 to m/z 194 in the spectra from both solids. The ions appeared in the spectra over a broad range of probe temperatures, indicating that they arose from surface desorption and by covalent bond rupture, i.e., by pyrolysis.

Many molecular and fragment ions from aromatic hydrocarbons were detected in the spectra from the filterable sediment and tube deposit. Alkylbenzene homologues were identified in the sediment to 190 amu and in the tube deposit to 162 amu. Indans and tetralins were found in both solids with molecular masses extending to 188 amu. Aromatics with a greater degree of unsaturation were evident in both sets of spectra. Six members of the naphthalene series (Z number of -12) were identified in the sediment spectra and five members in the spectra from the tube deposit. The most highly aromatic types identified in either set of spectra were the fluoranthenes and pyrenes (Z number of -22). One member of the series, the parent compound at m/z 202, was identified in the spectra of the sediment, and three members (m/z 202, 216, and 244) were found in the tube-deposit spectra.

A number of molecular and fragment ions containing one oxygen were identified in the spectra from the filterable sediment and tube deposit. These are seen in Table VI. Molecular ions for aliphatic and alicyclic types (e.g., tetrahydrofurans) were almost nonexistent in the spectra, and they were not expected based on the known fragmentation of these compounds. However, a number of fragment ions for aliphatic and alicyclic oxygen-containing types were detected, as noted in the table.

Aromatics containing one oxygen were readily detected in both sets of spectra. Several phenols were identified, as well as a number of more unsaturated types, including naphthols and dibenzofurans. Compounds with a greater degree of unsaturation appeared to be partitioned more toward the filterable sediment than toward the tube deposit. As an illustration, four fluorenones and phenalenones (parent mass of 180) were detected in the sediment, but none were found in the tube deposit.

Compound types containing two oxygens were identified in the spectra of the filterable sediment and tube deposit, including nonaromatic and aromatic carboxylic acids and dihydroxyaromatics (results not shown). The aromatics were decidedly partitioned more toward the sediment. For example, six benzoic acids and benzodioxoles were found in the spectra of the sediment ranging from the parent compound (m/z 122) to homologues having five alkyl carbons attached (m/z 192). On the other hand, in the spectra of the tube deposit only one fragment ion attributable to these compound types was detected (m/z 149). Although molecular ions containing two oxygens were detected in Z series as negative as -18 in the spectra of the sediment, no molecular ions in series more negative than -4 were detected in the tube-deposit spectra.

Table VII shows ions detected in homologous series for compounds containing three oxygens. Because of the more complex nature of these types, names are omitted except to note that the ions are attributable to multifunctional compounds. Phthalates are indicated by m/z 149 in the -11 Z series. These compounds, especially dioctylphthalate, are common artifacts seen in mass spectra.

A very prominent peak appeared in the spectra of the tube deposit at m/z 129, corresponding to a fragment ion of elemental formula $C_6H_9O_3$. It must have arisen from a nonaromatic oxygen-containing compound, such as an alcohol, ether, or peroxide. None of these compound types would produce a significant molecular ion. At first glance, m/z 129 might appear to have an elemental formula of C_9H_7N, corresponding to quinoline or isoquinoline. However, the accurately measured mass of the peak was consistently closer to the value expected for the CHO_3 combination (129.0552) than for the CHN combination (129.0578). Therefore, a formula of C_9H_7N was ruled out. The $C_6H_9O_3$ ion at m/z 129 was much weaker in the spectra of the filterable sediment, showing that the corresponding compound(s) was strongly partitioned toward the tube deposit.

Except for compound(s) producing the m/z 129 peak, types containing three oxygens were partitioned more toward the sediment than toward the tube deposit. This is evident from the larger number of molecular and fragment ions found for the sediment as compared with the number found for the tube deposit. The difference is not easily explainable, but it may result from the relatively low thermal stability of compounds containing alcohol or ether groups; that is, these compounds may have appeared in smaller quantities in the tube deposit because they may have been thermally decomposed on the hot metallic surface of the tube.

A number of compounds containing one nitrogen were identified in the filterable sediment, but only a few were found in the tube deposit, as seen by comparing results in Table VIII. The difference may have been a consequence of thermal decomposition of nitrogenous compounds on the hot tube surface. Compound types prominent in the spectra of the filterable sediment included pyrrolines (molecular ions from m/z 69 to 125 and 153) and aromatic types such as pyridines (or anilines), showing molecular ions from m/z 79 to m/z 149. Indolines, indoles, and quinolines (or isoquinolines) were abundant, as indicated by the number of molecular and fragment ions detected in homologous series for these types.

Analysis of Filterable Sediment and Tube Deposit from Petroleum-derived Fuel. In spite of the different origins of fuel 2987 (coal liquid) and fuel 2955 (petroleum), mass-spectral analyses of solids formed by thermally stressing the two fuels produced surprisingly similar results. Therefore, discussion of the compositions of the filterable sediment and tube deposit from fuel 2955 is limited mainly to differences found between the solids formed from the two fuels.

Numerous hydrocarbons were identified in the filterable sediment and tube deposit from fuel 2955. When these were compared with hydrocarbons from fuel 2987, it became evident that the compositions of the hydrocarbons in the solids from the two fuels were very similar. This observation suggests that the same hydrocarbons were contributing to the formation of the solids in both fuels.

Compound types having one oxygen were identified in the filterable sediment and tube deposit from fuel 2955. When compared with the same types identified in the solids from fuel 2987, only slight differences were seen that may not be significant. For example, only one dibenzofuran (mass 196) was detected in the sediment from fuel 2955, but in the sediment from fuel 2987 four homologues were found (masses 168 to 210), as noted in Table VI. Several fluorenones and phenalenones were detected in the tube deposit from fuel 2955 but not in the sediment from the same fuel. The opposite was found for fuel 2987, i.e., fluorenones and phenalenones were detected in the sediment but not in the tube deposit (Table VI).

Fewer compounds containing two oxygens were found in the filterable sediment from fuel 2955 than in the sediment from fuel 2987. Differences were particularly evident for the more unsaturated species. No types with Z numbers more negative than -12 (coumarins and dihydroxynaphthalenes) were detected in the 2955 sediment, whereas in the sediment from fuel 2987, types with Z numbers as negative as -18 were identified (biphenylene carboxylic acids and hydroxyfluorenones). In contrast, by comparing results from the two tube deposits, it was evident that more types containing two oxygens, especially aromatics, were detected in the tube deposit from fuel 2955 than in the 2987 deposit.

A very similar distribution of compound types containing three oxygens was found between the filterable sediments from the two fuels as well as between their tube deposits. As mentioned previously, a very strong m/z 129 peak of elemental formula $C_6H_9O_3$ was found in the spectra of the tube deposit from fuel 2987 (Table VII). This same peak was present in the spectra of the 2955 tube deposit although its intensity was not as strong as in the 2987 spectra. The $C_6H_9O_3$ ion was also detected in the spectra of the filterable sediment from fuel 2955; however, its intensity was much weaker than in the spectra of the tube deposit from the same fuel.

Ions containing one nitrogen were identified in the spectra of the filterable sediment and tube deposit from fuel 2955. The corresponding compound types were seen to be distributed more toward the sediment than toward the tube deposit. This same observation was noted in the discussion of solids formed during thermal stressing of fuel 2987 (Table VIII). Although the compositions with respect to nitrogen-containing compounds were similar in the sediments from the two fuels, fewer highly aromatic types were detected in the spectra of the sediment from fuel 2955. For example, only one homologue

for acridines and phenanthridines (mass 193) was identified in the 2955 spectra, but three were found in the spectra of the 2987 sediment (masses 179, 193, and 221), as noted in Table VIII. A few nitrogen-containing species were detected in the tube deposit from fuel 2955 as compared to virtually none in the spectra of the 2987 deposit (Table VIII). In this respect, several quinolines (or isoquinolines) were identified in the tube deposit from fuel 2955, but the presence of this compound type in the 2987 deposit was doubtful.

SUMMARY AND CONCLUSIONS

Storage and thermal stabilities of a JP-8 fuel produced from GPGP liquid by-products were compared with those of a conventional petroleum-derived JP-8 fuel. Initial characterization and simulated distillation of the two fuels showed that the coal-derived fuel contained more lower-boiling components, a longer filtration time, and a higher particulate content than the petroleum-derived fuel. Also, the coal-derived fuel possessed a slight color. Nevertheless, for the most part both fuels met JP-8 specifications.

Both fuels exhibited good oxidation stability through 40 hours of aging according to ASTM D 2274, with the coal-derived fuel showing less sediment and color formation but somewhat higher peroxide content than the petroleum-derived fuel. Storage stability (aging at 80° C under 100 psig oxygen) gave approximately the same results for both fuels through three weeks of aging. However, between the third and fourth week, the coal-derived fuel deteriorated rapidly and exceeded the petroleum fuel in sediment and color formation as well as peroxide content.

Fractionation of the 80° C aged sediment from the coal-derived fuel by HPLC indicated that the sediment was composed primarily of carboxylic acids and difunctional acids.

Both fuels easily met thermal-stability specifications with the coal-derived fuel showing a higher breakpoint temperature than the petroleum-derived fuel.

Mass spectra of the filterable sediments and JFTOT-tube deposits formed during thermal stressing of the coal-derived and petroleum-derived fuels were remarkably similar, indicating that the same compound types were responsible for solids formation in both fuels.

When spectra of the filterable sediment from either fuel were compared with those of the tube deposit from the same fuel, a number of similarities were found as well as some significant differences. Both sets of spectra showed molecular- and fragment-ion peaks for aromatic and nonaromatic hydrocarbons and for compounds containing one to three oxygens. Strong peaks were observed in the spectra of the filterable sediment corresponding to aromatic compounds containing one nitrogen. These peaks were much weaker or absent in the spectra from the tube deposit. No spectra of the sediment or tube deposit from either fuel showed more than traces of sulfur-containing compounds.

An intense, nonaromatic fragment ion containing three oxygens was identified in the spectra the tube deposits from both fuels. This ion was also found in the spectra of the filterable sediments from both fuels although its intensity was much weaker. The ion could not be correlated with a

molecular ion from any particular compound type, but it may have originated from an alcohol, ether, or some other type that does not produce a significant molecular ion.

Although structural information obtained through mass-spectral analysis of solids formed during thermal-stressing experiments has not specifically identified precursors responsible for solids formation in either fuel, the results demonstrate the value of the method for identifying compound types associated with fuel degradation under conditions of high temperature, such as those encountered in turbine engines.

ACKNOWLEDGMENTS

Appreciation is expressed to F. L. Tilley, S. K-T. Yu, and M. White for technical assistance. This work was supported by the U.S. Department of Energy under Contract DE-FC22-83FE60149 and by the Pittsburgh Energy Technology Center through Military Interdepartmental Purchase Request FY1455-86-N0657.

LITERATURE CITED

(1) Farlong, M., Fox, J., and Masin, J., AFWAL-TR-87-2042, Vol. IX, "Production of Jet Fuels from Coal-Derived Liquids, Results of Bench-Scale and Pilot-Plant Testing," AMOCO Oil Company, Naperville, IL, June, 1989.

(2) Whisman, M. L., Cotton, F. O., Goetzinger, J. W., and Ward, C. C., "Radiotracer Study of Turbine Aircraft Fuel Stability," Bureau of Mines Report of Investigation 7493, Bartlesville, OK, March, 1971.

(3) Goetzinger, J. W., Thompson, C. J., and Brinkman, D. W., "A Review of Storage Stability Characteristics of Hydrocarbon Fuels, 1952-1982," Report No. DOE/BETC/IC-83/3, Bartlesville Energy Technology Center, Bartlesville, OK, October, 1983.

(4) Loeffler, M. C. and Li, N. C., Fuel, 64, 1047-1053 (1985).

(5) Smith, R. O., Udseth, H. R., and Hazlett, R. N., Fuel, 64, 810-815 (1985).

(6) Mayo, F. R. and Lan, B. Y., Ind. Eng. Chem. Prod. Res. Div., 25, 333-348 (1986).

(7) Taylor, W. F. and Frankenfeld, J. W., Proceedings, 2nd International Conference on Long-Term Storage Stabilities of Liquid Fuels, ed. by L. L. Stavinoha, Southwest Research Institute, San Antonio, TX, 1986, pp. 496-511.

(8) Malhotra, R. and St. John, G. A., Proceedings, 2nd International Conference on Long-Term Storage Stabilities of Liquid Fuels, ed. by L. L. Stavinoha, Southwest Research Institute, San Antonio, TX, 1986, pp. 327-335.

(9) Wright, B. W., Kalinoski, H. T., Udseth, H. R., and Smith, R. D., Proceedings, 2nd International Conference on Long-Term Storage Stabilities of Liquid Fuels, ed. by L. L. Stavinoha, Southwest Research Institute, San Antonio, TX, 1986, pp. 526-539.

(10) Bhan, O. K., Brinkman, D. W., Green, J. B., and Carley, B., Fuel, 66, 1200-1214 (1987).

(11) Sutterfield, F. D., Brinkman, D. W., Bhan, O. K., Green, J. B., Goetzinger, J. W., Sturm, G. P., Jr., Speck, G., and Turner, L., Proceedings, 3rd International Conference on Stability and Handling of Liquid Fuels, ed. by R. W. Hiley, R. E. Penfold, and J. F. Pedley, The Institute of Petroleum, London, U.K., 1988, pp. 321-337.

(12) Brinkman, D. W., Bhan, O. K., Green, J. B., Goetzinger, J. W., Grigsby, R. D., and Kamin, R., Proceedings, 3rd International Conference on Stability and Handling of Liquid Fuels, ed. by R. W. Hiley, R. E. Penfold, and J. F. Pedley, The Institute of Petroleum, London, U.K., 1988, pp. 796-807.

(13) Mayo, F. R., Stavinoha, L. L., and Lee, G. H., Ind. Eng. Chem. Res., 27, 362-363 (1988).

(14) Reddy, K. T., Cernansky, N. P., and Cohen, R. S., Energy & Fuels, 2, 205-213 (1988).

(15) Bhan, O. K., Tang, S. Y., Brinkman, D. W., and Carley, B., Fuel, 67, 227-237 (1988).

(16) Pedley, J. F., Hiley, R. W., and Hancock, R. A., Fuel, 67, 1124-1130 (1988).

(17) Green, J. B., J. Chromatogr., 358, 53-75 (1986).

(18) Green, J. B., Yu, S. K-T., Green, J. A., Doughty, D. A., Vogh, J. W., Grigsby, R. D., Chapter 3 in "Analysis of Heavy Oils: Method Development and Application to Cerro Negro Heavy Petroleum, Final Report," NIPER-452 (Vol. 1) (DE90000200). IIT Research Institute, National Institute for Petroleum and Energy Research, Bartlesville, OK, December, 1989.

(19) Schronk, L. R., Grigsby, R. D., and Scheppele, S. E., Anal. Chem., 54, 748-755 (1982).

(20) Grigsby, R. D., Sturm, G. P., Jr., Green, J. B., Goetzinger, J. W., and Kamin, R. A., PREPRINTS, Div. of Petrol. Chem., ACS, 34 (4), 825-831 (1989).

(21) Sturm, G. P., Jr., Grigsby, R. D., Goetzinger, J. W., Green, J. B., and Anderson, R. P., AFWAL-TR-87-2042, Vol. XIII, "Production of Jet Fuels from Coal-Derived Liquids, Evaluation of Storage and Thermal Stability of Jet Fuels Derived from Coal Liquids," IIT Research Institute, National Institute for Petroleum and Energy Research, Bartlesville, OK, May, 1990.

TABLE I

INITIAL CHARACTERIZATION OF JP-8 FUELS DERIVED FROM PETROLEUM (2955) AND COAL (2987)

Property	Method	Fuel 2955	Fuel 2987	Specification maximum
Color, Saybolt	D 156	+29	+14	---
Viscosity, -20 oC, cSt	D 445	4.8	4.4	8.0
Particulate, mg/mL	D 2276	0.26	1.2	1.0
Filtration time, min.	MIL-T-83133B, Appendix A	6.5	28	15
Peroxide, ppm	D 3703	0	0.5	---

TABLE II

STORAGE-STABILITY RESULTS FOR PETROLEUM-DERIVED FUEL (2955) AND COAL-DERIVED FUEL (2987)

Aging Time	1 week		2 weeks		3 weeks		4 weeks	
Fuel	2955	2987	2955	2987	2955	2987	2955	2987
Property								
Filterable sediment, mg/100 mL	0.8	0.3	1.3	0.5	1.5	1.0	2.7	9.1
Adherent sediment, mg/100 mL	0.5	0.2	0.5	0.1	0.6	0.7	1.1	398
Total sediment, mg/100 mL	1.3	0.5	1.8	0.6	2.1	1.7	3.8	407
Peroxide, ppm (D 3703)	3.5	9.5	6.6	39.0	8.9	757	12.8	334
Color (D 1500)	L1.0	L0.5	L1.0	L0.5	L1.0	L0.5	L1.0	2.5

TABLE III

SEPARATION OF SEDIMENT FROM COAL-DERIVED FUEL (2987) BY HPLC. YIELDS AND TYPICAL COMPOSITIONS.

Fraction	Yield, wt%	Typical composition
1	0.77	very weak acids, polynuclear aromatic hydrocarbons
2	1.21	2-3 ring pyrrolic benzologs
3	1.21	4-5 ring pyrrolic benzologs and hindered hydroxyaromatics
4	7.84	hydroxyaromatics
5	13.03	carboxylic acids
6	54.68	difunctional acids
Recovery	78.74	

TABLE IV

THERMAL STABILITY RESULTS (ASTM D 3241) FOR PETROLEUM-DERIVED FUEL (2955) AND COAL-DERIVED FUEL (2987)

Property	Fuel		Specification maximum
	2955	2987	
Tube deposit rating at tube temp. of 260° C	1	1	3
Pressure drop, mm HG	0	0	25
Breakpoint, °C	275	295	---

TABLE V

MASS-SPECTROMETRIC ANALYSIS OF FILTERABLE SEDIMENT AND TUBE DEPOSIT FROM THERMALLY STRESSED FUEL 2987. IDENTIFICATION OF HYDROCARBONS.

Suggested origin[1]	Elemental composition: C_nH_{2n+z}	Homologous ions detected Filter	Tube
	z = +2	---	---
	+1	71-155	71-183
Olefins, cycloalkanes (70)	0	70-140[2]	70-140,168[2]
	-1	69-167	69-153
Dienes, cycloalkenes (68), bicycloalkanes	-2	68-194	68-194
	-3	81-207	81-179
Cyclic dienes (66), tricycloalkanes	-4	80-178	80-192
	-5	79-191	79-205
Alkylbenzenes (78)	-6	92,106,134, 148,176,190	78-162
	-7	77-189	77-203
Indans (118), tetralins	-8	76-188[3]	76-188[3]
	-9	75-173	75-187
Indenes (116), dihydronaphthalenes	-10	74-200[3]	74-186[3]
	-11	73-157	87-185,213
Naphthalenes (128)	-12	114-142 170-212[3]	114-184[3]
	-13	113-211	113-197
Acenaphthenes (154), biphenyls	-14	126,154[3]	126,154-196[3]
	-15	125-195	139-195
Acenaphthylenes (152), phenalenes, fluorenes	-16	152-194	152-208
	-17	151-193	151-207
Anthracenes (178), phenanthrenes	-18	150-206[3]	164-220[3]
	-19	163,191,205	163,205
Methylenephenanthrenes (190), phenylnaphthalenes	-20	176,190[3]	176,204,218[3]
	-21	189,203	133,189-217
Fluoranthenes, pyrenes (202)	-22	202	202,216,244
	-23	215	145,215,229

[1]Molecular mass of first member of homologous series in parentheses.
[2]Series may contain rearrangement ions.
[3]First members of series may represent rearrangement ions.

TABLE VI

MASS-SPECTROMETRIC ANALYSIS OF FILTERABLE SEDIMENT AND TUBE DEPOSIT FROM THERMALLY STRESSED FUEL 2987. IDENTIFICATION OF COMPOUNDS CONTAINING ONE OXYGEN.

Suggested Origin[1]	Elemental Composition: $C_nH_{2n+z}O$	Homologous Ions Detected Filter	Tube
	z = +2	---	---
	+1	73	---
Tetrahydrofurans (72)	0	---	72
	-1	71-113,239	71-127
Dihydrofurans (70)	-2	70-112	70-126
	-3	69-139	69-139
Furans (68)	-4	68-110,138	68-152
	-5	81-151	81-165
Phenols (94)	-6	94-150	94-122
	-7	93-163,191	107-135
Dihydrobenzofurans (120),	-8	120-162	106-162[2]
hydroxyindans	-9	105-175	105-161
Benzofurans (118),	-10	104-188[2]	104-188[2]
indanones	-11	131-201	131-173
Naphthols (144)	-12	130-214[2]	144-200
	-13	143-199	157-185
Acenaphthenols (170)	-14	156-226[2]	184,198
	-15	155-211,253	155-197
Dibenzofurans (168)	-16	168-210	182,196
	-17	181-209	181-209
Fluorenones (180),	-18	180-222	---
phenalenones	-19	207	---
	...	...	...
	-22	218, 246	---

[1]Molecular mass of first member of homologous series in parentheses.
[2]First member of series may represent rearrangement ion.

TABLE VII

MASS-SPECTROMETRIC ANALYSIS OF FILTERABLE SEDIMENT AND TUBE DEPOSIT FROM THERMALLY STRESSED FUEL 2987. IDENTIFICATION OF COMPOUNDS CONTAINING THREE OXYGENS.[1]

Suggested Origin[2]	Elemental Composition: $C_nH_{2n+z}O_3$	Homologous Ions Detected Filter	Tube
	z = +2	78,162	---
	+1	119-147	---
	0	104,146-174	---
	-1	131,145	---
	-2	116-172	242
	-3	129,157	129[3],143, 185,241
	-4	100,128,170	100,128,142
	-5	141-183	127
	-6	154,182	---
	-7	167,181	---
	-8	166,208,222	152
	-9	221,235	151
	-10	150-178,220	---
	-11	149-191	149

[1]Peaks overlap with those containing one nitrogen.
[2]Multifunctional compounds.
[3]Very strong peak at m/z 129.

TABLE VIII

MASS-SPECTROMETRIC ANALYSIS OF FILTERABLE SEDIMENT AND TUBE DEPOSIT FROM THERMALLY STRESSED FUEL 2987. IDENTIFICATION OF COMPOUNDS CONTAINING ONE NITROGEN.[1]

Suggested Origin[2]	Elemental Composition: $C_nH_{2n+z}N$	Homologous Ions Detected Filter	Tube
Aliphatic amines	z = +3	---	---
	+2	72-100	268,296[4]
Pyrrolidines (71), piperidines	+1	85	---
	0	70-112	294[4]
Pyrrolines (69)	-1	69-125,153	---
	-2	68-152	---
Pyrroles (67)	-3	81,95,123	---
	-4	80-150	---
Pyridines (79), anilines	-5	79-149	---
	-6	78-162	---
Indolines (119)	-7	91-175[3]	---
	-8	76-174	---
Indoles (117)	-9	75,103-173[3]	---
	-10	88-158,228	242[4]
Quinolines (129), isoquinolines	-11	129-171	185,241[4]
	-12	114-184	---
Phenylpyridines (155)	-13	127-183[3]	---
	-14	140-196	---
Carbazoles (167)	-15	153-181[3]	---
	-16	152,194,208	---
Acridines (179), phenanthridines	-17	179,193,221	---
	-18	178,220	---
	-19	163-191	---
	-20	162-204,232	---
Aminofluoranthenes (217), aminopyrenes	-21	217	---
	-22	188,216-244	---

[1]Peaks overlap with those containing three oxygens.
[2]Molecular mass of first member of homologous series in parentheses.
[3]First members of series may represent rearrangement ions.
[4]Ions probably originate from different molecular structure.

TABLE V

MASS-SPECTROMETRIC ANALYSIS OF FILTERABLE SEDIMENT AND TUBE DEPOSIT FROM THERMALLY STRESSED FUEL 2987. IDENTIFICATION OF HYDROCARBONS.

Suggested origin[1]	Elemental composition: C_nH_{2n+z}	Homologous ions detected Filter	Tube
	z = +2	---	---
	+1	71-155	71-183
Olefins, cycloalkanes (70)	0	70-140[2]	70-140,168[2]
	-1	69-167	69-153
Dienes, cycloalkenes (68), bicycloalkanes	-2	68-194	68-194
	-3	81-207	81-179
Cyclic dienes (66), tricycloalkanes	-4	80-178	80-192
	-5	79-191	79-205
Alkylbenzenes (78)	-6	92,106,134, 148,176,190	78-162
	-7	77-189	77-203
Indans (118), tetralins	-8	76-188[3]	76-188[3]
	-9	75-173	75-187
Indenes (116), dihydronaphthalenes	-10	74-200[3]	74-186[3]
	-11	73-157	87-185,213
Naphthalenes (128)	-12	114-142, 170-212[3]	114-184[3]
	-13	113-211	113-197
Acenaphthenes (154), biphenyls	-14	126,154[3]	126,154-196[3]
	-15	125-195	139-195
Acenaphthylenes (152), phenalenes, fluorenes	-16	152-194	152-208
	-17	151-193	151-207
Anthracenes (178), phenanthrenes	-18	150-206[3]	164-220[3]
	-19	163,191,205	163,205
Methylenephenanthrenes (190), phenylnaphthalenes	-20	176,190[3]	176,204,218[3]
	-21	189,203	133,189-217
Fluoranthenes, pyrenes (202)	-22	202	202,216,244
	-23	215	145,215,229

[1]Molecular mass of first member of homologous series in parentheses.
[2]Series may contain rearrangement ions.
[3]First members of series may represent rearrangement ions.

SYMPOSIUM ON THE STABILITY AND OXIDATION CHEMISTRY OF MIDDLE DISTILLATE FUELS, DIVISION OF FUEL AND PETROLEUM CHEMISTRY, AMERICAN CHEMICAL SOCIETY, WASHINGTON D.C. MEETING, AUGUST 1990

THE THERMAL DEGRADATION OF AVIATION FUELS IN JET ENGINE INJECTOR FEED-ARMS: RESULTS FROM A HALF-SCALE RIG

By

R.H. Clark* and P.A. Stevenson

Shell Research Ltd., Thornton Research Centre, P.O. Box 1, Chester CH1 3SH

INTRODUCTION

Aviation kerosine undergoes significant heating within the fuel system of an aviation gas turbine. Heating occurs because, firstly, fuel is used as a coolant for the engine lubricating oil and for other heat exchanger systems (e.g. avionics, air conditioning, etc.) and, secondly, because certain regions have a high intrinsic temperature (e.g. injector feed-arms). The feed-arms, which pass fuel directly into the combustor, represent the most severe fuel system environment in that the combination of high fuel inlet temperatures and very hot metal surface can promote a very high degree of thermal degradation. In this event, the small apertures within the fuel atomisers can become obstructed, causing flow restriction or fuel spray pattern distortion, and leading ultimately to engine malfunction. Thus, the thermal stability of aviation fuels within the feed-arm environment is crucial for the safe operation of gas turbine engines.

Whilst the thermal degradation of aviation fuels is well documented[1], relatively few researchers have addressed the specific problem of deposition within burner feed-arms[2-4]. Two such investigations were collaborative projects[3-4] between Shell Research and Rolls-Royce plc., Derby. A full-scale rig simulation[4], the IFAR (Injector Feed-Arm Rig), was used to look at the effects on fouling of fuel flow rate and fuel pressure, the addition of additives, and rig repeatability. However, the large appetite of the rig (50,000 litres of fuel per test) prevented a more detailed examination of the contribution of fuel chemistry to the fouling.

The study reported here used a half-scale rig, the MIFAR (Mini Injector Feed-Arm Rig), which is similar in design to the IFAR and operates at identical temperatures. The use of this scaled-down rig with its significantly decreased fuel appetite - a reduction from 50,000 litres to 2,000 litres/test - has enabled the effects of fuel processing and chemistry on feed-arm fouling to be evaluated for a wide range of fuels. In addition, it has permitted correlations to be drawn between the MIFAR and other thermal stability rigs.

The objectives of the research program were as follows:

- To make a direct comparison of fuel performance in large- and small-scale injector feed-arm rigs, and thence to pursue the initial findings about the feed-arm deposition process.

- To relate a fuel's deposition tendency to its chemical composition and to correlate the MIFAR with other predictors of fuel thermal stability, in particular to the JFTOT (Jet Fuel Thermal Oxidation Tester).

- To gain greater insight into the action of one additive, the approved metal deactivator, Du Pont's MDA, specifically to confirm related findings[5] on its dual action as metal chelator and metal passivator.

EXPERIMENTAL

Mini Injector Feed-Arm Rig (MIFAR)

The philosophy underlying the aviation fuel thermal stability testing pursued at Shell Research Ltd has been always to construct simulation rigs, using actual engine components where possible, and to measure fuel deposition quantitatively at well characterised temperatures. The MIFAR, illustrated in Figure 1, is a realistic, half-scale simulation of an aircraft fuel system. Fuel is supplied from external storage tanks via a 0.45 μm filter to a glass reservoir (to simulate a wing tank); in the current programme, the reservoir was left unheated to simulate the absence of fuel recirculation in civil aviation practice. On leaving the reservoir, the fuel is pressurised to 250 psi by a Lucas high-pressure piston pump and supplied to a fuel line heater, comprising two stainless-steel sheathed electrical cartridge heaters in series; the heaters simulate the avionic and engine cooling components of a gas turbine engine. The hot (165°C), pressurised fuel is then fed to a model feed-arm mounted in a fluidised sandbath, which simulates the hot compressor discharge air environment. Thereafter, the fuel passes through filters, is cooled and dumped to waste. A DEC micro PDP-11 computer provides automatic control of the rig operating conditions via process control software; the same software also provides data logging and reporting functions.

At Shell Research the model feed-arms are designed to simulate the burner stems that lead to the nozzle assemblies and are plain, thick-walled steel tubes (0.25" O.D. x 0.090" I.D.), corresponding to a half-scale system. The tubes are instrumented with thermocouples mounted in grooves along the arms to allow the temperature of the inner wall (TIW) to be measured. Only the central 10 cm of the arm (corresponding to 7.2 cm^2) are immersed in the sandbath. Bulk fuel temperatures at the inlet and outlet of the arm are determined by the associated thermocouples.

Deposition Monitoring

The deposition process is monitored "on-line" during a test by measuring the rise in the inner wall temperature (ΔTIW) of the feed-arm; this rise occurs because of the deposit's insulating effect on heat transfer. After a test has been completed, the deposit mass is calculated from the amount of carbon (W_C) recovered as carbon dioxide from the controlled combustion of the deposit. Empirical data have shown that the weight of carbon recovered is 70% of the original deposit weight; this allows W_C values to be converted into deposit weight (W_D) values, thus providing an "off-line" reference of fouling rate.

Test conditions

As with the IFAR[4], the tests were targetted to reflect severe thermal conditions; therefore a bulk fuel inlet temperature of 165°C and an inner wall temperature of 300°C were selected. The fuel pressure was 250 psi, and a flowrate of 300 ml/min was chosen to give a turbulent flow regime (Reynold's Number, Re = 8000).

The 300°C TIW was achieved by adjusting the temperature of the fluidised sandbath within the range 410°-450°C at the start of each test; thereafter the sand bath was maintained at a constant temperature.

Test fuels

The ten fuels studied included examples of the three main process types: sweetening, hydrotreating and hydrocracking. Most were Jet A/A-1 type fuels meeting the DERD 2494/ASTM D1655 specifications, but some were chosen because of their poor/borderline stability. The fuels and their inspection properties are listed in Table 1. The fuels encompass a wide range of sulphur contents and responses in the JFTOT specification thermal stability test. These fuels were used in a series of 16 tests (detailed in Table 2).

RELATED THERMAL STABILITY TESTS/RESULTS

Fuel performance within the MIFAR was not considered in isolation; the wide range of thermal stability tests available at Shell Research enabled fuel performance in the MIFAR to be compared with other measures of stability. From these data, two complementary pieces of information were derived: firstly, the ability of other tests to predict fuel performance - as determined in a realistic environment; secondly, the prediction of fuel performance from more fundamental compositional information.

The IFAR

The IFAR was built as part of a programme undertaken jointly by Shell Research and Rolls-Royce to study injector feed-arm fouling[4]. The rig, whilst similar in principle to the MIFAR, is essentially a full-scale simulation. The operating principles, test temperatures and measurements made are directly comparable and essentially identical to those of the MIFAR. Insights gained from the IFAR into feed-arm fouling have been published in the literature[4,5]

The single tube heat transfer rig (STHTR)

The STHTR realistically simulates fuel degradation within an oil-cooler[6]. It is Shell's principal benchmark of fuel thermal stability in service, insofar as it duplicates the dimensions, fuel flow rates and metallurgy of an oil-cooler. In the rig, the fuel undergoes three stages of heating to simulate those heat sources encountered in an aircraft fuel system:

- Fuel tank heating (aerodynamic heating, fuel transfer/recirculation)
- Heating from hydraulics/avionics/environmental system heat exchangers
- The engine oil-cooler (i.e., that component simulated by the test heat-exchanger)

Fuel degradation is monitored via the reduction in heat-transfer coefficient of the test element.

JFTOT testing

For commercial purposes, the thermal stability of aviation fuels is generally assessed in the Jet Fuel Thermal Oxidation Tester[7] (JFTOT, ASTM method D3241) at a defined temperature. In essence, fuel is passed over a heated metal tube and then through a filter; the fuel is rated on a go/no go basis by the tube lacquer or the blockage of the filter. For research purposes this is not very informative. Accordingly, in the current work, fuels were ranked using the breakpoint temperature (i.e., the highest temperature sustainable without causing the fuel to fail on the tube lacquer or filter blockage criterion.) In addition, the degree of carbon deposition in the tests carried out at a 350°C tube temperature was also determined.

Flask oxidation studies

The flask oxidation test (FOT) is an in-house method of measuring the liquid phase oxidation rate of fuels and thereby determining their other oxidation characteristics[8]. Perturbing the system with a radical initiator (t-butyl peroxide) enables a fuel's intrinsic radical initiation rate to be determined. This rate has been found to be a good predictor of a fuel's deposition tendency within our oil-cooler simulation.

MIFAR RESULTS: DEPOSITION RATES

The raw MIFAR test results comprise two types of measurement:

(i) The tube wall temperature, TIW, recorded as a function of time throughout the test;

(ii) The total weight of deposit formed on the feed-arm wall, W_D, at the end of test.

By plotting, in log-log form, the end-of-test increase in wall temperatures, ΔTIW, against the weight of deposit, W_D, for each test, an empirical linear relationship between the two parameters has been identified:

$$W_D = Y(\Delta TIW)^Z \qquad \ldots (1)$$

The value of Y is 1.82 and that of Z is 1.0, resulting in a linear relationship. This compares with the near quadratic form of relationship (i.e. $W_D \alpha (\Delta TIW)^{2.2}$) found in the full-scale IFAR. The reason

for the differing exponents in the expression is obscure. One supposition is that the lower sandbath temperature of the MIFAR (400°C versus 540°C) has resulted in different heat-transfer characteristics between the sandbath and the feed-arm. However, there could well be other consequences of reducing scale.

The relationship has been used to convert the ΔTIW recorded during the test to the equivalent W_D, so generating a picture of the build-up of deposit as a function of duration (Figures 2 - 4). Now, assuming that deposition occurs only on the directly heated surface of $7.2cm^2$ area, deposition rates have been calculated for each test (Table 2).

The main points are as follows:

(1) The form of the curves confirms our earlier findings as to the nature of the deposition process; namely, it comprises three distinct phases:

- A finite, variable-duration "induction period", during which no significant deposition occurs.
- A period of near-constant deposition rate.
- In some tests, a decrease in deposition rate towards the end of test.

(2) Deposition rates span a factor of 25. The sweetened fuels (excluding off-grade Fuel A) encompass the range 0.1 - 0.5 mg $cm^{-2}h^{-1}$ and the hydrotreated fuels are all less than 0.05 mg $cm^{-2}h^{-1}$.

(3) The highest deposition rate was that of the off-grade Fuel A, which was consistent with its high metal content. However, addition of MDA restored this high rate to that more typical for a sweetened fuel.

DISCUSSION

The nature of the deposition process

The graphs of the temporal evolution of deposits on the feed arms (Figure 2 - 4) show features identical to those in the IFAR study[4], i.e. the three main phases in the deposition process noted above,

- Finite hold-up or induction period, during which little or no deposition is detected. This corresponds to the low deposition rate on a clean steel surface.

Followed by:

- A higher constant rate of deposition on a fouled surface.

Ultimately

- A reduction in deposition rate due to the insulating effect of the cumulative deposit.

However, the current studies, with the large suite of fuels, have given a much clearer insight into the deposition process. Examination of the data reveals an obvious link between the length of the induction period (τ_{ip}) and the post-induction deposition rate (r_p); i.e. the less stable a fuel is, the shorter its induction period and the higher its deposition rate. In fact, it is reasonable that there should be a relationship between these two parameters; the reciprocal induction period ($1/\tau_{ip}$) is a measure of fuel deposition rate on a clean metal surface, whereas the post-induction rate is a measure of deposition rate on a fouled surface. In Figure 5, the plotting of deposition rate versus $1/\tau_{ip}$ yields a straight line passing through the origin, illustrating the relationship between two measures of deposition. The data can be interpreted further, by making certain assumptions. Examination of the W_D versus duration plots suggests that the induction period is the time taken for 5 mg of deposit to build up. From this, an estimation can be made of the relative fuel deposition rates on a clean surface versus those on a lacquered one; the ratio obtained is 1:4.

The influence of MDA

The mechanism by which the metal deactivator additive (MDA) affects fuel performance can be resolved into two components[5]:

- Metal chelation, the claimed role of the additive, whereby dissolved metals within the fuel are rendered catalytically inactive. In this mode, bulk fuel reactivity is affected, thus increased chelation is manifested as a decrease in deposition rate.
- Metal passivation, in which the MDA adsorbs onto and, thereby, modifies a clean metal surface, thus inhibiting formation of the first layer of deposit. Increased passivation is evident from an increase in induction periods.

These feed-arm studies have provided an excellent illustration of the above mechanisms. Consider the test sequence 1 - 4 (Figure 2 - 4), in which an off-grade fuel (Fuel A) contaminated with catalytic metal is progressively doped with higher concentrations of the MDA additive (0, 5.7 and 12 mg l^{-1}). (i) The base fuel gave the highest deposition rate 1.1 mg cm^{-2} h^{-1} and the shortest induction period of 3 hours. (ii) At 5.7 mg l^{-1}, MDA is present in excess relative to the metal contamination (0.25 mg l^{-1} of MDA would be required). Thus, all metals are chelated and the deposition rate decreases to 0.3 mg cm^{-2} h^{-1} via the chelation mechanism. However, in tandem, the induction period increases from 3 to 8 hours via the passivation mechanism. (iii) At 12 mg l^{-1} there can be no extra benefit from chelation over and above that seen at the 5.7 mg l^{-1} level, which was already an excess of MDA. In consequence, the deposition rate remains essentially unaffected. However, this additional MDA can affect the passivation mechanism and increase the induction period from 8 to 20 hours.

From our previous work[4] using metal-free fuel to avoid the chelation mechanism, it can be estimated from the induction period data that deposition rates on a clean steel surface are reduced by two-thirds by the MDA passivation associated with the 5.7 mg l^{-1} doping level.

Comparing the MIFAR with other measures of thermal stability

A major aim of the research programme was to predict fuel performance within the MIFAR from compositional data, and to relate the performance to other thermal stability rigs. Six potential predictors of fuel thermal stability were considered:

(1) Radical initiation rate (FOT)
(2) JFTOT breakpoint
(3) JFTOT carbon deposit determination
(4) Oil-cooler rig (i.e. STHTR) data
(5) Fuel sulphur content
(6) Total acid content (TAC) via ion-exchange

Accordingly, MIFAR test results in the form of deposition rates were correlated with these other measures. The resultant statistical information is illustrated in Table 3 and the correlation graphs in Figures 6 and 7.

Two striking features can be observed from the statistics:

(i) The lack of a significant correlation between the oil-cooler rig and the MIFAR (correlation confidence is well below the significant level of 95%)

(ii) The superiority of all the analytically derived predictors (i.e. sulphur, R_i and TAC), when compared to rig-based tests, in forecasting MIFAR deposition rates.

In fact these two points are probably related. The MIFAR, in its current configuration, simulates a fuel system that is not subject to wing tank heating. Thus, the fuel is not resident in any heated component for any length of time, and as a consequence one would expect deposition to be influenced by fuel chemistry in a straightforward manner, i.e. oxidation followed by reaction of intermediates with fuel polar species (acids and sulphur compounds). It is seen that the statistical data are in accord with such a mechanism. The poor correlation with the STHTR may well relate to the more complex chemistry associated with the multi-stage heating system of the rig whereby the fuel is pre-heated in a simulated wing tank for a comparatively long residence time (ca. 1 hour) before encountering the test section.

The poor correlation of the MIFAR with either JFTOT measure could result from the JFTOTs' lack of realism in utilising a laminar fuel flow condition and thus not responding solely to fuel chemistry[7].

Overall, the best prediction of fuel thermal stability in both the large-scale rigs, i.e. the MIFAR and STHTR, is given by total acid content (TAC) via ion-exchange chromatography[9].

CONCLUSIONS

- A half-scale injector feed-arm fouling rig, the MIFAR, provides clear confirmation of the deposition mechanisms first observed in full-scale

rig (i.e. the IFAR) measurements, namely, the three distinct deposition phases of induction, constant rate deposition and tail-off. However, working with a large suite of fuels enables the mechanism to be resolved at a greater level of detail. In particular, relationships have been drawn up between fuel deposition on a clean steel surface (estimated from the induction period length) and deposition on a fouled surface (post induction).

- MIFAR data provide an excellent illustration of the mode of action of the two mechanisms by which the approved thermal-stability-enhancing additive MDA affects fuel-deposition tendency: metal chelation and metal passivation. Chelation is measured as a change in the post-induction deposition rate, whereas passivation is measured in terms of the length of the induction period.

- Simple chemical composition parameters are superior to other measures for predicting the thermal stability performance of fuels in the MIFAR. These three parameters, radical initiation rate, fuel total sulphur and total acid content (TAC), are in accord with our current understanding of the chemistry of the degradation mechanism. TAC by ion-exchange chromotography is considered the best measure.

- The poor MIFAR/STHTR correlation suggests that the more complex heating stages within the STHTR have a significant effect on the chemistry of the decomposition process.

ACKNOWLEDGEMENTS

The authors thank Mr. G. Houlbrook and Mrs L. Smith for their assistance in the experimental work and Dr. D.R. Kendall for helpful discussions.

REFERENCES

1. CRC Report No. 509, April 1979, CRC, Boca Raton, Fl.

2. C.A. Moses, M.W. Shayeson and P.A. Karpovich, ASME Paper 86-GT-94.

3. A.E. Peat, ASME Paper 82-GT-27.

4. D.R. Kendall, G. Houlbrook, R.H. Clark, S.P. Bullock and C. Lewis, Injector Feed Arm Fouling - Part 1 Results from a Full-scale Rig, presented at the 30th International Gas Turbine Congress Tokyo, Oct 1987.

5. R.H. Clark, Paper #47, p283, presented at the 3rd International Conference on the Stability and Handling of Liquid Fuels, London, Sept 1988, Institute of Petroleum (1989).

6. J.S. Mills and D.R. Kendall, ASME paper 85-GT-33.

7. R.H. Clark and L. Thomas, SAE Paper 881533.

8. D.R. Kendall and J.S. Mills, Ind. Eng. Chem. Prod. Res. Dev., Vol 25, June 1986, pp 360-366.

9. R.H. Clark and L. Smith, Paper #46, p268, presented at the 3rd International Conference on the Stability and Handling of Liquid Fuels, London, Sept 1988, Institute of Petroleum (1989).

Table 1

Inspection properties of fuels used in the MIFAR fouling studies

FUEL	A	B	C	D	E	F	G	H	I	J
PROCESS TYPE	SWEETENED	MEROX SWEETENED	MEROX SWEETENED	~50/50 STRAIGHT RUN/ HYDROCRACKED	MEROX SWEETENED (FUEL F) +12%v UNTREATED LCCO	MEROX SWEETENED	MEROX SWEETENED	HYDROCRACKED PRODUCT	HYDROTREATED	HYDROTREATED
AROMATICS, %v	18.8	19.2	19.2	16.4	27.7	17.5	17.4	8.6	16.0	14.7
OLEFINS, %v	0.7	0.3	0.8	0.2	0.4	0.5	0.3	0.4	<1	0.4
MERCAPTAN SULPHUR, %w	0.0002	0.0003	0.0005	0.0004	0.0008	0.0017	0.0002	0.0001	-	0.0001
TOTAL SULPHUR, %w	0.14	0.03	0.10	0.01	0.30	0.21	0.133	0.013	0.002	0.004
ACIDITY, mgKOH g^{-1}	0.001	0.001	<0.001	0.007	0.005	0.003	0.001	0.001	0.004	0.001
*Total Acids, mg l^{-1}	-	196	123	112	273	153	281	27	47	16
Distillation										
IBP, °C	163	151	148	153	154	141	147	171	155	160
50%, °C	199	203	190	197	223	194	190	210	200	199
FBP, °C	265	259	252	286	350	260	259	279	259	263
Density, kg l^{-1}	0.8078	0.8110	0.7908	0.8032	0.8214	0.7960	0.7878	0.8033	0.7960	0.8016
Copper, µg l^{-1}	47	2	7	<2	52	16	<2	<2	2	<2
Antioxidant, mg l^{-1}	Nil	Nil	Nil	18	Nil	Nil	Nil	20	20	20
JFTOT Breakpoint, °C	250	285	265	290	245	250	285	305	285	285

* Total Acid Content, TAC, extracted by ion exchange chromatography

Table 2

Comparison between MIFAR deposition rates and some other thermal stability indices

MIFAR Test no.	Fuel	MIFAR deposition rate mg cm^{-2} h^{-1}	IFAR deposition rate mg cm^{-2} h^{-1}	Single tube rig ΔHTC, % h^{-1}	JFTOT breakpoint, °C	JFTOT carbon deposit, µg	Radical initiation rate mol l^{-1} s^{-1} x 10^7
1,2	A	1.04, 1.18	-	0.33	250	-	26.9
3,4	A + MDA 5.7 ppm, 12 ppm	0.31, 0.50	-	-	-	-	-
5,6	B	0.29, 0.37	0.43	1.3	285	143	2.5
7,8	C	0.18, 0.36	0.43	0.6	265	138	5.8
9	D	0.15	0.47	1.9	290	71	4.9
10	E	0.41	0.63	12.3	245	553	4.9
11,12	F	0.11, 0.10	-	1.3	250	307	6.3
13	G	0.22	-	5.4	285	87	0.5
14	H	0.046	-	0.2	305	59	0.70
15	I	0.049	-	0.19	285	54	0.93
16	J	0.046	-	0.002	285	25	0.76

Table 3

The correlation of MIFAR deposition rates with some other thermal stability indices

Test	Correlation Confidence, %	|R|	MSE*	Gradient$	Intercept$
R_i, 10^{-7} mole l^{-1} s^{-1}	99.7	0.730	0.106	0.62 ± 27%	-1.0 ± 12%
JFTOT, B.P., °C	95.5	0.542	0.160	-7.9 ± 45%	1.8 ± 46%
STHTR, ΔHTC, % h^{-1}	85.4	0.409	0.189	0.21 ± 64%	-0.66 ± 18%
S, % M	48.2	0.620	0.140	0.41 ± 37%	-0.16 ± 19%
# JFTOT, C.D. μg	96.3	0.601	0.090	0.58 ± 41%	-2.0 ± 25%
# TAC, mg l^{-1}	99.9	0.843	0.049	0.77 ± 20%	-2.39 ± 13%

+ MSE: Mean square error, |R| : Correlation Coefficient

$ Values in the expression

$$\log_{10} (\text{MIFAR}) = \text{Intercept} + \text{Gradient} * \log_{10} (\text{Test index})$$

Data set for these indicies comprise 12 measurements. All others 14 measurements

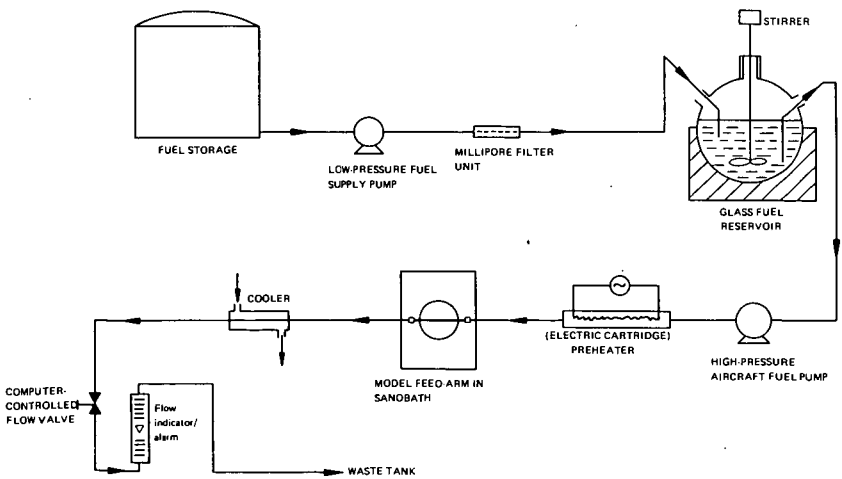

FIG. 1 – Schematic diagram of the Mini Injector Feed-Arm Rig (MIFAR)

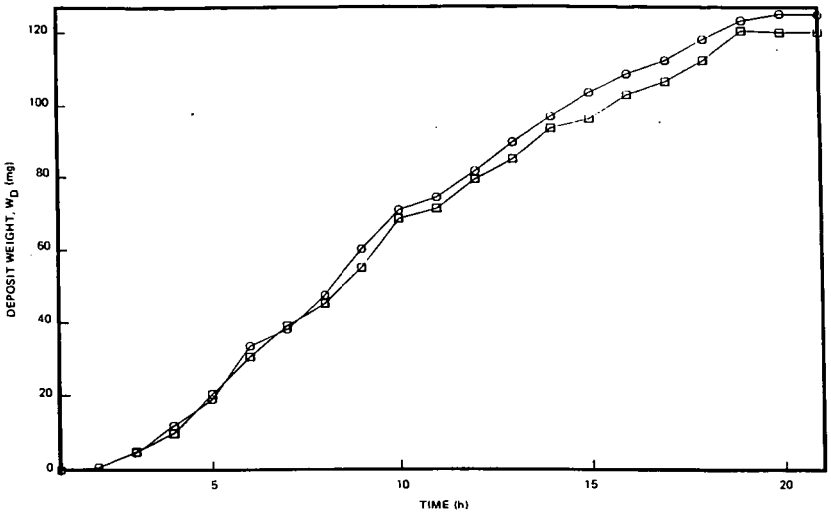

FIG. 2 — The evolution of feed-arm deposition for Fuel A, Test 2

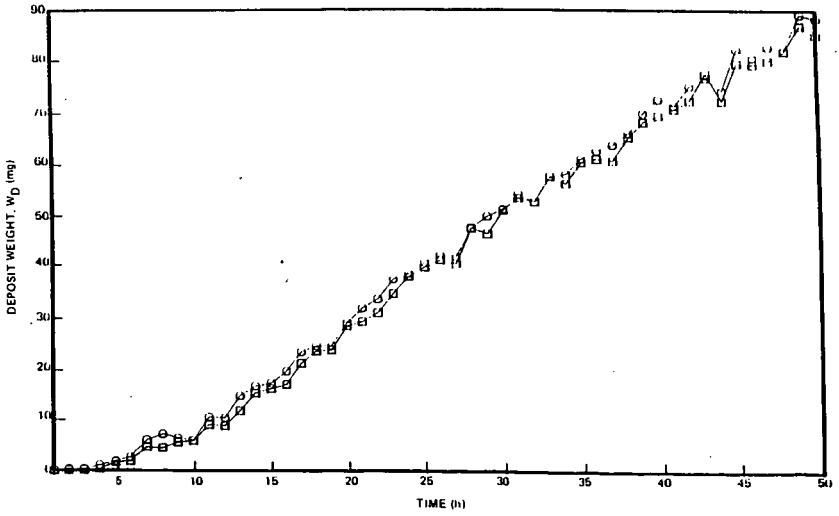

FIG. 3 — The evolution of feed-arm deposition for Fuel A + 5.7 mg l^{-1} MDA

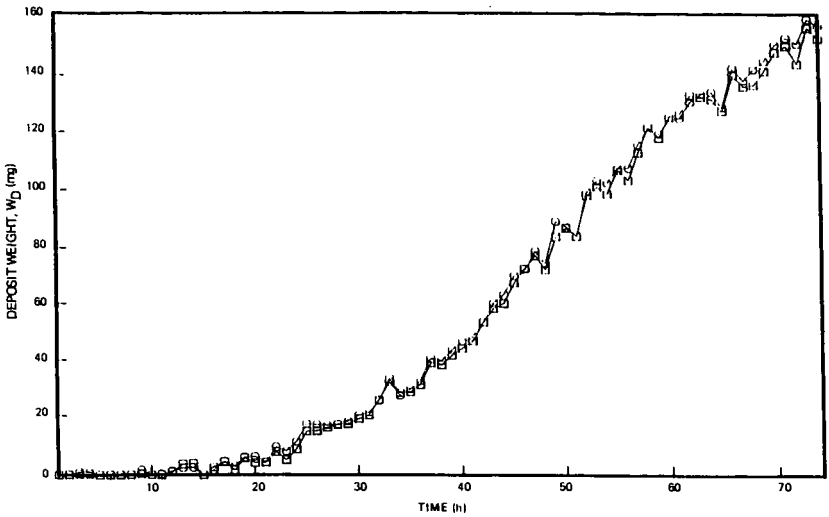

FIG. 4 — The evolution of feed-arm deposition for Fuel A + 12 mg l^{-1} MDA

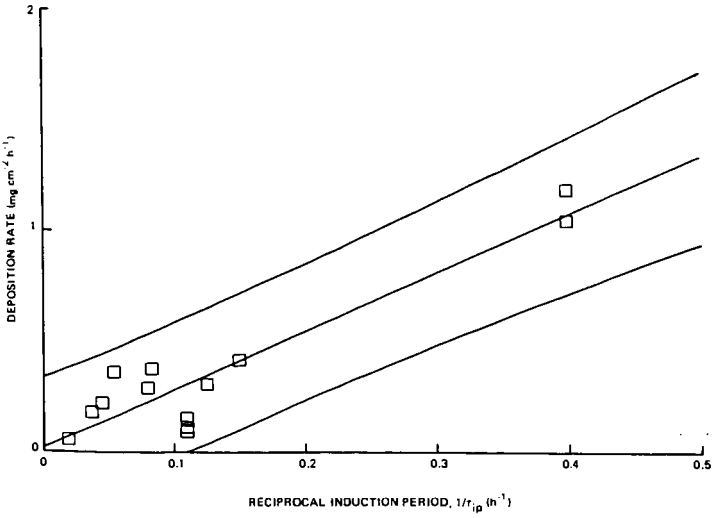

FIG. 5 — The relationship between feed-arm deposition rate and induction period

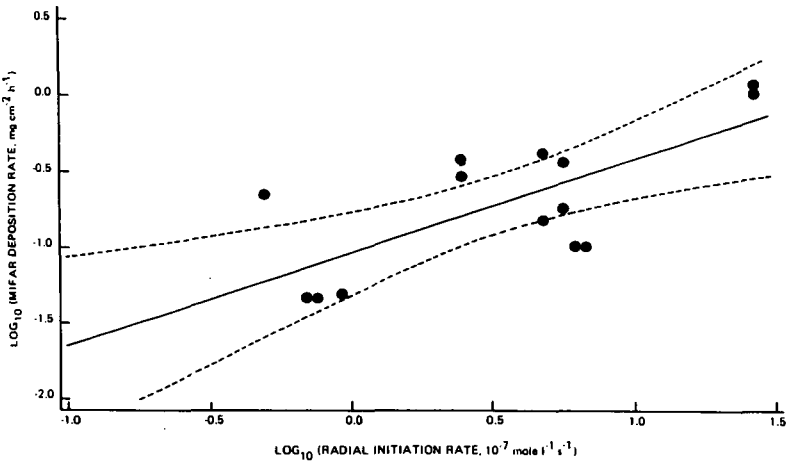

FIG. 6 — The correlation between feed-arm deposition rate in the MIFAR and fuel radical initiation rate

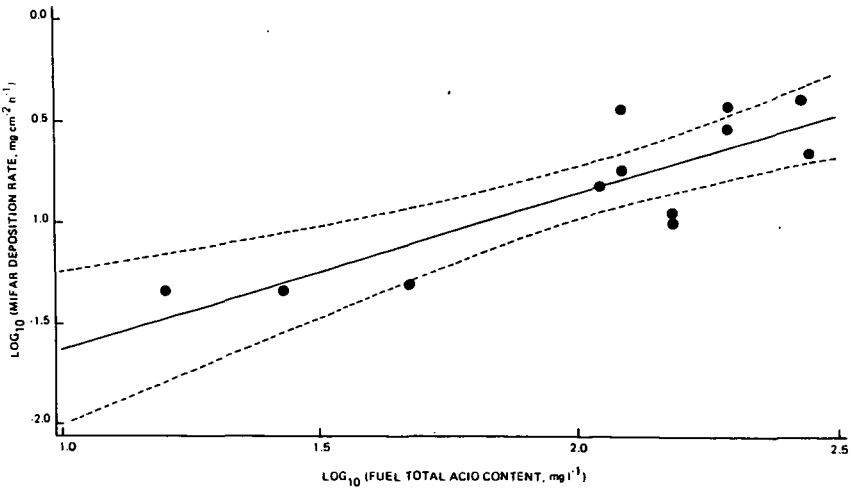

FIG. 7 — The correlation between feed-arm deposition rate in the MIFAR and fuel total acid content

THE ROLE OF SURFACE COMPOSITION IN FUEL DEPOSITION

L.L. Stavinoha, D.W. Naegeli and L. McInnis
Belvoir Fuels and Lubricants Research Facility
Southwest Research Institute
San Antonio, Texas 78238

Keywords: Thermal stability, JFTOT, deposit, metal catalyst

Abstract: Experiments were performed in a Hot Liquid Process Simulator (HLPS) configured and operated such that it performed under conditions similar to Jet Fuel Thermal Oxidation Tester (JFTOT) ASTM D 3241 requirements. The JFTOT heater tubes used were 316 stainless steel (SS), 304 SS, and 304 SS tubes coated with aluminum, magnesium, gold, and copper. A low sulfur Jet A fuel with a breakpoint temperature of 254°C was used to create deposits on the heater tubes at temperatures of 300°, 340°, and 380°C. Deposit thickness was measured by dielectric breakdown voltage and Auger ion milling. Auger ion milling of the deposits showed the order of deposition to be copper > magnesium = 316 SS > gold > aluminum. The dielectric strength method indicated that 316 SS > 304 SS > gold > magnesium = aluminum = copper. The pronounced differences between the deposit thickness measuring techniques suggest that the dielectric strength of the deposit is strongly affected by metal ions that become included in the bulk of the deposit. The results show that the surface temperature and composition play an important role in deposition.

Introduction: The effect of fuel system metallurgy on fuel stability is an important concern in the development of high efficiency/advanced engine technology such as adiabatic, low heat rejection engines and hypergolic injection systems. Several studies have shown that trace metals adversely affect the thermal stability of hydrocarbon fuels.(1,2) Metal concentrations as low as 15 ppb of copper, 25 ppb of iron, 100 ppb of zinc, and about 200 ppb of lead have been found to cause significant change in the thermal stability of jet fuels. These studies suggest that the slightest metallic contamination could cause a significant change in the thermal oxidative stability of hydrocarbon fuels. In fact, the theory has been advanced that all hydrocarbon autoxidations are trace metal catalyzed.(3)

Recent work (4), in which only limited data are available, suggests that aluminum tubes with magnesium-enriched surfaces tend to have lower deposit buildups than the standard aluminum tubes. If such minor changes in surface metallurgy cause significant changes in the rate of deposit formation, major changes in surface composition could dramatically effect processes such as deposit adherence and oxidation catalysis.(5) Experiments with metal deactivator in dodecane using JFTOT equipment suggest that the effect on deposit reduction may be a consequence of interactions in the liquid-phase rather than a reduced adherence to the hot metal surface.(6)

One measure of the thermal stability of aviation fuels is the quantity of deposits formed on heated metal surfaces.(7) In accelerated stability tests conducted in accordance with the JFTOT procedure (ASTM D 3241) (8), the rating methods currently employed involve either visual comparisons or measurements of reflected light by the tube deposit rater (TDR), both of which are sensitive to deposit color and surface texture. In the research reported in reference 7, deposits formed on stainless-steel JFTOT heater tubes were examined by the TDR, a gravimetric carbon combustion method, and two new nondestructive techniques for determining deposit volumes based on measurements of dielectric strength and optical interference. Measurements of total carbon content by combustion were used as a reference. It was found that the dielectric and interference methods correlated well with the combustion analyses and each other, while the total TDR often yielded misleading results. The purpose of the present study was to investigate the role of JFTOT metal surface composition in deposit formation.

Experimental: Experiments were performed in an Alcor model HLPS300 Hot Liquid Process Simulator (HLPS), which is a modular version of the JFTOT apparatus used for the ASTM D 3241 method. The HLPS was operated to give conditions equivalent to D 3241 requirements except that Triton-treated fuel prefilters were not used. In the development of the experimental technique, there was a desire to achieve a more isothermal temperature profile over the length of the tube so that greater accuracy could be achieved in the measurement of rate parameters such

as activation energies for deposit formation. In the first attempt to broaden the hot zone over the tube, a "heated line transformer with line clips" was used to preheat the fuel. Figure 1 shows the result of fuel preheating on the longitudinal temperature profile of the JFTOT heater tube. In Figure 1, station 0 in the fuel inlet and station 60 is where the fuel leaves the JFTOT heater tube jacket. Preheating the fuel to 150°F (66°C) and 200°F (93°C) at heater tube temperatures of 300° and 340°C did not demonstrate any significant hot zone broadening advantages over fuel at room temperature. Figure 2 shows the results of a second approach to broadening the temperature profile using a reverse fuel flow by the JFTOT heater tube. The reverse flow approach did, in fact, achieve a much higher degree of isothermal tube temperature behavior, but because it was less standard and could possibly hinder comparisons with other studies, it was not used in the experiments reported here.

Procedure for Coating Heater Tubes. Aluminum, gold, carbon, magnesium, and copper were deposited on sets of three each 304 SS heater tubes. Basically, the objective was to make coatings on the heater tubes thick enough to cover the surface completely yet thin enough to minimize possible effects of both electrical and thermal conductivity. The coatings were accomplished with a Denton model DV-502 vacuum deposition apparatus that was set up to produce a thin layer of the test element onto standard 304 SS JFTOT heater tubes. In developing the procedure for coating the tubes, it was found that the success of the method depended greatly on the cleanliness of the heater tube surface. Quality adherence of the coatings was achieved when the heater tubes were cleaned with trichloroethane in a sonic bath for about two minutes and dried in a laboratory specimen dryer.

Deposit Measurement Device. The deposit thickness measurement device (DMD) determines the thickness of a deposit on a conductive surface by applying a voltage across the deposit while measuring the dielectric breakdown of the layer at various points.(9) The DMD used in this work was first reported in reference.(10) The DMD voltage measurements were shown to relate thickness of deposits with 350 volts equal to 1 micrometer.(10) Methods for calculating deposit volume on JFTOT heater tubes were also discussed in reference.(10) This procedure was used to develop DMD data correlations to carbon burn-off values reported in reference 7.

Auger Milling Technique. The raw data from Auger ion milling are given in units of time. To determine thickness repeatably, it is necessary to make the appropriate calibration. For the deposit thickness measurements, a piece of tantalum foil with a layer of tantalum oxide of known thickness was ion-milled at a given rate until the oxide was removed. For a given milling rate, it was then possible to measure thickness in terms of time. JFTOT deposit thicknesses were determined assuming that the rates of material removal from the deposit and the tantalum oxide standard were equivalent. However, it was expected that the deposit would mill at a somewhat faster rate since it is primarily carbon and hydrogen, i.e., lighter elements than the oxygen and tantalum. Since the mass removal rate for the deposit could be faster than that of the standard, the actual deposit thicknesses may have been somewhat larger than those reported in this paper.

Test Fuel. The objective in choosing a test fuel was to find one that could provide assessable deposits on 304 SS heater tubes at test temperatures of 300°, 340° and 380°C. After evaluating several fuels, a West Coast Jet A fuel was found to give measurable levels of deposit on 304 SS heater tubes at all three of the chosen test temperatures. This fuel met ASTM D 1655 specification at the time of manufacture; it had a code 3 breakpoint temperature of 254°C when the work was started.

Test Procedure. Stainless steel (304) tubes were evaluated using the West Coast Jet A fuel and test durations of 0.5, 1.0, 1.5 and 2.5 hours at maximum heater tube temperatures of 300°, 340°, and 380°C. These data are summarized in Table 1. The 1.5-hour test period was selected for use in the metal surface evaluations because it produced a deposit that was relatively nascent, yet assessable by the DMD and Auger measuring techniques.

Results and Discussion: The results in Figure 3 show the longitudinal temperature profile of the heater tubes at controlled maximum temperatures of 300°, 340°, and 380°C. These data were used as a reference to determine the temperature at a particular heater tube station. Figures 4 through 9 summarize the deposit thickness by DMD for the West Coast Jet A using the 316 SS heater tube, the 304 SS heater tube, and the 304 SS heater tubes coated with aluminum, magnesium, gold, and copper. Auger milling measurements of deposit thickness were made at

several of the heater tube stations for the various surfaces as shown in Figures 4 through 9. Note that Auger results were not available for the 304 stainless steel.

All the DMD deposit profiles were consistent in that they each exhibited a shift toward the fuel inlet (station 0) as the maximum heater tube temperature was raised. General comparison of Auger milling values to DMD thickness values suggest:

* Auger milling gives much greater thicknesses for deposits formed on copper coated tubes. The two methods give similar deposit profiles and locations of maximum thickness.
* Magnesium coated tube deposit values by Auger were increasingly higher than DMD values at higher heater tube temperatures.
* 316 SS tube deposit values by Auger were increasingly higher than DMD values at higher heater tube temperatures.
* Aluminum coated tube deposit thickness by Auger was approximately one-half of that by DMD.
* Gold coated tube deposit thickness by Auger milling was essentially equal to DMD measured values.

Auger ion milling of the deposits showed the order of deposition to be copper > magnesium = 316 SS > gold > aluminum. The dielectric strength method indicated that 316 SS > 304 SS > gold > magnesium = aluminum = copper.

The pronounced differences between the deposit thickness measuring techniques suggest that the dielectric strength of the deposit is strongly affected by metal ions that become included in the bulk of the deposit. The results show that the surface temperature as well as composition plays an important role in deposition. Other than for variation in the thickness of deposits formed during 1.5-hour tests using various metal surfaces, the most dramatic effect observed was that the bulk of deposits moved to lower tube temperature as the maximum tube temperature was increased from 300° to 380°C. These data suggest that this fuel is unique in that it deposits over a relatively narrow temperature range; compared to the other surface materials, copper tends to shift this temperature to somewhat lower limits (See Table 2).

Basically, there are two theories on the role of metals in fuel stability. When fuels are exposed to hot metal surfaces, it is believed that naphthenic acids react with surface oxides and produce fuel-soluble metal naphthenates. In solution, the trace metals may either initiate autoxidation reactions or enhance reaction rates by decomposing hydroperoxides and producing more reactive free radicals. The other theory is that gums formed in the autoxidation process have different affinities for surface materials and thus adhere to some surfaces more than others. If it is simply the adherence of gums to the surface that matters, the effect would be expected to be important only in the formation of nascent deposits, and the composition of the deposit would not be changed by the metal. If the mechanism is based solely on the dissolution of metals by acidic constituents in the fuel, one would not anticipate a change in the rate of deposition as the deposit builds up. Also, metal ions would probably become incorporated homogeneously in the deposit since metals tend to form chelates with the relatively polar gum molecules in the fuel.

In ASTM D 3241-88a, note 8 states: "**Heater tubes should not be reused.** Tests indicate that magnesium migrates to the heater tube surface under normal test conditions. The enriched magnesium surface may reduce adhesion of deposits to re-used heater tubes." The topography of the deposit formed on the magnesium surface was found to be somewhat different than that of the other metal surfaces. A cursory examination of photographs taken with the scanning electron microscope (SEM) at magnifications of 1000X and 2000X showed hemispherical deposits on the magnesium surface and flat platelet-type deposits on the other metal surfaces. Before the tests, the magnesium coatings showed no apparent abnormalities; all of the metal coatings were made with essentially the same thickness. After the test, the deposit thickness profiles appeared to be similar to those formed on the other metal surfaces. The results indicate either adhesion of agglomerated insolubles or the formation of deposits from soluble gums at particular sites on the magnesium surface. The adhesion of agglomerated insolubles seems to be a more likely candidate because the Auger deposit thickness measurements were higher than those with the DMD and the difference tended to increase with rising temperature. The results indicate that greater amounts of

magnesium become incorporated into the structure of the deposit as the temperature is raised. This suggests, as mentioned above, that magnesium dissolution is an important process as the fuel is prestressed on its journey to the hot section of the heater tube. Perhaps the dissolved magnesium initiates nucleation of soluble gums and causes agglomerates to form which then deposit (adhere) on the surface.

Conclusion: Under JFTOT D 3241 test conditions thickness profiles of deposits formed on a variety of surfaces, 316 SS, 304 SS, Al, Mg, Cu and Au, were compared using the DMD (dielectric breakdown voltage) and Auger milling. Except for gold and aluminum, the deposit thicknesses measured by DMD were substantially lower than those measured by Auger milling, and the disparity in the two methods seemed to grow with increased deposit thickness. Some deposits, especially those on the copper coated tubes, gave particularly low DMD thickness values compared to Auger milling values. Metal dissolution and subsequent inclusion into the deposit is thought to be responsible for the increased conductivity of the deposit, an effect which becomes more pronounced at higher tube temperatures. Aside from variations in the thickness of deposits due to metallurgy, the most dramatic effect observed was that the bulk of deposits moved to tube locations of lower temperature as the maximum temperature of the tube was increased from 300° to 380°C. These results suggest that the fuel used in this study forms its deposit over a relatively narrow temperature range; compared to the other surfaces this effect was observed at lower temperatures on the copper coated tubes. A cursory examination of photographs taken with the scanning electron microscope (SEM) showed hemispherical deposits on the magnesium surface and flat platelet type deposits on the other metal surfaces. Deposit morphology will be further studied and new experiments are planned using heater tube surfaces under more isothermal conditions with fuel flow across the tube (as opposed to longitudinal flow).

Acknowledgement: This work was conducted under DOD Contract No. DAAK70-87-C-0043, administered by the Fuels and Lubricants Division of the Materials, Fuels, and Lubricants Laboratory, U.S. Army Belvoir Research, Development and Engineering Center, Fort Belvoir, Virginia 22060-5606, with Mr. T.C. Bowen, STRBE-VF, serving as contracting officer's representative and Mr. M.E. LePera, STRBE-VF, serving as technical monitor. Approved for publication, this paper represents only the views of the authors.

References

(1) Cuellar, Jr., J.P., Russell, J.A., "Additive Depletion and Thermal Stability Degradation of JP-5 Fuel Shipboard Samples," Report No. NAPC-PE-141C.
(2) CRC Literature Survey on the Thermal Oxidation Stability of Jet Fuel, CRC Report NO.509, April 1979.
(3) Uri, N.; ACS Advances in Chemistry Series, #36, Chapt.10, p. 102, 1962.
(4) Hazell, L.B., Baker, C., David, P., and Fackerel, A.D., "An AES Depth Profiling Study of the Deposits on Aluminum During the Jet Fuel Thermal Oxidation Test," Surface and Interface Analysis 1, pp. 507-513, 1986.
(5) Clark, R.H., "The Role of a Metal Deactivator in Improving the Thermal Stability of Aviation Kerosines," 3rd International Conference on Stability and Handling of Liquid Fuels, London, UK, 13-16 September 1988.
(6) Schreifels, J.A., Morris, R.E.,Turner, N.H., and Mowery, R.L., "The Interaction of a Metal Deactivator With Metal Surfaces," American Chemical Society, Division of Fuel Chemistry, Preprints, 35, No.2, pp. 555-562, 22-27 April, 1990.
(7) Morris, R.E. and Hazlett, R.N., "Methods for Quantifying JFTOT Heater Tube Deposits Produced From Jet Fuels," Energy and Fuels, Vol. 3, No. 2, pp. 263-267, 1989.
(8) ASTM Thermal Oxidation Stability of Aviation Turbine Fuels (JFTOT Procedure). In Annual Book of ASTM Standards; ASTM: Philadelphia, PA, 1989; Part 5.02, ASTM D 3241-88a.
(9) U.S. Patent No. 4,791,811, "Deposit Thickness Measurement," J.G. Barbee, Southwest Research Institute, Granted Dec. 20, 1988.
(10) Stavinoha, L.L., Barbee, J.G., and Buckingham, J.P., "Thermal Stability Deposit Measuring Device," Proceedings of 2nd International Conference on Long-Term Storage Stabilities of Liquid Fuels, San Antonio, TX, 29 July - August 1986.

TABLE 1. Summary of Deposit Measuring Device (DMD) Evaluation of JFTOT Tubes Along With Standard ASTM D 3241 Ratings

Test No.	Tube Metal	Total Test Time, hr	Prefilter	Temp, °C	Pressure Drop, mm of Hg at Time	TDR Spun Rating at Station, mm	Visual Rating	DMD, Max. Thickness, cm × 10^{-7} at Station, mm	DMD, Vol. of Deposit, $cm^3 \times 10^{-7}$
253-H	304 SS	2.5	No	300	125 at 46.5 min	50+ at 44-58	>4 Peacock	2394 at 54	3785
254-H	304 SS	2.5	No	340	125 at 38.1 min	50+ at 32-50	>4 Peacock	2277 at 40	2999
255-H	304 SS	2.5	No	380	125 at 52.1 min	50+ at 26-58	>4 Peacock	2005 at 32	3226
157-T	Al	2.5	Yes	260	2 at 148.7 min	12 at 38-45	<4	42 at 54	54
256-H	304 SS	1.5	No	340	125 at 36.0 min	50+ at 34-58	>4 Peacock	1862 at 40	2282
257-H	304 SS	1.5	No	300	125 at 31.2 min	50+ at 45-58	>4 Peacock	1968 at 50	2255
258-H	304 SS	3.5	No	300	125 at 63.3 min	50+ at 40-58	>4 Peacock	2742 at 54	2742
259-H	304 SS	0.5	No	300	5.3 at 30.0 min	47 at 50-52	4	345 at 54	439
260-H	304 SS	1.0	No	300	125 at 56.1 min	50+ at 45-58	>4	1811 at 54	1835
261-H	304 SS	0.5	No	340	19.5 at 30.0 min	50 at 38-42	>4	591 at 42	651
262-H	304 SS	1.0	No	340	125 at 48.0 min	50+ at 36-49	>4	1845 at 42	2091
257-H	304 SS	1.5	No	300	125 at 31.2 min	50+ at 45-58	>4 Peacock	1968 at 50	2255
263-H	Al/304 SS	1.5	No	300	125 at 56.0 min	36 at 54	4 Peacock	1168 at 52	1256
264-H	Au/304 SS	1.5	No	300	125 at 66.3 min	50+ at 50-56	>4 Peacock	1411 at 52	1294
266-H	Mg/304 SS	1.5	No	300	125 at 52.1 min	Too Dark to Rate	4	1082 at 54	1558
267-H	Cu/304 SS	1.5	No	300	125 at 18.5 min	50+ at 38-58	4 Peacock	862 at 46	1164
279-H	316 SS	1.5	No	300	125 at 58.2 min	50+ at 28-58	>4 Peacock	2211 at 54	2669
256-H	304 SS	1.5	No	340	125 at 36.0 min	50+ at 34-58	>4 Peacock	1862 at 40	2282
268-H	Al/304 SS	1.5	No	340	125 at 33.5 min	50+ at 40-45	>4 Peacock	1200 at 42	1649
269-H	Au/304 SS	1.5	No	340	125 at 31.5 min	50+ at 40-45	>4 Peacock	1917 at 42	2048
270-H	Mg/304 SS	1.5	No	340	125 at 40.5 min	Too Dark to Rate	>4	1297 at 42	1944
271-H	Cu/304 SS	1.5	No	340	125 at 30.0 min	50+ at 29-58	>4 Peacock	751 at 36	682
278-H	316 SS	1.5	No	340	125 at 40.9 min	50+ at 24-56	>4 Peacock	2668 at 40	2440
272-H	304 SS	1.5	No	380	125 at 52.4 min	50+ at 30-40, 49-54	>4 Peacock	2137 at 34	2191
273-H	Al/304 SS	1.5	No	380	125 at 48.1 min	50+ at 32-36	>4 Peacock	1805 at 34	1633
274-H	Au/304 SS	1.5	No	380	125 at 56.9 min	50+ at 32-36	>4 Peacock	2248 at 34	1824
275-H	Mg/304 SS	1.5	No	380	125 at 58.3 min	Too Dark to Rate	>4	1237 at 36	1782
276-H	Cu/304 SS	1.5	No	380	125 at 31.2 min	50+ at 24-58	>4	1148 at 30	812
277-H	316 SS	1.5	No	380	125 at 35.5 min	50+ at 18-58	>4 Peacock	2477 at 34	1757

(LAM.F)

Table 2. Tube Locations of Maximum Deposit For Three Control Temperatures

	Deposit Peak Locations, mm		
Tube control temp. =	300°C	340°C	380°C
Metal Surface			
316 SS	52	40	32
Mg/304 SS	52	40	34
Cu/304 SS	46 (301°C)*	36 (325°C)*	30 (340°C)*
Au/304 SS	52	40	32
Al/304 SS	52	44	34
304 SS	50 (298°C)*	40 (335°C)*	34 (345°C)*

* Approximate Tube Temperature, °C, at location, estimated from Figure 3.

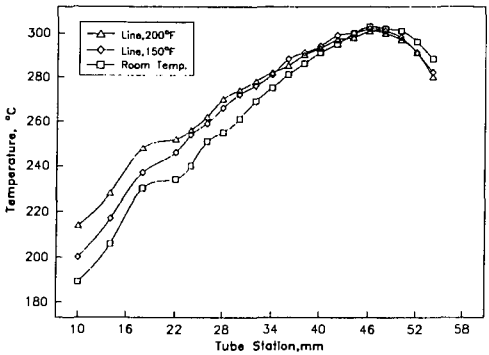

Figure 1. HLPS temperature profiles at 300°C

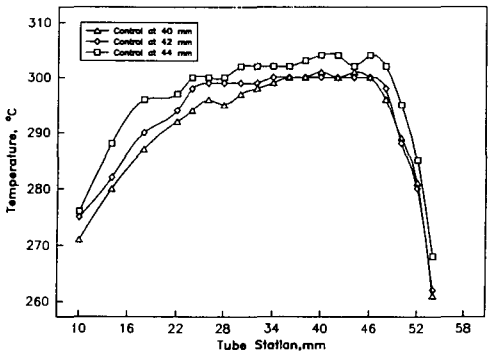

Figure 2. HLPS temperature profile with fuel flow through top of the 304 stainless steel heater tube at 300°C

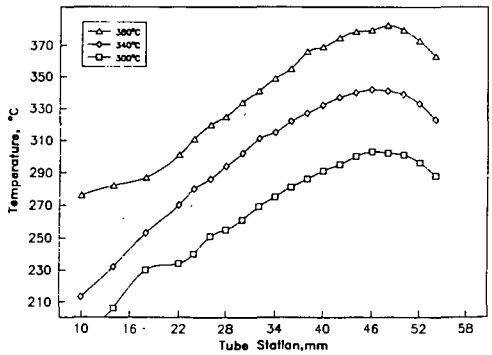

Figure 3. HLPS temperature profile of three temperatures using 304 stainless steel heater tubes

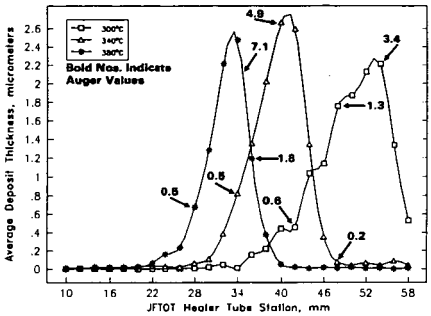

Figure 4. Deposit thickness on 316 stainless steel heater tube run at 300°C, 340°C, and 380°C

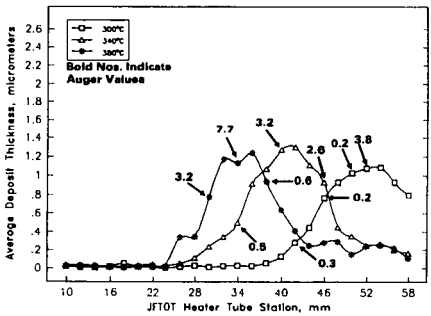

Figure 5. Deposit thickness on magnesium plated heater tube run at 300°C, 340°C, and 380°C

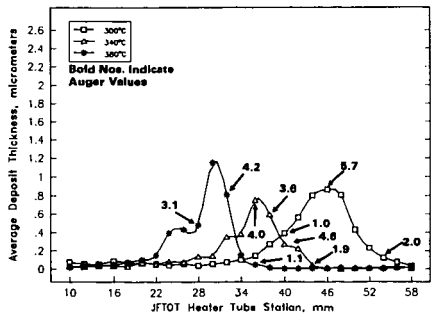

Figure 6. Deposit thickness on copper plated heater tube run at 300°C, 340°C, and 380°C

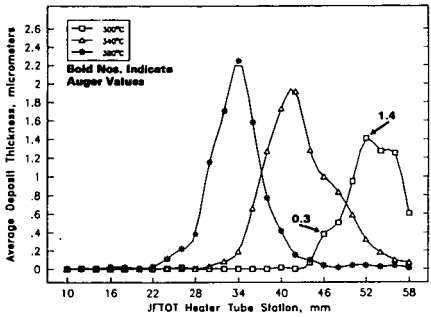

Figure 7. Deposit thickness on gold plated heater tube run at 300°C, 340°C, and 380°C

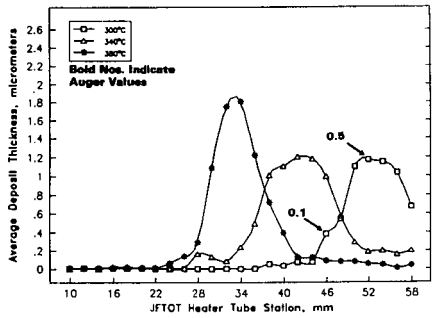

Figure 8. Deposit thickness on aluminum plated heater tube run at 300°C, 340°C, and 380°C

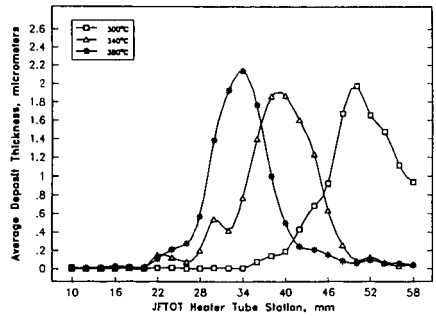

Figure 9. Deposit thickness on 304 stainless steel heater tube run at 300°C, 340°C, and 380°C

HIGH TEMPERATURE GAS PHASE PYROLYSIS OF JP-8

by

Jeffrey L. Moler*†, Ellen M. Steward†, and Philip H. Taylor‡

†Aero Propulsion and Power Laboratory (WRDC/POSF), Aeronautical Systems Division, Air Force Systems Command, United States Air Force, Wright-Patterson Air Force Base OH 45433-6563 (U.S.A.)

‡University of Dayton Research Institute, Dayton OH 45469 (U.S.A.)

Gas phase pyrolysis of JP-8 (NATO designation F-34), neat and with a thermal stability additive (JFA-5) is reported. Experiments were conducted in a quartz test cell to minimize catalytic effects. Data were collected isothermally at 50 degree intervals from 350°C (662°F) to 850°C (1562°F) and at mean residence times in the range of 0.3 to 3.0 seconds. Products were analyzed using gas chromatography with mass selective and flame ionization detectors, GC/MS and GC/FID, respectively. The low molecular weight decomposition products, from C_1 to C_7, are identified. The onset of decomposition and formation of decomposition products were observed under these conditions. The products of thermal decomposition and the time and temperature relationship of the decompositions are discussed and compared to the decomposition products of pure compounds. The results obtained from the jet fuel thermal oxidation tester (JFTOT) for the same fuels are also discussed. The JFA-5 additive had almost no effect on the thermal decomposition over this temperature range.

INTRODUCTION

The chemical composition of aviation fuels determines the thermal stability of the fuel. The temperatures and times required for a fuel to degrade determine the limits of aircraft performance and how much of the advantage gained from more efficient engines can actually be achieved. Thermal stability and thermal decomposition products of aviation fuels will play an important role in the design of future aircraft systems.

The thermal stability of aviation turbine fuels was first recognized as a problem in the 1950's. In conventional turbine engines, aviation fuels encountered high temperatures in the lubrication oil heat exchanger and the combustor manifold and nozzles[1]. Exposure of the fuel to these high temperatures resulted in the thermal degradation of the fuel and formation of deposits on critical engine parts.

With the development of high-Mach aircraft and more efficient engines, thermal stability of fuels has become even more crucial. The fuel in these aircraft and systems may reach temperatures of 538°C (1000°F), or higher[2]. This increased thermal stress may increase the thermal degradation and the deposits formed on critical engine parts and in fuel systems. Therefore, a better understanding of the thermal stability characteristics of current United States Air Force and NATO jet fuels is needed.

Previously, the pyrolysis of several alkanes, branched alkanes, and alkylated cycloalkanes within a carbon number range of 8 to 14 was reported[3]. These classes were chosen for study because they number among the major components of a typical JP-8. Comparison of individual component pyrolysis behavior with the pyrolysis behavior of JP-8 will yield a better understanding of JP-8 thermal stability.

A systematic study of the thermal decomposition of JP-8 (NATO designation F-34) from 600°C to 1000°C has been accomplished. JP-8 is typically a petroleum distillate cut from 177°C to 266°C (kerosenes) and commonly contains certain classes of compounds that may lower thermal stability. The rates at which individual components decompose and products form, *i.e.*, the temperatures and times necessary for pyrolysis to occur, are important factors in understanding the general thermal stability of a jet fuel.

EXPERIMENTAL

Apparatus

The system for thermal diagnostic studies (STDS)[4], developed at the University of Dayton Research Institute, is a continuous system consisting of three in-line units: the thermal decomposition unit, an analytical gas chromatograph (GC) for separation of parent compounds and pyrolysis products, and hydrogen flame ionization and mass selective detectors (FID and MSD, respectively)[5][6].

The thermal decomposition unit has a test-cell control module and an interchangeable test-cell assembly. The test-cell assembly has a quartz reaction cell heated by a hinged tube furnace (Linberg) over a temperature range of 250°C to 1150°C. The test-cell assembly is housed in a GC oven (Hewlett-Packard 5890A) for temperature control of the transfer lines, e.g., -100°C to +400°C.

Chromatographic separation was performed in a GC (Hewlett-Packard 5890A) with two separate chromatographic columns. Initial experiments were performed on a 30-meter Hewlett-Packard Ultra-5 column that was fed from the reactor cell assembly to the MSD (Hewlett-Packard 5970B). The Hewlett-Packard Ultra-5 column was then replaced with a 12-meter Hewlett-Packard Ultra-1 column that was fed from the reactor cell assembly to the FID. Ultra-high purity helium (99.999%) was used in the reactor cell assembly and as the carrier gas for chromatographic analysis.

Reagents

Thermal stability enhanced JP-8 was prepared from a WRDC/POSF standard JP-8 and 30 mg/l of JFA-5, obtained from the DuPont Company. Standard mixtures of C_2 to C_6 alkenes and C_1 to C_6 normal alkanes were obtained from Scott Specialty Gases for identification standards and quantitation.

Procedure

A 0.03 μl sample was injected into the test-cell assembly resulting in a gas-phase concentration of 1.78 x 10^{-4} moles/l. Both a neat JP-8 and a JP-8 standard containing 30 mg/l of JFA-5 were tested. The reaction temperature was governed by the tube furnace temperature. Temperatures were monitored before, within, and after the reaction zone using chromel/alumel thermocouples. The sample was held at 200°C before and after isothermal exposure ($\pm$1°C) to the experimental temperature in the reactor. Residence time at temperature was controlled by changing the mass flow. Unreacted sample and decomposition products were swept through a heated transfer line—to prevent condensation—after emerging from the test-cell and were captured at the head of the analytical chromatographic column, held at -60°C. During the first 6 minutes, separation of the C_1 to C_4 products occurred on the column. After the initial 6 minutes, the analytical GC was temperature programmed at 15°C/min to 285°C to allow for chromatographic separation of the remaining decomposition products and the jet fuel sample. The GC eluents were detected qualitatively by the MSD and quantitatively by the FID.

RESULTS AND DISCUSSION

JP-8 is composed of thousands of compounds, among which normal alkanes, branched alkanes, and alkylated cycloalkanes have the largest concentration, with smaller amounts of aromatic and unsaturated compounds. Trace components, such as nitrogen-, sulfur-, and oxygen-containing species and dissolved oxygen and metals, are present in the fuel and may act as initiators in free radical decomposition of the fuel components[7][8]. Thermal decomposition of JP-8 was not observed at temperatures below 650°C. Thermal decomposition of alkanes at high temperatures (500°C or higher)[9] occurs via a radical-chain mechanism[10]. Other pyrolysis experiments with low molecular weight alkanes at 660°C[11][12] produced the same products as JP-8, but the higher molecular weight hydrocarbons in JP-8 require higher temperatures to produce similar decompositions[13]. This is supported by the trends observed for individual component decomposition[3].

JP-8 was subjected to pyrolysis to determine its overall thermal decomposition and the thermal decomposition characteristics of individual components in a complex mixture at various mean residence times. In Table 1, the reactor residence times necessary for one, five, ten, fifteen, and twenty percent decomposition of neat JP-8 have been calculated from the experimental data for temperatures from 600°C to 1000°C. In Figure 1, the gas chromatograms of the neat JP-8, subjected to temperatures from 500°C to 1000°C with a mean residence time of 1 second, illustrate typical behavior observed from the thermal decomposition. Additional chromatograms showing similar behavior were collected at reactor residence times between 0.3 and 3.0 seconds.

While data were collected over a range of residence times, 0.3 to 3.0 seconds, within the temperature range of 500°C to 1000°C, the typical patterns of formation and decomposition observed are shown in Figures 2 through 9, using a residence time of 1.0 second. The C_1 to C_6 compounds in Figures 2 to 5 are not present in the unstressed JP-8. The C_7 and higher carbon number compounds in Figures 5 to 9 are present at differing

concentrations in the unstressed JP-8. The concentrations of the decomposition products relative to the initial JP-8 concentration are also given in Figures 2 through 9.

Inspection of Figures 2 through 4 indicates that for temperatures less than 750°C, the lighter hydrocarbons (C_1 through C_4) are the principal products. At higher temperatures, the rate of decomposition for C_2 and higher carbon number compounds competes with their rate of formation until the formation of methane dominates above ~900°C. Higher molecular weight aromatic compounds are observed chromatographically, but were not quantitatively measured. These higher molecular weight compounds include alkylated benzenes, naphthalenes, and multiple-aromatic-ring compounds identified by the MSD.

Methane and ethene increase in concentration up to 800°C, where the rate of formation no longer increases with temperature (Figure 2). Propene and propyne each reach a maximum at 800°C and 900°C, respectively, and then fall off in concentration (Figure 3). 1,3-Butadiene and 1-butene reach maxima at 750°C and 800°C, respectively, before decreasing in concentration (Figure 4). Finally, the two primary aromatic species formed are benzene and methylbenzene (Figure 5). These aromatic species reach their maxima at 750°C and 825°C, respectively. Their formation is a potential indicator of deposit precursor formation[14], and may provide a link to the degradation kinetics.

The normal and branched alkanes found in JP-8 show similar behavior in most cases. Nonane and decane can be formed through pyrolysis of higher molecular weight alkanes, and therefore show maxima before rapidly decreasing at 650°C (Figure 6). Slightly higher in molecular weight and thermal stability, the concentrations of undecane and dodecane are fairly constant until they reach a breakpoint after which their concentration decreases (Figure 7). The branched alkanes shown in Figure 8 have very different behavior resulting from their formation from the decomposition of higher molecular weight species. 2-Methyldodecane behaves similar to nonane and decane, with a maximum at 650°C. At 800°C, 2-methylundecane coeludes with naphthalene, which begins to dominate as a more favorable by-product of decomposition and addition reactions at higher temperatures, because the naphthalene concentration increases up to 1000°C. The concentrations of tetradecane and pentadecane decrease linearly in concentration as temperature increases (Figure 9).

The addition of 30 mg/l of the JFA-5 additive into JP-8 increased the JFTOT breakpoint temperature from 280°C to 360°C using a 2.5 hour duration test[15]. Comparisons of 1.0 second residence time data within the 650°C to 1000°C temperature range show a slightly greater decomposition occurring for the JP-8 with additive compared to the neat JP-8 (Figure 10). Other thermal oxidative inhibitors have been reported to enhance thermal stability at moderate temperatures and decrease stability at much higher temperatures[16]; inhibiting radical formation at moderate temperatures and acting as a radical initiator at much higher temperatures. Additional tests above 650°C with varied amounts of the radical-inhibitor JFA-5 will be needed to determine its effectiveness for extremely high temperatures.

Although the STDS contained an oxygen-free environment, as noted previously, oxygen was most likely present as small amounts of dissolved oxygen and oxygenated species, approximately 55 ppm. This results in an oxygen concentration of approximately 1.65 ppb in the reactor. The presence of oxygen affects the pyrolysis behavior; oxygen readily supports the formation of radical species that are important in the decomposition of hydrocarbon compounds. Even so, the typical behavior of an average JP-8 at these temperatures was observed. The kinetics of thermal decomposition of JP-8 are complex, and remain unresolved.

CONCLUSIONS

The maximum temperature and minimum times at various temperatures, at which a fuel will resist thermal degradation in the presence of small amounts of oxygen, have been approximately determined. To obtain a ten percent decomposition using reactor residence times of 0.3 to 3.0 seconds, temperatures from 680°C to 600°C, respectively, were required. For a one second residence time, a temperature of 636°C was needed for ten percent decomposition of JP-8. The addition of 30 mg/l of the JFA-5 additive did not change the temperature required for equivalent decomposition in the neat JP-8. This information will provide the basis for determining the limits of thermal stability and developing methods that will be used to enhance thermal stability of future jet fuels[17].

The major components of JP-8 are normal and branched alkanes. The majority of other components have alkyl groups attached to them. The decomposition products are formed by the cracking of alkanes and

cleaving alkyl groups. Additionally, dehydrogenation and isomerization occurs at temperatures above 850°C and reformed products undergo further cracking and cleavage. The major low molecular weight products formed from 600°C to 1000°C are the methane, ethene, propene, propyne, and the butenes. From 600°C to 700°C, terminal alkenes are formed preferentially. From 700°C to 850°C, alkylated cycloalkanes and alkenes dominate the higher molecular weight products. Above 850°C, the major products become alkylated benzenes, naphthalenes, and multiple-aromatic-ring compounds.

Further work needs to be accomplished before the kinetics can be resolved. The pyrolysis studies of more single components and simple mixtures of these single components are required before the mechanisms and kinetics will be understood. Pure compound studies are planned to attempt to unravel the kinetic complexity of JP-8 decomposition.

The JFA-5 additive had the effect of increasing the thermal oxidative stability at lower temperatures (up to 350°C); yet, it had almost no effect on the thermal stability of JP-8 from 600°C to 1000°C at a residence time of 1.0 second.

LITERATURE CITED

1. S. M. Cohen, *Aircraft Research and Technology for Future Fuels Symposium*, NASA Conf. Pub. 2146, april 16-17, 1980.
2. A. C. Nixon, Performance Report Battelle Subcontract No. F-4186(8827)-484 under U. S. Air Force Contract No. F33615-84-C-2410, January, 1986.
3. J. L. Moler and E. M. Steward, *ACS, Div. Pet. Chem.*, PREPRINTS, **34**, (4), 837 (1989).
4. W. R. Rubey and R. A. Grant, *Rev. Sci. Instrum.*, **59**, (2), 265 (1988).
5. H. S. Hertz and S. N. Chesler, *Trace Organic Analysis: A New Frontier in Analytical Chemistry*, (NBS, Washington, 1979).
6. W. A. Rubey and R. A. Carnes, *Rev. Sci. Instrum.*, **56**, 1795 (1985).
7. E. W. Pitzer and E. M. Steward, AFWAL-TR-86-2043, 1986. (Available through NTIS.)
8. C. Martel, WRDC-TR-89-2021, 1989. (Available through NTIS.)
9. F. O. Rice, *J. Am. Chem. Soc.*, **55**, (7), 3035-3040 (1933).
10. A. Kossiakoff and F. O. Rice, *J. Am. Chem. Soc.*, **65**, (4), 590-595 (1943).
11. A. N. Rumyantsev and E. Yu. Oganesova, *Kimiya i Tekhnologiya Topliv i Masel*, No. 1, 29-30, January, 1987.
12. A. N. Rumyantsev and E. Yu. Oganesova, *Kimiya i Tekhnologiya Topliv i Masel*, No. 3, 29-31, March, 1987.
13. B. M. Fabuss, J. O. Smith, and C. N. Satterfield, *Advances in Petroleum Chemistry and Refining*, (Interscience, New York, Vol IX, Chapter 4, 1964).
14. I. C. Lewis, E. M. Dickinson, D. J. Miller, and J. Amos, *ACS, Div. Pet. Chem.*, PREPRINTS, **33**, (3), 404 (1988).
15. P. D. Liberio and M. R. Swensen, Unpublished Data, June, 1989.
16. R. E. Morris and R. N. Hazlett, *ACS, Div. Pet. Chem.*, PREPRINTS, **33**, (2), 364 (1988).
17. A. C. Nixon, G. H. Ackerman, R. D. Haawthorn, H. T. Henderson, and A. W. Ritchie, Technical Documentary Report No. APL TDR-64-100, Part II, September, 1966.

Table 1. Temperature Versus Reactor Residence Time Required for One, Five, Ten, Fifteen, and Twenty Percent Decomposition of Neat JP-8.

T (°C)	$t_{(1\%)}$	$t_{(5\%)}$	$t_{(10\%)}$	$t_{(15\%)}$	$t_{(20\%)}$
600	0.56	1.64	2.38	2.64	2.75
650	0.06	0.37	0.71	0.92	1.13
700	<0.01	0.02	0.21	0.32	0.47
750	<0.01	<0.01	0.06	0.11	0.19
800	<0.01	<0.01	0.02	0.04	0.08

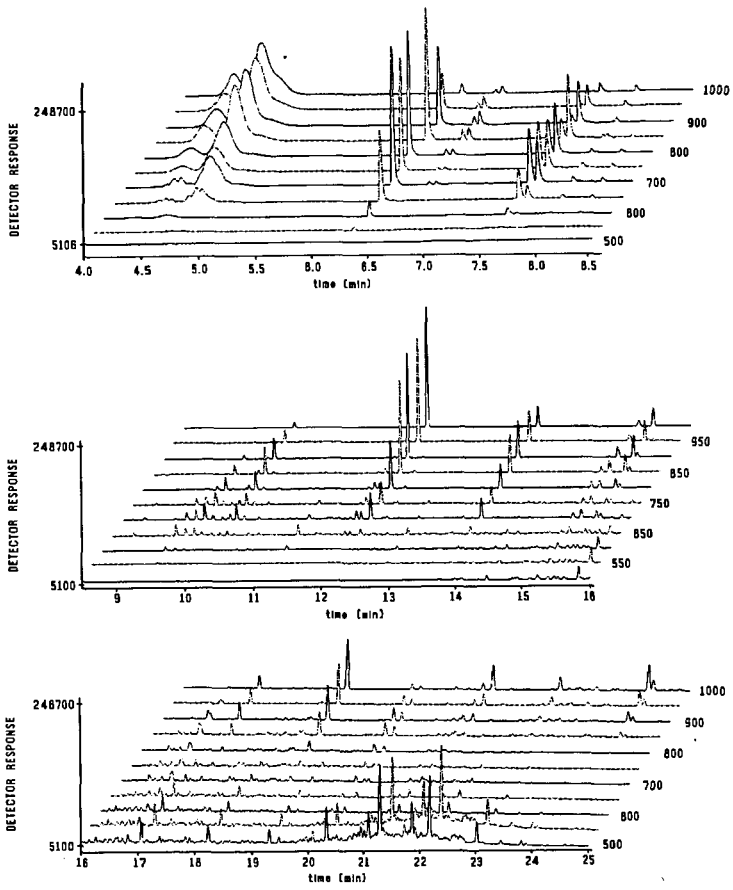

Figure 1. Gas Chromatograms of JP-8 from 500°C to 1000°C with a 1 Second Residence Time.

Compounds not initially present in JP-8.

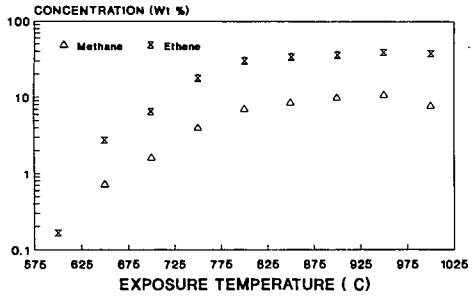

Figure 2. Formation of CH4 and C2H4.

Compounds not initially present in JP-8.

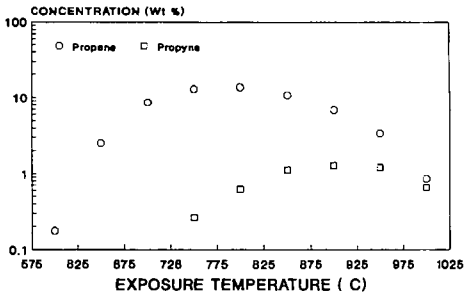

Figure 3. Formation of C3 Species.

Compounds not initially present in JP-8.

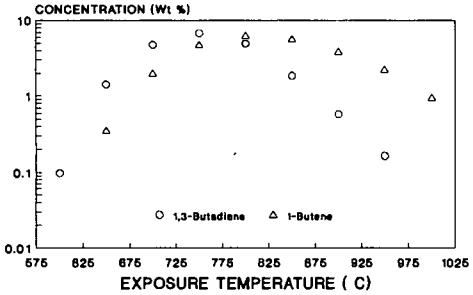

Figure 4. Formation of C4 Species.

Benzene is not initially present in JP-8

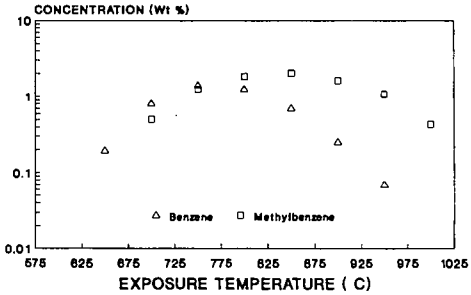

Figure 5. Formation of C6-C7 Aromatics.

Changes in amounts present in JP-8.

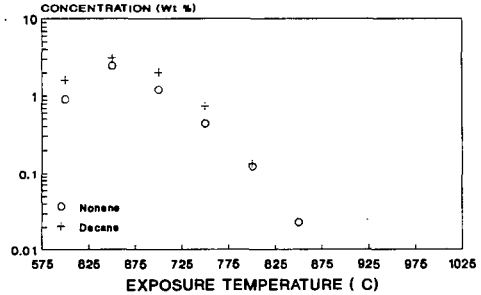

Figure 6. Decomposition of C9 and C10.

Changes in amounts present in JP-8.

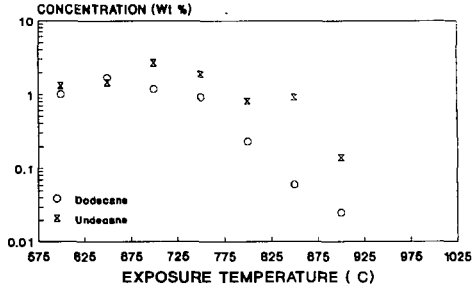

Figure 7. Decomposition of C11 and C12.

Changes in amounts present in JP-8.

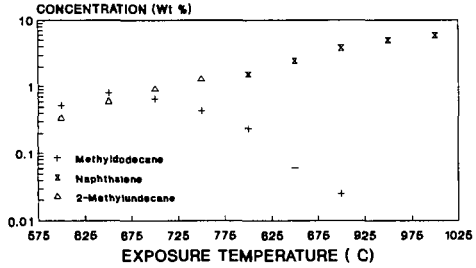

Figure 8. Behavior of Branched Alkanes and Formation of Naphthalene.

Changes in amounts present in JP-8.

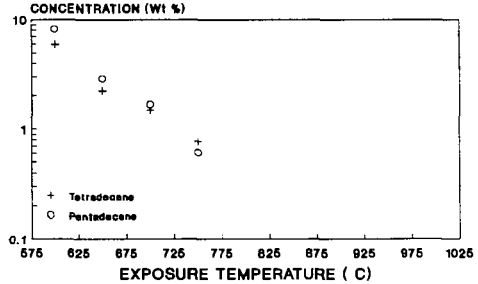

Figure 9. Decomposition of C14 and C15.

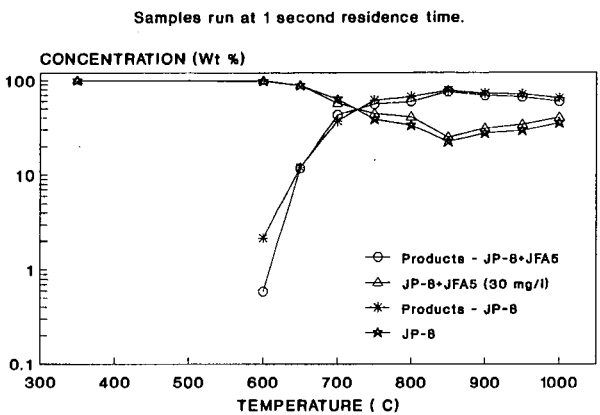

Figure 10. JP-8 versus JP-8 + JFA-5.

SYMPOSIUM ON THE STABILITY AND OXIDATION CHEMISTRY
OF MIDDLE DISTILLATE FUELS
PRESENTED BEFORE THE DIVISIONS OF FUEL
AND PETROLEUM CHEMISTRY, INC.
AMERICAN CHEMICAL SOCIETY
WASHINGTON MEETING, AUGUST 26-31, 1990

A THREE-DIMENSIONAL ANALYSIS OF THE FLOW AND TEMPERATURE DISTRIBUTIONS IN THE JFTOT

By

J. A. Pearce and W. M. Roquemore
WRDC Aero Propulsion and Power Laboratory, Wright-Patterson AFB, Ohio, 45433

and

C. H. Oh, B. J. Merrill, and R. P. Wadkins
Idaho National Engineering Laboratory, P. O. Box 1625, Idaho Falls, Idaho 83415

ABSTRACT

This paper provides an insight into the detailed flow and temperature distributions in the Jet Fuel Thermal Oxidation Tester (JFTOT), a test device that has been used for many years to quantify the thermal stability of aircraft fuels. Though the JFTOT has found wide application as a qualification test device, very little is known about the many intricacies and nuances of the JFTOT flow field. Of particular interest is the possibility that variations in the flow field could be manifested in terms of changes in deposition on the JFTOT heater tube. To quantify the flow and temperature distributions, a three-dimensional numerical analysis is applied using the KIVA code. Also included in the analysis is a simplified model for jet fuel thermal degradation. Due to the limited amount of quantitative data available from JFTOT experiments, the deposition model used in the study is a global type Arrhenius equation with "calibration" data derived from tests with the Fiber Optic Modified JFTOT (FOM-JFTOT).

NOMENCLATURE

a_i constants in temperature curve fit
A_d Arrhenius preexponential factor
A_e exit flow area
A_i inlet flow area
D characteristic diameter

E_d	Arrhenius activation energy
i	grid representation of r
j	grid representation of θ
k	grid representation of z
K	deposit thermal conductivity
l	starting length
r	radial direction
r_i	inner radius
r_o	outer radius
Δr	$r_o - r_i$; channel width
Re_D	Reynolds number based on hydraulic diameter
t	time
T	temperature
u_r	radial velocity component
u_z	axial velocity component
u_θ	azimuthal velocity component
z	axial direction
θ	azimuthal direction
τ	deposit thickness

INTRODUCTION

Thermal stability of jet fuels is a research area which has received significant attention for more than 30 years. Current interest in the field is high due to the prospects for future thermal stability challenges. These challenges arise primarily from the practice of using fuel to cool critical on-board aircraft systems. Large thermal stresses on the fuel are the consequence of this practice, and this condition is expected to worsen with increasingly sophisticated aircraft design. To further aggravate the problem, crude stock quality is expected to decrease in the future with possible deleterious effects on fuel thermal stability (1). At this juncture it has become critical to better understand the mechanisms that affect a fuel's thermal stability. The consequences of failing to gain a better understanding of thermal stability could include limiting aircraft performance envelopes for lack of suitably stable fuels.

A long standing tool of the thermal stability researcher is the Jet Fuel Thermal Oxidation Tester (JFTOT). This device has long been used by laboratories in the qualification of jet fuel thermal stability. Full details on the test procedures are not

necessary for the current discussion but can be found in the literature (2,3). A qualification test for a typical aviation fuel such as JP-4, JP-5, or JP-8 consists of flowing the given fuel around an electrically heated tube for a period of 150 minutes at a peak heater tube temperature of 260°C. The test is evaluated by comparing the color of the deposit on the heated tube to a standard reference. A numerical value or rating is assigned to the test results based on the tube coloration. Based on this rating a fuel either "passes" or "fails" the test. Unfortunately, the qualification test yields little or no data which can be used to better understand the various detailed mechanisms contributing to the degradation of fuel within the device.

In an attempt to try to increase the research value of JFTOT testing, variations on the standard qualification test have been devised (4). A common practice is to run tests at progressively higher tube temperatures until a "failure" is recorded. The temperature at which a fuel "fails" the test has been designated as the *Breakpoint Temperature*. Though this type of test certainly has more value than the qualification test, it still provides little information which could be valuable in the study of detailed degradation mechanisms.

Recent attempts have been made to try to quantify the results of JFTOT tests in terms which are more valuable to researchers (4-6). These tests have focused on examining the effects that various subprocesses have on the overall deposition process. Among the factors examined in these studies are fuel flow rate, tube temperature, and heater tube metallurgy. One of the more interesting results taken from the tests of Warner and Biddle (4) was a marked azimuthal asymmetry in the deposition on the tube. This trend was repeated in subsequent testing and is believed to be strongly linked to the complex flow field which exists within the JFTOT. Therefore, an exercise which may help to elucidate deposit mechanisms within the JFTOT is a determination of the detailed flow field within the device. The work presented here is focused on obtaining a description of the flow field within the JFTOT.

JFTOT GEOMETRY AND BOUNDARY CONDITIONS

JFTOT Geometry

A thorough understanding of the JFTOT geometry is necessary to comprehend the results which will be subsequently presented. The JFTOT is intended to be a simple flowing device for the qualification of jet fuels; however, a close examination of the flow passage reveals much about the JFTOT flow which is not simple. The Reynolds number at the tube entrance, based on the hydraulic diameter, is $Re_D \cong 13$. This Reynolds number places this flow firmly in the domain of laminar flow. The low Reynolds number is a

product of both the low flow rate through the JFTOT (3 ml/min) and the small annular flow channel ($\Delta r < 1$ mm). A schematic representation of the JFTOT is provided as Figure 1 to aid in demonstrating this point; also, the coordinate system (cylindrical) which is utilized for all subsequent discussions is provided as Figure 2.

The primary flow direction in the JFTOT is the axial (+z) direction; however, the flow is not a simple annular pipe flow as one might expect. Complexities arise in the JFTOT flow which are directly attributable to the orientation of the fuel inlet and exit. The fuel enters the JFTOT in the radial direction; consequently, the entry is normal to the primary flow direction (+z). This orientation of the flow, as it is introduced to the JFTOT, then provides a great deal of complication to the otherwise simple flow field. Also note that the entering flow impinges on a step in the JFTOT tube which further complicates the flow. Therefore, components of velocity in the r and θ directions in the lower region of the tube are introduced by the incoming fuel.

The flow is similarly perturbed by the fuel exit which is again situated normal to the primary flow direction. Since the JFTOT flow is elliptic in nature, the influence of a downstream disturbance will be manifested upstream of the exit; therefore, the effects of the exit orientation should be apparent in the region of the JFTOT upstream from the exit. Also, in a manner similar to the entering flow, the exiting flow must flow past a step on leaving the flow channel.

A further element complicating the JFTOT geometry is the respective orientation of the inlet and exit planes. The fuel is introduced in the $-r$ direction at the location $\theta = 0°$, while the fuel exits in the $+r$ direction at the location $\theta = 90°$. Therefore, there is a 90° rotation in the azimuthal plane from the inlet to the exit and an azimuthal (θ) component of velocity must be introduced to the flow to account for this rotation. In light of the previous discussions, it should now be apparent that the flow in the JFTOT is three-dimensional and quite complex, and the analysis of the flow field is not a trivial problem.

Boundary Conditions

One aspect critical to the determination of the JFTOT flow field is the application of proper boundary conditions. The primary quantities of interest are the velocity components and the fuel temperature. The following boundary conditions apply at the tube inlet:

$$r = r_o = 2.3125\text{x}10^{-3}\text{ m};\ \theta = 0°;\ z = 0$$
$$u_r = -0.01\text{ m/s};\ u_\theta = 0;\ u_z = 0$$
$$T = T_{amb} = 300\text{ K} \qquad 1)$$

Conditions at the tube exit ($r = r_o$, $\theta = 90°$, $z = 0.06$ m) are determined by the code and are unspecified at the outset. However, there is a constraint that the exiting velocity be in the $+r$ direction.

At the outer radius of the tube (excepting the inlet and exit), the following conditions apply:

$$r = r_o = 2.3125\text{x}10^{-3}\ \text{m}$$
$$u_r = u_\theta = u_z = 0$$
$$T = T_{amb} = 300\ \text{K} \qquad 2)$$

Admittedly, the temperature boundary condition at the outer radius is likely incorrect. In reality, the outer surface is exposed to ambient air, but it is certainly heated by both conduction through the test apparatus and convection from the heated fuel. However, since no reliable measurements of the outer housing temperature were available, the boundary was fixed at the ambient air temperature.

Finally, at the inner radius (JFTOT heater tube outer surface) the following conditions apply:

$$r = r_i = 1.40\text{x}10^{-3}\ \text{m}$$
$$u_r = u_\theta = u_z = 0$$
$$T\ (\text{see (3)}) \qquad 3)$$

Note that the ASTM (3) description of the JFTOT test provides axial temperature profiles along the heater tube. There is no azimuthal variation in these prescribed temperature profiles. For the particular case modeled in this study (maximum heater tube temperature of 550°F), a curve fit of the heater tube temperature profile was employed with the following form:

$$T(\text{K}) = a_1 + a_2 z + a_3 z^2 + a_4 z^3 \qquad 4)$$

where z is in mm and the constants a_i are

$a_1 = 519.6$ K
$a_2 = -3.676$ K/mm
$a_3 = 0.2718$ K/mm^2
$a_4 = -0.003857$ K/mm^3

NUMERICAL MODEL

Computational Fluid Dynamics

The fluid flow in the JFTOT was modeled using the KIVA code developed at the Los Alamos National Laboratory. The partial differential equations solved in the KIVA code are the Navier-Stokes, conservation of mass, and internal energy equations. The code is both three-dimensional and transient. For these calculations, JP-5 fuel was the fluid of interest; consequently, temperature dependent curve fits of the fluid properties were derived from existing data (7) and implemented into the code. Details of the numerical scheme employed in the code can be found in the literature (8-12), and their inclusion here is unnecessary.

The computational grid applied to the given problem is shown in Figures 3 and 4. Figure 3 shows a three-dimensional representation of the grid which consists of 8 radial cells, 24 azimuthal cells, and 24 axial cells (4,608 total cells). The coordinate orientations are supplied in the figure, as are the general locations of the fuel inlet and exit. Figure 4, which depicts an r-θ plane of the grid, further clarifies the geometry. Fuel is inlet in the azimuthal (j) cells between $j = 3$ and $j = 7$. The fuel exits between cells $j = 9$ and $j = 13$. Logically, the inlet is at the bottom of the computational grid at axial (k) cells $k = 1$ and $k = 2$, and the exit is at the top of the computational grid at $k = 24$ and $k = 25$. All fuel enters and exits the flow domain at the outer radius which corresponds to the radial (i) location $i = 9$. By specifying the inlet and exit regions in this manner, the correct flow areas of $A_i = A_e = 4.91 \times 10^{-6}$ m^2 are preserved in the model.

Jet Fuel Thermal Degradation

The calculation of jet fuel thermal degradation, in terms of a deposit thickness on the JFTOT heater tube, was accomplished separately from the KIVA code. A number of assumptions were made regarding the deposition on the heater tube; primarily that the deposition was solely a function of the temperature at the deposit/fuel interface and that the local flow field had *no* effect on the deposition. Due to a severe lack of quantitative deposition data from the JFTOT, a simple global Arrhenius expression was used to model the accumulation of deposits on the heater tube. The expression governing deposit growth is given by

$$\frac{d\tau}{dt} = A_d \, exp\left(\frac{-E_d}{T}\right) \qquad 5)$$

The preexponential factor (A_d) and activation energy (E_d) were determined from data provided by Warner and Biddle (4) with the Fiber Optic Modified JFTOT (FOM-JFTOT). From this data the following constants for the preexponential factor and activation energy were determined:

A_d = 155,970 m/s
E_d = 19,920 K

The temperature used in Equation 5 is the temperature at the fuel/deposit interface. This temperature is determined by analyzing the following energy equation for heat transfer in the deposit layer:

$$\left[\frac{1}{r}\frac{\partial}{\partial r}\left(Kr\frac{\partial T}{\partial r}\right)+\frac{1}{r^2}\frac{\partial}{\partial \theta}\left(K\frac{\partial T}{\partial \theta}\right)\right]=0 \qquad 6)$$

The boundary conditions for this equation, which is solved separately from KIVA, are taken from the KIVA temperature field for a given time step in the calculation.

RESULTS

JFTOT Flow Field

Though the KIVA code calculates the flow field in a transient sense, all of the velocity vectors and temperature contours displayed are for an instant in time subsequent to the system achieving a steady state. The first depiction of the flow field is provided as Figure 5. On the left are contours of the fluid temperature and on the right are velocity vectors. The three slices of the flow field shown are r-θ planes at the bottom (z = 0), mid-height (z = 0.03 m), and top (z = 0.06 m) of the flow domain. Note the orientation of the inlet and exit with respect to the plots which are shown (refer to Figures 3 and 4).

First considering the plots of the isotherms, note that for each plot the minimum and maximum temperatures are given below the figure and the contours are evenly spaced throughout the given temperature range. At the bottom of the domain note how the contour lines are bunched near the surface of the tube on the side corresponding to the fluid inlet. This bunching indicates steep thermal gradients and is a consequence of the entering fluid. On the side of the tube opposite from the inlet, note how the contour lines are much more widely spaced indicating the penetration of thermal energy into the flow. This is a consequence of the nearly stagnant flow in this region of the domain.

The temperature contours at the mid-height appear to be evenly distributed both radially and azimuthally. This is apparently because the thermal energy has sufficiently penetrated the fuel to eliminate any significant radial or azimuthal variations in the temperature field which were caused by the inlet. Furthermore, at this plane the flow is farthest from any of the influences which tend to perturb the flow (i. e., the inlet and exit). Moving to the exit, the contours are evenly spaced excepting the region where the fuel is exiting. At the exit, the contours appear to be stretched by the influence of the exiting flow.

Before discussing the velocity vectors depicted in Figure 5, some explanatory notes are necessary. First, since these depictions are r-θ planes, no axial velocity component is visible in these plots. Second, the plot routine scales the vectors independently for each plot; therefore, the length of the vectors is an indicator of velocity magnitude only for a given plot. The magnitudes of vectors *are not* directly related from plot to plot.

In the plot at the bottom of the domain, the influence of the incoming fluid can clearly be seen. There is an expected high radial component of velocity near the inlet, and there is also a high azimuthal velocity away from the inlet. However, on the side of the tube opposite the inlet the radial and azimuthal velocity components are very small. Moving to the mid-height, the flow is considerably more complex. Even at the mid-height, the influence of the exit can already be seen in terms of an outward radial component of velocity. However, note that the magnitude of these vectors is approaching the limits of the code's numerical accuracy. Directly opposite the azimuthal location of the exit, the azimuthal velocity component is again very small. Away from this location in both directions is a large azimuthal component of velocity. In some regions, there is also evidence of recirculation.

Finally, moving to the tube exit, the flow appears to be much more well ordered. There is a strong outward radial component of velocity at the exit, and there is also a significant azimuthal component of velocity on the side of the tube corresponding to the exit. However, on the opposite side of the tube, both the radial and azimuthal velocity components appear to be minute.

Moving to another view of the flow field, Figure 6 depicts radial profiles of temperature and axial velocity at the same axial locations used in Figure 5. Note that each of the plots in Figure 6 is at the azimuthal location corresponding to the fuel exit ($\theta = 90°$). In the three temperature plots, the penetration of thermal energy can be seen progressively as one moves up the tube. At the bottom of the tube, there is a large radial gradient in temperature near the heater tube surface, and this effect is diminishing at the mid-height. At the tube exit, the slope is in fact very shallow, indicating a low rate of heat transfer to the fluid.

The velocity plots show basically an expected result. Note that the influences of radial and azimuthal velocity components are not present in this figure. At both the bottom of the tube and the mid-height, the velocity profiles are basically parabolic. This is the type of behavior that would be expected in a developed laminar pipe flow. Note that for laminar pipe flows, the length required for a flow to develop is approximately

$$l = 0.058\, Re_D\, D \qquad 7)$$

which for $Re_D \cong 13$ equates to approximately $0.75D$ (13). Assuming D is the hydraulic diameter, the entire length of the JFTOT is approximately $160D$. This implies that the flow becomes developed a short distance from the inlet. Admittedly, the geometry of the JFTOT is not the specific geometry to which this relationship applies; however, even if this relationship were in error by two orders of magnitude, the flow would still be developed at the tube mid-height. Finally, the profile at the top of the domain appears to have an anomaly at the outer radius where the velocity is not zero. This is simply due to the presence of the fuel exit.

The final figure of the flow field is given as Figure 7. This plot depicts the velocity vectors in an r-z plane of the flow domain. The plot on the left represents the azimuthal positions corresponding to the exit ($\theta = 90°$ and 270°) and the plot on the right represents the positions corresponding to the inlet ($\theta = 0°$ and 180°). At the inlet ($\theta = 0°$), the influence of the entering fluid can clearly be seen, as can the flow stagnation in all other regions. Through the middle section of the tube there is little to note. Due to the great magnitude of the axial velocity with respect to the radial velocity ($u_z/u_r >> 1$) in most regions of the flow field, the influence of the radial velocity is not apparent. Finally, at the exit ($\theta = 90°$) the influence of the exiting flow is evident, and the flow is basically stagnant in all other regions.

Jet Fuel Thermal Degradation

The results of the calculation of deposit thickness on the JFTOT heater tube are given in Figure 8. Axial profiles of both the deposit thickness and wall temperature are shown. The results clearly show that the growth of the deposit layer follows the increase in wall temperature along the tube length. One would certainly expect this when considering that the model for deposit growth is based solely on the temperature of the fuel/deposit interface (Equation 5). The maximum deposit occurs at the location of the maximum temperature, and the maximum deposit thickness of 0.13 μm compares favorably with the measured value of 0.14 μm (4). It appears that this deposition model does a reasonable job of

approximating the JFTOT deposition for the specific case for which it was devised. However, its applicability to any other thermal stability experiments is questionable, and further studies would have to be accomplished to make any determination.

The premise that the local fluid flow has no influence on the deposition process is most certainly incorrect. Though many experiments have substantiated the significant role that surface temperature plays in the deposition process, it is not the sole contributing factor in jet fuel degradation. Some models have recently been presented that have addressed the issue of including multiple reaction steps in the degradation chemistry and allowing for the influence of fluid flow and bulk fuel temperature on the overall deposition process (14-16). However, the complexity of these models was beyond the scope of the current modeling effort, which was primarily focused on a determination of the JFTOT flow field.

CONCLUSIONS AND RECOMMENDATIONS

The results presented here have clearly demonstrated that the flow field in the JFTOT is quite complex. Due to the orientation of the flow inlet and exit, elements of flow in the radial and azimuthal directions are evident throughout the entire flow field. If one assumes that the flow field has some bearing on the deposition process, this complication of the flow could have a significant effect on the deposition observed on the JFTOT heater tube. However, the effects that the radial and azimuthal flow disturbances have on the deposition are not clear.

Further experimental efforts are necessary to elucidate the various mechanisms of fuel thermal degradation. Both the complex degradation chemistry and the effects of fluid mechanics and heat transfer must be addressed to better understand the overall deposition process. The most difficult task appears to be designing experiments that can isolate particular chemical and transport processes. Clearly the JFTOT is not such a device. Even though the JFTOT has been of great value in the qualification of fuel thermal stability, its use as a research tool is of questionable value.

ACKNOWLEDGEMENTS

This effort was jointly supported by the WRDC Aero Propulsion and Power Laboratory and the Department of Energy (DOE) Pittsburgh Energy Technology Center. The authors wish to thank Dr. Nand K. Narain, the DOE-Pittsburgh Program Manager, and William E. Harrison III, the U. S. Air Force Program Manager,.for their guidance in this effort.

LITERATURE CITED

(1) TeVelde, J. A. , and Glickstein, M. R. , United Technologies/Pratt & Whitney, NAPC-PE-87C (1983).

(2) Alcor, Inc., Report No. 75-167 (1975).

(3) ASTM D 3241-82, *1985 Annual Book of ASTM Standards: Petroleum Products, Lubricants, and Fossil Fuels,* Volume 05.03, 150-172 (1985).

(4) Warner, P. A. and Biddle, T. B., United Technologies/Pratt & Whitney, Report No. FR 19032-11 (1988).

(5) Clark, R. H. and Thomas, L., "An Investigation of the Physical and Chemical Factors Affecting the Performance of Fuels in the JFTOT," SAE Aerospace Technology Conference and Exposition (1988).

(6) Kendall, D. R. and Mills, J. S., SAE Paper 851871 (1985).

(7) Nixon, A. C., Ackerman, G. H., Faith, L. E., Henderson, H. T., Ritchie, A. W., Ryland, L. B. , and Shryne, T. M., Shell Development Company, AFAPL-TR-67-114, Pt. III, Vol. II (1970).

(8) Amsden, A. A., Ramshaw, J. D., O'Rourke, P. J., and Dukowicz, J. K., Los Alamos National Laboratory, LA-10245-MS (1985).

(9) Amsden, A. A., Ramshaw, J. D., Cloutman, L. D., and O'Rourke, P. J., Los Alamos National Laboratory, LA-10534-MS (1985).

(10) O'Rourke, P. J. and Amsden, A. A., Los Alamos National Laboratory, LA-10849-MS (1986).

(11) Amsden, A. A., O'Rourke, P. J., and Butler, T. D., Los Alamos National Laboratory, LA-11560-MS (1989).

(12) Oh, C. H., Merrill, B. J., and Wadkins, R. P., Idaho National Engineering Laboratory, WRDC-TR-89-2138 (1989).

(13) Shames, Irving H., *Mechanics of Fluids*, New York, McGraw-Hill Book Company, 270 (1982).

(14) Roquemore, W. M., Pearce, J. A., Harrison, W. E., III, Krazinski, J. L. , and Vanka, S. P., *Preprints - Division of Petroleum Chemistry 34* (4), 841-849 (1989).

(15) Deshpande, G. V., Serio, M. A., Solomon, P. R., and Malhotra, R., "Modeling of the Thermal Stability of Aviation Fuels," Symposium on the Chemical Aspects of Hypersonic Propulsion, 198th National Meeting of the ACS, Miami, FL (1989).

(16) Krazinski, J. L., Vanka, S. P., Pearce, J. A. , and Roquemore, W. M., ASME Paper No. 90-GT-33 (1990).

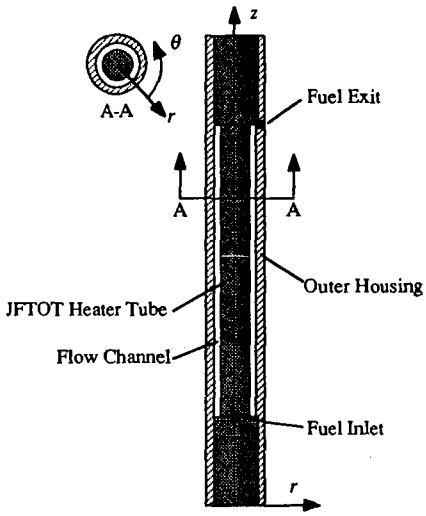

Figure 1: Schematic Representation of the JFTOT (Not to Scale)

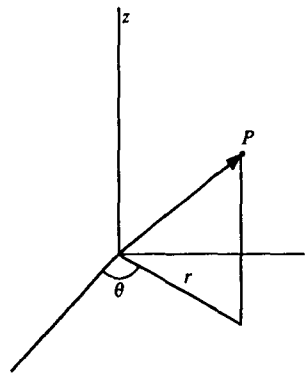

Figure 2: Cylindrical Coordinate System Used in KIVA Calculations

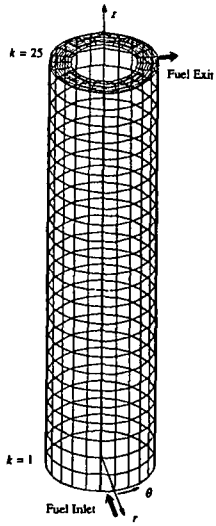

Figure 3: Three-Dimensional View of 8 x 24 x 24 Computational Grid

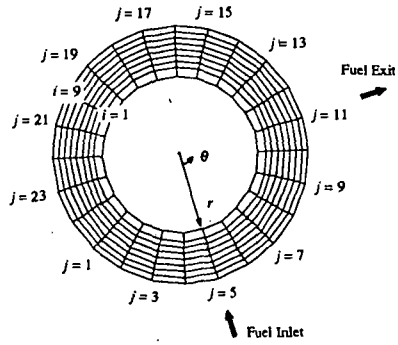

Figure 4: Top View of Computational Grid

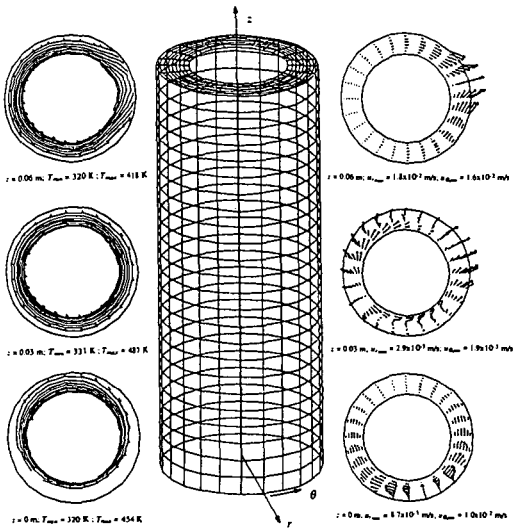

Figure 5: Calculated Temperature Contours and Velocity Vectors at the Bottom, Mid-Height, and Top of the JFTOT

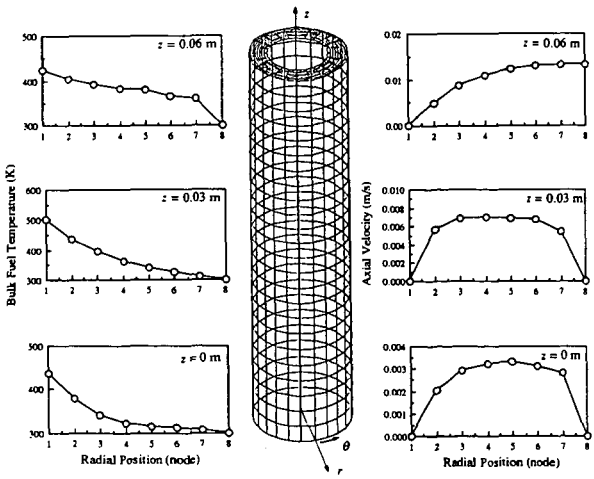

Figure 6: Calculate Radial Temperature and Axial Velocity Profiles at the Bottom, Mid-Height, and Top of the JFTOT

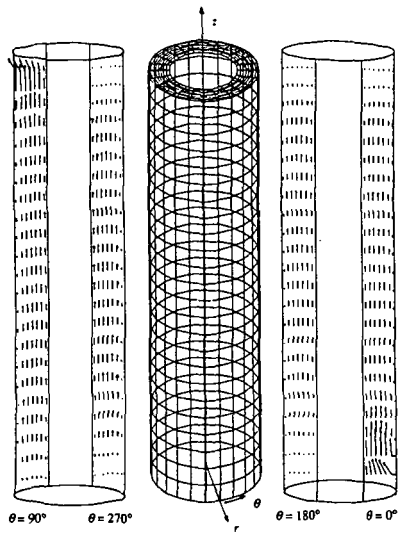

Figure 7: Calculated Velocity Vectors in the r-z Plane for Azimuthal Positions Corresponding to the Fuel Inlet and Exit

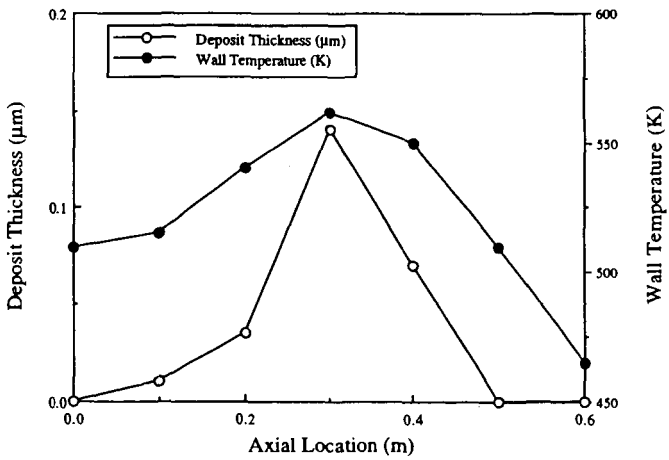

Figure 8: Predicted Axial Profiles of Deposit Thickness and Wall Temperature in the JFTOT

SYMPOSIUM ON THE STABILITY AND OXIDATION CHEMISTRY
OF MIDDLE DISTILLATE FUELS
PRESENTED BEFORE THE DIVISIONS OF FUEL
AND PETROLEUM CHEMISTRY, INC.
AMERICAN CHEMICAL SOCIETY
WASHINGTON MEETING, AUGUST 26-31, 1990

A TIME-DEPENDENT MODEL WITH GLOBAL CHEMISTRY FOR DECOMPOSITION AND DEPOSITION OF AIRCRAFT FUELS

By

K. V. Reddy and W. M. Roquemore
WRDC/Aero Propulsion and Power Laboratory,
Wright-Patterson Air Force Base, OH 45433-6563

Abstract

The complicated decomposition processes of a thermally stressed aircraft fuel are mathematically treated using a computational fluid dynamics (CFD) base model with global chemistry. Recently Krazinski et al. (6) proposed a time-averaged CFD model with global chemistry for predicting the deposition rate of jet fuel. This model has proven to give reasonable results when calculations are compared to heated tube experiments lasting 25 hours or less. However, longer duration heated tube experiments have shown that the deposition rate increases with test time. This cannot be adequately treated by the time-average model since it assumes that the deposition rate is independent of time. This paper presents a time-dependent CFD model with global chemistry that directly accounts for deposit build-up and the impact this has on the fuel velocity and heat transfer rate and, thus their effect on deposition rate. The time-dependent incompressible Navier-Stokes equations along with the species continuity and energy equations are solved in an uncoupled manner using a fully implicit scheme. The model uses the global chemistry model proposed by Krazinski et al., but also assumes that the surface deposition reaction rate increases as a power of the deposit thickness. Comparisons of predictions with data from long duration tests, show that the model gives reasonable results for test durations of 150 hours or less but begins to deviate substantially for longer test times. Future improvements to the chemistry in the model are needed to correctly account for the effects of very long test times on deposition rate.

Introduction

The thermal stability of future jet fuels and the processes that result in fouling of fuel system components are of increasing concern. Thermal stability refers to the potential of a fuel to thermally decompose into insoluble products that can adher to solid surfaces. Exceeding the thermal stability limit of a fuel in an aircraft fuel system can result in sticking of fuel control valves, poor performance of heat exchangers, clogging of fuel nozzles and hot streaks in the combustor due to an alteration of fuel nozzle spray pattern (1). Although these fouling problems occur sporadically in today's engines, they are expected to be more serious in future high performance aircraft due to the higher heat loads that the fuel will experience as it is used to cool the engine lube oil, avionics, environmental systems, and the fuel controls (2).

The thermal stability of jet fuels has been studied for many years. Quality control methods and empirical design information for hot fuel system components such as heat exchangers and fuel nozzles have resulted from these studies (1). Also, a considerable quantity of data have been collected for different experimental conditions and test apparatus. However, the overall complexity and a lack of fundamental understanding of the processes leading to fouling has hindered the development of a general theoretical framework that can be used to interpret or predict different experimental results. Two empirically based fouling models with similar global kinetics for fuel decomposition chemistry have been developed (3,4). One of the models (4) contains heat and mass transport expressions, which makes it potentially applicable to many engineering problems. However, the empirically based models do not provide, in a fundamental way, the general mathematical framework necessary for predicting the thermal deposition of different jet fuels for radically different experimental apparatus with a wide range of operating conditions. Thus, they do not have the general theoretical framework needed to interpret and predict the results for many different types of experiments. On the other hand, recently proposed computational fluid dynamics based models with global chemistry (CFDC) (5,6) do have the potential of being generally applicable for different test section geometries and a wide range of test conditions. Furthermore, the CFDC models can serve as an aid in designing meaningful experiments, interpreting experimental results in terms of fundamental processes, evaluating theories, providing insights into coupled processes, and estimating the relative sensitivity of parameters associated with fouling.

This paper extends the CFDC thermal stability modeling approach by solving the time-dependent Navier-Stokes equations instead of the Reynolds or time-averaged equations as done in Refs. 5 and 6. The model takes into account the build-up of deposits with time and the impact this has on the fluid velocity and heat transfer rate at the fuel/solid interface. The global chemistry model of Krazinski (6) is used in the present analysis along with the preexponential and activation energies determined therein. These global kinetic parameters were determined by curve fitting procedures using data from short duration tests of 25 hours or less.

Effects of Long Duration Testing on Deposition Rate

The importance of time on the deposition rate was demonstrated in long duration tests conducted by Giovanetti and Szetela (4) and Marteney (7). The average deposition rate at 500 hours is a factor of approximately two greater than that at 400 hours and is approximately four times that at 100 hours (7). This increase is larger at lower wall temperatures than at higher wall temperatures. Since clean fuel is always entering the test section, these changes in deposition rate with exposure time suggest that changes in surface reactivity and changes in fluid dynamics and heat transfer due to deposit blockage might be important factors. A microscopic analysis of deposit surfaces revealed that they are highly irregular and granular (7). The surface irregularity and the structure of the cavities depend mainly on the fluid velocity and the deposit thickness. This rough surface might affect the deposit growth rate by trapping fuel in the cavities and altering the surface sticking properties. Because of the constant heat flux used in heating the fuel, the trapped fuel may experience higher temperatures and residence times than the surrounding flowing fuel thereby, yielding more deposits. Blockage of the tube also becomes significant for long duration tests. At a fuel velocity of 0.076 m/s, Marteney (7) observed only a 43 percent open area after 50 hours of testing. This dropped to 16 percent after 150 hours. The blockage is not evenly distributed along the length of the tube because of the way the deposition rate depends on temperature. The large blockage with uneven distribution of deposits alters the fuel velocity and the heat transfer rate which can, in turn, change the deposition rate. These factors are considered in the time-dependent CFDC thermal stability model.

Mathematical Approach

The time dependent Navier-Stokes equations along with the turbulent energy and species conservation equations are used to describe the fuel motion in a long thin circular tube that is heated electrically with a constant heat flux. To advance the calculations with large time steps (to complete the hundreds of hours of real time within a few minutes of computational time), the governing equations are discretized into finite-difference equations and then are integrated using a fully implicit scheme. At each time step, the oxygen and precursor conservation equations are solved simultaneously with the other governing equations in an uncoupled manner.

The present formulation allows the deposit to grow on the wall surface with test time. In other words, after every time step, the geometry of the fuel/deposit interface, is allowed to change as part of the solution procedure. The computational domain is bounded between the axis of symmetry and the fuel-deposit interface and the grid system is reconstructed after every time-step for the changes in the boundary shape.

The mass, momentum and energy transport equations of the governing equations contain several coefficients related to molecular diffusion, viscosity, and thermal conductivity, respectively. Since a wide range of temperatures exists within the test section, the transport properties of the fuel vary significantly. A fresh JP-5 fuel is used as the fluid in the present calculations and the transport properties, along with the enthalpy and density at the given temperature, are obtained from the curve fits, just as done in Ref. 6.

Chemical Kinetics

Although there is only a limited understanding of the thermal decomposition processes in jet fuels, it is widely believed that they involve oxidation and pyrolysis of hydrocarbon fuel molecules and the formation of radical species (8,9). Autoxidation of the fuel, which is promoted by dissolved oxygen, occurs at temperatures up to about 540 K. Krazinski, et al. (6) used a global kinetics model with two reaction steps to account for the autoxidation reaction. This model did well in predicting the deposition rates in different heated tube experiments and is used in the present analysis. The two reaction steps of this model, which are assumed to to occur in the bulk fuel, can be written as follows:

Fuel + Oxygen ==> Precursor

Precursor + Fuel ==> Fuel + Solubles

Step 1 generates the important deposit forming precursor species through an autoxidation process. The removal of precursors from the deposition process is assumed to occur at higher temperatures through the second reaction step. A wall reaction, that is similar to the oxidation reaction but, with different reaction rate constants, is also used as a surface reaction mechanism.

To take into account the effects of test duration on the wall reaction, the rate constant for the wall autoxidation reaction is assumed to be a function of both temperature and deposit thickness. Experimental observation (7) indicates that the deposition rate, thickness and granularity of the deposits increase with test duration. This suggests that the number of sites on which the deposit can form increases with time. As a first approximation, the wall reaction rate is assumed to be:

$$\text{Reaction Rate} = k\,(\Delta h/R)^m \exp(-Ea/R_0T) \qquad 1)$$

Here, Δh is the deposit thickness at any given axial location on the tube with initial inner radius R, m is a constant to be determined and k is the pre-exponential constant used in Ref. 6. In the above global reaction model, all the precursors produced on the wall surface and those transported from the bulk fuel to the wall, are assumed to stick to the wall instantaneously and form a deposit. After the (n+1) time-step, the deposit thickness is calculated by updating the deposit geometry at the nth time-step using the expression:

$$\Delta h^{n+1} = \Delta h^n + (\Delta t)\,P\,/\,\text{Density of the Deposit} \qquad 2)$$

where P is the rate of generation of precursor particles on the wall surface due to the wall reaction and molecular transport mechanisms.

Results

The time-dependent CFDC model was initially evaluated by repeating the CFDC time averaged calculations presented in Ref. 6. Using the same rate boundary conditions and global reaction model, the time-dependent calculations of wall and fuel temperatures, fuel velocity,

turbulent intensities, deposition rate, and concentrations of precursor and oxygen converged to steady-state values that were in agreement with the time-averaged calculations performed using the model in Ref. 6. For this initial check out of the model the influence of deposit growth on the flow field and heat transfer rate, nor the increase of the surface reaction rate with deposit thickness, these capabilities were not activated. This was necessary to simulate the conditions in the time-average CFDC model.

Marteney (7) conducted a series of experiments to investigate the dependence of deposition rate and deposit morphology on test time duration. The fuel was thermally stressed as it flowed through electrically heated stainless steel tubes with an inner radius of 1.08 mm. A constant heat flux along the 914.4 mm tube length was maintained for the duration of a test. Steady-flow test were conducted from 25 to 500 hours. Tests were run at fuel inlet velocities of 0.0762 m/s and 0.3048 m/s. These test results are used to investigate the capabilities of the time-dependent CFDC model. The ability of the model to correctly determine the dependence of deposition rate and deposit thickness on test duration are of prime interest in the following results.

Figure 1 is presented to demonstrate how the deposit thickness and deposition rate change with wall temperature for test durations of 50 and 150 hours and a fuel velocity of 0.0762 m/s. Two types of calculations are presented. Both have m = 0 in the surface deposition rate equation (Eq. 1). In one calculation, the influence of deposit blockage on the fluid dynamics and heat transfer processes is not taken into account. In this case, the time-dependent calculations converged to a steady-state solution shown in Fig. 1. In this case the solution is the same as would be obtained by using the time averaged model in Ref. 6. For the steady-state solution, the total deposition rate is the mass of deposit divided by the test time. By using a deposit density of 0.9 g/cc, as recommended in Ref. 7, this linear relationship can be used to calculate the deposit thickness for the two test times. The deposit thickness results are also shown as steady-state solutions in Fig. 1.

The second type of calculation presented in Fig. 1 considers the influence of deposit blockage as a function of time on the fluid dynamics and the heat transfer processes. These calculations show that the deposition rate is not influenced at the low wall temperatures and only weakly influenced at the higher wall temperatures. The model does, however, give the correct trends. The model predicts that the deposition rate should increase more rapidly at the lower wall temperatures than for the higher wall temperatures, and that after 150 hours the deposition rate reaches a saturation value at a wall temperature of about 550 K. These trends are also observed in the experiments. Figure 1 also shows that the predicted deposit thickness is also only weakly

influenced by the effects of blockage on deposit formation. However, there is a significant discrepancy in the two measured thicknesses and the calculated values.

The experimental deposition rates shown in Fig. 1 for the 50 and 150 hours tests have a larger separation than the calculated rates. This indicates that the deposition rate mechanism is different from that used in the model. In Fig. 2, calculations are presented in which the deposition rate in Eq. 1 is assumed to go as the deposit thickness to a power m = 0.8. This assumption appears to improve the agreement between the calculated and measured deposition rates as compared to those in Fig. 1. The deposit thicknesses are also in better agreement but the calculated values are lower than the measured values. This is inconsistent with the fact that the calculated deposition rates are consistently higher than the measured values. The deposit thickness appears to be a sensitive function of deposit density. This opinion was reached by repeating the calculations for different deposit densities. It was determined that with a deposit density of 0.15 g/cc, the deposit thickness would agree with the measured values. However, the value of m had to be limited to 0.8 in order to keep deposition rate from becoming unrealistically high. The sensitivity of deposit thickness to density illustrates the importance of having accurate measurements of deposit density.

Calculations have also been made with the same tube but at a higher inlet fuel velocity (0.3048 m/s) and using a value of m = 0.8. At this velocity, the flow inside the tube is transitional. Since the present CFDC code can only simulate either a completely laminar or a fully turbulent flow, two calculations are made at this velocity; one with the assumption that the flow is laminar, and the other with a fully turbulent flow assumption. In the heated-tube section, the laminar flow assumption yields more accurate values of wall temperatures but the predicted bulk temperature is very low compared to the experimental data. On the other hand, the overall temperature distribution is better for the turbulent flow simulation and fairly accurate bulk fuel temperatures are obtained; but, agreement for the wall temperatures is poor near the entrance region up to 500 K. These results are shown in Fig. 3. Since the experimental data for deposition rate are available only up to 500 K, laminar flow simulations are used to predict the deposit growth.

The predicted and measured deposition rates are plotted in Fig. 4 for long duration tests with a fuel velocity of 0.3048 m/s. For test durations up to 300 hours, the predicted deposition rate curves closely follow the experimental data. For very long exposure times and low wall temperatures, however, the computed deposition rates are significantly lower than the measured values and at the higher temperatures the deposition rates undergo rapid increases. This trend is not observed in the experimental results.

Summary and Conclusions

A time-dependent CFDC model for predicting the thermal autoxidation decomposition and deposition characteristics has been developed. This model is used to estimate the effects of long duration tests on deposition rate as measured by Marteney (7). The experimental result that the deposition rate increases significantly with time, suggests that the deposition rate depends in some way on the deposits that are already present. It was assumed in the model that the surface deposition rate increases with deposit thickness. This resulted in fair agreement of deposition rates for test times of less than 150 hours but poor agreement for longer times. The calculated deposit thicknesses were also in poor agreement with measured values for the shorter duration tests. In conclusion, additional work must be performed on the model to better account for the effects of test time duration on deposition rate and deposit thickness.

ACKNOWLEDGMENT

The first author wishes to thank the National Research Council, Washington for supporting him to carry-out this research through the NRC-Air Force Systems Command Research Associateship.

LITERATURE CITED

(1) Anon: CRC Literature Survey on the Thermal Oxidation Stability of Jet Fuel. CRC Report No. 509, Coordinating Research Council, Inc., Atlanta, GA, April 1979.

(2) Koff, Bernard L., The Next 50 Years of Jet Propulsion, The Global Anniversary of Jet Powered Flight:1939 -1989, Dayton and Cincinnati AIAA Meeting, Dayton,OH, August 1989.

(3) Deshpande, G. V., Serio, Michael A., Solomon, Peter R. and Malhotra, Ripudaman, Modeling of the Thermal Stability of Aviation Fuels, , ACS Division of Petroleum Chemistry, Inc., Washington D. C., Vol. 34, No. 3, p. 955, Sept. 1989.

(4) Giovanetti, A. J., and Szetela, E. J., Long Term Deposit Formation in Aviation Turbine Fuel at Elevated Temperature, AIAA Paper 86-0525, 24th Aerospace Sciences Meeting, Reno, January 6-9, 1986

(5) Roquemore W. M., Pearce, J. A., Harrison III, W. E., Krazinski, J. L., and Vanka, S. P., Fouling in Jet Fuels: A New Approach, Preprints-Symposia in the Structure of Jet Fuels II, ACS Division of Petroleum Chemistry, Inc., Washington D. C., Vol. 34, No. 4, p. 841-849, Sept. 1989.

(6) Krazinski, J. L., Vanka, S. P., Pearce, J. A., and Roquemore W. M., A Computational Fluid Dynamics and Chemistry Model for Jet Fuel Thermal Stability, ASME Paper No. 90-GT-33, Proceedings of the 35th ASME International Gas Turbine and Aeroengine Congress and Exposition (Combustion and Fuels Committee), Brussels, Belgium, 11-14 June 1990.

(7) Marteney, P. J., Thermal Decomposition of JP-5 in Long Duration Tests, United Technologies Research Center, R88-957403-23, 1988.

(8) Taylor, W. F., Deposit Formation from Deoxygenated Hydrocarbons, Part I - General Features, Ind. and Eng. Chem., Prod. Res. and Devel., Vol. 13, No. 2, pp. 133-138, 1974.

(9) Hazlett, R. N., Hall, J. M., and Matson, M., Reactions of Rerated n-Dodecane Liquid Flowing Over Heated Metal Tubes, Ind. and Eng. Chem., Prod. Res. and Devel., Vol. 16, No. 2, p.171-177, 1977.

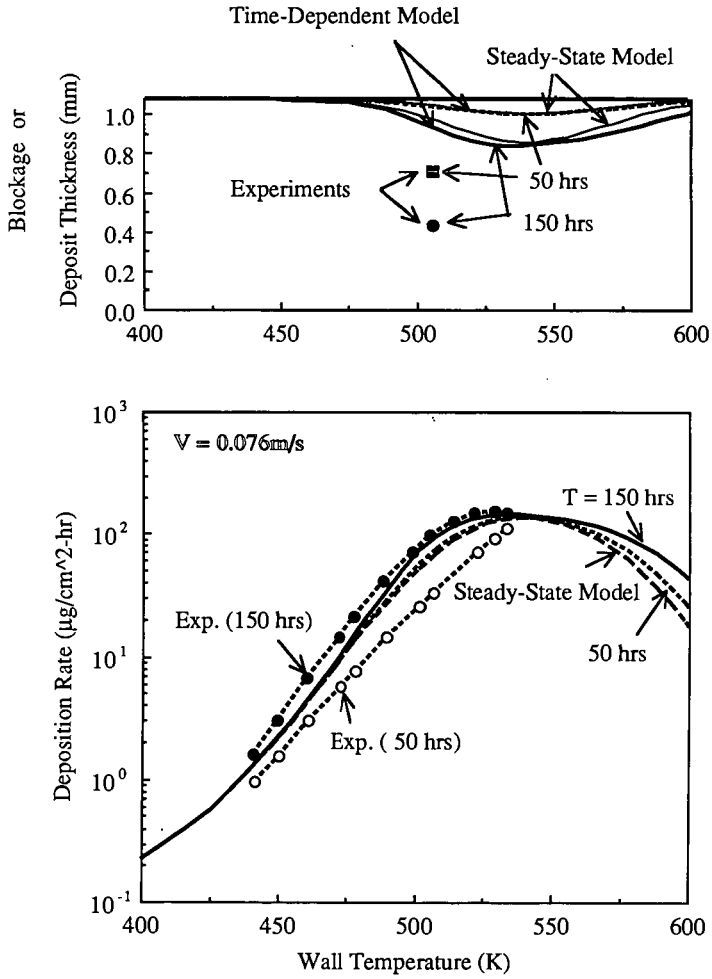

Figure 1. Predicted (without Changing Wall Reaction) and Measured Deposition Rates and Blockages for Long Duration Heated Tube Experiments of Marteney (1989).

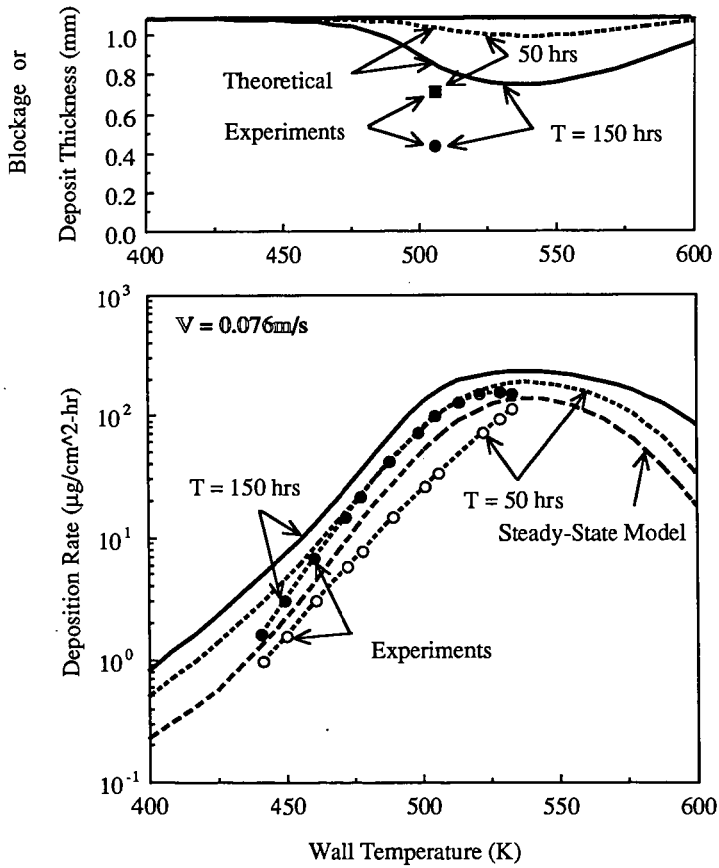

Figure 2. Predicted and Measured Deposition Rates and Blockages for Long Duration Heated Tube Experiments of Marteney (1989).

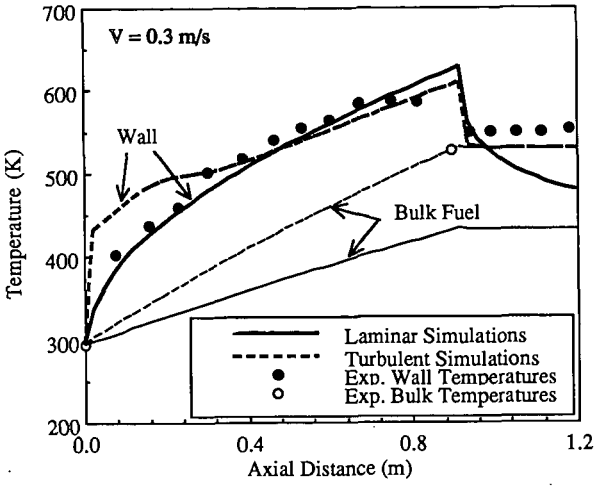

Figure 3. Comparision Between Predicted (Laminar and Turbulent Simulations) and Experimental Data for the Wall and Bulk Fuel Temperatures in the Heated Tube Experiment of Marteney (1989).

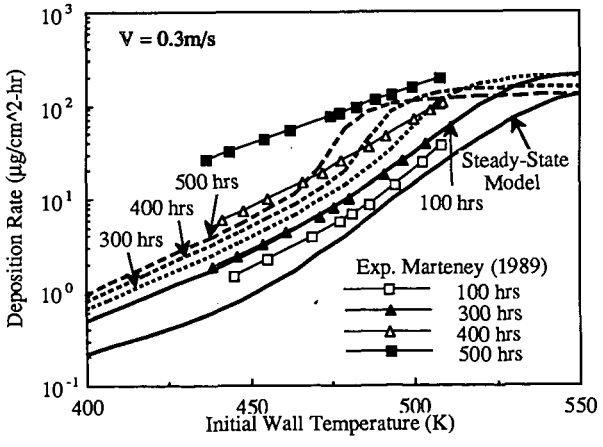

Figure 4. Predicted and Measured Deposition Rates for Long Duration Heated Tube Experiments of Marteney (1989).

CLEAN COAL TECHNOLOGIES, CLEAN AIR LEGISLATION, AND NATIONAL ENERGY STRATEGY

by

C. Lowell Miller, Ph.D.
Associate Deputy Assistant Secretary for Clean Coal
Office of Fossil Energy (FE-22)
U.S. Department of Energy
Washington, D.C., 20585

Introduction

Over the last year or two, several new phrases have become part of our lexicon, and have become so well known that they are now "household words"; included are phrases like:

- Acid rain,
- Ozone depletion, and
- Global warming.

These words all conjur up a frightening image of withering trees, dying lakes, sunburn, rising oceans, and flooded coasts. As a response, however, in 1989 the Bush Administration strove to familiarize the American public with two more phrases; these were:

- The Clean Air Act Amendments of 1989, and
- National Energy Strategy.

If the job is done right, the image that these words will conjur up will be reduced pollution, environmental protection, and a reliable supply of energy at an affordable price. That's where the Clean Coal Technology (CCT) Program comes in, because the CCT Program is the single most potent means at our disposal with which to overcome the global dilemma of how to use our abundant fossil fuels — not just America's, but indeed the world's — without simultaneously impairing the very quality of life we are working to improve with readily available electrical and other forms of energy.

There is no point in pretending that coal is what it is not, nor that it is not what it is. Coal is naturally endowed with the elements and minerals of the living organisms that define its primordial origins, and that means the carbon for which it is valued. But, to some degree, it also must mean sulfur, and nitrogen, and incombustible impurities. It is an incontrovertible fact that the uncontrolled burning of coal will release into the environment carbon dioxide (CO_2), sulfur dioxide (SO_2), oxides of nitrogen (NO_x), particulate matter, and ash.

It is the business of the CCT Program to develop the means of burning this coal with attendant minimal emissions of these undesirable pollutants; we know that there can never be none. So, if not literally "clean" coal, then certainly we mean "cleaner" coal, and it is in this sense that the Program uses the shorthand term, Clean Coal Technology.

What Are Clean Coal Technologies?

Now, having said that, what are Clean Coal Technologies? When we refer to CCTs, we mean advanced coal-based systems that can offer significant benefits when used to generate power, control pollution, or to convert coal into other alternative energy products.

For electric utilities, the characteristics of these technologies, including such attributes as higher thermal efficiency, modular construction, improved environmental performance, fuel flexibility, and repowering capability, will help them adapt to the decade of the 90's — a time of difficult and even conflicting pressures from regulatory reform, uncertain growth in power demand, environmental concerns, and increasing competition from independent power producers and cogenerators.

With regard to pollution control, CCTs have the ability to produce less, or to directly remove from the combustion process, SO_2 and NO_x acid rain precursors, and to reduce the amount of CO_2 generated by coal combustion. The types and quantities of pollutants removed will, of course, be a function of the specific CCT under consideration. In fact, some CCTs (e.g., pressurized fluidized bed combustion [PFB] and integrated gasification combined cycle [IGCC]) even have the ability to remove SO_2 and NO_x while at the same time increasing the power output of the facility itself from 50-150 percent. Table 1 lists the environmental performance of CCTs as compared to conventional (uncontrolled) pulverized coal-fired power plants.

Finally, CCTs can afford us the opportunity to produce coal-derived liquid fuels to replace oil and gas in numerous important applications. This capability could permit coal to play a much greater role in providing energy to the industrial, commercial, and transportation sectors.

The Projects That Comprise the CCT Program

On December 19, 1985, Congress passed Pub. L. No. 99-190, *An Act Making Appropriations for the Department of the Interior and Related Agencies for the Fiscal Year Ending September 30, 1986, and for Other Purposes*. Included in this Act were provisions for funds to conduct cost-shared, clean coal technology, projects for constructing and operating facilities demonstrating the feasibility of future commercial clean coal applications.

ENVIRONMENTAL PERFORMANCE OF CLEAN COAL TECHNOLOGIES RELATIVE TO CONVENTIONAL COAL-FIRED POWER PLANTS

Technology	SO2 Reduction	NOx Emissions	Waste Characteristics
Coal Cleaning:	10 - 30%	No change.	Solids disposal.
Flue Gas Desulfurization:	90+ %	No change.	Sludge disposal.
Advanced Flue Gas Cleaning	90+ %	Large reduction.	Usable byproduct.
Lime. Inj. Ms. Burner (LIMB):	50 - 60 %	Moderate reduction.	Dry pwdr. ok for landfill.
Slagging Combustor:	50 - 90 %	Moderate reduction.	Dry pwdr. ok for landfill.
Gas Reburning:	10 - 20 %	Moderate reduction.	None produced.
In-duct Sorbent Injection:	50 - 70 %	No change.	Dry pwdr. ok for landfill.
Advanced Coal Cleaning:	30 - 90 %	No change.	Solids disposal.
Int. Gas. Cmb. Cycle (IGCC):	95 - 99 %	Moderate reduction.	Slag, S, min. addl solids
Pressurized FBC:	90 - 95 %	Moderate reduction.	Dry gran. nontox. solids
Atmospheric FBC:	85 - 90 %	Moderate reduction.	Dry gran. nontox. solids

This first solicitation was open to all market applications of CCTs that applied to any segment of the United States coal resource base; the solicitation also encompassed both "new" and "retrofit" applications. DOE issued a Program Opportunity Notice (PON) on February 17, 1986, and received of 51 proposals by the April 18, 1986, deadline.

The outcome was the selection, on July 25, 1986, of nine initial projects for negotiation of Cooperative Agreements, and the identification of 14 alternate projects to be considered should negotiations not be successfully completed with any of the initial candidates. As of this writing, 8 of the alternate projects eventually entered into negotiations. Seven Cooperative agreements have now been executed, while three additional projects are in various stages of negotiation. These ten CCT-I projects now in the Program, and their locations, are shown in Figure 1.

While CCT-I was directed at demonstrating technologies that could, through increased efficiency and flexibility, increase the role of coal as an energy option, CCT-II was more focused and directed specifically on demonstrating technologies that can address the environmental aspects of coal use associated with the issue of acid rain. The objectives were derived principally from the efforts and results of the Special Envoys on Acid Rain. (In March 1985, the President appointed Drew Lewis to be the United States Special Envoy on Acid Rain, and, at the same time, Prime Minister of Canada Brian Mulroney appointed William Davis as the Canadian Special Envoy. The Special Envoys were charged with the responsibility to assess the international environmental problems associated with transboundary air pollution, and then recommend actions that would solve them.)

In January 1986, the Envoys presented their findings, including their recommendation that the United States initiate a 5-year, $5-billion, program for commercial demonstration of control technology projects recommended by industry and jointly funded by government and industry. In March 1986, the President endorsed the Special Envoys' recommendations, hence setting in motion the development of an expanded CCT Program that would build on the CCT-I effort, reflect ongoing State and privately funded initiatives, and be fashioned as fully as practicable from the guidelines recommended by the Special Envoys.

Accordingly, a second solicitation (CCT-II) was prepared and released on February 22, 1988, and, on September 28, 1988, 16 additional projects were selected for the Program; as of this writing, 9 of the projects have consummated Cooperative Agreements, while one project has withdrawn. The remaining 15 CCT-II projects and their locations are shown in Figure 2.

Figure 1

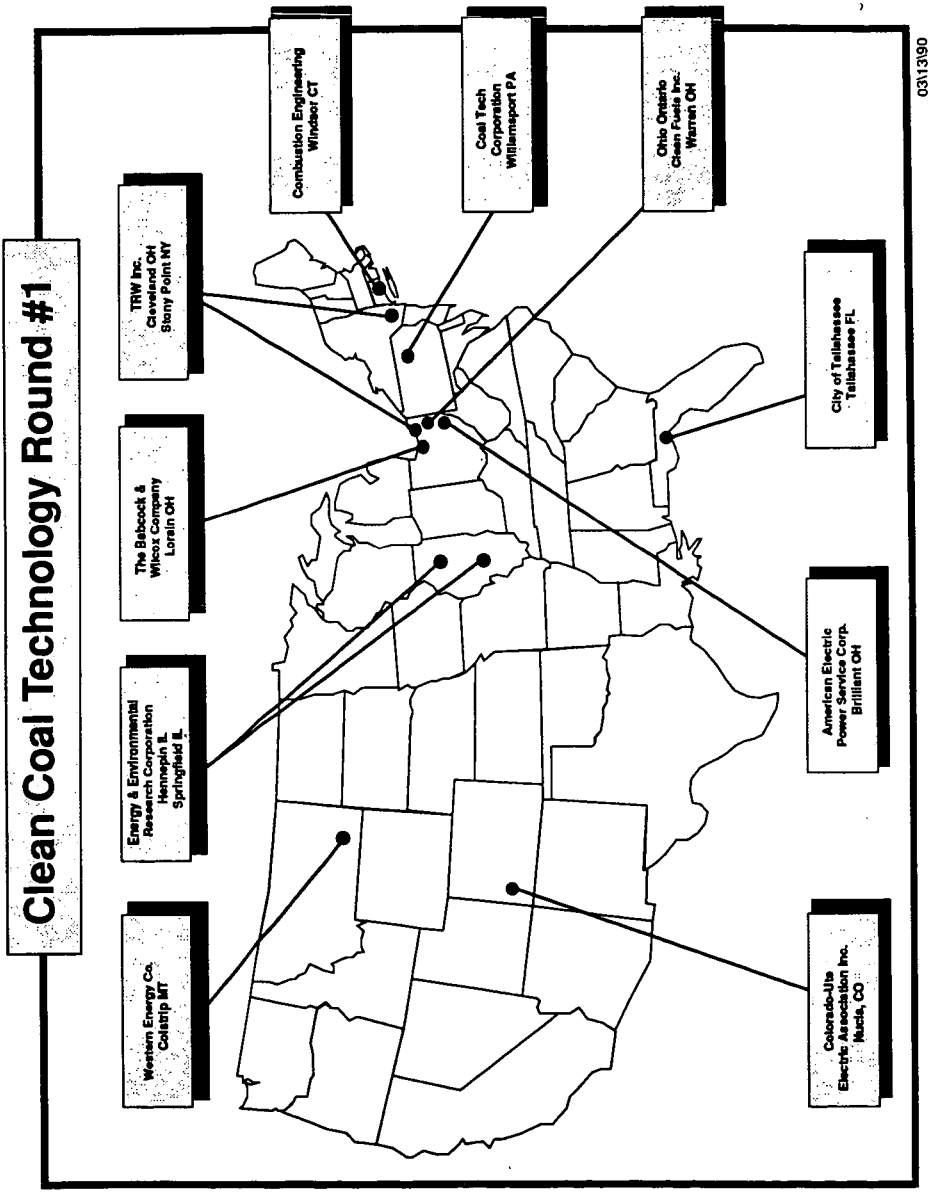
Clean Coal Technology Round #1
Western Energy Co.
Colstrip MT
Energy & Environmental
Research Corporation
Hennepin IL
Springfield IL
The Babcock &
Wilcox Company
Lorain OH
TRW Inc.
Cleveland OH
Stony Point NY
Combustion Engineering
Windsor CT
Coal Tech
Corporation
Williamsport PA
Ohio Ontario
Clean Fuels Inc.
Warren OH
City of Tallahassee
Tallahassee FL
American Electric
Power Service Corp.
Brilliant OH
Colorado-Ute
Electric Association Inc.
Nucla, CO
03113190

Figure 2

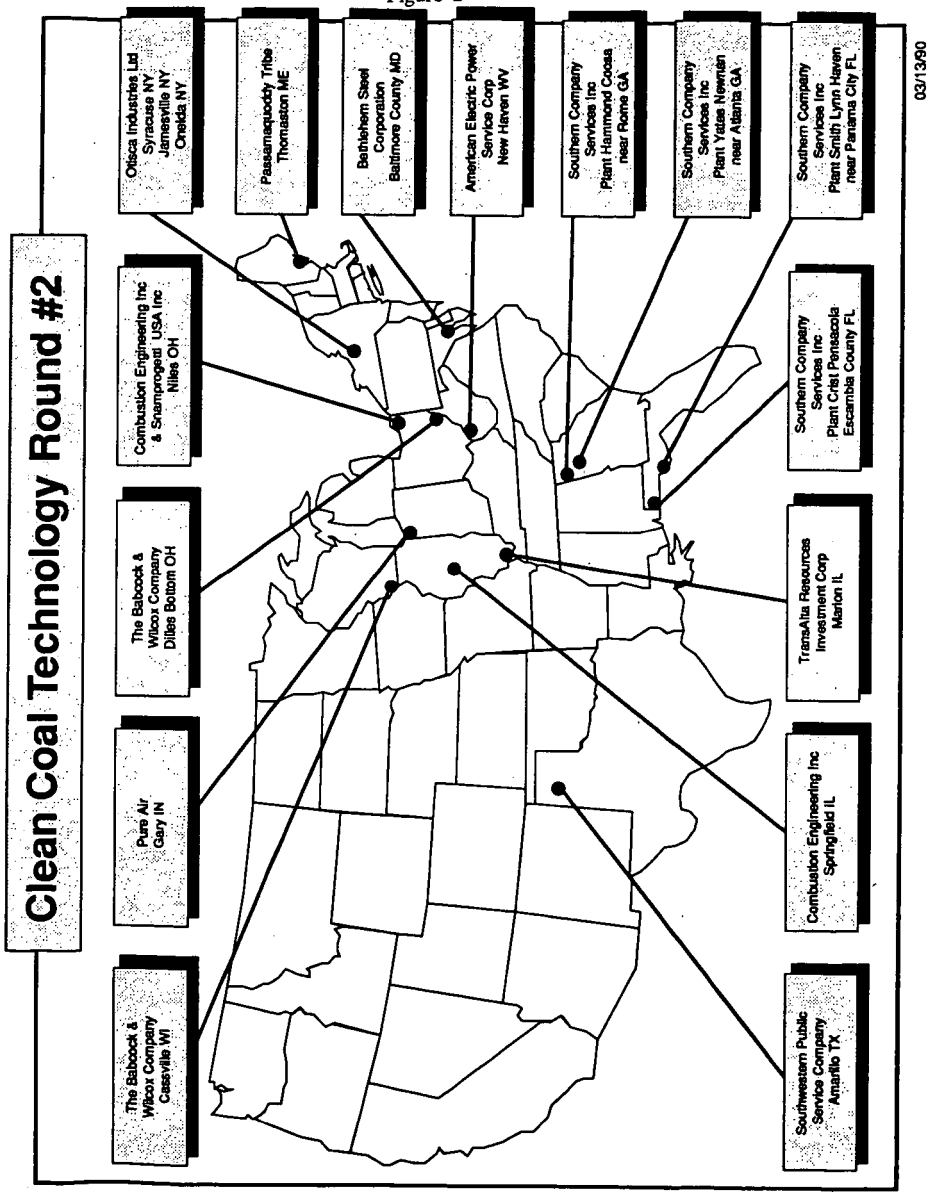
Clean Coal Technology Round #2
Otisca Industries Ltd
Syracuse NY
Jamesville NY
Oneida NY
Passamaquoddy Tribe
Thomaston ME
Bethlehem Steel
Corporation
Baltimore County MD
American Electric Power
Service Corp
New Haven WV
Southern Company
Services Inc
Plant Hammond Coosa
near Rome GA
Southern Company
Services Inc
Plant Yates Newnan
near Atlanta GA
Southern Company
Services Inc
Plant Smith Lynn Haven
near Panama City FL
Combustion Engineering Inc
& Snamprogetti USA Inc
Niles OH
Southern Company
Services Inc
Plant Crist Pensacola
Escambia County FL
The Babcock &
Wilcox Company
Dilles Bottom OH
TransAlta Resources
Investment Corp
Marion IL
Pure Air
Gary IN
Combustion Engineering Inc
Springfield IL
The Babcock &
Wilcox Company
Cassville WI
Southwestern Public
Service Company
Amarillo TX
03/13/90

The cost-shared CCT-II projects will demonstrate technologies that are more cost-effective than existing technologies, and are capable of achieving significant reductions in SO_2 and/or NO_x emissions from existing coal burning facilities, particularly those that contribute to transboundary and interstate pollution. Of the 15 projects, 12 technologies can be retrofitted to existing coal-burning plants, and three can be used to repower existing facilities. Analyses show that the generic technologies represented by the CCT-I and -II projects, if adopted by much of the market to which they are applicable, would result in significant National reductions in SO_2 and NO_x emissions by the year 2010.

Language in Pub. L. No. 100-446, *Making Appropriations for the Department of the Interior and Related Agencies for the Fiscal Year Ending September 30, 1989, and for Other Purposes*, established the schedule for the third CCT Program solicitation (CCT-III). The PON was issued on May 1, 1989, and, on December 21, 1989, 13 additional projects were selected for the Program. Seven of the projects are advanced retrofit pollution control technologies, three are utility repowering technologies, and three are new coal-based fuel form technologies. The CCT-III projects and their locations are shown in Figure 3.

Regardless of the specific CCT technology, the Program can contribute to improving the world in which we live, as discussed below. As Secretary of Energy Watkins has noted, environmental issues transcend national, socioeconomic, ethnic, and cultural boundaries. We must curb emissions of pollutants that contribute to acid rain and urban smog. The past decade has also seen rising concerns over the potential for global climatic change, although, at present, our science is not conclusive regarding this threat. As a result, there is great uncertainty regarding the possible consequences of these changes.

Coal Use and Global Warming

One of the critical environmental issues that has gained National attention is the possibility of global climatic change in response to increases in atmospheric concentrations of "greenhouse gases" – most notably carbon dioxide (CO_2), methane (CH_4), nitrous oxide (N_2O), and chlorofluorocarbons (CFCs). The atmospheric concentration of CO_2 increased 9.5 percent between 1960 and 1986. It generally is recognized that combustion of fossil fuels is the primary contributor, although global deforestation is an important contributing factor. In 1986, the United States contributed 22 percent of the global CO_2 emissions from burning fossil fuels; of these 22 percent, electric power generation contributed 35 percent, transportation 30 percent, industrial sources 24 percent, and the remaining 11 percent was contributed by the residential and commercial sectors. Approximately 37 percent of the CO_2 emitted in the United States, which accounts for 8 percent of global CO_2 emissions, is attributable to the combustion of coal.

Figure 3

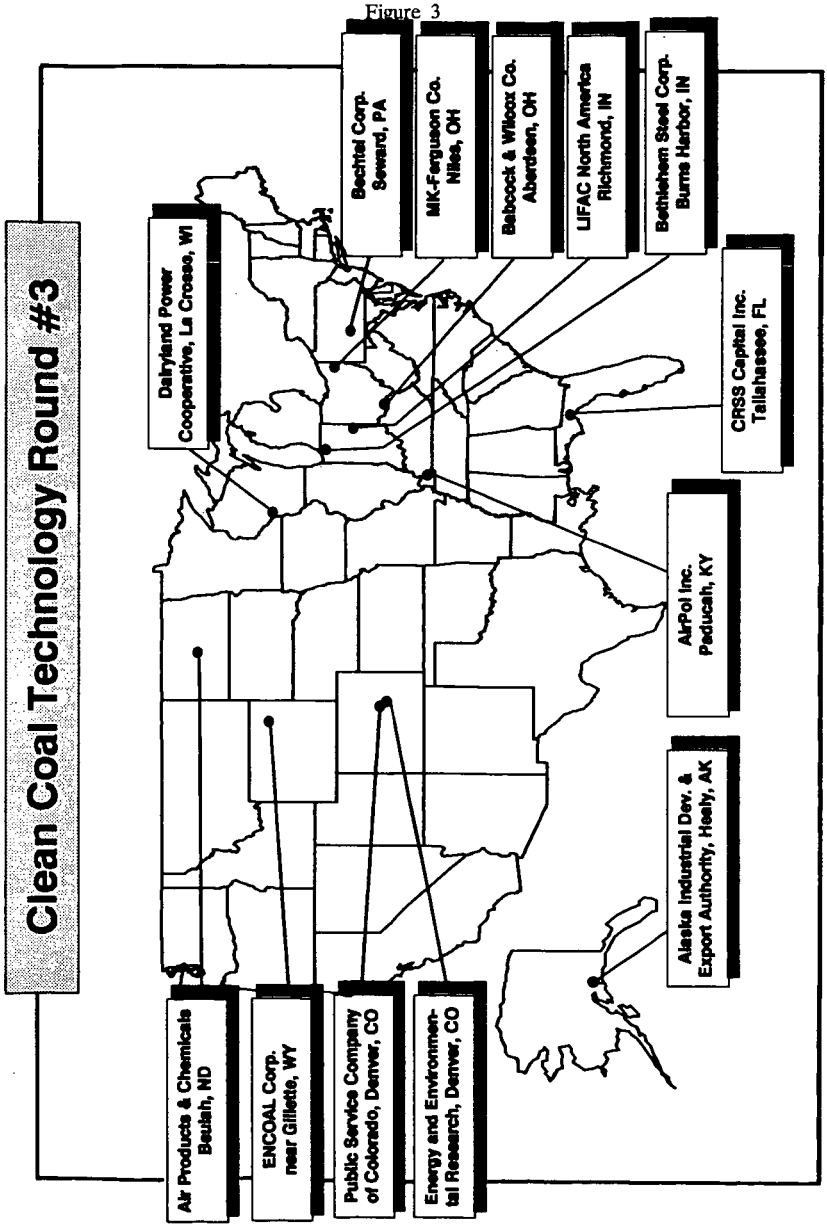
Clean Coal Technology Round #3
Air Products & Chemicals Beulah, ND
ENCOAL Corp. near Gillette, WY
Public Service Company of Colorado, Denver, CO
Energy and Environmental Research, Denver, CO
Dairyland Power Cooperative, La Crosse, WI
Bechtel Corp. Seward, PA
MK-Ferguson Co. Niles, OH
Babcock & Wilcox Co. Aberdeen, OH
LIFAC North America Richmond, IN
Bethlehem Steel Corp. Burns Harbor, IN
CRSS Capital Inc. Tallahassee, FL
AirPol Inc. Paducah, KY
Alaska Industrial Dev. & Export Authority, Healy, AK

Another greenhouse gas produced by the combustion of fossil fuels is nitrous oxide(N_2O), which is a product of both combustion conditions and fuel nitrogen content; recent data suggest that the N_2O production rate is correlated directly with NO_x production rates.

CCTs can impact the emissions of greenhouse gases in two fundamental ways: with respect to CO_2, many of the CCTs improve the efficiency of the conversion of coal to useful energy. Technologies such as pressurized fluidized bed combustion, integrated gasification combined cycle, and fuel cells consume less coal per unit of useful energy produced, thus lowering the amount of CO_2 emitted. Furthermore, these repowering technologies in addition to low NO_x burners, selective catalytic reduction, and other NO_x-reduction technologies, will reduce NO_x emissions, which should in turn result in N_2O emissions reductions. For example, gas reburning technology reduces NO_x emissions by up to 60 percent, and can reduce CO_2 emissions from 5-10 percent since combustion of natural gas produces less CO_2 than coal combustion.

It is not unexpected that reductions of greenhouse gases emissions will become more common as an international policy objective, and the worldwide commercial deployment of clean coal technologies will take on commensurately added significance.

The Clean Air Act Amendments of 1989

On June 12, 1989, President Bush fulfilled a major campaign commitment by proposing a comprehensive program to provide clean air for all Americans. The President's plan, known as ***The Clean Air Act Amendments of 1989*** and formally proposed to the Congress on July 21, 1989, called for the first sweeping revisions to the Clean Air Act since 1977, and represented the first time an Administration had put forward a proposal since that time. The President's plan was designed to curb three major threats to the Nation's environment and to the health of millions of Americans: acid rain, urban air pollution, and toxic air emissions.

Five goals underlied the President's clean air proposals and the means for accomplishing them:

- **Protecting the Public's Health.** To prevent public exposure to cancer-causing agents and to protect those who live in cities with dirty air that does not conform to National health standards.

- **Improving the Quality of Life.** To improve the quality of life for all Americans by exercising responsible stewardship over the environment for future generations.

- **Achieving Early Reductions and Steady Progress.** Established realistic timetables to meet air quality standards, but cut substantial amounts of air pollution in the near term, while requiring steady reductions of harder to control emissions.

- **Harnessing the Power of the Marketplace.** The use of marketable permits to achieve acid rain reductions, and emissions trading to achieve reductions from automobile pollution, so as to clean the air to a definite standard while minimizing the burden on the American economy.

- **Employing Innovative Technologies.** Encouraged development of Clean Coal Technology, alternative fuel systems for automobiles, and other cost-effective means of using new technology to cut pollution.

The "Acid Deposition Control" (Title V) provisions of the President's bill, with emphasis on those aspects of greatest interest to the CCT Program, are highlighted below:

- A reduction of 10 million tons of SO_2 by the year 2000, using a baseline year of 1980 for tons of SO_2 emitted, primarily from coal-fired power plants.

- A two-phase program in order to ensure early reductions. A reduction of five million tons was required during the first phase, by the end of 1995. (All dates had assumed enactment of this legislation by December 31, 1989.)

- A 2 million ton reduction of NO_x in Phase II. The plan would have allowed utilities to trade reductions of NO_x for reductions of SO_2 and vice versa, and thus represented a call for a total reduction of 12 million tons in acid rain-causing pollutants.

- A 3-year extension of the Phase II deadline for plants adopting CCT repowering technologies, combined with regulatory incentives designed to smooth their transition into the marketplace. This would allow the United States to "make good" on the major investment in the CCT Program that the President has called for, and would ensure that coal continues to play an important role in America's energy future.

- Freedom of choice in cutting pollution. The plan required all plants above a certain size in affected States to meet the same emissions standard, but did not dictate to plant managers how the standard should be met. The plan required the largest polluting plants to make the greatest cuts in pollution. The emissions standard would be set at the rate necessary to achieve 5 million tons in the first phase. The plan envisioned a standard of 2.5 lb SO_2/million Btu, which would affect 107 plants in 18 states. The standard would subsequently be tightened to approximately 1.2 lb/million Btu so as to achieve a 10 million ton reduction of SO_2 in Phase II.

- Maximum flexibility in obtaining reductions. The plan allowed utilities to trade required emissions reductions so that they would be achieved in the most optimal manner. In the first phase, trading would be allowed among electric plants within a State or within a utility system. In addition, full interstate trading would be allowed in Phase II.

- The estimated cost of the President's proposal would have been about $700 million per year in the first phase, and $3.8 billion annually in the second phase. While this represents an increase of over 2 percent by the year 2000 in the Nation's $160 billion a year electricity bill, the flexibility built into the President's plan reduced, by up to half, the cost of various competing proposals mandating the use of specific technologies.

One important provision in the proposed bill, Section 508, "Repowered Sources," established the availability of a 3-year extension of the stage II compliance date (i.e., until the end of 2003, instead of 2000) for *any unit being repowered with one of the following CCTs:*

- Atmospheric (AFB) or Pressurized Fluidized Bed (PFB) Combustion
- Integrated Gasification Combined Cycle (IGCC)
- Magnetohydrodynamics
- Direct and indirect coal-fired turbines
- Integrated gasification fuel cells
- or a "derivative of one of these technologies, as determined by the Administrator of the Environmental Protection Agency (EPA), in consultation with the Secretary of Energy."

Such a repowered source would be exempt from meeting EPA New Source Performance Standards (NSPS) for SO_2 and would benefit from streamlined New Source Review (NSR) procedures if their potential emissions were expected to increase.

Section 515 of the bill, entitled, "Clean Coal Technology Regulatory Incentives," also was very important to the CCT Program. Here, CCTs were defined as:

> any technology, including technologies applied at the precombustion, combustion, or postcombustion stage, at a new or existing facility which will achieve significant reductions in air emissions of SO_2 or NO_x associated with the utilization of coal in the generation of electricity, process steam, or industrial products, which is not in widespread use as of the date of enactment of this title.

In order to encourage the use of such CCTs, the Federal Energy Regulatory Commission (FERC) was required here to adopt regulations for a 5-year CCT demonstration program that would include establishment of an incentive rate of return and a 10- to 20-year amortization period. This proposal also required FERC to develop a process whereby it would negotiate a prudent level of investment for CCTs and other "innovative emission control technology."

This Section also exempted temporary and permanent CCT demonstration projects from NSR requirements under Section 111 (*Standards of Performance for New Stationary Sources*) and Parts C (*Prevention of Significant Deterioration of Air Quality*) and D (*[State Implementation] Plan Requirements for Nonattainment Areas*) of the current Clean Air Act, so long as the demonstration project would not increase the original facility's potential to emit any pollutant regulated under the Act.

Finally, States were encouraged to provide additional utility regulatory incentives for the promotion of CCTs, and several examples were provided.

The CCT Program and National Energy Strategy

On July 26, 1989, the Secretary of Energy, Admiral James D. Watkins, appeared before the Senate Committee on Energy and Natural Resources to discuss the President's plan for development of a National Energy Strategy (NES). In his opening remarks, the Secretary noted that:

> Environmental concerns are putting new pressures on our ability to use our most abundant domestic fuel, coal. Electricity reserve margins are shrinking across the country. Voltage reductions have already been required in the Northeast, and right here in Washington. Meanwhile, New York State officials are rushing to pull fuel rods from a completed, safe nuclear power plant. ... Our country needs a clear energy blueprint to take the United States into the next century — a National Energy Strategy.
>
> The President has directed me to lead the development of this National Energy Strategy — an action plan essential to providing this Nation, in the years to come, with adequate supplies of competitively priced, clean energy. This strategy will serve as a blueprint for energy policy and government program decisions. It will contain specific short-term, mid-term,

> and long-term recommendations. This strategy will chart our course, set our pace, and provide mileposts by which to evaluate our progress in providing the energy our economy needs, while protecting the Nation's health, safety, and environment.
>
> ... I have committed the Department to extensive consultations with the Governors and State officials of this Nation, with Congress, with industry, and with the American people.

The Secretary observed that, "If the National Energy Strategy is to gain the support of the American people, it must be built on a reliable foundation of data, analytical tools, and forecasting capability." Accordingly, he has instructed DOE to work closely with the Energy Information Administration to develop a National Energy Modeling System (NEMS); he has also asked the National Academy of Sciences "to examine our plans for the development of the NEMS and ensure that it will, to the maximum extent possible, address the critical energy issues before us. These include major environmental issues, strategic considerations and technology research and development."

The goals of the CCT Program are germane to and supportive of many of the recurring themes in the NES development process. For example, the National Laboratories were asked to assist DOE with the analyses of key issues and the preparation of special white papers, completed this past autumn, on such subjects as:

- The science of global climate change and the scope of uncertainty. This subject area encompasses CO_2 releases, and pertains to the increased efficiency of some of the CCTs, with attendant reduced emissions.

- Options available to enhance DOE technology transfer to the broader development community. Technology transfer is important not only to meet National energy and environmental objectives, but to assure that lesser developed nations — which are the fastest growing energy users — will do the same.

  The subject of technology transfer is "near and dear" to the CCT Program, which considers this activity as vital to the promulgation and deployment of mature CCTs into the marketplace, both home and abroad. We believe that CCTs offer the opportunity for export of U.S. coal together with the know-how to consume it cleanly and cost-effectively to the mutual benefit of both the consumers and the vendors.

On April 2, 1990, the Secretary of Energy announced the completion of the first phase — information gathering — of the development of the NES, and released for public comment the *Interim Report on the Development of a National Energy Strategy, A Compilation of Public Comment*. The Secretary noted that the report "will provide a baseline for for development and analysis of energy options, and public comment on the report is invited." As was noted in the accompanying News Release, since August 1989, DOE has held 15 public hearings, received more than one thousand written submissions, and compiled twelve thousand pages of public hearing record. The *Interim Report* conveys the results of that public participation, presenting a compendium of public concern, and a series of publicly identified goals, obstacles to progress, and options for overcoming them.

This was followed almost immediately by the announcement on April 12, 1990, of the completion and release for review by the public of five National Laboratory "white papers" that had been commissioned by DOE to assist in the development of the NES:

- *Energy Efficiency: How Far Can We Go?*
- *The Potential of Renewable Energy.*
- *Energy and Climate Change.*
- *Energy Technology for Developing Countries.*
- *The Technology Transfer Process.*

Finally, some of the remarks about CCTs and the CCT Program, that were offered by panelists in the course of discussing the NES, are noteworthy, as follows:

> Clean coal program of DOE is important for removing constraints to coal use, given current old technology and environmental concerns.
>
> **- State government official**

> Energy and environmental policy should be coordinated. Clean coal technology to reduce NO_x and SO_2 emissions is good example.
>
> **- Public utilities commissioner**

> Coal is the largest domestic resource, however its viability as an energy source is seriously constrained by air quality regulations and cost of compliance; by the need for federal support of clean coal technology development; and proposed acid rain legislation capping SO_2 and NO_x emissions.
>
> **- Electric utility executive**

> Coal is the most plentiful resource but is underutilized; energy research on effective and clean use of coal is needed ... Promotion of coal exports should be undertaken, and clean coal technology should be promoted.
>
> - **Energy company executive**

> Clean coal program R&D is now addressing containment of CO_2 emissions ... Progress being made in environmental protection is not being communicated to the public. Public information program is needed as part of the strategy of NES to inform public on environmental health and safety.
>
> - **Coal company executive**

The Future; CCT-IV and -V

On October 23, 1989, President Bush signed Public Law No. 101-121, "Department of the Interior and Related Agencies Appropriations, Fiscal Year 1990." Among other things, this Bill provided $1.2 billion for the 4th and 5th rounds of CCT solicitations ($600 million for each in FY 1991 and FY 1992), and specified dates for release of the solicitations, submittal of proposals, and selections of projects.

The language in the accompanying Conference Report (No. 101-264) included the guidance that the word "replacing" should be added to the definition of "clean coal technology," and noted that:

> ... the inclusion of "replacing" for clean coal IV and V is intended to cover the complete replacement of an existing facility if, because of design or site specific limitations, repowering or retrofitting of the plant is not a desirable option.

Although the original schedule called for release of the CCT-IV solicitation on or before June 1, 1990, on May 15, 1990, DOE announced that it intended to delay issuance of the solicitation "until uncertainties regarding Congressional action have been resolved." The News Release of that date noted that the Secretary of Energy had "informed Congress that unresolved issues in the pending Supplemental Appropriations Act and the Clean Air Act Amendments make it premature for the Energy Department to begin asking industry for new CCT proposals." The Release also pointed out that this delay will provide time for a draft of the solicitation to be issued for public comment prior to its official release. It is anticipated that, with the passage of the Clean Air Bill, PON-IV, revised as appropriate to accomodate the provisions of the Bill, will be released.

THERMOGRAVIMETRIC STUDY OF NOVEL SORBENTS FOR FLUE GAS CLEANUP*

Sheila W. Hedges and R. A. Diffenbach
Pittsburgh Energy Technology Center
U. S. Department of Energy, Pittsburgh, PA 15236

Keywords: flue gas cleanup, regenerable sorbents, cerium oxide

INTRODUCTION

Several promising new processes are being developed at the Pittsburgh Energy Technology Center (PETC) to remove the sulfur and nitrogen oxides from the flue gas of coal-fired utility boilers. The Fluidized-Bed Copper Oxide Process developed at PETC is one such new technology for the simultaneous removal of 90% of both SO_2 and NO_x from the flue gas[1]. This process involves the absorption of SO_2 by copper oxide on an alumina support in conjunction with sorbent catalyzed reduction of NO_x by ammonia addition. Alternate sorbents to CuO/Al_2O_3 are also being considered at PETC for possible improvements in reactivity toward SO_2, regenerability, attrition resistance, and sorbent costs. A similar process concept based on a CeO_2/Al_2O_3 sorbent[2] has been studied recently at PETC and is the subject of this report.

Cerium oxide is a particularly promising new sorbent because ceria imparts resistance to thermal loss of surface area to alumina[3]; CeO_2 has potential for the uptake of two moles of sulfur per mole of metal to form $Ce(SO_4)_2$; CeO_2 sorbent reacts with SO_2 over a fairly wide range of temperature; and when regenerated under the appropriate conditions, CeO_2/Al_2O_3 sorbent produces an off-gas stream that can be used conveniently in a Claus plant for conversion into elemental sulfur[2]. The natural abundance of cerium is slightly higher than copper, and extensive deposits are located in the western United States, as well as in Australia, Brazil, India, and China. Rare earth minerals are mined both as a primary product and as a by-product of the mining of such metals as iron (in China), tin, titanium, and zirconium. Cerium is produced as a by-product of the isolation of other rare earths. The current price of cerium oxide is approximately \$1.50-\$2.00 per pound at 90-95% purity.[4]

The effects of sorbent preparation on the reactivity of CeO_2/Al_2O_3 sorbents toward SO_2 and on the regenerability of the sorbents have been examined using a thermogravimetric (TG) technique with simulated flue gas and hydrogen, respectively. Potassium-modified CeO_2/Al_2O_3 and composite oxides of Co/Ce and Mn/Ce on alumina have also been investigated. Incorporation of potassium into CeO_2/Al_2O_3 has been reported to decrease the CeO_2 crystallite size and improve sorbent performance[5]. Several recent catalysis studies on Co/Ce and Mn/Ce composite oxide systems have described high redox properties[6,7] and catalytic activity for the CO + SO_2 reaction[8] and the CO + NO reaction[9]. Both cobalt and manganese oxides have been previously identified as

*Reference in this paper to any specific commercial product, process, or service is to facilitate understanding and does not imply endorsement or favoring by the United States Department of Energy.

promising supported sorbents (on alumina) for SO_2 absorption[10]. Manganese oxides have been investigated by several researchers for sulfur removal at a number of different conditions. Investigations of MnO_x/Al_2O_3 for flue gas desulfurization have been promising but problems have been identified with low manganese loading and some loss of capacity has been observed on repeated cycles of regeneration[11,12]

EXPERIMENTAL

Sorbent samples were prepared by aqueous impregnation of 1/16 inch alumina spheres. Reagent-grade, water-soluble cerium salts that can be decomposed thermally at moderate temperatures were selected for testing. The salts selected were ceric ammonium nitrate, cerous ammonium nitrate, cerous nitrate hexahydrate, and cerous acetate. The alumina spheres were obtained from three commercial catalyst manufacturers. After soaking in excess solution, the sorbent pellets were drained, dried in air overnight at 120°C, and calcined in N_2 at 650°C for 6 hours. Metal loadings on the sorbents were varied by changing the concentration of the impregnation solution and were determined by elemental analysis at Huffman Laboratories, Inc., using atomic absorption techniques. Surface areas were determined by the multipoint BET method using an automated Micromeritics Digisorb 2500 instrument with N_2 as adsorbate. Potassium nitrate was added to the K-modified CeO_2/Al_2O_3 sorbents by an incipient wetness technique prior to calcination of the sorbent. Composite oxide sorbents were prepared in the same manner as the Ce-only sorbents by simply combining cobalt or manganese nitrate with the cerium nitrate to form a mixed metal impregnation solution (eg. $Co(NO_3)_2 + Ce(NH_4)_4(NO_3)_6$ and $Mn(NO_3)_2 + Ce(NO_3)_3$).

Reactivity of the varous sorbent preparations toward SO_2 was measured in a modified Perkin-Elmer TGS-2 Thermogravimetric Analyzer that has been previously described[13]. For these tests, the sample-shielding tube was refabricated using quartz and a large external furnace was used for temperature control. Simulated flue gas was blended from certified gas mixtures and humidified using a sparger. The calculated typical gas composition was 2800-3000 ppm SO_2; 480-500 ppm NO; 2.8-3.0 % O_2; 13.7-14.7 % CO_2; 4.0, 7.0, or 18 %(vol.) H_2O; and N_2 as the balance. A sample size of 50 mg of sorbent was selected to just fill the quartz sample pan; this corresponds to about 18-20 pellets. A typical TG test sequence was composed of four steps: 1) the sample was heated to the desired reaction temperature at 10°C/minute in dry N_2; 2) after allowing the sample to come to equilibrium at the test relative humidity a "dry" sample weight was obtained and the sample was exposed to humidified simulated flue gas for one hour; 3) the sample was regenerated by reduction in H_2 for 30 minutes followed by reoxidation in air for 10 minutes; and 4) the sample was re-exposed to flue gas for 60 minutes.

From the TG thermal curves, the sorbent capacity was calculated from the weight gain after 60 minutes of exposure to simulated flue gas which was sufficient to completely saturate most of the sorbents. For samples with high metal loadings, although the reaction had not completely stopped after 60 minutes, the rate of reaction had dropped to one percent or less of its initial value. The rate of SO_2 uptake was calculated from the weight gain averaged for the first 10 minutes of absorption. This somewhat long time interval was selected for comparison purposes to minimize the relative

uncertainty in measuring small weight gains. [Note: this estimated rate underestimates the true rate since the TG thermal curves show some deviation from linearity after about 5 to 8 minutes. The conversion of the solid is typically 30+ % after 10 minutes.]

RESULTS AND DISCUSSION

The sorbent capacity for SO_2 uptake as a function of temperature is shown in Figure 1 for several different metal loadings. Since cerium nitrates are thermally unstable above 250°C and hydrated ceric sulfate is completely dehydrated at approximately 350°C[14], all of the weight gain observed during the TG test has been attributed to sulfate formation. X-ray diffraction results for several of the spent CeO_2/Al_2O_3 sorbent samples showed weak lines not present in the fresh sorbent. However, these lines could not be assigned to known cerium sulfate compounds and suggested that the CeO_2 is converted to an amorphous or highly dispersed sulfate on exposure to flue gas. Examination of fresh and spent sorbent by FTIR (Fourier transform infrared spectroscopy) clearly showed the presence of sulfate on the spent sorbents, but specific product compounds could not be identified.

As can be seen in Figure 1, at low metal loadings, the sorbent is essentially saturated at 550°C before 60 minutes of exposure to synthetic flue gas. For sorbents at moderate and high metal loading the capacity continues to increase up to 600°C. However, the TG curves are essentially flat for these sorbents after 60 minutes of exposure even though the sorbent has not reached the calculated, theoretical capacity (complete conversion of CeO_2 to $Ce(SO_4)_2$). The rate of SO_2 uptake also decreases steadily below about 600°C as shown in Figure 2. Complete regeneration of these CeO_2/Al_2O_3 sorbents occurred in 30 minutes or less in hydrogen at temperatures above 550°C. Figure 3 shows the weight loss after 30 minutes of exposure to H_2 expressed as a percentage of the gain during absorption. Some of the sorbents show weight loss on reduction in excess of 100 %, which is probably due to the partial conversion of CeO_2 to Ce_2O_3 or $CeAlO_3$[15,16]. Based on these observations of the temperature dependence of absorption and regeneration, a temperature of 600°C was selected to compare the various methods of sorbent preparation.

Comparison of the various CeO_2/Al_2O_3 sorbents prepared with differing precursor salts showed little or no difference in sorbent capacity between samples with comparable cerium loadings. A slightly higher rate of SO_2 uptake was observed for sorbents prepared using $Ce(NH_4)_4(NO_3)_6$ as the precursor salt. Although $Ce(NH_4)_4(NO_3)_6$ has been shown to produce a highly porous CeO_2 when decomposed at low temperature[17], $Ce(NO_3)_3 \cdot 6H_2O$ has been reported to produce CeO_2 of smaller crystallite size when calcined at higher temperature[14]. The somewhat higher rate of SO_2 uptake observed for sorbents prepared using $Ce(NH_4)_4(NO_3)_6$ as the precursor salt suggests that the crystallite size of the CeO_2 supported on alumina may not follow the same trends observed for pure, unsupported compounds[14]. X-ray diffraction results for several of the CeO_2/Al_2O_3 sorbent samples were consistent with highly dispersed CeO_2, but no estimation of crystallite size was made. It should be pointed out that these differences in rate are small and, when experimental uncertainties are taken into consideration, the differences may not be statistically significant. All of the

precursor salts resulted in sorbents with high BET surface areas, 150 to 200 m^2/g. However, no correlation was found between total surface area and sorbent capacity or rate of SO_2 uptake. The sorbent capacity and rate of SO_2 uptake were also found to be unaffected by increasing the water content of the simulated flue gas from 4 % to 18 % or by removing nitric oxide from the gas mixture.

Figure 4 shows the SO_2 to CeO_2 mole ratio (stoichiometry) after 60 minutes of exposure to simulated flue gas for sorbents prepared using various precursor salts on three different aluminas. For metal loading below about 5 %, the observed uptake is greater than the amount required to completely convert all the CeO_2 to $Ce(SO_4)_2$, indicating some uptake by the alumina support. For sorbents with loadings above about 15 %, the utilization drops to below one mole of SO_2 per mole CeO_2. No difference was observed in the utilization of the CeO_2 on alumina from different suppliers. One of the aluminas did have a lower affinity for cerium uptake, that is, the metal retained on this support was significantly lower at a given impregnation solution concentration than for the other two aluminas. Figure 5 shows that the rate of SO_2 uptake was also lower on sorbents prepared using the third support. Simple grinding in a ball mill showed sorbent prepared on this support to be much less rugged than sorbents prepared on the other two supports and no further testing was done with this alumina. The small differences in the measured rate of SO_2 uptake for sorbents prepared on the same support material have been attributed to differences in sample preparation, ie., the specific precursor cerium salt used.

As noted above, the CeO_2/Al_2O_3 sorbents undergo weight loss during hydrogen reduction at 600°C of 100+ % of the amount of SO_2 uptake. Since some reduction of Ce(IV) to Ce(III) also occurs, the sorbent samples were reoxidized in air prior to subsequent SO_2 absorption measurements. Following this regeneration procedure, the weight percent of any residual material remaining on the sorbent was recorded. The results of these measurements are summarized in Figure 6. For the CeO_2/Al_2O_3 sorbents, the residual was less than one percent of the total sorbent weight. The sorbent was pale yellow in color after regeneration. Ce_2S_3 is reddish-purple or brown. However, there was not sufficient sample produced in these TG tests for a detailed characterization of the residual material. For the CuO/Al_2O_3 sorbent with a 6-7 % Cu loading, a residual of 3-3.5 percent of the total sorbent weight was measured in the TGA test after a similar regeneration, however, both absorption and regeneration of the CuO/Al_2O_3 sorbent were at 400°C. Following regeneration, the CeO_2 sorbent samples were exposed a second time to simulated flue gas. A small decrease in sorbent capacity was observed, but the rate of SO_2 uptake was the same as that measured for the freshly prepared sorbents as can be seen by comparing Figures 5 and 7. For laboratory prepared samples of the CuO/Al_2O_3 sorbent with a 7 % Cu loading, the rate of SO_2 uptake measured in the TGA using the same gas compositions and reaction times but at 400°C, is 1.7 mg SO_2 per g sorbent per minute.

A series of K-modified CeO_2/Al_2O_3 sorbents was prepared with metal loadings of 4 to 12 % Ce and 0.8 % K to investigate reported[5] improvements in sorbent performance. The rate of SO_2 absorption measured for each of these sorbents at 600°C was the same as for the Ce-only sorbents. The K-modified sorbents have approximately 10-20 % higher mole ratio of SO_2 absorbed to CeO_2 present at comparable metal loadings than

the Ce-only sorbents. No increase in the residual material remaining on the sorbent after regeneration, as compared to the Ce-only sorbents, was observed for the K-modified CeO_2/Al_2O_3 sorbents. Figure 8 compares the capacity of a K-modified CeO_2/Al_2O_3 sorbent with a Ce-only sorbent, both with 4 % Ce loading. As pointed out above, at this low metal loading the observed sorbent capacity of CeO_2/Al_2O_3 at temperatures above 550 °C corresponds to a sulfur to cerium stoichiometry of greater than 2 to 1. This effect is even more pronounced for the K-CeO_2/Al_2O_3 sorbent. At 600°C, the excess corresponds to a 115 % utilization of the CeO_2 on the Ce-only sorbent and a 123 % utilization of the sum of CeO_2 and K_2O on the K-CeO_2/Al_2O_3 sorbent. Both types of sorbent show the same temperature dependence of SO_2 capacity and show evidence of a mechanism change below about 300°C.

Composite oxides of Co/Ce and Mn/Ce were prepared on the same alumina support to investigate whether the redox properties of these materials[6-9] would improve the SO_2 reactivity or regenerability of the Ce-containing flue gas sorbent. $CeO_2/MnO_x/Al_2O_3$ sorbents were prepared containing 8 and 13 percent cerium with manganese loadings ranging from 0.3 to 3.7 weight percent (mole fraction of manganese in the composite oxides ranged from 0.07 to 0.43). These sorbents had SO_2 reactivities comparable to the Ce-only sorbents of similar Ce loading and maintained their reactivity after regeneration. (The test was carried out for only one regeneration cycle.) However, a substantial amount of residual material (1 to 4 % of the total sorbent weight) was observed to be left on these sorbents after regeneration. No advantage was found in the $CeO_2/MnO_x/Al_2O_3$ sorbents as compared to the Ce-only sorbent. $CeO_2/CoO_x/Al_2O_3$ sorbents were prepared containing 5, 10, and 14 percent cerium with cobalt loadings ranging from 0.2 to 2.0 percent (mole fraction of cobalt in the composite oxides ranged from 0.06 to 0.39). Reactivity measurements on these sorbents showed them to be essentially the same as the Ce-only sorbents. In this case no difference in residual material after regeneration in H_2 was observed. The temperature dependence of the SO_2 absorption by the $CeO_2/CoO_x/Al_2O_3$ sorbent was also examined and found to be essentially the same as for the Ce-only sorbents.

A comparison of the SO_2 reactivity measurements for all four types of sorbents is shown in Figures 9 and 10. The K-modified CeO_2/Al_2O_3 and CeO_2/Al_2O_3 prepared from $Ce(NH_4)_4(NO_3)_6$ have slightly higher rates of absorption (Figure 9) but the differences are small. The K-modified CeO_2/Al_2O_3 sorbents have somewhat higher capacities (Figure 10), but once again the improvement is modest. For laboratory prepared samples of the CuO/Al_2O_3 sorbent with a 7 % Cu loading, the rate of SO_2 uptake measured in the TGA using the same gas compositions and reaction times but at 400°C is 1.7 mg SO_2 per g sorbent per minute and the sorbent capacity is 59 mg SO_2 per g sorbent.

CONCLUSIONS

CeO_2/Al_2O_3 sorbents have been prepared that have SO_2 reactivity comparable to or slightly higher than the CuO/Al_2O_3 sorbent, and can be regenerated in hydrogen with essentially complete removal of sulfur. Residual material remaining on the CeO_2/Al_2O_3 sorbents was about one fifth the amount typically seen for the CuO/Al_2O_3 sorbent with similar metal loading under similar experimental conditions (TG testing was performed using the same gas compositions and reaction times for both types of sorbents).

However, the temperature of operation is higher for the CeO_2, 600°C compared to 400°C for CuO. $CeO_2/MnO_x/Al_2O_3$ and $CeO_2/CoO_x/Al_2O_3$ sorbents were also prepared that gave quite comparable SO_2 reactivity to the Ce-only sorbent. However, these composite oxide sorbents do not appear to offer an advantage to the Ce-only sorbent when H_2 is the reducing gas. K-modified CeO_2/Al_2O_3 sorbents exhibited approximately 10-20 % higher absorption capacity at comparable metal loadings than did the Ce-only sorbents, but the rate of SO_2 uptake was essentially the same.

ACKNOWLEDGEMENTS

The authors would like to thank Dr. S.S. Pollack for providing the X-ray diffraction analysis and Michael Hilterman, Michael Ferrer, and Frank McCown for assistance in obtaining the TG data.

REFERENCES

1. Plantz, A.R.; Drummond, C.J.; Hedges, S.W.; Gromicko, F.N. "Performance of the Fluidized-Bed Copper Oxide Process in an Integrated Test Facility," presented at the 79th Annual Meeting and Exhibition of the Air Pollution Control Association, Minneapolis, Minnesota, June 1986.
2. Longo, J.M. U.S. Patent 4 001 375, 1977 and Longo, J.M.; Neville, L.C. U.S. Patent 4 251 496, 1981.
3. Yao, H.C.; Yao, Y.F.Yu *J. Catal.* 1984, *86*, 254-65.
4. Hedrick, J.B. "Rare-Earth Minerals and Metals" in "Minerals Yearbook 1986"; Bureau of Mines; U.S. Government Printing Office: Washington, 1988; Vol. 1, pp. 771-782.
5. Lewis, P.H.; Dai, E.P.; Holst, E.H. U.S. Patents 4 600 898 and 4 626 419, 1986.
6. Imamura, S.; Doi, A.; Ishida, S. *Ind. Eng. Chem. Prod. Res. Dev.* 1985, *24*(1), 75-80.
7. Imamura, S.; Nakamura, M.; Kawabata, N.; Yoshida, J.I; Ishida, S. *Ind. Eng. Chem. Prod. Res. Dev.* 1986, *25*(1), 34-37.
8. Bazes, J.G.I.; Caretto, L.S.; Nobe, K. *Ind. Eng. Chem. Prod. Res. Dev.* 1975, *14*(4), 264-8.
9. Deremince-Mathieu, V.; Collette, H.; Nagy, J.B.; Deriyabem E.G.; Verbist, J.J. *Inorg. Chim. Acta* 1987, *140*(1-2), 41-43.
10. Koballa, T.E.; Dudukovic, M.P. *AIChE Symp. Ser.* 1978, *73*(165), 199-228.
11. Van den Bosch, P.J.W.M.; De Jong, W.A. *Adv. Chem. Ser.* 1974, *133*, 571-87.
12. Van den Bosch, P.J.W.M.; De Jong, W.A. *Prep. Catal., Proc. Int. Symp. 1975* (Pub. 1974), 651-62.
13. Diffenbach, R.A.; Hedges, S.W.; Friedman, S. *Thermochim. Acta* 1988, *127*, 57-71.
14. El-Adham, K.A.; Gadalla, A.M.M. *Interceram* 1977, *26*(3), 223-6.
15. Miki, T.; Ogawa, T.; Ueno, A.; Matsuura, S.; Sato, M. *Chem. Lett.* 1988, 565-568.
16. Shyu, J.Z.; Weber, W.H.; Gandhi, H.S. *J. Phys. Chem.* 1988, *92*(17), 4964-70.
17. Zaki, M.I.; Baird, T. *React. Solids* 1986, *2*, 107-23.

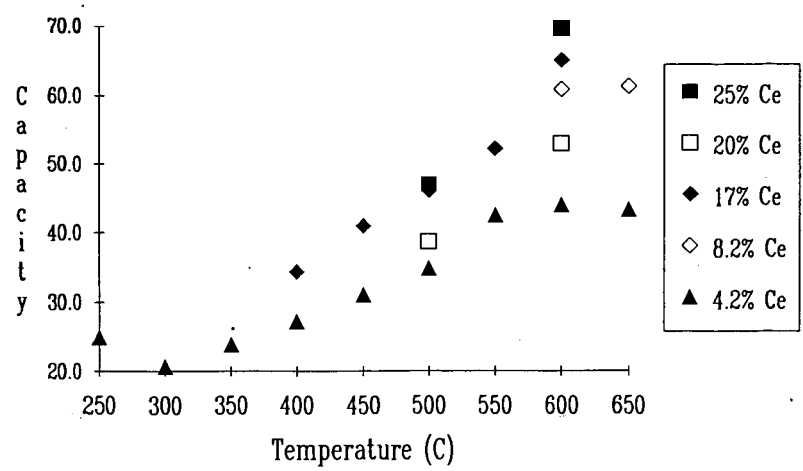

Figure 1. Capacity of CeO_2/Al_2O_3 sorbents expressed in mg SO_2 per g sorbent as a function of temperature.

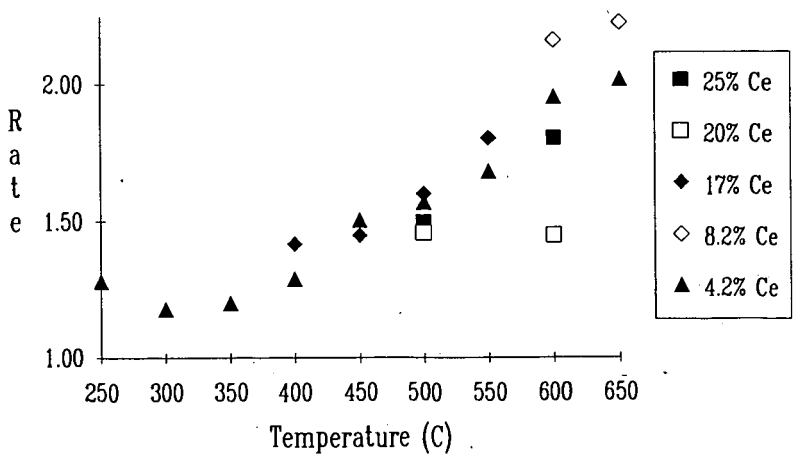

Figure 2. Rate of SO_2 uptake by CeO_2/Al_2O_3 sorbents expressed in mg SO_2 per g sorbent per minute as a function of temperature. See text for discussion.

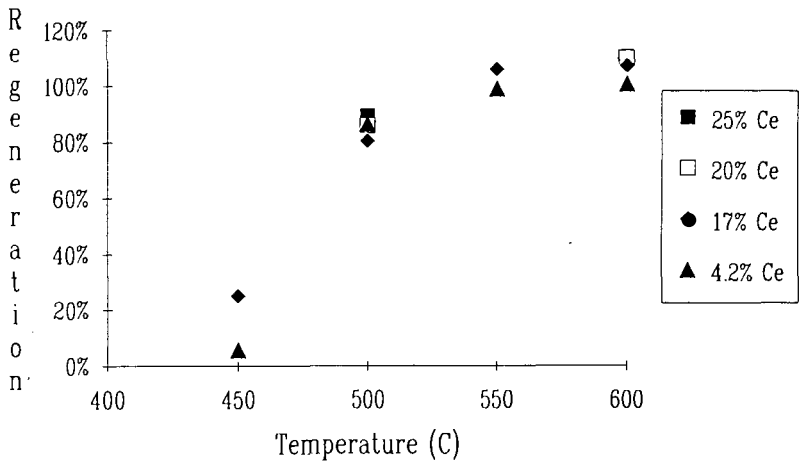

Figure 3. Reduction of spent CeO_2/Al_2O_3 sorbents in hydrogen expressed as a percentage of the weight gain observed during SO_2 absorption as a function of temperature.

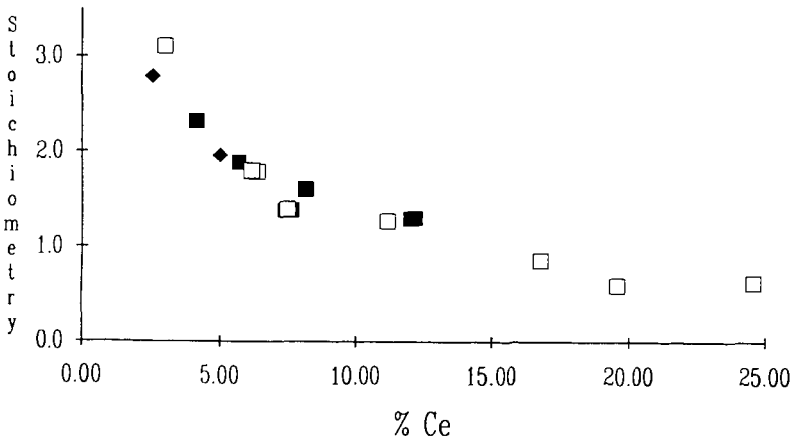

Figure 4. Mole ratio of SO_2 absorbed at saturation at 600°C to CeO_2 on the sorbent as a function of metal loading. Different point symbols represent aluminas from different commercial suppliers.

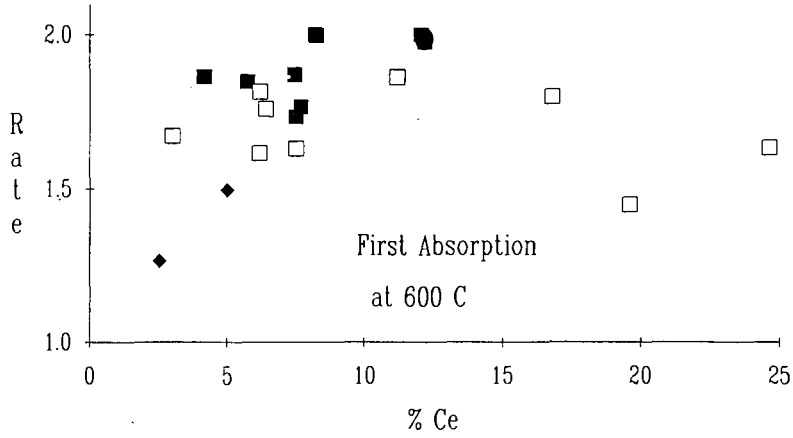

Figure 5. Rate of SO_2 uptake by CeO_2/Al_2O_3 sorbents expressed in mg SO_2 per g sorbent per minute as a function of Ce loading. The standard deviation of the rates determined was 0.1 or less. Different point symbols represent aluminas from different commercial suppliers. See text for discussion.

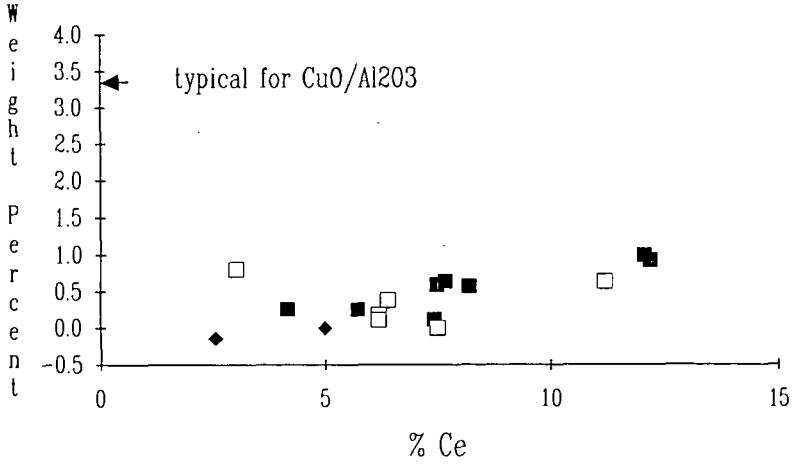

Figure 6. Residual remaining on CeO_2/Al_2O_3 sorbents after regeneration in H_2 in the TGA test unit. The value observed for CuO/Al_2O_3 under similar conditions is shown for comparison.

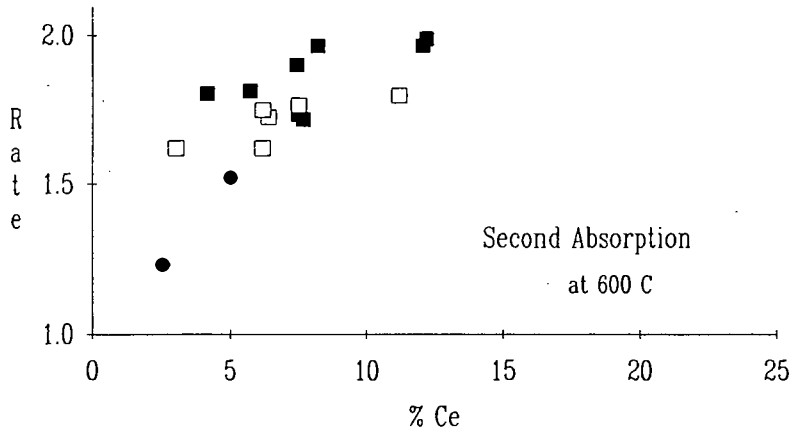

Figure 7. Rate of SO_2 uptake by CeO_2/Al_2O_3 sorbents during a second exposure to simulated flue gas after regeneration in H_2 expressed in mg SO_2 per g sorbent per minute as a function of Ce loading. The standard deviation of the rates determined was 0.1 or less. Point shapes represent aluminas from different commercial suppliers. See text for discussion.

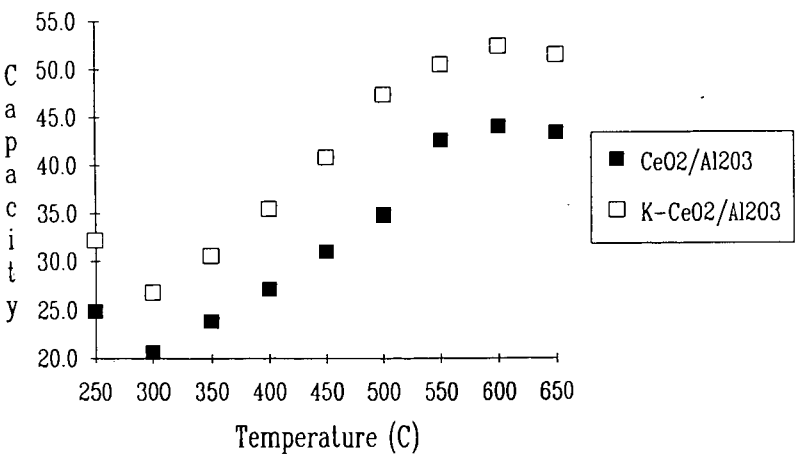

Figure 8. Comparison of SO_2 capacity as a function of temperature of a K- modified and a Ce-only sorbent, both of which contain 4 % Ce. Capacity is expressed in mg SO_2 per g sorbent.

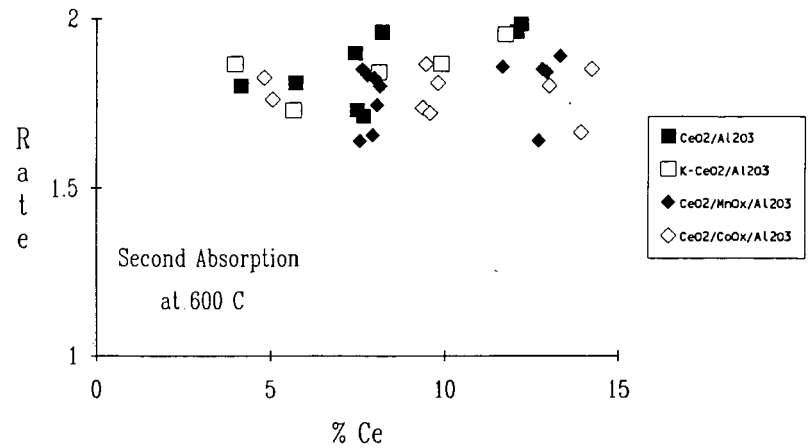

Figure 9. Rate of SO_2 uptake by Ce-containing sorbents during a second exposure to simulated flue gas after regeneration in H_2 expressed in mg SO_2 per g sorbent per minute as a function of Ce loading. The standard deviation of the rates determined was 0.1 or less.

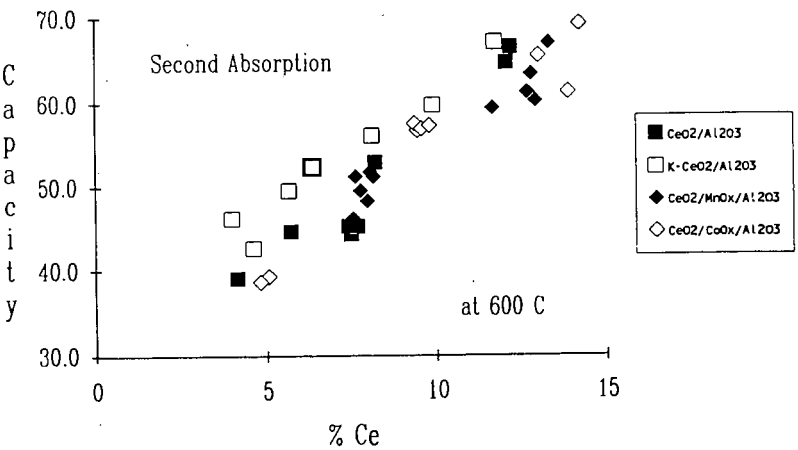

Figure 10. Comparison of SO_2 capacity of Ce-containing sorbents during a second exposure to simulated flue gas after regeneration in H_2 expressed in mg SO_2 per g sorbent as a function of Ce loading. The standard deviation of the capacities determined was 2 or less.

THE PHYSICAL NATURE AND THE CHEMICAL REACTIVITY OF A HETEROGENEOUS MgO/VERMICULITE FLUE-GAS SORBENT

Richard J. Ruch, Carl J. Knauss, William E. Bacon, and Scott Miller
Department of Chemistry
Kent State University, Kent, OH 44242

Sidney G. Nelson, Brian W. Nelson, and Sidney G. Nelson, Jr.
Sanitech, Inc.
1935 East Aurora Road, Twinsburg, OH 44087

INTRODUCTION

Many advancing new technologies for removing SO_2 and NO_x from flue gas emissions involve dry scrubbing, in contrast to wet scrubbing, the most widely used technology today [1]. These developments are being encouraged by a real need to reduce costs, to increase overall efficiency, and to avoid major problems relating to water pollution and to sludge handling and disposal. Cost reductions and increased efficiency can be achieved by using regenerable, high-capacity sorbents, and the water and waste-disposal problems can be alleviated by handling sorbents dry and by generating useful by-products from the wastes produced. Recently, a new family of dry, regenerable sorbents, called NelSorbents, has reached the stage of pilot-scale testing.

The reactivity of unsupported MgO for removal of flue-gas components has been studied extensively [2]. Studies have also been done on inert supports for MgO and other oxides [3]. In addition, the reactivity and catalytic activity of such support-type materials as aluminates, silicates, and zeolites, have been studied [4].

The present study was undertaken to determine the physical nature and the chemical reactivity of a promising NelSorbent material having vermiculite as a support for hydrated MgO. This patented sorbent has been shown to effectively remove SO_2 and NO_x from flue gases in the laboratory and in pilot-scale operations. A fundamental scientific investigation of the material was performed to improve current methods of preparation, conditioning, utilization, and regeneration.

EXPERIMENTAL

NelSorbent Preparation

The NelSorbent used in the studies was prepared by Sanitech, Inc. using the techniques described in U.S. Patent Number 4,721,582. Vermiculite was variously coated with several grades of MgO, $Mg(OH)_2$, or $MgCO_3$. The samples were both bench- and batch-processed at 45% by weight MgO and conditioned at temperatures of 400, 550, and 800°C.

Sample Preparation

Sanitech exposed NelSorbents both in a dry and in a moistened condition to side-streams of flue-gas at the Gorge Power Plant of Ohio Edison in Akron, Ohio. In the laboratory, vermiculite and NelSorbents were exposed to synthetic flue-gas mixtures and to SO_2 or NO_x under varying relative humidities.

NelSorbent Regeneration

Flue-gas exposed samples were regenerated at 800°C in either air or in a 40% CH_4/60% N_2 mixture.

Gas Adsorption

Nitrogen adsorption and desorption measurements were made in a classical gas adsorption apparatus at liquid nitrogen temperature. Pressures were measured with a mercury manometer and masses were measured to ±0.01 milligrams with a Cahn electromagnetic balance. Adsorption and desorption for SO_2 and NO_X, both in the presence and in the absence of added moisture, were measured to ±0.2 milligrams with a quartz spring balance.

Water adsorption isotherms were carried out over a period of weeks. Samples in desiccators were exposed to specific relative humidities achieved by various saturated salt solutions. Weight gains in these trials were determined with an analytical balance.

Infrared Spectra

Fourier transform infrared spectra (FTIR) were measured with an IBM model 32 spectrophotometer. Both powder samples in a nitrogen atmosphere and solution spectra in silver chloride cells were measured. A Spectra-Tech high temperature environmental chamber was used to run series of spectra at elevated temperatures.

X-Ray Diffraction

Samples were packed in Lindeman glass capillaries and exposed to Cu radiation at 35 kilovolts and 15 milliamps for about seven hours. The interlayer spacings were calculated from the resultant powder patterns.

Electron Micrographs

Electron micrographs were made with several microscopes. Due to static charge phenomena, the best results were obtained at very low amperages and gave good resolution to the nanometer range.

RESULTS AND DISCUSSION

Nitrogen Isotherms

The classical BET theory was used to analyze adsorption isotherms such as those shown in Figures 1 and 3. Moisture variability is a problem in establishing a reliable mass baseline for minerals such as vermiculite. To minimize this variability, the samples were outgassed under a vacuum as the sample was heated to 200°C. Although this procedure reduced the baseline variability, it was necessary to plot the data in the form shown in Figures 2 and 4 to get reproducible results.

For the N(1-X) ordinate of Figures 2 and 4, N represents the mass reading in milligrams obtained from the Cahn balance. When X=P/Po=0, the intercept gives the correct baseline. Adding the baseline to the slope of the plot gives the mass in milligrams for a monolayer by the BET theory.

Surface Areas

BET surface areas with N_2 are shown in Table 1. The value of 4 M^2/gram represents the external surface area of vermiculite.

TABLE 1
BET SURFACE AREAS - M^2/gram Sample

SAMPLE	TEMPERATURE	NITROGEN	WATER
Conditioned:			
Vermiculite	550°C	4	
MgO	550°C	50	
NelSorbent-Bench	550°C	55	270
NelSorbent-Bench	800°C	11	
NelSorbent-Batch	550°C	16	52
Regenerated NelSorbents:			
Batch-Air	800°C	12	57
Batch-CH_4/N_2	800°C	8	
Previous Sample in Air	500°C	2	45

The surface area of MgO varies considerably depending on how it is prepared [7,8]. The NelSorbent bench-processed at 550°C had a surface area of 55 M^2/gram of sample. Since this NelSorbent is only 45% MgO by weight, this corresponds to a surface area for this MgO of over 100 M^2/gram or more than twice that of the original MgO. Special treatment of MgO has been shown to give areas in excess of 500 M^2/gram [9].

Exposure to high temperatures caused surface areas to drop. Surface areas of NelSorbent conditioned at 800°C and NelSorbent batch-processed at 550°C, where hot-spots may exist, dropped below 20 M^2/gram. After gas exposure, the batch-processed NelSorbents were regenerated and the surface areas dropped even more, to 12 and 8 M^2/gram. The sample regenerated in a CH_4/N_2 atmosphere had a grey color which disappeared on heating in air to 500°C. However, the surface area then dropped even more to 2 M^2/gram. The grey colored sample gave a positive sulfide test with lead acetate paper.

The 550°C bench-processed NelSorbent was sieved into fractions >1400, 500-1400, 250-500, and <250 microns. The surface areas ranged from 23-36 M^2/gram sample, considerably below the 55 M^2/gram for the unsieved sample. In the unsieved sample, the larger vermiculite particles may protect the MgO from being sintered.

Water Isotherms

Table 1 also shows the surface areas determined by the adsorption of water on four selected samples. These water areas exceed the nitrogen areas by greater than three-fold. The most dramatic effect was for the regenerated sample which went from 2 to 45 M^2/gram. This shows that the conditioning water can penetrate the interlayers of the vermiculite even if external surface area has been previously reduced.

NO_x Adsorption

Table 2 shows that a NelSorbent conditioned at 550°C and exposed to NO_x under ambient conditions had an 11.2% weight gain which was retained on evacuating the system. After heating to 200°C in vacuum, the weight gain dropped to 7.0%. Vermiculite on the other hand, gained only 2.2%

by weight NO_x under similar conditions and lost almost all of the weight by pumping in a vacuum without the addition of heat. Hence, there is a much stronger interaction of NO_x with the NelSorbent than with the vermiculite, the former being akin to chemical adsorption and the latter to physical adsorption.

TABLE 2

NO_x/SO_2 ADSORPTION - PERCENTAGE WEIGHT GAIN

SAMPLE	AMBIENT EQUILIBRIUM	VACUUM 20°C	VACUUM 200°C
NO_x ADSORPTION			
550°C NelSorbent[a]	11.4%	11.4%	7.0%
Vermiculite[a]	2.2%	0.3%	--
SO_2 ADSORPTION			
550°C NelSorbent[b]	4.0%	--	--
Vermiculite[a]	1.0%	0.5%	--
550°C NelSorbent[a]	4.5%	3.4%	--
550°C NelSorbent[c]	94%[d]	57%	30%
Vermiculite[c]	24%[e]	2%	--

a. Prepared at ambient conditions b. Prepared by pumping to vacuum
c. Prepared at 100% relative humidity d. Weight gain includes 37% water e. Weight gain includes 12% water

SO_2 Adsorption

NelSorbent conditioned at 550°C gained nearly 5% by weight when exposed to SO_2 under ambient conditions and dropped a few percent when pumped down in a vacuum. However, when the NelSorbent was pre-conditioned for a week in 100% relative humidity, there was over a 50% weight gain of SO_2 which remained on evacuating the system under ambient conditions. Even on heating to 200°C in a vacuum, 30% by weight SO_2 remained indicating a strong chemical interaction.

Vermiculite gained little weight under ambient conditions when exposed to SO_2 and the weight gain dropped to near the original sample weight when pumped to a vacuum under ambient conditions. Although there was a larger weight gain when the vermiculite was first saturated with water vapor for a week at 100% relative humidity, most of the weight gain was lost on pumping to a vacuum. This suggests a very weak physical interaction between SO_2 and vermiculite even in the presence of a large amount of pre-absorbed water.

FTIR Solid Spectra

Raw vermiculite and 550°C conditioned vermiculite gave bands at 3000-3500 cm^{-1} and at 1650 cm^{-1}. Silicon-oxygen absorption near 1000 cm^{-1} interfered with sulfite and sulfate analyses.

Conditioned NelSorbent gave a strong $Mg(OH)_2$ band at 3700 cm^{-1} which disappeared as the temperature of conditioning was increased. $MgCO_3$ peaks at 1500 cm^{-1} and 850 cm^{-1} became evident on heating as well as 1400 and 400-700 cm^{-1} peaks for MgO. Batch-processed material did not as effectively reduce the $Mg(OH)_2$ peaks as did bench-processing. When $MgCO_3$ was used as the starting material, the carbonate peaks remained strong even after conditioning indicating that insufficient energy was added to the system to break down the carbonate.

When the NelSorbent was exposed to SO_2, a sulfite peak at 950 cm^{-1}, a sulfate peak at 1100 cm^{-1}, and bisulfite/bisulfate peaks at 2250 cm^{-1} were noted in addition to the previously discussed peaks and bands. $MgCO_3$ was particularly dominant when NelSorbents were run under dry conditions at the power plant suggesting that CO_2 strongly competes in adsorption under these conditions.

In general, the concentration of NO_X was not high enough in the flue-gas streams to be absorbed to such an extent to be detected by FTIR. One NelSorbent sample exposed to NO and superheated steam showed the presence of nitrite at 1250 cm^{-1}.

The spent NelSorbents regenerated in air showed MgO, $MgCO_3$, and $MgSO_4$ peaks. The sample regenerated in CH_4/N_2 suggested the presence of magnesium compounds not previously seen in other samples, perhaps Mg or MgS. Subsequent heating of the sample in air eliminated these compounds and peaks were observed for MgO and $MgSO_4$. Also, a particularly large $MgCO_3$ peak appeared which may have been previously masked.

A NelSorbent well-spent with flue-gas was heated in situ in the FTIR environmental chamber. The sample was mixed with KBr and heated in a stream of nitrogen. Bisulfite/bisulfate peaks disappeared by 200°C, water peaks reached a minimum at 300°C, MgO and $MgCO_3$ disappeared by 500°C, and $MgSO_4$ increased in intensity at 400°C and remained constant up to 660°C, the maximum temperature of analysis.

FTIR Solution Spectra

Aqueous extracts of NelSorbents spent with flue-gas indicated the sulfate ion at 1100 cm^{-1}. No sulfite was detected, perhaps due to its oxidation to sulfate.

A NelSorbent sample saturated in the laboratory with moisture and with NO_X gave a nitrite peak at 1240 cm^{-1}. The nitrate peak was absent.

Basal Plane X-Ray Spacings

The raw and the 550°C processed vermiculite gave a 14 angstrom interlayer spacing expected for two layers of water. When conditioned at 550°C for 30 minutes in the NelSorbent preparation, the interlayer distance dropped to 12 angstroms expected for one interlayer of water. When conditioned at 800°C for 30 minutes, the interlayer collapsed to a 9 angstrom distance which indicates the complete loss of interlayer water.

The interlayer distance expanded back to 14 angstroms for the NelSorbent in the flue-gas stream indicating the presence of enough water to re-expand the lattice.

Interplanar X-Ray Spacings

Table 3 shows interlayer distances and compound assignments found for a NelSorbent which was used at the power plant during a week of heavy rains.

TABLE 3
NELSORBENT EXPOSED TO FLUE GAS

COMPOUND	ANGSTROMS	COMPOUND	ANGSTROMS
$MgCO_3 \cdot 3H_2O$	6.49	$MgSO_4 \cdot 2H_2O$	2.03, 4.39
$MgSO_4 \cdot 7H_2O$	5.91	$MgSO_3 \cdot 6H_2O$	2.76
$MgSO_4 \cdot 6H_2O$	2.89	$MgSO_3 \cdot 3H_2O$	4.19
$MgSO_4 \cdot 4H_2O$	3.93, 5.41	MgO	3.04
$MgSO_4 \cdot 3H_2O$	2.49	$Mg(OH)_2$	1.49, 1.57, 1.79, 2.39

The 2.10 angstrom spacing for MgO in the freshly processed NelSorbent disappears on flue-gas exposure but reappears on regeneration. Some residual $MgSO_4$ is present under all methods of regeneration. Several unidentified spacings were found when the NelSorbent was regenerated in CH_4/N_2 but disappeared when the material was reheated in air. Any sulfides, for example, would be oxidized to the sulfate and/or the oxide in air.

NelSorbent exposed to superheated steam and NO_X in the laboratory developed a red-orange color. X-Ray spacings showed MgO, $Mg(OH)_2$ and $Mg(NO_3)_2$. The nitrate occurred at 3.34 angstroms and was not found in any flue gas exposed samples of NelSorbent.

Electron Micrographs

At 100,000 magnifications of the NelSorbent, the MgO or $Mg(OH)_2$ patches were observed to be sparsely but uniformly distributed on the vermiculite. As the magnification increased, the patches appeared as crystalline clusters with a high degree of porosity. At the highest magnification, the clusters seemed to be composed of needles several hundred nanometers in length and about 50 nanometers in cross-section.

SUMMARY

The surface area of the NelSorbents is larger than would be expected from the collective surface areas of the constituent vermiculite and MgO suggesting that the vermiculite support is enhancing surface area development of the MgO. There is evidence of a mesoporous structure in the NelSorbent from the electron micrographs and by the hysteresis of some of the desorption isotherms. Difficulty in establishing baseline weights of the NelSorbents also suggests the existence of a microporous structure. MgO is a better starting material than either $Mg(OH)_2$ or $MgCO_3$ for preparation of the NelSorbent. The carbonate does not seem to completely decompose in the conditioning process.

There is a loss of surface area when the NelSorbents are subjected to too high a temperature. This can happen during conditioning or regeneration or when hot spots develop in batch conditioning or when sieved fractions tend to fuse. The vermiculite basal plane structure can also be collapsed by the higher temperatures.

Sulfites, sulfates, and sulfides are detected by FTIR, X-Ray, or qualitative tests. The sulfite tends to oxidize to the sulfate over longer periods of time. Some sulfate tends to remain even under fairly rigorous regeneration techniques. Any sulfides produced by a reducing regeneration atmosphere are reoxidized to sulfate or oxide by heating in air.

Nitrites or nitrates were not detected in pilot plant NelSorbent samples due to the small concentration of NO_X in the flue-gas. They were variously detected in laboratory treated samples by FTIR, X-Ray, and qualitative tests.

Moisture plays an extremely important role in the adsorption process. Burning wet coal or adding moisture to the sorbent bed increased the adsorption efficiency of the NelSorbent for SO_2 and NO_X. This observation is confirmed by laboratory studies under static conditions. X-Ray studies and adsorption studies with water substantiated the penetration of the vermiculite interlayers.

Dynamic studies have shown larger percentage utilizations of the NelSorbents than have static studies in the laboratory. Future studies will need to address what factors in the dynamic systems are responsible for this difference.

ACKNOWLEDGMENT

This work was funded by a Thomas Edison Seed Grant from the state of Ohio. The space for the pilot-plant operations was donated by the Ohio Edison Company.

REFERENCES

[1] Chemical & Engineering News, 67, No. 20, 20(1989); 67, No. 50, 17(1989); 68, No. 3, 5(1990).

[2] Egan, B.Z. and Felker, L.K., Ind. Eng. Chem. Process Des. Dev., 25, 558(1986).

[3] Kocaefe, D., Karman, D., and Steward, F.R., Canadian J. Chem. Eng., 63, 971(1985).

[4] Marier, P. and Ingraham, T.R., Mines Branch Information Circular IC 263, Department of Energy, Mines and Resources, Mines Branch, Ottawa, February, 1971.

[5] Haggin, J., Chemical & Engineering News, 68, No. 3, 38(1990).

[6] Marier, P. and Dibbs, H.P., Thermochimica Acta, 8, 155(1974).

[7] De Vleesschauwer, W.F.N.M. in "Physical and Chemical Aspects of Adsorbents and Catalysts", B.G. Linsen, ed., Academic Press, N.Y., pp. 265-314, 1970.

[8] Hartman, M. and Svoboda, K., Ind. Eng. Chem. Process Des. Dev., 24, No. 3, 613(1985).

[9] Beruto, D., Rossi, P.F., and Searcy, A.W., J. Phys. Chem., 89, 1695(1985).

Key Words: sorption, flue-gas, vermiculite

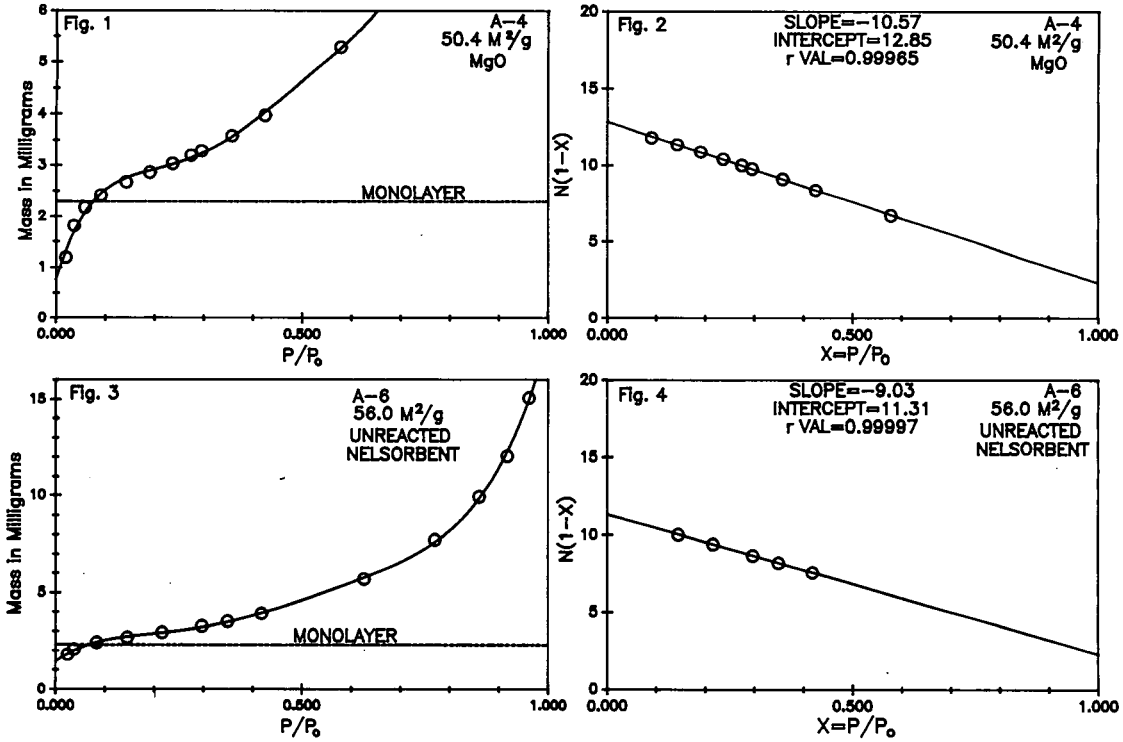

Figure 1 – Adsorption isotherm of MgO processed at 550°C.
Figure 2 – Variation of BET plot to determine mass of A-4 monolayer.
Figure 3 – Adsorption isotherm of NelSorbent processed at 550°C.
Figure 4 – Variation of BET plot to determine mass of A-6 monolayer.

PRODUCTION AND APPLICATION OF THIOSULFATE IN LIME-BASED WET FGD

Y. Joseph Lee[a], Lewis B. Benson[a], and Robert O. O'Hara[b]
a. Dravo Lime Company, Pittsburgh, PA 15225
b. Duquesne Light Company, Pittsburgh, PA 15279

Key Words: sulfur, alkaline hydrolysis, thiosulfate, oxidation inhibition, lime

INTRODUCTION

Thiosulfate has been identified as a free radical scavenger which inhibits sulfite oxidation effectively (Owens and Rochelle, 1985). In flue gas scrubbers, excessive oxidation could cause some serious reliability problems such as scaling on scrubber internals and mist eliminators. Emulsified sulfur has been used in many limestone scrubbers (Moser et al., 1988) since it was found that sulfur could react with sulfite in scrubbing liquor to form thiosulfate feasibly (Rochelle et al., 1987). However, the reaction rate is very slow primarily because of the low solubility of sulfur in aqueous solution. Alkaline hydrolysis of sulfur is a potential alternative to synthesize thiosulfate by sulfur addition. At high pH and high temperature, sulfur can be converted to thiosulfate and polysulfides which react with sulfite readily to form thiosulfate. This paper is focused on the kinetics of the alkaline hydrolysis of sulfur and its effect on the overall performance of lime-based wet FGD.

BACKGROUND

Several reactions related to the production of thiosulfate from sulfur are collectively listed in Table 1. Thiosulfate has been produced commercially by the reaction of sulfur and sulfite in neutral or alkaline media (rxn 1). Because of the equilibrium between sulfite and bisulfite (rxn 2), alkalinity is necessary to enhance reaction 1 by removing the proton released from bisulfite. The reaction rate is independent of pH or sulfite concentration and is first order in sulfur solids concentration when pH is above 5.0 and sulfite is greater than 1 mM (Donaldson and Johnston, 1969). At 55°C, typical for lime/limestone slurry scrubbers and recycle tanks, 0.04 hr^{-1} was suggested for this first order kinetic constant (Rochelle et al., 1987).

One way to facilitate the production of thiosulfate is by using sulfide or polysulfides instead of sulfur (rxn 4). Polysulfides may be formed by dissolving sulfur in sulfide solutions (Gould, 1962). Reaction 4 is so fast that the proton released by reaction 2, in some instances, cannot be neutralized immediately. Besides, the pH at gas-liquid interface is low due to SO_2 dissolution. The consequence is the formation of "local" low pH spot despite the alkaline bulk solution and the generation of hydrogen sulfide that may cause serious odor problems. Because of this reason, ploysulfide was abandoned in the EPA limestone scrubbing pilot plant at Research Triangle Park (Rochelle et al., 1987). However, if polysulfides are introduced to scrubbers together with lime slurries, the high pH of the feeding slurry and the scrubbing liquor as well as the fast dissolution of lime will neutralize the proton in reaction 2 effectively and therefore prevent the formation of H_2S.

Boiling sulfur-lime slurry is a commercial process for polysulfide production.

Alkaline hydrolysis of sulfur is therefore a logical approach to synthesize thiosulfate in situ because of the highly exothermic reaction of lime slaking. The polysulfides will react readily with sulfite to form thiosulfates (rxn 7-9). The unreacted sulfur leaving the lime slurry storage tank will react with sulfite in the scrubbers and in the recycle tanks to produce additional thiosulfate (rxn 1). Another "reactor" for thiosulfate production is the thickener. Therefore, the conversion of sulfur to thiosulfate is expected to be substantially higher in lime-based FGD than in linestone-based FGD.

EXPERIMENTAL METHODS

Jacketed reactors were used to perform experiments at the desired temperature. The solutions were agitated by magnetic stirrers. When thiosulfate formation in slakers/lime tanks was studied, 500 ml of 3.3 wt% or 10 wt% lime slurry was used to react with sulfur. The slurry samples (25 ml) were quenched by adding 50 ml cold 0.2M sodium sulfite. The resulting mixtures were allowed to react 10 minutes to completely convert polysulfides to thiosulfate. Clarified filtrates were then analyzed for thiosulfate by iodometric titration after blocking sulfite with formaldehyde. The thiosulfate measured in this way was dubbed "available thiosulfate."

When the formation of thiosulfate by reacting sulfur with sulfite was studied, a calcium sulfite slurry available from a power station's (Elrama, PA) recycle tank was used as the source of sulfite. Fritted glass spargers were used to introduce gas containing SO_2 to the reacting solutions. Lime slurries (10 wt%) were used to neutralize the absorbed SO_2 and to keep the pH between 6.5 and 7.5. Both emulsified sulfur and powdered sulfur were used for this study. Emulsified sulfur had no problem getting into slurry solution while 2000X dilute Triton X-100 was needed to wet powdered sulfur first.

A schematic diagram of the flow system used for studying the impact of sulfur addition to a lime slurry scrubbing system is given in Figure 1. Nitrogen, air, and SO_2 were metered and mixed in a mixing chamber to simulate the flue gas. In most cases, both nitrogen and air were set at 1.0 scfm to give ~10% O_2 in the simulated flue gas. Sulfur dioxide was set at a rate slightly lower than necessary to neutralize the 5 wt% lime slurry fed at 12 ml/min. An auxiliary SO_2 flow was activated by a pH controller when the pH value of the scrubbing liquor was higher than 7.2. The scrubber pH was thus maintained between 7.0 and 7.2 throughout all experiments. The temperature of the scrubbing liquor was maintained at 55°C by circulating the liquor through a heat exchanger. The simulated thickener overflow (TOF) was fed to the scrubber at 100 ml/min. The composition of the simulated TOF is also given in Figure 1. Sodium thiosulfate or available thiosulfate was fed to the scrubber at 16 ml/min. The volume of the absorber was maintained at 5.5 liters by a level controller. Samples were taken once an hour and analyzed for both sulfite and thiosulfate by iodometric titration.

RESULTS AND DISCUSSIONS

Sulfur to Thiosulfate and Polysulfides in Slakers and Lime Tanks

Boiling a slurry mixture of lime and sulfur is a general practice to

manufacture polysulfides commercially. This process prompted the testing of thiosulfate production by feeding sulfur to the slaker or the lime slurry storage tank because of the fast conversion of polysulfides to thiosulfate and the highly exothermic reaction of lime slaking. According to the reactions 6-9 listed in Table I, one mole of sulfur will generate one mole of thiosulfate stoichiometrically. The calculation of sulfur conversion is based on the formation of the available thiosulfate.

Both powdered sulfur and emulsified sulfur were tested for the production of available thiosulfate. It is very clear that the conversions of powdered sulfur (Figure 2) and emulsified sulfur (Figure 3) to available thiosulfate are strongly dependent on reaction temperature. The dramatic difference between 70°C and 80°C in converting powdered sulfur to available thiosulfate is probably not exclusively due to the activation energy of reaction 6. A possible contribution is the dissolution of powdered sulfur in sulfide or polysulfide solutions. As a matter of fact, one way to produce polysulfide is dissolving powdered sulfur in sodium sulfide solution (Hartler et al., 1967; Arntson et al., 1958). Therefore, when the concentration of sulfide or polysulfide is high, the conversion of sulfur to available thiosulfate will be accelerated. The ceiling conversion is probably controlled by the thermodynamic equilibrium and the coprecipitation with lime solids.

Figure 2 indicates that higher concentrations (1.0 g S/500 ml lime slurry) of sulfur are subjected to lower conversion rates. Probably the agglomeration of sulfur particles, that reduces the available surface area for reactions, is more severe at higher concentrations. Emulsified sulfur is a lot more reactive than powdered sulfur for alkaline hydrolysis. Compared to powdered sulfur (>30μ), emulsified sulfur (<5μ) is at least 100 times more reactive at 70°C primarily due to its smaller particle size.

It is well known that thiosulfate is not stable in acidic solution (rxn 3). It is also known that thiosulfate decomposes to sulfate and sulfide in alkaline media (Kirk-Othmer, 1969). To investigate the stability of thiosulfate in lime slurry, sodium thiosulfate was added to 3.3 wt.% lime slurry. The samples at different "seasoning" time were analyzed for thiosulfate. The results indicate that 20% and 30% of the sodium thiosulfate are not accounted for in the filtrate for 12.5 mM and 25 mM sodium thiosulfite solutions respectively, however the thiosulfate concentrations did not change with time. Another study, mixing lime slurry (3.3 and 10 wt%) with varying amounts of sodium thiosulfate (up to 25.3 mM) for one hour at 80°C, indicated that the unaccounted for fraction was larger when using more concentrated lime slurry. These results imply that the major source of unaccounted thiosulfate is the "coprecipitation" with lime, while the decomposition of thiosulfate in lime saturated solutions is probably not significant. This was verified by analyzing the available thiosulfate in the filtered lime solids. Nevertheless, thiosulfate incorporation into lime solids should not cause any problems in lime slurry scrubbing systems because as the lime dissolves the coprecipitated "available thiosulfate" will be released.

Sulfur to Thiosulfate in Scrubbers and Recycle Tanks

Scrubbers and recycle tanks are the major reactors for the conversion of sulfur to thiosulfate (rxn 1) in limestone slurry scrubbing systems. For lime slurry scrubbing systems, the unreacted sulfur leaving from lime slurry storage tank

will contribute additional thiosulfate generation in scrubbers and recycle tanks. The reaction rate can be expressed empirically as first order in sulfur solids concentration (eq. 10)

$$\frac{d[S]}{dt} = -k[S] \qquad (10)$$

Based on reaction 1 and equation 10, equation 11 can be derived.

$$\ln\left(1 - \frac{[S_2O_3]_t - [S_2O_3]_o}{[S]_o}\right) = -kt \qquad (11)$$

Where subscripts t and o denote time t and time zero respectively. Plotting the experimental data as $\ln\ (1-([S_2O_3]_t-[S_2O_3]_o)/[S]_o)$ versus time should then give a straight line of slope -k. The results are summarized in Table 2.

The conversion of sulfur to thiosulfate by reacting with sulfite decreased with increasing sulfur loading just like what was observed in the study of alkaline hydrolysis of sulfur. When sulfur solid concentration increased from 0.4 g to 1.2 g per 500 ml slurry, the empirical reaction rate constant decreased from 0.072 hr^{-1} to 0.040 hr^{-1} when N_2 blanket was applied above the reaction solutions. Similar results were reported by Rochelle et al. (1987). However, no significant differences were observed with different sulfur loadings (0.17-1.2 g) when gases were sparged through the solutions. Probably, the gas sparging helps the dispersion of sulfur solids and enhances the solid-liquid reactions.

In reacting with sulfite to form thiosulfate, emulsified sulfur has significantly larger initial conversion rate while powdered sulfur has an "incubation" period. The latter was also observed by Rochelle et al. (1987). The reaction rate constant measured after incubation period is 0.087 hr^{-1} for powdered sulfur. The corresponding kinetic constant for emulsified sulfur is 0.090 hr^{-1}. In other words, there is no significant difference between emulsified sulfur and powdered sulfur except for the much faster initial rates of emulsified sulfur and the long incubation time of powdered sulfur.

Previous studies suggested a kinetic constant of 0.04 hr^{-1} at 55°C in the absence of sulfite oxidation (Rochelle et al., 1987). Thiosulfate decomposition is coupled with sulfite oxidation. Table 2 indicates that the kinetic constants are well above that value even in the presence of significant sulfite oxidation caused by 15% O_2. Perhaps some unidentified chemistry facilitated the conversion of sulfur to thiosulfate in Elrama slurries more effectively.

Impact of Available Thiosulfate on the Performance of Wet Scrubber

In a laboratory scale slaker, elemental sulfur (32 g powdered sulfur or 45.7 g 70 wt% emulsified sulfur was mixed with 10 liter preheated water (46°C) first and 2 kg pebble lime was then fed to the water-sulfur mixture. The slurry temperature rose and then dropped from 81.5°C to 72°C over 25 minutes. The slurry was then diluted with water make 8.4 wt% solids. The temperature was maintained at 44°C by a heating tape and the slurry was gently stirred for one hour. The slurry was then quenched with water to make 5.0 wt% slurry. The conversions of sulfur to available thiosulfate were 78% and 21% for emulsified sulfur and powdered sulfur, respectively.

A bench scale absorber was used to evaluate the effect of the available thiosulfate on the general performance of magnesium-enhanced lime slurry scrubber. During the experiments, lime slurry and available thiosulfate were fed to the absorber separately. Separate feeding made the control of thiosulfate concentration independent of the lime slurry feed rate. A very light odor of emulsified sulfur was detected during the process of conducting experiments, but no H_2S odor problem was encountered.

The result indicated that the oxidation of sulfite could be suppressed by thiosulfate when thiosulfate concentration was higher than a certain level, the so-called threshold concentration. For example, 0.63 mM thiosulfate gave a calcium sulfite/sulfate solid with 87% oxidation, which was essentially the same as the solid oxidation in the absence of thiosulfate. As low as 15% solid oxidation was achieved when 1.8 mM thiosulfate was present.

Two experiments were performed under similar conditions except one used $Na_2S_2O_3$ directly and the other used polysulfides, which were produced by alkaline hydrolysis of sulfur, as the source of thiosulfate. The results show practically no difference between these two experiments except polysulfides slightly decreased calcium and increased sulfate but kept the oxidation level in the solids (15%) essentially the same.

It seemed that polysulfides reacted with sulfite fast enough to provide thiosulfate reliably. Fortunately, the absorption of SO_2 into lime slurry to supply sulfite for thiosulfate production was even faster. Therefore, the concentration of sulfite in the solution was maintained nearly constant. Sulfite is important because SO_3^{-2} is the major source of alkalinity used to absorb SO_2.

Figure 4 shows the effect of thiosulfate concentration on its utilization. The utilization here is defined as the ratio of the measured thiosulfate concentration to the "maximal" thiosulfate concentration, which is obtained by assuming no decomposition and no coprecipitation. The results imply that the major loss of thiosulfate is due to coprecipitation with calcium sulfite hemihydrate when thiosulfate concentration is higher than 1.9 mM. (Because thiosulfate utilization in the absence of oxygen is 92%, which is not significantly higher than 85-88% utilization with 1.9-3.8 mM thiosulfate in the scrubbing liquor and 10.5% O_2 in the flue gas. And the thiosulfate degradation is supposed to be coupled with sulfite oxidation). Thiosulfate utilization increases with its concentration up to 1.9 mM thiosulfate. This trend implies that thiosulfate, at lower concentration, is subjected to more severe chemical degradation. It seems consistent with previous study (Maller et al. 1988), which correlated thiosulfate degradation rate (R_{deg}) and sulfite oxidation rate (R_{ox}) as:

$$R_{deg} = a(R_{ox} \times [S_2O_3^{2-}])^{0.5} \quad (12)$$

$$R_{ox} = b([SO_3^{2-}]/[S_2O_3^{2-}]) \quad (13)$$

Equations (12) and (13) can be combined to give equation (14):

$$R_{deg} = c[SO_3^{2-}]^{0.5} \quad (14)$$

Where a, b, and c are constants. In other words, the degradation of thiosulfate was predicted to be half order in sulfite but was independent of thiosulfate concentration. Equation (15) can be derived from equation (14) if the sulfite concentration is maintained constant:

$$\frac{[S_2O_3^{2-}]}{[S_2O_3^{2-}]_o} = 1 - \frac{[SO_3^{2-}]^{0.5}}{d[S_2O_3^{2-}]_o} \qquad (15)$$

Where d is a constant. Equation (15) indicates qualitatively that the utilization of thiosulfate increases with thiosulfate and decreases with sulfite. More research is needed to better understand the degradation and coprecipitation of thiosulfate in lime slurry scrubbing systems.

ACKNOWLEDGMENT

This research project was financially supported by Duquesne Light Company. Special appreciation is extended to Mr. John College, who helped initiate this research project. The authors would like to thank Mr. James Zahorchak, Ms. Pat Kerr, and Mr. Jerry Hoffman for their help in performing the experiments, typing the paper, and preparing the figures, respectively.

REFERENCES

Arntson, R. H., F. W. Dickson, and G. Tunell, "Saturation Curves of Orthohombic Sulfur in the System $S-Na_2S-H_2O$ at 25°C and 50°C," Science, Vol. 128, 716-718 (1958)

Donalson, G. W. and F. J. Johnston, "The Reaction of Colloidal Sulfur with Sulfite," J. Phys. Chem. Vol. 73, 2064-2068 (1969)

Gould, E. S., "Inorganic Reactions and Structure," Revised Ed. 291-292 (1962)

Hartler, N., J. Libert, and A. Teder, "Rate of Sulfur Dissolution in Aqueous Sodium Sulfide Solution," Ind. Eng. Chem. Proc. Dea. Dev. Vol. 6, 398-406 (1967)

Kirk-Othmer, "Encyclopedia of Chemical Technology," 2nd Ed. Vol. 20, 227-247 (1969)

Moser, R. E., J. D. Colley, J. G. Noblett, and A. F. Jones. "Control and Reduction of Gypsum Scale in Wet Lime/Limestone FGD Systems by Addition of Thiosulfate: Summary of Field Experiences," Presented at the First Combined FGD and Dry SO_2 Control Symposium, St. Louis, MO, October (1988)

Rochelle, G. T., Y. J. Lee, R. N. Ruiz-Alsop, J. C. S. Chang, and T. G. Brna, "Thiosulfate Additives for Lime/Limestone Scrubbing," EPA - 600/9-87-004b, February (1987)

TABLE I

THIOSULFATE FORMATIONS IN LIME SLURRY SCRUBBING SYSTEMS

$$S + SO_3^{-2} \longrightarrow S_2O_3^{-2} \quad (1)$$

$$HSO_3^- \longrightarrow H^+ + SO_3^{-2} \quad (2)$$

$$S_2O_3^{-2} + H^+ \longrightarrow S + HSO_3^- \quad (3)$$

$$S_x^{-2} + SO_3^{-2} \longrightarrow S_{(x-1)}^{-2} + S_2O_3^{-2} \quad (4)$$

$$S_x + 6OH^- \xrightarrow{>100°C} 2S^{-2}_{(x-2)/2} + S_2O_3^{-2} + 3H_2O \quad (5)$$

$$S_8 + 6OH^- \xrightarrow{>100°C} 2S_3^{-2} + S_2O_3^{-2} + 3H_2O \quad (6)$$

$$S_3^{-2} + SO_3^{-2} \longrightarrow S_2^{-2} + S_2O_3^{-2} \quad (7)$$

$$S_2^{-2} + SO_3^{-2} \longrightarrow S^{-2} + S_2O_3^{-2} \quad (8)$$

$$2S^{-2} + 4HSO_3^- \longrightarrow 3S_2O_3^{-2} + 2OH^- + H_2O \quad (9)$$

TABLE 2

SUMMARY OF KINETIC CONSTANTS OF THIOSULFATE FORMATION BY REACTING SULFUR WITH SULFITE AT 55°C

Sulfur (powdered) (g/500 ml slurry)	Reaction Rate Constant ($hour^{-1}$)		
	N_2 Blanket	1% SO_2 200 ml/min	2000 ppm SO_2 15% O_2 1 l/min
0.1668		0.081	0.042
0.336		0.087	0.049
		0.090*	0.052
0.40	0.072	0.059	
1.20	0.040	0.062	

*0.4766 g 70 wt% emulsified sulfur

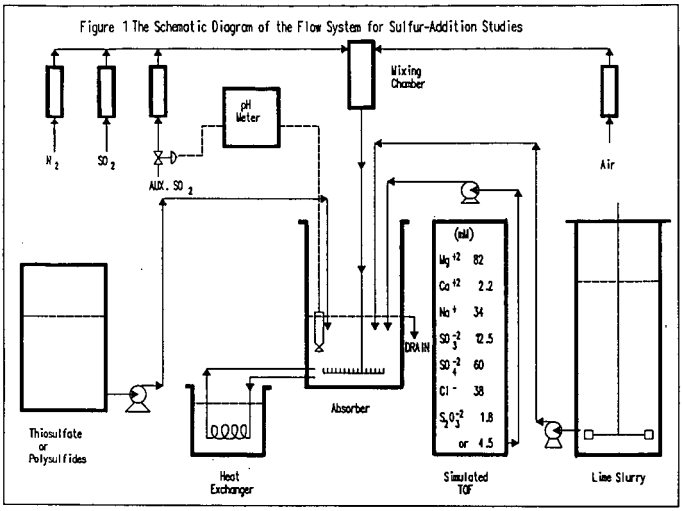

Figure 2 Temperature Effects on Alkaline Hydrolysis of Sulfur

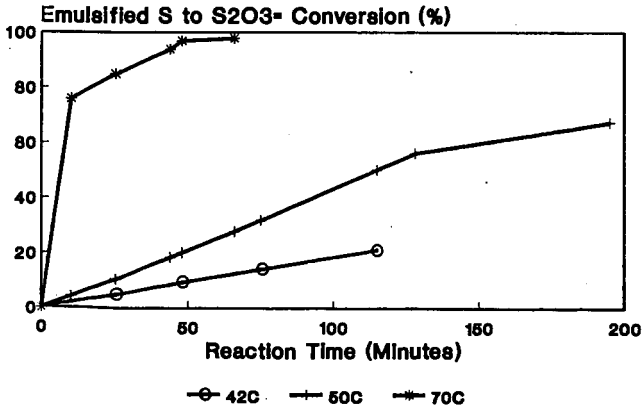

Figure 3 Temperature and Sulfur Loading Effects on Alkaline Hydrolysis of Sulfur

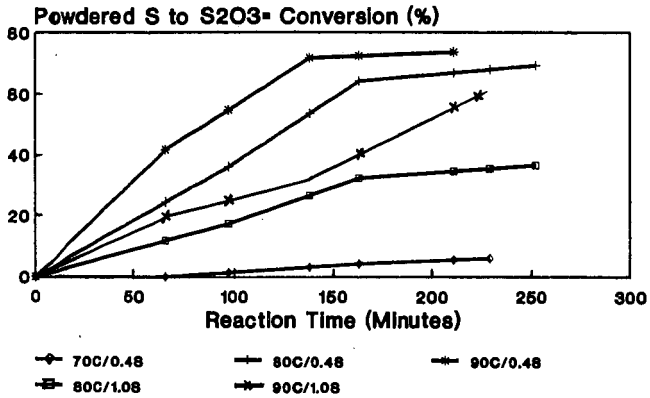

Figure 4 Utilization of Thiosulfate in Thiosorbic Lime Slurry Scrubbers

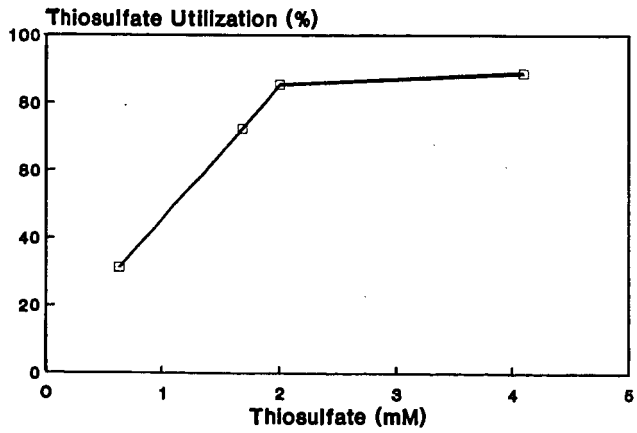

Enhanced Flue Gas Denitrification Using Ferrous*EDTA and a Polyphenolic Compound Having Combined Antioxidant and Reducing Properties

M. H. Mendelsohn and J. B. L. Harkness
Energy Systems Division
Argonne National Laboratory, Argonne, IL 60439

Keywords: NO_x-control, ferrous*EDTA, antioxidant/reducing agents

ABSTRACT

Previous work in this laboratory has involved studying the possibility of combined NOx/SOx scrubbing using various aqueous chemistries with a metal chelate additive. Recently, we have focused our work on the metal chelate ferrous*EDTA. A major problem encountered in the practical application of ferrous*EDTA is that the ferrous ion has been found to oxidize to the corresponding ferric species leading to a decrease of the NOx removal for the scrubbing solution containing the additive. We have found that addition of a polyphenolic compound leads to a sustained high NOx removal under various oxidizing conditions. We believe that the improved performance of ferrous*EDTA is due to the known capabilities of these organic compounds to both inhibit oxidation of ferrous chelates by dissolved oxygen and to rapidly reduce any ferric ions back to the original ferrous species. These effects are illustrated by the chemical reactions shown below:

$$O_2(l) + \text{organic} \longrightarrow \text{oxidized organic}$$

$$Fe(III) + \text{organic} \longrightarrow Fe(II) + \text{oxidized organic.}$$

INTRODUCTION

The use of metal chelate additives in an aqueous scrubbing environment for combined NO_x/SO_2 removal from oxygen-containing flue gases has been investigated in this laboratory for several years (1,2,3). Recent work with the metal chelate Fe(II)*EDTA has shown initially high NO_x removals which, however, decline with time as a function of the amount of oxygen gas in the feed gas stream. Because of this dependence on oxygen concentration in the feed gas, we have attributed the decline in NO_x removal to the oxidation of the Fe(II)*EDTA additive to the ferric form. One possible solution to this problem would be to add a secondary additive to the system which is either capable of preferentially reacting with any dissolved oxygen or capable of reducing any oxidized ferric species back to the ferrous form. These chemical reactions may be summarized simply as follows:

$$O_2(l) + \text{additive} \longrightarrow \text{oxidized additive}$$

$$Fe(III) + \text{additive} \longrightarrow Fe(II) + \text{oxidized additive.}$$

From an examination of previous work in the literature, we have found one class of compounds which is capable of performing both of the above stated reactions. Theis and Singer (4) found that certain polyphenolic compounds, which are products of natural vegetative decay, are capable of significantly affecting the rate of oxidation of ferrous iron. This study showed, for example, that an equimolar amount of tannic acid was able to maintain a ferrous iron concentration of 5×10^{-5} M unchanged for 7 days in the presence of 0.5 atm O_2. Also phenols, such as gallic acid, are well-known antioxidants (5).

Because of the above stated properties of polyphenolic compounds, we have investigated the effect of tannic acid, pyrogallol, and gallic acid as secondary additives in aqueous scrubbing

systems containing the primary additive Fe(II)*EDTA. Using these secondary additives, we have been able to maintain NO_x removals as high as 60-65% for up to 2 hours.

EXPERIMENTAL SETUP

The complete experimental setup has been described previously (1,2). Some recent modifications to the scrubbing section have been made and are described herein. Figure 1 shows a flow diagram of the aqueous scrubber system that was used. One major modification is that a disk and donut scrubber having four (4) stages was used instead of the previously described flooded column. A sieve plate having 3/16" diameter holes with a total open area of 10.3% was placed at the bottom of the scrubber in order to provide the capability of having some liquid holdup in the column. Also, an approximately 10 liter holding tank was added to the system and connected to the bottom of the scrubber column. Circulation rates from the holding tank to the top of the scrubber could be varied from about 330-1420 ml/min. For the experiments described below, an average circulation rate of 890 ml/min was used. However, the circulation rate was varied in the range of 790-985 ml/min in order to maintain a fixed liquid level in the scrubber. All of the experiments discussed below were performed in a sodium, double-alkali chemistry by using a 0.31 M sodium carbonate solution.

Although the feed gas system is basically unchanged from that reported earlier (1,2), we have modified the procedure for preparing the simulated feed gas mixture. For the experiments to be reported, simulated feed gas was prepared by first setting the NO level at 450 ppm in the presence of carbon dioxide, oxygen, and nitrogen gases only. In all runs, the feed gas mixture contained 14.5% CO_2, 5.4% O_2, and N_2 as the balance. After the metering valve for the NO gas was set to give 450 ppm, a shut-off valve was closed and nitrogen dioxide was then set in the same CO_2, O_2, and N_2 mixture. Nitrogen dioxide is calculated as a difference between measured NO_x and measured NO and except where noted below was set around 75 ppm. The preset amount of NO was then added to the nitrogen dioxide. Finally, sulfur dioxide was added to the feed gas mixture and adjusted to the desired level. This new feed gas preparation procedure has improved the reproducibility and reliability of our removal measurements compared to the previously used method (1,2). Except where noted, approximately 8% water vapor was also added to the simulated feed gas mixture.

RESULTS AND CONCLUSIONS

We note that all experimental comparisons in this paper are made using total NO_x removal data. This is because we have observed that the presence (as in the feed stream) or absence (as in the effluent stream) of sulfur dioxide can alter the NO or (NO_x - NO) value, but has little effect on the total NO_x value. This "SO_2 effect" depends on the amount of unmixed nitrogen dioxide in the feed gas mixture and most likely arises from a gas phase reaction between SO_2 and NO_2. Because of the relatively small amount of NO_2 that we are adding in our new feed gas preparation procedure, as described above, this effect is small. In fact, although we still consider NO_x removals more reliable, in all cases discussed below, NO removals were never more than a few percent different from the reported NO_x removals.

We first present our initial experiment which was performed with tannic acid as the secondary additive using the previously described flooded column scrubber (1,2). Figure 2 shows NO_x removal for a baseline run with 0.24 moles of Fe(II)*EDTA alone versus that of an identical run with the addition of 0.04 moles of tannic acid. This first try experiment showed a significant improvement in NO_x removal from about 14% to about 40% in the stable portions of both curves. After this experiment, the scrubber column was changed from the flooded type to the disk and donut type described above.

Because of several problems with tannic acid, including the viscosity changes it caused, its high molecular weight, and its relatively high cost; we performed the remaining experiments with the polyphenolics pyrogallol and gallic acid. After trying several ferrous:polyphenolic

ratios, the most effective ratio was found to be approximately 1:1. This ratio of primary additive to secondary additive was used in all the experiments which follow.

Figure 3 compares NO_x removal for Fe(II)*EDTA alone versus that with pyrogallol as a secondary additive. This figure clearly demonstrates the declining NO_x removal with Fe(II)*EDTA alone versus the slightly increasing removal with pyrogallol. After 90 minutes, NO_x removal with pyrogallol was about twice that of Fe(II)*EDTA alone (64% vs 32%). The tests represented by this figure are the only ones in this paper which did not have moisture added to the feed gas stream. Figure 4 compares NO_x removals with pyrogallol for feed gas mixtures with and without added moisture. NO_x removal with added moisture was consistently about 6% greater than without added moisture. This effect is probably indicative of gas phase interactions of NO and/or NO_2 with water vapor as discussed earlier (1).

The next three figures illustrate the effect on NO_x removal of various changes in the feed gas stream composition. Figure 5 compares NO_x removals with pyrogallol for feed gas mixtures containing 1500 ppm and 3000 ppm sulfur dioxide. Although NO_x removal was 9% higher, on average, with 3000 ppm sulfur dioxide; it is interesting to note that after two hours of scrubbing with 1500 ppm SO_2, the NO_x removal had increased to about 56% with no apparent peak. Figure 6 compares NO_x removals for feed gas mixtures with 0 ppm versus 75 ppm NO_2 and 0 ppm versus 150 ppm NO_2, respectively. Figure 6a shows the removals were virtually identical for the first 90 minutes of each test; but for the last 30 minutes, the run with no NO_2 showed removal about 4% higher than the test with 75 ppm NO_2. Figure 6b shows that the test with 150 ppm NO_2 had slightly improved NO_x removal for the 10 - 90 minute interval (about 3%); but, again as in Figure 6a, the run with no NO_2 had a removal about 3% higher for the last 30 minutes. The point to be stressed here is that NO_2 levels of 0-150 ppm make relatively little difference on total NO_x removal.

Finally, Figure 7 compares NO_x removals for the secondary additives gallic acid and pyrogallol under identical conditions. While NO_x removal with pyrogallol was slightly better in the 20 to 80 minute interval (3% higher on average), after 80 minutes their performances were comparable.

ACKNOWLEDGMENT

This work is supported by the U.S. Department of Energy, Assistant Secretary for Fossil Energy, under contract W-31-109-ENG-38, through the Pittsburgh Energy Technology Center (PETC). The authors wish to acknowledge the support provided by Perry Bergman and Charles Drummond of the PETC. In addition, the authors express their deep appreciation and gratitude to Sherman Smith for his invaluable contributions on the modifications and maintenance of the experimental apparatus as well as on the performance of the tests described herein.

REFERENCES

1. Harkness, J.B.L. and Doctor, R.D., Development of Combined Nitrogen Oxide/Sulfur Oxide Environmental-Control Technology, Argonne National Laboratory Report ANL/ECT-14, Argonne, Ill. (Aug. 1985) (also available through NTIS).

2. Harkness, J.B.L. and Doctor, R.D., Simultaneous NOx/SOx Removal In Aqueous Scrubber Chemistries, American Institute of Chemical Engineers National Meeting, New Orleans, La., April 1986.

3. Harkness, J.B.L., Doctor, R.D., and Wingender, R.J., U.S. Patent No. 4,612,175 (1986).

4. Theis, T.L. and Singer, P.C., Environ. Sci. Technol., 8, 569 (1974).

5. Loginova, L.F., Medyntsev, V.V., and Khomutov, B.I., Zh. Obsh. Khim., 42, 739 (1972).

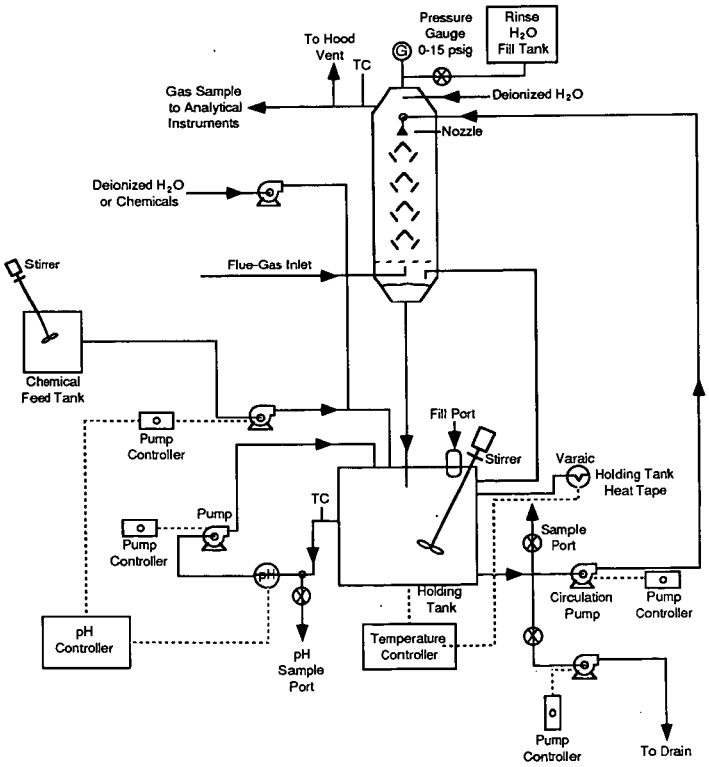

Figure 1. Flow diagram of laboratory aqueous scrubber system

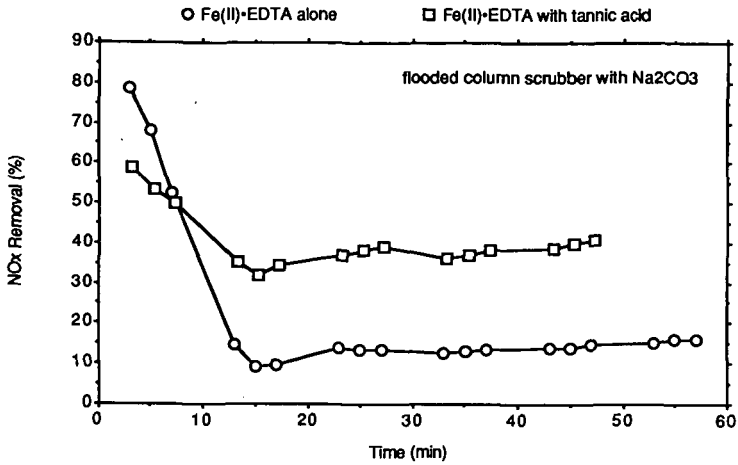

Figure 2. NOx removal for Fe(II)•EDTA alone vs Fe(II)•EDTA with tannic acid

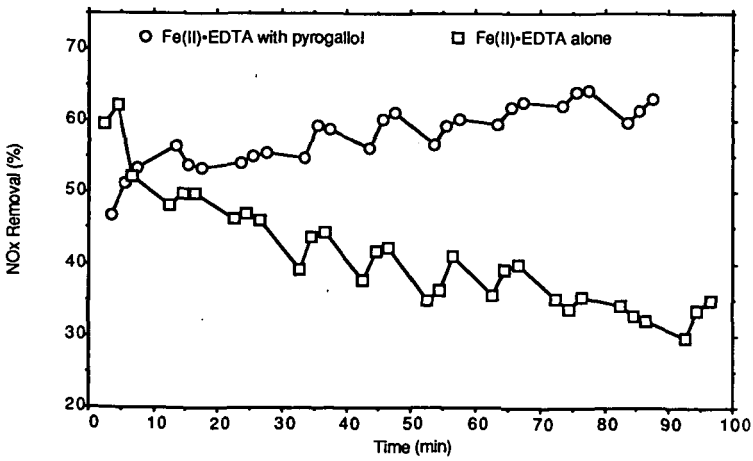

Figure 3. Comparison of NOx removals with or without the secondary additive pyrogallol

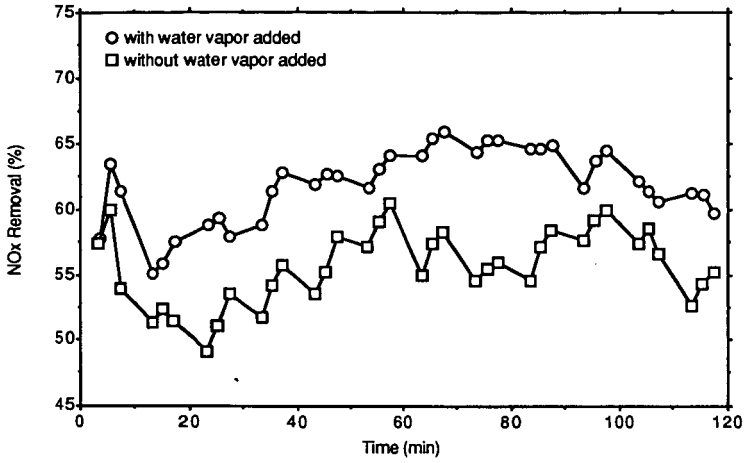

Figure 4. Comparison of NOx removal for Fe(II)•EDTA and pyrogallol with or without moisture

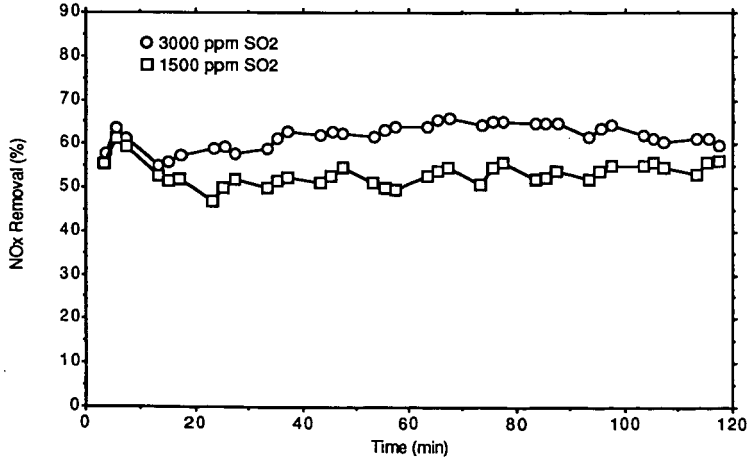

Figure 5. Comparison of NOx removal for Fe(II)•EDTA and pyrogallol with different SO2 levels

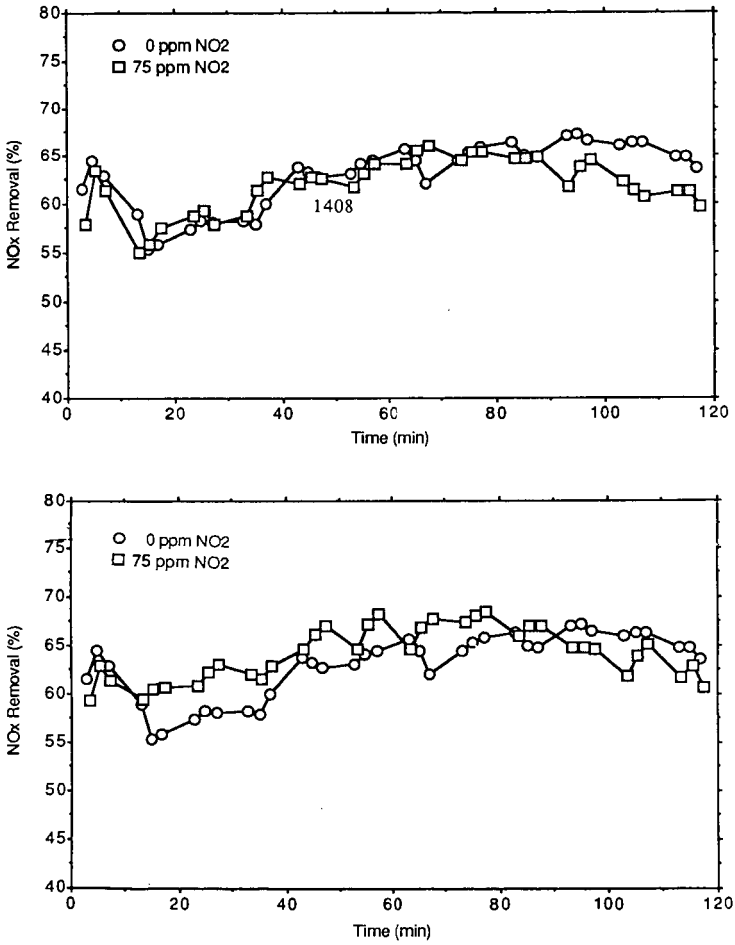

Figures 6a. and b. Comparison of NOx removals for three different NO2 levels

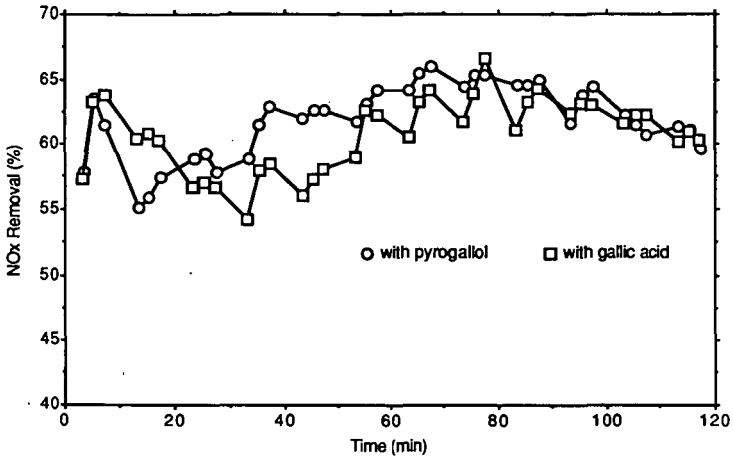

Figure 7. NOx removal comparison for secondary additives pyrogallol and gallic acid

IN-SITU X-RAY ABSORPTION STUDIES OF A CuO/Al_2O_3 SORBENT DURING SO_2 REMOVAL FROM COAL FLUE GASES

Yuqun Cao[1] and Pedro A. Montano[1,2]

1) Department of Physics, Brooklyn College of CUNY, Brooklyn, NY 11210
2) Department of Physics, West Virginia University, Morgantown, WV 26506

Keywords: X-ray absorption, copper oxide sorbent, coal cleaning

ABSTRACT

We have studied the local structure around the Cu ion in a CuO/Al_2O_3 sorbent using X-ray absorption (XAS) . This sorbent is commercially used for the removal of sulfur dioxide from flue gases. Pure oxides of CuO and Cu_2O were also studied as a function of temperature and in the presence of flue gases. The pure oxides were used as standards. The XANES and EXAFS spectra for the sorbent in nitrogen gas at the same temperatures did not show any significant changes. By contrast, we observed the appearance of a new near edge feature in the XANES spectra of the sorbent in the presence of flue gases. A strong peak appears at an energy characteristic of monovalent copper. The amount of Cu^+ reaches a maximum at about 200C and then decreases at higher temperatures. It is noted that the EXAFS spectra do not show any significant change in the nearest neighbors distance during reaction with the flue gases.

INTRODUCTION

The removal of sulfur dioxide from the coal flue gases is one of the major tasks in the electrical power industry. The deleterious effect of the pollutants resulting from the combustion of coal is a great concern in contemporary society. A common industrial practice is the use of a sorbent for the capture of the flue gas pollutants [1,2]. Copper oxide supported on alumina is commonly used as a commercial sorbent. This sorbent is used to remove SO_2 from the coal flue gases. Our major interest in this study is to investigate the Cu local environment in the presence of the flue gases. It is important to understand the undergoing processes in order to facilitate a most efficient use of the sorbent. The chemical environment at the transition metal site can be better studied using XAS , because of the penetration capabilities of X-ray in-situ studies become possible. X-ray Absorption Fine Structure (EXAFS) and X-ray Absorption Near Edge Structure (XANES) have been used in recent years to study local structures [3,4,5]. We report here a series of in situ EXAFS and XANES measurements of a CuO/Al_2O_3 sorbent and model compounds. We investigated the evolution of the structure at the Cu site as a function of temperature in the presence or absence of flue gases. In the following paragraphs we describe the methodology employed and summarize the results of our measurements.

EXPERIMENTAL

The measurements were carried out at beamline X-18B at the National Synchrotron Light Source. The beamline is equipped with a double crystal monochromator. The two crystal monochromator has the advantage that the exit beam path is fixed [6]. Two ion chambers are used to measure the incident and transmitted beam intensities. They were

filled with 30 KPa of Ar. A third ion chamber is placed at the end of the second ion chamber with a thin Cu foil to obtain accurate energy calibrations. The data collecting procedure is automatic and controlled by a PDP 11/24 computer. The energy range covered in these measurements was 200 eV below and 1200 eV above the Cu K-edge (E=8.979 KeV). The experimental setup is schematically shown in Fig. 1. The sample chamber has two windows sealed with thin Capton films to let the X-ray beam go through. The flue gas passes though the sorbent in the chamber. A Chromel/Alumel thermocouple is attached to the sample holder for temperature monitoring. A variable transformer and a temperature controller are used for setting up the desired sorbent temperature. The coal is burned in a separate combustion chamber. It has an inlet for air and an outlet for the flue gas. A thermocouple is used here to measure the combustion temperature. We burned a West Virginia Blacksville #2 coal. This coal sample has 3.4% by weight of total sulfur (organic and inorganic). The sorbent sample used in this measurement is CuO/Al_2O_3. The fresh sample is in the form of small sphere of 2mm in diameter. The sample is made into powder right before the measurement and put into the sample cell. The sample cell is a 0.5mm aluminum plate with a 5mmx15mm hole in the center. The powder is sandwiched between two thin aluminum foils. On the aluminum foils a matrix of tiny pinholes are punched to allow the flue gases to go through the sorbent. Careful measurements on the effects of the aluminum foils were conducted before we began collecting data. It is found out that the aluminum foil we used here does not have side effects to the XANES. However, it contains a very small amount of zinc impurities which can be seen on the EXAFS spectrum 680 eV above the Cu K-edge. In figure 2 we show the raw EXAFS data for the sorbent at room temperature. The measurements were performed from room temperature to 400C. The sample were measured in nitrogen gas flow and in the presence of flue gases. The measurements were repeated several times in order to evaluate their reproducibility. The same set of measurements were performed using model compounds, pure copper oxides (Cu_2O and CuO) and $CuSO_4$ and is shown in Fig. 3. The data was analyzed using the conventional methods described in the literatures [3,4].

RESULTS AND DISCUSSION

We choose the maximum of the 1st derivative of Cu metal foil at the K absorption edge as E_0. All the energy values are given with respect to this E_0. The most prominent energy peaks of the samples are given in Table 1. The XANES of the copper compounds consists two parts: (1) the discrete part below the continuum threshold, where the weak features are usually called pre-edge peaks, due to transitions to unoccupied bound antibonding orbitals and (2) the continuum part where the peaks are due to multiple-scattering of the photoelectron, which are sensitive to both coordination geometry and interatomic distances [4,7,8,9]. The K-edge XANES of Cu primarily represents electric dipole transitions (E1) from the 1s core level to final states with nonzero np components, which are governed by the electronic structure of the material [8,9,10]. Peak P corresponds to the 1s --> 3d transition and peak A corresponding to the 1s --> 4p transition. The absence of peak P for Cu metal and Cu_2O is attributed absence of vacancies in the 3d orbitals.

The XANES spectra and its 1st derivative for the sorbent at various temperatures before reaction with flue gases are shown in Fig. 4. There is no noticeable change when the temperature is raised to 300C from RT and then back to RT. Comparing the peak positions

with that of the CuO standard, the first major peak A shifts from 5.0 eV to 6.0 eV, the second one, B at 12.0 eV does no change and the third peak C at 17.5 eV does not exist. The EXAFS of the sorbent is significantly different from that of the CuO standard. We identify the first shell as due to Cu-O bond. The higher order shells (2nd, 3rd and 4th) are not clearly seen in the Fourier transform of the k3X(k) (Fig. 5). This makes us believe that the CuO in the sorbent is in highly dispersed form, very small clusters. The Cu-O interatomic distance is almost the same as that in bulk CuO. The magnitude of the Fourier transform of the 1st shell decreases with temperature (Fig. 6). This is understood to be related to thermal effects on the interatomic vibrations.

The most significant change happens when the sorbent is exposed to the flue gases (Fig. 7). A peak S at 1.5 eV characteristic of Cu^+ begins to appear. It reaches a maximum at about 200C. This feature disappears when the sample is returned to RT. For temperatures in excess of 300C there is a remnant small peak at about 1.5 eV. The remaining XANES features are the same as those before reaction with the flue gases. The new peak indicates that Cu^+ is formed during the SO_2 removal process. 200C seems to be an optimal temperature for the formation of this intermediate species. At this stage the reaction product is unlikely to be $CuSO_4$. The XANES spectrum of $CuSO_4$ is different from the sorbent. We suggest that the following process is taking place,

$$CuO + SO_2 == CuSO_3 \ (200\ C).$$

The SO_2 molecules are chemically absorbed by the CuO clusters. The Cu is in a mixed state of Cu^{++} and Cu^+. The EXAFS amplitudes also have a consistent change. It decreases with the increasing temperature until 200C then increases at higher temperature (Fig. 6). The magnitude also recovers at RT after the reaction. Table 2 shows the ratio of the oxygen coordination number surrounding Cu ion, $N_{CuO}/N_{Sorbent}$, and the deviation of the sorbent Debye-Waller factor from that of CuO. This gives us information on how the average oxygen coordination number around the Cu ion changes with temperature. The average oxygen coordination number for the sorbent becomes minimum at 200C. Our XANES measurements show strong evidence of mixed charge states (Cu^{++} and Cu^+).

CONCLUSIONS

We have measured XANES and EXAFS spectra of a commercial sorbent (CuO/Al_2O_3) used for the removal of SO_2 from coal flue gases. The studies shows that CuO in the sorbent is in the form of very small disordered clusters. The sorbent is thermally stable from RT to 400C in the nitrogen atmosphere. We observed a partial transformation of Cu^{++} to Cu^+ at 200C This happens only when the flue gases are present. The observed transformation is reversible if the temperature of the sorbent does not exceed 300C. Our result suggests that at 200C optimum conditions exist for the formation of this intermediate species.

ACKNOWLEDGMENT

We would like to express our appreciations to A. Bommannavar and M. Ramanathan for their help. This work was supported by the US DOE and Y. Cao acknowledge the financial support of the Division of Educational Program at Argonne National Laboratory .

REFERENCE

1. D.H. McCrea, A.J. Forney, J.G. Myers, J. Air Pollut. Control Assoc. 20, 819 (1970)

2. Sidney S. Pollack, William P. Chisholm Richard T. Obermyer, Sheila W. Hedges, Mohan Ramanathan, and Pedro A. Montano, I&EC Research, 27, 2276 (1988).

3. B.K. Teo, *EXAFS : Basic Principles and Data Analysis* (Springer, 1986).

4. *X-ray Absorption : Principles, Applications, Techniques of EXAFS, SEXAFS, and XANES.* edited by D.C. Konigsberger and R. Prinz, Chemical Analysis, Vol. 92 (1988).

5. R.B. Greegor, F.W. Lytle, E.C. Marques, E.M. Larson, A.J. Panson, and J. Stohr in *Electronic Materials and Processes*, edited by J.T. Hoggatt, W. Jensen, M. Kushner, and S. McCollough, 2nd international Sample Electronics Conference Series, Vol 2, P.179 (June 1988).

6. M. Ramanathan, PhD thesis, *X-ray Absorption Study of the Interaction of Coal Combustion Gases with Calcium Oxide*, 1988.

7. A. Bianconi, E. Fritsch, G. Calas, and J. Petiau, Phys. Rev. B32, P.4292 (1985).

8. L.S. Kau, D.J. Spira-Solomon, J.E. Penner-Hahn, K.O. Hodgson, and E.I. Solomon, J. Am. Chem. Soc. 109, 6433 (1989).

9. F.W. Lytle, R.B. Greegor, and A.J. Panson, Phys. Rev. B37, P.1550 (1988).

10. E.E. Alp, G.K. Shenoy, D.W. Capone II, L. Soderholm, H.B. Schuttler, J. Guo, D.E. Ellis, P.A. Montano, and M. Ramanathan, Phys. Rev. B35, P.7199 (1987).

Table 1 Characteristic Energies of the XANES (Unit is in eV)

	P	A	B	C	D
Cu	—	0.0	6.0	11.0	22.0
Cu_2O	—	1.5	6.0	—	—
CuO	-1.5	5.0	12.0	17.5	—
$CuSO_4$	-2.5	9.0	14.5	—	—
Sorbent	-3.5	6.0	12.0	—	—

Table1. Characteristic XANES energies for the samples in this experiment.

Table 2

	Temp	$N_{CuO}/N_{Sorbent}$	ΔDW (Å)
Sorbent Only	RT	0.62	0.058
	100C	0.59	0.060
	200C	0.68	0.062
	300C	0.68	0.067
	RT	0.62	0.058
Sorbent Flue Gas	RT	0.72	0.063
	100C	0.82	0.065
	200C	0.89	0.064
	300C	0.77	0.064
	RT	0.70	0.061

Table 2. The ratio of the average oxygen coordination number surrounding the Cu ion, $N_{CuO}/N_{Sorbent}$, and the deviation of the Debye-Waller factor from that of CuO, ΔDW, obtained by the ratio method of EXAFS.

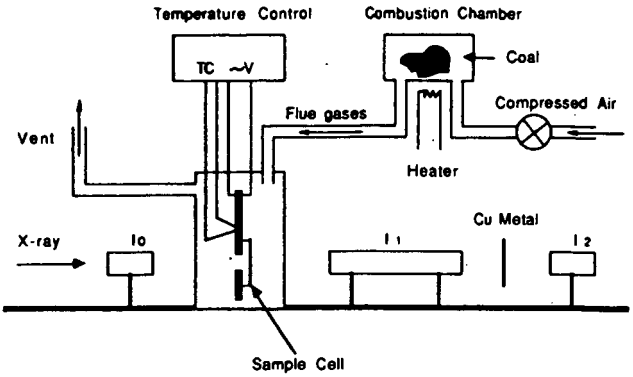

Fig. 1. Schematic drawing of the experimental setup inside the experiment hutch.

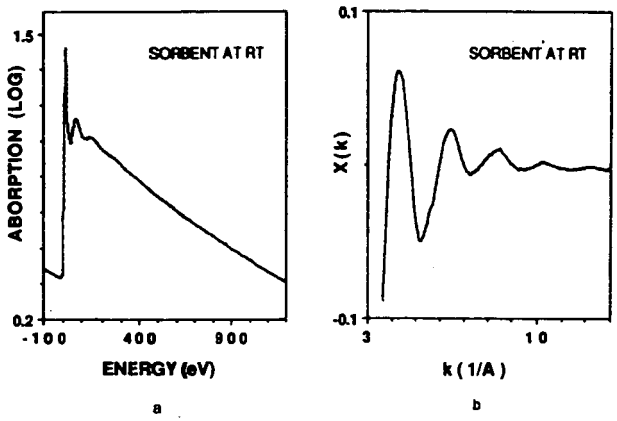

Fig. 2. a. EXAFS of the Sorbent at RT before the reaction.
b. X(k) after the EXAFS background subtraction and step height normalization.

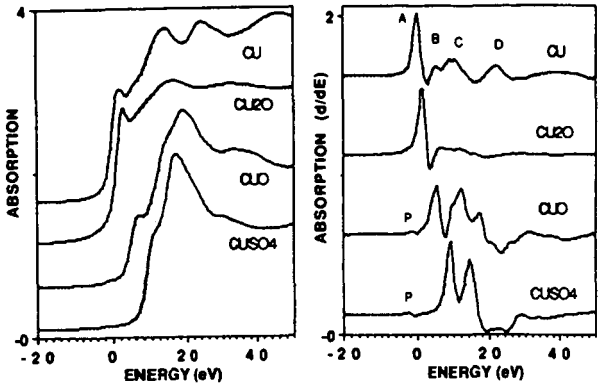

Fig. 3. XANES and 1st derivatives of pure Cu_2O, CuO and $CuSO_4$.

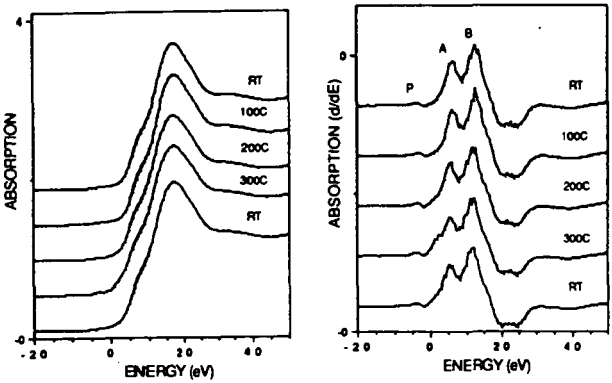

Fig. 4. XANES and 1st derivatives of the Sorbent at various temperatures under the N_2 environment.

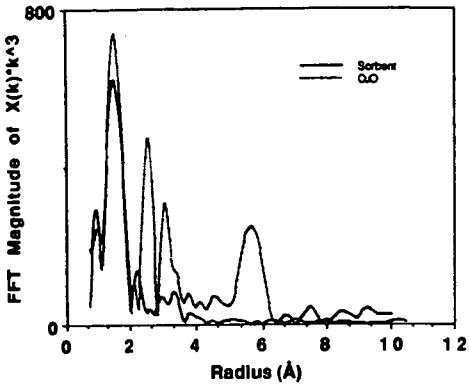

Fig. 5. Fourier transforms of the $k^3X(k)$ for the pure CuO and the sorbent at RT.

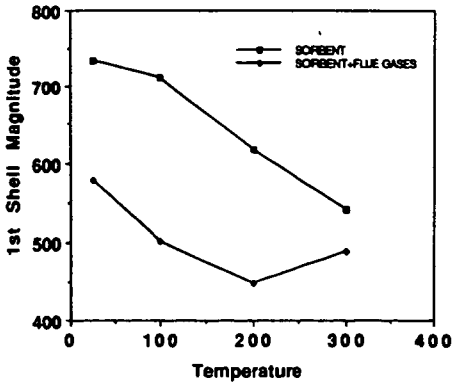

Fig. 6. Comparison of the 1st shell magnitude changes with the temperature for the sorbent with and without the flue gases.

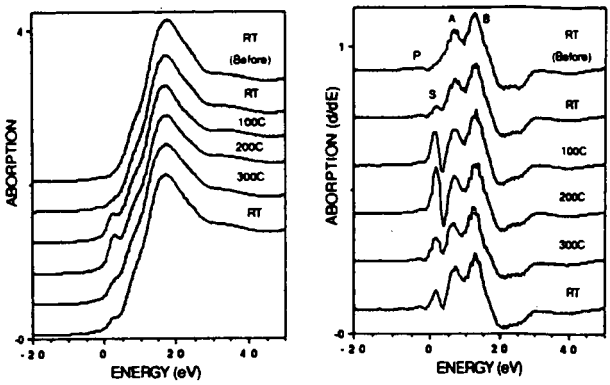

Fig. 7. XANES and 1st derivatives of the Sorbent at various temperatures in the presence of flue gases.

HIGH-SURFACE-AREA HYDRATED LIME FOR SO_2 CONTROL

M. Rostam-Abadi, D. L. Moran, Illinois State Geological Survey, Champaign, IL
V. P. Roman, R-C Environmental Services and Technologies, Irvine, CA
H. Yoon and J. A. Withum, Consolidation Coal Company, Library, PA

KEYWORDS: SO_2 removal, hydrated lime, dry sorbent injection

INTRODUCTION

For many site specific applications, dry sorbent injection technologies offer advantages over the wet flue gas desulfurization systems for controlling the emissions of SO_2 produced during combustion of high sulfur coal. These potential advantages include ease of retrofit, dry waste, and lower capital investment. The technologies that have been researched considerably in recent years include furnace sorbent injection (FSI), boiler economizer injection, and post furnace duct-injection/humidification (Coolside). The main factor which distinguishes the dry processes is that a calcium-based sorbent is injected into different locations within a pulverized coal boiler unit. In the FSI, limestone ($CaCO_3$) or hydrated lime ($Ca(OH)_2$) is injected into the upper furnace cavity where temperatures range from 1800-2200°F. The sorbent is rapidly calcined forming CaO which reacts with SO_2 to form $CaSO_4$. In the boiler economizer process, $Ca(OH)_2$ is injected in a location between the superheater and air preheater where the temperature is in the range of 800-1200°F.[1] Coolside desulfurization involves $Ca(OH)_2$ injection in the duct work downstream of the air preheater at about 300°F followed by flue gas humidification with a water spray.[2] SO_2 is removed by the entrained sorbent particles in the duct work and by the dense sorbent bed collected in the particulate removal system. Unlike the FSI where $CaSO_4$ is formed, under boiler economizer and Coolside conditions $CaSO_3$ is the major product.

Bench- and pilot-scale tests have shown that typical SO_2 capture efficiencies under FSI conditions are about 35 and 55% for $CaCO_3$ and commercial $Ca(OH)_2$, respectively,[3,4] and 30-50% with commercial $Ca(OH)_2$ under boiler economizer[5] and Coolside conditions[6] (all at Ca/S ratio of 2). In some Coolside process pilot tests, an additive such as sodium hydroxide or sodium carbonate has been injected with the humidification water resulting in SO_2 removal of about 70 to 80%.[6, 11] Because these SO_2 removal levels correspond to less than 50% of the theoretical saturation capacity for the sorbents, a major objective of research in the recent years has been to identify sorbent properties that result in enhanced SO_2 capture in order to reduce operating costs and the amount of waste products. In FSI studies, the superiority of $Ca(OH)_2$ over $CaCO_3$ has been attributed to the smaller mean particle size[7], higher surface area and porosity[7,8], larger pores[9] and plate-like grain structure[10] (vs. sphere-like) of the CaO derived from $Ca(OH)_2$ compared to that derived from $CaCO_3$. In boiler economizer and Coolside studies, improved SO_2 removal performance has also been reported for $Ca(OH)_2$ with high porosity, high surface area, and small particle size.[1,5,11]

This paper reviews recent work comparing the SO_2 removal performance of two commercial hydrated limes and a high-surface-area (HSA) hydrated lime under FSI, boiler economizer, and Coolside conditions. The properties of the sorbents and a discussion of the results are presented.

EXPERIMENTAL

Test Sorbents

The sorbents tested included a HSA hydrate and two commercial hydrated limes designated as A and B. The HSA hydrate and commercial hydrate A were made from the same lime. The HSA hydrated lime was prepared by a proprietary hydration process developed at the

Illinois State Geological Survey. Three hundred pounds of the sorbent was prepared using a bench-scale hydrator capable of producing seven pounds of products per batch. The HSA hydrate was not subjected to air classification or milling prior to being tested for sulfur removal efficiency.

Chemical compositions of sorbents were determined by X-ray fluorescence. Surface areas were obtained by N_2-adsorption in conjunction with the one point BET method. Pore volumes and pore size distributions (pores smaller than 0.25 micrometers) were determined by nitrogen porosimetry. Sorbent particle size analyses were performed on a Micromeritics sedigraph 5100 using Micromeritics dispersant. Hydrate A and the HSA hydrate were examined by X-ray diffraction (XRD) and the data were used for determination of crystallite size using the Scherrer equation.[12]

Pilot-Scale SO_2 Removal Tests

FSI tests - These experiments were performed in the Innovative Furnace Reactor (IFR) located at the U. S. Environmental Protection Agency, Research Triangle Park, North Carolina.[13] FSI tests were performed burning four Illinois coals from the Illinois Basin Coal (IBC) Sample Program. The analyses of the coals identified as IBC-101, -102, -106 and -109 are presented in table 1.

Testing in the IFR consisted of determining the SO_2 concentration in the flue gas during sorbent injection while burning each of the coals at feed rates sufficient to yield a thermal rating of approximately 14 kW. The tests were conducted with HSA hydrate and hydrate A at Ca/S ratios of approximately 1:1 and 2:1 and at a temperature of 2192°F. The details of test procedures and a description of the IFR are given elsewhere.[13]

Boiler economizer tests - The Research-Cottrell Environmental Services and Technologies (R-C EST) 150 kw pilot-scale furnace located in Irvine, California was used for boiler economizer tests. The experiments were conducted at a nominal input rate of 75 kw. A detailed description of the unit is given elsewhere.[5] The furnace is fired on natural gas and SO_2 is added at the proper concentration. A time-temperature history representative of a utility boiler backpass is generated by using the upper section of the furnace to reduce the flue gas temperature to approximately 1300°F. The gas temperature is then decreased from 1300 to 800°F in approximately 0.5 seconds in the section of the furnace where convective tube banks are located. The flue gas is continuously analyzed for oxygen, sulfur dioxide and carbon dioxide using the R-C EST continuous emissions monitor (CEM).

The test program involved testing HSA hydrate and hydrate A at injection temperatures of 900, 1000 and 1100°F, a Ca/S ratio of 2, and SO_2 concentrations of 500 and 3000 ppm. The flue gas composition was typically 4.0% O_2, 9.8% CO_2, and 50 ppm CO.

Coolside tests - These tests were conducted in a 100 kW pilot unit located in the Research and Development Department of the Consolidation Coal Company, Library, Pennsylvania. The Coolside pilot plant is described elsewhere.[2] Briefly, the exhaust from a natural gas burner is mixed with recycle gas, into which CO_2, SO_2, N_2, steam and fly ash are injected to produce the simulated flue gas from a coal-fired boiler. The humidifier is an 8.3-inch ID down-flow duct installed with a water-spray nozzle, and is 20 feet long from the nozzle location to the exit. The gas exiting the humidifier enters a baghouse which separates the solids from the gas. The gas is further cooled and dehumidified in a condenser, and the process fan recycles most of the flue gas for reuse. SO_2 removal is calculated from measurements of SO_2 and O_2 analyzers at the humidifier inlet and exit, and the baghouse exit.

HSA hydrated lime and hydrate B were tested at Ca/S ratios of 0.5 to 2.0 and 25°F approach to adiabatic saturation temperature. The conditions selected represent standard pilot plant tests for evaluating a new sorbent to provide SO_2 removal data at typical Coolside in-duct injection operating conditions. The common conditions were 300°F inlet flue gas temperature, 1500 ppm inlet SO_2 content (dry basis), and 125°F adiabatic saturation temperature. The flue gas flow rate was set at 175 scfm, which provided a 2.0 sec humidifier residence time.

RESULTS AND DISCUSSION

Test Sorbents

The chemical and physical properties of hydrates A and B, the HSA hydrate and lime A (from which hydrate A and the HSA hydrate were made) are presented in table 2. In the FSI and boiler economizer systems, the HSA hydrated lime was tested against the hydrate A. However, in the Coolside tests, HSA hydrate was tested against hydrate B, since this material has been shown to be the best-performing commercial sorbent under Coolside conditions.

Chemical analyses of hydrated limes indicate that the sorbents contained over 96 wt% CaO after ashing. The mass mean diameters and surface areas of the HSA hydrated limes varied between 1.6 and 2.7 micrometers and 35 to 44 m^2/g (except for one batch which was 31 m^2/g), respectively, depending on the hydration batch. These samples, however, had surface areas well above the 20-23 m^2/g surface areas typical for commercial hydrates. The pore volume of the HSA hydrate was 0.35 cm^3/g compared to only 0.08 cm^3/g for its commercial counterpart. The XRD results showed that the HSA hydrate had smaller $Ca(OH)_2$ grain size and lower crystallinities when compared to commercial material.

Pilot-Scale SO_2 Removal Tests

FSI tests - The results for FSI tests are presented in table 3. The average baseline SO_2 concentrations under the test conditions were 3140 ppm for IBC-101, 2410 ppm for IBC-102, 2890 ppm for IBC-106 and 1000 ppm for IBC-109. The trend in the SO_2 concentration is consistent with the total sulfur content of the coals reported in table 1. Figure 1 shows the estimated SO_2 removal percentages at Ca/S ratio of 2. The values were calculated by extrapolating linearly from the mean removals at both Ca/S ratios run for each coal/sorbent combination. For each coal tested, HSA hydrate removed more SO_2 than its commercial counterpart. SO_2 removal observed with the HSA hydrate ranged from 72 to 77% for the coals tested (excluding IBC-102) compared to 55 to 66% for hydrate A.

The SO_2 capture levels for the IBC-102 coal were only 57 and 42% with the HSA and commercial hydrates, respectively. The substantial decrease in SO_2 capture by the sorbents for this coal could be related to its higher pyritic sulfur content than for the other coals tested. The pyritic/organic sulfur ratio for IBC-102 was 2.3:1 compared to values less than 1:1 for the other coals. One explanation that could be offered is that a major fraction of the organic sulfur in coals is released as H_2S in the initial stages of the combustion and is rapidly captured by the fresh sorbent. The SO_2 released by the oxidation of the pyrite, which follows the pyrolysis stage, then reacts with the partially utilized sorbent at a much slower rate compared to the H_2S reaction.[14] Therefore, sulfur capture by the sorbent is lowered when coal with a high concentration of pyritic sulfur is burned. This suggests that FSI is most beneficial for coals that are high in organic sulfur which cannot be removed by physical coal cleaning.

The enhanced performance of the HSA hydrate could be related to its smaller particle size and higher initial surface area. Laboratory tests conducted under FSI conditions at 2012°F with CaO derived from $Ca(OH)_2$ have revealed that the CaO conversion to $CaSO_4$ is inversely related to particle diameter to the 0.2 to 0.35 power[7]. In a recent study, however, the initial sulfation rate of CaO (7 to 100 micrometers) derived from several limestones and dolomites varied roughly inversely with the particle size, indicating pore diffusion was the rate controlling step under these test conditions (1650°F).[9] Based on the data obtained in this work, SO_2 capture was inversely related to particle size to the 0.44 power (for capture values estimated at Ca/S ratios of 1 and 2).

The higher SO_2 capture of the HSA hydrate can also be attributed in part to its favorable pore structure. Pore volume analyses of raw sorbents, shown in figure 2, indicate the volume of pores between 0.01 and 0.1 micrometers (10 and 100 nm) is substantially higher for the HSA hydrate than for hydrate A. Pore volumes of hydrated limes are expected to correlate with pore volumes of the corresponding calcines. Due to the increase in molar volumes when converting from CaO to $CaSO_4$ (16.9 vs 46.0 cm^3/mole), pore plugging is known to limit the sulfation reaction. Therefore, sorbents with a high volume of larger pores are expected to capture more SO_2.

Boiler economizer tests - The results of these experiments are shown in figure 3. The HSA hydrate showed significantly greater SO_2 removals than hydrate A at all test conditions. The SO_2 reduction achieved with the HSA hydrate at 3000 ppm SO_2 and Ca/S of 2 was 58% at 900°F, 57% at 1000°F and 52% at 1100°F compared to only 32%, 30% and 28% for the commercial hydrate. At 500 ppm SO_2 and Ca/S ratio of 2, the average SO_2 removals for hydrate A and the HSA hydrate were 6.1 and 17%, respectively (an increase of 180%). The SO_2 removals observed for the HSA hydrate were also higher than for other commercial hydrates examined under similar test conditions.[5]

The superior performance of the HSA hydrate observed in this study is attributed, in part, to its high surface area and small particle size. The role of surface area and particle size can be explained in terms of two competing reactions under boiler economizer conditions,

$$Ca(OH)_2 + SO_2 \text{ ----> } CaSO_3 + H_2O \qquad (1)$$
$$Ca(OH)_2 + CO_2 \text{ ----> } CaCO_3 + H_2O \qquad (2)$$

The intrinsic rates (which are related to pore surface area of sorbent) of reactions (1) and (2) are very fast even at 900°F. However, because of the low concentration of SO_2 in the flue gas, reaction (1) is controlled by bulk diffusion of SO_2 for particles larger than 5 micrometers[1,5] (diffusion rate for spherical particles is inversely related to particle size to the second power), whereas reaction (2) is controlled by intrinsic rate. As a result, the relative rates for the reaction of $CaSO_3$ and $CaCO_3$ depend both on pore surface area and particle size of the sorbent. Increasing pore surface area would favor the carbonation reaction if particle diameter is held constant. Decreasing particle size and holding pore surface area constant would favor desulfurization reaction. Therefore, a sorbent with high pore surface area and small particle size would be expected to show high SO_2 removal efficiency under boiler economizer conditions. The average increase in sulfur capture observed for the two sorbents at 3000 ppm SO_2 and Ca/S ratio of 2 was 83%, which corresponds approximately to the difference in surface areas. However, at 500 ppm SO_2 and Ca/S ratio of 2, SO_2 captures were inversely related to particle diameter to the second power, indicating bulk diffusion limitation under these test conditions.

Coolside tests - Three different batches of HSA hydrate were examined in the Coolside pilot unit. The surface areas of the samples tested at Ca/S ratios of 0.54, 1.1 and

2.1 were 31, 34 and 39 m^2/g, respectively. Figure 4 shows the effect of the Ca/S molar ratio on SO_2 removal at 25°F approach to saturation. The value shown for hydrate B at 2.1 Ca/S was obtained in this study. The removals shown for the same hydrate at 1.0 and 1.5 Ca/S are from Reference 2. The HSA hydrated lime showed higher SO_2 removals than the best-performing commercial hydrate. With the HSA hydrate at Ca/S ratios of 0.54, 1.1 and 2.1, the SO_2 removals were 15, 25 and 46% in the humidifier and 18, 33 and 56% across the entire system (humidifier + baghouse). Comparison of the data at Ca/S of 2.1 indicate that the HSA sorbent captured 35% more SO_2 than hydrate B in the humidifier and 15% more across the entire system. The maximum percent calcium utilizations for the HSA hydrate were 33.3, 31.7 and 26.3 as Ca/S ratio increased from 0.54 to 2.1. For hydrate B a 23.2% utilization was observed at Ca/S ratio of 2.1.

Figure 4 shows a linear SO_2 removal behavior at the Ca/S ratios tested. Normally, as is exhibited by hydrate B, a plot of SO_2 removal vs Ca/S ratio is curved because the effect diminishes as the Ca/S ratio increases. The straight-line behavior for the HSA hydrate may be due to the sample surface area variations mentioned above.

The Coolside data suggest that a major fraction of the SO_2 capture occurred during the two second residence time in the duct work. The higher SO_2 capture achieved by the HSA hydrate in the humidifier section and across the entire system suggests higher overall activity of the sorbent relative to hydrate B.

SUMMARY AND CONCLUSIONS

The HSA hydrated lime prepared by a proprietary process had considerably higher surface area and porosity, smaller particle size, and finer $Ca(OH)_2$ grain size than typical commercial hydrated lime. The results of the pilot-scale testing under FSI, boiler economizer, and Coolside conditions indicate that the HSA hydrated lime removed, depending on the test system, 15-180% more SO_2 than the commercial hydrated limes tested under similar conditions. The superior performance of the HSA hydrate was attributed to its favorable physical properties.

ACKNOWLEDGEMENTS

This work was funded in part by grants from the Illinois Coal Development Board through the Center for Research on Sulfur in Coal. Dr. Brian K. Gullett of the U. S. Environmental Protection Agency provided the FSI data.

REFERENCES

1. Bortz, S.J.; Roman, V.; Offen, G. R. First Combined FGD and Dry SO_2 Control Symposium, St. Louis, MO, Oct. 25-28, 1988, Paper no. 10-7.

2. Yoon, H.; Stouffer, M. R.; Rosenhoover, W.A.; Withum, J.A.,; Burke, F.P. Eng. Prog. 1988, 7(1), 82-89.

3. Beittel, R.J.; Gooch, J.; Dismukes E.; Muzio, L. Proc. Symp. on Dry SO_2 and Simul. SO_2/NO_x Control Technol. 1985, 1, 16, EPA-600/0-85-020a (NTIS PB85-232353).

4. Snow, G.C.; Lorrain, J.M.; Rakes, S.L. Proc. Joint Symp. on Dry SO_2 and Simul. SO_2/NO_x Control Technol. 1986, 1, 6-1, EPA-600/9-86-029a (NTIS PB87-120465).

5. Bortz, S.J.; Roman, V.P.; Yang, C.J.; Offen, G.R. Proc. Joint Symp. on Dry SO_2 and Simul. SO_2/NO_x Control Technol. 1986, 2, 31.

6. Withum, J.A.; Lancet, M.S.; Yoon, H. Paper presented at the AIChE 1989 Spring Nat. Mtg, Houston, Texas. 1989

7. Gullett, B.K.; Bruce, K.R. First Combined FGD and Dry SO_2 Control Symposium, St. Louis, MO, Oct 25-28 1988, 6-7, EPA-600/9-89-0369(NTIS PB89-172159).

8. Newton, G.H.; Chen, S.L.; Kramlich, J.C. AIChE J. 1989, 35(6), 988-994.

9. Stouffer, M.R.; Yoon, H. AIChE J. 1989, 35(8), 1253-1262.

10. Bruce, K. R.; Gullett, B.K.; Beach, L.O. AIChE J. 1989, 35(1), 37-41.

11. Yoon, H.; Stouffer, M.R.; Rosenhoover, W.A.; Statnick, R.M. Proc. Second Pittsburgh Coal Conference, Pittsburgh, PA, Sept 16-18 1985, 223-242.

12. Klug, H.P.; Alexander, L.E. "X-ray Diffraction Procedures for Polycrystalline and Amorphous Materials," John Wiley and Sons, New York 1974, 657-659.

13. Gullett, B.K.; Briden, F.E. U. S. Environmental Protection Agency, AEERL, Research Triangle Park, NC, 1989, 62 pages, EPA-600/2-89-065.

14. Borgwardt, R.H.; Roache, N.F.; Bruce, K.R. Environ. Prog. 1984 3, 129.

Table 1. Average analyses of the coals (moisture free values).[1,2]

	IBC-101	IBC-102	IBC-106	IBC-109
Moisture	14.8	14.3	10.5	9.2
Vol Matter	40.7	39.9	39.7	35.0
Fixed Carbon	48.8	53.3	51.3	56.8
H-T Ash	10.5	6.8	9.0	8.2
Carbon	69.30	74.10	71.86	75.05
Hydrogen	5.18	5.32	4.93	4.89
Nitrogen	1.31	1.50	1.67	1.74
Oxygen	9.31	8.92	8.76	8.53
Sulfatic Sulfur	0.05	0.06	0.01	0.00
Pyritic Sulfur	1.22	2.26	1.86	0.50
Organic Sulfur	3.08	0.98	1.90	0.63
Py/Or Ratio	0.40	2.30	0.98	0.80
Total Sulfur	4.36	3.30	3.77	1.13
Total Chlorine	0.12	0.02	0.02	0.42
Btu/lb	12659	13628	13226	13324

[1] All values in wt% except where noted
[2] Analyses were performed by LECO analyzers and are different than those obtained by the ASTM methods and reported in reference 13.

Table 2. Properties of test sorbents

Sorbent	Ash Analyses, (wt%) CaO	MgO	Mean diameter (micrometers)	BET surface area (m^2/g)	Pore volume[1] (cm^3/g)	Crystallite size (angstroms)
Lime A	96.1	0.52	---	1.6	---	---
Hydrate A	99.0	0.57	3.5	20.6	0.08	220
HSA hydrate	96.5	1.20	2.0[2]	38.0[3]	0.35	150
Hydrate B	97.7	0.55	3.1	23.2	---	---

[1] Pores smaller than 0.25 micrometers.
[2] The value is an average. The range was 1.6 to 2.7 micrometers.
[3] The value is an average. The range was 35 to 44 m^2/g.

Table 3. Furnace Sorbent Injection (FSI) data.[1]

Coal (%)	Sorbents Ca/S	Baseline SO_2	Removal (ppm)	Ratio
IBC-101	Hydrate A	3161	28.8	0.85
	Hydrate A	3161	56.6	1.70
	HSA hydrate	3120	36.6	0.79
	HSA hydrate	3120	61.4	1.58
IBC-102	Hydrate A	2541	25.6	0.88
	Hydrate A	2541	42.1	1.75
	HSA hydrate	2288	32.8	0.85
	HSA hydrate	2288	50.3	1.70
IBC-106	Hydrate A	2918	36.5	1.10
	Hydrate A	2918	63.7	2.21
	HSA hydrate	2862	59.8	1.07
	HSA hydrate	2862	78.7	2.14
IBC-109	Hydrate A	1032	40.8	0.92
	Hydrate A	1032	52.7	1.84
	HSA hydrate	960	47.1	1.16
	HSA hydrate	960	80.6	2.32

[1] Data from reference 13.

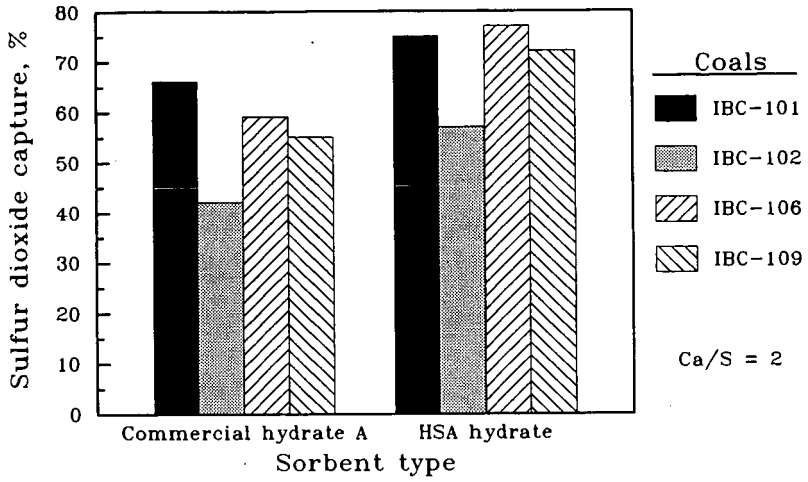

Figure 1. Furnace sorbent injection pilot-plant data

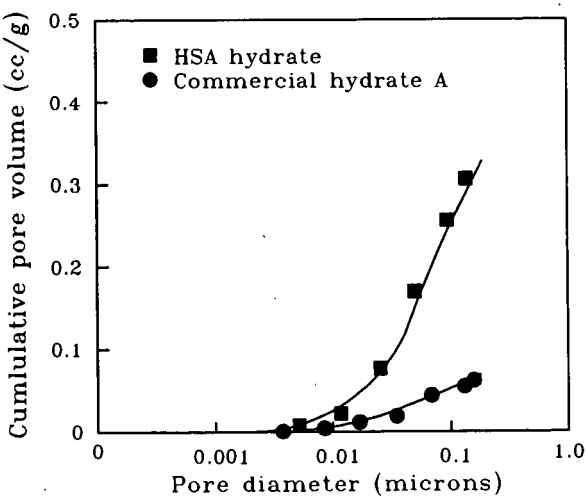

Figure 2. Pore size distribution data

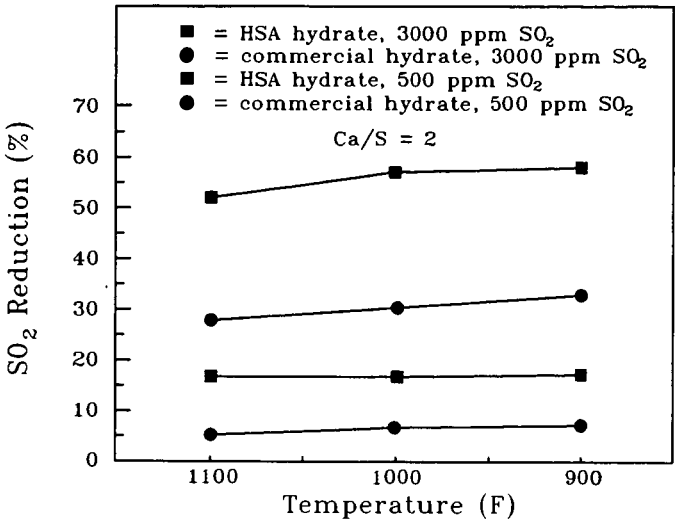

Figure 3. Boiler economizer pilot-plant data

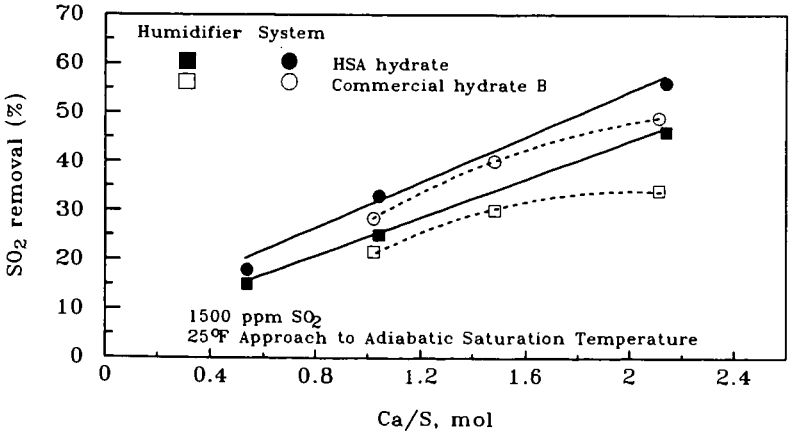

Figure 4. Coolside pilot-plant data

CHEMICAL REGENERATION OF FE(II)-EDTA IN WET SCRUBBERS

Y. Joseph Lee and Lewis B. Benson
Dravo Lime Company, Pittsburgh, PA 15225

Key Words: Fe(II)-EDTA, chemical reduction, NO_x removal

INTRODUCTION:

Transition metal chelates have attracted the attention of researchers for the past two decades primarily because of the effectiveness of Fe(II)-EDTA in removing nitric oxide (NO) from the flue gas and its likely compatibility with wet scrubbers. However, Fe(II)-EDTA tends to get oxidized in the scrubbers and Fe(III)-EDTA is not reactive for NO removals. Several reducing agents have been proposed. The purpose of this paper is to evaluate these reducing agents including sulfite or bisulfite, the most logical ones in wet scrubbers.

EXPERIMENTS:

Jacketed reactors were used to conduct experiments at desired temperatures. 1, 10-phenanthroline method was used to determine ferrous ions (Walker and Perry, 1989). Total iron was measured by atomic absorption. Ethylene diamine tetraacetic acid (10% excess), ferrous ammonium sulfate, and ferric ammonium sulfate were used to prepare Fe-EDTA. Sodium carbonate powder and dilute sulfuric acid were used to adjust pH.

RESULTS AND DISCUSSIONS:

Several reducing agents were tested in batch reactors for Fe(II)-EDTA regeneration. Table 1 lists the related redox potentials. As indicated by the redox potentials, several common metals such as Fe, Zn and Al, areexpected to be able to reduce Fe(III)-EDTA to Fe(II)-EDTA. Iron powder, aluminum powder and zinc dust were used to reduce 10 mM Fe(III)-EDTA. The results are summarized in Figure 1. Iron was capable of reducing Fe(III)-EDTA to Fe(II)-EDTA, which was tested and abandoned because of its poor utilization and ferric hydroxide precipitation problem (Staub, 1988). Compared to zinc or alumina, the reducing rate of Fe(III)-EDTA by iron powder was substantially lower probably due to the adverse effect of the magnetic stirring bar on iron powder distribution. Alumina was not reactive at pH 5.5. However, when the pH was raised to 9.0 its reactivity towards Fe(III)-EDTA reduction was substantially higher. Obviously, the higher pH helped dissolve the inert Al_2O_3 film on the surface of alumina. Zinc is much more effective in reducing Fe(III)-EDTA primarily because of the unit surface area of the zinc we used was substantially higher than those of iron and alumina. Although zinc and alumina are effective and efficient in reducing Fe(III)-EDTA to Fe(II)-EDTA, they are probably not adequate for Fe(II)-EDTA regeneration because the stability constants of Zn-EDTA and Al-EDTA are larger than that of Fe(II)-EDTA. If Zn-EDTA and Al-EDTA are reactive towards NO removal, they should be used in the first place because Zn-EDTA and Al-EDTA cannot be oxidized.

Hydrogen sulfide has been proposed to reduce Fe(III)-EDTA to Fe(II)-EDTA. This approach was not generally accepted because of the toxicity and the odor problem of H_2S. However, H_2S can be converted to CaS or Na_2S quite easily by reacting with $Ca(OH)_2$ and NaOH respectively. There are two possible reactions in scrubbing liquor when sulfide is added.

$$2S^{-2} + 4HSO3^- \quad 3S_2O_3^{-2} + 2OH^- + H_2O \qquad (1)$$
$$S^{-2} + 2Fe^{+3} \quad S + 2Fe^{+2} \qquad (2)$$
$$S + HSO3^- \quad H^+ + S_2O_3^{-2} \qquad (3)$$

Sulfite/bisulfite competes with ferric for sulfide. The results indicated that 5 mM sulfide converted 6 mM Fe(III)-EDTA to Fe(II)-EDTA instantaneously with or without the presence of 0.1 M sulfite. In other words, the utilization of sulfide in reducing Fe(III)-EDTA was around 60%. There might be some unidentified reactions that reduce the utilization of sulfide as a reducing agent for Fe(II)-EDTA regeneration. As indicated by equations 1-3, thiosulfate will be accumulated when sulfide is used to reduce Fe(III)-EDTA. Thiosulfate was recognized as an effective free radical scavenger and was applied to wet FGD to inhibit sulfite oxidation successfully (Owens and Rochelle, 1985). Still, the effect of accumulated thiosulfate on the performance of wet scrubbers needs further study.

Theoretically, alkaline hydrolysis of sulfur (Lee et al., 1990)

$$S_8 + 12OH^- \quad 4S^{-2} + 2S_2O_3^{-2} + 6H_2O \qquad (4)$$

can achieve a 50% conversion to sulfide as indicated by reaction 4. When the reaction is not complete, a polysulfide mixture instead of sulfide is the product. To investigate the possibility of using the sulfide/polysulfide product as the reducing agent for Fe(II)-EDTA regeneration, sodium tetrasulfide (Na_2S_4) was used to reduce Fe(III)-EDTA. The results indicated that the sulfide sulfur of the tetrasulfide was as good as sulfide in terms of reducing Fe(III)-EDTA to Fe(II)-EDTA. Unsurprisingly, the elemental sulfur of tetrasulfide did nothing except react with sulfite/bisulfite to form thiosulfate. Because alkaline hydrolysis of sulfur (reaction 4) is an inexpensive source of reducing agent, effects of accumulated thiosulfate on the performance of scrubbers deserve further investigation.

Obviously, the most ideal reducing agent for Fe(II)-EDTA regeneration in wet scrubbing system is sulfite/bisulfite. Unfortunately, the reaction rate at scrubber operating temperature (~50°C) is too slow to be practical. It is well known that the rate can be accelerated by raising the temperature, however, the effects of pH on the kinetics were reported inconsistently. Sada et al. (1984) judged that Fe(III)-EDTA reduction by sulfite/bisulfite should be enhanced by raising pH probably based on Le Chatelier principle and the following reaction.

$$Fe(III)\text{-}EDTA + HSO_3^- \quad Fe(II)\text{-}EDTA + 1/2S_2O_6^{-2} + H^+ \qquad (5)$$

Sada et al. (1988) reported later that reaction 5 was first order in both Fe(III)-EDTA and $HSO3^-$. In other words, Fe(III)-EDTA reduction by sulfite/bisulfite was supposed to be favored by lowering the pH of the

solution. It is contradictory to our result (Figure 2); and our result is consistent with data of Walker et al. (1988). Furthermore, Weisweiler et al. (1986) showed that NO removal was enhanced by raising pH in an ejector type 16-liter gas-liquid contactor. The mechanism is not clear yet, but our preliminary data (not shown) indicated that both Fe(II)-EDTA and dithionate suppressed the forward reaction of reaction 5. Furthermore the pH may significantly affect the activity of Fe(II)-EDTA and the stability of dithionate.

Since the regeneration of Fe(II)-EDTA by sulfite/bisulfite is not good enough to maintain high NO_x removal, the search for efficient and affordable additives or other reducing agents has been in progress. Sodium thiosulfate was tested. It itself did not show any capability for Fe(II)-EDTA regeneration. However, in the presence of sulfite/bisulfite (0.05 M S(IV)), at pH 7, 10 mM thiosulfate tripled the initial rate of Fe(II)-EDTA (10 mM) reduction. However, a couple hours later, the cumulative conversion of ferric to ferrous EDTA was not affected by the addition of thiosulfate.

Several organic "reducing agents" were also tested for the reduction of Fe(III)-EDTA to Fe(II)-EDTA. Most of these organic compounds were not satisfactory. For example, methanol can be oxidized to formaldehyde, which can then be oxidized to formic acid, and then decomposed to carbon dioxide. Based on standard redox potentials, one would predict that Fe(III)-EDTA could be reduced to Fe(II)-EDTA by each oxidation reaction mentioned above. Unfortunately, neither methanol, formaldehyde or formic acid showed any reducing capability. Both tartaric acid and maleic acid are apt to be oxidized in the air. Oxalic acid, when decomposed to carbon dioxide, was predicted to be able to reduce Fe(III)-EDTA. Unfortunately, none of these three organic acids gave positive results. However, some of the aforementioned organic compounds may act as antioxidants which will prolong the lifetime of Fe(II)-EDTA by sacrificing themselves. Maleic acid is of particular interest because it is available as waste products and it was reported to be easily oxidized under FGD conditions (Lee, 1986).

One of the most interesting organic reducing agents we studied so far is ascorbic acid or vitamin C. It was reported to be a good reducing agent for Fe(II)-EDTA regeneration, in the presence of dithionite (Holter et al., 1987). We found that ascorbic acid was a very good reducing agent even in the absence of dithionite. Furthermore, 1 molecule of ascorbic acid can reduce 10 molecule of Fe(III)-EDTA in a couple hours (figure 3). Also tested was the D-form or the optical isomer of ascorbic acid. The D-isomer demonstrated similar effect on Fe(III)-EDTA reduction as one would expect. In other words, the racemic mixture, which should be substantially cheaper than vitamin C, would be as good as L-ascorbic acid in terms of Fe(II)-EDTA regeneration. The mechanism and the products of this reaction are not clear to the authors yet.

ACKNOWLEDGMENT

The Authors would like to thank Mr. Jeff Henk, Ms. Pat Kerr and Mr. Jerry Hoffman for their help in performing the experiments, typing the paper and preparing the figures, respectively.

REFERENCE

Holter, H. et al., "Process for Stripping Nitrogen Oxides and Sulfur Oxides as Well as Optionally Other Noxious Elements of Flue Gas from Combustion Plants," United States Patent 4,670,234 (1987).

Lee, Y., L. Benson, and R. O'Hara, "Production and Application of Thiosulfate in Lime-Based Wet FGD," ACS Annual Meeting, Washington, D.C. (1990).

Lee, Y. and G. Rochelle, "Oxidative Degradation of Organic Acids Conjugated with Sulfite Oxidation in Flue Gas Desulfurization: Products, Kinetics, and Mechanism," Environ. Technol. 21 (3) 266-272 (1987).

Walker, R. and H. Pennline, "Optimization of a Flue Gas SO_2/NO_x Cleanup Process Utilizing Electrodialysis," AIChE 1988 Summer Meeting, Denver, Colorado, (1988).

Weisweiler, W., B. Retzlaff, and L. Raible, "Simultaneous Absorption of Sulfur Dioxide and Nitrogen Monoxide in Aqueous Solutions of Iron Chelate Complexes," Int. Chem. Eng. 26 (4), 574-581 (1986).

TABLE 1
RELATED STANDARD REDUCTION POTENTIALS FOR Fe(II)-EDTA REGENERATION

Reduction Reaction	Eo
$Fe(III)\text{-}(Phenanthroline)_3^{+3} + e^- \rightarrow Fe(II)\text{-}(Ph)_3^{+2}$	1.14
$Fe^{+3} + e^- \longrightarrow Fe^{+2}$	0.77
$S_2O_6^{-2} + 4H^+ + 2e^- \longrightarrow 2H_2SO_3$	0.6
$S_4O_6^{-2} + e^- \longrightarrow 2S_2O_3^{-2}$	0.09
$Fe(III)\text{-}EDTA^- + e^- \longrightarrow Fe(II)\text{-}EDTA^{-2}$	-0.177*
$2SO_4^{-2} + 4H^+ + 2e \longrightarrow S_2O_6^{-2} + 2H_2O$	-0.2
$CO_2 + 2H^+ + 2e^- \longrightarrow HCOOH$	-0.2
$Fe^{+2} + 2e^- \longrightarrow Fe$	-0.409
$S + H_2O + 2e^- \longrightarrow HS^- + OH^-$	-0.478
$2CO_2 + 2H^+ + 2e^- \longrightarrow H_2C_2O_4$	-0.49
$S + 2e^- \longrightarrow S^{-2}$	-0.508
$2SO_3^{-2} + 3H_2O + 4e^- \longrightarrow S_2O_3^{-2} + 6OH^-$	-0.58
$Zn^{+2} + 2e^- \longrightarrow Zn$	-0.76
$SO_4^{-2} + H_2O + 2e^- \longrightarrow SO_3^{-2} + 2OH^-$	-0.92
$2SO_3^{-2} + 2H_2O + 2e^- \longrightarrow S_2O_4^{-2} + 4OH^-$	-1.12
$Al^{+3} + 3e^- \longrightarrow Al$ (0.1F NaOH)	-1.706
$H_2AlO_3^- + H_2O + 3e^- \longrightarrow Al + 4OH^-$	-2.35

Sources
CRC Handbook of Chemistry and Physics 53rd Ed. (1972-1973)
*W. R. Grace Technical Information

Figure 1 Fe(II)-EDTA Regeneration by Al, Zn, and Fe Powdered Metals

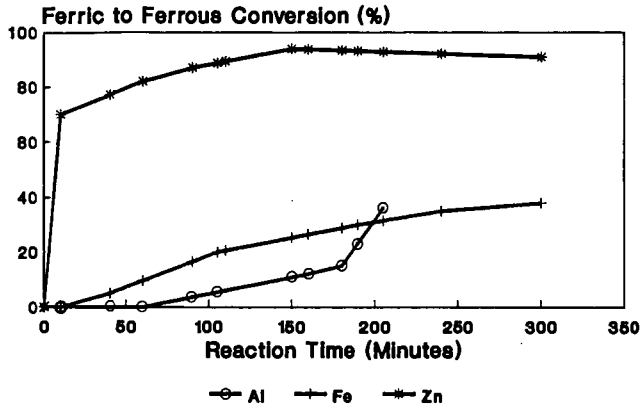

Figure 2 pH and Temperature Effects on Fe(II)-EDTA Regeneration by Sulfite

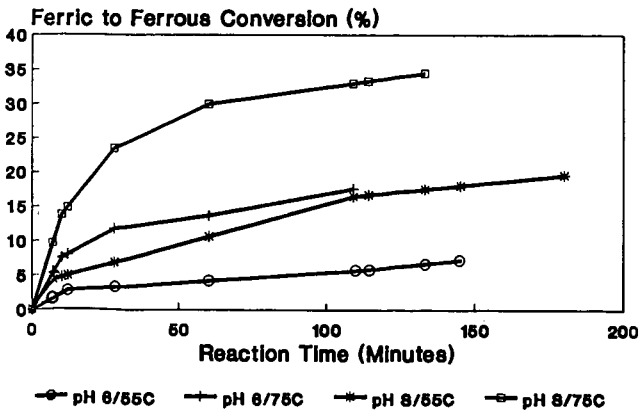

Figure 3 Fe(III)-EDTA Reduction
by L-Ascorbic Acid (Vitamin C)

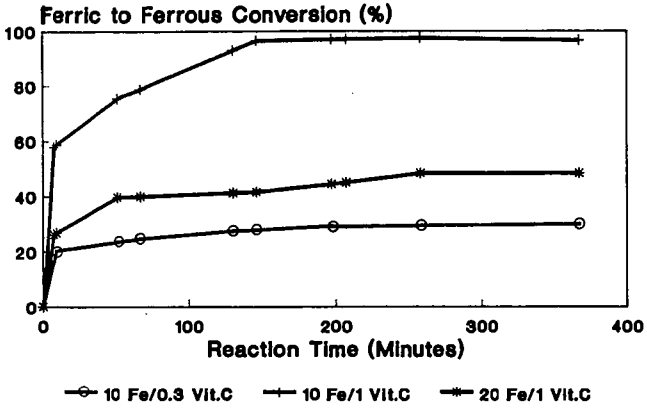

THERMOCHEMISTRY OF THE Fe-O-S SYSTEM AS A DESULFURIZER IN COAL COMBUSTION ATMOSPHERES: PART I - Fe-FeO-LIQUID EQUILIBRIUM

M. T. Hepworth, K. J. Reid, J. C. Wang and S. Zhong
Mineral Resources Research Center
University of Minnesota, 56 East River Road
Minneapolis, Minnesota 55455

Key words: Iron oxysulfide, slagging burner, desulfurization

INTRODUCTION

Development in slagging combustors for utility coal combustion is being driven by several factors:

* Removal of coal combustion residues as dense constituents at the source of combustion to reduce ash transfer to heat exchangers and down-stream fly ash capture devices,
* Incorporation of staged-combustion to minimize NO_x emissions,
* Utilization of added sorbents to reduce SO_x emissions,
* Capability of operation at elevated pressures suitable for combined cycle operation.

A recent survey[1] indicated that lime or limestone was currently the only sorbent being injected in slagging utility burners for those systems close to, or currently undergoing commercial development. Some researchers, notably Avco[2] have experimented with added iron as a sorbent material with initial success. The results of some preliminary studies by AMAX on iron oxide additions to the reducing stage of a small coal burner was reported[3] to result in up to 90 percent sulfur removal into a compact residue. This residue appeared to be relatively inert with respect to sulfur re-emission when exposed to moisture. Avco confirm these preliminary findings in experiments conducted late in 1989.

This paper is written entirely from a thermodynamic point of view. It compares the degree of desulfurization which can be achieved using an iron system with a calcium-based system operating under both reducing conditions (to produce calcium sulfide) and oxidizing conditions (to produce calcium sulfate). For this study calculations were made on an Illinois #2 coal as the fuel. They are restricted to those sulfur potentials which occur for the four phase equilibrium: gas + iron + wustite (FeO) + liquid iron oxysulfide.

Iron may be considered a potential competitor to lime as a sorbent for several reasons:

* It forms a series of low-melting-point liquid solutions with iron and oxygen under reducing conditions. These liquids should be highly reactive with respect to absorption of sulfur in the gases which they contact. Because they are liquids rather than solids, good internal mixing under the high shear conditions of cyclonic burners should enhance the kinetics of absorption and also achieve sulfur absorption closer to the predicted stoichiometry than would occur with a solid sorbent.

* However, lime, being a solid, has been shown to require from two-to-five times the stoichiometric ratio of calcium-to-sulfur[4] in order to produce a high degree of desulfurization.
* Iron in the form of taconite concentrates (magnetite) is cost-competitive with lime at locations close to Great Lakes' ports (approximately $30/short ton, FOB).

THERMODYNAMIC ANALYSIS

Calculations are based upon a Western Illinois Coal (Illinois No. 2), described as "Colchester, low ash, high pyritic sulfur" from sample IBC 102[5]. This coal, of the assay given below, was factored into the calculations as 100 grams of coal on dry basis plus 14.2 grams moisture:

Constituent	% by Wt.	
Carbon	73.92	
Hydrogen	5.29	
Nitrogen	1.52	
Total sulfur	3.29	
Oxygen	9.02	(not included in ash)
Ash	6.9	
Total	100.0	(dry basis)
Moisture	14.2	
BTU/lb	13,582	

An interactive computer program was developed which enables coal assays to be varied as well as combustion conditions including temperature, total pressure coal composition, moisture content, volume of air, etc. Data were taken from Kubaschewski and Alcock[6] for the thermodynamics of the gas phase interactions and for the stabilities of the calcium compounds. The iron oxygen-sulfur systems incorporates data from Darken and Gurry[7], Bog and Rosenqvist[8], Rosenqvist and Hartvig[9], and Burgmann et al.[10] as reported by Turkdogan and Kor.[11]

The results of these calculations are shown in Figure 1 for the system Ca-S-O. This figure is a predominance diagram in which the equilibrium phase regions are designated on a logarithmic plot of partial pressures of sulfur (taking the dimer as the predominant elemental sulfur species) on the ordinate and log oxygen partial pressure as a measure of the chemical potential of oxygen on the abscissa. The solid lines represent conditions at 1000° C. and the dashed lines at 1300° C., respectively. As is expected, calcium sulfide is oxidized upon increasing the oxygen potential to the sulfate form and can only be maintained under the reducing conditions shown. As temperature is increased (dashed lines) the transition from sulfide to sulfate occurs under more oxidizing conditions. Also as temperature is increased the equilibrium between sulfide and oxide occurs at lower sulfur pressures in the equilibrium between CaS and CaO; however, the sulfur pressures for the equilibrium between CaO and $CaSO_4$ phases occur for higher sulfur pressures as temperature is raised.

Using the interactive program and the coal composition given above, the calculations in Figure 2 on the CaO/CaS/gas system show the anticipated equilibrium sulfur concentration reported as pounds of SO_2 per million BTU against temperature. For this plot the partial pressure of oxygen was arbitrarily taken at 10^{-12} atmospheres with a total gas pressure of 1 atmosphere. The thermodynamic conditions are for the reducing stage of a two-stage combustor; however, the calculations for the sulfur dioxide emissions (ordinate) are based upon stoichiometric conditions existing in the second stage of the combustor. Figure 2 substantiates the conditions borne out in Figure 1; that is, high temperatures for the calcium sulfide system yield better desulfurization.

The converse is true for lime used as a sorbent under oxidizing conditions; i. e., with calcium sulfate as the product of reaction. Figure 3 shows that for temperatures much above 1150° C., the sulfur pressure rises rapidly. The conditions chosen were for an oxygen pressure of 0.05 atmospheres, or a slight excess of oxygen over stoichiometric requirements. In Figures 2 and 3 the theoretical dosage of lime is also plotted. As the lime reacts with sulfur, the dosage of lime required, of course, increases (Figure 1); whereas, the converse is true for Figure 3 where lime becomes less effective as a desulfurizer.

Figure 4 is a ternary projection of the liquidus surfaces in the Fe-O-S system showing the phase pyrrhotite (FeS) at the lower right hand corner. The liquid phase is seen to be in the thermal "trough" with a ternary eutectic of 920° C. From this ternary eutectic the labeled isotherms diverge outward to form the steep walls of this valley. The region in this paper for which calculations were made is the heavy diagonal line toward the left-hand wall of this trough which marks the boundary between the regions of iron/wustite/and liquid.

Data summarized by Turkdogan and Kor have been employed in our calculations. Figure 5 is a plot of the conditions of oxygen and sulfur potential as a function of temperature to maintain this four phase equilibrium (three condensed phases plus gas). This plot is not for a system of constant composition but for the composition along the solid line shown in the previous figure. As temperature rises, the oxygen partial pressure is shown to rise, but interestingly, the sulfur partial pressure shown on a log scale drops sharply. Part of this drop can be attributed toward the increasing solubility limit of the liquid phase (closer to lower sulfur concentrations); nevertheless, the rapid drop in sulfur partial pressure is steeper than would be predicted merely by a shift in composition to lower sulfur contents. Even at 1300°C the chemical potential of sulfur, as measured by the parameter, $-RT\ln P_{S2}$, is about 45,000 calories per gram mole corresponding to a partial pressure of sulfur of 5.58×10^{-7} atm. This is a fortuitous aspect of the iron-oxygen-sulfur system; i e., the thermodynamic calculations on desulfurization show improvement with higher temperatures. Figure 6 is a plot for the Fe-O-S system similar to those for the lime-based systems in which this improved degree of desulfurization with increasing temperature is shown. The increased dosage of iron is also shown. For example at 1300°C an iron dosage for the coal composition for these calculations would be 15 grams per 100 grams of coal.

One of the objectives of this study is to develop an interactive computer program such that an operator of a slagging combustor can enter coal compositions and combustion conditions and determine the optimum process conditions required. Figure 7 shows the air requirements for 100 grams of dry coal and the theoretical percent sulfur removal which can be achieved.

Figure 8 shows the calculated concentrations of the major gas species as a function of temperature for the equilibrium between Fe/FeO/liquid/gas. The predominant species for these reducing conditions (corresponding to a combustion stoichiometry of approximately 55% of the required air for complete combustion) are N_2 and CO followed by CO_2, H_2, and H_2O in that order. The total sulfur pressure is the sum of all the sulfur-bearing species with H_2S being the predominant sulfur carrier. Lower rank coals with higher hydrogen water vapor contents would be expected to carry more sulfur into the gas phase. Since the pressure of the sulfur species, S_2, is fixed by the Fe-O-S equilibria, the actual amount of sulfur in the gas phase is determined principally by the equilibrium:

$$H_2(g) + 1/2S2_2(g) = H_2S(g).$$

This equilibrium has an equilibrium constant somewhat greater than unity. Also the pressure of H_2S is proportional only to the square root of the sulfur pressure but varies linearly with hydrogen pressure. It follows, then, that iron oxysulfide would perform best on dry, high-rank coals.

CONCLUSIONS

The following can be concluded from this analysis:

* In the Fe-O-S system for the four-phase contact, Fe/FeO/liquid/gas, higher temperatures result in greater degrees of desulfurization for the range of temperatures studied.
* Lime added under oxidizing conditions to form sulfate as a reaction product is not practical as a sulfur sorbent at temperatures above 1175°C.
* Inference is made that for iron oxysulfide as a sorbent, this liquid phase should exhibit a higher degree of utilization in liquid droplets than solid lime sorbents. Furthermore the kinetics of liquid/gas interactions should be more favorable than solid/gas interactions. This hypothesis will require further study in a dynamic burner system.
* Further calculations are required to determine the process conditions to achieve effective sulfur removal for the two phases, liquid/gas. These calculations should be made for a range of coals of varying hydrogen and water contents.

REFERENCES

1. Hepworth, M. T. and Reid, K. J.: Slagging Combustor Review, Final Report MRRC, University of Minnesota December, 1988.

2. Private Communication: R. Diehl Avco Research Laboratories, Everett, Mass.

3. Hepworth, M. T. and Wicker G. R., "Iron Oxide as a Desulfurizing Agent in a Slagging Coal Combustor", Pyrometallurgy '87, Institution of Mining and Metallurgy, London, 1987, and Hepworth, M. T., U. S. Patents 4,572,085 (2/25/86), 4,598,652 (7/8/86), and 4,599,955 (7/15/86).

4. Lachapelle, David G.:"EPA's LIMB Technology Development Program," Chemical Engineering Progress, May 1985 pps. 56-62.

5. Harvey, Richard D.: Illinois Geological Survey, Letter of 9/8/89 to M.T. Hepworth.

6. Kubaschewski, O. and Alcock, C. B.: Metallurgical Thermochemistry, Pergamon Press, 1979.

8. Bog, S. and Rosenqvist: The Physical Chemistry of Metallic Solutions and Intermetallic Compounds, Paper 6B, NPL Symposium No 9, Vol II, 1959.

7. Darken, L. S. and Gurry, R. W., J. Am. Chem. Soc., 1945, Vol 67. pps. 1398-1412; 1946, Vol 68, pps. 798-816.

9. Rosenqvist, T. and Hartvig, T.: Roy. Norweg. Concil Sci. and Ind. Res., Rep. No 12, Part II, 1958.

10. Burgmann, W., Urbain, G., and Frohberg, M. G.: IRSID Saint Germain-en-Laye, France, January 1968.

11. Turkdogan, E. T. and Kor, G. J. W.: "Sulfides and Oxides in Fe-Mn Alloys: Part I, Phase Relations in the Fe-Mn-S-O System", Metallurgical Transactions, Vol 2, June 2971 pps 1561-1578.

ACKNOWLEDGEMENT

The authors wish to express their appreciation to the Department of Energy contract #DOE/DE-FG22-89PC89778 for funding this study.

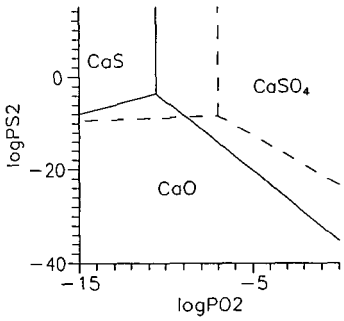

Figure 1. Predominance Diagram Ca-S-O System.

Solid Lines - 1000° C.
Dashes Lines - 1300° C.

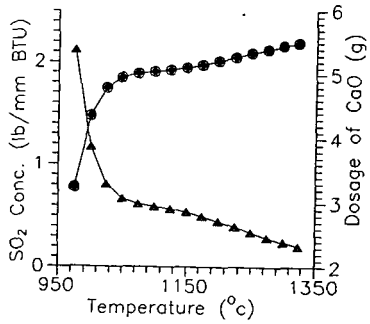

Figure 2. CaO/CaS/Gas Stoichiometric SO_2 Conc. vs. Temp at Oxygen Pressure: 10^{-12} Atm.
△ SO_2
O Dosage of CaO

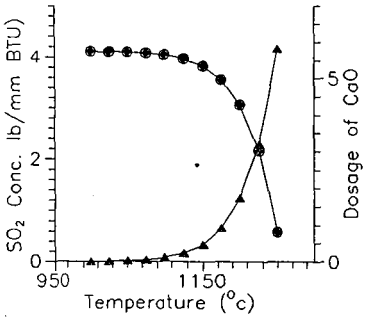

Figure 3. $CaO/CaSO_4$/Gas Stoichiometric SO_2 at Oxygen Pressure: 0.05 Atm.
△ SO_2
O Dosage of CaO

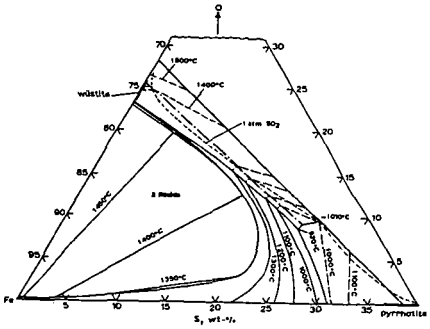

Figure 4. Ternary Section Fe/FeS/O System: Projection Liquidus Surface.

After: Bog and Rosenqvist[8] and Hilty and Crafts[12]

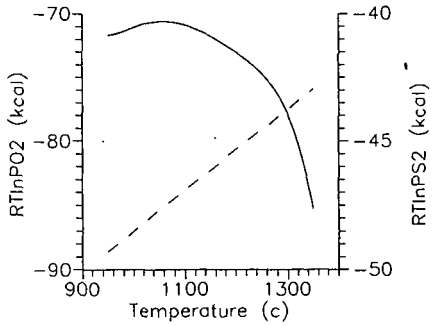

Figure 5. Fe/FeO/Liquid/Gas System
Chemical Potentials S, O.
— Sulfur
--- Oxygen

After: Turkdogan et al.[11]

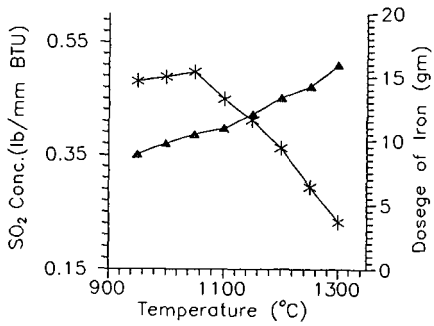

Figure 6. Fe/FeO/Liquid/Gas System
Stoichiometric SO
Conc. vs. Temp.
✱ SO_2 Concentration
△ Dosage of Iron

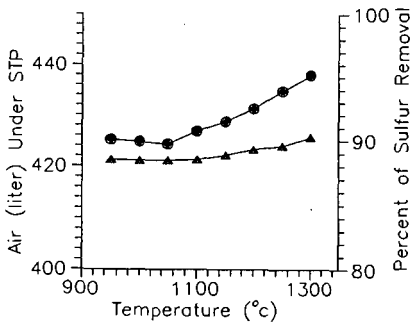

Figure 7. Fe/FeO/Liquid/Gas System
△ Air Dosage/100g Dry Coal &
O % Sulfur Removal vs Temp.

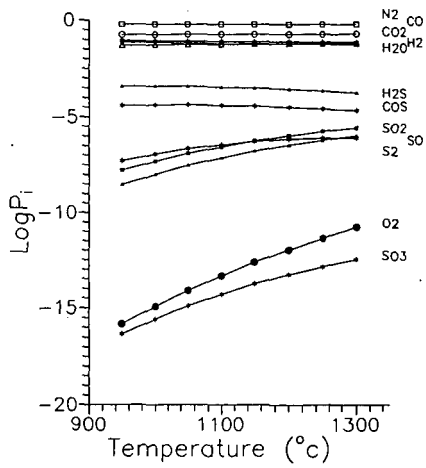

Figure 8. Calculated Partial Pressure (atm.) vs. Temperature for Coal Combustion Products in Equilibrium with Fe/FeO/Liquid

COMPUTER MODELING OF THE CHEMISTRY OF AQUEOUS SCRUBBER SYSTEMS

David Littlejohn and Shih-Ger Chang
Lawrence Berkeley Laboratory
1 Cyclotron Road
Berkeley, CA 94720

Abstract

The chemistry occurring in aqueous flue gas scrubbing solutions can be quite complicated, due to the large number of chemical species present and the many physical processes involved. These include gas absorption into solution, gas and solution kinetics involving both nitrogen oxides and sulfur oxides, oxidation and hydrolysis reactions in solution, and liquid-solid interactions. Simple models that neglect the solution kinetics which can occur in scrubbers cannot be expected to accurately model aqueous-based scrubber chemistry. We have developed a computer model which incorporates the aqueous solution kinetics of nitrogen oxyanions, sulfur oxyanions, nitrogen-sulfur compounds, and other species. The model can be adapted to predict the chemistry in a wide range of aqueous-based scrubber systems. It can be used to study the effect of changes in the operating conditions of the scrubbers. The results of the model can be compared with experimental observations to determine how well the chemistry of the solutions is understood.

Key Words: Wet scrubber chemistry, nitrogen sulfur compounds, computer modeling

Introduction

A good understanding of the chemistry occurring in wet flue gas scrubbing systems is inportant. The chemistry will influence the NO_x and SO_2 removal and the product distribution, as well as factors such as scaling. A large number of compounds can be formed in scrubber solutions.[1] The compounds present depend, in part, on the type of scrubber chemistry utilized. Nitrogen-sulfur compounds will form under neutral to acidic conditions when both nitrite ion and bisulfite ion are present in significant quantities.[1] The term nitrogen-sulfur compound is used to collectively refer to hydroxyimidodisulfate (HADS), hydroxysulfamic acid (HAMS), nitridotrisulfate (ATS), imidodisulfate (ADS), sulfamate, and hydroxylamine. The compounds have been observed in a number of wet scrubber solutions.[2,3] These compounds can interfere with the recovery of desirable byproducts from scrubber solutions. They will also build up in scrubber solutions and must eventually be treated or removed.

To develop an understanding of the solution chemistry of wet scrubbers, a chemical kinetic computer modeling program has been developed. It allows simulation of the known reactions occurring in solution and calculation of reaction rates and concentration of aqueous species.

The Model

Exact equations for calculating the concentrations of species involved in chemical reactions can only be established for the simplest reaction systems. Approximations, such as the steady-state approximation, permit estimation of concentrations and rates of reaction in more complicated chemical systems under suitable conditions, provided that the system is not too complicated. A different approach is required to accurately calculate concentrations and rates in complex reaction systems, particularly where conditions are rapidly changing.

In the 1970's, work by Whitten[4] and others led to the development of matrix-based computer calculations to simulate complicated chemical kinetic systems. The system of chemical reactions is converted into a series of ordinary differential equations . A method to integrate a sytem of ordinary differential equations was developed by Gear[5] and modified by Hindmarsh[6] at Lawrence Livermore National Laboratory. This routine is the basis for most chemical kinetic modeling schemes. The program performing the Gear routine has subsequently been modified to handle sparse matrices and improve its operating efficiency.[7] This version of the Gear routine is the basis of the chemical kinetic modeling program used in this work. It is similar to modeling routines that have been used to simulate air pollution chemistry for a number of years.[8]

Results and Discussion

The chemistry of the nitrogen-sulfur compounds in solution has been studied extensively for many years, and is, for the most part, reasonably well understood. The rate constants for the reactions involving nitrogen-sulfur compounds, along with those for other important reactions, are incorporated into the computer model. The initial conditions for the calculation are also included as input. These include temperature or temperture vs time profile, initial concentration of species, pH and length of time of the calculation. The program generates a list of reaction rates vs time and concentration vs time for all species included in the calculation. In this way, we can explore the effect of variables such as temperature, pH, concentrations, and additives on the scrubber chemistry.

The chemical reaction database used as input into the model is listed in Table 1. Depending on conditions, some of the reactions are unimportant and are not included in the calculation to reduce the processing time. Tests are performed to ensure the absence of a reaction does not significantly alter the results of the calculation. Updated or additional reaction rate constants can be incorporated into the database as new measurements become available.

Examples of the calculations are shown in Figure 1 and Figure 2. Figure 1 illustrates the effect of pH on the generation and interconversion of nitrogen-sulfur compounds. Calculations were done at pHs of 3, 5 and 7 at a temperature of 40°C for a batch reactor exposed to concentrations of SO_2 = 2000 ppm, NO = 450 ppm and NO_2 = 50 ppm. Increasing the solution pH significantly increases the total concentration of nitrogen-sulfur compounds and favors ATS and ADS as products. Figure 2 illustrates the effect of temperature on the system of nitrogen-sulfur compounds. Calculations were done at temperatures of 20°C (68°F), 40°C (104°F), and 60°C (140°F) at a pH of 5 for a batch reactor exposed to concentrations of SO_2 = 2000 ppm, NO = 450 ppm, and NO_2 = 50 ppm. Increasing the solution temperature

also increases the total concentration of nitrogen-sulfur compounds. Higher temperatures increase the concentrations of ATS and ADS relative to HADS and HAMS.

These calculations illustrate what can be studied using the computer model. The influence of a number of scrubbing system parameters can be investigated relatively rapidly. The model does require accurate information on kinetics, gas concentrations, and solubilities for all compounds that have a significant influence on the chemistry to provide realistic results.

The chemical kinetics modeling program is still under development to increase its versatility. We are in the process of incorporating precipitation processes in the model to simulate the formation of solids. This will allow more accurate investigation of some scrubber chemistries, such as lime/limestone-based scrubbing systems. Measurement of the solubilities of the nitrogen-sulfur compounds is currently in progress,[9] and the results of this study will be incorporated into the model.

The model is also being developed to incorporate the effects of ionic strength and activities of the ions in solution on the reactions used. Scrubbing solutions are generally at conditions that are far from those of ideal solutions. By incorporating ionic strength and ionic interactions into the model, we should be able to obtain more accurate simulation of the chemistry of scrubbing solutions.

This work was supported by the Assistant Secretary for Fossil Energy, Office of Coal Utilization Systems, U.S. Department of Energy under Contract No. DE-AC03-76SF00098 through the Pittsburgh Energy Technology Center, Pittsburgh, PA.

References

1. Chang, S.G.; Littlejohn, D.; Lin, N.H. Flue Gas Desulfurization; Hudson, J.L.; Rochelle, G.T., Eds.; ACS Symposium Series 188; American Chemical Society: Washington, DC, 1982; pp 127-152.

2. Littlejohn, D.; Chang, S.G. "Identification of Species in a Wet Flue Gas Desulfurization and Denitrification System by Laser Raman Spectroscopy". *Environ. Sci. Technol.* **1984**, *18*, 305-310.

3. Littlejohn, D.; Chang, S.G. "Determination of Nitrogen-Sulfur Compounds by Ion Chromatography". *Anal. Chem.* **1986**, *58*, 158-160.

4. Whitten, G.Z."Rate Constant Evaluations Using a New Computer Modeling Scheme". Presented at the 167th National Meeting of the American Chemical Society, San Francisco, CA.

5. Gear, C.W. Numerical Initial Value Problems in Ordinary Differential Equations; Prentice Hall, Englewood Cliffs, NJ, 1971.

6 Hindmarsh, A.C. "GEAR: Ordinary Differential Equation System Solver" Report UCID-30001, rev.3; Lawrence Livermore National Laboratory, Livermore, CA, 1974.

7. Spellman, J.W.; Hindmarsh, A.C. "GEARS: Solution of Ordinary Differential Equations Having a Sparse Jacobian Matrix" Report UCID-30116; Lawrence Livermore National Laboratory, Livermore, CA, 1975.

8. Whitten, G.Z.; Hogo, H. "CHEMK; A Computer Modeling Scheme for Chemical Kinetics". Report No. EF78-107R, Systems Applications, Inc., San Rafael, CA, 1979.

9. Littlejohn, D.; Chang, S.G. to be published.

Table 1

Chemical Reactions Related to Aqueous Scrubber Chemistry

Reaction			k,K or H[a]	E_{act}[b]
1. SO_2(gas)	<=>	SO_2(aq)	1.24	
2. NO(gas)	<=>	NO(aq)	.0019	
3. NO_2(gas)	<=>	NO_2(aq)	.007	
4. CO_2(gas)	<=>	CO_2(aq)	.034	
5. HNO_2(gas)	<=>	HNO_2(aq)	60	
6. NO + NO_2 + H_2O (gas)	<=>	HNO_2 + HNO_2	5.3×10^{-2}	
7. SO_2(aq)	<=>	HSO_3^- + H^+	1.5×10^{-2}	
8. CO_2(aq)	<=>	HCO_3^- + H^+	4.3×10^{-7}	
9. HSO_3^-	<=>	SO_3^{2-} + H^+	1.2×10^{-7}	
10. HNO_2(aq)	<=>	NO_2^- + H^+	5.8×10^{-4}	
11. HSO_4^-	<=>	SO_4^{2-} + H^+	1.2×10^{-2}	
12. HSO_3^- + HSO_3^-	<=>	$S_2O_5^{2-}$ + H_2O	6.5×10^{-2}	
13 NO(aq) + NO_2(aq)	—>	HNO_2(aq) + HNO_2(aq)	1.6×10^{8}	
14. HNO_2(aq) + HNO_2(aq)	—>	NO(aq) + NO_2(aq)	14	
15 H^+ + HNO_2(aq)	—>	NO^+ + H_2O	4.08×10^{2}	11.5
16. HNO_2 + HSO_3^-	—>	$ONSO_3^-$ + H_2O	2.43	12.1
17 NO^+ + HSO_3^-	—>	$ONSO_3^-$ + H^+	c	
18. $ONSO_3^-$ + HSO_3^-	—>	$HON(SO_3)_2^{2-}$	c	
19 $HON(SO_3)_2^{2-}$ + H^+	—>	$HONHSO_3^-$ + H^+ + HSO_4^-	2.1×10^{11}	17.6
20 $HON(SO_3)_2^{2-}$	—>	$HONHSO_3^-$ + HSO_4^-	1.67×10^{11}	23.0

Table 1
(continued)

21. $HONHSO_3^- + H^+$	-->	$NH_2OH + H^+ + HSO_4^-$	6.2×10^{12}	26.3
22. $HON(SO_3)_2^{2-} + HSO_3^-$	-->	$N(SO_3)_3^{3-} + H_2O$	3.4×10^{10}	19.2
23. $N(SO_3)_3^{3-} + H^+$	-->	$HN(SO_3)_2^{2-} + HSO_4^-$	1.5×10^{13}	16.5
24. $HN(SO_3)_2^{2-} + H^+$	-->	$H_2NSO_3^- + HSO_4^-$	2.54×10^{14}	23.5
25. $HON(SO_3)_2^{2-} + HSO_3^-$	-->	$HN(SO_3)_2^{2-} + HSO_4^-$	1.5×10^{10}	19.0
26. $HONHSO_3^- + HSO_3^-$	-->	$HN(SO_3)_2^{2-} + H_2O$	1.4×10^{13}	24.5
27. $HONHSO_3^- + HSO_3^-$	-->	$H_2NSO_3^- + HSO_4^-$	6.0×10^{12}	24.5
28 $NH_2OH + SO_2(aq)$	-->	$H_2NSO_3^- + H_2O + H^+$	1.74×10^{11}	13.4
29. $NH_2OH + SO_2(aq)$	-->	$NH_4^+ + HSO_4^-$	1.06×10^{2}	3.0
30. $H_2NSO_3 + HNO_2$	-->	$HSO_4^- + H_2O$	1.13×10^{2}	11.3
31. $NO(aq) + HSO_3^-$	-->	$^-ONSO_3^- + H^+$	2.6×10^{14}	17.6
32. $NO(aq) + SO_3^{2-}$	-->	$^-ONSO_3^-$	3.2×10^{10}	10.6
33. $NO(aq) + {}^-ONSO_3^-$	-->	$^-ON(NO)SO_3^-$	c	
34. $^-NO(NO)SO_3^-$	-->	$N_2O + SO_4^{2-}$	1.55×10^{-3}	
35. $NO_2(aq) + NO_2(aq)$	-->	$HNO_2(aq) + NO_3^- + H^+$	8.4×10^{7}	
36. $HSO_3^- + 2NO_2(aq)$	-->	$2NO_2^- + 3H^+ + SO_4^{2-}$	1.2×10^{7}	

a. k in units of M^{-1} sec^{-1} or sec^{-1}; K in units of M; H in units of M atm^{-1}

b. In units of kcal mol^{-1}

c. reactions 17,18 and 33 are assumed to be fast.

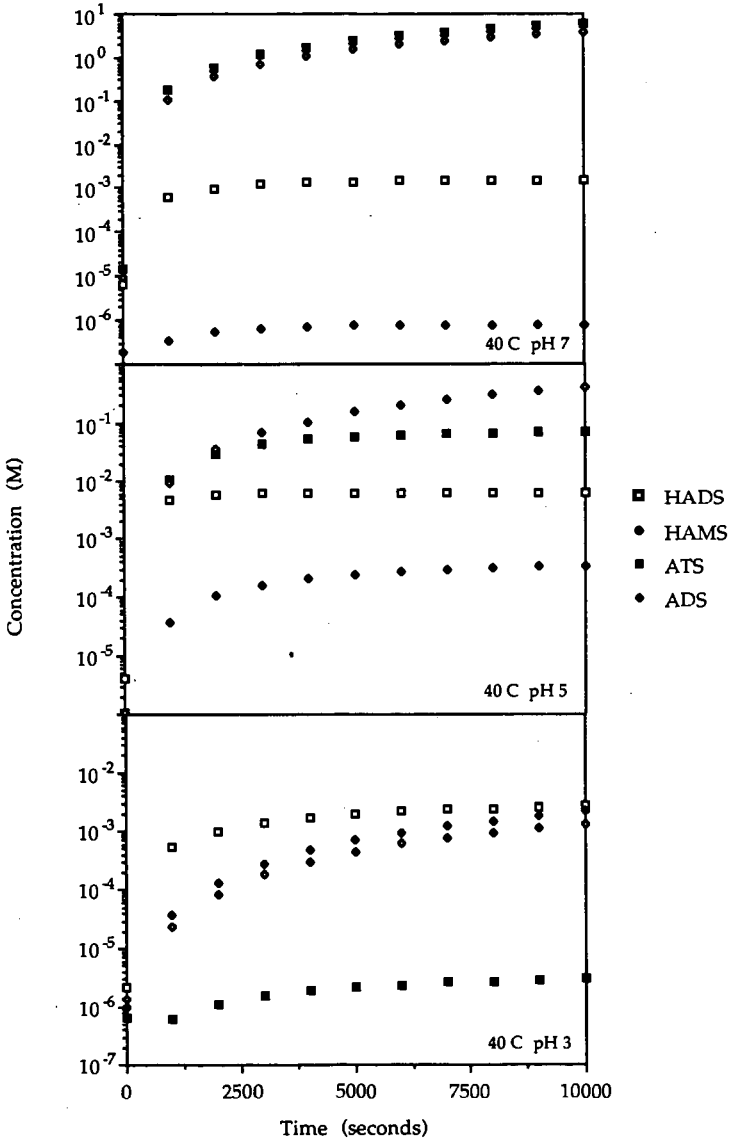
Concentration (M)
40 C pH 7
40 C pH 5
40 C pH 3
HADS
HAMS
ATS
ADS
0
2500
5000
7500
10000
Time (seconds)

Figure 1

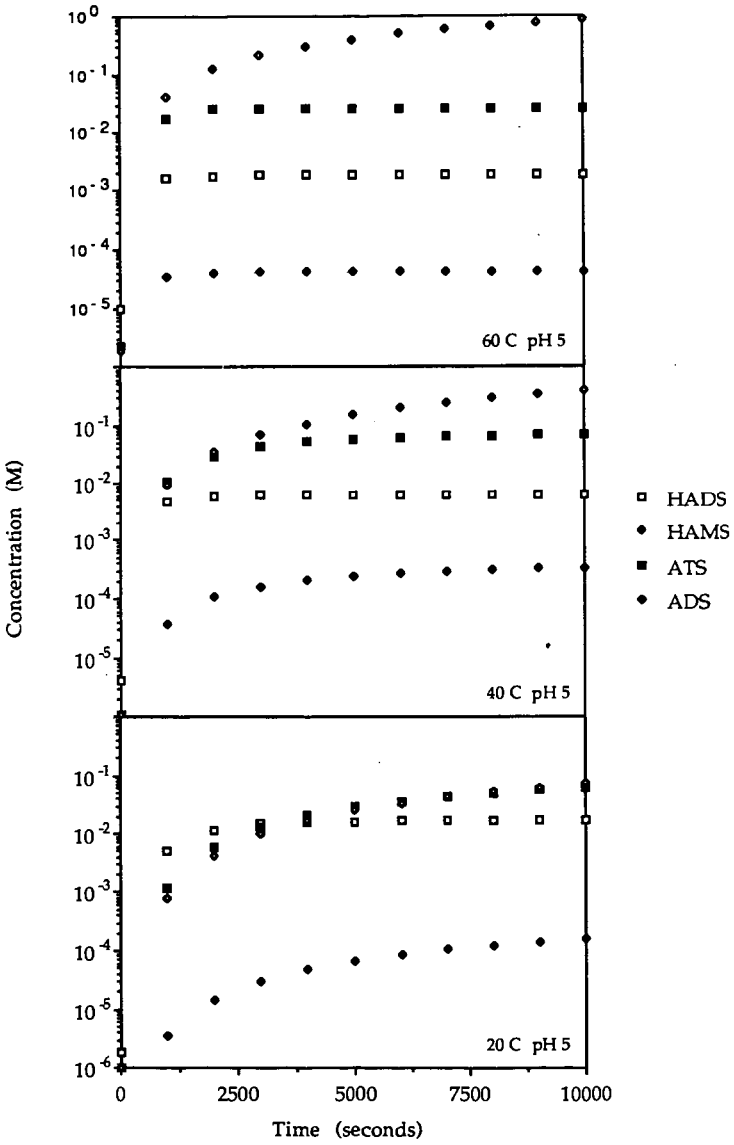
Concentration (M)
60 C pH 5
40 C pH 5
20 C pH 5
HADS
HAMS
ATS
ADS
Time (seconds)
0
2500
5000
7500
10000

Figure 2

NITROGEN OXIDE REBURNING WITH HYDROCARBON FUELS

Thomas E. Burch, Franz R. Tillman, Wei-Yin Chen*, and Thomas W. Lester

Department of Mechanical Engineering, Louisiana State University, Baton Rouge, LA 70803
**Corresponding Author; Present Address: Department of Chemical Engineering, University of Mississippi, University, Mississippi 38677*

Keywords: Nitrogen Oxides, Reburning, Fuel Effects

Introduction:

Reburning (or fuel staged combustion) is a in furnace NO_x control process that utilizes the reduction powers of hydrocarbons. This concept and the term reburning were first proposed by Wendt, et al. (1973). However, reburning was not established as a practical NO_x reducing method until Takahashi, et al. (1983) reported greater than 50% reduction of NO in tests at Mitsubishi Heavy Industries. Reburning comprises three zones in the combustion process. The primary zone is the main heat release zone in which approximately 80% of the fuel is burned in a fuel lean (SR = 1.1) environment. This is followed by a reburning zone where additional fuel is added to give an overall fuel rich stoichiometry (ca. SR = 0.9). Finally additional air is provided in the burnout zone to complete the combustion process by burning off residual hydrocarbons in a fuel lean environment.

This study addresses the mechanisms of NO reduction in pulverized coal combustion using reburning. The interactions between NO and hydrocarbon constituents in the fuel, and the fate of fuel nitrogen are the focal points of this research. Nitrogen oxide reduction and formation mechanisms in reburning stage are investigated with a laboratory scale flow reactor. Feed to the reactor includes simulated flue gas and reburning fuels (methane, benzene, hexane, coal, and lignite). This paper discusses the implications of nitrogen product distribution as functions of second stage stiochiometry and reburning fuel type. In addition, a unique GC/MS technique established for the systematic analysis of flue gas will be presented.

Experimental:

The experiments reported here were carried out in a ceramic flow reactor (Figure 1) with a simulated flue gas consisting of 16.8% CO_2, 1.95% O_2, and 0.1% NO in a helium base. These concentrations of CO_2, O_2, and NO were chosen to be consistent with those of a coal primary flame operated at a stoichiometric ratio of 1.1. Helium, instead of nitrogen, was used as the base gas to minimize heating time due to its low heat capacity.

The flow reactor used for this research was an alumina tube (Coors Ceramics Co.) with an inside diameter of 0.75 in. and an overall length of 24 in the central portion of the reactor tube was enclosed in a 12 in. long electrically heated furnace (Lindberg Model 55035) which provided tube temperatures up to 1150°C.

For experiments using coal as a reburning fuel, the delivery system was modified to incorporate a laboratory scale coal feeder shown schematically in Figure 2. Details of this device have been reported elsewhere (Burch, et al. 1990). The coal feeder required part of the gas flow (usually helium) to be diverted through the coal feeder for use as carrier gas.

The sampling train consisted of 0.25 in stainless steel transfer lines and switching manifold with stainless steel valves. Transfer lines from the reactor tube exit to the impinger were heat traced to prevent absorption of HCN and NH_3. The effluent was desiccated with anhydrous calcium sulfate before transfer to the instrument package through 0.25 in teflon tubing. For coal experiments, the sampling train was modified to allow the gaseous products (and particulate matter) to pass straight through the end of the reactor tube into a paper filter before entering the transfer lines. The filter was enclosed in a glass housing and heated to 100°C. Revoery tests showed no loss of HCN or NH_3 in the filter. A 10 μm filter was also added upstream of the desiccant dryer for coal experiments. The flow reactor was maintained near atmospheric pressure by providing an atmospheric vent downstream of the instrument package and monitoring the supply gas pressure in the mixing chamber.

HCN and NH_3 were collected by diverting the reactor effluent through a straight tube impinger filled with 0.5 L of 0.1N HNO_3 aqueous solution for a specified time interval. The captured solutions were pH adjusted using NaOH

and analyzed for CN- and dissolved ammonia with specific ion electrodes (Orion Research). Poisoning of the cyanide electrode by sulfur ions from coal combustion was prevented by adding an aqueous solution of $PbNO_3$ prior to adding the NaOH. Sulfide ions were precipitated as PbS. Recovery of HCN and NH_3 by this method was tested using known standards and found to be near quantitative for NH_3 but only 70% for HCN. Thus NH_3 values have been presented as measured while HCN values reported have been corrected for collection efficiency.

Qualitative analysis or separation of nitrogenous species were also performed by GC/MS. Samples of the reactive effluent were captured in 300 cm^3 stainless steel containers. To eliminate contamination from past runs the containers were heated under vacuum between runs to remove HCN and NH_3 absorbed into the walls.

Two chromatographic columns were used for separation of the nitrogen compounds. N_2 and NO were effectively separated from other fixed gases on a 20 ft x 1/8 in S.S. Hayesep D_B column (Hayesep separations) at 25°C isothermal. Separation of NH_3 and HCN was accomplished using an 8 ft x 1/8 in. S.S. Hayesep C column operated at 80°C for NH_3 and 120°C for HCN. Due to active sites on the column. Low concentrations of these specifics (less than 200 ppm) required several saturation injections and isothermal conditions to give quantifiable mass peaks. Lower concentrations of NH_3 and HCN (less than 75 ppm) were analyzed by "loading" the column with repeated injection onto a cold column (25°C). The oven temperature was then rapidly raised to the desired operating temperature to facilitate elution. This procedure was repeated until the yields of the HCN and NH_3 were stabilized, signifying that active sites were filled with species from the current sample.

GC/MS samples were injected via evaluated and heated static injection loops. For fixed gas analysis, a 10 cm^3 S.S. loop was used. For HCN and NH_3 analysis a 40 cm^3 S.S. loop was used to help overcome low concentrations and active column sites.

Results and Discussion:

- Gaseous Fuels Results

Reburning experiments were conducted for methane, hexane and benzene at a reburning temperature of 1100°C and an estimated reaction time of 0.2 seconds. The stoichiometry for these tests was varied from SR = 0.7 to 1.0. The resulting TFN (total fixed nitrogen; ie, all nitrogen species except N_2) speciation profiles are illustrated in cumulative fashion by the curves in Figure 3 through 5.

The minimum TFN for each of these fuels occurred near SR = 0.95 under these conditions. However, the minimum value attained and the sensitivity to stoichiometry were found to be considerably different for the three fuels. Also, the TFN speciation in the neighborhood of the minimum TFN was radically different.

For methane the dominant fixed nitrogen species at the optimum stiochiometry was NO which accounted for more than 85% of the total. In benzene reburning, the contribution of NO at the optimum stoichiometry was only 2% of the total with HCN making up 75%. Hexane fell in between these two extremes with NO and HCN contributions of 33% and 60% respectively. It is interesting to note that hexane exhibited the lowest TFN.

Employing the mechanisms and senstivity analysis of Miller and Bowman (1989) along with calculations conducted by Chen et al. (1989) it seems resonable to view reburning as possessing two major kinetic barriers. The first barrier is the conversion of NO to HCN by combination with various hydrocarbon fragements such as

$$C + NO \rightarrow CN + O$$
$$CH + NO \rightarrow HCN + O$$
$$CH_2 + NO \rightarrow HCNO + H$$

The accepted rate constants for these reactions are all within roughly one order of magnitude so the dominant mechanism in the conversion of NO to HCN is strongly dependent on the relative concentrations of the reducing species produced. Regardless of which mechanism dominates, there is general agreement that the end product is HCN, whether formed directly of by rapid conversion of intermediates such as CN.

The second major kinetic obstacle appears to be oxidation of HCN via one of the following reactions:

$$HCN + OH \rightarrow HOCN + H$$
$$HCN + OH \rightarrow HNCO + H$$
$$HCN + O \rightarrow NCO + H$$
$$HCN + O \rightarrow NH + CO$$

Having accomplished this step the subsequent conversion to N atoms is rapid. N atoms are then recycled to form NO or react with NO to form N_2.

Using this two barrier concept many of the salient feactures of reburning can be interpreted. First the concentration and longevity of reducing species at near stoichiometric conditions is so low that substantial quantities of the initial NO remains unreacted. As the stoichiometry is shifted to more fuel rich conditions, competition from other oxidizing species decreases allowing concentrations of reducing species to build and react with NO. Thus at richer stoichiomctries, most of the NO is converted to HCN. Actually the concentration of reducing species appears to peak somewhere around SR = 0.9, then slowly declines as the stochiometry becomes more fuel rich. However, the general trend described above appears valid.

The concentration of oxidizing species needed to overcome the second barrier follows an opposite trend. At lean stoichiometries the populations of O and OH are high, effectively converting most form HCN to subsequent species. As the stoichiometry becomes richer the concentration of oxidizing species is depleted by reaction with abundant reducing species.

Thus, in leaner stoichiometries, the dominant kinetic barrier appears to be the initial reduction of NO whereas in rich stoichiomctries the conversion of HCN to subsequent species is the major obstacle. The optimum stoichiometry is then defined by a compromise between these processes. Based on this admittedly simplistic arguement the behaviour exhibited in Figures 3 through 5 can be interpreted.

For methane, the fact that the minimum TFN contains primarily NO indicates that reduction of NO to HCN is the limiting factor. The carbon to hydrogen ratio of methane (1 to 4) may not provide enough of the appropriate reducing species to effectively convert NO to HCN until the stoichometry becomes too fuel rich to sustain good populations of O and OH.

Although any comments on the breakup of hexane and benzene is somewhat speculative, one might expect these fuels which are more carbon rich to produce CH_i ($i > 0, 1, 2$) fragments in greater numerous at stoichiometries lean enough to still support subtantial O and OH populations. The hexane curves (Figure 4) seem to follow this reasoning in that more of the NO has apparently been converted to HCN at SR = 0.95 where a substantial quantity of the HCN produced was converted to subsequent species leading to N_2.

Benzene shown in Figure 5, continued the trend of increasing reduction of NO to HCN as the carbon content of the fuel increased. However, the expected attending conversion of HCN to N_2 at this relatively lean stoichiometry was not observed. Perhaps the benzene oxidation mechanism is such that O and OH species are consumed too rapidly (or not produced at all) to allow for the conversion of HCN.

The timing of peak concentrations of important species is also critical. Since the conversion of HCN to N_2 by necessity succeeds the reduction of NO to HCN, high populations of NO reducing species occuring after O and OH have been depleted serve to reduce NO but not TFN.

One final observation is that the true optimum stoichiometry for benzene (or methane) may not have been found. The high levels of HCN at SR = 0.95 would seem to suggest that a leaner stoichiometry might yield a better conversion of HCN to N_2 without seriously impairing the reduction of NO to HCN. Similarly, the high NO and low HCN exhibited by methane at SR = 0.95 would indicate a slightly richer stoichiometry might improve overall TFN levels.

Coal Results

Reburning experiments were conducted for a Pittsburgh #8 bituminous coal and a North Dakota lignite with reburning conditions identical to those used for gaseous fuels. The analyses of the two coals used are given in Table 1.

Each of the coals were sieved between 200 and 270 mesh to provide a uniform particle size for feeding and to eliminate particle size considerations in comparison of results.

Char samples were collected from reburning experiments ranging from SR = 0.7 to SR = 1.0. Analysis of these samples for each coal showed no more than a statistical variation in nitrogen retained in the char. On average, lignite char retained 50% of the notrogen contained in the coal whereas bituminous char contained 58% of the original nitrogen. Apparently, reburning with these conditions involves primary devolatilization with little or no char oxidation taking place. Average data were used to determine char nitrogen with ash as a tracer.

The cumulative TFN speciation for the Pittsburgh #8 coal is shown in Figure 6. The most notable feature of this graph is that the minimum gas phase TFN occurs at SR2 = 0.85 whereas for gaseous fuels SR = 0.95 produced minimum TFN. This is reasonable if reburning is considered to be controlled primarily by homogeneous gas phase reactions. Since part of the hydrogen were retained in the solid phase as char, the gas phase stoichiometry was somewhat leaner than the overall stoichiometry.

The gas phase TFN exhibited by the Pittsburgh #8 coal appears very similar to a stretched version of the hexane distribution both in minimum TFN value and speculation. However, the retained char nitrogen added considerably to the fixed nitrogen pool and accounted for more than 65% of the total at SR = 0.85.

Lignite reburning produced more novel results as shown in Figure 7. The minimum TFN for lignite occurred at SR = 0.9 owing partially to higher volatility of combustible species. Surprisingly, reduction of NO was nearly complete for stoichiometries below SR = 0.85 achieving levels below 1 ppm. Another unusual feature is that for all stoichiometries below SR = 0.90 the gas phase TFN is totally dominated by NH_3. HCN levels never exceeded 17 ppm at any stoichiometry.

Although fuel rich combustion and pyrolysis experiments reported in the literature (eg. Chen, et al., 1982) have shown high levels of NH_3 from lignites the results presented here differ in that much of the gas phase nitrogen in these experiments did not originate in the coal. The extremely low NO and HCN levels (normally the dominant species in reburning) suggest that most of the original NO has been converted to either NH_3 or N_2. These peculiar results spanned an effort to isolate the reason for this behavior and to see if the low NO, low HCN, and high NH_3 levels were related.

Heterogeneous reactions of NO are usually discounted in reburning as too slow to be of any consequence. However, a suitable gas phase mechanism could not be found so the search was directed toward heterogeneous mechanisms. The following sequence of tests was conducted and the corresponding results given.

The effect of char addition rate on surviving NO levels with varying gas composition was studied. The char was collected from lignite reburning at SR = 0.85. First, the standard gas composition used for other reburning experiments (i.e. 16.8% CO_2, 1.95% O_2, 1000 ppm NO, balance He) was used. For reference a char feed rate of 0.029 gm/min corresponds to the char loading found in lignite reburning at SR = 0.9. The results are shown in Curve 1 of Figure 8. As the char feed rate was increased, the surviving NO levels gradually decreased and then abruptly fell to less than 10 ppm. This precipition decline was accompanied by the disappearance of measurable O_2 in the reactor effluent. This suggested competition for active sites on the char surface.

The results shown in Curve 2 of Figure 8 were obtained by replacing the O_2 in the feed gas with helium so that CO_2 remained the only oxidizer competing with NO for active sites. The elimination of O_2 had a profound effect in that very low surviving NO levels were measured with significantly reduced char feed rates. However, some competition for active sites persisted as evidenced by the reduction of CO_2 to CO when char was fed.

Finally, the effect of char on surviving NO with only NO and He in the feed gas is shown in Curve 3 of Figure 8. Eliminating the CO_2 from the feed gas further reduced the required char feed rate to the point that any char feed resulted in almost total elimination of NO from the reactor effluent.

In all of the above tests only low levels of HCN and NH_3 were formed because of the absence of available hydrogen. Also, the reaction was almost certainly heterogeneous instead of surface catalyzed gas phase since gas phase reactants were almost non existent. DeSoete (1980) gives an excellent review of possible mechanisms.

Next attention was turned to the unusually high production of NH_3 in lignite reburning. Again heterogeneous effects were suspected. To confirm this, a methane reburning experiment was conducted at SR = 0.9 with char addition at a rate of approximately 0.0194 gm/min. The results of this experiment (shown in Table 2) were very similar to those from lignite reburning. The only difference of note was the lower NO level produced by methane/char reburning because of the richer gas phase stoichiometry.

Next, lignite ash was produced by burning char in excess O_2 at 1100°C and fed with methane at SR = 0.9. Again, high levels of NH_3 were produced as shown in Table 2. However, in this experiment the surviving NO level was similar to that when reburning with methane alone. Also, the NH_3 level was almost twice that of methane/char reburning.

Since the ash contained very little carbon, the direct heterogeneous reduction of NO on carbon was eliminated. This caused more of the nitrogen to be converted to HCN as in reburning with methane alone.

In the final experiments, (shown in Table 2) NO was replaced with approximately 500 ppm of HCN in methane/char reburning. Again the final TFN distribution was weighted heavily in favor of NH_3. Although not conclusive, these tests strongly inidicate that increased NH_3 production with lignite reburning was the result of HCN conversion in an ash catalzed reaction. However, direct conversion by addition of H_2 would seem unlikely. A mechanism such as the sequence

$$\begin{aligned} HCN + OH &\xrightarrow{\text{catalyst}} HOCN + H \\ HOCN + H &\rightarrow HNCO + H \\ HNCO + H &\rightarrow NH_2 + CO \\ NH_2 + H_2 &\rightarrow NH_3 + H \end{aligned}$$

would be more plausible. In the mechanism, some of the HCN converted to NH_2 would be subsequently converted to N_2 via

$$\begin{aligned} NH + NH_2 &\rightarrow N_2H_2 + H \\ N_2H_2 + M &\rightarrow NNH + H + M \\ N_2H_2 + M &\rightarrow NNH + H_2 \\ NNH + M &\rightarrow N_2 + H + M. \end{aligned}$$

Thus the lower total fixed nitrogen found in methane/ash versus methane alone would be accounted for.

The usually strong heterogeneous and/or catalytic effects observed with lignite char are particularly interesting in light of the apparent absence of such effects with bituminous char. The reason for this disparity is not known and may be due to differences in the nature of the chars.

The lignite ash (PSOC 1507) composition as reported by the Pennsylvania State University Coal Research Section was unusually rich in calcium oxide (23.2%), barium (6570 ppm), and strontiom (4900 ppm). On the basis of concentrations alone, these seem to be the most likely candidates for catalysts.

The heterogeneous reduction of NO is most likely due to the large surface area of the very porous and friable lignite char. However, this may also be a catalytic effect. Several authors including Walker et al. (1968) have observed enhancement of char oxidation rates when the chars were impregnated with various transition metal compounds.

Conclusions

The choice of fuels has a very definite impact on the TFN speciation and minimum TFN achievable in reburning. The estimated NO concentrations after burnout for the fuels tested in this work can be calculated based on 80% conversion of gas phase fixed nitrogen and 20% conversion of char nitrogen to NO. From these calculations, it would appear that the lignite has the greatest potential in spite of its fuel bound nitrogen.

The strong hetereogeneous/catalytic activity of the lignite char could have important consequences for practical reburning enhancement. It appears that lignite char at least partially removes the current kinetic barriers in reburning

by directly converting NO to N_2 and by converting HCN to other nitrogeneous species that are more readily converted to N_2.

Addition of lignite char in methane, reburning reduced gas phase TFN by 71%. If the char could be produced with low nitrogen constant or used in smaller quantities without adversely affecting the desirable characteristics, overall TFN could be reduced to extremely low levels. Even the simple addition of lignite ash in methane reburning reduced TFN levels by 39% over methane alone. Although termperature, scale up, and mixing effects need to be studied and may impact the utility of this scheme, enhanced reburning by injection of suitable char/ash may show some promise.

Acknowledgenemts

The work reported in this paper was funded by the U.S. Department of Energy, Pittsburgh Energy Technology Center under contract No. DE-AC22-88PC88859.

References

Burch, T.E., R.B. Conway, and W.Y. Chen, "A Practical Coal Feeder for Bench-Scale Combustion Requiring Low Feed Rates", submitted to Review of Scientific Instruments, Feb., 1990.

Chen, S.L., M.P. Heap, D.W. Pershing, and G.B. Martin, "Fate of Coal Nitrogen during Combustion," Fuel, 61(12), 1218 (1982)

Chen, W.Y., T.W. Lester, L.M. Babcock, T.E. Burch, and F.R. Tillman, "Formation and Destruction of Nitrogen Oxides in Coal Combustion", Sixth Quarterly Report, DOE Contract No. DE-AC22-88PC88859, July 1989.

DeSoete, G.G., "Mechanisms of Nitric Oxide Reduction on Solid Particles", Fifth EPA Fundamental Combustion Research Workshop, Newport Beach, January, 1980.

Miller, J.A. and C.T. Bowman, "Mechanism and Modelling of Nitrogen Chemistry in Combustion", Prog. Energy Combustion Science, Vol. 15, p. 287, 1989.

Takahashi, Y., T. Sengoku, F. Nakashima, S. Kaneko, and K. Tokuda, "Evaluation of Tangential Fired Low NO_x Burner", Proc. 1982 Joint Symposium Stationary NO_x Control, Vol. 1, "EPRI Report No. CS-3182, July, 1983.

Walker, P.L., M. Shelef, and R.T. Anderson, "Catalysis of Carbon Gasification", Chemistry and Physics of Carbon, Vol. 4 (Walker, P.L., Ed.), Marcel Dekker, New York, NY, 287, 1968.

Wendt, J.O.L., C.V. Sternling, and M.A. Matovich, "Reduction of Sulfur Trioxides and Nitrogen Oxides by Secondary Fuel Injection", Fourteenth Symposium (International) on Combustion, p. 897, The Combustion Institute, 1973.

Table 1. Analysis of Coals

	Pittsburgh #8, Bituminous	North Dakota Lignite (PSOC 1507)
Moisture*	2.02	33.57
Carbon	70.48	62.61
Hydrogen	4.66	4.41
Oxygen (Diff)	8.53	18.23
Nitrogen	1.44	0.83
Sulfur	3.35	1.43
Ash	11.54	12.49
Vol. Matter	33.25	40.77
Fixed Carbon	55.21	46.75

*Moisture is reported on an as recieved basis all other results are on a dry basis.

Table 2. Total Fixed Nitrogen Speciation with Addition of Lignite Char/Ash.

Reburning Fuel	CH_4	Lignite	CH_4/char	CH_4/ash	CH_4/char
N in Feed	NO	NO	NO	NO	HCN
Concentration, ppm	1000	1000	1000	1000	500
Effluent Species					
NO, ppm	90	32	5	70	1
HCN, ppm	308	12	9	10	12
NH_3, ppm	105	135	130	227	51

Gas phase SR = 0.9 for all tests.

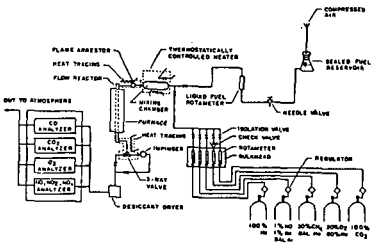

Figure 1. Schematic of experimental facility.

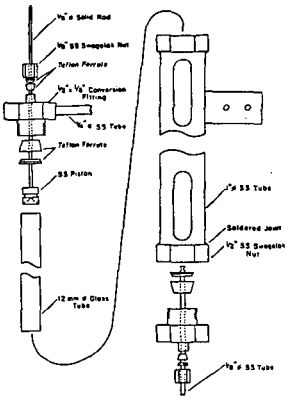

Figure 2. Exploded view of coal feeder assembly.

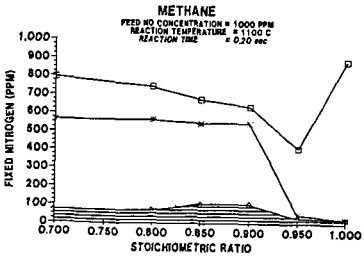

Figure 3. Cumulative total fixed nitrogen for methane reburning.

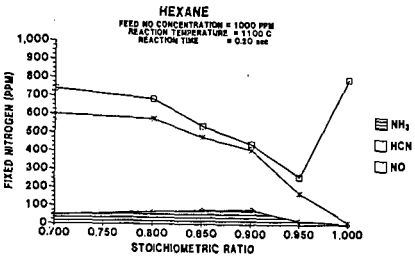

Figure 4. Cumulative total fixed nitrogen for hexane reburning.

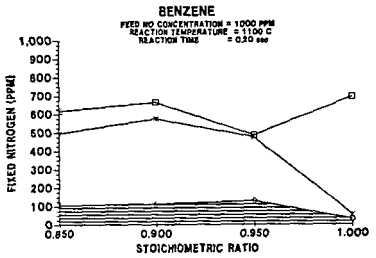

Figure 5. Cumulative total fixed nitrogen for benzene reburning.

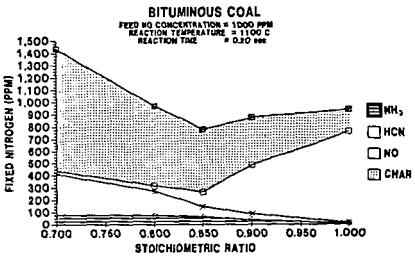

Figure 6. Cumulative total fixed nitrogen for reburning with Pittsburgh #8 bituminous coal.

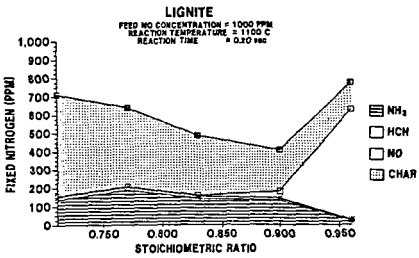

Figure 7. Cumulative total fixed nitrogen for reburning with Zap, North Dakota lignite.

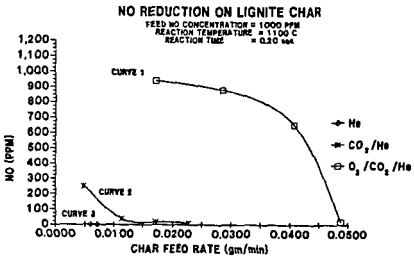

Figure 8. Influence of gas composition on heterogeneous reduction of NO with lignite char.

PROCESS DESIGN AND CHEMISTRY OF THE NOXSO PILOT PLANT DEMONSTRATION

Rita E. Bolli, John L. Haslbeck[1], B. Dwight Coffin[2], and L. G. Neil[1]

Ohio Edison Company
Environmental and Special Projects Dept.
76 South Main Street
Akron, OH 44308

[1]NOXSO Corporation, Library, PA
[2]MK-Ferguson Company, Cleveland, OH

Key Words: NOXSO, FGT (flue gas treatment), pollution (control technology).

ABSTRACT

Ohio Edison Company, NOXSO Corporation, MK-Ferguson, and W. R. Grace Co. are conducting a Proof-of-Concept (POC) test of the NOXSO flue gas treatment system at Ohio Edison's Toronto Plant in Toronto, Ohio. The project is co-funded by the U.S. Department of Energy's (DOE) Pittsburgh Energy Technology Center (PETC), the Ohio Coal Development Office and the project team. The pilot plant treats flue gas from either Boiler No. 10 or No. 11 at Toronto containing approximately 2300 ppm SO_2 and 350 ppm NO_x. The pilot plant treats a volume of flue gas equivalent to 5 MW of power production, which makes the pilot plant roughly 1/20 the size of a commercial process module. This paper presents the design and process chemistry of the pilot test facility.

Background

On May 10, 1989, a consortium consisting of Ohio Edison, NOXSO Corporation, MK-Ferguson, and W. R. Grace Co. signed a cost-shared contract with the DOE/PETC to conduct a Proof-of-Concept (POC) test of the NOXSO process. The POC project will take approximately three years to complete, and the test will be conducted at Ohio Edison's Toronto Plant at Toronto, Ohio.

POC Test Site

The POC unit will treat flue gas from either Boiler No. 10 or No. 11 at Ohio Edison's Toronto Plant. Two sources of flue gas will be tapped so that the POC test can continue as long as one of the boilers is operating. A slipstream of flue gas will be taken from either boiler in the amount of 12,000 SCFM. The slipstream will be taken downstream of the Toronto Plant's electrostatic precipitators (ESPs) which remove 99 percent of the particulate matter from the flue gas. The Toronto boilers are pc-fired and burn Ohio coal containing 3.7 percent sulfur. The flue gas typically contains 2300 ppm SO_2 and 350 ppm NO_x.

POC Test Schedule

Detailed design engineering has been completed and the major pieces of equipment have been ordered. Construction began in March 1990 and will be completed in November 1990. The test is scheduled to begin in January 1991 and will run through August 1991.

POC Process Flow Diagram

The process flow diagram for the POC is shown in Figure 1. The system is best described by following the flow of flue gas, sorbent, and regeneration gas through the process.

Flue gas will be available from either Boiler No. 10 or No. 11 at the Toronto facility and will be taken downstream of the respective ESP. The base case condition will treat 12,000 SCFM of flue gas, equivalent to approximately 5 MWe. The flue gas, once past the ESP, will enter the NOXSO flue gas treatment system. The flue gas first passes through the adsorber feed blower and then is cooled by vaporizing a water stream sprayed directly into the duct work. The cooled flue gas then passes through the fluidized bed adsorber where SO_2 and NO_x are simultaneously removed. The clean flue gas then enters a cyclone that returns entrained sorbent larger than 20 microns back to the adsorber fluid bed. Attrited sorbent smaller than 20 microns diameter will pass through the cyclone along with any flyash remaining in the flue gas, and the entire stream will pass through a baghouse for final particulate removal.

After the sorbent is to loaded with SO_2 and NO_x, it is removed from the adsorber and feeds the dense phase pneumatic conveying system. Fresh make-up sorbent is also added to the dense phase conveying system from the make-up sorbent bin. Compressed air is then used to lift the sorbent to the sorbent heater. The sorbent passes through a disengaging chamber where the lift air is separated from the sorbent. The sorbent heater is a three-stage fluidized bed where a hot air stream is passed countercurrent through the reactor raising the sorbent temperature from the adsorber temperature of 250°F to the regeneration temperature of 1220°F. During the heating process, loosely bound SO_2 and NO_x are desorbed and transported away in the heating gas stream. The hot gas stream exiting the sorbent heater passes through a cyclone which returns entrained sorbent larger than 20 microns to the top bed. Finally, the hot air is combined with the clean flue gas from the adsorber and the combined streams pass through the baghouse for final particulate removal. Alternatively, the hot air from the sorbent heater may bypass the baghouse and combine with the clean flue gas downstream of the baghouse. The combined streams are then returned to the downstream side of the plant ESP from where the gas will exit the plant stack.

Once the sorbent reaches the regeneration temperature of 1220°F, it is fed by means of a J-valve to the moving bed regenerator. The J-valve is used to both control the solid feed rate to the regenerator and to isolate the sorbent heater from the regenerator. In the regenerator, sorbent is contacted with natural gas in a countercurrent fashion. The off-gases from both sections of the regenerator are then sent to an incinerator where all the sulfur species are oxidized to SO_2. Any excess CH_4 that passes through the regenerator will also be oxidized to CO_2 and H_2O. Both combustion air and natural gas are provided to maintain the incinerator flame. The incinerator exhaust is cooled with air to 1200°F and returned to the power plant duct.

From the steam treatment vessel, the sorbent is again transferred by means of a J-valve to the sorbent cooler. The sorbent cooler is also a three-stage fluidized bed and is also operated in a countercurrent manner. Ambient air passes first through the cooling air blower and then through the three fluid beds. The warm air exiting the cooler is further heated in a natural gas-fired

air heater before being used to heat the sorbent in the sorbent heater. The sorbent temperature is reduced in the cooler to the adsorber bed temperature (248°F) and is then gravity fed to the sorbent surge bin. Finally, by means of another J-valve, the sorbent is fed from the surge bin to the adsorber completing one full cycle.

The POC facility differs from a commercial application of the NOXSO technology in two important areas. First, the POC facility does not include a Claus plant, which in the commercial design would be used to produce a sulfur by-product from the concentrated stream of SO_2 and H_2S produced in the regenerator. This is because Claus technology is commercially available and, therefore, does not require testing at pilot scale. Second, the POC does not include NO_x recycle to the coal combustor. In the commercial design, NO_x in the air leaving the sorbent heater is recycled to the combustor as part of the combustion air. Since NO_x formation in the coal combustor is a reversible reaction, addition of NO_x to the combustion air suppresses the formation of NO_x in the combustor. Since this is an important feature of the NOXSO process, the results of tests on NO_x recycle are presented in this paper. However, NO_x recycle is impractical in the POC test, since the POC treats less than 10 percent of the flue gas produced by Toronto Boiler 10 or 11.

NOXSO PROCESS CHEMISTRY

The NOXSO process chemistry is relatively simple. It involves the chemistry of adsorbing the SO_2 and NO_x pollutants and the chemistry of regenerating the sorbent for reuse using natural gas as shown below.

Adsorption

The NOXSO sorbent consists of $NaAlO_2$ on the surface of a gamma alumina substrate. Sodium aluminate adsorbs SO_2 according to the following reaction mechanism:

$$2NaAlO_2(s) + H_2O(g) \longrightarrow 2NaOH(s) + Al_2O_3(s) \quad (1)$$

Sodium hydroxide reacts with SO_2 in the flue gas as follows:

$$NaOH(s) + SO_2 \longrightarrow NaHSO_3(s) \quad (2)$$

The sodium bisulfite is subsequently converted to bisulfate in a reaction with O_2 in the flue gas with NO_x acting as a catalyst.

$$NaHSO_3(s) + 1/2\ O_2(g) \xrightarrow{NO_x} NaHSO_4(s) \quad (3)$$

The bisulfate combines with a neighboring active site to form sodium sulfate.

$$NaHSO_4(s) + NaOH(s) \longrightarrow Na_2SO_4(s) + H_2O(g) \quad (4)$$

By a similar mechanism, sodium hydroxide adsorbs NO_x from the flue gas to form NaNO2 and NaNO3.

Regeneration

Regeneration is accomplished by heating the spent sorbent in air followed by treatment with a reducing gas. The reducing gas is used solely to reduce sorbed sulfur compounds. Treatment with the reducing gas produces a mixture of sulfur compounds: SO_2, H_2S, and elemental sulfur.

The chemistry of the regeneration step is complex, involving the reduction of sodium-sulfur and alumina-sulfur compounds. Reactions involving the reduction of sodium-sulfur compounds with hydrogen are as follows:

$$Na_2SO_4(s) + Al_2O_3(s)\ H_2(g) \longrightarrow 2NaAlO_2(s) + H_2O(g) + SO_2(g) \quad (5)$$

$$Na_2SO_4(s) + Al_2O_3(s) + 4H_2(g) \longrightarrow 2NaAlO_2(s) + 3H_2O(g) + H_2S(g) \quad (6)$$

$$Na_2SO_4(s) + 4H_2(g) \longrightarrow Na_2S(s) + 4H_2O(g) \quad (7)$$

Reaction (7) above produces a sulfide which remains on the sorbent after it has been treated with the reducing gas. In tests to date, the sorbent has been treated with steam, following treatment with the reducing gas, to hydrolyze the sulfide to form H_2S according to reaction (8):

$$Na_2S(s) + Al_2O_3(s) + H_2O(g) \rightleftharpoons 2NAlO_2(s) + H_2S(g) \quad (8)$$

The product of NO_x chemisorption, in the case of both the sorbent and the alumina, is unstable at temperatures in the range 350-400°F. Therefore, the sorbent's activity toward NO_x is completely restored as the sorbent is heated to the sulfur regeneration temperature of 1220°F. The sorbent is heated with air in a fluidized bed. The concentrated stream of NO_x in air produced on heating the spent sorbent is recycled to the boiler with the combustion air.

The technical feasibility of returning the NO_x to the combustor was evaluated in two previous pilot tests. The data show that 65 percent and 75 percent of the NO_x returned to the combustor, depending upon the combustor configuration is reduced in the combustor. These tests proved that the technique is feasible although its use will result in a slightly higher equilibrium concentration of NO_x in the flue gas relative to the concentration prior to NO_x recycle.

POC TEST UNIT DESIGN

Adsorber

Internals for the POC adsorber were designed by Dr. Frederick Zenz, a noted expert in the field of fluid bed engineering. The adsorber grid (gas distributor) is a flat perforated plate containing 72,700, 1/16" diameter holes spaced 0.45" center to center on a square pitch. To ensure smooth fluidization, the grid pressure drop was set at 30 percent of the pressure drop across the sorbent bed. The grid pressure drop sets the gas velocity through the grid plate and the grid hole area (given flue gas flow rate). The size of the grid holes is predicated on the observation that holes no larger than four times the particle diameter (d_p = 1409 microns) will not weep on complete shutdown but will inevitably seal off by particle interference or blockage at the lip of the grid hole. A similar approach was used to design the grid plates in the three-staged fluid bed sorbent heater and cooler.

Sorbent is fed to the adsorber through a 6" line entering below bed level and sloped 60° for the horizontal to minimize attrition by minimizing the force of impact as sorbent particles "fall" into the bed. Sorbent leaves the bed by overflow into a 6" downcomer with a detachable section that may be changed to test different bed heights in the adsorber.

Flue gas enters the adsorber at a flow rate of 14,780 ACFM at 233°F. The chemical reactions in the adsorber are exothermic so that the adsorber bed temperature is 250°F. The superficial gas velocity in the adsorber is 2.8 ft/sec, approximately 2.4 times greater than the minimum fluidization velocity and a factor of three less than the terminal velocity of the smallest particle in the bed. At baseline conditions, the sorbent circulation rate is 9,673 pounds per hour into the adsorber. The adsorber settled bed height is two feet, and the sorbent residence time is 45 minutes.

Fluidized Bed Sorbent Heater/Cooler

A fluidized bed is used heat and cool the sorbent because of its extraordinarily effective thermal conductivity. In previous tests, a single stage fluidized bed was used. However, multistaged fluidized beds are preferred since adding more beds increases the efficiency at which the heat in gas and solids is utilized. Energy efficiency was not a primary concern in previous tests. Energy efficiency is a major concern in the POC test, since the POC unit is intended to duplicate the design of the commercial unit.

The fluidized bed internals (i.e., pipes to transport sorbent in and out, standpipes, gas distributor plates, etc.) were designed by Dr. Frederick Zenz in a manner similar to that discussed previously in connection with the fluidized bed adsorber.

Regenerator

Regeneration of the NOXSO sorbent consists of three steps: Heating to 1220°F, contacting with a reducing gas, and contacting with steam. In the first step, heating the sorbent, adsorbed NO_x is desorbed from the sorbent surface. Measurements made during the LCTU tests show that from 76 percent to 99 percent of the adsorbed NO_x was detected in the sorbent heater offgas. Within limits of measurement error, this represents complete regeneration of the sorbent with respect to NO_x.

Besides NO_x, some adsorbed SO_2 is released in the sorbent heater. Based on LCTU results, from 2.2 percent to 8.6 percent of the adsorbed SO_2 was detected in the sorbent heater offgas stream with an average of 6 percent.

After reaching the regeneration temperature of 1220°F, the sorbent is transferred from the sorbent heater to the moving bed regenerator. The adsorbed sulfur compounds are regenerated by contacting the sorbent with a reducing gas followed by steam. During the three completed test programs, H_2, CO, H_2 + CO, H_2S, and natural gas were used as the reducing gas. The offgas from the regenerator contains SO_2, H_2S, and elemental sulfur with the relative proportions dependent on the reducing gas used.

Each of the reducing gases, when coupled with steam treatment, successfully regenerated the sorbent. Natural gas required a higher temperature for regeneration (1130°F) compared to H_2 (1050°F) or H_2S (950°F). Nonetheless, natural gas was chosen as the regenerant for the POC based on economic considerations, availability, and the fact that natural gas generates the most favorable product mix for a Claus plant feed.

Sorbent residence times were determined from laboratory experiments performed at W. R. Grace and NOXSO using methane followed by steam to regenerate the sorbent in a fixed-bed reactor. The required sorbent contacting time with reducing gas was found to be 30 minutes and with steam 20 minutes. With residence time and sorbent circulation rate fixed, the regenerator inventory and hence volume can be calculated according to:

$$V = I/ = W(RT_S)/\rho$$

where V = sorbent volume, ft^3
I = sorbent inventory, lbs
ρ = sorbent bulk density, lb/ft^3
W = sorbent circulation rate, lb/hr
RT_S = sorbent residence time in regenerator, hr

THE POC regenerator consists of two distinct moving bed reactors encased in a single, cylindrical shell, four feet in diameter and approximately 40 feet high. (Note: The POC regenerator is intentionally sized larger than required to allow testing of sorbent circulation rates and residence times beyond the range of baseline conditions.) Sorbent moves through the upper section of the regenerator and into a conical section which separates the natural gas and steam treatment sections of the reactor. To guard against "rat-holing," i.e., sorbent moving through the center of the reactor faster than along the walls, the angle of the cone is 70° which is greater than the sorbent's angle of internal friction. Natural gas in fed into the conical section through a series of concentric rings hung inside the cone. The rings provide a gas space between the moving bed of sorbent and the reactor wall and serve to distribute the gas within the bed.

The rings are placed at an angle of 45° to the horizontal. The sorbent's angle of repose is 23°. Sorbent leaving the upper section of the regenerator passes through a six-inch pipe into the steam treatment section. The steam treatment section is also a cylindrical vessel with a 70° cone at the bottom. Steam is fed into the cone through a series of rings identical to those in the upper section of the regenerator.

The POC will use a dense phase lift to convey the sorbent and no valves will open or close on the sorbent.

The transport system will be a dense phase pneumatic lift that should be much less attriting than the conveying system used in previous tests. The attrition rate of 0.03 percent/hr of the fluid bed inventory gives an attrition rate at the POC of about 6 lbs/hr at base case conditions.

PROCESS SUMMARY

The NOXSO process has the following operating advantages over both existing and developing sulfur removal processes:

* Simultaneous removal of SO_2 and NO_x in a single reaction vessel.

* Produces no secondary pollution in the form of solid or liquid waste.

* Applicable to all coal types and sulfur contents.

* Completely dry process with no need for stack gas reheat.

* Cost effective when compared to conventional technology, i.e., flue gas desulfurization plus selective catalytic reduction.

* Applicable to new and retrofit installations

Figure 1
Proof-of-Concept Process Flow Diagram

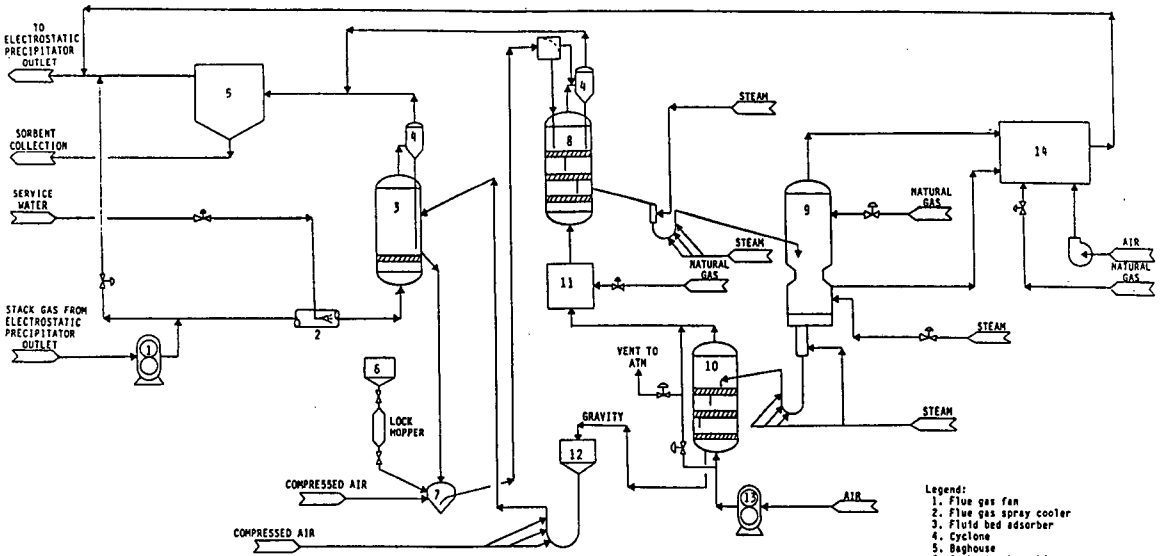

Legend:
1. Flue gas fan
2. Flue gas spray cooler
3. Fluid bed adsorber
4. Cyclone
5. Baghouse
6. Sorbent makeup bin
7. Pneumatic transport receiving hopper
8. Fluid bed sorbent heater
9. Regenerator
10. Fluid bed sorbent cooler
11. Air heater
12. Sorbent surge bin
13. Cooling air fan
14. Incinerator

COOLSIDE DESULFURIZATION DEMONSTRATION AT OHIO EDISON EDGEWATER POWER STATION

J. A. Withum, R. M. Statnick, H. Yoon, and F. P. Burke
CONSOLIDATION COAL COMPANY
Research & Development
4000 Brownsville Road
Library, PA 15120

KEYWORDS: FGD, Retrofit SO_2 Control, Duct Sorbent Injection

ABSTRACT

The Coolside Process is a duct sorbent injection process developed for retrofit SO_2 control in a coal-fired boiler. The attractive features of the process for retrofit use include low capital cost, low space requirements, and short construction time. The demonstration project was conducted on the 104 MWe Unit 4-Boiler 13 at the Ohio Edison Edgewater Power Plant, Lorain, Ohio, under a partial sponsorship of the U.S. Department of Energy (DOE) Clean Coal Technology Program. The full-scale test results confirmed the SO_2 removal capability of the process, as previously observed in pilot plant tests, and the soundness of the basic process design concept for operation in a utility environment. Additionally, the demonstration provided information on process equipment design improvements required for commercial operation.

This paper focuses on the process SO_2 removal performance observed in the demonstration. Potential research areas for improving the process performance based on the full-scale results are discussed.

INTRODUCTION

In 1986, Babcock & Wilcox, Consolidation Coal Company (Consol), the State of Ohio Coal Development Office, and Ohio Edison Company, under the sponsorship of the DOE Clean Coal Technology Program, agreed to demonstrate the Coolside and LIMB processes at the Ohio Edison Edgewater Station. The demonstration of the Coolside process was conducted from late July 1989 to mid-February 1990, using compliance (1.4 wt % S) and non-compliance (3 wt % S) bituminous coals from Ohio (Table 1). The objectives of the full-scale program were to verify the process performance in regard to short-term operability and SO_2 removal, to determine factors which could affect long-term operations, and to develop a data base to establish process economics and design parameters. The demonstration program included sorbent once-through and sorbent recycle operations. Key process variable effects were evaluated in short-term (6-8 hr) parametric tests and longer-term (1-14 day) process operability tests. Two different hydrated limes (Table 2) were tested. Prior to the demonstration, pilot-scale tests were conducted to select the hydrated limes to be tested and to develop process performance data applicable to the Edgewater site-specific conditions. The pilot data were used for demonstration program planning and data interpretation. This paper discusses full-scale Coolside desulfurization results at the Edgewater Station Unit 4-Boiler 13 in Lorain, Ohio. The discussion of the results is limited to the observations from once-through process tests. Recycle process tests (in which a portion of the collected ash is reinjected into the flue gas to increase overall sorbent utilization) were performed but the data are not included here because data analysis was not completed at the time this paper was written. Coolside pilot-scale process performance (1-5) and full-scale design and operation (6) were described elsewhere.

PROCESS DESCRIPTION

Coolside desulfurization technology involves dry injection of hydrated lime into the flue gas downstream of the air preheater and flue gas humidification by water sprays (Figure 1). SO_2 is captured by reaction with the entrained sorbent particles in the humidifier and by the dense sorbent bed collected in the particulate removal system. The humidification water serves a dual purpose. First, it activates the sorbent to enhance SO_2 removal and, second, it conditions the flue gas and particulate matter to maintain efficient electrostatic precipitator (ESP) performance. Spent sorbent is removed from the gas along with fly ash in the existing particulate collector (ESP or baghouse). The sorbent activity can be significantly enhanced by dissolving sodium hydroxide (NaOH) or sodium carbonate (Na_2CO_3) in the humidification water (3-5). Sorbent recycling can be used to improve the sorbent utilization if the particulate collector can handle the resulting increased solids loading. For reasons of convenience and cost, NaOH was used as the additive in the Edgewater demonstration.

EDGEWATER HUMIDIFIER DESCRIPTION

The Edgewater equipment and process operations were described in detail elsewhere (6). Because humidification is crucial to the Coolside process, a short description of the Edgewater humidifier follows. The Edgewater humidifier was designed to avoid forming wet deposits on the walls. Figure 2 shows a drawing of the humidifier and the ductwork connecting it to the existing plant equipment. The humidification chamber was erected on the roof of the boiler house. Its dimensions were 14-feet 7-inches x 14-feet 7-inches, and 56-feet long. A 10 x 10 array of Babcock & Wilcox Company Mark 12 atomization nozzles at the humidifier entrance provided the fine water sprays for the flue gas humidification. The hydrated lime injector ports were located at the same vertical plane as the atomizer array. The humidifier was designed for a flue gas flow rate of one million pounds per hour, which gives about a 2.5 second humidifier residence time. However, air in-leakage through the air preheater resulted in a higher-than-design flue gas rate (1.3 million pounds per hour at full boiler load of 104 MWe). This increased flow necessitated that, at full load, a portion of the flue gas by-pass the humidification chamber. The original plant ductwork between the air preheater and the ESP was used for the flue gas by-pass. The data reported here, however, are only from tests at lower load in which all of the flue gas passed through the humidification chamber.

Thermocouples to measure flue gas temperature were located at the humidifier inlet and exit and at the ESP inlet. Humidification was controlled by varying the water flow rate to maintain a preset humidifier outlet temperature based on the thermocouples located at the humidifier exit. The flue gas was continuously monitored at the humidifier inlet and the ESP exit (stack) for SO_2 and O_2.

PROCESS DESULFURIZATION PERFORMANCE

Desulfurization Performance Overview

The Edgewater program demonstrated that the Coolside process can routinely achieve up to 70% SO_2 removal at the design conditions of 2.0 Ca/S and 0.19 Na/Ca molar ratios and 20°F approach to adiabatic saturation temperature using a commercial hydrated lime (Lime A). Use of an alternate hydrated lime (Lime B) gave somewhat lower SO_2 removals, as did a 25°F approach; these effects will be discussed in detail later in this paper. A range of SO_2 removals between 30 and 70% was achieved by controlling the Ca/S and Na/Ca molar ratios and the approach to adiabatic saturation temperature. The SO_2 removals measured in these tests were confirmed by ash analysis results, as discussed in a later section. The SO_2

removal results were consistent with projections based on Consol 0.1 MWe pilot plant and 1 MWe field test data.

Sorbent once-through utilizations of up to 35% were observed. This indicates that there is room for significant process improvement if the sorbent utilization can be increased through process optimization, including sorbent recycle. When calculating sorbent utilization, NaOH is included as a co-sorbent since it also captures SO_2 as Na_2SO_3 or Na_2SO_4.

The process was operated round-the-clock. During most operations, the ESP was able to handle the increased solids loading resulting from the sorbent injection and kept the flue gas opacity level below 5%. The acceptable performance of the ESP was largely the result of flue gas humidification. Without humidification, the ESP would not have been able to handle the increased solids loading and particle resistivity caused by sorbent injection (7).

Variable Effects

Ca/S Ratio. The data obtained at Edgewater show an increase in SO_2 removal with Ca/S ratio for the two hydrated limes tested (Figure 3). The SO_2 removal using hydrated lime B at 23 to 26°F approach to adiabatic saturation are shown as squares, while the removals using hydrated lime A are shown as crosses for tests at 23 to 26°F approach, and as circles for 19 to 22°F approach to adiabatic saturation. No tests were performed using hydrated lime B at 19 to 22°F approach because, by this point in the test program, the humidification performance had deteriorated to the point where operation at 20°F set point caused the formation of large droplets, leading to wet deposits formation at the humidifier outlet. Using hydrated lime A, SO_2 removals were 40, 50 and 70% at average Ca/S molar ratios of 1.1, 1.4 and 2.0, respectively. The process conditions were 19 to 22°F approach to adiabatic saturation; 0.17 to 0.24 Na/Ca molar ratio; and coal sulfur content between 2.0 to 2.8 wt %. The SO_2 removals with hydrated lime B showed a similar trend, although they were lower than those with hydrated lime A. Although the observed SO_2 removals at similar Ca/S ratios had some variation, Figure 3 clearly shows the trend of higher SO_2 removals at higher Ca/S ratios. The Ca/S ratio is an important process variable to maintain SO_2 removal at a desired level. As was shown in pilot plant (4,5) and other field tests (1), SO_2 removal increases in a predictable manner with increasing Ca/S ratio.

The SO_2 removals were calculated from the SO_2 concentrations measured at the humidifier inlet and ESP outlet using continuous gas analyzers which were corrected to dry, excess-air-free conditions. Corrections for air in-leakage were made using continuous oxygen analyzer data collected at both locations. The moisture content was calculated based on measured wet bulb and dry bulb temperatures. The Ca/S ratio was calculated based on the measured SO_2 concentration in the flue gas entering the humidifier, the measured flue gas flow rate into the humidifier, and the measured hydrated lime feed rate to the humidifier.

Approach to Adiabatic Saturation Temperature. At a constant Ca/S and Na/Ca molar ratio, SO_2 removal was higher when the process was operated at closer approach to adiabatic saturation (or wet bulb) temperature. The effect of only a few degrees variation in the approach to adiabatic saturation can be observed by comparing the circles (19 to 22°F approach) with the crosses (23 to 26°F approach) in Figure 3. This comparison shows that, at equivalent Ca/S ratios, the observed SO_2 removals were 6 to 10 percentage points (absolute) higher in the tests at 19 to 22°F approach than in tests at 23 to 26°F approach over the range of Ca/S ratios in the figure. The effect of larger variation in the approach to adiabatic saturation is given by Figure 4, which shows SO_2 removal as a function of the approach to the

adiabatic saturation temperature using hydrated lime A at Ca/S molar ratios of 1.4 and 2.0; the Na/Ca molar ratio was 0.17 to 0.24. Although some variation occurred in the observed SO_2 removals at similar approach temperatures, the data demonstrate that the SO_2 removal is higher at closer approaches to adiabatic saturation temperature.

Variations in the approach to adiabatic saturation were not intended as part of the demonstration test program. The variations shown in Figure 4 occurred for two reasons. First, the approach varied because of variations in the humidifier exit temperature from the control point and some fluctuations in the flue gas wet bulb temperature. Second, the set point for the approach was increased from 20 to 25°F during the tests with lime A. This change was necessary because of the change in the humidifier performance.

Na/Ca Ratio. At constant Ca/S and approach to adiabatic saturation, the SO_2 removal was higher when NaOH was added to the humidification water. Using hydrated lime A at a 2.0 Ca/S molar ratio and 23 to 26°F approach to adiabatic saturation temperature, SO_2 removals were 60 to 65% in tests with additive (0.19 Na/Ca molar ratio) but only 35 to 45% in tests without additive. Since NaOH additive significantly enhances SO_2 removal, and demonstration of maximum SO_2 removal was the project goal, tests without NaOH were limited. Thus, no data were obtained at 1.0 Ca/S without additive, nor were data obtained at higher approaches without additive. The effect of sodium additive on SO_2 removal performance was established in previous pilot plant studies (3-5). The full-scale results were in good agreement with pilot data on the additive effect.

Effect of Different Hydrated Limes. Hydrated lime A gave higher SO_2 removals than hydrated lime B at similar process conditions. This is shown for the conditions 0.17 to 0.24 Na/Ca molar ratio and 23 to 26°F approach to adiabatic saturation temperature by comparing the crosses (Lime A) with the squares (Lime B) in Figure 3. This comparison shows that, at equivalent Ca/S ratios, the observed SO_2 removals were 5 to 10 percentage points (absolute) higher when using hydrated lime A than when using hydrated lime B over the range of Ca/S ratios in the figure. These results are consistent with pilot plant results that showed higher SO_2 removals when using hydrated lime A than when using hydrated lime B (5). Both are high calcium (>88% $Ca(OH)_2$ by wt) hydrated limes. Differences in physical properties, such as surface area, may have contributed to the performance differences. The BET surface areas were 22 to 24 m^2/g for hydrated lime A and 15 to 18 m^2/g for hydrated lime B. Previously reported work showed a correlation between sorbent surface area and SO_2 removal performance (5).

Comparison with Pilot Plant and Field Tests

In preparation for the demonstration tests at Edgewater, Consol conducted pilot plant tests on a 0.1 MWe scale and a 1 MWe scale. Figure 5 compares the SO_2 removals at Edgewater with those observed in the 0.1 MWe pilot plant (4,5) and 1 MWe field tests (1) for the conditions of 2.0 Ca/S and 0.19 Na/Ca molar ratios. The data shown from the Edgewater and the 1 MWe field tests were from tests at 20°F approach; the data from the pilot plant were from tests at 25°F approach to adiabatic saturation. The sorbent was hydrated lime A for the Edgewater and pilot plant data and a third lime, hydrated lime C for the field test data. In pilot plant tests, the SO_2 removals using hydrated lime C were about 5 to 10% (relative) lower than those using hydrated lime A (5). The 70% SO_2 removal achieved at Edgewater compares well with the 75% SO_2 removal observed in the 1 MWe field tests. In both of these tests, an ESP was used for particulate control. These removals were lower than the 85% SO_2 removal observed in pilot plant tests. However, a baghouse was used for particulate collection in the pilot plant. Because a

baghouse provides more effective gas-sorbent contact than an ESP, the SO_2 removals were expected to be somewhat lower at Edgewater than in the pilot plant tests. These results, along with the consistency in the variable effects of the pilot and Edgewater tests, as discussed above, indicate that the 0.1 MWe pilot plant unit is a reliable device for simulating process performance, for evaluating improved sorbents, or for conducting site-specific simulations.

In addition to the difference in the particulate removal device, differences in other design/operating factors of the Edgewater Coolside system from the pilot plant may have affected the comparison of SO_2 removal performances at Edgewater and at the pilot plant. These factors include water droplet size distribution, water droplet and hydrated lime distributions in the gas, and flue gas velocity and flow distribution. However, the effects of these differences on SO_2 removal were not quantifiable from the current Edgewater data.

Edgewater Data Reliability

Table 3 compares the sorbent utilizations based on the sulfur, Ca, and Na contents of the ESP hopper samples with the sorbent utilizations calculated from the process run data for tests using hydrated lime A. Samples also were taken during tests using hydrated lime B, but the analyses were not completed when this paper was written. The average difference between the two methods was 0.87% (absolute). This agreement is good, considering the relatively small size of the ESP samples (50-100 lbs) taken from a single ESP hopper, of which 100 grams was submitted for analysis, compared with the large amount of solids (2 to 10 tons/hr) collected by the ESP which had a total of twelve hoppers. A standard statistical F Test (8) on the data in Table 3 shows that the differences between the results of the two methods of determining sorbent utilization were not significant. Using the twelve process runs and the two methods of determining utilization in Table 3 as the sources of variance, the F-number for the method variance/residual variance was 0.87 for 1/11 degrees of freedom. This indicates that the probability that the two methods gave truly different results was not significant.

Directions for Desulfurization Performance Improvement

Since the observed sorbent utilization is low (25-35%), there is a significant potential for improving process economics by optimizing the process design for maximum SO_2 removal efficiency. Process optimization is possible in several areas. Improved dispersion of the sorbent in the flue gas may improve the SO_2 removal. Sorbent recycle, involving reinjection of spent sorbent recovered from the ESP, offers a straightforward means of enhancing the sorbent utilization as long as the ESP and the waste handling system installed in the plant can handle the increased solids loading. Sorbent recycle tests were performed during the Edgewater demonstration, but the data analysis was not completed at the time this paper was written.

In the longer term, optimization of the sorbent (hydrated lime) properties for SO_2 capture is expected to lead to an improved sorbent. Pilot plant tests have shown a positive correlation of hydrated lime surface area with sorbent utilization. Lime hydration methods that produce high surface area hydrates are being studied at Consol R&D (9) and elsewhere (10). Additive incorporation during lime hydration also may provide more reactive sorbents (2,11).

CONCLUSIONS

The Edgewater Coolside testing demonstrated SO_2 removals up to 70% in an electric utility boiler burning an eastern United States high-sulfur coal.

- Sorbent utilizations at these SO_2 removals were typically 30 to 35%. The spent sorbent analyses confirmed the sorbent utilizations based on the continuous flue gas analyzers.
- The full-scale SO_2 removals were similar to pilot-scale SO_2 removals. This indicates that appropriate pilot-scale tests are a good predictor of full-scale performance for this technology.
- As observed in the pilot-scale tests, the process SO_2 removal depends on the primary process variables: Ca/S and Na/Ca molar ratios and the approach to adiabatic saturation.
- Differences in the hydrated lime affect the SO_2 removal level.

LEGAL NOTICE/DISCLAIMER

This report was prepared by Consolidation Coal Company, pursuant to a contract with Babcock & Wilcox Company. This report was prepared in accordance with a cooperative agreement partially funded by the U.S. Department of Energy, and neither Babcock & Wilcox Company, nor any of its subcontractors nor the U.S. Department of Energy, nor any person acting on behalf of either: a) makes any warranty or representation, express or implied, with respect to the accuracy, completeness, or usefulness of the information contained in this report, or that the use of any information, apparatus, method, or process disclosed in this report may not infringe privately-owned rights; or b) assumes any liabilities with respect to the use of, or for damages resulting from the use of, any information, apparatus, method or process disclosed in this report.

Reference herein to any specific commercial product, process, or service by trade name, trademark, manufacturer, or otherwise, does not necessarily constitute or imply its endorsement, recommendation, or favoring by the U.S. Department of Energy. The views and opinions of authors expressed herein do not necessarily state or reflect those of the U.S. Department of Energy.

REFERENCES

1. Yoon, H.; Ring, P.A.; Burke, F. P. "Coolside SO_2 Abatement Technology: 1 MW Field Tests". Proceedings, Coal Technology '85 Conference, Pittsburgh, PA, November 1985; Vol. V, pp 129-151.
2. Yoon, H; Stouffer, M. R.; Rosenhoover, W. A.; Statnick, R. M. "Laboratory and Field Development of Coolside SO_2 Abatement Technology". Proceedings, Second Annual Pittsburgh Coal Conference, Pittsburgh, PA, September 1985; pp 235-236.
3. Withum, J. A.; Rosenhoover, W. A; Yoon, H. "A Pilot Plant Study of the Coolside Desulfurization Process with Sorbent Recycle". Proceedings, Fifth Annual Pittsburgh Coal Conference, Pittsburgh, Pa, September 1988; pp 84-96.
4. Yoon, H; Stouffer, M. R.; Rosenhoover, W. A.; Withum, J. A.; Burke, F. P. "Pilot Process Variable Study of Coolside Desulfurization". *Environmental Progress* **1988**, *7*(2), 104-111.
5. Stouffer, M. R.; Rosenhoover, W. A; Yoon, H. "Pilot Plant Process and Sorbent Evaluation Studies for 105 MWe Coolside Desulfurization Process Demonstration". Third International Conference on Processing and Utilization of High Sulfur Coals, Ames, IA, November 1989; paper A-52.
6. Kanary, D. A.; Statnick, R. M.; Yoon, H.; McCoy, D. C.; Withum, J. A.; Kudlac, G. A. "Coolside Process Demonstration at the Ohio Edison Company Edgewater Unit 4-Boiler 13". Proceedings, 1990 EPA/EPRI SO_2 Control Symposium, New Orleans, LA, May 1990.
7. Fink, C. E.; McCoy, D. C.; Statnick, R. M. "Flue Gas Humidification With Boiler Limestone Injection for Improved ESP Performance and Increased SO_2 Removal". Proceedings, Coal Technology '85 Conference, Pittsburgh, PA, November 1985.

8. Miller, R. E. "CE Tutorial: Statistics. 4. Means and Variances". *Chemical Engineering* **1985**, 107-110.
9. Withum, J. A.; Yoon, H. "Treatment of Hydrated Lime with Methanol for In-Duct Desulfurization Sorbent Improvement". *Environmental Science and Technology* **1989**, *23*(7), 821-827.
10. Moran, D. L.; Rostam-Abadi, M; Harvey, R. D.; Frost, R. R.; Sresty, G. C. "Sulfur Dioxide Sorption Reactivity of Hydrated Lime: Effect of Hydration Method". *Prepr., Div. Fuel Chem., Am. Chem. Soc.* **1987**, *32*(4), 508-516.
11. Yoon, H.; Withum, J.A.; Rosenhoover, W. A.; Burke, F. P. "Sorbent Improvement and Computer Modeling Studies for Coolside Desulfurization". Proceedings, Joint Symposium on Dry SO_2 and Simultaneous SO_2/NO_x Control Technology, Raleigh, NC; U.S. Environmental Protection Agency. U.S. Government Printing Office: Washington, DC, 1986; EPA-600/9-86-029b.

TABLE 1

TYPICAL COAL ANALYSES*

		Proximate Analysis			Ultimate Analysis					
Coal	Btu/lb	Moisture	Volatile Matter	Fixed Carbon	Ash	C	H	N	S	O (by diff.)
Compliance	13204	4.18	34.75	54.74	10.51	74.48	4.92	1.39	1.42	7.29
Non-Compliance	12695	4.12	37.98	48.91	13.11	70.72	4.88	1.25	3.02	7.02

*All analyses except moisture are wt % dry basis.

TABLE 2

TYPICAL HYDRATED LIME ANALYSES

Hydrated Lime	BET Surface Area, m^2/g	TGA Data, dry wt %	
		$Ca(OH)_2$	$CaCO_3$
A	23.2	93.0	2.5
B	16.7	88.0	2.5

TABLE 3

COMPARISON OF ESP ASH ANALYSES AND PROCESS RUN DATA

			% Sorbent Utilization Based on		
Ca/S (mol)	Na/Ca (mol)	% SO_2 Removal	SO_2 Removal, Ca/S and Na/Ca*	Ash Analysis**	Difference
1.56	0.00	41.1	26.3	30.0	-3.7
1.89	0.19	58.6	28.3	22.9	5.4
1.21	0.28	46.9	33.9	34.6	-0.7
1.29	0.17	44.7	32.5	31.8	0.7
1.45	0.18	52.7	34.2	32.3	1.9
1.45	0.18	53.7	34.9	33.8	1.1
1.40	0.21	48.2	32.0	33.0	-1.0
2.05	0.23	57.8	26.7	29.2	-2.5
1.49	0.11	45.7	29.6	24.7	4.9
1.96	0.23	60.8	29.2	32.9	-3.7
1.03	0.00	29.1	28.3	21.4	6.9
2.17	0.00	27.1	12.5	11.4	1.1
Average					0.87

* $\frac{\%\ SO_2\ \text{Removal}}{Ca/S + 0.5\ (Na/S)}$

** $\frac{\text{Total Sulfur}/32}{CaO/56 + Na_2O/62}$, CaO and Na_2O corrected for calcium and sodium in coal ash

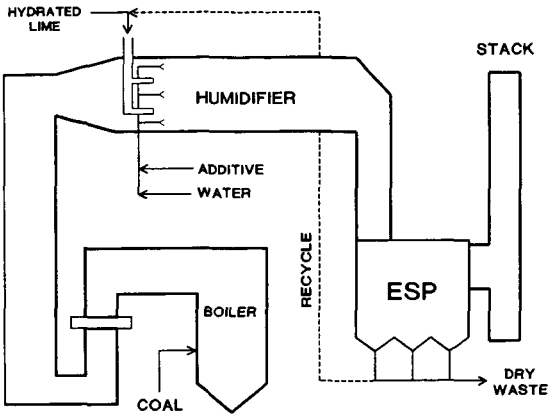

Figure 1. Coolside Process Schematic..

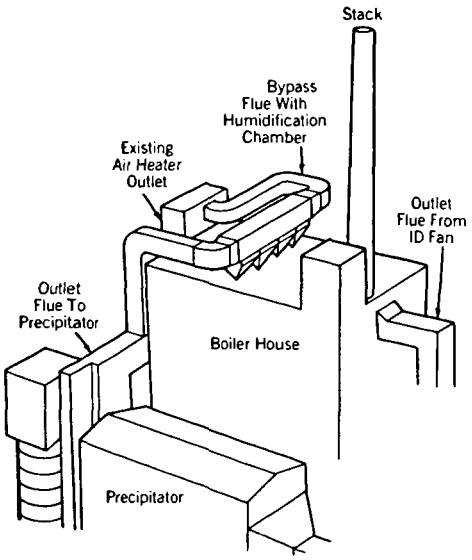

Figure 2. Edgewater Coolside Demonstration Process Equipment Layout.

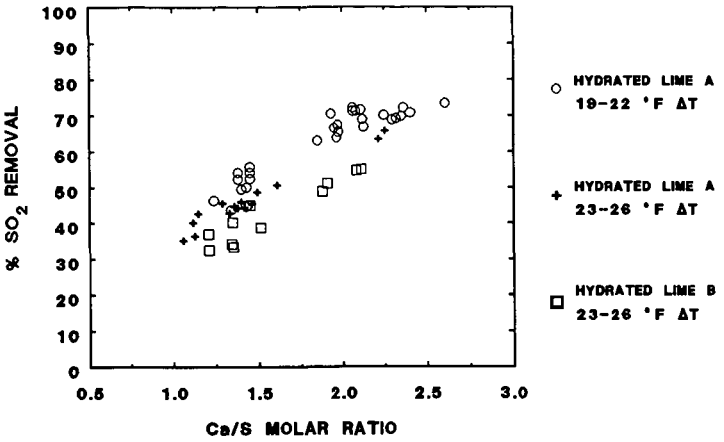

Figure 3. SO_2 Removal vs Ca/S Ratio. These data were obtained at a nominal Na/Ca mol ratio of 0.19. ΔT is the approach to adiabatic saturation at the humidifier outlet.

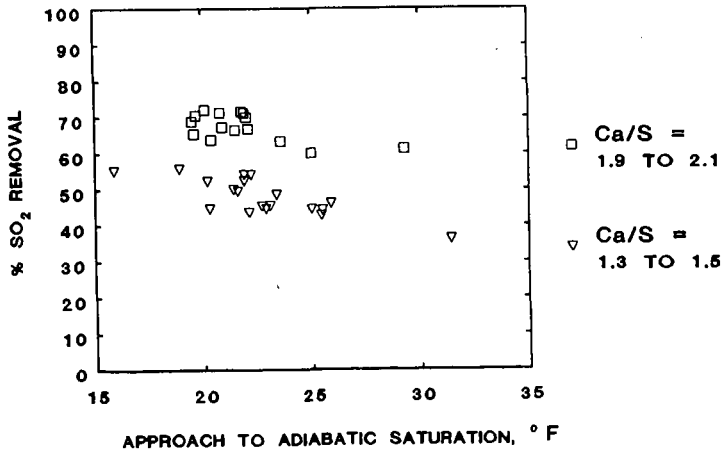

Figure 4. SO_2 Removal vs Approach to Adiabatic Saturation for Operation With Hydrated Lime A. The Na/Ca molar ratio was 0.17-0.24 in these tests.

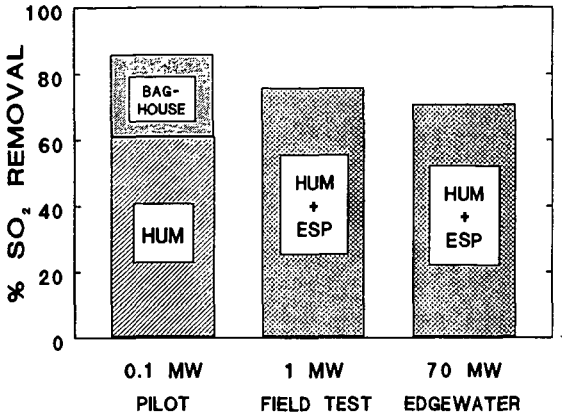

Figure 5. Comparison of Pilot, Field and Demonstration Test SO_2 Removal Performance: Ca/S - 2 mol ratio, Na/Ca = 0.19 mol ratio, 20-25°F approach to adibatic saturation.

EVALUATION OF CALCIUM COMPOUNDS AS SORBENTS FOR IN-SITU DESULFURIZATION WITH TEXACO COAL GASIFICATION PROCESS

Mitri S. Najjar and Dick Y. Jung
Texaco Inc.
P. O. Box 509
Beacon, NY 12508

Keywords: in-situ desulfurization; coal gasification; calcium

SUMMARY

The feasibility of using calcium-based compounds as potential sulfur-capturing sorbents for in-situ desulfurization in combination with partial oxidation of coal in a slagging mode was examined using thermodynamic calculations and bench-scale experimental tests. Although pure calcium compounds are excellent sorbents for capturing sulfur, problems may be encountered when other compounds which are commonly found in coal slags are present. Under the simulated reaction conditions used in Texaco coal gasifiers, calcium compounds were found to preferentially react with the silicates commonly found in coal slags rather than capture sulfur.

INTRODUCTION

To utilize coal in an environmentally safe manner, it is necessary to remove the gas phase sulfur compounds released during the combustion and/or gasification of coal. In recent years, integrated gasification-combined cycle (IGCC) processes have been demonstrated which gasify coal to produce synthesis gas (syngas) which is fired in a turbine to generate electrical power. Typically, these processes separate the reaction step (where coal is converted to raw syngas under reducing conditions at high temperatures) from the acid gas removal step (where physical solvents are generally used to scrub hydrogen sulfide and carbonyl sulfide from the crude syngas). This approach requires significant capital investments as well as operating utility costs since the hot syngas must be cooled to the low temperatures commonly needed for physical solvents and subsequent reheated prior to its introduction into the gas turbine.

A potentially more efficient alternative is to combine coal combustion with the sulfur removal step in the same vessel. However, the solubility of sulfur in coal slags is quite low (typically between 0.01 and 0.5 weight percent). One possible approach to enhance sulfur solubility in coal slags is the addition of sulfur-capturing sorbents along with the coal feed to the gasifier. The ideal sorbent should be an inexpensive additive that chemically reacts with the sulfur compounds in the gas (primarily hydrogen sulfide with smaller amounts of carbonyl sulfide) to form a disposable sulfide that is encapsulated in the resultant slag but this additive should not cause any complications for slag flow from the gasifier.

Although calcium-based compounds have been commercially used in fluidized bed combustion to perform in-situ desulfurization,

only bench scale work has been reported using these potential sorbents to study high temperature desulfurization in conjunction with an entrained bed coal gasifier. It was hoped that the sulfur from the gas phase would be captured in the slag as calcium sulfide under the reducing atmosphere commonly found in these coal gasifiers. Whitney, et al.[1] have suggested that the use of concentrated coal-water slurries mixed with finely divided lime (CaO) or limestone ($CaCO_3$) represents a promising avenue for coal conversion with simultaneous sulfur capture but they reported evidence of mass transfer limitations. Freund and Lyon[2] performed thermodynamic calculations that indicate a range of attainable conditions where high levels of sulfur capture could be achieved for fuel-rich combustion of coals containing calcium-based sorbents. However, they also point out that even though the thermodynamics of sulfur sorption may be favorable, there are no assurances that the kinetics will be fast enough for practical use. In addition, neither group of researchers consider the interactions among calcium compounds and other components in the coal slag (such as aluminosilicates) or the effect of these additives on slag removal from the gasifier. To explore the possibility of using calcium-based compounds to capture sulfur in the more reducing atmosphere typically found in Texaco coal gasifiers with coal-water slurry feeds operating in a slagging mode, theoretical thermodynamic calculations as well as bench scale drop tube furnace equilibrium experimental runs were performed.

METHODS

Calculations

Thermodynamic equilibrium calculations were performed using a multiphase free energy minimization computer program by an in-house version of SOLGASMIX[3] augmented with additional thermodynamic data[4]. The systems considered in this study include calcium compounds alone as well as with inorganic species (e. g. silicon-, iron- and aluminum-based compounds) commonly found in coal slags under simulated syngas compositions expected in Texaco coal gasifiers with coal-water slurry feeds operating in a slagging mode.

Experiments

To validate these equilibrium predictions, bench scale drop tube furnace equilibrium experiments were performed for selected coal slag-additive systems. These tests were conducted at atmospheric pressure using temperatures and gas compositions selected to simulate gasifier conditions using the apparatus shown schematically in Figure 1. The principal units for high temperature testing are two identical LeMont Scientific quench furnaces capable of reaching 3000°F. Samples of the slag and sorbent (50-100 mg) were placed in a crucible that is suspended in the furnace by a thin platinum wire which is then equilibrated by exposure to a flowing gas mixture for at least 18 hours. Gaseous mixtures of CO, CO_2 and 1 vol %SO_2 in Argon were selected to simulate the S_2 and O_2 partial pressures at the desired temperatures and ambient pressure based on the thermodynamic equilibrium calculations using an in-house version of SOLGASMIX[3]. The suspended slag-sorbent sample was then rapidly quenched by dropping the crucible into a pool of water or simulated syngas. This was

accomplished by passing an electrical current through the suspending platinum wire which causes the wire to break.

The quenched sample was recovered and characterized by petrographic examination using a Leitz Orthoplan microscope and electron microprobe analysis. An Amray 1645 scanning electron microscope equipped with secondary and backscattered electron detectors for imaging as well as a Tracor Northern TN-5500 energy dispersive X-ray microanalysis system with 40 MByte data storage capacity and color display were used to obtain SEM photomicrographs to show phase morphologies as well as EDX multielement semiquant chemical analysis to confirm phase identifications.

RESULTS

Equilibrium calculations based on the calcium oxide/calcium sulfide system with simulated syngas from a Texaco coal gasifier initially looked quite promising for sulfur capture. Phase diagrams indicate that calcium sulfide (in the absence of other coal slag compounds) is stable over the temperature range as well as oxygen and sulfur partial pressures commonly expected in Texaco coal gasifiers. The calculations suggest that in-situ sulfur capture with calcium (when there is no interactions with the coal slag) is favored by lower temperatures and/or more reducing conditions.

However, when other compounds from the coal slag are incorporated into these calculations, the situation is now altered. For example, if silica (SiO_2) is added to this calcium oxide/sulfide system, new phases[5] must now be taken into account which form via chemical reactions. Consider $CaSiO_3$ which is formed by the following reaction:

$$CaS + SiO_2 + \frac{1}{2} O_2 = CaSiO_3 + \frac{1}{2} S_2 \qquad (1)$$

Note CaS is now stable only below the CaS-SiO_2-$CaSiO_3$ region shown in Figure 2. The now smaller CaS stability region would translate into a reduced sulfur capture for this system in comparison to the system without silica added. Note that a much lower oxygen partial pressure is now needed for a stable CaS phase which may not be possible for a Texaco coal gasifier with a coal-water slurry feed operating in a slagging mode. If one now further considers the addition of iron and aluminum compounds (which are commonly found in most coal slags) to this system, the situation becomes even more complex with a plethora of new phases that must now be considered. A sample calculation result is shown in Table 1 which indicates that with even a relatively high calcium additive loading, most of the calcium is predicted to appear in various aluminosilicate compounds rather than the desired CaS under oxygen and sulfur partial pressures expected in Texaco coal gasifiers. Hence, calcium would be a less effective sorbent for sulfur capture under these conditions.

To qualitatively confirm these predictions, bench scale equilibrium drop tube furnace runs were performed using simulated oxygen and sulfur partial pressures selected to match those expected in Texaco coal gasifiers. The EDX semiquant chemical analyses for several silicate phase grains from these experimental runs are listed in Table 2. Note that the sulfur content for these silicate particles is relatively low even though the calcium and silicon content were relatively high. No calcium sulfide grains were identified. Hence, these experimental data support the

prediction that under the simulated syngas conditions for a Texaco coal gasifier with a coal-water slurry feed operating in a slagging mode, calcium compounds preferentially react with the silicate compounds in the coal slag rather than the sulfur compounds in the gas phase.

CONCLUSIONS

The feasibility of adding calcium-based compounds as potential sulfur capturing sorbents during coal gasification is being examined using theoretical equilibrium calculations as well as bench scale equilibrium drop tube furnace experiments. Although it is predicted that calcium-based compounds can be effective agents for desulfurization when used alone under simulated syngas conditions commonly encountered in Texaco coal gasifiers with a coal-water slurry feed operating in a slagging mode, thermodynamic calculations suggest calcium compounds can preferentially interact with other common coal slag components, especially the silicates, which limit their usefulness as in-situ sulfur sorbents during coal gasification. EDX semiquant chemical analyses for silicate phase grains obtained from experimental bench scale equilibrium drop tube furnace runs are presented which are consistent with these predictions.

ACKNOWLEDGEMENTS

The authors gratefully acknowledge financial support for this work under the five year Texaco/Department of Energy Cooperative Program (Contract No. DE-FC21-87MC23277) on "Integration and Testing of Hot Desulfurization and Entrained Flow Gasification for Power Generation Systems" with METC's Dr. J. Beeson as Contract Manager. Uygur Kokturk assisted in designing and troubleshooting the bench scale drop tube furnace units. Ron McKeon performed most of the experimental runs while Tris Laurion provided EDX analyses of the slag samples.

REFERENCES

1. G. M. Whitney, Z. Yunming, M. M. Denn and E. E. Petersen, "Sulfur Capture during Partial Coal Combustion", Chem. Engineering Comm., 55 (1987) 83-93.
2. H. Freund and R. K. Lyon, "The Sulfur Retention of Calcium-Containing Coal during Fuel-Rich Combustion", Combustion and Flame, 45 (1982) 191-203.
3. G. Eriksson, Acta Chem. Scand., 25 (1971) 2651.
4. R. A. Robie, B. S. Hemingway and J. R. Fisher, "Thermodynamic Properties of Minerals and Related Substances at 298.15 K and 1 Bar (10^5 Pascals) Pressure and at Higher Temperatures", U. S. Geological Survey Bulletin 1452, U. S. Government Printing Office, Washington (1979).
5. J. W. Larimer, "An experimental investigation of oldhamite, CaS; and the petrologic significance of oldhamite in meteorites", Geochimica et Cosmochimica Acta, 32 (1968) 965-82.

TABLE 1
Calculated equilibrium compositions at 1600 K (2420 F) and 38 atm. to check for stable phases in a system with coal slag and calcium additive under simulated Texaco coal gasifier syngas conditions

GAS PHASE COMPOSITION

Gases	Mole Fraction	Mole	Partial Pressure (atm)
CO	0.410	0.687	15.6
CO_2	0.0987	0.165	3.75
H_2	0.278	0.466	10.6
H_2O	0.199	0.334	7.58
COS	1.38E-04	2.32E-04	5.26E-03
H_2S	2.79E-03	4.67E-03	0.106
O_2	5.98E-13	1.00E-12	2.27E-11
N_2	0.0102	0.0170	0.386
SO_2	2.52E-07	4.21E-07	9.56E-06

EQUILIBRIUM SOLID PHASES

Solid	Mole	Solid	Mole	Solid	Mole
FeO	0.00400	CaS	0.00270	$Ca_3Al_2Si_3O_{12}$	0.0
FeS	0.0	$CaSiO_3$	0.0	Fe_2SiO_4	0.0
Fe	0.0	$Ca_2Al_2SiO_7$	0.00180	Al_2SiO_5	0.0
CaO	0.0161	Ca_2SiO_4	0.00490	$CaAl_2Si_2O_8$	0.0
SiO_2	0.0	Al_2O_3	0.0	$Ca_2Fe_2O_5$	0.0

TABLE 2
EDX chemical analysis for particles from bench scale drop tube furnace runs at 2200°F with calcium added to Pittsburgh #8 slag

Grain	Na	Al	Si	S	Ca	Fe
1	1.40	21.02	43.97	0.32	19.23	11.91
2	3.14	12.87	54.01	0.34	12.13	14.50
3	3.23	13.34	53.39	0.25	12.84	13.50
4			40.93		58.87	
5	0.64	12.15	34.86		43.80	4.28

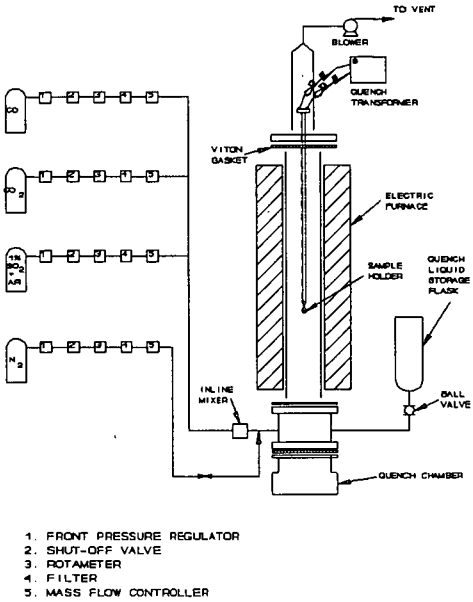

FIGURE 1 Schematic for Equilibrium Furnace

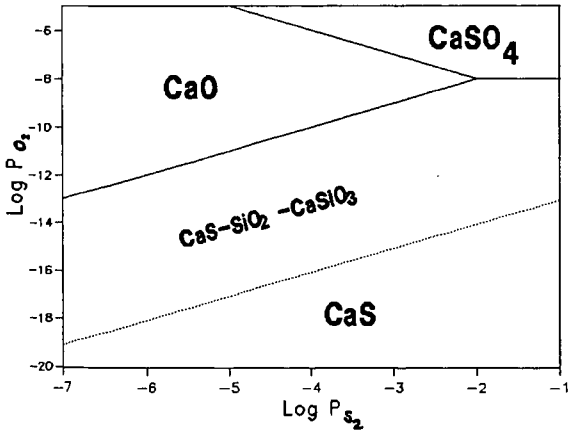

FIGURE 2 Silicate-sulfide-oxide equilibrium for Calcium at 2200°F

PREDICTION OF SO_2 REMOVAL FOR POWER PLANTS USING INDUCT INJECTION OF LIME SLURRY

*Peter Harriott, John Ruether and **Fred Sudhoff

U.S. Department of Energy
Pittsburgh Energy Technology Center
Pittsburgh, PA 15236

*At Cornell University, Ithaca, NY
**Burns and Roe Services Corporation

Keywords: duct, lime, sulfur dioxide

More than half of SO_2 emissions in the United States come from older coal- fired power plants that have no scrubbers or other devices for SO_2 removal. Pending legislation may require at least 50 percent SO_2 reduction, but it would be difficult to retrofit many of these older plants with large scrubbers of the type used for new plants. Induct injection of lime slurry is a promising method for achieving moderate SO_2 removal by simply spraying lime slurry into the flue gas between the air preheater and the solids collection equipment. The SO_2 is absorbed and neutralized in the short time that it takes for the drops to evaporate, and the nearly dry solids are collected with the fly ash in the existing electrostatic precipitator or baghouse. A flow diagram is shown in Figure 1.

Simple Model for SO_2 Removal

Several studies of induct sorbent injection were recently carried out in pilot units using a slipstream of flue gas from an operating coal-fired utility boiler (Murphy and Samuel, 1988; Murphy et al., 1988; Drummond and Babu, 1988). Extent of SO_2 removal depends on the approach to adiabatic saturation temperature of the flue gas and on parameters describing the reaction of lime and SO_2. The results were correlated using a simple model based on the fundamentals of mass and heat transfer to and within the drops plus some empirical factors (Harriott, 1989a). The equation for fractional removal of SO_2 is:

$$E_{SO_2} = 1 - e^{-X} \quad (1)$$

where

$$X = \frac{A(SR)}{B+SR} \ln \frac{T_{in} - T_{as}}{T_{out} - T_{as}} \quad (2)$$

SR = stoichiometric ratio = $Ca(OH)_2/SO_2$ (molar)

T_{AS}= adiabatic saturation temperature, °F

The factors A and B were obtained by fitting the data and depend on the type of lime and the SO_2 concentration in the gas. A value of A = 1.25 was found for calcitic lime. Based on limited data, B was found to depend on the SO_2 content of the entering flue gas and was correlated as:

$$B = 0.05 \ (\text{ppm } SO_2)^{0.5} \quad (3)$$

The predicted SO_2 removal for different values of SR, T_{in}, and (T_{out} - T_{as}) for 1600 ppm SO_2 is shown in Figure 2.

For given inlet conditions, the SO_2 removal can be improved by increasing the stoichiometric ratio or by decreasing the approach to the saturation temperature. However, too close an approach will lead to incomplete drying and deposition of wet solids in the duct or the particulate collection device. Plants that have long ducts or low flue gas velocities to give 2-3 seconds residence time in the longest straight duct could operate with a close approach to saturation and achieve good SO_2 removal with moderate excess of lime. Plants with less than 1 second residence time in a straight length of duct would have to use a larger approach to insure dry solid at the exit and might not get 50% SO_2 removal even with a large excess of lime.

Duct Survey and FORTRAN Program for Utility Boilers

Data on duct dimensions, flue gas velocities, and gas temperatures are available for 316 utility boilers in a Duct Survey data base at PETC (Sarkus and Henzel, 1988). The units surveyed have capacities of at least 50 MWe and SO_2 emissions of 1.8 lb SO_2/MM Btu or greater and are less than 35 years old. Further information on the size rating of the boilers, the coal used, and the coal properties are contained in the ORACLE data base at PETC. This information was used along with the simple model (Equations 1-3) to develop a FORTRAN program for predicting the expected SO_2 removal for each boiler in the survey at different operating conditions and stoichiometric ratios.

A key part of the computation is estimating the permissible approach to saturation. A typical spray was assumed to have a surface mean droplet size of 30 microns and a maximum size of 70 microns. The calculated drying times based on plug flow of gas and zero slip was correlated with the equations:

$$t_{dry} = \frac{60\ F_D\ F_S}{\Delta\ T_{lm}} \qquad (4)$$

where

$$F_D = 1 + 0.05\ \frac{(T_{in} - T_{as})}{(T_{out} - T_{as})} \qquad (5)$$

$$F_S = \left(\frac{d_{max}}{70}\right)^2 \qquad (6)$$

and T_{lm} is the log mean temperature difference between the spray and flue gas at the beginning and end of the straight length of duct. The factor F_D allows for the effect of drop size distribution, which makes the largest drops evaporate more slowly than they would in a monodispersion (Harriott, 1989b). The factor F_S is used if the largest drop size is greater than 70 microns.

The first step in the program is the calculation of the approximate gas residence time based on the inlet velocity and the longest straight duct length. Space in the straight duct required for atomization equipment is neglected, and the complete gas residence time is assumed to be available for droplet drying. Then the outlet gas temperature is calculated by trial to make the drying time from Eq. (4) match the residence time. The approach to saturation is specified to be at least 20 F^o to insure that the particles are dry enough to prevent sticking on the duct walls. The closest approach to adiabatic saturation that will yield stable operation is yet to be firmly established in full scale operation. The amount of water to be added is then determined by a heat balance. The Ca/S ratio is set at arbitrary values such as 1.5 or 1.8 and the SO_2 removal calculated, or the SO_2 removal is fixed and the Ca/S ratio determined.

Results for Normal and Part-Load Operation

The distribution of residence times in the longest straight duct at full load for the boilers in the survey is shown in Figure 3. Residence time for most boilers falls in the range 0.4 - 1.6 seconds. The projected SO_2 removals for a few plants with residence times ranging from 0.40 - 1.98 seconds at full load are given in Table 1. Over 50% SO_2 removal is possible at SR = 1.8 except for the two plants with the lowest residence times.

To illustrate how SO_2 removal depends on some of the independent variables, a typical boiler has been chosen as a baseline for a process variable study. The boiler chosen, at the Genoa Station in Wisconsin, has a capacity of 350 MWe and a straight duct residence time of 0.60 seconds at full load. Its flue gas contains about 1395 ppm SO_2. The effect of residence time on SO_2 is shown in Figure 4, where the residence time at Genoa Station is treated as if it were an independent variable. The calculations have been performed such that the maximum amount of water was injected

subject to the drying conditions and minimal allowable approach to adiabatic saturation described above. It is seen that for all stoichiometries considered, the SO_2 removal would increase significantly at Genoa Station if the duct residence time were increased from 0.60 s to about 1.0 s. The increased removal is due not only to longer reaction time, but also to a closer approach to saturation that is possible with the longer drying time. For times above about 1.2 s little additional SO_2 removal is predicted. This is because the system at 1.2 s residence time is already operating at the closest approach to saturation permitted, and the model predicts little further reaction with almost dry lime particles.

The importance of the approach to saturation is further illustrated in Table 2, where the effect of operating under reduced load conditions is shown for the Genoa Station. Operation of a boiler at part load increases the gas residence time but decreases the gas temperature at the injection point. The increased gas residence time permits operation at a closer approach to adiabatic saturation as well as providing longer reaction time. Both effects improve SO_2 removal. Compared to full load, operation at 80% load is predicted to increase the SO_2 removal by 7 percent absolute.

The increase in SO_2 removal with decreasing approach to saturation is similar to that observed in the dry scrubbing process, where flue gas is contacted with lime slurry in a spray dryer. However, the contact time in the spray dryer is about 10 seconds, in contrast to the typical residence times of 0.5-2 seconds in the duct. When the residence time in the duct is sufficient to allow a 20 F° approach to saturation, the predicted SO_2 removal is still less than that reported for a spray dryer. The difference is probably caused by additional SO_2 absorption in the almost dry solid during the last 8-9 seconds of residence time.

Total Emissions Reduction

The 316 power plant boilers in the survey data base have a total capacity of 85,400 MWe and had uncontrolled emissions of 7.9

million tons SO_2/year in 1985. Using induct injection of lime slurry at Ca/S = 1.8, the model was used to estimate SO_2 removal in each boiler. The total SO_2 removed is computed to be 4.7 million tons/year for an average removal of 57 percent.

The predictions given here are estimates based on limited data. A more thorough laboratory, pilot-plant, and modeling study of the induct process is now being carried out under DOE sponsorship, and a design handbook for the process will be prepared. However, the simple model used here, with corrections to fit current data, may still be useful for quick comparisons or for predicting the effects of changes in plant operation on SO_2 removal.

REFERENCES

1. Harriott, P., "A Simple Model for the Induct Injection Process for SO_2 Removal," 1989a, submitted to JAPCA.

2. Harriott, P., "Drying Times for Slurry Droplets in the Duct Injection Process," 1989b, U.S. Department of Energy.

3. Murphy K.R., and E.A. Samuel, "In-duct Scrubbing Pilot Study," Fourth Annual Coal Preparation, Utilization, and Environmental Control Contractors Conference, Pittsburgh, PA, August, 1988.

4. Murphy, K.R., E.A. Samuel, and A. Demian, "In-duct Scrubbing Process," First Combined FGD and Dry SO2 Control Symposium, St. Louis, MO, Oct. 1988.

5. Drummond, C.J., and M. Babu, "Duct Injection Technologies for SO2 Control," ibid.

6. Sarkus, T.A. and D.S. Henzel, "DOE's Duct Injection Survey," presented at Fourth Annual DOE Coal Preparation, Utilization, and Environmental Control Contractor's Conference, Pittsburgh, Aug. 8-11, 1988.

TABLE 1

Predicted SO2 Removal for Selected Plants at SR= 1.8

Station	MWe	PPM	Tin	Tout-Tas	t	ESO2
			°F	°F	sec	%
Gibson	668	1874	320	51	0.68	53
Hutsonville	81	1927	300	48	0.73	52
JM Stuart	610	1032	288	29	1.00	70
Joppa	183	1337	320	84	0.50	40
JP Pullian	125	1526	350	108	0.40	34
Lansing	36	2165	305	40	0.77	58
New Castle	105	1008	256	20	1.98	72

TABLE 2

SO_2 REMOVAL EFFICIENCY AT REDUCED FIRING RATES*

Firing Rate	Inlet Temp °F	Residence Time, Sec	Approach to TAS °F	SO_2 Removal Efficiency %
Full	380	0.6	54	54
80%	348**	0.75	37	61
50%	330	1.2	20	71

Notes:

*SO_2 Concentration 1395 PPM, Ca/S Ratio = 1.4.

**Estimated Values

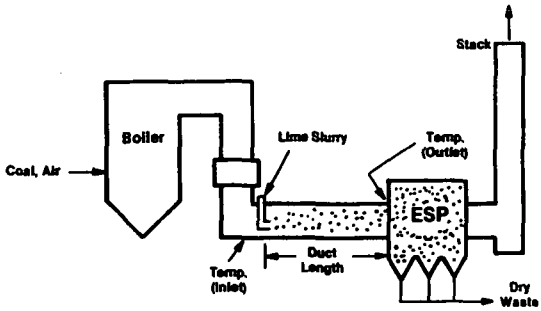

FIGURE 1. INDUCT LIME SLURRY INJECTION PROCESS FLOW DIAGRAM.

DJ19,378

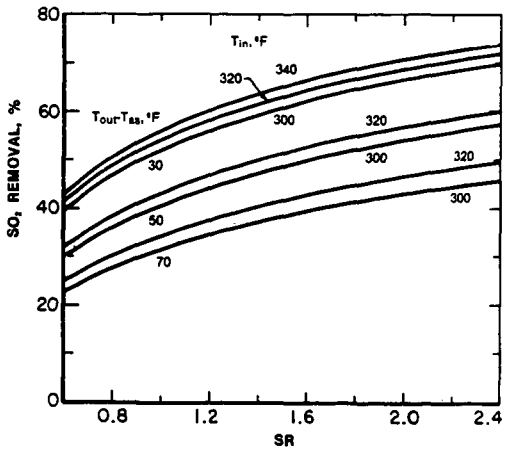

Figure 2. Dependence of SO_2 Removal on Stoichiometric Ratio.

NO/18,898

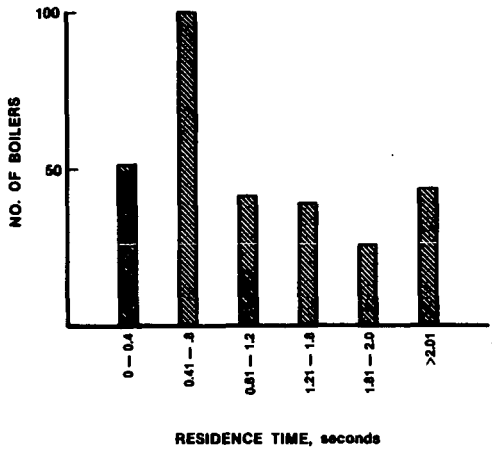

Figure 3. Residence Times in Longest Straight Duct at Full Load for Survey Data.

NO/19,565

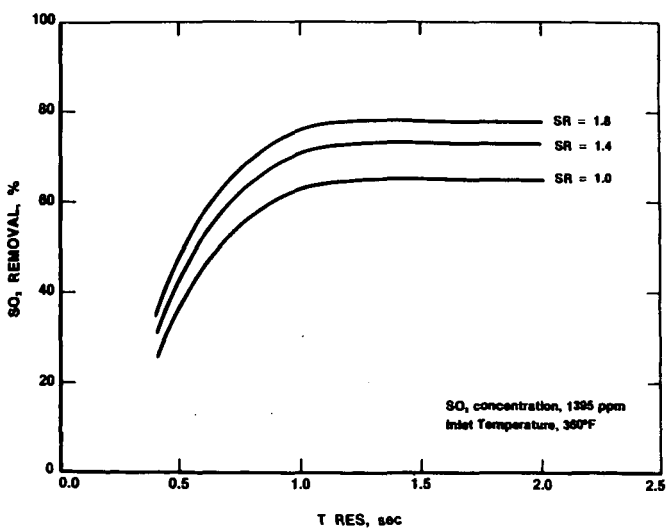

Figure 4. Dependence of SO_2 Removal on Residence Time.

NO/19,564